

Polish Chitin Society

**PROGRESS ON CHEMISTRY
AND APPLICATION OF CHITIN
AND ITS DERIVATIVES
(PCACD)**

Volume XXIX

Łódź, Poland 2024

Editor-in-Chief: Magdalena Gierszewska

Faculty of Chemistry,
Nicolaus Copernicus University in Toruń,
ul. Gagarina 7, 87-100 Toruń, Poland
e-mail: mgd@umk.pl

International Editors:

C. M. Caramella, University of Pavia, Italy
H. Ehrlich, TU Bergakademie Freiberg, Germany
S. Hudson, North Carolina State University, USA
S. Ifuku, Tottori University, Japan
H. Pospieszny, Institute of Plant Protection, Poland
S. Rossi, University of Pavia, Italy
S. Senel, Faculty of Pharmacy, Hacettepe University, Turkey
V. Varlamov, Russian Academy of Science, Russia



We would like to inform that the development, publication, and dissemination of the XXVII volume (2022), XXVIII volume (2023), and XXIX volume (2024) of the journal ‘Progress on Chemistry and Application of Chitin and its Derivatives’ (PCACD) is funded from the state budget under contract RCN/SN/0122/2021/1 from the resources of the Minister of Education and Science in the frame of the program ‘The development of scientific journals’

Co-financing: 50 000 zł Total value: 50 000 zł

ISSN 1896-5644

All rights reserved

©Copyright by the Polish Chitin Society



Printed by: Media-Press, Lodz, Poland

CONTENT

<i>Review</i> Bożena Losiewicz, Patrycja Osak, Delfina Nowińska	7
Recent advances in the electrophoretic deposition of chitosan-silver nanocomposite coatings on metallic implants with enhanced biocidal properties	
<i>Review</i> Olga Marchut-Mikołajczyk	21
Endophytic fungi as chitin-modifying enzymes producers	
<i>Review</i> Patrycja Osak, Bożena Losiewicz, Delfina Nowińska	30
Chitosan as a drug carrier	
<i>Review</i> Marcin Przybyła, Barbara Dolińska, Aneta Ostróżka-Cieślik	44
Progress of knowledge in the development of chitosan formulations with insulin to promote skin wound healing	
<i>Review</i> Julia Rypińska, Justyna Kozłowska	60
Applications of chitosan in the preparation of care cosmetics	
<i>Review</i> Shuhrat Shamsiddinovich Khudoyberdiyev, Noira Rakhimovna Vokhidova, Sayyora Sharafovna Rashidova	75
Synthesis and properties of binary and ternary interpolyelectrolyte complexes of chitosan	
Volodymyr Antonyuk, Nazar Manko, Lidiia Panchak, Semen Khomyak, Oleksandr Gromyko, Rostylav Stoika	99
Synthesis of chitosan composites with methylene blue, malachite green and acid fuchsin dyes for enhancement of their antimicrobial action	
Mateusz Data, Danuta Ciechańska, Lukasz Hojarski, Bogumil Brycki, Maria Wiśniewska-Wrona, Ewa Kopania, Justyna Wietecha, Dorota Kaźmierczak, Jagoda Jóźwik-Pruska	113
Hygienic papers modified by functional biopolymer-biocide compositions in a pilot research installation	

Joanna Dziedzic, Dorota Biniś, Włodzimierz Biniś	128
Study of the kinetics of copper ion sorption by chitosan spheres	
Urszula Filipkowska, Tomasz Józwiak	140
The combination of waste products from chitin and sawdust to remove anionic and cationic dyes	
Marcelina Krupa-Malkiewicz, Ireneusz Ochmian	156
Comparison of the effectiveness of chitosan and auxin on <i>in vitro</i> and <i>ex vitro</i> rooting of <i>Vaccinium corymbosum</i> L.	
Macelina Krupa-Malkiewicz, Ireneusz Ochmian	166
Alleviative effects of chitosan and nanosilver on <i>Solanum pimpinellifolium</i> under heavy metal stress <i>in vitro</i>	
Katarzyna Malolepsza-Jarmołowska, Hanna Bazan	178
Protection of the oesophageal mucosa with chitosan gels	
Katarzyna Malolepsza-Jarmołowska, Hanna Bazan	186
Studies on chitosan gels with polyvinyl alcohol to protect the oesophageal mucosa	
Rakiya Yunusovna Milusheva, Ilnar Nakipovich Nurgaliev, Sayora Sharafovna Rashidova	194
Features of the interaction and formation of nanostructured chitosan systems during ionotropic gelation	
Krzysztof Nowacki, Maciej Galiński	213
<i>o</i> -Phthalaldehyde cross-linked chitosan membrane as a quasi-solid-state electrolyte for supercapacitors	
Ireneusz Ochmian, Marcelina Krupa-Malkiewicz	231
Response of the 'polesie' raspberry cultivar to foliar application of chitosan with different molecular weights	
Anna Rył, Piotr Owczarz	244
Dynamic light scattering-based microrheology of thermosensitive chitosan hydrogels: preliminary studies	

Piotr Salachna, Agnieszka Zawadzińska	254
Foliar application of depolymerised chitosan enhances the growth and content of polyphenols and L-ascorbic acid in <i>Eucomis autumnalis</i> , an ornamental and medicinal plant	
Barbara M. Stencel, Małgorzata M. Jaworska	263
pH stability and kinetics of pH deactivation of chitin deacetylase produced by <i>Absidia orchidis</i>	
Katarzyna Struszczyk-Świta	270
The use of enzymes from <i>Mucor circinelloides</i> IBT-83 in the synthesis of chitoooligosaccharides – preliminary research	
Klaudia Szafran, Małgorzata Jurak, Robert Mrocza, Katarzyna Pastuszak, Agnieszka Ewa Wiącek	276
Polyethylene terephthalate (PET) coated with chitosan and cyclosporine A layers as a potential stent material and drug-delivery system	
Marta Wiśniewska-Wrona, Monika Sikora, Monika Owczarek	289
Polymer biocomposites in the form of hydrogel used for the treatment of pressure sores	
Agnieszka Zawadzińska, Piotr Salachna	306
Effect of chitosan with different molecular weight on the growth and bulb yield of oriental lily ‘Mona Lisa’	

REVIEW

RECENT ADVANCES IN THE ELECTROPHORETIC DEPOSITION OF CHITOSAN-SILVER NANOCOMPOSITE COATINGS ON METALLIC IMPLANTS WITH ENHANCED BIOCIDAL PROPERTIES

Bożena Łosiewicz^{1,a,*}, Patrycja Osak^{1,b}, Delfina Nowińska¹

¹ – Institute of Materials Engineering, Faculty of Science and Technology, University of Silesia in Katowice, 75 Pułku Piechoty 1A Str., 41-500 Chorzów, Poland

^a – ORCID: 0000-0001-9472-1893; ^b – ORCID: 0000-0002-0628-6367

*corresponding author: bozena.losiewicz@us.edu.pl

Abstract

This review covers the latest issues related to the development of medical technologies based on chitosan coatings. The progress of modern implantology requires medicine to adapt constantly to new opportunities and challenges. Infections may occur at the implantation site or in the body and may require treatment with antibiotics or surgery to resolve them. Due to its unique properties, such as biocompatibility, biodegradability, non-toxicity and antibacterial activity, chitosan has been proposed to be co-deposited with biocidal silver nanoparticles in the form of nanocomposite coatings on the surface of metallic implants to extinguish local inflammations. The mechanism of co-deposition of chitosan with metal ions and particles using electrophoretic deposition has not yet been thoroughly explained. This, among others, results from a number of factors that influence the process and their mutual relations. Therefore, the present review aims at a deeper understanding of the mechanism of creating chitosan-silver nanocomposite coatings.

Keywords: biocide, chitosan, electrophoretic deposition, metallic implants, nanocomposite, silver nanoparticles

Received: 28.02.2024

Accepted: 13.05.2024

1. Introduction

Metallic biomaterials are one of the fastest developing groups of biomaterials due to their biocompatibility, high corrosion resistance in the environment of bodily fluids, good mechanical properties, the possibility of modifying properties by creating alloys, the possibility of modifying the structure by changing the size of grains and precipitates, and the possibility of modifying the surface by selecting the appropriate roughness or applying coatings [1–4]. Metallic biomaterials are used in orthopaedics, craniofacial surgery, dentistry, heart surgery and endovascular surgery [4]. They are mainly used to produce implants to stabilise bone fragments and to treat bone defects, and also as heart valves, stents, endoprostheses and dental prostheses. Some of the most commonly used metals and alloys for implants include titanium [5, 6] and titanium alloys [7–11], cobalt-chromium alloys [12], austenitic steel [13], nickel-titanium alloy [14, 15] and magnesium alloys [16]. The choice of metallic biomaterial for an implant depends on various factors, including the specific application, the patient's medical history and the surgeon's experience and preferences.

The biocompatibility of metallic biomaterials can be increased by using chitosan (Chit) coatings; Chit is one of the most promising natural polymers, especially in tissue engineering and regenerative medicine [17–21]. On an industrial scale, Chit is produced by deacetylation of chitin [18, 22, 23]. The sources of chitin – the shells of red crabs, shrimp, krill and other crustaceans – are obtained during processing sea fishing for food. Chit can also be isolated from the cell walls of the filamentous fungi belonging to the class Zygomycetes (the *Mucor*, *Absidia*, *Rhizopus* and *Gongronella* genera) [24]. By adding the appropriate enzymes to the fungi and using the optimal composition of the medium, with the help of alkaline separation of the insoluble fraction in bases, it is possible to separate Chit from fungal biomass. Thanks to continuous mushroom cultivation, it is possible to obtain a large amount of raw material for the production of Chit in a relatively short time.

In an environment with low ionic strength, Chit takes the form of an extended structure of macromolecules due to electrostatic repulsion between segments of the chain. When the ionic strength tends to infinity, it completely neutralises the proton groups, causing the electrostatic repulsion forces to disappear, and the structure of Chit becomes a compact zone regardless of differences in molecular weight. The presence of free protonated amino groups in the Chit structure allows the formation of complexes with derivatives with a negative charge, such as polymers, proteins or dyes. In addition, Chit may bind selectively to cholesterol, fat, cancer cells, DNA and RNA. Chit also has the ability to form chelates with metal ions, which requires the special involvement of –OH and –O– groups in D-glucosamine residues, and amine ions in Chit complex metal ions more effectively than acetyl groups in chitin [17].

Chit is used in medicine as a component of dressing materials, as it stops bleeding; accelerates wound healing; and exerts anti-inflammatory, analgesic, antiviral, antifungal and antibacterial effects [17, 18, 25–27]. Chit has the ability to adsorb strongly on mucous membranes, which allows it to be used as a carrier in mucoadhesive drug-delivery systems, thanks to which drugs are bound to the site of their action, that is, mucous membranes [28]. This natural biopolymer also has the ability to create a variety of morphological structures such as films, membranes, nanoparticles, fibres and knitted and nonwoven fabrics made from them, and hydrogels [17–22, 28]. Moreover, the chemical composition of Chit is similar to the composition of the extracellular matrix of biological systems [29]. In addition to biocompatibility, Chit also shows biodegradability, bioactivity, non-toxicity, water wettability, the ability to chelate and bind metal ions and organic substances, easy miscibility, and can also be a matrix for dispersed solid particles [17–19, 21, 28, 30–32]. Particularly interesting is the possibility of producing Chit-based

nanocomposite coatings with dispersed silver nanoparticles (Ag NPs), which show high antibacterial activity [33]. Ag NPs production methods, their properties and their possible mechanisms of antibacterial activity have been discussed in detail in previous studies [33–36]. Ag NPs used in medicine are nanomaterials that have a size of 1–100 nm in at least one dimension or at least 50% of the particles in the particle size distribution are in the nanometre scale. They exhibit significant antibacterial activity due to their high surface-area-to-volume ratio, which increases as their size decreases [34, 35]. Smaller Ag NPs show an increased active surface, which consequently leads to greater antibacterial activity. Moreover, by selecting appropriate reaction conditions, the shape of Ag NPs can be controlled. Ag NPs in the form of spheres (e.g. a diameter of 5–100 nm [35], 40–80 nm and 120–180 nm [34]), platelets (e.g. 20–60 nm [34]), cubes (e.g. 140–180 nm [34]), rods (e.g. a diameter of 80–120 nm and a length of > 1000 nm [34]) and triangular (e.g. 31 nm [35]), have been prepared. The published reports regarding the influence of the shape of Ag NPs on their antibacterial activity are contradictory [34–36]. Some authors claim that among different shapes of Ag NPs, those in the triangular form have the highest antibacterial activity due to their sharp edges and vertices, and the largest active surface area [36]. Others have proved that spherical Ag NPs have the highest antibacterial activity [34, 35]. Co-deposition of Ag NPs with these unique physicochemical properties and the Chit matrix on metallic substrates using electrophoretic deposition (EPD) enhances the biocidal properties of Chit-Ag NP nanocomposite coatings due to the synergistic effect of both the Chit matrix and the embedded Ag NPs composite component [37, 38].

This review discusses the latest research of Chit-Ag NP nanocomposite coatings on metallic implants, especially dental implants, obtained using the EPD method. The main goal of this review is to provide a deeper understanding of the mechanism by Chit-Ag NP nanocomposite coatings are formed; it has yet to be fully understood due to numerous factors that influence the EPD process. The studies included in this review were retrieved from the Scopus database, with a publication range covering the last 5 years.

2. Inflammation and Complications After Implantation

Biomaterials should be biocompatible, which means harmony of interactions within living matter [1–4]. Biocompatible implants do not initiate toxicological and immunological reactions and do not irritate tissues in the host's body. However, inflammation occurs after each implantation because mechanisms are stimulated in a living organism to reject the implant as a foreign body [2, 3, 20]. After the implant is detected by the immune system, the body starts producing antibodies that have a strong oxidising effect. As a result of the body's defensive reaction, proteins accumulate near the implant and are absorbed into it, which initiates the degradation of the implant. Protein dissociation and reactions at the cellular level cause changes in the pH of the blood and bodily fluids, which constitute a strong corrosive environment with a high concentration of chloride anions. Bodily fluids are buffer solutions with a stable pH in the range of 7.00–7.35. After implanting a metal biomaterial into the bone, the pH in the area surrounding the implant decreases to approximately 5.20 and returns to the physiological value of 7.35–7.45 only after 2 weeks. Additionally, the concentration of dissolved oxygen in bodily fluids is unfavourable – four times lower than the concentration in air – which delays the regeneration of the self-passive oxide layer and increases the amount of metal ions released from the surface of the metal implant into the body [4–9, 12–15, 30, 31]. Other reasons why inflammation may occur after implantation include surgical trauma causing tissue damage, infection as a result of bacteria or other pathogens entering the body during the implantation process, an allergic reaction to the biomaterials used in the implant or the biomaterials applied

during the surgical procedure, and implant malposition leading to irritation or pressure on surrounding tissues [1, 3, 4].

Although implantation has a high success rate of up to 98%, the invasiveness of commonly performed implant procedures also carries the risk of complications after implantation, which is an inherent element of the osseointegration process [39]. Complications may occur at the early and late stages of osseointegration. Complications in the early stages include infection; swelling; haematomas; petechiae; and bleeding occurring in the maxilla and mandible, sinuses and soft tissues around the implant, which are caused by a surgical approach that is too traumatic, overheating of bone tissues during the procedure or bacterial infection of the wound. Late-stage complications are a consequence of complications of the early stage of osseointegration and are manifested by mucosal perforation, maxillary sinusitis, mandibular fractures, failure of osseointegration, bone defects and periapical implant failure. Of note, bacterial contamination during the procedure and improper oral hygiene after implantation increase the risk of complications. Peri-implant infections are initiated mainly by bacteria attaching to implants in the form of biofilm and can be classified based on the route of spread, the time of implant contamination, the period of symptom onset and the course of infection [39–41].

Post-implantation complications can be divided into mechanical, technical and biological [40]. The main cause of mechanical complications after implantation implant placement that is too tight, implant displacement or excessive force loading the implant, as is the case, for example, in the case of bruxism (Figure 1a) [42]. One of the most common mechanical complications after implantation is overloading the implants, leading to their loosening or fracture. Implant fractures occur due to manufacturing defects or as a result of loading the implant too quickly with a prosthesis or bridge.

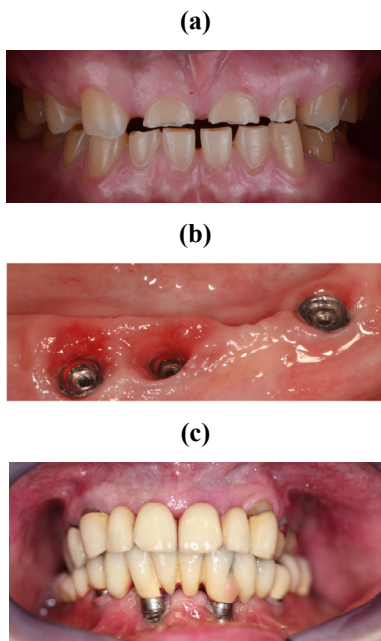


Figure 1. (a) Chipped and worn teeth as a result of bruxism [42] (the image is from stock.adobe.com and has been reproduced under the terms and conditions of a standard license), (b) peri-implant mucositis [41] (this image has been reproduced under the terms and conditions of a Creative Commons Attribution [CC BY] license) and (c) peri-implantitis [43].

When occlusal forces are too high – approximately 200–300 N, there is damage to the implant connector and subsequent loosening of the shaft [40]. Technical complications often occur with implant-supported fixed partial dentures and include fractures of the veneering porcelain and fractures of the framework. The group of biological complications includes sensory disturbance, progressive bone loss, formation of bacterial plaque and bacterial infections.

Peri-implant diseases include inflammation of the mucosa around implants with clinical symptoms of redness, swelling and bleeding [41, 44]. They are classified into curable peri-implant mucositis and incurable peri-implantitis. Figure 1b shows a clinical case of peri-implant mucositis with inflammation induced by abutment loosening [41]. Marginal inflammation of the peri-implant mucosa is visible without loss of supporting bone after initial bone remodelling. When the extent of inflammation increases and exceeds the gum–bone border with bone destruction, the disease progresses to peri-implantitis (Figure 1c) [43]. This destructive inflammatory process affects both soft and hard tissues surrounding dental implants. The longer peri-implantitis lasts, the greater the bone loss, which may lead to the loss of implants along with the prosthetic restoration. Therefore, there is a need to develop innovative dental implants with enhanced osteoinductive properties with the possibility of intelligent and controlled drug delivery directly to the site of inflammation.

3. Production Methods of Chitosan-Silver Nanocomposite Coatings

Chit-Ag NP nanocomposite coatings are biodegradable, biocompatible and environmentally friendly biomaterials that have attracted significant attention in recent years due to their potential applications in medicine [37, 38]. The production of these coatings involves the incorporation of Ag NPs into the Chit matrix to enhance their properties, such as mechanical strength, thermal stability and barrier properties. Table 1 lists several methods developed for the production of Chit-Ag NP nanocomposite coatings along with a description of the basis of each method.

Each method has its advantages and disadvantages, and the choice of method depends on the specific application and desired properties of the nanocomposite coating. Chit-Ag NP nanocomposites are advanced and multifunctional biomaterials composed of Ag NPs dispersed in a polymer matrix and/or covered with a polymer (core shell) [45]. Regarding the use of EPD to produce Chit-Ag NP nanocomposite coatings, the advantages are it requires relatively inexpensive and simple equipment; it is easy to control the properties, thickness and porosity of thin films by changing EPD parameters; sensitive biomaterials such as Chit can be co-deposited at room temperature; substrates with complex shapes can be coated homogeneously; it requires a short amount of time; easy scalability; and high production efficiency. The main disadvantage of EPD include Ag NP agglomeration in the suspension bath during the production of Chit-Ag NP nanocomposite coatings, which requires the use of surfactants and nanoparticle stabilisers [17].

Table 1. Methods for the production of chitosan silver nanoparticle (Chit-Ag NP) nanocomposite coatings.

Type of method	Description of the method	Reference
Solvent casting	Chit and Ag NPs are dispersed in a suitable solvent, such as acetic acid or water, to form a homogeneous solution, which is then cast onto a substrate and allowed to dry, forming a thin nanocomposite coating. The solvent is evaporated, leaving behind the nanocomposite coating on the substrate.	[46]
Electrospinning	An electric field is used to generate a jet of Chit-Ag NP solution, which is then collected on a grounded collector to form a nanofibrous mat. The electrospinning process allows for the formation of nanofibers with high surface area and tunable pore size, which can be tailored for specific applications.	[46]
Layer-by-layer assembly	Alternating deposition of Chit and Ag NPs onto a substrate is used to form a multilayer coating. The process is typically carried out by dipping the substrate into a solution containing Chit and Ag NPs, followed by rinsing with a suitable solvent to remove any unbound species. The desired number of layers is achieved by repeating the process.	[46]
In situ polymerisation	Chit is mixed with a monomer and a cross-linker, and Ag NPs are added to the mixture. The mixture is then heated or irradiated to initiate the polymerisation process, resulting in the formation of a nanocomposite coating. This method can be used to prepare coatings with high mechanical strength and improved barrier properties.	[46]
Co-precipitation	Chit and Ag NPs are mixed in a suitable solvent, and a precipitating agent is added to form a nanocomposite precipitate, which is then collected by filtration, washed with a suitable solvent, and dried to form a nanocomposite coating.	[46]
Spray-drying	Dispersion of Chit and Ag NPs in a suitable solvent is used, followed by the introduction of the solution into a spray dryer. The solvent is evaporated in the spray dryer, forming a powder of the nanocomposite coating. The powder can then be collected and used for various applications, such as encapsulation or coating.	[46]
Electrophoretic deposition	Synthesis of thin nanocomposite Chit-Ag NPs films and coatings on various substrates is available. This method relies on the movement of charged particles under an electric field to deposit them on a metallic electrode.	[38, 45–49]

4. Chitosan-Silver Structure

Chit-Ag NPs are a nanocomposite biomaterial where Ag NPs are embedded into a Chit matrix (Figure 2). When the natural polymer Chit is combined with Ag NPs, which have antimicrobial properties, the resulting Chit-Ag NP nanocomposite exhibits enhanced antibacterial activity [50–52]. The structure of the Chit-Ag NP nanocomposite involves Ag NPs distributed within the Chit polymer matrix [53].

Chit is a linear polysaccharide composed of randomly distributed β -(1 \rightarrow 4)-linked D-glucosamine (a deacetylated unit) and N-acetyl-D-glucosamine (an acetylated unit). The presence of amine groups is responsible for many of the unique properties of Chit, including biocompatibility, biodegradability and the ability to form films [45, 54]. The structure does not indicate the degree of polymerisation or the ratio of deacetylated to acetylated units, which affect the physicochemical properties of Chit. The presence of amino and hydroxyl groups in the Chit structure allows it to form stable interactions with Ag NPs [53]. Chit's affinity for Ag NPs may be due to the formation of chemical bonds between electron-rich nitrogen atoms and the lone pairs in the silver orbitals, which is important for creating new Chit-Ag NP nanocomposite structure. The amino groups of Chit can change the permeability of bacterial cells by reacting with anionic groups on the surface of bacterial cells [19, 20, 22, 23, 45].

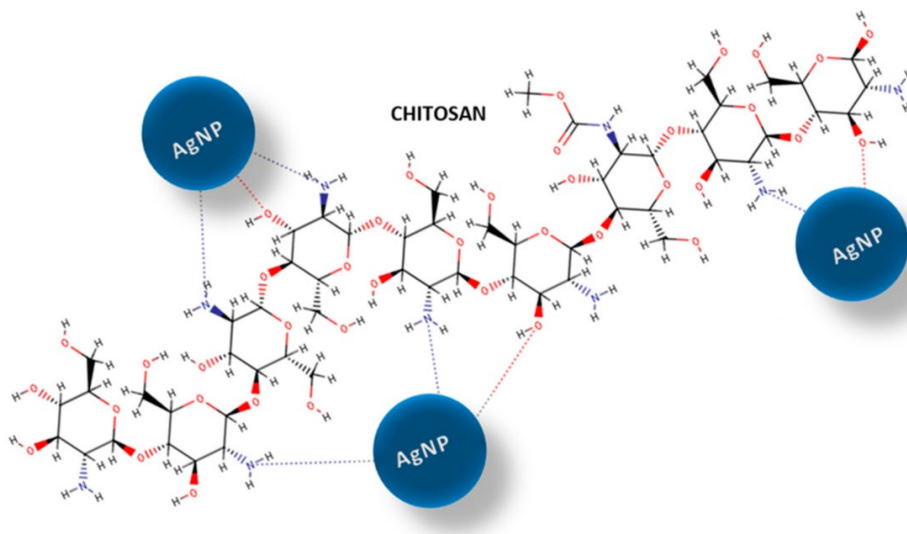


Figure 2. A schematic illustration of how silver nanoparticles (Ag NPs) are embedded into the chitosan (Chit) matrix [53]. This figure has been reproduced under the terms and conditions of a Creative Commons Attribution (CC BY) license (<https://creativecommons.org/licenses/by/4.0/>).

Such properties of Chit-Ag NP nanocomposites result in a growing interest in these biomaterials for the needs of modern medicine. Chit-Ag NP nanocomposites may be used in the future as therapeutic agents to fight pathogenic microorganisms whose drug resistance is increasing. According to the literature, Chit-Ag NP nanocomposites have biocidal properties against *Escherichia coli*, *Escherichia bacillus*, *Enterococcus faecium*, *Candida albicans*, *Klebsiella pneumoniae*, *Pseudomonas aeruginosa* and *Staphylococcus aureus*, among other microorganisms [45, 51]. There is also a need to develop innovative metallic implants with increased osteoinductive properties with the possibility of intelligent

and controlled drug delivery directly to the site of inflammation. The use of such implants would result in a gentler course of treatment for patients and a reduction in the amount of anti-inflammatory drugs they take. This is especially important for older people, who are often additionally burdened with oral drug supplementation, which is required in the treatment of other age-related diseases, such as hypertension, diabetes, rheumatological diseases and others [1–3, 6, 8–13].

5. Electrophoretic Deposition Mechanism of Chitosan-Silver Nanocomposite Coatings

EPD is used to deposit particles, such as colloids or suspensions, onto a substrate using an electric field [55]. The particles to be deposited are suspended in a liquid medium, such as water, and the mixture is stirred or agitated to obtain a homogenous suspension (Figure 3a). The pH of the suspension is also adjusted to ensure that the particles have stable electrophoretic mobility.

Researchers have proposed EPD for green synthesis of Chit-Ag NP nanocomposite coatings based on chemical reduction from a dilute acetic acid using silver nitrate (AgNO_3) as a precursor to obtain Ag NPs [31, 37, 50, 56]. According to research, citric acid yields a more compact Chit matrix structure compared with acetic acid due to less intense electroevolution of hydrogen [57–59]. The crystalline component of the Chit-Ag NP nanocomposite has also been used in the form of Ag NPs [37, 38, 60, 61].

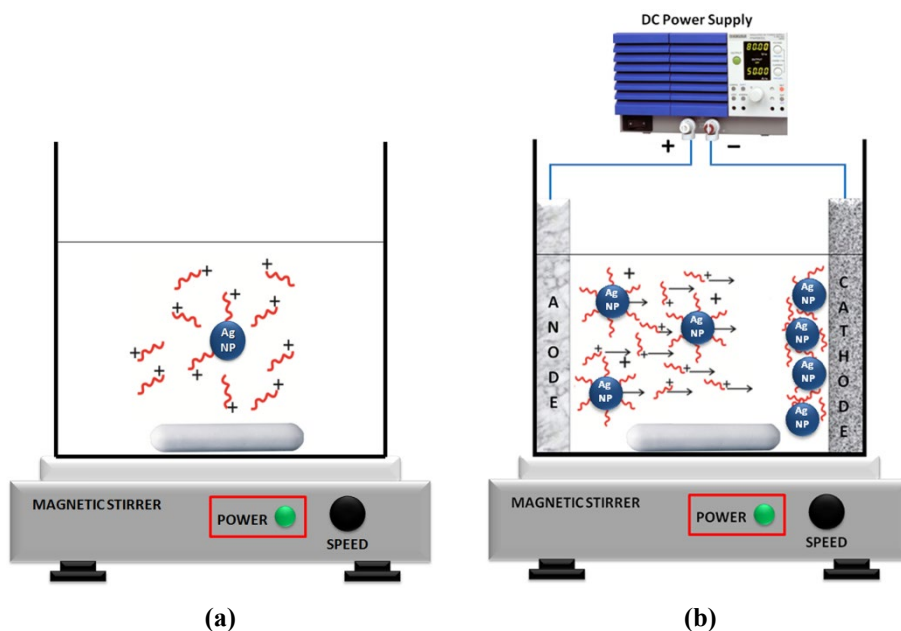


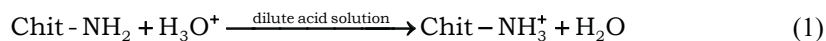
Figure 3. A schematic illustration of (a) chitosan (Chit) protonation and Chit adsorption on silver nanoparticles (Ag NPs) in a dilute solution of acid and (b) electrophoretic co-deposition of Ag NPs with Chit as a cationic polymer.

Several factors can influence the efficiency and quality of EPD, including the key EPD process parameters: the concentration of Ag NPs in the suspension (e.g. 0.05 g of Ag NPs with an average powder grain 30 nm dispersed in 1 dm³ of 1% acetic acid [38],

and 0.005 or 0.01 g Ag NPs with an average powder grain 30 nm dispersed in 100 ml of 1 vol% acetic acid [61]), the applied voltage (e.g. 10 V [38, 61], 15 V [60], 20 V [38] and 30 V [61]), the duration of the EPD process (e.g. 1 min [38, 61], 3 min [61], 10 min [60] and 30 min [31]), the pH of the suspension (e.g. 4.6 [60]) and the substrate type (e.g. Co-Cr-Mo alloy [31], a nanotubular TiO₂ layer on the Ti13Zr13Nb alloy [38], additively manufactured Ti6Al4V ELI alloy [60] and Ti Grade 2 [61]). The effects of key EPD process parameters on the improvement of microstructural homogeneity; mechanical and electronic properties; adhesion; and *in vitro* corrosion resistance, biocompatibility and biological activity of the Chit-Ag NP nanocomposite coatings on metallic implants have been reported [31, 38, 60, 61]. The EPD method has allowed researchers to produce Chit-Ag NP nanocomposite coatings with about 2 wt% Ag, which ensures maximum antibacterial activity [31], and to develop drug-delivery systems, for example, the Chit/Eudragit E 100/Ag NP nanocomposite coating [61].

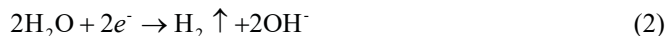
An adsorption mechanism can be proposed to explain co-deposition of Ag NPs and amorphous Chit matrix on the metallic substrate (Figure 3b). Electrode reactions do not participate in the EPD of solid particles, despite the fact that the solid particles in a colloidal solution may have a positive or negative charge depending on the pH of the solution [62]. Solid particles in a colloidal solution behave like charge carriers and provide current flow. The electric field strength in the EPD process is too weak to overcome the mutual repulsion of particles, but it is large enough for a higher number of particles to accumulate near the electrode with the opposite charge [63]. The introduction of dispersing agents or polyelectrolytes into the solution can provide the right charge for colloidal particles and ensure their correct dispersion in the solution. In cataphoresis, polyelectrolytes with a protonated –NH₂ group, such as Chit, are used; they are applied during cataphoretic co-deposition of solid particles. Chit is used as a binding agent for Ag NPs, which enable their co-deposition to obtain composite coatings on the surface of a metallic electrode. Polyelectrolytes show significant non-electrostatic interactions with solid particle surfaces [64]. Therefore, adsorption of Chit onto Ag NPs in the entire suspension volume can be assumed. Figure 3a presents a schematic illustration of the protonation of Chit and Chit adsorption on Ag NPs in a dilute acid solution. Chit adsorption may be associated with the formation of Ag-Chit chelates. Ag NPs can also interact with amino groups, between which hydrogen bonds are formed and are tightly wrapped in Chit chains (Figure 2). Ag NPs surrounded by Chit chains have a positive charge; therefore, in the EPD process under the influence of applied voltage they move towards the cathode, on which they are embedded in the coating (Figure 3b). It is worth noting that increasing the pH of the cathode area during cataphoresis may reduce electrostatic repulsion and promote chelation in the obtained coatings [62].

Based on the above, the mechanism of co-deposition of the Chit matrix with Ag NPs on a metallic substrate proceeds in two stages. In the first stage, polymer protonation occurs in the colloidal solution – a mixture of well-dispersed Ag NPs and Chit – to generate Chit macromolecules with a positive charge (Figure 3a). Chit amino groups are only protonated at pH < 6.5 [19]. Only under such conditions does Chit become a cationic polyelectrolyte according to reaction (1):

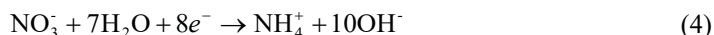


Then, the Chit chains are adsorbed onto the surface of Ag NPs, giving them a positive charge. In the EPD process, an electric field applied from an external power source causes the electrophoretic movement of positively charged Ag NPs with adsorbed Chit on the surface and free polymer chains, which move towards the cathode, on the surface of which they are co-deposited in the form of a Chit-Ag NP nanocomposite coating.

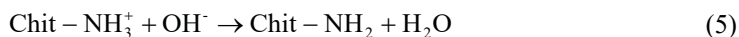
The deprotonation of positively charged Chit chains occurs at the cathode, and in the electrode space there is a local pH increase associated with the water electrolysis according to reaction (2) [65]:



Reactions (3) and (4) occur on the cathode surface:



An increase in the pH of the solution results in a decrease in charge and at pH = 6.5, the amino groups of Chit are deprotonated according to reaction (5):



As a result of neutralisation of the protonated amino groups of the Chit chain in the presence of OH^- ions, an insoluble nanocomposite coating with the Chit matrix and co-deposited crystalline component in the form of Ag NPs forms on the surface of the cathode. The deposition efficiency and quality of the deposited Chit-Ag NP nanocomposite coatings are affected by the cataphoresis conditions. It can be expected that as the concentration of Ag NPs in the colloidal solution increases, the mass of deposited polymer and co-deposited Ag NPs increases, and thus the thickness of the deposited coating increases.

6. Conclusions

Chit, a biopolymer derived from chitin, has been widely studied for its biocidal properties and biocompatibility. Ag NPs have also been recognised for their strong antimicrobial activity. There has been a marked increase in the attention directed towards the use of Chit-Ag NP nanocomposite coatings due to their potential applications in modern medicine. The combination of Chit and Ag NPs in a nanocomposite coating has shown enhanced biocidal properties, making it a promising biomaterial for antimicrobial applications to modulate inflammation and to prevent complications after implantation. Among the production methods of Chit-Ag NP nanocomposite coatings, EPD seems to be a low-cost, effective, easily scalable and promising method due to its ability to produce uniform and adherent coatings on substrates with a complex shape. However, there is a need for further research to optimise the EPD process and to understand the relationship between the deposition parameters and the biocidal properties of the Chit-Ag NP nanocomposite coatings. Considering that the antibacterial activity of Ag NPs is influenced by their shape, size, concentration, synthesis time and surface charge, the incorporation of a composite component in the form of Ag with a particle size below 1 nm, silver Ångstrom particles (Ag ÅPs), into the Chit matrix would generate a new Chit-Ag ÅP composite with superior antibacterial activity due to higher effective contact and anticancer properties of Ag ÅPs for applications in tissue engineering and drug-delivery systems.

7. References

- [1] Bayindir-Buchhalter I; (2024) Nanomedicine, Bioengineering and Biomaterials Research for Everyone. *Adv NanoBiomed Res* 4(1), 2300172. DOI:10.1002/anbr.202300172

- [2] Jana S, Jana S; (2022) *Functional Biomaterials: Drug Delivery and Biomedical Applications*. 1st ed, Springer Verlag, Singapore.
- [3] Bhaskar B, Sreenivasa Rao P, Kasoju N, Nagarjuna V, Raju Baadhe R; (2021) *Biomaterials in Tissue Engineering and Regenerative Medicine: From Basic Concepts to State of the Art Approaches*, Springer Nature, Singapore.
- [4] Wen C; (2020) *Metallic Biomaterials Processing and Medical Device Manufacturing*. 1st ed, Woodhead Publishing Series in Biomaterials, Sawston.
- [5] Łosiewicz B, Osak P, Maszybrocka J, Kubisztal J, Stach S; (2020) Effect of Autoclaving Time on Corrosion Resistance of Sandblasted Ti G4 in Artificial Saliva. *Materials* 13(18), 4154. DOI:10.3390/ma13184154
- [6] Osak P, Maszybrocka J, Kubisztal J, Ratajczak P, Łosiewicz, B; (2021) Long-term assessment of the *in Vitro* corrosion resistance of biomimetic ACP coatings electrodeposited from an acetate bath. *J Funct Biomater* 12(1), 12. DOI:10.3390/jfb12010012
- [7] Aniołek K, Łosiewicz B, Kubisztal J, Osak P, Stróż A, Barylski A, Kaptacz S; (2021) Mechanical properties, corrosion resistance and bioactivity of oxide layers formed by isothermal oxidation of Ti-6Al-7Nb alloy. *Coatings* 11(5), 505. DOI:10.3390/coatings11050505
- [8] Smółka A, Dercz G, Rodak K, Łosiewicz B; (2015) Evaluation of corrosion resistance of nanotubular oxide layers on the Ti13Zr13Nb alloy in physiological saline solution. *Arch Metall Mater* 2015(1), 2681–2686. DOI:10.1515/amm-2015-0432
- [9] Szklarska M, Dercz G, Łosiewicz B, Rak J, Simka W; (2015) The influence of passivation type on corrosion resistance of Ti15Mo alloy in simulated body fluids. *Arch Metall Mater* 60(4), 2681–2686. DOI:10.1515/amm-2015-0433
- [10] Smółka A, Rodak K, Dercz G, Dudek K, Łosiewicz B; (2014) Electrochemical formation of self-organized nanotubular oxide layers on Ti13Zr13Nb alloy for biomedical applications. *Acta Phys Pol* 125(4), 932–935. DOI:10.12693/APhysPolA.125.932
- [11] Stróż A, Dercz G, Chmiela B, Stróż D, Łosiewicz B; (2016) Electrochemical Formation of Second Generation TiO₂ Nanotubes on Ti13Nb13Zr Alloy for Biomedical Applications. *Acta Phys Pol* 130(4), 1079–1080. DOI:10.12693/APhysPolA.130.1079
- [12] Łosiewicz B, Osak P, Kubisztal J, Górka-Kulikowska K; (2023) Effect of Artificial Saliva Modification on the Corrosion Resistance and Electronic Properties of Bego Wirobond® C Dental Alloys. *Appl Sci* 13(22), 12185. DOI:10.3390/app132212185
- [13] Łosiewicz B, Osak P, Górka-Kulikowska K, Goryczka T, Dworak M, Maszybrocka J, Aniołek K; (2023) Effect of Artificial Saliva Modification on Pitting Corrosion and Mechanical Properties of the Remanium®-Type Orthodontic Archwire. *Materials* 16(20), 6791. DOI:10.3390/ma16206791
- [14] Dudek K, Dulski M, Łosiewicz B; (2020) Functionalization of the NiTi shape memory alloy surface by HAp/SiO₂/Ag hybrid coatings formed on SiO₂-TiO₂ glass interlayer. *Materials* 16(20), 6791. DOI:10.3390/ma13071648
- [15] Osak P, Łosiewicz B; (2018) EIS Study on Interfacial Properties of Passivated Nitinol Orthodontic Wire in Saliva Modified with Eludril® Mouthwash. *Prot Met Phys Chem Surf* 54, 680–688. DOI:10.1134/S2070205118040226
- [16] Zhang T, Wang W, Liu J, Wang L, Tang Y, Wang K; (2022) A review on magnesium alloys for biomedical applications. *Front Bioeng Biotechnol* 10, 953344. DOI:10.3389/fbioe.2022.953344
- [17] Avcu E, Baştan FE, Abdullah HZ, Ur Rehman MA, Yıldırım Avcu Y, Boccaccini AR; (2019) Electrophoretic deposition of chitosan-based composite coatings for biomedical applications: a review. *Prog Mater Sci* 103, 69–108. DOI:10.1016/j.pmatsci.2019.01.001

- [18] Szulc M, Lewandowska K; (2023) Biomaterials based on chitosan and its derivatives and their potential in tissue engineering and other biomedical applications – review. *Molecules* 28(1), 247. **DOI:**10.3390/molecules28010247
- [19] Hasnain MS, Beg S, Nayak AK; (2021) *Chitosan in Drug Delivery*. 1st ed, Elsevier Science.
- [20] Tan H, Ma R, Lin C, Liu Z, Tang T; (2013) Quaternized chitosan as an antimicrobial agent: antimicrobial activity, mechanism of action and biomedical applications in orthopaedics. *Int J Mol Sci* 14(1), 1854–1869. **DOI:**10.3390/ijms14011854
- [21] Shariatinia Z; (2019) Pharmaceutical applications of chitosan. *Adv Colloid Interface Sci* 263, 131–194. **DOI:**10.1016/j.cis.2018.11.008
- [22] Nuc Z, Dobrzycka-Kraheil A; (2021) From chitin to chitosan – a potential natural antimicrobial agent. *Prog Chem Appl Chitin Deriv* 26, 23–40. **DOI:**10.15259/PCACD.26.003
- [23] Riaz Rajoka MS, Mehwish HM, Wu Y, Zhao L, Arfat Y, Majeed K, Anwaar S; (2020) Chitin/chitosan derivatives and their interactions with microorganisms: a comprehensive review and future perspectives. *Crit Rev Biotechnol* 40(3), 365–379. **DOI:**10.1080/07388551.2020.1713719
- [24] Ferreira JA, Lennartsson PR, Edebo L, Taherzadeh MJ; (2013) Zygomycetes-based biorefinery: present status and future prospects. *Bioresour Technol* 135, 523–532. **DOI:**10.1016/j.biortech.2012.09.064
- [25] Raafat D, Sahl HG; (2009) Chitosan and its antimicrobial potential – a critical literature survey. *Microb Biotechnol* 2(2), 186–201. **DOI:**10.1111/j.1751-7915.2008.00080.x
- [26] Qin Y, Li P; (2020) Antimicrobial Chitosan Conjugates: Current Synthetic Strategies and Potential Applications. *Int J Mol Sci* 21(2), 499. **DOI:**10.3390/ijms21020499
- [27] Kong M, Chen XG, Xing K, Park HJ; (2010) Antimicrobial properties of chitosan and mode of action: a state of the art review. *Int J Food Microbiol* 144(1), 51–63. **DOI:**10.1016/j.ijfoodmicro.2010.09.012
- [28] Jiang WZ, Cai Y, Li HY; (2017) Chitosan-based spray-dried mucoadhesive microspheres for sustained oromucosal drug delivery. *Powder Technol* 312, 124–132. **DOI:**10.1016/j.powtec.2017.02.021
- [29] Yang H, Wang S, Bian H, Xing X, Yu J, Wu X, Zhang L, Liang X, Lu A, Huang C; (2022) Extracellular matrix-mimicking nanofibrous chitosan microspheres as cell micro-ark for tissue engineering. *Carbohydr Polym* 292, 119693. **DOI:**10.1016/j.carbpol.2022.119693
- [30] Łosiewicz B, Osak P, Kubisztal J; (2023) The effect of a composite chitosan/copper(II) ion coating on the corrosion resistance of grade 4 titanium in saline: preliminary results. *Prog Chem Appl Chitin Deriv* 28, 89–102. **DOI:**10.15259/PCACD.28.008
- [31] Łosiewicz B, Osak P, Kubisztal J; (2023) The effect of a composite chitosan-silver(I) ion coating on the corrosion resistance of the cobalt-chromium-molybdenum alloy in saline solution. *Prog Chem Appl Chitin Deriv* 28, 75–88. **DOI:**10.15259/PCACD.28.007
- [32] Vokhidova VR, Ergashev KH, Rashidova SSH; (2022) Synthesis and application of chitosan hydroxyapatite: a review. *Prog Chem Appl Chitin Deriv* 27, 5–34. **DOI:**10.15259/PCACD.27.001
- [33] Siddiqi KS, Husen A, Rao RAK; (2018) A review on biosynthesis of silver nanoparticles and their biocidal properties. *J Nanobiotechnology* 16(1), 14. **DOI:**10.1186/s12951-018-0334-5
- [34] Helmlinger J, Sengstock C, Groß-Heitfeld C, Mayer C, Schildhauer TA, Köller M, Epple M; (2016) Silver nanoparticles with different size and shape: equal cytotoxicity, but different antibacterial effects. *RSC Adv* 6, 18490–18501. **DOI:**10.1039/c5ra27836h

- [35] Xu L, Wang Y-Y, Huang J, Chen C-Y, Wang Z-X, Xie H; (2020) Silver nanoparticles: Synthesis, medical applications and biosafety. *Theranostics* 10(20), 8996–9031. **DOI:**10.7150/thno.45413
- [36] Kelly JM, Keegan G, Brennan-Fournet ME; (2012) Triangular silver nanoparticles: their preparation, functionalisation and properties. *Acta Phys Pol A* 122(2), 337–345. **DOI:**10.12693/APhysPolA.122.337
- [37] Kumar-Krishnan S, Prokhorov E, Hernández-Iturriaga M, Mota-Morales JD, Vázquez-Lepe M, Kovalenko Y, Sanchez IC, Luna-Bárceñas G; (2015) Chitosan/silver nanocomposites: synergistic antibacterial action of silver nanoparticles and silver ions. *Eur Polym J* 67, 242–251. **DOI:**10.1016/j.eurpolymj.2015.03.066
- [38] Bartmański M, Pawłowski Ł, Zieliński A, Mielewczyk-Gryń A, Strugała G, Cieślik B; (2020) Electrophoretic Deposition and Characteristics of Chitosan-Nanosilver Composite Coatings on a Nanotubular TiO₂ Layer. *Coatings* 10(3), 245. **DOI:**10.3390/coatings10030245
- [39] Annibali S, Ripari M, LA Monaca G, Tonoli F, Cristalli MP; (2008) Local complications in dental implant surgery: prevention and treatment. *Oral Implantol (Rome)* 1(1), 21–33.
- [40] Hanif A, Qureshi S, Sheikh Z, Rashid H; (2017) Complications in implant dentistry. *Eur J Dent* 11(1), 135–140. **DOI:**10.4103/ejd.ejd_340_16
- [41] Scarano A, Khater AGA, Gehrke SA, Serra P, Francesco I, Di Carmine M, Tari SR, Leo L, Lorusso F; (2023) Current Status of Peri-Implant Diseases: A Clinical Review for Evidence-Based Decision Making. *J Funct Biomater* 14(4), 210. **DOI:**10.3390/jfb14040210
- [42] The chipped and worn teeth; Designed by Freepik. Available online: www.freepik.com (accessed on 26 February 2024).
- [43] ZWP online. Periimplantitis: Implantate professionell managen. Available online: <https://www.zwp-online.info/fachgebiete/prophylaxe/therapie/periimplantitis-implantate-professionell-managen> (accessed on 26 February 2024).
- [44] Al-Sabbagh M, Shaddox LM; (2019) Is Peri-Implantitis Curable? *Dent Clin North Am* 63(3), 547–566. **DOI:**10.1016/j.cden.2019.02.003
- [45] Regiel-Futyra A, Kyzioł A, Arruebo M; (2013) Chitosan-silver nanocomposites – modern antibacterial materials. *CHEMIK* 67(8), 683–692.
- [46] Thomas S, AR A, Jose Chirayil C, Thomas B (eds); (2023) *Handbook of Biopolymers*. Springer, Singapore.
- [47] Khubiev OM, Egorov AR, Kirichuk AA, Khrustalev VN, Tskhovrebov AG, Kritchenkov AS; (2023) Chitosan-Based Antibacterial Films for Biomedical and Food Applications. *Int J Mol Sci* 24(13), 10738. **DOI:**10.3390/ijms241310738
- [48] Kumar S, Mukherjee A, Dutta J; (2020) Chitosan based nanocomposite films and coatings: Emerging antimicrobial food packaging alternatives. *Trends Food Sci Technol* 97, 196–209. **DOI:**10.1016/j.tifs.2020.01.002
- [49] Alduwaib SM, Salih SA, Al-den-Fakar DJ; (2023) Synthesis and characterization of TiO₂-Ag-chitosan nano-composites in order to surface modification and bone tissue engineering using dip coating method. *JTAP* 18(1), 1–12. **DOI:**10.57647/JTAP.2024.1801.07
- [50] Nate Z, Moloto MJ, Mubiayi PK, Sibiyi PN; (2018) Green synthesis of chitosan capped silver nanoparticles and their antimicrobial activity. *MRS Advances* 3, 2505–2517. **DOI:**10.1557/adv.2018.368
- [51] Zheng LY, Zhu JF; (2003) Study on antimicrobial activity of chitosan with different molecular weights. *Carbohydr Polym* 54, 527–530. **DOI:**10.1016/j.carbpol.2003.07.009

- [52] Bartmański M, Ronowska A, Mania S, Banach-Kopeć A, Kozłowska J; (2024) Biological and antibacterial properties of chitosan-based coatings with AgNPs and CuNPs obtained on oxidized Ti13Zr13Nb titanium alloy. *Mater Lett* 360, 135997. **DOI:**10.1016/j.matlet.2024.135997
- [53] Zienkiewicz-Strzałka M, Deryło-Marczewska A, Skorik YA, Petrova VA, Choma A, Komaniecka I; (2020) Silver Nanoparticles on Chitosan/Silica Nanofibers: Characterization and Antibacterial Activity. *Int J Mol Sci* 21(1), 166. **DOI:**10.3390/ijms21010166
- [54] Piotrowska-Kirschling A, Brzeska J; (2020) Review of chitosan nanomaterials for metal cation adsorption. *Prog Chem Appl Chitin Deriv* 25, 51–62. **DOI:**10.15259/PCACD.25.004
- [55] Dickerson JH, Boccaccini AR, Eds.; (2012) *Electrophoretic Deposition of Nanomaterials*. Springer, New York, NY, USA.
- [56] Govindan S, Nivethaa EAK, Saravanan R, Narayanan V, Stephen A; (2012) Synthesis and characterization of chitosan-silver nanocomposite. *Appl Nanosci* 2, 299–303. **DOI:**10.1007/s13204-012-0109-5
- [57] Łosiewicz B, Dercz G, Szklarska M, Simka W, Łęźniak M, Krząkała A, Swinarew A; (2013) Characterization of electrophoretically deposited chitosan coatings on Ti13Zr13Nb alloy for biomedical applications. *Solid State Phenom* 203–204, 212–215. **DOI:**10.4028/www.scientific.net/ssp.203-204.212
- [58] Szklarska M, Łosiewicz B, Dercz G, Maszybrocka J, Rams-Baron M, Stach S; (2020) Electrophoretic deposition of chitosan coatings on the Ti15Mo biomedical alloy from a citric acid solution. *RSC Adv* 10(23), 13386–13393. **DOI:**10.1039/d0ra01481h
- [59] Kowalski P, Łosiewicz B, Goryczka T; (2015) Deposition of chitosan layers on NiTi shape memory alloy. *Arch Metall Mater* 60(1), 171–176. **DOI:**10.1515/amm-2015-0027
- [60] Ghalayani Esfahani A, Sartori M, Bregoli C, Fiocchi J, Biffi CA, Tuissi A, Giavaresi G, Presentato A, Alduina R, De Luca A, Cabrini A, De Capitani C, Fini M, Gruppioni E, Lavorgna M, Ronca A; (2023) Bactericidal Activity of Silver-Doped Chitosan Coatings via Electrophoretic Deposition on Ti6Al4V Additively Manufactured Substrates. *Polymers* 15(20), 4130. **DOI:**10.3390/polym15204130
- [61] Pawłowski Ł, Bartmański M, Mielewczyk-Gryń A, Cieślik BM, Gajowiec G, Zieliński A; (2021) Electrophoretically Deposited Chitosan/Eudragit E 100/AgNPs Composite Coatings on Titanium Substrate as a Silver Release System. *Materials* 14(16), 4533. **DOI:**10.3390/ma14164533
- [62] Joshi AG, Sahai S, Gandhi N, Krishna YGR, Haranath D; (2010) Valence band and core-level analysis of highly luminescent ZnO nanocrystals for designing ultrafast optical sensors. *Appl Phys Lett* 96, 123102. **DOI:**10.1063/1.3354025
- [63] Vasile BS, Oprea O, Voicu G, Fica A, Andronescu E, Teodorescu A, Holban A; (2014) Synthesis and characterization of a novel controlled release zinc oxide/gentamicin-chitosan composite with potential applications in wounds care. *Int J Pharm* 463(2), 161–169. **DOI:**10.1016/j.ijpharm.2013.11.035
- [64] Zhitomirsky I, Hashambhoy A; (2007) Chitosan-mediated electrosynthesis of organic-inorganic nanocomposites. *J Mater Process Technol* 191(1–3), 68–72. **DOI:**10.1016/j.jmatprotec.2007.03.043
- [65] Pang X, Zhitomirsky I; (2005) Electrodeposition of composite hydroxyapatite-chitosan films. *Mater Chem Phys* 94(2–3), 245–251. **DOI:**10.1016/j.matchemphys.2005.04.040

REVIEW

ENDOPHYTIC FUNGI AS CHITIN-MODIFYING ENZYMES PRODUCERS

Olga Marchut-Mikolajczyk

*Institute of Molecular and Industrial Biotechnology, Faculty of Biotechnology
and Food Sciences, Lodz University of Technology,
Stefanowskiego 2/22 Str., 90-537 Lodz, Poland
ORCID: 0000-0003-2041-3980
corresponding author: olga.marchut-mikolajczyk@p.lodz.pl*

Abstract

Chitosan and chitoooligosaccharides, which are products of chitin modification, have wide industrial applications. An improved understanding of the structure and properties of chitin-modifying enzymes has increased the interest in obtaining them from microbial sources and using them in the biotechnological production of these essential sugars. Endophytic fungi include a diverse group of microorganisms that inhabit the intercellular and intracellular areas of plant tissues, thus exerting beneficial effects on host species. They are considered an extremely valuable source of biologically active secondary metabolites and enzymes with high application potential. This review presents the potential of endophytic fungi to produce chitin-modifying enzymes and discusses the role of chitin modification by enzymes produced by fungal endophytes in their survival in the plant host.

Keywords: *endophytic fungi, chitin modification, enzymes*

Received: 08.04.2024

Accepted: 10.06.2024

1. Introduction

Chitin, a linear homopolymer composed of *N*-acetylglucosamine linked by β -(1,4)-glycosidic bonds, is a prevalent biopolymer that is frequently encountered in the cell walls of fungi and the exoskeletons of crustaceans, invertebrates and insects [1]. Chitosan, which is a form of chitin that has undergone deacetylation, possesses antibacterial properties and is utilised in the management of plant diseases [2]. Both of these polymers possess non-toxic, biodegradable and biocompatible properties, making them suitable for many applications in the fields of food, cosmetics, agriculture and pharmaceuticals [3, 4]. Interestingly, chitooligosaccharides, which are oligomers produced from chitin or chitosan, exhibit substantial potential for application in wound healing, as antibacterial agents and as carriers in gene therapy [4].

To produce functional chitin derivatives, including chitooligosaccharides and chitosan, the original biopolymer must be modified. The enzymatic conversion of chitin into chitosan and chitooligosaccharides offers numerous benefits in comparison to chemical approaches [1, 5]. Chitin-modifying enzymes, such as chitin deacetylases (EC 3.5.1.41), chitinases (EC 3.2.1.14) and chitosanase (EC 3.2.1.132), can be used to produce products with the required molecular weight and degree of deacetylation [4, 6]. In this context, there is an increasing interest in chitin-modifying enzymes, which are produced by both bacteria and fungi. Considering the existing habitat and evolved mechanisms of adaptability, fungal endophytes appear to be a highly potential reservoir of novel enzymes, including chitin-modifying enzymes.

2. Endophytic Microorganisms

Endophytes are microorganisms, mainly bacteria or fungi, that inhabit plant tissues without causing any damage to the plant host. The term ‘endophyte’ was first used in literature in the nineteenth century. Endophytic microbes are primarily classified into two groups: facultative and obligatory. This classification is based on the way in which the microbes colonise the plant. While facultative endophytes do colonise plants at certain points in their life cycles, they can also live outside of plants at other points in their lives and establish a relationship with the soil in the host plants’ immediate rhizosphere. Obligate endophytes, on the other hand, are plant-dependent throughout their duration. Typically, they modify metabolic processes and plant products to ensure their own survival, or they reproduce between plant generations by means of vertical transmission and exploitation [7].

For many decades, researchers have been intensively studying the plant microbiome. It is now known that endophytic microorganisms benefit the plant by allowing it to survive in unfavourable environmental conditions, and they also serve as a valuable reservoir of bioactive compounds [8, 9].

2.1. Endophytic Fungi

Endophytic fungi are unique in that they only inhabit plant tissues, as opposed to mycorrhizal fungi that can grow into the rhizosphere and colonise plant roots [10]. Endophytic fungi have been the subject of extensive research due to their potential as a rich reservoir of novel biologically active compounds. These microorganisms have the ability to stimulate plant growth, work as biological protection agents and activate resistance to biotic and abiotic factors. Furthermore, certain endophytic fungi are capable of generating cytotoxic, antibacterial and anticancer compounds [7, 11–13].

These organisms can be divided based on their life cycle, plant hosts, phylogenetic features and ecological functions (Figure 1). The first group includes clavicipitaceous

fungal endophytes that reside in some grasses located in both warm and cool regions. Non-clavicipitaceous endophytic fungi are a distinct group that inhabit the tissues of non-vascular plants, ferns, conifers, and angiosperms. They are commonly classified within the Ascomycota or Basidiomycota families [8, 10, 14].

2.2.1. *Clavicipitaceous Fungal Endophytes*

Clavicipitaceous endophytes are frequently observed in the shoots of plants, particularly grasses that thrive in both cold and warm climates [7]. Typically, these microorganisms are related phylogenetically, and plants harbour a single genotype of the fungus. This category includes species that are symptomatic (type I), symptomatic-pathogenic (type II) and asymptomatic (type III) [15]. The colonisation of the plant by fungal endophytes from this particular group has the potential to enhance both drought resistance and biomass yield. Additionally, endophytes generate active chemicals that exhibit toxicity towards animals, perhaps imposing restrictions on herbivory. The specific impact is dependent on various elements, including the plant host species and prevailing environmental conditions [9]. Unfortunately, cultivating this category of fungal endophytes is very difficult, making it challenging to evaluate their potential for industrial application [7].

2.2.2. *Non-Clavicipitaceous Fungal Endophytes*

The ecological roles of non-clavicipitaceous endophytes, which are primarily ascomycetous fungi, are poorly understood despite their great diversity. This group of fungi can be isolated from almost all plants that thrive in terrestrial habitats under a variety of conditions, including extreme ones. Non-clavicipitaceous endophytes harbour an extensive variety of fungal species primarily classified within the ascomycetous group. Due to their extensive diversity, there is limited knowledge regarding their ecological functions. These endophytes exhibit a remarkable capacity to transition between endophytic and free-living lifestyles. The remarkable variety of this group of endophytes and the diverse ecological roles they carry out make these microorganisms the centre of attention of numerous research studies [9, 16, 17].

Non-clavicipitaceous fungal endophytes can be classified into three separate classes. This categorisation was established by considering the host colonisation method, the intergenerational transmission mechanism, the levels of plant diversity and the ecological significance. Class 1 endophytes possess the capacity to thrive in both above-ground and below-ground tissues, and the diversity of this class within individual host plants is generally limited [10, 18]. Conversely, class 2 and 3 endophytes are limited to the above-ground tissues and the roots, respectively. The host plant or tissue can harbour a significant variety of class 2 endophytes, with more than 20 species recorded from a single leaf tropical plant, as reported by Arnold et al. [18]. There has been insufficient research on the diversity of class 3 endophytes inside individual plants [10, 19].

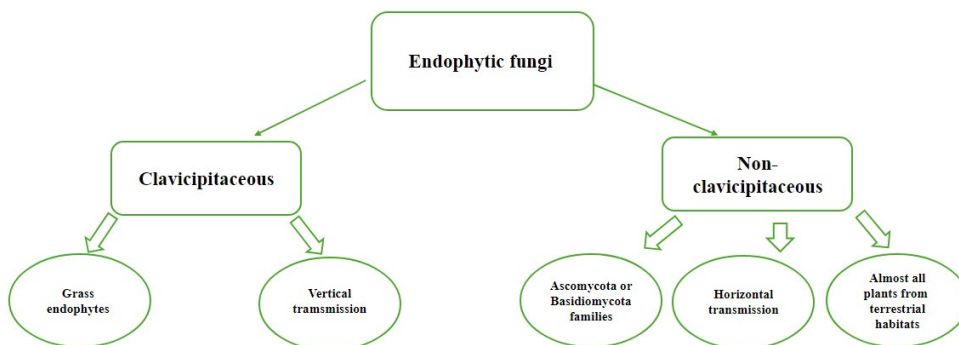


Figure 1. A descriptive scheme for endophytic fungi [10, 20].

3. Chitin-Modifying Enzymes Produced by Endophytic Fungi

Throughout the process of evolution, plants have developed an effective immune system that enables them to defend against harmful pathogens like fungi and insects. One of the key strategies involves detecting the presence of foreign compounds, such as chitin. With the help of specialised enzymes, plants have the ability to break down fungal cell walls and generate certain compounds that serve as triggers during the breakdown of chitin [21–23].

The environment in which endophytes live is not conducive to the growth of fungi due to the presence of tannins, phenols and other substances with biocidal activity, as well as the high salinity that often prevails in plant tissues. However, the ability of endophytic fungi to grow in these challenging conditions enables them to produce a wider variety and a greater number of enzymes. Moreover, compared with enzymes of the same classes produced by non-endophytic fungus, these enzymes are typically extracellular and show a spectrum of activity throughout a greater range of pH and salinity. However, the scientific literature on this topic is still quite limited [24].

3.1. Chitin Deacetylase

Despite the fact that fungal endophytes and pathogenic fungi share the same ecological niche, plant hosts exhibit distinct responses to infection caused by microorganisms from these two categories. To colonise plant tissue, endophytic fungi produce enzymes that facilitate the colonisation process, such as cellulases, laccases, pectinases and xylanases, which degrade the cell wall [25]. Nevertheless, this procedure activates the plant's immune responses. Thus, to survive in plants, endophytes require specific strategies to avoid detection by the plant's immune system. One such approach involves deacetylating chitin to chitosan to conceal its presence in the cell wall [26]. Chitin oligomers can be inactivated through various methods such as binding, degrading or deacetylating them. Of note, chitosan oligomers that have been completely deacetylated do not activate plant receptors, thus preventing any immune response [23, 26]. Research has indicated that the key enzymes responsible for the conversion of chitin into chitosan are chitin deacetylases (CDA) [23].

The first characterised CDA, namely PesCDA, was isolated from the endophytic fungus *Pestalotiopsis* sp. in 2016 [23]. The researchers identified the gene in *Pestalotiopsis* sp. that encodes CDA and then expressed it heterologously in *Escherichia coli*. Then, they examined the enzyme's substrate specificity and the chemical structure and biological activity of its reaction products. The study revealed that PesCDA is capable of modifying chitin oligomers, resulting in the formation of partially deacetylated chitosan oligomers with a distinct acetylation pattern: $\text{GlcNAc-GlcNAc-(GlcN)}_n\text{-GlcNAc}$ ($n \geq 1$) [23]. Incubation of rice cells with the PesCDA products demonstrated that the chitosan oligomer products failed to induce an immune response. The findings suggest that the presence of endophytic CDA may prevent the plant's immune system from recognising the endophyte. The results further demonstrate that the use of recombinant CDA, which exhibits well-established regioselectivity in generating chitosan oligomers with distinct acetylation patterns, is a promising technique for the biotechnological synthesis of potentially effective bioactive compounds [23].

3.2. Chitinase

Mendrofa et al. [27] evaluated the ability of an endophytic fungus derived from the indigenous *Hedychium coronarium* J. Koenig to produce chitinase. Out of the 12 endophytic fungal isolates that were examined, only two strains

Aspergillus fumigatus JRE 4B and *Trichoderma afroharzianum* JRE 1A – demonstrated the capacity to generate extracellular chitinase (Table 1). Furthermore, the researchers analysed the antibacterial efficacy of the isolates against the pathogenic fungus *Fusarium oxysporum*. The tested pathogen led to growth inhibition in only two isolates, namely *T. afroharzianum* (> 70%) and *A. fumigatus* (> 30%), the same isolates that exhibited chitinase activity. The tested endophytic chitinases showed activity up to pH 4; however, at pH > 7, there was a significant decrease in activity. The chitinases from microbiological sources showed activity in the pH range of 5–8 [27]. The chitinase from *T. afroharzianum* JRE 1A was more stable than the chitinase from *A. fumigatus* JRE 4B. It retained > 80% activity in the pH range of 4–6, which indicates its tolerance to an acidic environment and its potential use in industrial processes operating at a low pH.

Depending on the chitinolytic strain, chitinase activity can be inhibited or stabilised by the presence of metal ions. Mendrofa et al. [27] also demonstrated that most tested metal ions slightly inhibited (>80%) the chitinases, especially the enzyme isolated from *A. fumigatus* JRE 4B. Conversely, the presence of various metal ions widely stimulated the activity of chitinase from *T. afroharzianum* JRE 1A, with only potassium (K^+) and calcium (Ca^{2+}) showing inhibition. Furthermore, the addition of manganese (Mn^{2+}) and zinc (Zn^{2+}) stimulated the activity of chitinase from both fungi, with Mn^{2+} providing the most pronounced stimulation. Additionally, other researchers have demonstrated that the crude chitinases derived from endophytes exhibited inhibitory effects on the growth of the phytopathogenic fungi *F. oxysporum* [28, 29].

Endophytic fungi belonging to the genus *Epichloë* (part of the Clavicipitaceae family) are symbionts of cool-season grasses and produce a variety of bioactive secondary metabolites that provide biotic stress resistance to the host. Noorifar et al. [28] documented the interactions between the endophytic *Epichloë festucae* and the perennial ryegrass (*Lolium perenne*). While the mechanisms by which *E. festucae* colonises ryegrass tissues are well understood, little is known about the means by which the fungus avoids inducing an immune response in the host through direct physical contact between its cell walls and the plant. Chitin is recognised as a significant constituent of the cell wall in *E. festucae* cultivated in axenic culture, but it is not present in the cell wall of endophytic hyphae, despite its evident presence in the septa [30–32]. *E. festucae* exhibits the capacity to reproduce both within plant tissue and as an epiphyte on the surface of grass leaves [30, 33]. Epiphytic hyphae originate from and remain connected to endophytic hyphae within the leaf. The composition of the cell wall of epiphytic hyphae undergoes changes during differentiation, resulting in the dominance of chitin within various divisions. These findings suggest that the chitin–chitosan substance in the cell wall of *E. festucae* undergoes changes when transitioning from free-living to endophytic hyphae and from endophytic to epiphytic hyphae. The genome analysis of *E. festucae* revealed the presence of three genes, *cdaA*, *cdaB* and *cdaC*, which encode proteins containing domains that are highly similar to CDA. These domains include a Zn-binding motif and catalytic-site amino acid residues that are essential for the activities of peptidoglycan and CDA. The data obtained from the study demonstrated that the conversion of cell wall chitin to chitosan, facilitated by chitin deacetylase, plays a vital role in sustaining the mutualistic symbiotic association between *E. festucae* and its grass host [30].

Malto et al. [32] investigated the capacity of three endophytic fungi derived from bamboo to break down chitin and to synthesise chitinases. Each of the three endophytic fungi demonstrated the capacity for growth on minimum media containing colloidal chitin as the sole carbon source. However, the strains *Aspergillus tubingensis* JB11 and *Daldinia eschscholzii* D12 had the fastest growth rate.

The investigated isolates demonstrated the capability to degrade chitin within 3–5 days of incubation. Although the three endophytic fungi exhibited similar levels of total chitinolytic activity (~0.35 U/ml), *A. tubingensis* JB11 showed the highest exochitinase activity (0.25 U/ml) [24, 27, 34]. The chitinase (GH18) genes of *A. tubingensis* JB11 and *D. eschscholzii* D12 were subjected to bioinformatic analysis. The analysis revealed variations in the GH18 chitinase sequences and the presence of additional domains. According to the scientists, a biochemical analysis of recombinantly produced chitinases is necessary to establish a connection between the chitinolytic activity of secreted fungal proteins and the GH18 genes found in these fungi. Furthermore, they suggest that the presence of sequence variation in the catalytic domain of GH18 chitinase with JB11 and D12 renders them very suitable as chitinase sources for biotechnological applications [24].

Table 1. Chitin-modifying enzymes produced by endophytic fungi.

Fungal endophyte	Host	Chitin-modifying enzyme	Activity	Reference
<i>Aspergillus fumigatus</i> JRE 4B	<i>Hedychium coronarium</i> J. Koenig	Chitinase	4.76 U/ml	[29]
<i>Trichoderma afroharzianum</i> JRE 1A		Chitinase	4.15 U/ml	
<i>Pestalotiopsis</i> sp.	Tea (<i>Camellia sinensis</i>)	Chitin deacetylase	n.d.	[23]
<i>Daldinia eschscholzii</i> D12	Bamboo (<i>Bambuseae</i> sp.)	Chitinase	0.35 U/ml	[24]
<i>Aspergillus tubingensis</i> JB11		Chitinase	0.38 U/ml	
<i>Fomitopsis</i> sp. JB10		Chitinase	0.35 U/ml	
<i>Epichloë festucae</i>	<i>Lolium perenne</i>	Chitin deacetylase	n.d.	[30]
<i>Penicillium</i> sp.	Seagrass <i>Cymodocea serrulata</i>	Chitinase	9 U/mg	[4]
<i>Cladosporium</i> sp.	Seagrass <i>Halophila ovalis</i>	Chitinase	5.9 U/mg	

Note. Abbreviation: n.d., not determined.

Venkatachalam et al. [4] conducted an interesting study. They examined the capacity of endophytic fungi isolated from seagrasses and algae to generate chitin-modifying enzymes. They obtained a total of 117 isolates, of which more than 14% exhibited chitinase activity, whereas nearly 40% displayed chitosanase activity. The isolates with the greatest chitinase activity were *Penicillium* sp. (9 U/mg) and *Cladosporium* sp. (5.9 U/mg). This work was the first to identify endophytic fungi of marine plants as a novel source of enzymes that alter chitin [4].

4. Conclusions

The demand for enzymes in various industrial processes remains significant. However, there is a need to establish techniques that produce enzymes with specified characteristics, such as long-lasting stability in terms of pH and temperature. Industrial applications also favour enzymes that demonstrate metal ion-independent activity and do not interfere with inhibitory compounds.

Because of their unique living conditions, endophytic fungi can serve as a valuable reservoir of enzymes with distinct features. The capacity to thrive in challenging environments such as high salinity and drought, along with the ability to utilise complex molecules as a carbon source, can lead to a wider range of enzymes being generated with increased stability. Although the ability of endophytic fungi to produce bioactive metabolites and new drugs with potential use in the environment, agriculture, medicine and the food industry has been explored widely, little attention has been paid to their use as a source of industrial enzymes.

Chitin and chitosanolytic enzymes have unique properties that make them useful to obtain new chitosan oligosaccharides with a specific structure and to biodegrade chitin waste, which brings benefits by minimising environmental contamination [35]. The knowledge of chitin-modifying enzymes produced by fungal endophytes remains limited. The predominant studies in this field have focused on understanding the endophyte-plant relationship and the significance of chitin-modifying enzymes in these interactions. It appears that chitin-modifying enzymes play a crucial role in facilitating symbiotic associations between fungal endophytes and plants [30]. The intriguing ability of endophytic fungi to use mechanisms that mask or transform chitin present in the cell wall into its derivatives, thereby facilitating compatible interactions with host plants, renders this taxonomic group a promising reservoir of enzymes capable of modifying chitin.

5. References

- [1] Kaczmarek MB, Struszczyk-Swita K, Li X, Szczęśna-Antczak M, Daroch M; (2019) Enzymatic modifications of chitin, chitosan, and chito oligosaccharides. *Front Bioeng Biotech* 7, 243. DOI:10.3389/fbioe.2019.00243
- [2] Govinda Rajulu MB, Thirunavukkarasu N, Suryanarayanan TS, Ravishankar JP, el Gueddari NE, Moerschbacher BM; (2011) Chitinolytic enzymes from endophytic fungi. *Fungal Divers* 47, 43–53. DOI:10.1007/s13225-010-0071-z
- [3] Dutta PK, Dutta J, Tripathi VS; (2004) Chitin and chitosan: chemistry, properties and applications. *J Sci Ind Res* 63, 20–31.
- [4] Venkatachalam A, Govinda Rajulu MB, Thirunavukkarasu N, Suryanarayanan TS; (2015) Endophytic fungi of marine algae and seagrasses: a novel source of chitin modifying enzymes. *Mycosphere* 6(3), 345–355. DOI:10.5943/MYCOSPHERE/6/3/10
- [5] Tsigos I, Martinou A, Kafetzopoulos D, Bourioti V; (2000) Chitin deacetylases: new, versatile tools in biotechnology. *Trends Biotechnol* 18, 305–312. DOI:10.1016/S0167-7799(00)01462-1
- [6] Liu H, Bao X; (2009) Overexpression of the chitosanase gene in *Fusarium solani* via *Agrobacterium tumefaciens*-mediated transformation. *Curr Microbiol* 58, 279–282. DOI:10.1007/s00284-008-9334-2
- [7] Alam B, Li J, Gě Q, Khan MA, Gōng J, Mehmood S, Yuán Y, Gōng W; (2021) Endophytic fungi: from symbiosis to secondary metabolite communications or vice versa? *Front Plant Sci* 12, 791033. DOI:10.3389/fpls.2021.791033

- [8] Jalgaonwala RE, Mahajan RT; (2011) Evaluation of hydrolytic enzyme activities of endophytes from some indigenous medicinal plants. *J Agric Technol* 7(6), 1733–1741.
- [9] Rutkowska N, Drożdżyński P, Ryngajłło M, Marchut-Mikolajczyk O; (2023) Plants as the extended phenotype of endophytes – the actual source of bioactive compounds. *Int J Mol Sci* 24(12), 10096. **DOI:**10.3390/ijms241210096
- [10] Rodriguez RJ, White JF, Arnold AE, Redman RS; (2009) Fungal endophytes: diversity and functional roles. *New Phytologist* 182(2), 314–330. **DOI:**10.1111/j.1469-8137.2009.02773.x
- [11] Uzma F, Mohan CD, Hashem A, Konappa NM, Rangappa S, Kamath PV, Singh BP, Mudili V, Gupta VK, Siddaiah CN, Chowdappa S, Alqarawi AA, Abd_Allah EF; (2018) Endophytic fungi - alternative sources of cytotoxic compounds: a review. *Front Pharmacol* 9, 309. **DOI:**10.3389/fphar.2018.00309
- [12] Poveda J, Eugui D, Abril-Urías P, Velasco P; (2021) Endophytic fungi as direct plant growth promoters for sustainable agricultural production. *Symbiosis* 85, 1–19. **DOI:**10.1007/s13199-021-00789-x
- [13] Poveda J, Baptista P; (2021) Filamentous fungi as biocontrol agents in olive (*Olea europaea* L.) diseases: Mycorrhizal and endophytic fungi. *Crop Prot* 146, 105672. **DOI:**10.1016/j.cropro.2021.105672
- [14] Gouda S, Das G, Sen SK, Shin HS, Patra JK; (2016) Endophytes: A treasure house of bioactive compounds of medicinal importance. *Front Microbiol* 7, 1538. **DOI:**10.3389/fmicb.2016.01538
- [15] Clay K, Schardl CL; (2002) Evolutionary origins and ecological consequences of endophyte symbiosis with grasses. *Am Nat* 160, S99–S127. **DOI:**10.1086/342161
- [16] Gakuubi MM, Munusamy M, Liang ZX, Ng SB; (2021) Fungal endophytes: a promising frontier for discovery of novel bioactive compounds. *J Fungi* 7(10), 786. **DOI:**10.3390/jof7100786
- [17] Bamisile BS, Dash CK, Akutse KS, Keppanan R, Wang L; (2018) Fungal endophytes: Beyond herbivore management. *Front Microbiol* 9, 544. **DOI:**10.3389/fmicb.2018.00544
- [18] Arnold AE, Herre EA; (2003) Canopy cover and leaf age affect colonization by tropical fungal endophytes: ecological pattern and process in *Theobroma cacao* (Malvaceae). *Mycologia* 95, 388–398. **DOI:**10.1080/15572536.2004.11833083
- [19] Rodriguez RJ, Henson J, Van Volkenburgh E, Hoy M, Wright L, Beckwith F, Kim Y, Redman RS; (2008) Stress tolerance in plants via habitat-adapted symbiosis. *ISME J* 2, 404–416. **DOI:**10.1038/ismej.2007.106
- [20] Mishra Y, Singh A, Batra A, Sharma MM; (2014) Understanding the biodiversity and biological applications of endophytic fungi: a review. *J Microb Biochem Technol* 2014, 1–11. **DOI:**10.4172/1948-5948.S8-004
- [21] Grover A; (2012) Plant Chitinases genetic diversity and physiological roles. *Crit Rev Plant Sci* 31, 57–73. **DOI:**10.1080/07352689.2011.616043
- [22] Sanchez-Vallet A, Mesters JR, Thomma BPHJ; (2015) The battle for chitin recognition in plant-microbe interactions. *FEMS Microbiol Rev* 39, 171–183 **DOI:**10.1093/femsre/fuu003
- [23] Cord-Landwehr S, Melcher RLJ, Kolkenbrock S, Moerschbacher BM; (2016) A chitin deacetylase from the endophytic fungus *Pestalotiopsis* sp. efficiently inactivates the elicitor activity of chitin oligomers in rice cells. *Sci Rep* 6, 38018. **DOI:**10.1038/srep38018

- [24] Chow YY, Ting A SY; (2019) Influence of fungal infection on plant tissues: FTIR detects compositional changes to plant cell walls. *Fungal Ecol* 37, 38–47. **DOI:**10.1016/j.funeco.2018.10.004
- [25] Jha P, Kaur T, Chhabra I, Panja A, Paul S, Kumar V, Malik T; (2023) Endophytic fungi: hidden treasure chest of antimicrobial metabolites interrelationship of endophytes and metabolites. *Front Microbiol* 11(14), 1227830. **DOI:**10.3389/fmicb.2023.1227830
- [26] El Gueddari NE, Rauchhaus U, Moerschbacher BM, Deising HB; (2002) Developmentally regulated conversion of surface-exposed chitin to chitosan in cell walls of plant pathogenic fungi. *New Phytol* 156, 103–112. **DOI:**10.1046/j.1469-8137.2002.00487.x
- [27] Mendrofa A, Munir E, Yurnaliza Y, Lutfia A, Hartanto A; (2021) Chitinase and Antifungal Activity of Endophytic Fungi Isolated from *Hedychium coronarium* J. Koenig. *Agric Conspec Sci* 86(2), 131–137.
- [28] Noorifar N, Savoian MS, Ram A, Lukito Y, Hassing B, Weikert TW, Moerschbacher BM, Scott B; (2021) Chitin deacetylases are required for *Epichloë festucae* endophytic cell wall remodeling during establishment of a mutualistic symbiotic interaction with *Lolium perenne*. *Mol Plant Microbe Interact* 34(10), 1181–1192. **DOI:**10.1094/MPMI-12-20-0347-R
- [29] Becker Y, Eaton CJ, Brasell E, May KJ, Becker M, Hassing B, Cartwright GM, Reinhold L, Scott B; (2015) The fungal cell-wall integrity MAPK cascade is crucial for hyphal network formation and maintenance of restrictive growth of *Epichloë festucae* in symbiosis with *Lolium perenne*. *Mol Plant Microbe Interact* 28(1), 69–85. **DOI:**10.1094/MPMI-06-14-0183-R
- [30] Becker M, Becker Y, Green K, Scott B; (2016) The endophytic symbiont *Epichloë festucae* establishes an epiphyllous net on the surface of *Lolium perenne* leaves by development of an expressorium, an appressorium-like leaf exit structure. *New Phytol* 211, 240–254. **DOI:**10.1111/nph.13931
- [31] Moy M, Belanger F, Duncan R, Freehoff A, Leary C, Meyer W, Sullivan R, White JF; (2000) Identification of epiphyllous mycelialnets on leaves of grasses infected by clavicipitaceous endophytes. *Symbiosis* 28(4), 291–302.
- [32] Malto ZBL, Bacal C, Diaz MJS, Yu ET; (2019) Local fungal endophytes as rich sources of chitinase genes. *Phillip J Sci* 148, 575–582.
- [33] Brzezinska-Swiontek M, Jankiewicz U; (2012) Production of antifungal chitinase by *Aspergillus niger* LOCK 62 and its potential role in the biological control. *Curr Microbiol* 65(6), 666–672. **DOI:**10.1007/s00284-012-0208-2
- [34] Liu D, Li J, Zhao S, Zhang R, Wang M, Miao Y, Shen Y, Shen Q; (2013) Secretome diversity and quantitative analysis of cellulolytic *Aspergillus fumigatus* Z5 in the presence of different carbon sources. *Biotechnol Biofuels* 6(1), 149. **DOI:**10.1186/1754-6834-6-149
- [35] Vega-Portalatino EJ, Rosales-Cuentas MM, Valdiviezo-Marcelo J, Arana-Torres NM, Espinoza-Espinoza LA, Moreno-Quispe LA, Cornelio-Santiago HP; (2023) Antimicrobial and production of hydrolytic enzymes potentials of bacteria and fungi associated with macroalgae and their applications: a review. *Front Mar Sci* 10, 1174569. **DOI:**10.3389/fmars.2023.1174569

REVIEW

CHITOSAN AS A DRUG CARRIER

Patrycja Osak^{1,a,*}, Bożena Łosiewicz^{1,b}, Delfina Nowińska¹

¹ – Institute of Materials Engineering, Faculty of Science and Technology,
University of Silesia in Katowice, 75 Pulku Piechoty 1A Str., 41-500 Chorzów

^a – ORCID: 0000-0002-0628-6367, ^b – ORCID: 0000-0001-9472-1893

*corresponding author: patrycja.osak@us.edu.pl

Abstract

The review discusses the latest issues related to using chitosan, a biocompatible and biodegradable polymer derived from chitin, as a carrier in intelligent drug-delivery systems. The continuous development of medicine and rapid technological progress pose new challenges in designing new therapeutic agents. Chitosan has properties that make it suitable for drug-delivery applications, such as its ability to form nanoparticles and its mucoadhesion that enhance drug absorption. Chitosan can be combined with antibiotics, analgesics and other ingredients with specific properties. While chitosan is not medicinal substance, it can be a carrier in controlled drug-release systems.

Keywords: chitosan, drug-delivery system, antibiotics, painkillers

Received: 15.03.2024

Accepted: 20.06.2024

1. Introduction

Chitosan belongs to a group of natural polymers obtained from chitin [1, 2]. It is an essential polysaccharide [2] characterised by a linear structure and high molecular weight (Figure 1a). It can be obtained from plant and animal sources. Chitosan most often occurs in the exoskeleton of crustaceans and molluscs and in fungal biomass [3, 4]. Chitosan is of particular importance in drug-delivery systems (DDS) due to its biocompatibility, low toxicity [5], biodegradability in the biological environment and adhesion to the mucosa [2, 6–9] (Figure 1b).

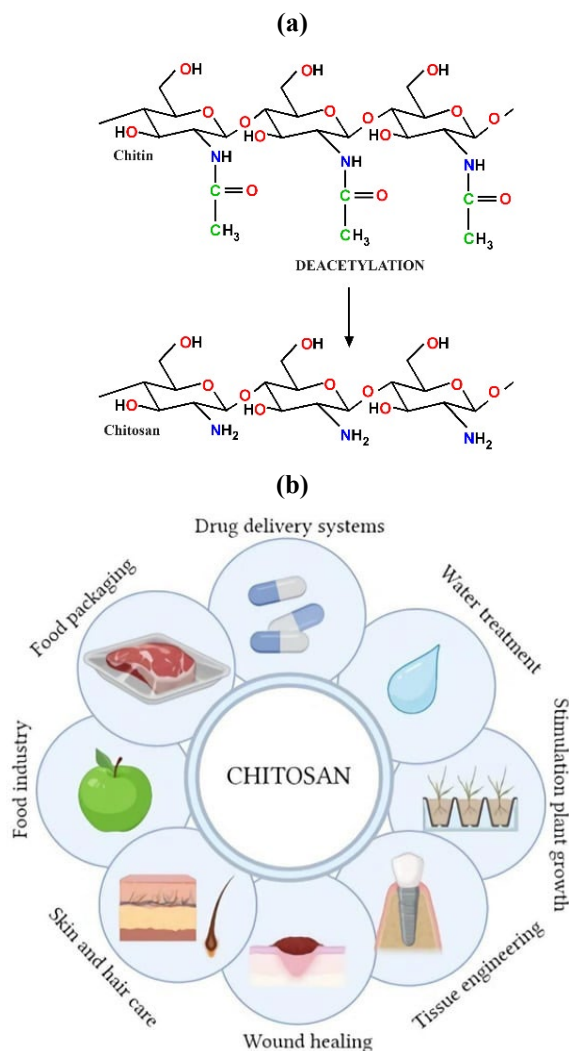


Figure 1. (a) Preparation of chitosan via chitin deacetylation. (b) The physicochemical properties of chitosan-based hydrogel [10]. This figure is distributed under the terms and conditions of a Creative Commons Attribution (CC BY) license (<https://creativecommons.org/licenses/by/4.0/>).

Target DDS are used to administer therapeutic agents to the body in a controlled and target manner. They optimise the therapeutic effects of drugs – increasing the bioavailability

and pharmacokinetics stability – while minimising side effects. They can be classified as oral, intravenous, transdermal or implantable. Chitosan-based drug carriers can improve the pharmacokinetics and therapeutic efficacy of various drugs [11]. In intelligent DDS, chitosan can be in the form of nanoparticles [2, 12, 13], coatings [6, 7, 14, 15], scaffolds [16] or in the form of a hydrogel [17].

Chitosan nanoparticles can encapsulate drugs, protecting them against degradation and improving their transport across biological barriers. Such nanoparticles have better antibacterial, anti-inflammatory and antioxidant properties [8, 18]. The kinetics of drug release from such nanoparticles depends on the site of drug targeting, the pH of the environment and the stability of the drug. In laboratory conditions, drug release kinetics is studied based on experimental data obtained during *in vitro* experiments and mathematical models such as the Korsmeyer–Peppas, Higuchi, and zero- and first-order kinetics models [18]. According to recent reports, chitosan nanoparticles are used widely in dentistry, especially in periodontology, implantology and endodontics [8, 15]. Chitosan supports the formation of osteoblasts and the regeneration of bone tissue. In combination with silver and hydroxyapatite nanoparticles, it supports the regeneration of the alveolar ridge. It inhibits the action of oral bacteria such as *Streptococcus mutans* and *Porphyromonas gingivalis* through the action of positively charged silver ions on the negatively charged bacterial cell wall [6, 19].

The use of DDS based on chitosan dressings is a current subject of research by scientists. These dressings allow for the local delivery of drugs – for example, in the case of healing wounds after burns or skin infections, ensuring transdermal transport. This DDS produces a systemic effect by changing the barrier properties of the skin. Chitosan dressings soaked in a medicinal substance create a tight patch–skin connection, facilitating the penetration of drugs. This is due to the mucoadhesive properties of chitosan, extending the contact time of the transdermal preparation with the skin. The therapeutic success of chitosan in transdermal applications depends largely on the type of drug administered, the formulation and the duration of drug delivery. In one study, researchers created a chitosan dressing with fat-soluble clobetasol, which released 80% from the patch within 2 h. The rapid release of the drug resulted in rapid inhibition of the development of bacteria immediately after applying the dressing to the wound [19]. In another study, the authors produced a patch consisting of chitosan, polyvinyl acetate and water-insoluble curcumin with antibacterial properties [20]. The delivery of medicinal substances from chitosan-based dressings resulted in faster healing of wounds and skin surface lesions and reduced the need for more frequent replacement of dressings due to the absorption properties of chitosan.

Chitosan-based hydrogels also demonstrate the ability to release drugs in a controlled manner. They create three-dimensional hydrophilic networks that can absorb and retain water, thus imitating the action of natural tissues in the human body. Chitosan hydrogels enable the use of many types of drugs, peptides and other therapeutic agents. This type of drug carrier can be designed to respond to changes in environmental conditions, such as changes in pH and temperature and reaction to enzymes [20].

Drug release kinetics can follow several mechanisms, including diffusion and dissolution. Designing DDS requires knowledge of these mechanisms and absorption times. Understanding the desired release profile, the physicochemical properties of the drug and the intended route of administration is crucial in selecting the appropriate drug release mechanism for a particular formulation. Scientists are constantly exploring innovative DDS to optimise the therapeutic outcomes and to minimise the side effects. The main goal of pharmacological treatment is to obtain and receive the optimal therapeutic dose of the therapeutic drug. The range from the minimum to maximum drug concentration is called the therapeutic window (Figure 2a) [18, 21], which represents the

safe dosage. Figure 2a shows drug release from DDS with immediate release (black curve) and delayed release (blue curve) [21]. Immediate and delayed release from DDS indicate a higher risk of toxicity from the drug [21]. However, the use of prolonged extraction of the drug substance from DDS means that the optimal therapeutic dose is maintained [21]. Conventional oral administration of a drug does not fully utilise its therapeutic dose. When the drug is administered, the dose increases dramatically, reaching a toxic dose. Over time, the therapeutic dose decreases gradually, reaching a dose that is too low to work effectively (e.g. fight bacteria and viruses or reduce pain; Figure 2b) [21]. The use of chitosan in controlled DDS means that the drug dose remains within the therapeutic window for as long as possible.

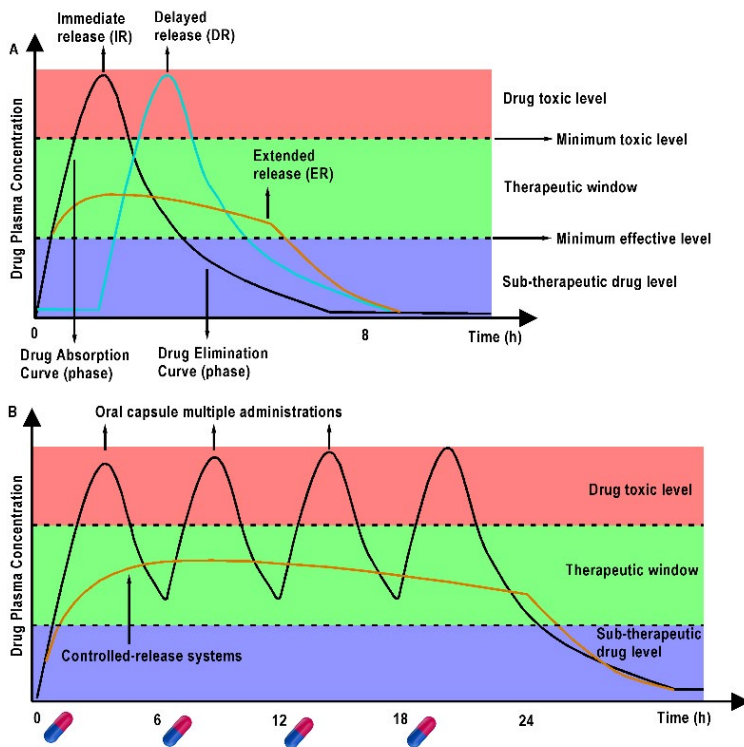


Figure 2. (a) A schematic illustration of the blood concentration of a drug (a) after traditional oral administration and (b) from a controlled drug-release system [21]. This figure is distributed under the terms and conditions of a Creative Commons Attribution (CC BY) license (<https://creativecommons.org/licenses/by/4.0/>).

The choice of a DDS depends mainly on factors such as the nature of the drug, including analgesics [22], anti-inflammatory, antiviral, antibiotics, antihypertensive drugs [23], anticoagulants and natural substances supporting treatment [24]. This review briefly discusses using chitosan as a drug carrier in intelligent DDS to release these compounds.

2. Drug-Delivery Systems Based on Chitosan Carrying Analgesics

Chitosan itself is not an analgesic – a compound that reduces pain – but it can carry other compounds that exert an analgesic action, including paracetamol, ibuprofen, ketoprofen, naproxen and the anaesthetic lidocaine. These are safe preparations provided

that the permissible therapeutic dose is not exceeded; this phenomenon depends on age, weight and comorbidities, among other factors.

Ibuprofen is a non-steroidal anti-inflammatory drug (NSAID). It works by inhibiting cyclooxygenases (COX), which produce prostaglandins, hormones responsible for pathogenic processes. Of note, ibuprofen inhibits all COX isoforms; other NSAIDs such as celecoxib can selectively inhibit COX-2 and thus eliminates prostaglandins more effectively [25]. Ibuprofen may cause side effects such as heartburn, nausea and abdominal pain. It has low solubility in the biological environment, fast-acting kinetics and a short period of biological activity [26]. As a result, oral administration of ibuprofen leads to underutilisation of the therapeutic dose of the drug. Despite the potential risk of chitosan inhibiting the action of ibuprofen, using this polymer as a drug carrier could help control the release of ibuprofen, increase its bioavailability and potentially reduce side effects. Such carriers may be designed to release ibuprofen in response to specific conditions in the body [26]. Chitosan-based transdermal patches containing ibuprofen improves the absorption of ibuprofen through the skin. Moreover, chitosan has antibacterial properties, preventing infections at the site where the patch is applied. This local ibuprofen administration system reduces the risk of systemic side effects such as gastric irritation [26].

Paracetamol is another NSAID that is widely used throughout the world due to its antipyretic effectiveness and low risk of side effects. Similarly to ibuprofen, it also inhibits COX to exert analgesic effects, but it does not have anti-inflammatory effects. Paracetamol has a low molecular weight of 151.16 g/mol, which means it can be released in a long-term manner. Indeed, it can be encapsulated in chitosan-coated alginate beads or in nanocomposites as part of DDS [27–30]. This approach is particularly useful for analgesic patches containing it [31]. Chitosan fibre scaffolds obtained from electrospinning act as drug carriers without the need to use additional chemicals [32]. Moreover, chitosan can undergo an encapsulation process, which makes it extremely attractive for use in microspheres with the addition of NSAIDs such as ibuprofen [33–37] and in the form of a hydrogel [38, 39].

Implantation procedures are associated with great pain, which is often alleviated with ketoprofen, another NSAID. Depending on the form, it works for 6–24 h. Ketoprofen, like other NSAIDs, blocks COX and may also irritate the gastric mucosa [25]. In one study, researchers showed that chitosan could be used successfully to form a film to carry ketoprofen [40]. In a rat model of rheumatoid arthritis, this preparation reduced disease-related oedema.

Chitosan can be used to cover anodically oxidised surfaces. Oxide nanotubes are usually produced on the surface of titanium and its alloys [41, 42]. Analgesics can be applied inside the oxide nanotubes and subsequently released rapidly from inside the nanotubes. Covering such a surface with a chitosan coating slows down the release of drugs, which helps achieve therapeutic effects. In one study, the authors compared the effectiveness of analgesic therapy with ibuprofen delivered in the form of microspheres directly into the socket and in a conventional oral manner [36]. The group receiving ibuprofen in the form of chitosan microspheres experienced significantly less pain and visibly less swelling of the operated site compared with the group receiving ibuprofen administered orally. Taken together, chitosan-containing systems that control analgesics such as NSAIDs have the ability to relieve pain and reduce inflammation [36, 37, 43]. The biocompatible properties of chitosan mean that these preparations can be applied directly to the mucous membranes [44].

3. Drug-Delivery Systems Based on Chitosan Carrying Antibiotics

Antibiotics are used to fight bacterial infections: they can kill bacteria or inhibit their growth. There are numerous classes of antibiotics, each with distinct mechanisms of action and spectrum of activity against bacteria. The most common classes of antibiotics are penicillins [45, 46], cephalosporins [47, 48] and tetracyclines. After implantation, there is local inflammation at the site of the implant. In the first days after implantation, growth factors are released locally, and platelets, proteins and blood plasma are released, causing a clot to form. Factors activating the healing process include histamine; prostaglandins; cytokines such as tumour necrosis factor (TNF), interleukin 1 (IL-1), IL-6 and IL-10; chemokines such as chemokine (C-X-C motif) ligand 3 (CXCL3), chemokine (C-C motif) ligand 2 (CCL2), CCL5, CC17, CXCL12 and CXCL3CL1; and bone matrix proteins with osteoinductive properties [49]. The pH of the tissues surrounding the implant is reduced from 7–7.35 to approximately 5.2 immediately after implantation, and then returns to the original level after approximately 2 weeks [49]. Such an environment is ideal for developing bacteria, resulting in peri-implant infection and subsequent related complications. Treating such infections requires broad-spectrum antibiotic therapy. Moreover, modifications to the implant surface have been proposed to accelerate their osseointegration and increase biological activity [6, 7]. Controlled DDS are being used with increasing frequency to reduce severe inflammatory reactions by releasing the therapeutic concentration of the drug at the target site [50].

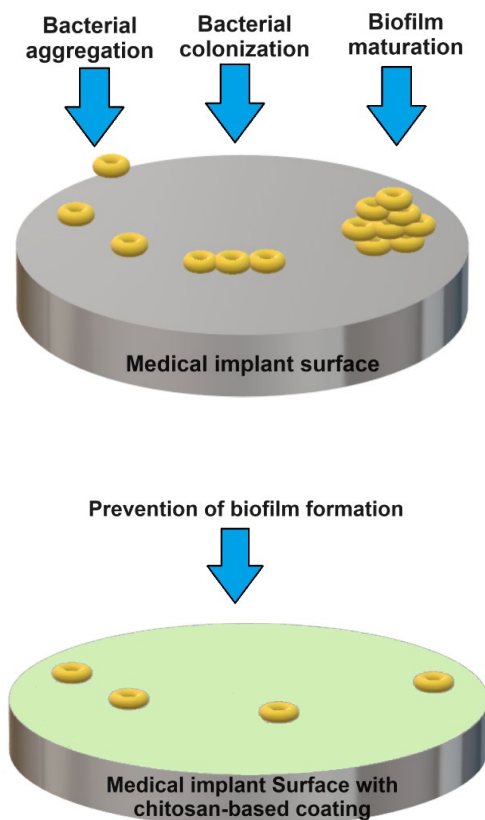


Figure 3. A schematic illustration of the process of bacterial colonisation on (a) the surface of implants without a chitosan coating and (b) an implant covered with a chitosan coating, which prevents the adhesion of bacteria.

According to the World Health Organization, a major problem in medicine is the overuse of antibiotics, which has resulted in increased antibiotic resistance among bacteria. In the human body, a biofilm forms on the implant surface; this coating consists of microorganisms that adhere closely to each other. It comprises polysaccharides, proteins and lipids, which makes it difficult for the antibiotic to reach and penetrate bacterial cells. Implants could be covered with coating containing biopolymers such as chitosan [51]. The use of biopolymer coatings based on chitosan supports the early stage of inhibiting bacterial growth by disturbing the development of biofilm (Figure 3) [52]. Chitosan coatings combined with an antibiotic inhibit the adhesion of bacteria to a natural biofilm that does not contain bacterial cells. This effect is due in part to the natural antimicrobial properties of chitosan [53].

Penicillin is a broad-spectrum antibiotic that disrupts the synthesis of bacterial cell membranes. It inhibits the enzyme transpeptidase, which is involved in cross-linking peptidoglycan chains in bacterial cell walls. This inhibition weakens the cell wall and thus inhibits bacterial growth [46]. However, many bacteria have developed resistance to penicillin-based antibiotics, which is why DDS that use chitosan to carry these antibiotics are being developed less and less frequently.

A recent study demonstrated the increased effectiveness of antibiotics loaded into chitosan magnetic microspheres. These microspheres ensure prolonged release and targeted delivery of the antibiotic to bacteria [47]. The magnetic properties of the microspheres enable external control over the movement of particles and their location in the human body. This method of targeted drug delivery is particularly beneficial to ensure the highest antibiotic concentration occurs at the site of infection, thus increasing its effectiveness and simultaneously minimising systemic side effects.

4. Drug-Delivery Systems Based on Chitosan Carrying Other Medicinal Substances

As mentioned above, the widespread use of antibiotics had led to the development of drug-resistant bacterial strains. One of the possibilities to overcome this issue is to increase the antibiotic dose, but this approach can disrupt the natural bacterial microflora of the treated person and lead to toxicity. An alternative approach is to use other bactericidal agents such as chlorhexidine [54], peptides, organic and inorganic substances.

Chlorhexidine, a commonly used antiseptic and antibacterial agent, is used in oral hygiene products and/or to inhibit bacteria responsible for inflammation in the mouth [55, 56]. The combination of chitosan as an adhesive agent with chlorhexidine enhances the antimicrobial effects, inhibits the formation of biofilm and thus reduces the risk of bacterial growth, in particular streptococci [57, 58]. Researches developed chlorhexidine-releasing liposomes containing chitosan that showed high cell compatibility and reduced inflammatory reactions by 60% in murine macrophages [54].

The latest research focuses on the search for new antibacterial agents based on antimicrobial peptides. These natural molecules affect the cell membrane of bacteria, inhibiting their further development. Chitosan-based hydrogel systems saturated with peptides are also being generated. One of them is histidine, which in the human body stimulates the immune system to combat viruses and bacteria [59]. There are also known natural products with antibacterial activity such as honey, propolis and bee pollen. The latest research shows the possibility of isolating jelleine-1, a bactericidal compound, from royal jelly. The use of this peptide applied in a carrier such as chitosan inhibits the release of pro-inflammatory cytokines and thus reduce inflammation (Figure 4) [59–62].

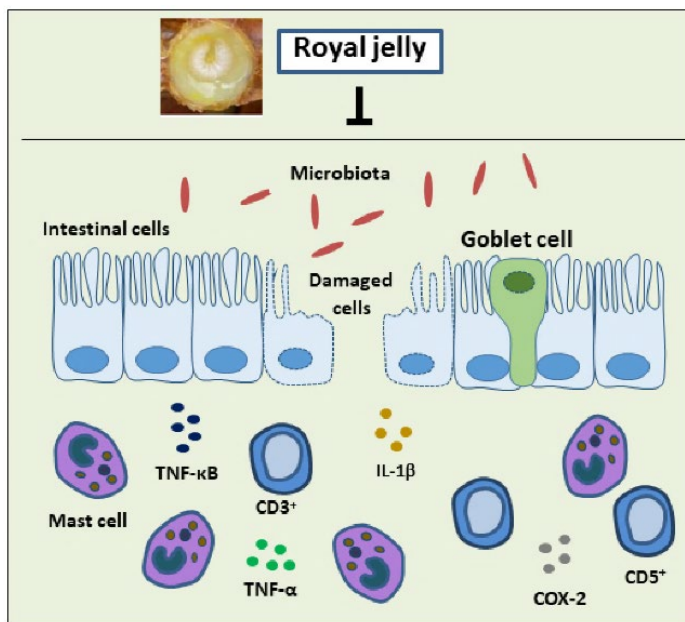


Figure 4. A schematic illustration of the inhibition of lymphocyte growth and pro-inflammatory cytokines by the peptide jelleine-1, which is isolated from royal jelly [62]. Abbreviations: CD, cluster of differentiation; COX, cyclooxygenase; IL, interleukin; TNF, tumour necrosis factor. This figure is distributed under the terms and conditions of a Creative Commons Attribution (CC BY) license (<https://creativecommons.org/licenses/by/4.0/>).

Chitosan combined with copper, silver or gold nanoparticles has antibacterial properties against *Staphylococcus aureus*, *Listeria monocytogenes*, *Escherichia coli* and *Salmonella Typhimurium*. The most commonly used chitosan–metal complexes contain silver in the form of ions or nanoparticles. In one study, researchers examined chitosan coatings saturated with silver nanoparticles or silver ions as a bactericidal agent against *S. aureus* and *E. coli* [63]. A chitosan coating saturated with 1% (w/w) silver nanoparticles or 2% (w/w) silver ions exerted a bactericidal effect. Their research showed that the chitosan–silver complex had better antibacterial properties than silver nanoparticles or its ions alone.

The combination of chitosan with micelles takes advantage of the mucoadhesion of chitosan and could be used to treat inflammatory eye diseases [64]. The development of the production of antibacterial agents by mixing chitosan with a copolymer of ethylene and vinyl alcohol is also being investigated [55]. Vinyl alcohol is a synthetic polymer with excellent barrier properties. Mixing these two polymers creates a composite with high antibacterial activity and increased mechanical and barrier properties.

5. Models of Drug Release From Chitosan-Based Carriers

Polymer materials used in the human body are exposed to bodily fluids as well as changes in temperature, pH and the oxygen concentration. Polymer-based drug carriers degrade in the biological environment. Indeed, chitosan swells and degrades in bodily fluids due to breakage of the polymer chain and alterations in the position and number of bonds [65].

This degradation allows the release of the carried drug to the target site. The rate of drug release depends on the type of matrix in which the drug is embedded. The use of chitosan as a drug carrier in controlled DDS requires knowledge of the kinetics of the release of the drug from the polymer. The drug release process has multiple stages. The primary stage in the case of polymers is the diffusion process [65].

The zero-order drug-release model describes a system in which the drug release rate does not depend on its concentration in the system. The drug is released slowly from the system. However, the drug adsorption rate depends on its concentration [66]. In the case of drug release from a flat/solid surface, the kinetics mainly follow the Higuchi model [67]. Specifically, the drug concentration used is much higher than the solubility of the drug in the carrier. The drug concentration gradient in the matrix and the resulting diffusion process occur in the direction perpendicular to the interface of the carrier and the therapeutic agent. Therefore, classic, one-dimensional diffusion occurs. Drug release from hydrogel coatings or hydrogels is mainly based on Fickian diffusion. In such a case, when the active substance is surrounded by a polymer, the drug release model is based on Fick's first law, defined by equation (1) [66]:

$$N_A = -D_{AB} \frac{dC_A}{dx} \quad (1)$$

The terms in equation (1) mean the following:

- N_A – stream of active agent [kg·A/(m²·s)];
- D_{AB} – drug diffusion coefficient [m²/s];
- C_A – drug concentration [kg·A/m³];
- x – dimensional coordinate [m].

If the drug is incorporated into the pores formed on the surface of the coating, then the diffusion of the drug follows Fick's second law, described in equation (2) [66]:

$$\frac{\partial C_A}{\partial x} = \frac{\partial}{\partial x} (D_{AB} (C_A) \frac{d^2 C_A}{dx^2}) \quad (2)$$

Currently, the Peppas model is frequently used to describe drug diffusion [67]. It is represented in equation (3):

$$\frac{M_t}{M_\infty} = kt^n \quad (3)$$

The value of n depends on the geometry of the carrier and the release mechanism (Table 1) [67]. k is a constant whose value depends on the structure of a given drug carrier.

Table 1. The value of the exponent n according to the Peppas model for various geometries of the drug-release system [67].

Exponent n / geometry			Release mechanism
Flat plate	Cylinder	Ball	
0.5	0.45	0.43	Fick's diffusion
0.5 < n < 1.0	0.45 < n < 0.89	0.43 < n < 0.85	Anomalous diffusion
1.0	0.89	0.85	Polymer swelling

The mechanism of drug release strongly depends on the wettability of a given release coating. Chitosan coatings have a strong ability to absorb bodily fluids, leading to faster desorption of the drug substance from the coating (Figure 5).

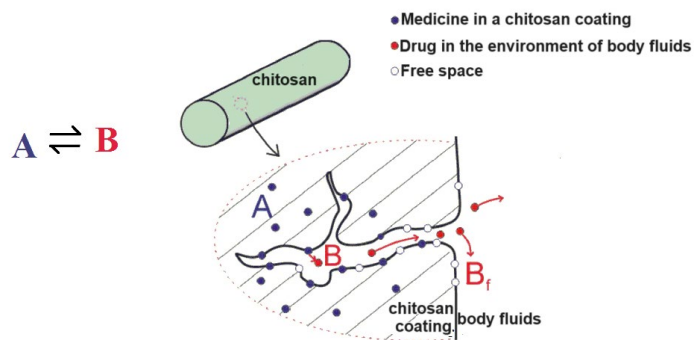


Figure 5. A schematic illustration of the mechanism of drug release from fibres.

Drug-release models from coatings are important for verifying experimental data. In the case of dental implants, it is necessary to release the drug gradually over approximately 14 days. A thorough analysis of the amount of the drug released enables the appropriate selection of the drug dose.

6. Conclusions

Chitosan is a universal carrier of various types of medicinal substances. There has been an increase in research on chitosan-based preparations that carry medicinal substances because chitosan has antibacterial properties, low toxicity, mucoadhesion and low allergenic potential. A controlled and targeted DDS is an excellent way to deliver the optimal therapeutic dose of a drug to the required place, bypassing the oral route and reducing side effects. Chitosan-based drug carriers can increase the solubility of insoluble drugs by creating a stable complex, and thus ensure better biodistribution of drugs. However, there is a need for further research into using chitosan as a carrier for medicinal substances and a detailed determination of their biocidal and therapeutic properties.

7. References

- [1] Yuan Y, Chesnutt BM, Haggard WO, Bumgardner JD; (2011) Deacetylation of Chitosan: Material Characterization and in Vitro Evaluation via Albumin Adsorption and Pre-Osteoblastic Cell Cultures. *Materials* 4, 1399–1416. DOI:10.3390/ma4081399
- [2] Suginta W, Khunkaewla P, Schulte A; (2013) Electrochemical Biosensor Applications of Polysaccharides Chitin and Chitosan. *Chem Rev* 113, 5458–5479. DOI:10.1021/cr300325r
- [3] Huq T, Khan A, Brown D, Dhayagude N, He Z, Ni Y; (2022) Sources, production and commercial applications of fungal chitosan: a review. *J Bioresour Bioprod* 7, 85–98. DOI:10.1016/j.jobab.2022.01.002
- [4] Trang TTC, Takaomi K; (2021) Chitosan and Its Biomass Composites in Application for Water Treatment. *Curr Opin Green Sustain Chem* 29, 100429. DOI:10.1016/j.cogsc.2020.100429
- [5] Amiri H, Aghbashlo M, Sharma M, Gaffey J, Manning L, Moosavi Basri SM, Kennedy JF, Gupta VK, Tabatabaei M; (2022) Chitin and Chitosan Derived from Crustacean Waste Valorization Streams Can Support Food Systems and the UN Sustainable Development Goals. *Nat Food* 3, 822–828. DOI:10.1038/s43016-022-00591-y

- [6] Łosiewicz B, Osak PA, Kubisztal J; (2023) The Effect of a Composite Chitosan-Silver(I) Ion Coating on the Corrosion Resistance of the Cobalt-Chromium-Molybdenum Alloy in Saline Solution. *Prog Chem Appl Chitin Deriv* 28, 75–88. **DOI:**10.15259/PCACD.28.007
- [7] Łosiewicz B, Osak PA, Kubisztal J; (2023) The Effect of a Composite Chitosan/Copper(II) Ion Coating on the Corrosion Resistance of Grade 4 Titanium in Saline: Preliminary Results. *Prog Chem Appl Chitin Deriv* 28, 89–102. **DOI:**10.15259/PCACD.28.008
- [8] Agrawal A, Reche A, Agrawal S, Paul P; (2023) Applications of chitosan nanoparticles in dentistry: a review. *Cureus* 15, e49934. **DOI:**10.7759/cureus.49934
- [9] Jurak M, Wiącek AE, Ładniak A, Przykaza K, Szafran K; (2021) What Affects the Biocompatibility of Polymers? *Adv Colloid Interface Sci* 294, 102451. **DOI:**10.1016/j.cis.2021.102451
- [10] Kulka K, Sionkowska A; (2023) Chitosan based materials in cosmetic applications: a review. *Molecules* 28, 1817. **DOI:**10.3390/molecules28041817
- [11] Wiranowska M; (2024) Advances in the use of chitosan and chlorotoxin-functionalized chitosan polymers in drug delivery and detection of glioma – a review. *Carbohydr Polym Technol Appl* 2024, 100427. **DOI:**10.1016/j.carpta.2024.100427
- [12] Saberi Rishh R, Vatankhah M, Hassanisaadi M, Varma RS; (2024) A Review of Chitosan Nanoparticles: Nature’s Gift for Transforming Agriculture through Smart and Effective Delivery Mechanisms. *Int J Biol Macromol* 260, 129522. **DOI:**10.1016/j.ijbiomac.2024.129522
- [13] Yan K, Xu F, Wei W, Yang C, Wang D, Shi X; (2021) Electrochemical Synthesis of Chitosan/Silver Nanoparticles Multilayer Hydrogel Coating with pH-Dependent Controlled Release Capability and Antibacterial Property. *Colloids Surface B* 202, 111711. **DOI:**10.1016/j.colsurfb.2021.111711
- [14] Hu B, Guo Y, Li H, Liu X, Fu Y, Ding F; (2021) Recent Advances in Chitosan-Based Layer-by-Layer Biomaterials and Their Biomedical Applications. *Carbohydr Polym* 271, 118427. **DOI:**10.1016/j.carbpol.2021.118427
- [15] Paradowska-Stolarz A, Mikulewicz M, Laskowska J, Karolewicz B, Owczarek A; (2023) The Importance of Chitosan Coatings in Dentistry. *Mar Drugs* 21, 613. **DOI:**10.3390/md21120613
- [16] Nezamabadi M, Balali E, Qomi M; (2023) A Sumanene-Chitosan Scaffold for the Adsorption of Niraparib Anticancer: DFT Insights into the Drug Delivery. *Inorg Chem Commun* 155, 111098. **DOI:**10.1016/j.inoche.2023.111098
- [17] Medha, Sethi S; (2024) RSM Optimized Chitosan Based Composite Hydrogel for Sustained Drug Delivery Applications. *Mater Today Commun* 38, 108029. **DOI:**10.1016/j.mtcomm.2024.108029
- [18] Herdiana Y, Wathoni N, Shamsuddin S, Muchtaridi M; (2022) Drug Release Study of the Chitosan-Based Nanoparticles. *Heliyon* 8, e08674. **DOI:**10.1016/j.heliyon.2021.e08674
- [19] Hallmann L, Gerngroß M-D; (2022) Chitosan and Its Application in Dental Implantology. *J Stomatol Oral Maxillofac Surg* 123, e701–e707. **DOI:**10.1016/j.jormas.2022.02.006
- [20] Raza ZA, Khalil S, Ayub A, Banat IM; (2020) Recent Developments in Chitosan Encapsulation of Various Active Ingredients for Multifunctional Applications. *Carbohydr Res* 492, 108004. **DOI:**10.1016/j.carres.2020.108004
- [21] Geraili A, Xing M, Mequanint K; (2021) Design and Fabrication of Drug-delivery Systems toward Adjustable Release Profiles for Personalized Treatment. *VIEW* 2, 20200126. **DOI:**10.1002/VIW.20200126
- [22] Lal N, Dubey J, Gaur P, Verma N, Verma A; (2017) Chitosan Based in Situ Forming Polyelectrolyte Complexes: A Potential Sustained Drug Delivery Polymeric Carrier for High Dose Drugs. *Mater Sci Eng C* 79, 491–498. **DOI:**10.1016/j.msec.2017.05.051

- [23] Imran M, Sajwan M, Alsuwayt B, Asif M; (2020) Synthesis Characterization and Anticoagulant Activity of Chitosan Derivatives. *Saudi Pharm J* 28, 25–32. **DOI:**10.1016/j.jsps.2019.11.003
- [24] Naeimi A, Ghadi FE, Parizi ZP, Rezakhani MS; (2023) ⁶⁸Ga Radiolabeled Chitosan/ Curcumin/Biotin Nanocomposite as a Drug Carrier and Early-Stage Cancer Detection. *Int J Biol Macromol* 235, 123619. **DOI:**10.1016/j.ijbiomac.2023.123619
- [25] Qureshi O, Dua A; (2024) COX Inhibitors. In: *StatPearls*; StatPearls. Publishing, Treasure Island.
- [26] Li C, Wang K, Xie D; (2021) Green Fabrication and Release Mechanisms of pH-Sensitive Chitosan-Ibuprofen Aerogels for Controlled Transdermal Delivery of Ibuprofen. *Front Chem* 9, 767923. **DOI:**10.3389/fchem.2021.767923
- [27] Pramanik S, Sali V; (2021) Connecting the Dots in Drug Delivery: A Tour d’horizon of Chitosan-Based Nanocarriers System. *Int J Biol Macromol* 169, 103–121. **DOI:**10.1016/j.ijbiomac.2020.12.083
- [28] Anirudhan TS, Gopal SS, Sandeep S; (2014) Synthesis and Characterization of Montmorillonite/N-(Carboxyacyl) Chitosan Coated Magnetic Particle Nanocomposites for Controlled Delivery of Paracetamol. *Appl Clay Sci* 2014 (88–89), 151–158. **DOI:**10.1016/j.clay.2013.11.039
- [29] Ibrahim MA, Alhalafi MH, Emam EM, Ibrahim H, Mosaad RM; (2023) A Review of Chitosan and Chitosan Nanofiber: Preparation, Characterization, and Its Potential Applications. *Polymers* 15, 2820. **DOI:**10.3390/polym15132820
- [30] Ali M, Mir S, Abid O-U-R, Ajlouni A, Ghafoor Alvi S, Bibi S; (2023) Applications of chitosan based bionanocomposites in drug-delivery and anticancer treatment – a review. *Eur Polym J* 201, 112576. **DOI:**10.1016/j.eurpolymj.2023.112576
- [31] Sami AJ, Khalid M, Jamil T, Aftab S, Mangat SA, Shakoori AR, Iqbal S; (2018) Formulation of Novel Chitosan Guar gum Based Hydrogels for Sustained Drug Release of Paracetamol. *Int J Biol Macromol* 108, 324–332. **DOI:**10.1016/j.ijbiomac.2017.12.008
- [32] Lemraski EG, Alibeigi S, Abbasi Z; (2022) Ibuprofen@silver Loaded on Poly(Vinyl Alcohol)/Chitosan Co-Polymer Scaffold as a Novel Drug Delivery System. *Mater Today Commun* 33, 104311. **DOI:**10.1016/j.mtcomm.2022.104311
- [33] Valle JAB, Valle R de CSC, Bierhalz ACK, Bezerra FM, Hernandez AL, Lis Arias MJ; (2021) Chitosan Microcapsules: Methods of the Production and Use in the Textile Finishing. *J Appl Polym Sci* 138, 50482. **DOI:**10.1002/app.50482
- [34] Aycan D, Yayla NA, Aydin YA; (2020) Chitosan Polyvinyl Alcohol Blend Films for Ibuprofen Encapsulation: Fabrication, Characterization and Kinetics. *Polym Degrad Stab* 181, 109346. **DOI:**10.1016/j.polymdegradstab.2020.109346
- [35] Bensouiki S, Belaib F, Sindt M, Magri P, Rup-Jacques S, Bensouici C, Meniai A-H; (2020) Evaluation of Anti-Inflammatory Activity and In Vitro Drug Release of Ibuprofen-Loaded Nanoparticles Based on Sodium Alginate and Chitosan. *Arab J Sci Eng* 45, 7599–7609. **DOI:**10.1007/s13369-020-04720-2
- [36] Kp K, R B; (2021) Evaluation and Comparison of Anti-Inflammatory Properties of Ibuprofen Using Two Drug Delivery Systems after Third Molar Surgery: Using Chitosan Microspheres as a Carrier for Local Drug Delivery into the Third Molar Socket and through the Oral Route. *Br J Oral Maxillofac Surg* 59, 191–196. **DOI:**10.1016/j.bjoms.2020.08.025
- [37] Najafabadi AH, Abdouss M, Faghihi S; (2014) Synthesis and Evaluation of PEG-O-Chitosan Nanoparticles for Delivery of Poor Water Soluble Drugs: Ibuprofen. *Mater Sci Eng C Mater Biol Appl* 41, 91–99. **DOI:**10.1016/j.msec.2014.04.035
- [38] Yang Y, Wu H, Fu Q, Xie X, Song Y, Xu M, Li J; (2022) 3D-Printed Polycaprolactone-Chitosan Based Drug Delivery Implants for Personalized Administration. *Mater Des* 214, 110394. **DOI:**10.1016/j.matdes.2022.110394

- [39] Mohseni M, Shokrollahi P, Barzin J; (2024) Gelatin/O-Carboxymethyl Chitosan Injectable Self-Healing Hydrogels for Ibuprofen and Naproxen Dual Release. *Int J Biol Macromol* 263, 130266. **DOI:**10.1016/j.ijbiomac.2024.130266
- [40] Oh DW, Kang JH, Lee HJ, Han SD, Kang MH, Kwon YH, Jun JH, Kim DW, Rhee YS, Kim JY, Park ES, Park CW; (2017) Formulation and in Vitro/in Vivo Evaluation of Chitosan-Based Film Forming Gel Containing Ketoprofen. *Drug Deliv* 24, 1056–1066. **DOI:**10.1080/10717544.2017.1346001
- [41] Smółka A, Rodak K, Dercz G, Dudek K, Łosiewicz B; (2014) Electrochemical Formation of Self-Organized Nanotubular Oxide Layers on Ti13Zr13Nb Alloy for Biomedical Applications. *Acta Phys Pol A* 125, 932–935. **DOI:**10.12693/APhysPolA.125.932
- [42] Smółka A, Dercz G, Rodak K, Łosiewicz B; (2015) Evaluation of Corrosion Resistance of Nanotubular Oxide Layers on the Ti13Zr13Nb Alloy in Physiological Saline Solution. *Arch Metall Mater* 60, 2681–2686. **DOI:**10.1515/amm-2015-0432
- [43] Balde A, Kim SK, Abdul NR; (2022) Crab (Charybdis Natator) Exoskeleton Derived Chitosan Nanoparticles for the in Vivo Delivery of Poorly Water-Soluble Drug: Ibuprofen. *Int J Biol Macromol* 212, 283–293. **DOI:**10.1016/j.ijbiomac.2022.05.131
- [44] Tang C, Guan Y-X, Yao S-J, Zhu Z-Q; (2014) Preparation of Ibuprofen-Loaded Chitosan Films for Oral Mucosal Drug Delivery Using Supercritical Solution Impregnation. *Int J Pharm* 473, 434–441. **DOI:**10.1016/j.ijpharm.2014.07.039
- [45] Choudhury AJ, Gogoi D, Kandimalla R, Kalita S, Chaudhari YB, Khan MR, Kotoky J, Chutia J; (2016) Penicillin Impregnation on Oxygen Plasma Surface Functionalized Chitosan/Antheraea Assama Silk Fibroin: Studies of Antibacterial Activity and Antithrombogenic Property. *Mater Sci Eng C* 60, 475–484. **DOI:**10.1016/j.msec.2015.11.070
- [46] Wiegand TJ; (2024) The Penicillins. In: Wexler P (ed), *Encyclopedia of Toxicology*, 4th edn. Academic Press, Oxford.
- [47] Chifiriuc CM, Grumezescu AM, Saviuc C, Croitoru C, Mihaiescu DE, Lazar V; (2012) Improved Antibacterial Activity of Cephalosporins Loaded in Magnetic Chitosan Microspheres. *Int J Pharm* 436, 201–205. **DOI:**10.1016/j.ijpharm.2012.06.031
- [48] Cigu TA, Vasiliu S, Racovita S, Lionte C, Sunel V, Popa M, Cheptea C; (2016) Adsorption and Release Studies of New Cephalosporin from Chitosan-g-Poly(Glycidyl Methacrylate) Microparticles. *Eur Polym J* 82, 132–152. **DOI:**10.1016/j.eurpolymj.2016.07.011
- [49] Guéhenec LL, Soueidan A, Layeolle P, Amourin Y; (2007) Surface Treatments of Titanium Dental Implants for Rapid Osseointegration. *Dent Mater* 23, 844–854. **DOI:**10.1016/j.dental.2006.06.025
- [50] Lengyel M, Kállai-Szabó N, Antal V, Laki AJ, Antal I; (2019) Microparticles, Microspheres, and Microcapsules for Advanced Drug Delivery. *Sci Pharm* 87, 20. **DOI:**10.3390/scipharm87030020
- [51] Mattioli-Belmonte M, Cometa S, Ferretti C, Iatta R, Trapani A, Ceci E, Falconi M, De Giglio E; (2014) Characterization and Cytocompatibility of an Antibiotic/Chitosan/Cyclodextrins Nanocoating on Titanium Implants. *Carbohydr Polym* 110, 173–182. **DOI:**10.1016/j.carbpol.2014.03.097
- [52] de Oliveira WF, Sales Albuquerque PB, Ribeiro Rodrigues NE, dos Santos Silva PM, Kennedy JF, dos Santos Correia MT, Breitenbach Barroso Coelho LC; (2024) Pharmaceutical Applications of Chitosan on Medical Implants: A Viable Alternative for Construction of New Biomaterials? *Carbohydr Polym Technol Appl* 7, 100407. **DOI:**10.1016/j.carpta.2023.100407
- [53] Khoshnood N, Frampton JP, Alavi Zaree SR, Jahanpanah M, Heydari P, Zamanian A; (2024) The Corrosion and Biological Behavior of 3D-Printed Polycaprolactone/

- Chitosan Scaffolds as Protective Coating for Mg Alloy Implants. *Surf Coat Technol* 477, 130368. **DOI:**10.1016/j.surfcoat.2023.130368
- [54] Hemmingsen LM, Panchai P, Julin K, Basnet P, Nystad M, Johannessen M, Škalko-Basnet N; (2022) Chitosan-Based Delivery System Enhances Antimicrobial Activity of Chlorhexidine. *Front Microbiol* 13, 1023083. **DOI:**10.3389/fmicb.2022.1023083
- [55] Fernandez-Saiz P, Ocio MJ, Lagaron JM; (2010) Antibacterial Chitosan-Based Blends with Ethylene-Vinyl Alcohol Copolymer. *Carbohydr Polym* 80, 874–884. **DOI:**10.1016/j.carbpol.2009.12.046
- [56] Osak P, Łosiewicz B; (2018) EIS Study on Interfacial Properties of Passivated Nitinol Orthodontic Wire in Saliva Modified with Eludril® Mouthwash. *Prot Met Phys Chem Surf* 54, 680–688. **DOI:**10.1134/S2070205118040226
- [57] Torres-Rosas R, Torres-Gómez N, Moreno-Rodríguez A, García-Contreras R, Argueta-Figueroa L; (2020) Anti-Inflammatory and Antibacterial Activity of the Chitosan/Chlorhexidine Gel Commercial Preparation for Postexodontia Treatment: An In Vitro Study. *Eur J Dent* 14, 397–403. **DOI:**10.1055/s-0040-1714453
- [58] Decker E-M, Von Ohle C, Weiger R, Wiech I, Brex M; (2005) A Synergistic Chlorhexidine/Chitosan Combination for Improved Antiplaque Strategies. *J Periodontal Res* 40, 373–377. **DOI:**10.1111/j.1600-0765.2005.00817.x
- [59] Riaz Z, Baddi S, Feng C-L; (2024) Supramolecular Co-Assembled Hybrid Hydrogels for Antibacterial Therapy. *Supramol Mater* 3, 100064. **DOI:**10.1016/j.supmat.2024.100064
- [60] Lima WG, Brito JCM, Verly RM, de Lima ME; (2024) Jelleine a Family of Peptides Isolated from the Royal Jelly of the Honey Bees (*Apis Mellifera*), as a Promising Prototype for New Medicines: A Narrative Review. *Toxins* 16, 24. **DOI:**10.3390/toxins16010024
- [61] Zhou J, Zhang L, He Y, Liu K, Zhang F, Zhang H, Lu Y, Yang C, Wang Z, Fareed MS, Liang X, Yan W, Wang K; (2021) An Optimized Analog of Antimicrobial Peptide Jelleine-1 Shows Enhanced Antimicrobial Activity against Multidrug Resistant *P. Aeruginosa* and Negligible Toxicity in Vitro and in Vivo. *Eur J Med Chem* 219, 113433. **DOI:**10.1016/j.ejmech.2021.113433
- [62] El-Seedi HR, Salama S, El-Wahed AAA, Guo Z, Di Minno A, Daglia M, Li Ch, Guan X, Buccato DG, Khalifa SAM, Wang K; (2024) Exploring the Therapeutic Potential of Royal Jelly in Metabolic Disorders and Gastrointestinal Diseases. *Nutrients* 16, 393. **DOI:**10.3390/nu16030393
- [63] Kumar-Krishnan S, Prokhorov E, Hernández-Iturriaga M, Mota-Morales JD, Vázquez-Lepe M, Kovalenko Y, Sanchez IC, Luna-Bárceñas G; (2015) Chitosan/Silver Nanocomposites: Synergistic Antibacterial Action of Silver Nanoparticles and Silver Ions. *Eur Polym J* 67, 242–251. **DOI:**10.1016/j.eurpolymj.2015.03.066
- [64] Yang Q, He C, Xu Y, Liu B, Shao Z, Zhu Z, Hou Y, Gong B, Shen Y-M; (2015) Chitosan Oligosaccharide Copolymer Micelles with Double Disulphide Linkage in the Backbone Associated by H-Bonding Duplexes for Targeted Intracellular Drug Delivery. *Polym Chem* 6, 1454–1464. **DOI:**10.1039/C4PY01473A
- [65] Lao LL, Peppas NA, Boey FYCh, Venkatraman SS; (2011) Modeling of Drug Release from Bulk-Degrading Polymers. *Int J Pharm* 418, 28–41. **DOI:**10.1016/j.ijpharm.2010.12.020
- [66] Costa P, Sousa Lobo JM; (2001) Modeling and Comparison of Dissolution Profiles. *Eur J Pharm Sci* 13, 123–133. **DOI:**10.1016/S0928-0987(01)00095-1
- [67] Peppas NA; (2013) Historical Perspective on Advanced Drug Delivery: How Engineering Design and Mathematical Modeling Helped the Field Mature. *Adv Drug Deliv Rev* 65, 5–9. **DOI:**10.1016/j.addr.2012.09.040

PROGRESS OF KNOWLEDGE IN THE DEVELOPMENT OF CHITOSAN FORMULATIONS WITH INSULIN TO PROMOTE SKIN WOUND HEALING

Marcin Przybyła¹, Barbara Dolińska^{1,a}, Aneta Ostróżka-Cieślik^{1,b,*}

¹ – Department of Pharmaceutical Technology, Faculty of Pharmaceutical Sciences in Sosnowiec, Medical University of Silesia, Kasztanowa 3 Str., 41-200 Sosnowiec, Poland

^a – ORCID: 0000-0003-3035-7417, ^b – ORCID: 0000-0002-5179-1370

*corresponding author: aostrozka@sum.edu.pl

Abstract

The treatment of difficult-to-heal wounds is a major problem in modern medicine. The search for new materials and ways to treat wounds is important and timely. Insulin stimulates proliferation, differentiation and migration of skin fibroblasts and keratinocytes. Chitosan has beneficial biological properties and can be an effective carrier of insulin. This review discusses research into the development of chitosan formulations with insulin to aid local treatment of chronic wounds. The PubMed, Google Scholar, Scopus and Web of Science databases were searched for studies on chitosan preparations with insulin in terms of their efficacy in wound healing. Twelve original English-language articles published in peer-reviewed scientific journals were included in the analysis. Insulin preparations in a chitosan matrix in the form of gel, hydrogel, injection and non-woven dressing are highly effective at all stages of the wound-healing process. They show anti-inflammatory and antimicrobial effects. Insulin from the formulations is released in a prolonged or controlled manner. However, it seems necessary to learn more about the mechanisms of insulin action within lesions. Of note, the data are mainly from basic and preclinical studies. Only one clinical study has been conducted.

Keywords: chitosan, insulin, hydrogel, dermal drug delivery, wound dressing

Received: 23.02.2024

Accepted: 23.04.2024

1. Introduction

One of the greatest challenges of the 21st century is the epidemic of non-communicable diseases. Chronic diseases are characterised by a slow progression of lesions, with the risk of many complications, including the development of difficult-to-heal wounds. The treatment of venous and arterial ulcers and diabetic foot represents a major challenge for modern medicine. The healing of these wounds does not follow a physiological pattern. Most chronic wounds stop in the inflammatory phase, with no tendency to progress to the proliferative phase. There are similar difficulties in effective treatment of burn wounds. It is estimated that 1.5–2 million people in Europe struggle with difficult-to-heal wounds [1], including 500,000 in Poland [2].

Insulin is a peptide hormone with hypoglycaemic effects that accelerates wound healing (in both people with diabetes and healthy individuals) [3]. It exhibits antioxidant and anti-inflammatory properties. Its application to the skin stimulates the migration and proliferation of keratinocytes, which have selective receptors for insulin on their surface. Insulin binding to receptors on the cell surface activates phosphoinositide 3-kinase (PI3K) and the Akt-dependent pathway, which influences normal endothelial function and vascular homeostasis [4–6]. It induces early neutrophil recruitment and increases M2 macrophage and interleukin-10 (IL-10) levels at the wound site. *In vitro*, it has been shown to affect the secretion of inflammatory mediators by regulating monocyte chemoattractant protein-1 (MCP-1) expression [7]. Insulin has been confirmed to reduce the wound-healing time. It accelerates neovascularisation, epithelialisation and remodelling. At the same time, no systemic (hypoglycaemia, hypokalaemia and hypoaminoacidosis) or local (pain, allergy and infection) side effects have been reported [8]. Research is currently underway to develop a topical insulin preparation that exhibits prolonged release of bioactive insulin.

The development of an innovative dermatological form of insulin – a hydrogel – has recently received increased attention. Hydrogels are hydrophilic substrates that are obtained by gelation using polymers. They exhibit adhesive properties and can therefore be applied to wounds with exudate and as a form of dressing. This review focuses on the use chitosan, a potential insulin carrier, whose properties allow the development of a hydrogel with extended active pharmaceutical ingredient (API) release.

Chitosan is a natural polymer that is biodegradable; biocompatible with the skin; and exhibits antimicrobial, haemostatic and antioxidant activity. It is formed by the deacetylation of chitin (a component of insect and arthropod exoskeletons, among others) and can be used both as a drug carrier and as a material for the creation of dressings or scaffolds in tissue engineering [9, 10]. It shows potential in wound care as a component of controlled drug-delivery systems, sponges, membranes, polymer films and nanofibers. Chitosan-based formulations promote wound healing by acting as an anti-inflammatory and antimicrobial agent. The main mechanism of chitosan's antimicrobial action is thought to be its interaction with negatively charged bacterial cell membranes/walls, which can lead to cell lysis. Other possible mechanisms include interference with bacterial DNA, inhibition of protein synthesis and chelation of nutrients from the bacterial environment (mainly divalent cations necessary for microbial growth) [10, 11]. In the initial stage of wound healing, chitosan promotes the migration of neutrophils and macrophages and subsequently stimulates the secretion of growth factors and collagen, which accelerates the wound-closure process. It also affects platelet and erythrocyte aggregation and inhibits fibrinolysis. During the proliferation

phase, it promotes the growth of granulation tissue. Chitosan can reduce the intensity of the scarring process, resulting in a visibly smaller scar [12–14]. Hydrogel dressings based on chitosan are characterised by oxygen permeability and high exudate absorption, keeping the wound site environment moist. This has the effect of accelerating the healing process [15]. Moreover, chitosan–basic fibroblast growth factor (bFGF) matrices promote epithelial regeneration and inhibit bacterial growth [16].

2. Methods

2.1. Research Question

The aim of this study was to review the literature on chitosan formulations containing insulin in terms of their efficacy in wound healing. The research question was: can chitosan-based hydrogels be effective insulin carriers for topical application?

2.2. Eligibility Criteria

Two authors searched the PubMed, Google Scholar, Scopus and Web of Science databases to identify articles on efficacy studies on dermal chitosan preparations with insulin. The following keywords were used: chitosan, insulin, drug-delivery system, topical therapy, dermal drug delivery, transdermal penetration, hydrogel, injection, microneedle devices, microneedle patch, needle-free injection, polymeric particles, electrospinning, wound dressing, bioactive dressings, wound healing, and diabetic foot ulcers. The inclusion criteria were: original English-language articles published in peer-reviewed journals within the last 20 years that included data from basic, preclinical or clinical studies. Various formulation technologies developed exclusively for epidermal, transdermal and subdermal applications to produce a topical effect were included. The exclusion criteria were: articles in which the insulin chitosan preparation was applied by another route (e.g. oral, ocular, mucosal and body cavities), review articles, newsletters, abstracts from conference proceedings and studies published on websites or in books.

3. Review of Studies on the Development of Chitosan Formulations With Insulin to Promote Skin Wound Healing

Skin wound healing is a complex, multi-stage process involving haemostasis, inflammation, neovascularisation, epithelialisation, granulation tissue formation, extracellular matrix deposition and tissue remodelling [16]. The ideal preparation for treating and accelerating wound healing should have the ability to stop bleeding, to prevent bacterial infection, to absorb wound exudate and to allow gas exchange, and it should be biodegradable and non-toxic [17]. Developing an effective and inexpensive wound treatment for patients remains a challenge. Biomaterial-based formulations can provide a simple and safe therapeutic option. Chitosan has favourable biological properties and can be an effective insulin carrier. This biopolymer could be used to produce various dermal forms of the drug. An analysis of the available literature indicates that the challenge is to develop a chitosan formulation of insulin that will enable efficient release and permeation of the hormone through the skin and ensure efficacy (Table 1).

Table 1. Review of the studies on chitosan preparations with insulin.

Reference	Type of insulin/chitosan used	Form of the insulin/chitosan preparation	Insulin dosage	Research model	Effects of the insulin preparation
Basic studies					
Kempe et al. 2007 [18]	Spin-labelled insulin/chitosan (Chitoclear® FG95) with a degree of deacetylation of 95%	Insulin-loaded chitosan/glycerol-2-phosphate (β -GP); injectable hydrogel	0.2 mg/ml	<i>In vitro</i>	<ul style="list-style-type: none"> • Combination of chitosan with β-glycerol phosphate (β-GP, 8%–16%) resulted in low viscosity at room temperature with thermogelling properties • Despite high mobility of the protein inside gel, there was controlled release of insulin over several days • A higher β-GP content in gel resulted in faster gelation and insulin release
Preclinical studies					
Zhao et al. 2017 [19]	Bovine insulin/phenylboronic-modified chitosan (CSPBA)	Injectable, pH- and glucose-sensitive hydrogel made of modified chitosan, poly(vinyl alcohol) and bezaldehyde-capped poly(ethylene glycol) (OHC-PEG-CHO) loaded with insulin and live fibroblasts (L929)	0.3%	Streptozotocin-induced diabetic rats	<ul style="list-style-type: none"> • Sustained and pH/glucose-triggered insulin release, as well as fibroblast viability and proliferation in the hydrogel matrix • The <i>in vivo</i> study showed an enhanced wound closure rate and increased neovascularisation and collagen deposition

<p>Ehterami et al. 2018 [20]</p>	<p>Insulin (not specified)/ chitosan (not specified)</p>	<p>Electrospun poly (ϵ-caprolactone)/ collagen (PCL/COLL) wound dressing with insulin-loaded chitosan nanoparticles</p>	<p>1000 IU</p>	<p>Full-thickness excisional wound on male Wistar rats</p>	<ul style="list-style-type: none"> • Incorporation of chitosan nanoparticles onto PCL/COLL dressing enhanced hydrophilicity, water-uptake and blood compatibility • Sustained insulin release of up to 65% over 14 days • The wound closure reached 97% after 14 days
<p>Zhu et al. 2020 [21]</p>	<p>Insulin (not specified)/ chitosan with a degree of deacetylation of $\geq 95\%$</p>	<p>Insulin-loaded micelles embedded along with epidermal growth factor into oxidised hyaluronic acid/succinyl chitosan composite hydrogel</p>	<p>10 mg/ml</p>	<p>Streptozotocin-induced diabetic rats</p>	<ul style="list-style-type: none"> • Low biological cytotoxicity and good biocompatibility • Excellent wound healing properties • Promoted fibroblast proliferation and collagen deposition • Addition of epidermal growth factor into the hydrogel resulted in an even faster wound closure rate
<p>Ribeiro et al. 2020 [22]</p>	<p>Recombinant human insulin/ chitosan with a degree of deacetylation of $\geq 75\%$</p>	<p>Hydrogel with chitosan nanoparticles containing insulin</p>	<p>0.5 IU</p>	<p>Alloxan-induced diabetic rats</p>	<ul style="list-style-type: none"> • High stability of insulin-chitosan nanoparticles • Stimulation of inflammatory cells proliferation • Increased angiogenesis and wound maturation

<p>Li et al. 2021 [23]</p>	<p>Insulin glargine/ chitosan with a degree of deacetylation of ~ 95%</p>	<p>Insulin incorporated into <i>N</i>-carboxy-ethyl chitosan, hyaluronic acid-aldehyde and adipic acid dihydrazide injectable hydrogel</p>	<p>0.1 IU</p>	<p>Streptozotocin-induced diabetic rats</p>	<ul style="list-style-type: none"> Hydrogel presented pH-responsive, sustained insulin release for up to 14 days, while retaining its bioactivity Shortened the inflammatory phase Promoted collagen deposition, re-epithelisation and angiogenesis
<p>Chen et al. 2022 [24]</p>	<p>Bovine insulin/ chitosan (number average molecular weight = 10–30 kDa)</p>	<p>Carbon monoxide-releasing, quaternised chitosan/ benzaldehyde F108 micelles (F108-CHO) hydrogel dressing loaded with insulin</p>	<p>Not specified</p>	<p>Streptozotocin-induced diabetic rats</p>	<ul style="list-style-type: none"> Antibacterial, anti-inflammatory and antioxidative properties Sustained and controlled insulin release The released carbon monoxide neutralised reactive oxygen species Significant healing properties of the infected diabetic wound along with great biocompatibility
<p>Hussein et al. 2022 [25]</p>	<p>Long performing insulin/ chitosan (not specified)</p>	<p>Insulin subcutaneous injections topped with chitosan/ zinc oxide nanocomposite membrane</p>	<p>2 IU/rat per day</p>	<p>Excisional wound on streptozotocin-induced diabetic rats</p>	<ul style="list-style-type: none"> Accelerated angiogenesis and tissue repair by activating the phosphoinositide 3-kinase/mitogen-activated protein kinase signalling pathway Additional upregulation of miR-125 and miR-132

Gao et al. 2022 [26]	Insulin (not specified)/ maleilated chitosan (mCH)	Insulin-loaded poly (L-lactic acid) (PLLA) nanofibrous mats coated with maleilated chitosan cross-linked with thiolated hyaluronan (tHA)	100 μ M	Diabetic mice	<ul style="list-style-type: none"> • Addition of mCH/tHA layer improved mechanical properties, wetting and water-uptake of PLLA mats • Increased insulin uptake and its controlled release, resulting in greatly improved wound healing
Sharda et al. 2023 [27]	Recombinant human insulin/ chitosan (not specified)	Insulin-loaded chitosan nanoparticles	60 μ M	Burn wounds on Swiss albino mice	<ul style="list-style-type: none"> • Increased cell migration • Almost 30% wound area reduction in the initial days of the treatment, reaching up to 95% after 20 days • Significant re-epithelisation and collagen deposition • Effective interleukin 6 suppression
Zanchetta et al. 2024 [28]	Regular insulin (Novolin®)/ chitosan with a molecular weight of 190–310 kDa and a degree of deacetylation of $\geq 75\%$	Insulin-containing chitosan/ hydroxypropyl methyl cellulose hydrogel	2 IU/g	Human keratinocyte cells and diabetic mice	<ul style="list-style-type: none"> • Stimulated proliferation and migration of human keratinocytes • Hair follicle regeneration at the wound site • Faster wound healing without affecting blood glucose levels
Clinical studies					
Dawoud et al. 2019 [29]	Insulin crystals/ chitosan with a medium molecular weight	Liposomal insulin chitosan gel	2%	Human patients	<ul style="list-style-type: none"> • Reduction of erythema • Wound healing rate 16 times faster compared with the control group • Confirmed stability of insulin liposomes up to 6 months (at 4°C)

3.1. Formulations for topical application and lubrication

3.1.1. Preclinical Studies

Zanchetta et al. [28] prepared a hydrogel based on chitosan and hydroxypropyl methylcellulose with insulin (Chi/HPMC/Ins). The *in vitro* studies with a human keratinocyte cell line (HaCaT) demonstrated that the gel had no cytotoxicity and stimulated keratinocyte migration, resulting in faster wound closure. The formulation accelerated wound healing by influencing the granulation process and regenerating hair follicles. These results were also confirmed in an *in vivo* model. The authors monitored wound healing over 20 days and found that the wound area tended to regress more in the Chi/HPMC/Ins hydrogel group after days 3 ($p < 0.05$), 7 ($p < 0.01$) and 10 ($p < 0.05$) compared with the saline group, and on days 7 and 10 ($p < 0.01$) compared with the Chi/HPMC group. The authors also demonstrated that topical application of hydrogel with insulin does not affect blood glucose levels.

Zhu et al. [21] described a pH-sensitive hydrogel based on oxidised hyaluronic acid (OHA) and succinylated chitosan (SCS), in which insulin-containing micelles were embedded. They added epidermal growth factor (EGF), a wound healing stimulator, to the hydrogel as a bioactive ingredient. The resulting formulation showed biocompatibility and significant efficacy in wound healing in a rat model. After just 6 days of hydrogel application, the wound area had decreased by 75%, compared with 45.5% after gauze-placebo application. The authors also found improved collagen and myofibril deposition at the wound site. The developed formulation promoted fibroblast proliferation and the integrity of the internal tissue structure. In the case of the bioactive hydrogel, in addition to a faster healing rate of the lesional skin, there was formation of new blood vessels, glands and hair follicles on day 12 of therapy. The authors did not perform statistical analysis.

Ribeiro et al. [22] prepared chitosan nanoparticles containing insulin and then placed them in a hydrogel based on the finished product Sepigel®. The resulting nanoparticles were homogeneous in size and shape (particle size = 245.9 nm; zeta potential = 39.3 mv) and stable for up to 56 days at 4°C. The authors evaluated the hydrogel in a rat model of diabetes. There was more efficient migration of pro-inflammatory cells at the initial stage of wound healing, followed by stimulation of migration of keratinocytes, epithelial cells and fibroblasts. Angiogenesis and granulation were also stimulated. Histological examination of tissues after 3 days of treatment with insulin-chitosan nanoparticles and chitosan nanoparticles alone showed a polymorphic nuclear infiltrate. This indicates that chitosan was involved in cell chemotaxis. Of note, the authors found no difference in wound healing between rats treated with the insulin-chitosan nanoparticle-based preparation and those treated with insulin alone.

Sharda et al. [27] investigated the efficacy of chitosan nanoformulation containing insulin to treat burn wounds. The resulting nanoparticles were spherical with a diameter of ~30 nm and a zeta potential of 28.8 mV (at pH 6.0) and 23.2 mV (at pH 7.4). The *in vitro* release of hormone across the dialysis membrane at 37°C occurred in a rapid and prolonged manner. Within the first 2 h, 74% of the API dose had been released, while at the end of the 36-h study, 90% of the loaded insulin was released. The authors confirmed the therapeutic properties of the developed nanoformulation *in vitro* using human keratinocyte cultures and *in vivo* using a mouse model of a burn wound. Five days after application of the chitosan/insulin nanopreparation, there was a 29% reduction in wound size; all other treatments showed no progress in wound healing. After 20 days of nanoparticle therapy, the wound surface was 96% healed, insulin alone and a commercially available preparation had resulted in 68% and 77% wound healing, respectively. In addition, stimulation of collagen

deposition, suppression of the pro-inflammatory cytokine IL-6, activation of the anti-inflammatory cytokine IL-10 and modulation of the Nrf-2 pathway were confirmed.

3.1.2. Clinical Study

Dawoud et al. [29] developed a chitosan-based mucoadhesive hydrogel in which insulin was encapsulated in liposomes (particle size = 257.751 nm; zeta potential = 20.548 mv). This hydrogel showed a biphasic insulin release profile, with an initiating dose (rapid API release) and a prolonged release dose (up to 24 h). Stability testing showed that liposomes with insulin stored at 25°C lost approximately 30% of the active ingredient after 14 days, while those stored in aqueous dispersion at 4°C showed high stability for up to 6 months. The authors confirmed the efficacy of chronic wound therapy in a clinical study involving 15 patients with chronic wounds and aged between 21 and 75 years. They excluded patients diagnosed with severe infection (suppurative wounds, wound exudates and bleeding), those who smoked, those who were taking immunosuppressants and those with debilitating chronic diseases. The test group (10 patients) received liposomal chitosan gel loaded with insulin, while the control group (5 patients) received liposomal chitosan gel without insulin. The test group showed a reduction in erythema and a 16-fold faster wound healing rate compared with the control group. There were no adverse systemic effects (headaches dizziness and sweating) and no hypoglycaemia. The wounds healed properly and were not infected. None of the participants reported complaints of pain during treatment. The researchers concluded that liposomal chitosan gel with insulin is a promising API delivery system with high stability.

3.2. Injectable Hydrogel

3.2.1. Basic Study

Kempe et al. [18] developed a chitosan hydrogel in combination with insulin-containing glycerol-2-phosphate (β -GP). The addition of β -GP to chitosan gave the hydrogel thermosensitive properties. As a result, at room temperature, the formulation was in the form of a sol and when administered, at physiological temperature, it turned into a gel, making it suitable for injection. The minimum concentration of β -GP providing this property was 6%, and as its concentration increased, the gelation rate of the formulation increased. In an oscillatory rheology study, the authors confirmed the formation of strong elastic gels as a result of the thermo-gelation of chitosan- β -GP systems. The authors examined the insulin release profile from samples with 8% and 16% β -GP. During the first 48 h, there were no significant differences between the two samples: approximately 50% of the insulin was released. In the later stages of the study, the amount and rate of insulin release were greater in the sample with the higher β -GP concentration (16%). In the final stage of release, 85% of the hormone was released from the formulation containing 8% β -GP, while 90% of the API was released from the formulation containing 16% β -GP. The release occurred by diffusion from the gel matrix.

3.2.2. Preclinical Studies

Li et al. [23] used hydrogel injections to treat diabetic foot ulcers. They prepared an insulin carrier based on *N*-carboxyethyl chitosan (*N*-chitosan), hyaluronic acid-aldehyde (HA-ALD) and adipic acid dihydrazide (ADH). The authors developed an injectable formulation that was characterised by a self-healing structure and a sustained release of the active substance that was sensitive to environmental pH. The dynamic acylhydrazone bonds present in the gel were responsible for the increase in the rate of insulin release as the pH decreased. As a result, the active ingredient was released faster from the sample

at pH 6.5 than from the sample at pH 7.4, reaching approximately 60% of the released API dose after 10 and 14 days, respectively. The hydrogel exhibited high biocompatibility, low cytotoxicity and promoted migration and proliferation of the cells tested *in vitro*. In a rat model of induced diabetes, injection of the hydrogel with insulin resulted in significantly faster wound healing (as early as 16 days) compared with the control. The hydrogel shortened the duration of inflammation and promoted collagen synthesis, epithelial formation and the formation of new blood vessels. The bioactive dressing was effective in alleviating peripheral neuropathy of diabetic wounds.

Zhao et al. [19] developed a pH- and glucose-responsive injectable hydrogel to treat diabetic wounds. The formulation was based on phenylboronic-modified chitosan (CSPBA), polyvinyl alcohol and OHC-PEG-CHO based on the Schiff base reaction. As in a previous study, insulin release occurred in a prolonged manner, and the rate of release increased with decreasing pH and increasing glucose concentration. The addition of chitosan to the gel resulted in a decrease in the amount of insulin released from the formulation, which is due to the ability of chitosan to lower blood glucose concentrations. The addition of insulin and fibroblasts to the carrier promoted neovascularisation, and collagen deposition and promoted diabetic wound healing. The study confirmed the observations of Kondo et al. [30] that chitosan shows potential to prevent diabetes.

3.3. Hydrogel Dressing

3.3.1. Preclinical Studies

Hussein et al. [25] conducted a study in a rat model of streptozotocin-induced diabetic foot syndrome. Topical treatment was based on subcutaneous administration of insulin at a dose of 2 IU/rat per day and topical application of a chitosan/zinc oxide (ZnO) nanocomposite membrane. The developed membrane showed an increase in surface roughness as the percentage of chitosan and ZnO increased, leading to an increase in its surface area. The authors showed that the combination of the two therapies resulted in a significant increase in the expression of the phosphatidylinositol 3-phosphatidyl kinase (PI3K) and mitogen-activated kinase (MAPK) genes, which were suppressed in untreated diabetic wounds. PI3K and MAPK are involved in signalling pathways that lead to an enhanced anti-inflammatory response and, as a result, accelerated wound healing. Insulin, as a bioactive component of hydrogel formulations, can induce the expression of these genes [31]. The formulation also increased the expression of the microRNAs miR-125 and miR-132, which have anti-inflammatory effects and stimulate cell migration and proliferation at the wound site [25]. The authors concluded that the proposed treatment could activate the PI3K/MAPK signalling pathway and some of the miRNAs that promote diabetic wound healing.

Gao et al. [26] developed a composite dressing. The authors investigated the therapeutic efficacy of hyaluronan/chitosan multilayer-coated PLLA (poly(L-lactic acid) nanofibrous mats (P-mCH/tHA) loaded with insulin, providing an extended hormone release profile. The dressing was obtained using an electrospinning technique. The authors suggest that coating the PLLA dressing with additional bioactive layers may increase not only its physical resistance to mechanical factors, but also its degradation rate and water absorption capacity, which is important for the treatment of oozing wounds. The dressings showed antimicrobial activity against *Escherichia coli*, mediated by the chitosan incorporated into the formulation. Insulin release occurred over 9 days, initially rapidly over 3 h, then in an extended manner. The dressing significantly improved wound healing in a diabetic mouse model by promoting angiogenesis, re-epithelialisation and increased collagen deposition.

Ehterami et al. [20] used the electrospinning method to develop a polymer fibre-based dressing. They coated insulin-delivering chitosan nanoparticles (particle diameter = 294.5 nm; zeta potential = 17.89 mV) with electrospun poly(ϵ -caprolactone)/collagen (PCL/COLL). The tested dressing showed high mechanical strength, a good exudate absorption capacity and a prolonged insulin release profile. The formulation was biocompatible and exhibited antimicrobial properties. In a rat model, wounds covered with the PCL/COLL/Cs-Ins dressing for 14 days showed almost complete healing, while wounds covered with the control showed 45% healing.

Chen et al. [24] developed one of the most innovative hydrogel dressings. It is based on a quaternary chitosan derivative and F108 micelles coated with benzaldehyde groups. The micelles encapsulated CORM-401, which exhibited the ability to release carbon monoxide, which has antioxidant, anti-inflammatory and antimicrobial effects. An additional bioactive component was insulin, suspended in a three-dimensional hydrogel structure. The formulation exhibited the ability to absorb fluids over 40 times its weight, showing self-regenerative properties. In response to pro-inflammatory factors including oxidative stress, CORM-401 released carbon monoxide at the wound site, which effectively neutralised reactive oxygen species while increasing the expression of haem oxidase 1 (HO-1). The carbon monoxide released also exerted antimicrobial activity, which was enhanced by the negatively charged chitosan chains. Carbon monoxide released in the wound had an anti-inflammatory effect by inhibiting the expression of pro-inflammatory cytokines (IL-1 β and IL-6) and tumour necrosis factor (TNF). The release profile of insulin from the formulation was pH and oxidative stress dependent, reaching its highest value (more than 80% of the released API within 5 days at a low pH and high oxidative stress, conditions corresponding to the wound environment). There was a synergistic effect of insulin with released carbon monoxide. A parallel study in a rat model with induced diabetes confirmed the therapeutic properties of the developed hydrogel dressing. The wound, which was additionally infected with a methicillin-resistant *Staphylococcus aureus* strain, healed 97% after 15 days of therapy compared with 66% for the control (phosphate-buffered saline) sample. The hydrogel dressing promoted angiogenesis, collagen synthesis and more intense granulation of the wound.

4. Considerations When Developing an Insulin Preparation for Dermal Administration

The studies included in the review confirm that insulin is a hormone with a high potential to promote wound healing. It stimulates the proliferation, differentiation and migration of skin fibroblasts and keratinocytes. It is involved in the production of the extracellular matrix, including collagen [32]. However, there has been limited research on its mechanism of action. Wertheimer et al. [33] conducted studies in a mouse model lacking the insulin receptor (IR) in the skin. The authors observed reduced proliferation of rodent skin keratinocytes, suggesting that insulin, through the IR, regulates differentiation and glucose transport in keratinocytes. Moreover, impaired insulin secretion can lead to abnormalities in wound healing in patients with diabetes [34]. The properties of insulin predispose it to be used as an ingredient in dermatological preparations to promote wound healing [35, 36]. The challenge is to ensure the effective action of the hormone when applied to the skin. Insulin-degrading enzymes (IDEs), which are zinc metallopeptidases, are present in the skin and wound serous fluid [37, 38], so it is crucial to develop an optimal carrier for insulin to ensure API stability and safety of its application. It is also important that the matrix components do not affect the loss of insulin bioactivity. Studies suggest that hydrogels based on biodegradable polymers have the potential

to stabilise a hormone such as insulin and promote its prolonged and controlled release into the wound bed as the polymer degrades [39, 40]. It should be noted that according to pharmacopeia guidelines, wound and burn preparations should be sterile. Polymer preparations can be sterilised using an autoclave, but this process may lead to a loss of viscosity, which should be considered at the pre-formulation stage of the drug formulation [41].

5. Select Aspects of Innovative Chronic Wound Management

Many patients with chronic wounds undergo basic surgical treatment involving tissue debridement, wound dressing and subsequent tissue reconstruction or amputation of dead limbs. For several years, there has been intensive research to develop effective, safe and accessible treatments for chronic wounds. Despite promising results on the benefits of epidermal insulin administration, there are no dermatological preparations containing this hormone available on the market. This is undoubtedly due to the difficulty of developing a technological formulation of insulin and the need for more knowledge on its effective and safe use. Recently, off-the-shelf preparations for the treatment of chronic wounds containing growth factors – specialised proteins that stimulate cell growth and differentiation and tissue regeneration – have become available. A significant drawback of these therapies is their high cost to the patient. Regranex® Gel 0.01% was approved by the U.S. Food and Drug Administration (FDA) in 1997 as a formulation for the treatment of diabetic foot ulcers. This carboxymethylcellulose (CMC)-based formulation contains becaplermin, a recombinant human platelet-derived growth factor (rhPDGF-BB). The formulation is non-sterile. A number of clinical studies have confirmed its high efficacy, but an increased risk of cancer following its application has been suggested [42, 43]. In 2001, Japan launched Fiblast® Spray containing recombinant fibroblast growth factor (rhbFGF) for the treatment of diabetic foot ulcers and second-degree burn wounds. The very good results of the clinical trials have not been recognised internationally [44]. Currently, drugs containing recombinant human EGF (rhEGF) – Heberprot-P®, 60 Regen-D™ 150, and Easyef® – are also used clinically [45]. Hydrogel systems containing stem and epithelial cells are also undergoing clinical trials [46].

Another alternative therapy for chronic wounds is formulations based on silver nanoparticle (AgNPs). The FDA has approved several silver-based biocomposites for the treatment of chronic wounds, including Acticoat™, Bactigras™, Aquacel™, PolyMem Silver™ (Aspen) and Tegaderm™ (3M) [47]. Different materials are used to carry AgNPs; they act in a similar manner but differ in the intensity of bactericidal action in the wound. Nanosilver shows the ability to penetrate deep into the wound, while ionic silver acts at the wound bed surface. Preparations containing AgNPs are highly effective against many bacterial strains, including multidrug-resistant bacteria [48]. It should be emphasised that the use of these dressings for large wound areas is not recommended. Despite the great advances in knowledge in the development of formulations for the treatment of chronic wounds, many authors suggest the need to understand the mechanisms of action of protein-peptide substances within the affected tissues. This would allow the optimisation of polymeric peptide dressing technology. The results of studies discussed in this review indicate the great therapeutic potential of chitosan-based insulin preparations in the treatment of chronic wounds. Their undoubted advantage is the low cost of therapy for the patient. The FDA has approved chitosan for use in wound dressings [49], and formulations based on this polymer are commercially available (e.g. Axiostat®, Celox™ and ChitoFlex®). The association of chitosan and insulin can have a synergistic effect.

6. Conclusions

Chitosan preparations with insulin show great potential in treating difficult-to-heal skin wounds. Studies have confirmed their effectiveness in gels, hydrogels, injections and fibrous dressings. They have a positive effect at all stages of the wound healing process. However, it should be noted that the data are mainly from basic and preclinical studies. Only one clinical study has been conducted, in which the authors developed a liposome-based insulin carrier embedded in a chitosan-based mucoadhesive hydrogel. Due to the species differences between humans and animals, the available data regarding the benefits of chitosan formulations with insulin are insufficient. The reviewed literature indicates that when applied to the skin, insulin does not cause hypoglycaemia, suggesting that it is safe to use. At present, however, the mechanism of action of insulin in healthy and lesional skin has not been determined. It is likely that these factors, as well as the difficulties associated with ensuring insulin stability and product sterility, are the reasons why there is no dermatological preparation of insulin on the market. We suggest further research in this direction.

7. Acknowledgements

This research was financed by the Medical University of Silesia in Katowice: No. BNW-1-030/K/3/F.

8. References

- [1] Pytlak K, Szymańska P, Skórka M, Bazaliński D; (2023) Quality of life of patients covered by the complex treatment of chronic wounds. *Surg Vasc Nurs* 17(1), 38.
- [2] Malka M, Krakowiecki A, Chojak M, Pławski M, Wądołek M, Wołowicz A, Dyczewska A, Paż A, Stefaniuk E, Grzela T; (2023) Anaerobic isolates found in infected hard-to-heal wounds and their sensitivity to antimicrobial drugs. *Leczenie Ran* 20(2), 53. DOI:10.60075/lrpjwm.v20i2.28
- [3] Wang J, Xu J; (2020) Effects of topical insulin on wound healing: a review of animal and human evidences. *Diabetes Metab Syndr Obes* 13, 719–727. DOI:10.2147/DMSO.S237294
- [4] Ostróżka-Cieślak A, Przybyła M, Wójcik W, Birówka K, Majczyna M, Dolińska B; (2023) Review of research in developing hydrogels with insulin to promote wound healing. *Med Sci Forum* 21(1), 17. DOI:10.3390/ECB2023-14290
- [5] Przybyła M, Dolińska B, Ostróżka-Cieślak A; (2023) Research progress on insulin dressings to promote wound. *Healing Eng Proc* 56(1), 21. DOI:10.3390/ASEC2023-15344
- [6] Apikoglu-Rabus S, Izzettin FV, Turan P, Ercan F; (2010) Effect of topical insulin on cutaneous wound healing in rats with or without acute diabetes. *Clin Exp Dermatol* 35(2), 180–185. DOI:10.1111/j.1365-2230.2009.03419.x
- [7] Chen X, Liu Y, Zhang X; (2012) Topical insulin application improves healing by regulating the wound inflammatory response. *Wound Repair Regen* 20(3), 425–434. DOI:10.1111/wrr.2012.20.issue-3
- [8] Chen X, Zhang M, Wang X, Chen Y, Yan Y, Zhang L, Zhang L; (2017) Peptide-modified chitosan hydrogels promote skin wound healing by enhancing wound angiogenesis and inhibiting inflammation. *Am J Transl Res* 9(5), 2352-2362.
- [9] Abd El-Hack ME, El-Saadony MT, Shafi ME, Zabermawi NM, Arif M, Batiha GE, Khafaga AF, Abd El-Hakim YM, Al-Sagheer AA; (2020) Antimicrobial

- and antioxidant properties of chitosan and its derivatives and their applications: a review. *Int J Biol Macromol* 164, 2726–2744. **DOI:** 10.1016/j.ijbiomac.2020.08.153
- [10] Matica MA, Aachmann FL, Tøndervik A, Sletta H, Ostafe V; (2019) Chitosan as a wound dressing starting material: antimicrobial properties and mode of action. *Int J Mol Sci* 20(23), 5889. **DOI:** 10.3390/ijms20235889
- [11] Kassem A, Ayoub GM, Malaeb L; (2019) Antibacterial activity of chitosan nano-composites and carbon nanotubes: a review. *Sci Total Environ* 668, 566–576. **DOI:** 10.1016/j.scitotenv.2019.02.446
- [12] Patrulea V, Ostafe V, Borchard G, Jordan O; (2015) Chitosan as a starting material for wound healing applications. *Eur J Pharm Biopharm* 97(Pt B), 417–426. **DOI:** 10.1016/j.ejpb.2015.08.004
- [13] Feng P, Luo Y, Ke C, Qiu H, Wang W, Zhu Y, Hou R, Xu L, Wu S; (2021) Chitosan-based functional materials for skin wound repair: mechanisms and applications. *Front Bioeng Biotechnol* 9, 650598. **DOI:** 10.3389/fbioe.2021.650598
- [14] Dai T, Tanaka M, Huang YY, Hamblin MR; (2011) Chitosan preparations for wounds and burns: antimicrobial and wound-healing effects. *Expert Rev Anti Infect Ther* 9(7), 857–879. **DOI:** 10.1586/eri.11.59
- [15] Liu H, Wang C, Li C, Qin Y, Wang Z, Yang F, Li Z, Wang J; (2018) A functional chitosan-based hydrogel as a wound dressing and drug delivery system in the treatment of wound healing. *RSC Adv* 8(14), 7533–7549. **DOI:** 10.1039/c7ra13510f
- [16] Lefler A, Ghanem A; (2009) Development of bFGF-chitosan matrices and their interactions with human dermal fibroblast cells. *J Biomater Sci Polym Ed* 20(10), 1335–1351. **DOI:** 10.1163/092050609X12457417534295
- [17] Alven S, Aderibigbe BA; (2020) Chitosan and Cellulose-Based Hydrogels for Wound Management. *Int J Mol Sci* 21(24), 9656. **DOI:** 10.3390/ijms21249656
- [18] Kempe S, Metz H, Bastrop M, Hvilsom A, Contri RV, Mäder K; (2008) Characterization of thermosensitive chitosan-based hydrogels by rheology and electron paramagnetic resonance spectroscopy. *Eur J Pharm Biopharm* 68(1), 26–33. **DOI:** 10.1016/j.ejpb.2007.05.020
- [19] Zhao L, Niu L, Liang H, Tan H, Liu C, Zhu F; (2017) pH and glucose dual-responsive injectable hydrogels with insulin and fibroblasts as bioactive dressings for diabetic wound healing. *ACS Appl Mater Interfaces* 9(43), 37563–37574. **DOI:** 10.1021/acsami.7b09395
- [20] Ehterami A, Salehi M, Farzamfar S, Vaez A, Samadian H, Sahrapeyma H, Mirzaii M, Ghorbani S, Goodarzi A; (2018) *In vitro* and *in vivo* study of PCL/COLL wound dressing loaded with insulin-chitosan nanoparticles on cutaneous wound healing in rats model. *Int J Biol Macromol* 117, 601–609. **DOI:** 10.1016/j.ijbiomac.2018.05.184
- [21] Zhu J, Jiang G, Hong W, Zhang Y, Xu B, Song G, Liu T, Hong C, Ruan L; (2020) Rapid gelation of oxidized hyaluronic acid and succinyl chitosan for integration with insulin-loaded micelles and epidermal growth factor on diabetic wound healing. *Mater Sci Eng C Mater Biol Appl* 117, 111273. **DOI:** 10.1016/j.msec.2020.111273
- [22] Ribeiro MC, Correa VLR, Silva FKLD, Casas AA, Chagas ALD, Oliveira LP, Miguel MP, Diniz DGA, Amaral AC, Menezes LB; (2020) Wound healing treatment using insulin within polymeric nanoparticles in the diabetes animal model. *Eur J Pharm Sci* 150, 105330. **DOI:** 10.1016/j.ejps.2020.105330

- [23] Li Z, Zhao Y, Liu H, Ren M, Wang Z, Wang X, Liu H, Feng Y, Lin Q, Wang C; (2021) pH-responsive hydrogel loaded with insulin as a bioactive dressing for enhancing diabetic wound healing. *Mater Des* 210, 110104. **DOI:**10.1016/j.matdes.2021.110104
- [24] Chen J, Chen D, Chen J, Shen T, Jin T, Zeng B, Li L, Yang C, Mu Z, Deng H, Cai X; (2022) An all-in-one CO gas therapy-based hydrogel dressing with sustained insulin release, anti-oxidative stress, antibacterial, and anti-inflammatory capabilities for infected diabetic wounds. *Acta Biomater* 146, 49–65. **DOI:**10.1016/j.actbio.2022.04.043
- [25] Hussein S, Hassan alsayes S, Aziza S, Abozaid O, Abdel-Aziz G; (2022) Wound healing treatment of local insulin injection with topical chitosan/ Zinc oxide nanocomposite membrane in diabetic rats model. *Benha Vet Med J* 42(2), 70–75. **DOI:**10.21608/bvmj.2022.148169.1547
- [26] Gao X, Huang R, Jiao Y, Groth T, Yang W, Tu C, Li H, Gong F, Chu J, Zhao M; (2022) Enhanced wound healing in diabetic mice by hyaluronan/chitosan multilayer-coated PLLA nanofibrous mats with sustained release of insulin. *Appl Surf Sci* 576, 151825. **DOI:**10.1016/j.apsusc.2021.151825
- [27] Sharda D, Ghosh S, Kaur P, Basu B, Choudhury D; (2023) Chitosan-insulin nano-formulations as critical modulators of inflammatory cytokines and Nrf-2 pathway to accelerate burn wound healing. *Discov Nano* 18(1), 154. **DOI:**10.1186/s11671-023-03941-2
- [28] Zanchetta FC, De Wever P, Morari J, Gaspar RC, Prado TPd, De Maeseneer T, Cardinaels R, Araújo EP, Lima MHM, Fardim P; (2024) *In vitro* and *in vivo* evaluation of chitosan/HPMC/insulin hydrogel for wound healing applications. *Bioengineering* 11(2), 168. **DOI:**10.3390/bioengineering11020168
- [29] Dawoud MHS, Yassin GE, Ghorab DM, Morsi NM; (2019) Insulin mucoadhesive liposomal gel for wound healing: a formulation with sustained release and extended stability using quality by design approach. *AAPS PharmSciTech* 20(4), 158. **DOI:**10.1208/s12249-019-1363-6
- [30] Kondo Y, Nakatani A, Hayashi K, Ito M; (2000) Low molecular weight chitosan prevents the progression of low dose streptozotocin-induced slowly progressive diabetes mellitus in mice. *Biol Pharm Bull* 23(12), 1458–1464. **DOI:**10.1248/bpb.23.1458
- [31] Yu T, Gao M, Yang P, Liu D, Wang D, Song F, Zhang X, Liu Y; (2019) Insulin promotes macrophage phenotype transition through PI3K/Akt and PPAR- γ signaling during diabetic wound healing. *J Cell Physiol* 234(4), 4217–4231. **DOI:**10.1002/jcp.27185
- [32] Suire CN, Nainar S, Fazio M, Kreutzer AG, Paymozd-Yazdi T, Topper CL, Thompson CR, Leissring MA; (2018) Peptidic inhibitors of insulin-degrading enzyme with potential for dermatological applications discovered via phage display. *PLoS One* 13(2), e0193101. **DOI:**10.1371/journal.pone.0193101
- [33] Wertheimer E, Spravchikov N, Trebicz M, Gartsbein M, Accili D, Avinoah I, Nofeh-Moses S, Szyzakov G, Tennenbaum T; (2001) The regulation of skin proliferation and differentiation in the IR null mouse: implications for skin complications of diabetes. *Endocrinology* 142(3), 1234–1241. **DOI:**10.1210/endo.142.3.7988
- [34] Baltzis D, Eleftheriadou I, Veves A; (2014) Pathogenesis and treatment of impaired wound healing in diabetes mellitus: new insights. *Adv Ther* 31(8), 817–836. **DOI:**10.1007/s12325-014-0140-x

- [35] Ostróżka-Cieślak A, Wilczyński S, Dolińska B; (2023) Hydrogel formulations for topical insulin application: preparation, characterization and *in vitro* permeation across the Strat-M® membrane. *Polymers* 15(17), 3639. DOI:10.3390/polym15173639
- [36] Ostróżka-Cieślak A; (2022) The potential of pharmaceutical hydrogels in the formulation of topical administration hormone drugs. *Polymers* 14(16), 3307. DOI:10.3390/polym14163307
- [37] Tang WJ; (2016) Targeting insulin-degrading enzyme to treat type 2 diabetes mellitus. *Trends Endocrinol Metab* 27(1), 24–34. DOI:10.1016/j.tem.2015.11.003
- [38] Duckworth WC, Fawcett J, Reddy S, Page JC; (2004) Insulin-degrading activity in wound fluid. *J Clin Endocrinol Metab* 89(2), 847–851. DOI:10.1210/jc.2003-031371
- [39] Ostróżka-Cieślak A, Maciążek-Jurczyk M, Pożycka J, Dolińska B; (2021) Pre-formulation studies: physicochemical characteristics and *in vitro* release kinetics of insulin from selected hydrogels. *Pharmaceutics* 13(8), 1215. DOI:10.3390/pharmaceutics13081215
- [40] Mansoor S, Kondiah PPD, Choonara YE; (2021) Advanced hydrogels for the controlled delivery of insulin. *Pharmaceutics* 13(12), 2113. DOI:10.3390/pharmaceutics13122113
- [41] Jacyna B, Maciejewski B, Sznitowska M; (2020) Hydrogels: compounded dermatological preparations. *Farm Pol* 76(1), 57–62. DOI:10.32383/farmopol/118356
- [42] Blume P, Bowlby M, Schmidt BM, Donegan R; (2014) Safety and efficacy of Becaplermin gel in the treatment of diabetic foot ulcers. *Chronic Wound Care Manag Res* 2014(1), 11–14. DOI:10.2147/CWCMR.S64905
- [43] Moses RL, Prescott TAK, Mas-Claret E, Steadman R, Moseley R, Sloan AJ; (2023) Evidence for natural products as alternative wound-healing therapies. *Biomolecules* 13(3), 444. DOI:10.3390/biom13030444
- [44] Abdelhakim M, Lin X, Ogawa R; (2020) The Japanese experience with basic fibroblast growth factor in cutaneous wound management and scar prevention: a systematic review of clinical and biological aspects. *Dermatol Ther (Heidelb)* 10(4), 569. DOI:10.1007/s13555-020-00407-6
- [45] Liu M, Wei X, Zheng Z, Li Y, Li M, Lin J, Yang L; (2023) Recent advances in nano-drug delivery systems for the treatment of diabetic wound healing. *Int J Nanomed* 18, 1537. DOI:10.2147/IJN.S395438
- [46] Hartmeier PR, Pham NB, Velankar KY, Issa F, Giannoukakis N, Meng WS; (2021) Hydrogel dressings for chronic wound healing in diabetes: beyond hydration. *J Pharm Drug Deliv Res* 10(1), 1000197.
- [47] Paladini F, Połlini M; (2019) Antimicrobial silver nanoparticles for wound healing application: progress and future trends. *Materials* 12(16), 2540. DOI:10.3390/ma12162540
- [48] Siddique MH, Aslam B, Imran M; (2020) Effects of silver nanoparticles on biofilm formation and EPS production of multidrug-resistant *Klebsiella pneumoniae*. *Biomed Res Int* 2020(1), 6398165. DOI:10.1155/2020/6398165
- [49] Kean T, Thanou M; (2010) Biodegradation, biodistribution and toxicity of chitosan. *Adv Drug Deliv Rev* 62(1), 3. DOI:10.1016/j.addr.2009.09.004

REVIEW

APPLICATIONS OF CHITOSAN IN THE PREPARATION OF CARE COSMETICS

Julia Rypińska¹, Justyna Kozłowska^{1,a,*}

¹ – Faculty of Chemistry, Nicolaus Copernicus University in Toruń,
Gagarina 7 Str., 87-100 Toruń, Poland

^a – ORCID: 0000-0002-2482-339X

*corresponding author: justynak@umk.pl

Abstract

Cosmetics manufacturers are becoming increasingly interested in chitosan due to its interesting biological and technical properties, which include being a natural conditioning and moisturising agent for the skin and hair. Indeed, according to the European Commission database CosIng (<https://ec.europa.eu/growth/tools-databases/cosing/details/75065>), the functions assigned to chitosan in cosmetics are film forming and hair fixing. This review discusses the unique physicochemical and functional properties of chitosan, the market for chitosan-based skin care and hair products and recent advances. Finally, future perspectives regarding applications of this biopolymer in cosmetics are discussed.

Keywords: chitosan, cosmetics, moisturising, conditioning, skin, hair

Received: 26.02.2024

Accepted: 04.05.2024

1. Introduction

The modern cosmetics industry places great emphasis on producing products that are safe for humans and the environment [1, 2]. Legal regulations regarding the introduction of cosmetics to the European Union (EU) market are very restrictive and regulate the process at every stage [3]. Much attention has been paid to environmental pollution, to which the cosmetics industry also contributes. The ingredients approved for use in cosmetics are constantly monitored to minimise the adverse effects of these products on the environment. Recently, there has been a trend towards reducing ingredients used in cosmetics formulations, and some environmentally unfriendly ingredients have been banned for use in the production of cosmetics. For example, microplastics have been gradually removed from cosmetics and are not recommended as abrasives in scrubs, toothpaste or other product formulas [4, 5]. Cosmetics producers prefer to use raw materials of natural origin, including plant, animal and mineral raw materials. Natural ingredients are also sought after by consumers. The growing awareness of cosmetics users encourages them to analyse the composition of the product before purchasing it. A modern consumer pays attention not only to the presence of natural active ingredients, such as plant extracts, vitamins, plant oils and essential oils, but also to other ingredients that make up the product, including emulsifiers, thickeners, preservatives and humectants [6–8].

Polymers, especially those of natural origin, are a very interesting group of compounds used to produce many conventional and novel cosmetics. Natural polymers, also named biopolymers, represent a specific class of renewable and biodegradable materials that are important in high-performance production [9]. Among biopolymers, proteins and polysaccharides are the main ingredients used in cosmetics applications. Collagen [10, 11], gelatine [12], elastin [13], silk [14] and keratin [15] are very common in modern cosmetics used for skin, body, hair and oral care; as make-up; and as decorative products. Polysaccharides are also popular; the most frequently used in the cosmetics industry are sodium alginate [16], xanthan gum [17], starch [18], hyaluronic acid [19, 20], cellulose [21], carrageenan [22], pectin [23] and chitin and its derivatives [24, 25]. Biopolymers are safe for the skin, biocompatible, environmentally friendly, non-toxic and widely available, so their use in cosmetics has continued to grow [26]. In cosmetics formulations, biopolymers are utilised as rheology modifiers, thickeners, emulsifiers, hydrators, destabilisers, film formers and fixatives [27]. Of note, the presence of biopolymers affects the properties and effects of cosmetics. One of the most characteristic features of biopolymers and their derivatives is moisturising properties. They hydrate skin, reduce transepidermal water loss (TEWL) and act as a barrier due to film formation on the skin surface [28].

Chitin is a natural biopolymer that occurs in the shells of crabs, shrimp and insects and in the cell walls of fungi and algae [29]. However, chitin is more useful when transformed into chitosan following a partial deacetylation process under alkaline conditions [30]. Chitosan and its derivatives (e.g. carboxymethyl chitosan and hydroxypropyl chitosan) have physicochemical and biological properties that allow for their application in a broad range of hygiene products and personal care cosmetics [31].

Cosmetics ingredients present on the EU market are regulated by Regulation (EC) No 1223/2009 of the European Parliament and of the Council of 30 November 2009 on cosmetic products. Chitin and chitosan, as animal by-products, are not on the list of substances that are prohibited (Annex II – List of substances prohibited in cosmetic products) or allowed with restrictions (Annex III – List of substances which cosmetic products must not contain except subject to the restrictions laid down) for use in cosmetics [3]. Moreover, Annex 2 of Regulation (EC) No 1223/2009 in position 419 bans the use

of substances that meet the definition of Category 1 and 2 materials as defined in Articles 4 and 5, respectively, of Regulation (EC) No 1774/2002 of the European Parliament and of the Council of 3 October 2002, and ingredients derived there from. This regulation establishes the health rules concerning animal by-products not intended for human consumption, including animal by-products used in cosmetics. Thus, animal by-products are allowed in cosmetics manufacturing if they comply with purity, safety and hygiene requirements. This review summarises the existing knowledge about chitosan as a cosmetics ingredient.

2. Physicochemical Properties of Chitosan

Chitosan (Figure 1) is a linear polysaccharide derived from chitin (Figure 2), which is found in crustaceans and insects. To obtain chitosan, chitin must undergo deacetylation, which results in the removal of acetyl groups and repeating units of glucosamine and *N*-acetylglucosamine [32, 33]. Its molar mass varies based on the source and processing, influencing viscosity, mechanical properties and biological activities. Chitosan with a higher molecular mass from a few thousand to over a hundred thousand Daltons is linked to enhanced bioadhesive properties [34–36]. The degree of deacetylation, expressed as a percentage, signifies the extent of chitin conversion to chitosan, impacting solubility, charge density and bioactivity. Higher deacetylation increases the positive charge and improves solubility in acidic conditions [37]. Chitosan is initially insoluble in water at neutral pH due to positively charged amino groups but becomes soluble in acidic conditions (pH < 6.5) upon protonation, enabling interaction with negatively charged molecules [38, 39]. Chitosan's ability to form gels and to swell in aqueous solutions is utilised in drug delivery and hydrogel preparations [40]. It exhibits thermal stability up to a certain temperature, making it applicable in processes involving elevated temperatures. With absorption and adsorption capabilities, especially for heavy metals and dyes, chitosan contributes to environmental remediation and wastewater treatment [41]. Overall, the diverse physicochemical properties of chitosan make it a versatile material with applications in various fields.

Chitosan faces some limitations in its solubility depending on its molecular structure and pKa [42]. Chitosan and chitin have been defined and differentiated by their different solubility profiles. Chitin is insoluble in organic solvents, whereas chitosan has limited solubility: it is soluble in all acidic organic solvents like acetic acid (1%–3%), tartaric acid and citric acid (4%) at pH < 6.5. This limited solubility of chitosan is due to its highly crystalline structure, which enhances inter- and intra-molecular hydrogen bonding. However, tailoring chitosan based on chemical modifications and derivatisation makes it soluble in a wide range of pHs. Chitosan shows a strong cationic character when added to acidic solutions due to the presence of a primary amine group on its backbone. These positively charged groups interact with counter ions (e.g. drugs, excipients, ions and polymers) [43].

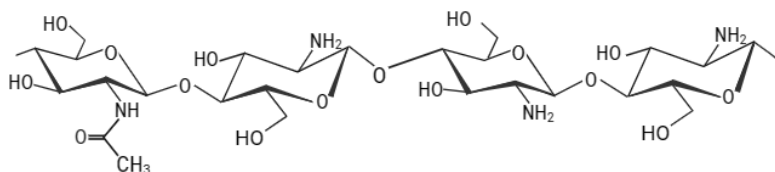


Figure 1. The chemical structure of chitosan.

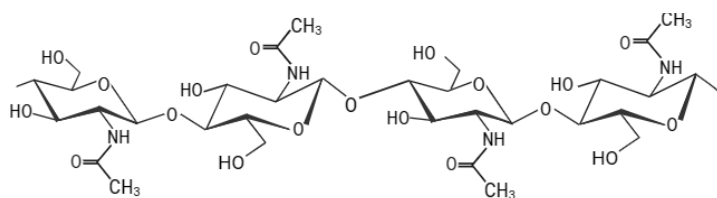


Figure 2. The chemical structure of chitin.

3. Functional Properties of Chitosan

Many physicochemical properties, such as solubility and charge, are pH dependent. Chitosan is positively charged in acidic conditions and suitable for applications like drug delivery and wound healing. Its low toxicity further enhances its suitability for medical use, ensuring safety in pharmaceuticals, medical devices and food preservation applications [44]. Chitosan's lack of immunogenicity is a significant advantage in scenarios where unwanted immune responses need to be minimised, particularly in the fields of tissue engineering and drug delivery [45]. The material's robust mechanical properties, including its film-forming ability and structural strength, enable its use to create films, membranes and scaffolds. These applications find relevance in areas such as wound dressings and controlled-release drug delivery. Chitosan's distinctive gel-forming ability and swelling capability are harnessed in the development of gel-based formulations and hydrogels, providing solutions for controlled-release drug-delivery systems and other biomedical applications [40]. The bioadhesive properties of chitosan allow it to adhere effectively to biological surfaces [46]. This adhesive ability is particularly valuable in drug-delivery systems requiring targeted and prolonged release. Inherent antimicrobial activity adds another dimension to chitosan's functionality. Its ability to inhibit the growth of bacteria and fungi makes it a sought-after material in wound dressings, food packaging and antimicrobial coatings. Chitosan's metal ion chelation capacity, facilitated by its amino and hydroxyl functional groups, renders it effective to remove heavy metals from water, contributing to environmental remediation efforts. Moreover, chitosan's absorption and adsorption capabilities, especially for heavy metals and dyes, find applications in environmental remediation and wastewater treatment, showcasing its multifaceted functional properties [47]. Figure 3 shows the many applications of chitosan, and Table 1 lists some of the functional properties of chitosan.

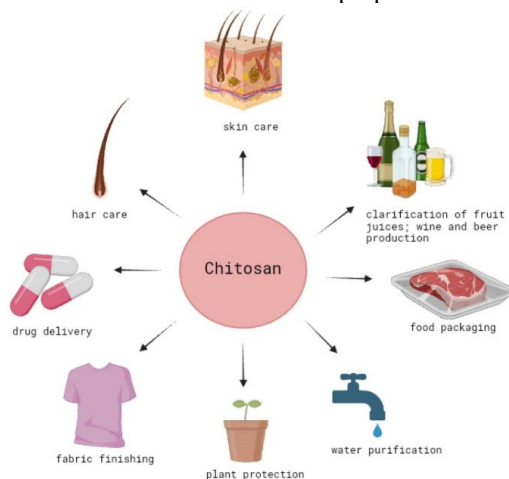


Figure 3. The major applications of chitosan.

Table 1. A list of some of the functional properties of chitosan.

Property	Reference
Biodegradability	[48]
Biocompatibility	[48, 49]
Antimicrobial activity	[50]
Antioxidant	[51]
Mucoadhesive	[52]
Antihyperglycaemic	[53]
Antibacterial and antifungal	[54, 55]
Wound healing	[56–59]
Antitumoural	[60]
Anti-inflammatory	[61]
Absorption and permeation enhancer	[62]
Film-forming ability	[63, 64]
Chelation	[65]
Drug delivery	[59, 52, 66–69]
Haemostatic effect	[70, 71]
Immunostimulation	[72]
Ability to absorb and retain water	[73, 74]

4. Chitosan in Skin Care Cosmetics

With its high molar mass, chitosan is widely utilised in the cosmetics industry to produce skin moisturisers, offering a cost-effective alternative to hyaluronic acid. It is incorporated into creams, lotions, anti-ageing cosmetics, nail care items and cleansing materials. The antimicrobial and antifungal properties of chitosan make it suitable for oral care products, such as toothpaste and mouthwashes, contributing to fresh breath and preventing plaque formation [75].

Chitosan can form a protective film on the skin's surface upon application and thus act as a barrier, reducing TEWL and enhancing skin hydration. Additionally, its hydrophilic nature attracts and binds water molecules, promoting skin moisturisation. Chitosan fills in fine lines and wrinkles upon application on the skin surface, improving their appearance for a temporary flawless and smooth effect [76]. Figure 4 shows the effect of chitosan applications on the skin.

Due to its cationic nature, chitosan exhibits inherent antibacterial properties. The positively charged amino groups interact with microbial cell membranes, disrupting their integrity and leading to microbial death or growth inhibition. This mechanism renders chitosan effective against acne-causing bacteria and other microbes, making it suitable for skincare products designed for acne-prone skin. Chitosan's multifaceted actions on skin physiology contribute to its anti-ageing effects. As a potent antioxidant, chitosan scavenges free radicals generated by environmental stressors, protecting skin cells from oxidative damage and premature ageing. Furthermore, chitosan stimulates collagen synthesis in the dermis, promoting skin elasticity and firmness. Its ability to induce cell proliferation and tissue regeneration aids in repairing damaged skin, further enhancing its anti-ageing effects. In wound healing, chitosan deposition on the skin surface creates a network

structure, stimulating collagen synthesis and supporting tissue regeneration, displaying biocompatibility, biodegradability and antibacterial properties. Its gentle exfoliating properties aid in removing dead skin cells, ensuring a smoother complexion and facilitating wound healing [56, 77, 78].

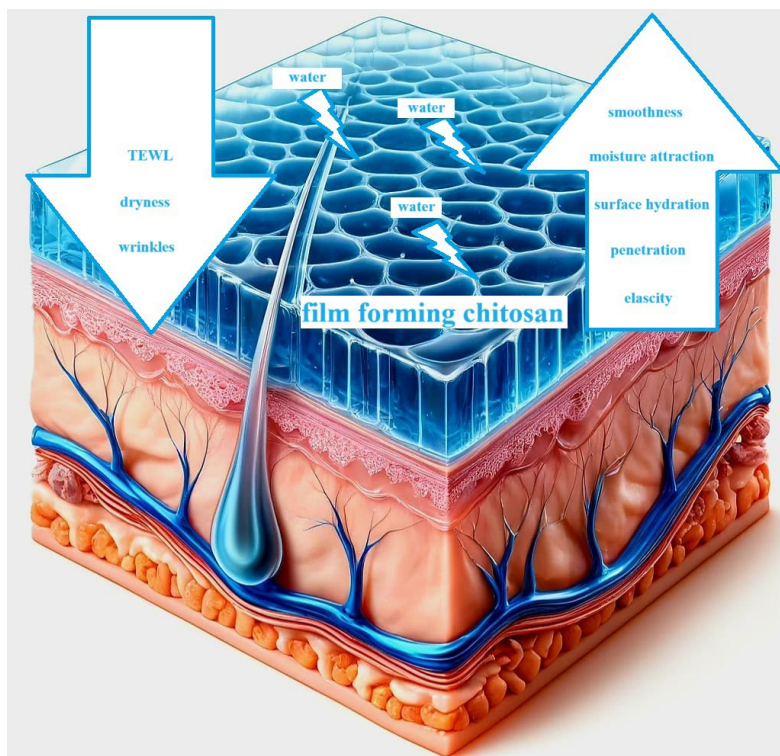


Figure 4. The effects of chitosan application to the skin surface.

Chitosan gel particles, with their moisturising properties, are adept at encapsulating hydrophilic cosmetics ingredients and penetrating the dermis for effective dermal delivery. Chitosan may have some ultraviolet-absorbing properties, making it a potential ingredient in sunscreens. Its potential as a sunscreen relies on its specific attributes, including the source, molar mass and degree of deacetylation. Although there has been insufficient research on how chitosan's characteristics influence its effectiveness as a sunscreen, applying a hybrid system film on the skin surface is a viable approach to mitigate the effects of ultraviolet (UV) radiation exposure. While it is not a replacement for dedicated sun protection ingredients, it can offer additional benefits and contribute to the overall formulation [79]. Chitosan's anti-inflammatory properties make it suitable for skincare products designed for sensitive skin. Moreover, research has shown a significant reduction in sebum levels after using cosmetics formulations containing chitosan, attributed to its ability to form complexes with sebum and thus hindering its accumulation on the skin's surface [76, 80].

Several brands use chitosan in their skin care cosmetics products [81]. Table 2 shows some commercially available skin care products with chitosan listed as an ingredient.

Table 2. Some examples of commercially available skin care cosmetics that contain chitosan [81].

Product	Manufacturer	Application
Under Eye Collagen 24k Gold Anti-Aging Eye Masks	Arlega (United States)	Mask
Intense Formula Day to Night Moisturiser	Mirabella (United States)	Facial moisturiser/ treatment
Moisturizing Hand Sanitizer, Uplifting Lemongrass	Babington Soap Co. (United Kingdom)	Hand sanitiser
Environmental Shield Essential – C Cleanser	Murad (United States)	Facial cleanser
Clarifying Cream Cleanser	Murad (United States)	Facial cleanser
High Amplify Wonder Boost	Matrix (United States)	Styling mousse/foam
Ultimate Miracle Worker Night Multi Rejuvenating Nighttime, Serum in Cream	Philosophy (United States)	Facial moisturiser/ treatment

5. Chitosan in Hair Care Cosmetics

With its positively charged amino groups, chitosan interacts with the negatively charged components of the hair, forming a complex. This interaction creates an elastic film on the hair surface, enhancing its softness, smoothness and mechanical strength. The film-forming ability of chitosan is attributed to its high molar mass and biopolymer structure, which allow it to adhere to the hair shaft and to provide structural support [76].

Chitosan's film-forming properties establish a protective layer on the hair shaft, reducing mechanical damage, such as breakage and split ends. By reinforcing the hair structure, chitosan helps to improve hair texture and resilience. Additionally, the film formed by chitosan adds thickness and volume to individual hair strands, enhancing the overall appearance and volume of hair. Its hydrophilic nature enables it to attract and retain moisture within the hair shaft, preventing excessive drying and maintaining optimal hydration levels. This moisture retention property softens the hair and reduces frizz by smoothing the hair cuticle and minimising static electricity. Chitosan's conditioning properties stem from its ability to form a protective film on the hair surface, smoothing out roughness and imparting a glossy finish. This film also helps to seal the hair cuticle, preventing moisture loss and enhancing the hair's overall texture and appearance [75, 76].

Chitosan's antimicrobial properties contribute to scalp health by inhibiting the growth of microorganisms, thus reducing the risk of scalp conditions such as dandruff [82]. Additionally, the protective film formed by chitosan on the hair surface helps to retain hair colour by minimising colour fading due to environmental factors such as UV radiation and washing. Chitosan's film-forming ability aids in detangling hair by reducing friction between hair strands, making combing easier and minimising breakage [83]. Furthermore, chitosan's potential to promote tissue repair is beneficial for addressing damaged hair, as it helps to strengthen the hair structure and improve overall hair health. In styling products like gels and mousses, chitosan's film-forming properties provide a flexible hold and structure to the hair, allowing for the creation of defined hairstyles. This film also helps to protect the hair from environmental stressors and maintain the desired hairstyle throughout the day [76].

Several brands use chitosan in their hair care cosmetics products [81]. Table 3 lists some commercially available hair care products with chitosan listed as an ingredient.

Table 3. Some examples of commercially available hair care cosmetics products that contain chitosan [81].

Product	Manufacturer	Application
Don't Despair, Repair Super Moisture Conditioner	Briogeo (United States)	Conditioner
Hair Care Don't Despair Repair! Super Moisture Conditioner	Briogeo (United States)	Conditioner
Instant Volume Volumizing Spray Gel	Aussie (United States)	Styling gel/ lotion
High Amplify Wonder Boost	Matrix (United States)	Styling mousse/foam
Instant Lift Volumizing Mousse	Kristin Ess (United States)	Styling mousse/foam
One Signature Shampoo with Avocado Oil + Castor Oil	Kristin Ess (United States)	Shampoo
Moisture Rich Curl Conditioner for Dry Damaged Curly + Wavy Hair	Kristin Ess (United States)	Conditioner
Touchable Hold Spray Gel, Scent Notes of Lily	Herbal Essences (United States)	Styling gel/ lotion
Pro-V Volume and Body Anti Frizz Hair Mousse	Pantene (Hong Kong)	Styling mousse/foam
Overnight Hair Mask	Orlando Pita Play (United States)	Hair treatment/ serum
Weightless Shine Working Hair Serum	Kristin Ess (United States)	Hair treatment/ serum
Curl Enhancer	Living Proof (United States)	Hair styling aide

6. Prospects and Challenges of Chitosan in Cosmetics Applications

According to contemporary global cosmetics trends, it is necessary to develop and obtain environmentally friendly cosmetics in terms of the product itself and the packaging. Care for the environment and the growing ecological awareness of consumers have required manufacturers to change the formulas of conventional cosmetics. Indeed, the shift from using ingredients from petrochemical sources to ingredients with a more ecological profile has been observed for a long time [1, 8]. Chitosan and its derivatives, which combine valuable physicochemical and biological qualities such as biocompatibility, biodegradability, non-toxicity, antibacterial activity and film-forming capabilities, are promising ingredients in this new trend in the cosmetics market. Chitosan is particularly helpful for preparing hair care formulations due to its electrostatic interaction capabilities with negatively charged substrates [24, 76]. So, it is an appropriate ingredient for treating damaged hair because it forms polymeric films that help condition hair. Moreover, chitosan is an ideal component for moisturising and anti-ageing skincare products due to its ability to create films, providing water while preventing dehydration. For this reason, chitosan

can be found in face, hand and body creams. Moreover, it is also an ingredient in deodorising products; dental care products; and coloured cosmetics such as lipstick, eye shadow and nail polish [84, 85].

A significant limitation related to the use of biopolymers, including chitosan, in the cosmetics industry is associated with the need to standardise and optimise chitosan isolation and purification on a large scale. Generally, it is highly challenging to obtain a biopolymer with sufficient purity and source reliability [24]. Chitosan isolated from different sources may have different physicochemical and biological properties, which constitutes a significant difficulty in the production of cosmetics. When changing the supplier of chitosan, the manufacturer cannot be sure that it will obtain a batch of the cosmetics with repeatable properties. The method of obtaining and purifying this polysaccharide also results in the relatively high price of this raw material as a cosmetics ingredient [86].

There has recently been a growing aversion among consumers towards animal-derived cosmetics ingredients because they can give rise to irritative or allergic reactions [87]. Moreover, many cosmetics producers have limited the use of raw materials of animal origin in the formulation of cosmetics due to the spread of animal diseases, such as bovine spongiform encephalopathy (BSE), widely referred to as ‘mad cow disease’, transmissible spongiform encephalopathy (TSE) and avian influenza (bird flu). Many cosmetics ingredients have been replaced by similar substances extracted from plants or of a biotechnological origin. In the case of chitosan, there has been an increase in interest in obtaining it from mushrooms for cosmetics purposes, especially in the production of increasingly popular vegan cosmetics. These products are created primarily without animal suffering, with ethical standards (cruelty free) and with respect for the entire ecosystem, emphasising the defence of biodiversity [88].

Chitosan has been widely used in biotechnology, agriculture, medicine and pharmacy, wastewater treatment, food and cosmetics despite its poor solubility. Its solubility can be improved by modifying its functional hydroxyl, amino and acetamide groups, which can form various new derivatives with improved physicochemical properties [38, 89]. According to the CosIng database (<https://ec.europa.eu/growth/tools-databases/cosing/details/74825>), chitosan derivatives are increasingly being used in the design of modern cosmetics preparations – for example, carboxymethyl chitosan as a film-forming, gel-forming and viscosity-controlling agent (<https://ec.europa.eu/growth/tools-databases/cosing/details/74825>). A very interesting example of modifying chitosan for cosmetics applications is adding hydrophobic moieties to its backbone. This modified chitosan is much more amphiphilic than the parent biopolymer, thus expanding its utility in cosmetics applications. The uses of *N*-alkylated or *N*-acylated chitosans with diverse degrees of substitution and hydrophobicity include, among others, mascara, moisturising creams, wrinkle-reducing products, shampoos, conditioners, blemish concealers and controlled-release matrices for fragrance [90]. Another example of innovative applications of chitosan and chitin are bioactive, biodegradable chitosan films containing chitin nanofibrils developed for face masks [91, 92]. Moreover, chitosan has been used to design nanoparticles for skin delivery. Chitosan nanoparticles can deliver the active and cosmetics components through the skin and can be used as a cosmetics delivery system [93, 94]. Even though chitosan is not as popular in the cosmetics industry as other biopolymers, interest in this polysaccharide as a cosmetics ingredient continues to grow. Thus, the use of this polysaccharide paves the way for a potential future in developing novel cosmetics formulations.

7. Conclusions

Natural polymers are ingredients that manufacturers use eagerly because they fulfil some of the main requirements of the green cosmetics industry. Consumers are increasingly paying attention to the composition of cosmetics and want them to be as natural as possible. Chitosan is not a particularly popular ingredient in cosmetics compared with other biopolymers, which means that the valuable properties of this polymer have not yet been fully exploited in the cosmetics industry. Perhaps the popularity of this ingredient will increase in the future. Inconveniences associated with introducing it into cosmetics formulations could be eliminated due to the possibility of modifying the properties of chitosan thanks to the presence of functional groups. Indeed, distributors of cosmetics ingredients already offer several chitosan derivatives, such as carboxymethyl chitosan, hydroxyethyl chitosan and chitosan lactate.

8. References

- [1] Martins AM, Marto JM; (2023) A sustainable life cycle for cosmetics: from design and development to post-use phase. *Sustain Chem Pharm* 35, 101178. DOI:10.1016/j.scp.2023.101178
- [2] Amberg N, Fogarassy C; (2019) Green Consumer Behavior in the Cosmetics Market. *Resour* 8(3), 137. DOI:10.3390/resources8030137
- [3] European Parliament Regulation (EC) No 1223/2009 of the European Parliament and of the Council of 30 November 2009 on Cosmetic Products Off. J. Eur. Union (2009)
- [4] Lim HY, Kwon KH; (2023) Sustainable Assessment of the Environmental Activities of Major Cosmetics and Personal Care Companies. *Sustainability* 15, 13286. DOI:10.3390/su151813286
- [5] European Chemicals Agency. ECHA's Proposed Restriction. Available online: <https://echa.europa.eu/hot-topics/microplastics> (accessed on 8 July 2023)
- [6] Faria-Silva C, Ascenso A, Costa AM, Marto J, Carvalho M, Ribeiro HM, Simões S; (2020) Feeding the skin: a new trend in food and cosmetics convergence. *Trends Food Sci Technol* 95, 21–32. DOI:10.1016/j.tifs.2019.11.015
- [7] Guzmán E, Lucia A; (2021) Essential Oils and Their Individual Components in Cosmetic Products. *Cosmetics* 8, 114. DOI:10.3390/cosmetics8040114
- [8] Rocca R, Acerbi F, Fumagalli L, Taisch M; (2022) Sustainability paradigm in the cosmetics industry: state of the art. *Cleaner Waste Systems* 3, 100057. DOI:10.1016/j.clwas.2022.100057
- [9] Mendoza-Muñoz N, Leyva-Gómez G, Piñón-Segundo E, Zambrano-Zaragoza ML, Quintanar-Guerrero D, Del Prado Audelo ML, Urbán-Morlán Z; (2023) Trends in biopolymer science applied to cosmetics. *Int J Cosmet Sci* 45, 699–724. DOI:10.1111/ics.12880
- [10] Avila Rodríguez MI, Rodríguez Barroso LG, Sánchez ML; (2018) Collagen: a review on its sources and potential cosmetic applications. *J Cosmet Dermatol* 17(1), 20–26. DOI:10.1111/jocd.12450
- [11] Amnuakit T, Shankar R, Benjakul S; (2022) Hydrolyzed Fish Collagen Serum from By-Product of Food Industry: Cosmetic Product Formulation and Facial Skin Evaluation. *Sustainability* 14, 16553. DOI:10.3390/su142416553
- [12] Al-Nimry S, Dayah AA, Hasan I, Daghmash R; (2021) Cosmetic, Biomedical and Pharmaceutical Applications of Fish Gelatin/Hydrolysates. *Mar Drugs* 19(3), 145. DOI:10.3390/md19030145
- [13] Kamaruzaman N, Yusop SM; (2021) Determination of stability of cosmetic formulations incorporated with water-soluble elastin isolated from poultry. *J King Saud Univ Sci* 33, 6, 101519. DOI:10.1016/j.jksus.2021.101519

- [14] Johnson W Jr, Bergfeld WF, Belsito DV, Hill RA, Klaassen CD, Liebler DC, Marks JG Jr, Shank RC, Slaga TJ, Snyder PW, Gill LJ, Heldreth B; (2020) Safety Assessment of Silk Protein Ingredients as Used in Cosmetics. *Int J Toxicol* 39(3_suppl), 127S–144S. **DOI:**10.1177/1091581820966953
- [15] Gavazzoni Dias MF; (2015) Hair cosmetics: an overview. *Int J Trichology* 7(1), 2–15. **DOI:**10.4103/0974–7753.153450
- [16] Łętocha A, Miastkowska M, Sikora E; (2022) Preparation and Characteristics of Alginate Microparticles for Food, Pharmaceutical and Cosmetic Applications. *Polymers* 14, 3834. **DOI:**10.3390/polym14183834
- [17] Petri DFS; (2015) Xanthan gum: a versatile biopolymer for biomedical and technological applications. *J Appl Polym Sci* 132, 42035. **DOI:**10.1002/app.42035
- [18] Olivato JB; (2024), Starch: a natural, safe, and multifunctional ingredient for cosmetic formulations. In: Pascoli Cereda M, Francois Vilpoux O (eds), *Starch Industries: Processes and Innovative Products in Food and Non-Food Uses*. Academic Press, 255–269. **DOI:**10.1016/B978-0-323-90842-9.00007-8
- [19] Ratajczak P, Maciejak O, Kopciuch D, Paczkowska A, Zaprutko T, Kus K; (2023) Directions of hyaluronic acid application in cosmetology. *J Cosmet Dermatol* 22(3), 862–871. **DOI:**10.1111/jocd.15485
- [20] Juncan AM, Moisă DG, Santini A, Morgovan C, Rus LL, Vonica-Țincu AL, Loghin F; (2021) Advantages of Hyaluronic Acid and Its Combination with Other Bioactive Ingredients in Cosmeceuticals. *Molecules* 26(15), 4429. **DOI:**10.3390/molecules26154429
- [21] Bianchet RT, Vieira Cubas AL, Machado MM, Siegel Moecke EH; (2020) Applicability of bacterial cellulose in cosmetics – bibliometric review. *Biotechnol Rep* 27, e00502. **DOI:**10.1016/j.btre.2020.e00502
- [22] Shafie MH, Kamal ML, Zulkiflee FF, Hasan S, Uyup NH, Abdullah S, Hussin NAM, Tan YC, Zafarina Z; (2022) Application of carrageenan extract from red seaweed (Rhodophyta) in cosmetic products: a review. *J Indian Chem Soc* 99(9), 100613. **DOI:**10.1016/j.jics.2022.100613
- [23] Roman-Benn A, Contador CA, Li MW, Lam HM, Ah-Hen K, Ulloa PE, Ravanal MC; (2023) Pectin: an overview of sources, extraction and applications in food products, biomedical, pharmaceutical and environmental issues. *Food Chem Adv* 2, 100192. **DOI:**10.1016/j.focha.2023.100192
- [24] Piekarska K, Sikora M, Owczarek M, Józwiak-Pruska J, Wiśniewska-Wrona M; (2023) Chitin and Chitosan as Polymers of the Future-Obtaining, Modification, Life Cycle Assessment and Main Directions of Application. *Polymers* 15, 793. **DOI:**10.3390/polym15040793
- [25] Anchisi C, Meloni MC, Maccioni AM; (2007) Chitosan beads loaded with essential oils in cosmetic formulations. *Int J Cosmetic Sci* 29, 485–485. **DOI:**10.1111/j.1468-2494.2007.00371_1.x
- [26] Pires PC, Mascarenhas-Melo F, Pedrosa K, Lopes D, Lopes J, Macário-Soares A, Peixoto D, Giram PS, Veiga F, Paiva-Santos AC; (2023) Polymer-based biomaterials for pharmaceutical and biomedical applications: A focus on topical drug administration. *Eur Polym J* 187, 111868. **DOI:**10.1016/j.eurpolymj.2023.111868
- [27] Gawade RP, Chinke SL, Alegaonkar PS; (2020) Polymers in cosmetics. In: AlMaadeed MAA, Ponnamma D, Carignano MA (eds), *Polymer Science and Innovative Applications*. Elsevier, 545–565. **DOI:**10.1016/B978-0-12-816808-0.00017-2
- [28] Maia Campos PMBG, de Melo MO, de Camargo Junior FB; (2014) Effects of Polysaccharide-Based Formulations on Human Skin. In: Ramawat K, Mérillon JM (eds), *Polysaccharides*. Springer, Cham. **DOI:**10.1007/978-3-319-03751-6_64-1

- [29] Pellis A, Guebitz GM, Nyanhongo GS; (2022) Chitosan: Sources, Processing and Modification Techniques. *Gels* 8(7), 393. **DOI:**10.3390/gels8070393
- [30] Younes I, Rinaudo M; (2015) Chitin and chitosan preparation from marine sources. Structure, properties and applications. *Mar Drugs* 13(3), 1133–74. **DOI:**10.3390/md13031133
- [31] Chen Q, Qi Y, Jiang Y, Quan W, Luo H, Wu K, Li S, Ouyang Q; (2022) Progress in Research of Chitosan Chemical Modification Technologies and Their Applications. *Mar Drugs* 20(8), 536. **DOI:**10.3390/md20080536
- [32] Bastiaens L, Soetemans L, D'Hondt E, Elst K; (2019) Sources of Chitin and Chitosan and their Isolation. In: van den Broek LAM, Boeriu CG (eds), *Chitin and Chitosan: Properties and Applications*. John Wiley & Sons Ltd., 1–34. **DOI:**10.1002/9781119450467.ch1
- [33] Vokhidova NR, Ergashev KH, Rashidova SS; (2022) Synthesis and application of chitosan hydroxyapatite: a review. *Prog Chem Appl Chitin Deriv* 27, 5–34. **DOI:**10.15259/PCACD.27.001
- [34] Petroni S, Tagliaro I, Antonini C, D'Arienzo M, Orsini SF, Mano JF, Brancato V, Borges J, Cipolla L; (2023) Chitosan-Based Biomaterials: Insights into Chemistry, Properties, Devices, and Their Biomedical Applications. *Mar Drugs* 21, 147. **DOI:**10.3390/md21030147
- [35] Aranda-Barradas ME, Trejo-López SE, Real AD, Álvarez-Almanazán S, Méndez-Albores A, García-Tovar CG, Conzález-Díaz FR, Miranda-Castro SP; (2022) Effect of molecular weight of chitosan on the physicochemical, morphological, and biological properties of polyplex nanoparticles intended for gene delivery. *Carbohydr Polym Technol Appl* 4, 100228. **DOI:**10.1016/j.carpta.2022.100228
- [36] Piegat A, Goszczyńska A, Idzik T, Niemczyk A; (2019) The Importance of Reaction Conditions on the Chemical Structure of N,O-Acylated Chitosan Derivatives. *Molecules* 24, 3047. **DOI:**10.3390/molecules24173047
- [37] Sorlier P, Denuzière A, Viton C, Domard A; (2001) Relation between the Degree of Acetylation and the Electrostatic Properties of Chitin and Chitosan. *Biomacromol* 2, 765–72. **DOI:**10.1021/bm015531+
- [38] Aranaz I, Alcántara AR, Civera MC, Arias C, Elorza B, Heras Caballero A, Acosta N; (2021) Chitosan: an overview of its properties and applications. *Polymers* 13, 3256. **DOI:**10.3390/polym13193256
- [39] Roy J, Salaün F, Giraud S, Ferri A, Guan J, Chen G; (2017) Solubility of Chitin: Solvents, Solution Behaviors and Their Related Mechanisms. **DOI:**10.5772/intechopen.71385
- [40] Ahmadi F, Oveisi Z, Samani SM, Amoozgar Z; (2015) Chitosan based hydrogels: Characteristics and pharmaceutical applications. *Res Pharma Sci* 10, 1–16.
- [41] Cai Z, Chen P, Jin H-J, Kim J; (2009) The effect of chitosan content on the crystallinity, thermal stability, and mechanical properties of bacterial cellulose-chitosan composites. *J Mech Eng Sci* 223, 2225–2230. **DOI:**10.1243/09544062JMES1480
- [42] Wu Q-X, Lin D-Q, Yao S-J; (2014) Design of Chitosan and Its Water Soluble Derivatives-Based Drug Carriers with Polyelectrolyte Complexes. *Mar Drugs* 12, 6236–6253. **DOI:**10.3390/md12126236
- [43] Wadhwa S, Paliwal R, Paliwal SR, Vyas SP; (2009) Chitosan and its Role in Ocular Therapeutic. *Mini Rev Med Chem* 9, 1639–1647. **DOI:**10.2174/138955709791012292
- [44] Victor RS, Santos ADM, Sousa BV, Neves GA, Santana LNL, Menezes RR; (2020) A Review on Chitosan's Uses as Biomaterial: Tissue Engineering, Drug Delivery Systems and Cancer Treatment. *Materials* 13, 4995. **DOI:**10.3390/ma13214995

- [45] Zaharoff DA, Rogers CJ, Hance KW, Schlom J, Greiner JW; (2007) Chitosan solution enhances both humoral and cell-mediated immune responses to subcutaneous vaccination. *Vaccine* 25(11), 2085–94. **DOI:**10.1016/j.vaccine.2006.11.034
- [46] Fan P, Zeng Y, Zaldivar-Siva D, Agüero L, Wang S; (2023) Chitosan-Based Hemostatic Hydrogels: The Concept, Mechanism, Application, and Prospects. *Molecules* 28(3), 1473. **DOI:**10.3390/molecules28031473
- [47] Upadhyay U, Sreedhar I, Singh SA, Patel CM, Anitha KL; (2021) Recent advances in heavy metal removal by chitosan based adsorbents. *Carbohydr Polym* 251, 117000. **DOI:**10.1016/j.carbpol.2020.117000
- [48] Maher ZE, Entsar SA; (2013) Chitosan based edible films and coatings: a review. *Mater Sci Eng C* 33(4), 1819–1841. **DOI:**10.1016/j.msec.2013.01.010
- [49] Rodrigues S, Dionísio M, López CR, Grenha A; (2012) Biocompatibility of Chitosan Carriers with Application in Drug Delivery. *J Funct Biomater* 3, 615–641. **DOI:**10.3390/jfb3030615
- [50] Ke C, Deng F, Chuang C, Lin C; (2021) Antimicrobial Actions and Applications of Chitosan. *Polymers* 13, 904. **DOI:**10.3390/polym13060904
- [51] Ngo DH, Kim SK; (2014) Antioxidant effects of chitin, chitosan and their derivatives. *Adv Food Nutr Res* 73, 15–31. **DOI:**10.1016/B978-0-12-800268-1.00002-0
- [52] Ways TMM, Lau WM, Khutoryanskiy VV; (2018) Chitosan and Its Derivatives for Application in Mucoadhesive Drug Delivery Systems. *Polymers* 10, 267. **DOI:**10.3390/polym10030267
- [53] Tzeng H-P, Liu S-H, Chiang M-T; (2022) Antidiabetic Properties of Chitosan and Its Derivatives. *Mar Drugs* 20, 784. **DOI:**10.3390/md20120784
- [54] Sikorski D, Bauer M, Frączyk J, Draczyński Z; (2022) Antibacterial and Antifungal Properties of Modified Chitosan Nonwovens. *Polymers* 14, 1690. **DOI:**10.3390/polym14091690
- [55] Zhang J, Tan W, Luan F, Yin X, Dong F, Li Q, Guo Z; (2018) Synthesis of Quaternary Ammonium Salts of Chitosan Bearing Halogenated Acetate for Antifungal and Antibacterial Activities. *Polymers* 10, 530. **DOI:**10.3390/polym10050530
- [56] Jonson NR, Wang Y; (2015) Drug Delivery Systems for Wound Healing. *Curr Pharm Biotechnol* 16(7), 621–629. **DOI:**10.2174/1389201016666150206113720
- [57] Tataru AM, Kontoyiannis DP, Mikos AG; (2018) Drug delivery and tissue engineering to promote wound healing in the immunocompromised host: current challenges and future directions. *Adv Drug Deliv Rev* 129, 319–329. **DOI:**10.1016/j.addr.2017.12.001
- [58] Yayehrad AT, Siraj EA, Matsabisa M, Birhanu G; (2023) 3D printed drug loaded nanomaterials for wound healing applications. *Regen Ther* 24, 361–376. **DOI:**10.1016/j.reth.2023.08.007
- [59] Saghazadeh S, Rinoldi C, Schot M, Kashaf SS, Sharifi F, Jalilian E, Nuutila K, Giatsidis G, Mostafalu P, Derakhshandeh H, Yue K, Swieszkowski W, Memic A, Tamayol A, Khademhosseini A; (2018) Drug delivery systems and materials for wound healing applications. *Adv Drug Deliv Rev* 127, 138–166. **DOI:**10.1016/j.addr.2018.04.008
- [60] Abedian Z, Moghadammia A, Zabih E, Pourbagher R, Ghasemi M, Nouri HR, Tashakorian H, Jenabian N; (2019) Anticancer properties of chitosan against osteosarcoma, breast cancer and cervical cancer cell lines. *Casp J Intern Med* 10, 439–446. **DOI:**10.22088/cjim.10.4.439
- [61] Friedman AJ, Phan J, Schairer DO, Champer J, Qin M, Pirous A, Blecher-Paz K, Oren A, Liu PT, Modlin RL, Kim J; (2012) Antimicrobial and anti-inflammatory activity of chitosan-alginate nanoparticles: a targeted therapy for cutaneous pathogens. *J Invest Dermatol* 133(5), 1231–1239. **DOI:**10.1038/jid.2012.399

- [62] Thanou M, Verhoef JC, Junginger HE; (2001) Chitosan and its derivatives as intestinal absorption enhancers. *Adv Drug Deliv Rev* 50, 91–101. **DOI:**10.1016/S0169-409X(01)00180-6
- [63] Lewandowska K, Szulc M; (2022) Rheological and Film-Forming Properties of Chitosan Composites. *Int J Mol Sci* 23, 8763. **DOI:**10.3390/ijms23158763
- [64] Zhang W, Cao J, Jiang W; (2022) Analysis of film-forming properties of chitosan with different molecular weights and its adhesion properties with different postharvest fruit surfaces. *Food Chem* 395, 133605. **DOI:**10.1016/j.foodchem.2022.133605
- [65] Verma C, Quraishi MA; (2021) Chelation capability of chitosan and chitosan derivatives: Recent developments in sustainable corrosion inhibition and metal decontamination applications. *Curr Res Green Sustain Chem* 4, 100184. **DOI:**10.1016/j.crgsc.2021.100184
- [66] Herdiana Y, Wathoni N, Shamsuddin S, Muchtaridi M; (2021) Drug release study of the chitosan-based nanoparticles. *Heliyon* 8(1), e08674. **DOI:**10.1016/j.heliyon.2021.e08674
- [67] Safdar R, Omar AA, Arunagiri A, Regupathi I, Thanabalan M; (2019) Potential of chitosan and its derivatives for controlled drug release application – a review. *J Drug Deliv Sci Technol* 49, 642–659. **DOI:**10.1016/j.jddst.2018.10.020
- [68] Prabakaran M, Mano JF; (2004) Chitosan-Based Particles as Controlled Drug Delivery System. *Drug Deliv* 12, 41–57. **DOI:**10.1080/10717540590889781
- [69] Farasati Far B, Omrani M, Naimi-Jamal MR, Javanshir S; (2023) Multi-responsive chitosan-based hydrogels for controlled release of vincristine. *Commun Chem* 6, 28(2023). **DOI:**10.1038/s42004-023-00829-1
- [70] Maksym PV, Sikora V; (2015) Chitosan as a Hemostatic Agent: Current State. *Eur J Med Ser B* 2, 24–33. **DOI:**10.13187/ejm.s.b.2015.2.24
- [71] Liu Z, Xu Y, Su H, Jing X, Wang D, Li S, Chen Y, Guan H, Meng L; (2023) Chitosan-based hemostatic sponges as new generation hemostatic materials for uncontrolled bleeding emergency: modification, composition, and application. *Carbohydr Polym* 311, 120780. **DOI:**10.1016/j.carbpol.2023.120780
- [72] Fong D, Hoemann CD; (2017) Chitosan immunomodulatory properties: perspectives on the impact of structural properties and dosage. *Future Sci OA* 4(1), FSO225. **DOI:**10.4155/fsoa-2017-0064
- [73] Mohamad N, Nadiah AHN, Jeefferie AR, Fairuz DM; (2013) Effect of Chitosan Gelatinization Temperature on Water Absorption and Water Retention of Chitosan-Based Urea Fertilizer. *Int J Automot Mech Eng* 8, 1357–1366. **DOI:**10.15282/ijame.8.2013.23.0111
- [74] [Trinh TH, KuShaari K; (2016) Dynamic of Water Absorption in Controlled Release Fertilizer and its Relationship with the Release of Nutrient. *Procedia Eng* 148, 319–326. **DOI:**10.1016/j.proeng.2016.06.444
- [75] Sreerag G, Sabu T, Anitha P; (2020) Chitin and Chitosan based Polymer Materials for Various Applications. In: Sreerag G, Sabu T, Anitha P (eds), *Handbook of Chitin and Chitosan*. Vol. 3. Elsevier, 71–88. **DOI:**10.1016/C2018-0-02998-9
- [76] Guzmán E, Ortega F, Rubio RG; (2022) Chitosan: A Promising Multifunctional Cosmetic Ingredient for Skin and Hair Care. *Cosmetics* 9, 99. **DOI:**10.3390/cosmetics9050099
- [77] Kulka K, Sionkowska A; (2023) Chitosan based materials in cosmetic applications: a review. *Molecules* 28, 1817. **DOI:**10.3390/molecules28041817
- [78] Ju S, Shin G, Lee M, Koo JM, Jeon H, Ok YS, Hwang DS, Kwang SY, Oh DX, Park J; (2021) Biodegradable chito-beads replacing non-biodegradable microplastics for cosmetics. *Green Chem* 23, 6953–6965. **DOI:**10.1039/D1GC01588E

- [79] Zhang X, Li Y, Guo M, Jin TZ, Arabi SA, He Q, Ismail BB, Hu Y, Liu D; (2021) Antimicrobial and UV Blocking Properties of Composite Chitosan Films with Curcumin Grafted Cellulose Nanofiber. *Food Hydrocoll* 112, 106337. **DOI:**10.1016/j.foodhyd.2020.106337
- [80] Aranaz I, Acosta N, Civera C, Elorza B, Mingo J, Castro C, Gandía ML, Caballero AH; (2018) Cosmetics and Cosmeceutical Applications of Chitin, Chitosan and Their Derivatives. *Polymers* 10, 213. **DOI:**10.3390/polym10020213
- [81] EWG's Skin Deep®. Your Guide to Safer Personal Care Products. Available online: EWG Skin Deep® Cosmetics Database
- [82] Firmansyah E, Hardiyanti R, Samosir AK, Sitepu MPB, Siagian NB; (2022) Preparation and Characterization of Chitosan from Golden Scales for Ani-dandruff Shampoo. *Rasayan J Chem* 15(2), 1340–1344. **DOI:**10.31788/RJC.2022.1526755
- [83] Luo C, Zhou L, Chiou K, Huang J; (2018) Multifunctional Graphene Hair Dye. *Chem* 4, 784–794. **DOI:**10.1016/j.chempr.2018.02.021
- [84] Abd El-Hack ME, El-Saadony MT, Shafi ME, Zaberemawi NM, Arif M, Batiha GE, Khafaga AF, Abd El-Hakim YM, Al-Sagheer AA; (2020) Antimicrobial and antioxidant properties of chitosan and its derivatives and their applications: a review. *Int J Biol Macromol* 164, 2726–2744. **DOI:**10.1016/j.ijbiomac.2020.08.153
- [85] Thambiliyagodage C, Jayanetti M, Mendis A, Ekanayake G, Liyanaarachchi H, Vigneswaran S; (2023) Recent advances in chitosan-based applications – a review. *Materials* 16(5), 2073. **DOI:**10.3390/ma16052073
- [86] Casadidio C, Peregrina DV, Gigliobianco MR, Deng S, Censi R, Di Martino P; (2019) Chitin and chitosans: characteristics, eco-friendly processes, and applications in cosmetic science. *Mar Drugs* 17(6), 369. **DOI:**10.3390/md17060369
- [87] Latheef F, Wilkinson M; (2020) Adverse skin reactions to cosmetics and skin care products. In: Johansen JD, Mahler V, Lepoittevin JP, Frosch PJ (eds), *Contact Dermatitis*. Springer, New York, 913–932. **DOI:**10.1007/978-3-030-36335-2_83
- [88] Cristiano L, Guagni M; (2022) Zoocuticals and Cosmetic Ingredients Derived from Animals. *Cosmetics* 9, 13. **DOI:**10.3390/cosmetics9010013
- [89] Yadav M, Kaushik B, Rao GK, Srivastava CM, Vaya D; (2023) Advances and challenges in the use of chitosan and its derivatives in biomedical fields: a review. *Carbohydr Polym Technol Appl* 5, 100323, **DOI:**10.1016/j.carpta.2023.100323
- [90] WO/2017/177027– Hydrophobically-modified chitosan for use in cosmetics and personal care applications (patent, publication date: 12.10.2017)
- [91] Kodolova-Chukhontseva VV, Dresvyanina EN, Nashchekina YA, Dobrovol'skaya IP, Bystrov SG, Ivan'kova EM, Yudin VE, Morganti P; (2022) Application of the Composite Fibers Based on Chitosan and Chitin Nanofibrils in Cosmetology. *J Funct Biomater* 13(4), 198. **DOI:**10.3390/jfb13040198
- [92] Kodolova-Chukhontseva VV, Rozova EY, Dresvyanina EN, Nashchekina YA, Dobrovol'skaya IP, Vlasova EN, Bystrov SG, Popova EN, Maslennikova TP, Yudin VE, Morganti P; (2023) New Composite Materials Based on Chitosan Films Reinforced with Chitin Nanofibrils for Cosmetic Application. *Cosmetics* 10, 51. **DOI:**10.3390/cosmetics10020051
- [93] Ta Q, Ting J, Harwood S, Browning N, Simm A, Ross K, Olier I, Al-Kassas R; (2021) Chitosan nanoparticles for enhancing drugs and cosmetic components penetration through the skin. *Eur J Pharm Sci* 160, 105765. **DOI:**10.1016/j.ejps.2021.105765
- [94] Sahudin S, Sahrum Ayumi N, Kaharudin N; (2022) Enhancement of Skin Permeation and Penetration of β -Arbutin Fabricated in Chitosan Nanoparticles as the Delivery System. *Cosmetics* 9, 114. **DOI:**10.3390/cosmetics9060114

REVIEW

SYNTHESIS AND PROPERTIES OF BINARY AND TERNARY INTERPOLYELECTROLYTE COMPLEXES OF CHITOSAN

Shuhrat Shamsiddinovich Khudoyberdiyev^{1,a},
Noira Rakhimovna Vokhidova^{2,b,*}, Sayyora Sharafovna Rashidova^{2,c}

¹ – Bukhara State University, M. Ikkal 11 Str., Bukhara 200114, Uzbekistan
^a – ORCID: 0000-0002-0696-3743

² – Institute of Chemistry and Physics of Polymers, Academy of Sciences
of the Republic of Uzbekistan, Tashkent 100128, Uzbekistan

^b – ORCID: 0000-0003-0477-3708, ^c – ORCID: 0000-0003-1667-4619
^{*}corresponding author: noira_vokhidova@yahoo.de

Abstract

This review provides a comprehensive summary of the results of research, published from 2002 to 2023, on the synthesis, physicochemical properties and medical applications of binary and ternary interpolyelectrolyte complexes (IPECs) based on chitosan, carboxymethylcellulose and collagen. The application of IPECs in the medical field mainly refers to their use in medical therapy and bone regeneration. In addition, we describe our original studies on IPECs based on chitosan and collagen.

Keywords: *chitosan, sodium carboxymethylcellulose, collagen, binary and ternary interpolyelectrolyte complexes, polyanion and polyampholyte*

Received: 26.01.2024

Accepted: 10.06.2024

Abbreviations

ALg-Na	– sodium alginate
BPE	– block polyelectrolyte
BSSE	– basis set superposition error
CAS	– cellulose acetate sulfate
CMC	– carboxymethylcellulose
CMCS	– carboxymethylchitosan
Coll	– collagen
CPLG	– colloidal polylactide glycolide
CS	– chitosan
FTIR	– Fourier-transform infrared
IL-2	– invitrogen (2 µg/ml biotinylated anti-IL-2)
IPEC	– interpolyelectrolyte complex
LPE	– lyophilised polyelectrolyte
MW	– mesoporous wollastonite
Na-CMC	– sodium carboxymethylcellulose
NISPEC	– non-stoichiometric interpolyelectrolyte complex
NPs	– nanoparticles
PEC	– polyelectrolyte complex
PF	– phosphate fibronectin
PLG	– polylactide glycolide
P(LLA-CL)	– poly(L-lactide-co-ε-caprolactone)
RT-PCR	– real-time polymerase chain reaction
SEC	– sulfoethylcellulose
TPP-Na	– sodium tripolyphosphate
ΔE_{inter}	– interaction energy

1. Introduction

Interpolyelectrolyte complexes (IPECs) are formed through the interaction of polycations and polyanions/polyampholytes. Polymer–polymer complexes have ordered and disordered structures. The actual structure of IPECs is between an ordered and a disordered structure [1]. IPECs are formed in aqueous dispersions, through spontaneous association of oppositely charged polyelectrolytes due to strong but reversible electrostatic interactions. Depending on the main characteristics of the chosen polymers, IPECs exhibit special physicochemical properties due to intermolecular electrostatic interactions and flexibility. For example, when mixing two or more aqueous solutions of polyelectrolytes in a stoichiometric ratio, the resulting IPECs are insoluble and precipitate, often in the form of a colloid [2].

IPECs are formed via hydrogen bonds and electrostatic interactions between oppositely charged functional groups, as well as changes in entropy during the release of counterions that were bound to free polyions. In stoichiometric IPECs, phase separation can be avoided if at least one of the polyelectrolytes contains non-ionic hydrophilic groups. This is the case in block ionomer complexes that form ‘core-shell’ structures with a PEC core stabilised by the hydrophilic shell of a non-ionic moiety [3]. The uniqueness of the IPEC formation method is associated with the simplicity of its technological design, the low cost of the process, low energy consumption and high efficiency. Non-stoichiometric complexes containing an excess of one polyion have increased sorption activity with respect to drugs, dyes and proteins, because they have a net charge [4].

An excess of polyanion complexation leads to the formation of non-stoichiometric IPECs (NIPECs), which are virtually block copolymers with hydrophilic areas represented by free anionic units and hydrophobic fragments of mutually neutralised anionic and cationic units. The negative charge confers colloidal stability on NIPECs in aqueous solutions, facilitating their binding to d-metal ions or positive dispersion particles [5]. At present, according to special terminology, an NIPEC comprises a lyophilising polyelectrolyte (LPE) and a counter-charged block polyelectrolyte (BPE). In IPECs, there is an excess of LPE relative to BPE units – that is, the [BPE]/[LPE] ratio is < 1 . Water-soluble IPECs can be obtained under varying conditions from oppositely charged synthetic and natural polyelectrolytes [6].

Given that CS can be modified in various ways to produce numerous complexes – in particular, binary and ternary IPECs – it is essential to study their physicochemical properties and application prospects. This review summarises the research on the preparation and use of IPECs in bone therapy and its engineering.

2. Preparation and Physicochemical Characteristics of Interpolyelectrolyte Complexes of Chitosan and Anionic Polyelectrolytes

Many researchers have prepared and characterised IPECs based on a cationic polyelectrolyte, chitosan (CS), and different anionic polyelectrolytes. Table 1 and the following text summarise the preparation methods and physicochemical properties of some IPECs.

Cerchiara et al. [7] obtained PECs based on CS and carboxymethylcellulose (CMC) for the delivery of vancomycin to the colon. They prepared various batches of PECs, using three different CS/CMC weight ratios (3:1 to 1:3) and collected them as microparticles by spray-drying. They also investigated microparticle water uptake and vancomycin release as well as its protection against gastric pepsin degradation. They selected the best formulation, CS/CMC 1:3, based on the encapsulation efficiency, water uptake and the drug-release rate [7].

In another study, the authors assessed the influence of the CS/CMC mixing ratio (1:0 to 0:1), temperature (25–85°C) and pH (3–4.5) during the preparation of macro- and micro-PEC. A mixing ratio of 1:2 and a temperature of 25°C maximised the interaction between the biopolymers and the formation of macro-PECs regardless of pH. Micro-PECs had a uniform appearance, while macro-PECs were porous mesh structures interspersed with vacuoles of different sizes. Macro-PECs were amorphous, which is optimal for encapsulating technologically important compounds [8].

CS/CMC complexes with a porous structure were obtained at a mass ratio of 1:1, after which the solution was poured into a glass beaker (1 mm thick) and the process continued in a water bath at 70°C for 12 h. The sample was lyophilised for 48 h [9].

IPECs based on CS and Na-CMC were synthesised and cross-linked with glutaraldehyde at pH 5.5 and a 1:1 mass ratio. Based on the zeta potential of the samples, the polymers interacted electrostatically [10].

CS/Na-CMC complexes were obtained by mixing a 1% solution of Na-CMC and a solution of CS in acetic acid by varying their ratios. Na-CMC and CS powders were added gradually to the solution with constant magnetic stirring for 1 h at 22°C to prevent gel formation. After complete dissolution, the studied solutions were titrated with hydrochloric acid (HCl) to pH 1 and then incubated in a cabinet for 12 h [11].

According to Zhao et al. [12], a CS/Na-CMC PEC was formed in solutions with the addition of 0.01 M CS and 0.01 M Na-CMC based on ionic interactions between

oppositely charged functional groups. The authors dried the PEC in vacuum at 60°C for 1 day and stored it in a nitrogen atmosphere.

A nanofibre based on a CS/Na-CMC ratio of 4:6 (w/w) was stable. The nanofibre made of a CS/Na-CMC ratio of 4:6 (w/w) presented the weakest fibroblast adhesion [13].

Using the method of sublimation drying, a biocomposite sponge was obtained containing CS/CMC with different concentrations of mesoporous wollastonite (MW) particles. Adding 0.5% MW to the CS/CMC sponge significantly improved the biomineralisation properties and adsorption of protein particles. The CS/CMC/MW sponge exhibited effective cytological properties against human osteoblasts, which is recommended for bone engineering. The osteogenic potential of the CS/CMC/MW scaffold was confirmed by calcium deposition and the enhanced expression of an osteoblast-specific microRNA, namely pre-mir-15b [14].

CS/CMC IPECs in a stoichiometric ratio of 1:1 (w/w) were obtained by titration to obtain thin films with antibacterial properties for biomedical use [15].

The thermal properties of CS/CMC IPECs were studied when glycerol or formaldehyde was added. The decomposition temperature of the initial CS was 120°C. The sample obtained by cross-linking with 0.2% formaldehyde exhibited high thermal stability at 220°C. Moreover, IPECs obtained with the addition of 0.4% formaldehyde in a mixture of CS/CMC (99:1) and glycerol (2%) were stable at 150°C [16].

At a CMC/CS ratio of 75:1, there was no blurring when CMC was added to the CS solution. When the CMC solution was added to the CS solution, the interaction between the polymers improved and a cloudy suspension was formed. When CMC was added to CS at a ratio of 75:1, agglomeration was observed under the microscope, and when CS was added to CMC, visible particles were formed [17].

Hydrogels based on CS and Na-CMC containing 1% hydrocortisone were prepared by mixing solid and liquid components. The solid components were hydrocortisone, Na-CMC and CS, and the liquid component was polyethylene glycol, obtained by mixing with paraffin, glycerine and distilled water [18]. In another study, researchers obtained CS/Na-CMC hydrogels [19], as presented schematically on Figure 1.

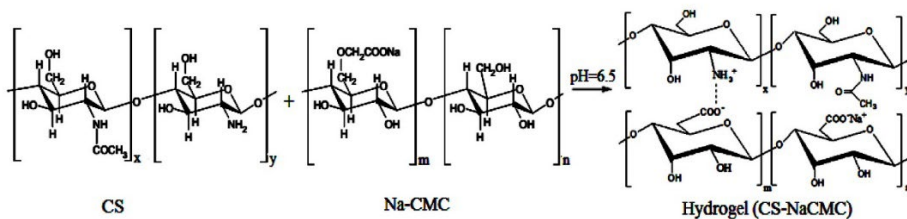


Figure 1. A scheme for the preparation of a hydrogel based on chitosan (CS) and sodium carboxymethylcellulose (Na-CMC).

The presence of intense absorption band at about 1600 cm^{-1} in the Fourier-transform infrared (FTIR) spectrum of a hydrogel showed that CS interacts with Na-CMC via positively charged $^+\text{NH}_3$ and negatively charged $-\text{COO}^-$ groups [20].

In another study, researchers prepared ionic gel microcomposites based on CS/CMC by adding various concentrations of the chelating agent sodium tripolyphosphate (TPP-Na) – 0.2%, 0.4% and 0.6% – dropwise to a 0.4% CS solution. Then, a 0.4% CMC solution was prepared and added dropwise to the CS solution chelated with TPP-Na.

They stirred the solution for 2 h and then isolated the target product by centrifugation for 15 min. The authors freeze-dried the microcarriers prepared with TPP-Na and named them CS/CMC-T1, CS/CMC-T2 and CS/CMC-T3 [21].

Inphonlek et al. [22] obtained colloidal polylactide-glycolide (PLG) particles and stabilised them by oppositely charged CS/Na-CMC complexes. They pre-emulsified dichloromethane containing dissolved PLG in the aqueous phase in mixtures of CS and Na-CMC. Evaporation of dichloromethane from the resulting emulsion forms PLG particles coated with CS/Na-CMC. The zeta potential varied from +54 to -50 mV, and the pH was 3–10.

CS and Na-CMC, as well as Egyptian clay, were used to prepare a composite hydrogel. A specific amount of clay (0–10 wt%) was added slowly to a 1 wt% CS solution, stirring for 1 day and then poured into a bottle. At 40°C, the membranes were incubated in a 1% Na-CMC solution for 24 h, repeatedly washed with distilled water and dried in a vacuum oven at 40°C [23].

In another study, the researchers obtained hydrogels with the solid components Na-CMC; methylcellulose (MC); and 3% Carbopol 934 P with 1% hydrocortisone and 1% CS. The liquid component was a hydrophilic agent (1,2-propylene glycol) mixed with dimethylacetamide and distilled water. They also obtained polymer hyaluronic acid gels containing various medicinal substances [24].

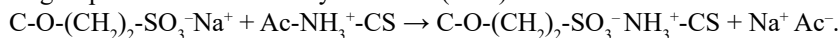
PECs based on CS and CMC were prepared by 'dry' thermomechanical mixing. The resulting films were stable and structurally intact (27% expansion and 94% weight increase after 1 day of hydration). The resulting films swelled sharply, increasing in volume by 138% and in weight by 913%, and were also brittle. The authors reported calculations for the formation of a PEC containing CS and CMC, the difference in the high hydrolytic stability of CS/CMC films with their high surface hydrophilicity and the contribution of CMC [25].

Researchers evaluated a two-layer polysaccharide coating containing CMC and CS regarding its effectiveness in preserving the post-harvest quality of tangerine and orange varieties. This CMC/CS coating was effective as a commercial polyethylene wax to improve the presentation of the fruit. Moreover, this CMC/CS coating did not negatively affect the taste of the fruit [26].

Researchers obtained a polymer-polymer mixture based on CS and Na-CMC with the trade name 'UZXITAN', which is used to encapsulate agricultural crop seeds. It is non-toxic, environmentally safe, helps suppress phytopathogens and stimulates plant growth and development [27].

In another study, researchers evaluated the effect of pH on the formation of CS/CMC IPECs and the viscosity and sorption–diffusion properties of the resulting films based on them. The IPEC films formed in an acidic medium (0.05 N) contained 2–2.5 times less water than films of the same composition obtained in an acetate-buffer medium [28].

According to Baklagina et al. [29], a PEC is formed due to the interaction of charged functional groups of CS and sulfoethylcellulose (SEC):



To obtain a stoichiometric insoluble complex, the authors mixed 2% solutions of polyions (CS and SEC) in an equimolar ratio. They stirred the solutions for 30 min, separated the PEC from the insoluble solvent, washed it, vacuum dried it and heated it at 100°C for 1 h [29].

An IPEC containing cellulose acetate sulfate (CAS) with a CS/CAS ratio of 1:1 (mol/mol) at pH 4.3 was obtained by mixing 0.1 M acetate buffer solutions of the starting components. The authors demonstrated that it was an effective additive for increasing the biovalue of chicken eggs and broiler meat during flocculation purification [30, 31].

Researchers studied the colloidal optical properties of IPECs containing CS and CAS (at a molar ratio of 1:1.5). In buffers, the particle size increased compared with acetic acid, and their concentration was reduced. The authors found that the addition of low-molecular-weight electrolytes to excess CS as well as an ionic strength of 0.2–0.3 led to the dissolution of IPECs. Complete dissolution occurred at an ionic strength of 1.5–2 [32].

In another study, the authors evaluated the thermal properties of an IPEC prepared with a CS/CAS molar ratio of 2:1. The derivative thermogravimetry (DTG) curve had a peak at 490 K – between 473 K (for CAS) and 563 K (for CS) – and the differential scanning calorimetry (DSC) curve was not exothermic at 566 K. Thermal studies showed that the formation of a new compound based on cadmium (Cd) and CAS reduced the influence on the DTG and DSC curves [33].

Researchers prepared IPECs containing CS and melanin prepared with ratios from 10:1 to 1:1. During thermal analysis of the initial components and complexes, there was mass change with the release of water for the range of 25–100°C [34].

The gelling properties of IPECs based on CS and sodium alginate (ALg-Na) were studied. Changes in the binding between ALg-Na and CS significantly affected the formation of the internal part of the cryogels. The densest gel, with ALg-Na/CS = 1.5 mol, had the most stable mesopore [35]. Based on scanning electron microscopy, the particles were 40–120 μm in size [36, 37]. The FTIR spectrum showed a CS absorption band at 1651 cm⁻¹ (δ-NH₂), characteristic of the NH₂ group, and ALg absorption bands at 1603 and 1412 cm⁻¹, characteristic of the carboxylate ion group. These results indicate electrostatic interactions between them that underlie IPEC formation [38].

When preparing IPECs, complexes tend to aggregate due to charge neutralisation. Therefore, to avoid aggregation and to control the size of nanoparticles, at least two conditions are mandatory: the PEC solutions must be diluted, and one of the polyions must be in excess to maintain the inequality ($n^+/n^- \neq 1$) (Figure 2) [39]. If the charge ratio is greater or less than unity, then the resulting nanoparticles have the same charge as the polyion in excess. Experiments have shown that at $n^+/n^- = 1$, particles are uncharged and large aggregates are formed as a result of agglomeration.

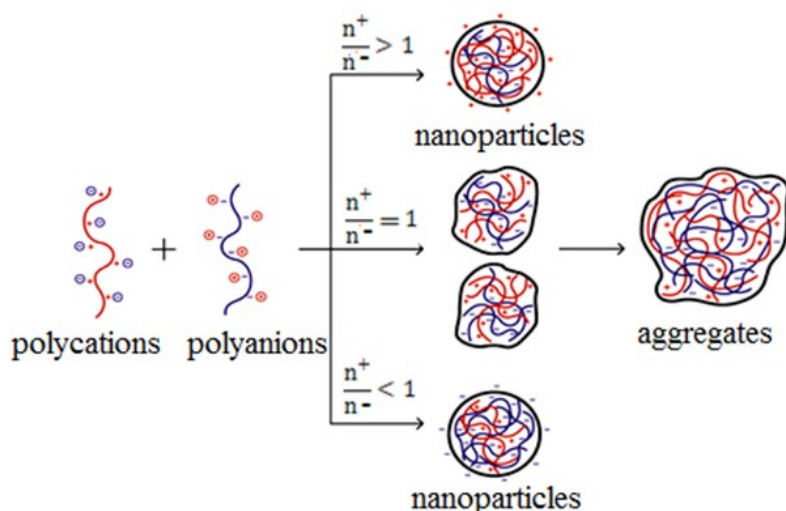


Figure 2. The influence of the charge ratio of polyelectrolytes on the size and charge of the formed polyelectrolyte complexes [39].

Researchers mixed solutions of CS-hyaluronic acid (CS molecular mass = 30×10^3 ; CS 0.1–8 wt%) and pectin (molecular mass = 26×10^3 ; 0.1–2 wt%) in phosphate buffer at pH 7.4 and 22°C to obtain IPEC hydrogels. The gel was formed due to the interaction between CS ($-\text{NH}_3^+$) and pectin ($-\text{COO}^-$) in solution [40]. The turbidimetric titration revealed that the CS/hyaluronic acid IPEC was stable at 573 nm. When mixing acetate-buffered solutions of the starting components, there was precipitation in the pH range of 3.6–6.5 [41].

Finally, researchers prepared CS/heparin complexes with mass ratios of 2:1 and 3:1. The particles were relatively small, with an average diameter of 176–192 nm. The most compact particles were obtained from a CS/heparin ratio of 2:1; they had low polydispersity and were stable for 72 h. These properties may be due to the strongest complexation of macromolecules [42].

3. Preparation of Interpolyelectrolyte Complexes Containing a Cationic Polyelectrolyte, Chitosan and Collagen

Researchers mixed 0.5% solutions of CS and collagen in different proportions (0:100 to 100:0) for 1 h, and degassed the mixture under a vacuum and then pipetted it into each cell of a 24-cell structure. They were freeze-dried by vacuum lyophilisation at -40°C for 24 h and created a porous structure and [43, 44].

CS and collagen were dissolved in 2% acetic acid at a concentration of 3 g/dl, stirred at room temperature for 6 h, poured into a mould and dried at -70°C . The resulting collagen/CS sponge was neutralised with a solution containing 0.5 N sodium hydroxide (NaOH) and ethanol, washed with a solution containing water and ethanol, and lyophilised [45].

In another study, the authors studied the morphology of cellular structures obtained from fibres based on CS/collagen complexes. Cells growing at the submicron level, especially films of CS and collagen fibres, had a greater length, up to 100 nm, compared with the control obtained on glass substrates [48].

Thin films were obtained based on solutions of CS, collagen and hyaluronic acid. First, the researchers obtained CS/hyaluronic acid complexes with three ratios (80:20, 50:50 and 20:80 wt%). Then, they added the CS/hyaluronic acid complex to the collagen solution in various ratios (10–90 wt%). The average thickness of the resulting films was 30 μm [49].

Researchers obtained IPECs with CS and gelatine. The interaction only occurred at a pH > 4.7 but < 6.2 . Natural polymers are involved in the healing of living tissues and skin restoration. Hydrogels obtained based on cross-linked natural polymers and PECs can be used for the prevention and treatment of trophic wounds and burns [50, 51].

The porous structure of CS-coated collagen membranes was characterised using scanning electron microscopy. The pore size was 20–50 μm [56].

In one study, researchers evaluated IPECs containing collagen and CS at a ratio of 7:3 and with or without 0.5% or 1% β -glycerol phosphate. The maximum strength of sponges was 8–10 MPa. The addition of β -glycerol phosphate to the collagen/CS complex increased the strength of the sponge [57].

The physicochemical and dielectric properties of collagen/CS films (100:0 to 0:100 wt%) were studied. The highest dielectric constant of the CS film was at 300 K, which increased the electrical conductivity from 2.4×10^{-19} to $3.4 \times 10^{-17} \text{ m}^{-1}$, and the activation energy ranged from 0.38 to 0.77 eV. When CS was added to the collagen film, the electrical conductivity of the collagen increased [58].

The catalytic activity of collagenase molecules available for binding, obtained from *Clostridium histolyticum*, under the influence of ultraviolet radiation

(151–6040 J/m²) showed greater modulation than in the case of immobilisation in a CS matrix. After ultraviolet irradiation of the enzyme solution at 3020 J/m², the activity of the biocatalyst solution decreased by ~9%. However, when collagenase was immobilised in an acid-soluble CS substrate, the efficiency of the enzyme at all studied doses did not change [60].

Table 1. Preparation and properties of interpolyelectrolyte complexes of chitosan (CS) and collagen and chitosan/gallic acid and collagen.

Preparation and composition of interpolyelectrolyte complexes	Properties	Ref.
Chitosan/collagen		
Collagen/CS matrices (weight ratio from 1:0 to 0:1) were obtained from 1% biopolymer gels by lyophilisation.	The porosity of the membranes was characterised by fractal geometry from scanning electron microscopy. It was dependent on the CS content.	[46]
Composite collagen/CS hydrogels (weight ratio from 0:1.0 to 1:0) were prepared by mixing 0.1 M CS solution in hydrochloric acid; they also contained fish collagen and disodium β -glycerophosphate.	Mechanical properties were studied by rotational rheometry. The presence of fish collagen negatively affected the mechanical strength of the obtained scaffolds. Only the lowest collagen concentration (0.25 g per 1 g of CS) improved mechanical properties.	[47]
Collagen/CS membranes were produced via the solvent evaporation method and exposed to gamma irradiation.	The water absorption of CS, collagen and CS/collagen membranes with and without gamma irradiation initially increased steadily and then reached a plateau.	[52]
Porous scaffolds for skin tissue engineering were prepared by freeze-drying a mixture of collagen and CS solutions treated with glutaraldehyde.	The presence of CS improved the biostability of the collagen/CS scaffold under glutaraldehyde treatment. Collagen/CS scaffold cross-linked by glutaraldehyde could be a potential candidate for dermal equivalent with enhanced biostability and good biocompatibility.	[53]
CS and collagen/CS (1:1, w/w) porous scaffolds were produced by freeze-drying and evaluated as potential skin substitutes.	The CS and CS/collagen samples were characterised with several methods. A miscible blend with intermediate thermal degradation properties was obtained. Collagen/CS scaffold was cytocompatible and showed the potential for skin tissue engineering.	[54, 55]

Genipin-cross-linked collagen/CS biodegradable porous scaffolds were prepared.	The CS and genipin concentrations influenced the physicochemical properties of the scaffolds.	[55]
Microspheres of CS and gallic acid were obtained by emulsification phase separation.	The product mimicked extracellular matrix and could be used as a topical healing agent for chronic wounds.	[59]
A collagen/CS complex was obtained by adding collagen solution in sodium hydroxide to a CS solution in acetic acid and the appropriate amount of sodium tripolyphosphate as a cross-linking agent (pH 6.5).	The complex was characterised and showed potential as an orally available protein-based drug to enhance antioxidant properties and to inhibit melanin synthesis.	[61]
Chitosan/gallic acid/collagen		
Microspheres of CS and gallic acid were obtained by emulsification phase separation and cross-linking with glutaraldehyde. CS/gallic acid microspheres incorporated collagen were prepared by collagen addition to cross-linked CS/gallic acid microspheres.	Gallic acid release from CS/gallic acid and CS/gallic acid/collagen microspheres was analysed. CS/gallic acid microspheres incorporated collagen matrix mimicked biomaterials as a topical healing agent for chronic wounds.	[59]

Collagen/CS complex nanoparticles were obtained using electrospinning. A mixture of 1,1,1,3,3,3-hexafluoro-2-propanol/trifluoroacetic acid (90:10, vol%) was found to be suitable for electrospinning [62].

CS/collagen sponges of 1:1 and 1:2 mass ratio were obtained. Cell growth in porous microstructures and sponges showed that porous sponges with a size of 80–100 μm were formed [63].

Collagen and CS were dissolved in 0.5 M acetic acid, transferred to a special flask (23 \times 18 cm) and frozen for 3 h at -20°C . Collagen fibres bended significantly when immersed in acid and were cross-linked by glutaraldehyde via covalent bond formation [64].

Analysis of the FTIR spectra of gelatine/CS PECs revealed the formation of hydrogen bonds within and between polymer chains and electrostatic interactions between the $-\text{COO}^-$ group of gelatine and the $-\text{NH}_3^+$ group of CS [65, 66].

Researchers prepared solutions of CS/collagen = 1:1, genipin and 25% glutaraldehyde and mixed all components in 2.5% acetic acid for 4 days. After this, they freeze-dried the aldehyde and genipin cross-linked scaffolds in a lyophilic chamber in liquid nitrogen (-196°C) [67].

The interaction between collagen and CS occurs due to the charged electron-donating functional groups of macromolecules. In addition, at $\text{pH} < 6.5$, most of the amino groups of CS are protonated, which contributes to the formation of electrostatic bonds between the $-\text{NH}_3^+$ groups of CS and the $-\text{COO}^-$ groups of aspartic and glutamine residues in collagen [54, 68].

Collagen/CS hydrogel scaffolds were prepared to model soft tissue. A mathematical model was developed to determine the mechanical properties of the scaffold obtained under various conditions. The elastic modulus of the collagen/CS scaffold (80/20, v/v%) was 3.69 kPa. The higher the CS content, the stiffer the frame became.

The elastic modulus of a scaffold consisting of 70% collagen and 30% CS was 11.6 kPa [69].

In another study, researchers used molecular dynamics simulations to describe the effect of pH and the presence of sodium and calcium cations on the stability of molecular complexes formed by type II collagen with chitin and CS oligosaccharides [70]. Based on the Gibbs free energy of binding, all the considered complexes were thermodynamically stable over the entire pH range. The affinity of CS oligosaccharide for collagen was highly dependent on pH, whereas oligomeric chitin did not have a pH-dependent effect on the stability of molecular assemblies with collagen. On the other hand, the presence of sodium and calcium cations had little effect on the affinity of chitin and CS for collagen.

Researchers summarised the modern developments in water-soluble non-stoichiometric PECs, which have such qualities as high stability and the ability to enter into competitive interpolyelectrolyte reactions. The complexes remain stable when external conditions (pH, ionic strength and temperature) vary over a wide range, but quickly respond with high sensitivity to changes in the environment outside this range by changing the phase state [71].

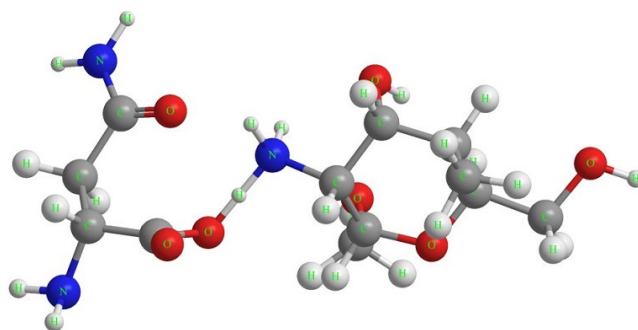
Finally, a study evaluated electrostatic complexation in an aqueous solution of cationic poly(diallyldimethylammonium chloride) with an excess of water-soluble anionic biopolymers. An NIPEC was formed: it was actually a block copolymer, with hydrophilic regions represented by free (unbound) anionic units and hydrophobic fragments of mutually neutralised anionic and cationic units [5, 72, 73].

4. Theoretical Calculations of the Formation of Interpolyelectrolyte Complexes

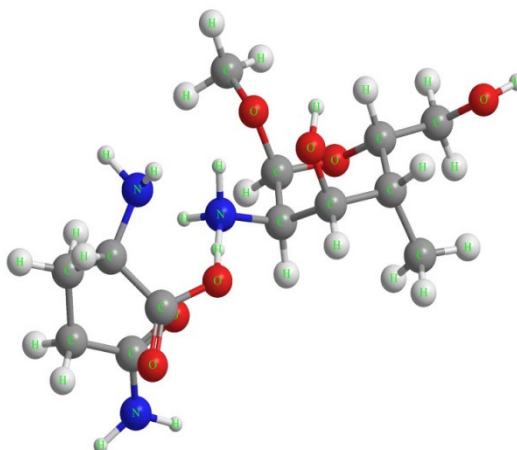
Theoretical calculations allow one to calculate possible interactions between compounds and to determine the possibility of the formation of various kinds of bonds, complexes, agglomerates, clusters and nanostructures. We have previously performed quantum-chemical density functional theory (DFT) studies of CS complexes with Na-CMC [74] or amino acids [75]. We analysed charge distribution of amino groups in CS chains of various lengths depending on the degree of deacetylation, the reactivity of acetamide and amino groups in CS, the interaction of CS with Na-CMC or CS and amino acids and the stability of their interpolymer complexes. We found that the main interaction between Na-CMC and CS changes from weak van der Waals interactions to strong electrostatic interactions, which link the two polymer chains into a compact structure. Moreover, we modelled interactions of the CS chain with Na-CMC during PEC formation [74]. The chains quickly approach each other in time, with the formation of electrostatic interactions between the polycation and the polyanion. The stability of the CS-CMC PEC is determined by the number of interactions between them, and, consequently, the chain becomes more compact.

The mechanism of PEC formation, identified using molecular dynamics simulation, is consistent with experimental data (conductometric measurements). Specifically, CS-CMC PECs are formed due to electrostatic interaction between the $-\text{NH}_3^+$ group of CS and the $-\text{COO}^-$ group of CMC. This process is affected by both the pH of the solution and the degree of deacetylation of CS [74]. The calculated group charge distribution for the tertiary hydrogen atom of the protonated amino group of CS is 1.54 e [76].

We previously performed theoretical calculations of the formation of PECs in solutions containing CS and amino acids such as asparagine and glutamine [75]. The optimised structures of these complexes are shown in Figure 3.



CS-asparagine



CS-glutamine

Figure 3. The optimised geometry of chitosan (CS) complexes with the amino acids asparagine and glutamine.

The DFT calculations revealed the presence of hydrogen bonds between the nitrogen atom of the $-\text{NH}_3^+$ group of CS and the oxygen atom of the $-\text{COO}^-$ group of the studied amino acids. According to Table 2, the distance between the H atom of the $-\text{NH}_3^+$ group of CS and the O atom of the $-\text{COO}^-$ groups of the amino acid is 1.001 Å (asparagine) and 0.999 Å (glutamine), which is typical for hydrogen bonds [77]. This indicates that CS forms hydrogen bonds with amino acids during the formation of complexes. Cationic or anionic amino acids are well known for their ability to form hydrogen bonds with oppositely charged species [78]; however, the formation of such a salt bridge in the gas phase of the complexes under consideration was not observed.

Moreover, based on interaction energy (ΔE_{inter}), the suitability of the carrier to a particular amino acid can be assessed. The calculated values of ΔE_{inter} in gas and aqueous phases are presented in Table 2. ΔE_{inter} is negative in all cases, contributing to the formation of the complexes formation. A high ΔE_{inter} for CS-glutamine may be due to the strong Coulomb force of attraction, which leads to hydrogen migration. The charge of the O atom in the $-\text{COO}^-$ group of glutamine is more negative (-0.64 e) than that of asparagine (-0.62 e).

Table 2. Hydrogen bond distance and basis set superposition error (BSSE) corrected interaction energy between chitosan (CS) and the amino acids asparagine and glutamine.

Complex	H-H bond length between N···O [Å] (aqueous phase)	ΔE_{inter} [kcal/mol] (gas phase)	ΔE_{inter} [kcal/mol] (aqueous phase)
CS-asparagine	1.001	-89.51	-18.96
CS-glutamine	0.999	-105.49	-23.1

Note. ΔE_{inter} , interaction energy.

CS/collagen complexes were formed in the aqueous phase. As seen in Table 2, the aqueous phase primarily affects the interaction energy of these systems. There is a progressive destabilisation of CS complexes with amino acids. The results show that molecules with opposite charges are indeed more separated and more stable than complexes in water, leading to a decrease in ΔE_{inter} . This can also be explained by the fact that in polar environments, the interaction with the environment (solvation) is probably more important than the electrostatic interaction between the two interacting molecules, leading to their preferential stabilisation [75].

The results indicate a strong interaction between CS and amino acids in a non-polar environment and a gradual weakening of the interaction in the aqueous phase. These results are significant for modelling the complex penetration process through a cell membrane that is non-polar in nature. The notably high ΔE_{inter} in the gas phase and very low ΔE_{inter} in the aqueous phase for the complexes indicate their suitability for use in biomedicine.

5. Application of Interpolyelectrolyte Complexes

CS-based PECs have found applications in drug delivery, wound healing, controlled-release systems, as enzyme and cell supports and bone scaffolds and tissue reconstruction, among others. Table 3 lists some examples of application of IPECs based on CS and collagen.

In an *in vivo* study using a rat model of spinal cord injury, the researchers transplanted a collagen/CS matrix immediately after a partial spinal cord injury. This transplantation restored sensory functions of the spine, maintained balance and prevented pathological physical activity [79].

There have been a wide range of experiments undertaken to evaluate CS/collagen IPECs. In one study, the researchers evaluated the biocompatibility of CS/collagen complex in composite vascular tissue engineering and performed real-time polymerase chain reaction (RT-PCR) in an effort to improve the morphogenesis, attachment, proliferation and phenotype of porcine iliac artery endothelial cells [98].

Poly(L-lactide-co- ϵ -caprolactone) [P(LLA-CL)] nanofibrils and collagen/CS complex were prepared using nanofibrillar electrospinning. The mechanical properties of collagen/CS complex nanofibrils varied depending on the collagen content of the complex. Biodegradation of P-nanofibrils (LLA-CL) occurred faster in collagen nanofibrils than in their membranes, and there was faster growth of P-nanofibrils in smooth muscle cells (LLA-CL) [99].

In another study, the researchers evaluated the effect of collagen and CS on the immune system. They analysed the number of T cells and their activation, wound antigen uptake and the cytokine profile in wound tissue and spleen cells. Animals treated with collagen/CS

had decreased invitrogen (2 µg/ml biotinylated anti-IL-2) (IL-2) secretion and increased IL-10 secretion in wound adhesive tissue and liver, respectively [102].

To prepare a three-dimensional nanoparticle gene delivery system based on collagen/CS sponges, body mesenchymal cells were transplanted in a mixture with plasmid-transformed β-1(PT-β1)/calcium phosphate fibronectin (PF). The glycosaminoglycan content of the three dimensional nanoparticle gene delivery system was comparable to that of those receiving PT-β1 as well as PT-β1 and dexamethasone, and was significantly higher than that of those receiving free plasmid and Lipofectamine 2000 [103].

Table 3. Application of interpolyelectrolyte complexes based on chitosan (CS) and collagen.

Material characteristics and drug used	Application area	Reference
Material tested on Wistar rats weighing 200–250 g	Wound coverings	[80, 81]
Bioeffective sponge containing Collahit-Bol and chitosan	Wound dressings for type IIIa and IIIb thermal skin burns	[82–85]
Sponges made of CS/collagen (50:50, weight ratio)	Used for osteoplasty in bone therapy	[86]
CS/collagen films (6:4, mass ratio)	Films for implants; adsorbed serum proteins on the surface the films evaluated by proteomics and bioinformatics	[68]
CS/collagen films (4:1, weight ratio) containing PLGA microspheres for VCR delivery (drug used in chemotherapy)	Implant films for the delivery of drugs in chemotherapy	[87]
CS/collagen 97.5:2.5, 95:5 and 90:10 (weight ratios)	Treatment of external epithelial damage	[88]
CS/collagen hydrogels	Treatment of myocardial infarction	[89]
CS/collagen sponges (50:50, mass ratio)	Targeted transport of medicinal substances	[90]
CS/collagen sponges (3:3, mass ratio)	Treatment of chronic wounds	[91, 92]
CS/collagen sponges (5 × 5 mm)	Wound coverings	[93]
Pills for drug, Collahit-G and Collahit-bol delivery	Treatment of various types of burns	[94, 95]
CS/collagen scaffolds (1:9, mass ratio)	Bone regeneration	[96]
CS/collagen membranes (1:1 to 1:4, mass ratio)	Bone regeneration	[97]

Note. PLGA, polylactic-co-glycolic acid.

Researchers developed a biomaterial consisting of a thin layer of fish collagen, one side of which was impregnated with a layer of CS. They used it as an artificial layer of skin for burn patients [104].

It was reported that porous collagen/CS sponge was used as a neurological indicator to restore nerve function. This transplantation contributed to change the parameters of neurological stress and improving the therapeutic effects of mesenchymal stem cells [105].

For osteochondral treatment, researchers used a mixture of collagen/CS (70:30, wt%) doped with magnesium hydroxyapatite (MgHA/collagen+CS) in the form of a three-dimensional scaffold [106]. Composite films CS collagen (a ratio of 1:0 to 0:1) accelerated the proliferation, differentiation and mineralisation of osteoblasts in MC3T3-E1 cells, the transcriptional activity of Runx2, and were recommended as a biomaterial for bone tissue engineering in bone diseases [107].

Sponges based on collagen/CS (a ratio of 1:9 to 9:1) and lauric acid were tested for use in skin tissue engineering for burns [108]. Collagen/CS hydrogels (a ratio of 1:1 to 50:1, wt %) increased the number of endothelial cells as well as angiogenesis when used in tissue engineering of the cardiovascular system [109].

Because of its cationic charge in solution, CS is prone to exhibit valuable physicochemical and biologically active properties. Despite its wide range of applications, due to lack of technology, CS is not very popular in the textile industry [110].

6. Preparation of Ternary Interpolyelectrolyte Complexes

Researchers studied the effect of the drying temperature (25 and 45°C) on the physical properties of gelatine/CMC/CS composite films (a ratio of 80:20:0 to 60:30:10). The 60:30:10 ratio was most suitable for food packaging due to its high vapour permeability and biodegradation rate [111].

Researchers obtained ternary IPECs by sequentially mixing a 0.25% solution of pectin and CS and 1% trypsin in a mass ratio of 2:1:2. They used it to carry biologically active substances. It prolonged the effects of these substances [112].

In another study, researchers reacted solutions of carboxymethylchitosan (CMCS), CMC, collagen and trans-glutaminase (T-Gase) in various mass ratios (40:40:20 to 25:25:50). They obtained anti-adhesion CMCS/CMC/collagen membranes [113].

Synthetic sponges based on collagen/Na-CMC/HA IPECS at a weight ratio of 2:1:8 wt% have been widely used in bone tissue engineering. Such sponges must have sufficient porosity to allow bone cells to grow and develop so that they can be used to treat bone defects and fractures [114–120].

IPEC nanoparticles based on CS, collagen and ALg-Na were obtained by electrospinning. A 4:1:1 mass ratio produced porous, bioresorbable three-dimensional matrices [121, 122]. In another study, the authors recommended collagen/CS/Na-hyaluronate IPEC as a suitable material for corneal tissue engineering [123].

Ternary IPECs are mainly used in medical practice. For example, biodegradable polymer CMCS/CMC/collagen membranes (40:40:20, 35:35:30 and 25:25:50) have been proposed as physical barriers to prevent peritoneal adhesions [116], and biomaterials have been obtained for bone engineering and regeneration. The effects of CS/collagen/glutaraldehyde [106, 114, 118, 124, 125] and CS/collagen/gelatine membranes on the activity of C3A cells was studied in an attempt to control cell growth and to improve growth rate *in vitro* for tissue engineering applications [126].

Three-dimensional scaffolds containing CS; collagen; and L-arginine, L-glutamic acid or L-lysine are used as biomaterials for tissue engineering and wound healing.

Their limitations include the toxicity of synthetic cross-linkers, poor mechanical stability, low biocompatibility and rapid biodegradation [127]. For skin regeneration, a CS/collagen/CMC complex was obtained, in which stem cells loaded into the studied scaffolds have proven their potential effect in improving skin healing and regeneration [128].

The collagen/CS/glycerol/hydroxypropyl methylcellulose complex as an artificial cornea was synthesised and characterised (functional cluster, cytotoxicity, morphological and antibacterial tests). All samples exerted minimal cytotoxicity (> 85% live cells) [129].

In another study, the authors evaluated the mechanical and physical effects of gelatine/CMC/CS composite films resulting from the addition of sorbitol. With glycerine as a plasticiser, solutions of gelatine/CMC/CS composite films containing graduated concentrations of sorbitol (0–30%). The results showed that an increase in the composite content resulted in a corresponding decrease in melting temperature and tensile strength. However, films with 25% sorbitol had increased tensile strength due to anti-plasticisation [130].

A hydrogel based on CS, collagen, hydroxypropyl- γ -cyclodextrin and polyethylene glycol was developed and characterised. Incorporation of nanohydroxyapatite and pre-encapsulated hydrophobic/hydrophilic model drugs reduced the porosity of the hydrogel from $81.62\% \pm 2.25\%$ to $69.98\% \pm 3.07\%$ [131].

7. Conclusions

Based on this review, we can draw the following conclusions:

1. Binary and ternary IPECs have indisputable utility: they are widely used for pharmaceutical and medical applications and in other areas.
2. Despite the huge amount of research, some fundamental aspects regarding how to obtain stable binary and ternary IPECs require additional research on regulating the charge of the surface layer of the complex and, accordingly, searching for areas of application of the synthesised complexes based on CS.
3. At present, the dependence of the initial ratios of polyions and the hydrodynamic characteristics of binary complexes CS/collagen and three-component IPECs with CS/collagen/Na-CMC has not been fully studied.

8. References

- [1] Bekturov EA, Kudaibergenov SE; (2015) A short course in the physical chemistry of polymers (In Russian). In: Almaty (ed), 'Ulagat' KazNPU named after Abai. Semey, 111–120.
- [2] Garipova V, Gennari C, Selmin F, Cilurzo F, Moustafine R; (2018) Mucoadhesive interpolyelectrolyte complexes for the Buccal delivery of Clobetasol. *Polymers* 10(1), 85. DOI:10.3390/polym10010085
- [3] Glagoleva AA, Larin DE, Vasilevskaya VV; (2020) Unusual structures of interpolyelectrolyte complexes: vesicles and perforated vesicles. *Polymers* 12(4), 871. DOI:10.3390/polym12040871
- [4] de Lima CRM, Gomes DN, de Moraes Filho JR, Pereira MR, Fonseca JLC; (2018) Anionic and cationic drug sorption on interpolyelectrolyte complexes. *Colloids Surf B Biointerfaces* 170, 210–218. DOI:10.1016/j.colsurfb.2018.05.071
- [5] Panova IG, Sybachin AV, Spiridonov VV, Kydralievva K, Jorobekova S, Zezin AB, Yaroslavov AA; (2017) Non-stoichiometric interpolyelectrolyte

- complexes: Promising candidates for protection of soils. *Geoderma* 307, 91–97. DOI:10.1016/j.geoderma.2017.08.001
- [6] Moon GA, Nurkeeva ZS, Khutoryansky VV, Urkimbaeva PI, Bekturov EA; (2018) Intermacromolecular complexes and composite materials based on them. Kazakh University, Almaty, 136.
- [7] Cerchiara T, Abruzzo A, Parolin C, Vitali B, Bigucci F, Gallucci MC, Luppi B; (2016). Microparticles based on chitosan/carboxymethylcellulose polyelectrolyte complexes for colon delivery of vancomycin. *Carbohydr Polym* 143, 124–130. DOI:10.1016/j.carbpol.2016.02.020
- [8] Mota Ferreira DC, Ferreira SO, Santiago de Alvarenga E, Ferreira Soares NF, Reis Coimbra JS, de Oliveira EB; (2022) Polyelectrolyte complexes (PECs) obtained from chitosan and carboxymethylcellulose: a physicochemical and microstructural study. *Carbohydr Polym Technol Appl* 3, 100197. DOI:10.1016/j.carpta.2022.100197
- [9] Chen H, Fan M; (2007) Chitosan/carboxymethyl cellulose polyelectrolyte complex scaffolds for pulp cells regeneration. *J Bioact Compat Polym* 22(5), 475–491. DOI:10.1177/0883911507081329
- [10] Roy JC, Ferri A, Giraud S, Jinping G, Salaün F; (2018) Chitosan-carboxymethylcellulose-based polyelectrolyte complexation and microcapsule shell formulation. *Int J Mol Sci* 19(9), 2521. DOI:10.3390/ijms19092521
- [11] Cai B, Zhong T, Chen P, Fu J, Jin Y, Liu Y, Tan L; (2018) Preparation, characterization and *in vitro* release study of drug-loaded sodium carboxy-methylcellulose/chitosan composite sponge. *PLoS One* 13(10), e0206275. DOI:10.1371/journal.pone.0206275
- [12] Zhao Q, Qian J, An Q, Gao C, Gui Z, Jin H; (2009) Synthesis and characterization of soluble chitosan/sodium carboxymethyl cellulose polyelectrolyte complexes and the pervaporation dehydration of their homogeneous membranes. *J Membr Sci* 333(1–2), 68–78. DOI:10.1016/j.memsci.2009.02.001
- [13] Kawasaki T, Nakaji-Hirabayashi T, Masuyama K, Fujita S, Kitano H; (2016) Complex film of chitosan and carboxymethyl cellulose nanofibers. *Colloids Surf B Biointerfaces* 139, 95–99. DOI:10.1016/j.colsurfb.2015.11.056
- [14] Sainitya R, Sriram M, Kalyanaraman V, Dhivya S, Saravanan S, Vairamani M, Sastry TP, Selvamurugan N; (2015) Scaffolds containing chitosan/carboxymethyl cellulose/mesoporous wollastonite for bone tissue engineering. *Int J Biol Macromol* 80, 481–488. DOI:10.1016/j.ijbiomac.2015.07.016
- [15] Ospanova AK, Savdenbekova BE, Iskakova MK, Omarova RA, Zhartybaev RN, Nussip BZ, Abdikadyr AS; (2017) Obtaining thin-films based on chitosan and carboxymethylcellulose with antibacterial properties for biomedical devices. *IOP Conf Ser Mater Sci Eng* 230, 012042. DOI:10.1088/1757-899x/230/1/012042
- [16] Thomas S, Soloman PA, Rejini VO; (2016) Preparation of chitosan - CMC blends and studies on thermal properties. *Procedia Technol* 24, 721–726. DOI:10.1016/j.protcy.2016.05.201
- [17] Mejia EH, Contreras H, Delgado E, Quintana G; (2019) Effect of experimental parameters on the formation of hydrogels by polyelectrolyte complexation of carboxymethylcellulose, carboxymethyl starch, and alginic acid with chitosan. *Int J Chem Eng* 2019(1), 3085691. DOI:10.1155/2019/3085691
- [18] Szcześniak M, Grimling B, Pluta J, Meler J; (2015) Effect of chitosan on the rheological properties of hydrogels based on sodium carboxymethylcellulose. *Prog Chem Appl Chitin Deriv* 20, 254–259. DOI:10.15259/PCACD.20.25

- [19] Ruiz-Matute AI, Cardelle-Cobas A, García-Bermejo AB, Montilla A, Olano A, Corzo N; (2013) Synthesis, characterization and functional properties of galactosylated derivatives of chitosan through amide formation. *Food Hydrocolloids* 33(2), 245–255. **DOI:**10.1016/j.foodhyd.2013.03.016
- [20] Benganem S, Chetouani A, Elkolli M, Bounekhel M, Benachour D; (2017) Effects of physical and chemical modification on biological activities of chitosan/carboxymethylcellulose based hydrogels. *J Chil Chem Soc* 62(1), 3376–3380. **DOI:**10.4067/S0717-97072017000100014
- [21] Samrot AV, Akanksha Jahnavi T, Padmanaban S, Philip SA, Burman U, Rabel AM; (2016) Chelators influenced synthesis of chitosan-carboxymethyl cellulose microparticles for controlled drug delivery. *Appl Nanosci* 6(8), 1219–1231. **DOI:**10.1007/s13204-016-0536-9
- [22] Inphonlek S, Sunintaboon P, Léonard M, Durand A; (2020) Chitosan/carboxymethylcellulose-stabilized poly(lactide-co-glycolide) particles as bio-based drug delivery carriers. *Carbohydr Polym* 242, 116417. **DOI:**10.1016/j.carbpol.2020.116417
- [23] Salah-El-Din TA, Elzatahry AA, Aldeyab SS, Kamoun EA; (2012) Preparation and characterization of water-absorbing composite membrane for medical applications. *Afr J Biotechnol* 11(66), 13058–13064. **DOI:**10.5897/ajb12.707
- [24] Meler J, Szcześniak M, Grimling B, Pluta J; (2013) Application of chitosan in the formulation of hydrogels applied on skin. *Prog Chem Appl Chitin Deriv* 18, 181–186.
- [25] Chen P, Xie F, Tang F, McNally T; (2020) Thermomechanical-induced polyelectrolyte complexation between chitosan and carboxymethyl cellulose enabling unexpected hydrolytic stability. *Compos Sci Technol* 189, 108031. **DOI:**10.1016/j.compscitech.2020.108031
- [26] Arnon H, Zaitsev Y, Porat R, Poverenov E; (2014) Effects of carboxymethyl cellulose and chitosan bilayer edible coating on postharvest quality of citrus fruit. *Postharvest Biol Technol* 87, 21–26. **DOI:**10.1016/j.postharvbio.2013.08.007
- [27] Rashidova D, Rashidova S; (2016) Application of chitosan *Bombyx mori* and its derivatives in cotton-growing. *Scholars Acad J Biosci* 4(7), 583–588. **DOI:**10.21276/sajb.2016.4.7.6
- [28] Suvorova AI, Tyukova IS, Borisova TS, Pletneva LV; (2005) Sorption of water vapor by interpolyelectrolyte complexes of chitosan and carboxymethylcellulose obtained from solutions, *Vysokomolekularnye Soedineniya, Ser A* 47(12), 1265–1270.
- [29] Baklagina YuG, Kononova SV, Petrova VA, Kruchinina EV, Nudga LA, Romanov DP, Klechkovskaya VV, Orekhov AS, Bogomazov AV, Arkhipov SN; (2013) Study of polyelectrolyte complexes of chitosan and sulfoethyl cellulose. *Kristallografiya* 58(2), 268–275. **DOI:**10.7868/S0023476113020033
- [30] Savitskaya T, Shibaylo T, Voronets E; (2008) Polymer chemistry: interpolyelectrolyte complexes based on chitin and cellulose derivatives - a special class of polymer substances. *Gamtamokslinis Ugdyimas/Natural Science Education (Belorussia)* 3(23), 50–57.
- [31] Savitskaya TA, Shibaila TN, Grinshpan DD; (2008) Interpolyelectrolyte complexes of chitosan and cellulose acetate sulfate (In Russian). *Bulletin of Belarusian State Univeristy*, 368–382.
- [32] Shibaila TN, Savitskaya TA, Kislyakova TA, Albulov AI, Grinshpan DD; (2008) Complexation of chitosan and cellulose acetate sulfate in acetic acid solutions. *Colloid J* 70(5), 661–665. **DOI:**10.1134/S1061933X08050165

- [33] Savitskaya TA, Shibayla TN, Selevich KA, Makarevich SE; (2008) Thermal properties of interpolyelectrolyte complexes of chitosan and cellulose acetate sulfate. *Bulletin of Belarusian State Univeristy, Series 2, No.3*, 38–41.
- [34] Bakulin AV, Kurchenko VP, Sushinskaya NV, Azarko II, Varlamov VP; (2009) Physicochemical characteristics of chitosan-melanin complexes (In Russian). *Proceedings of the Belarusian State University 4(2)*, 290–297.
- [35] Brovko OS, Palamarchuk IA, Valchuk NA, Chukhchin DG, Bogolitsyn KG, Boytsova TA; (2017) Gels of interpolyelectrolyte complexes based on sodium alginate and chitosan. *Russ J Phys Chem 91(8)*, 1580–1585. **DOI:10.1134/S0036024417080064**
- [36] Brovko OS, Palamarchuk IA, Valchuk NA, Boytsova TA, Bogolitsyn KG; (2018) Prospects for obtaining new film materials for biomedical purposes based on the alginate-chitosan interpolymer complex. *Proceedings of the Ufa Scientific Center of the Russian Academy of Sciences 2(3)*, 45–49. **DOI:10.31040/2222-8349-2018-2-3-45-49**
- [37] Brovko OS, Palamarchuk IA, Valchuk NA, Boytsova TA, Bogolitsyn KG, Chukhchin DG; (2016) Structure of interpolymer complexes based on sodium alginate and chitosan. *Proceedings of the Ufa Scientific Center of the Russian Academy of Sciences 3(1)*, 19–22.
- [38] Kassymova ZhS, Orazzhanova LK, Bayakhmetova BB, Gaisina BS, Kassenova NB, Yelemessova GT; (2019) Preparation of interpolymer complexes of chitosan and sodium alginate. *Journal of Moscow University. Series „Chemistry” 1(93)*, 17–24. **DOI:10.31489/2019Ch1/17-24**
- [39] Quiñones JP, Peniche H, Peniche C; (2018) Chitosan based self-assembled nanoparticles in drug delivery. *Polymers 10(3)*, 235. **DOI:10.3390/polym10030235**
- [40] Vildanova RR, Sigaeva NN, Fayanova EA, Kukovinets OS, Vlasova NM, Kolesov SV; (2017) Interpolyelectrolyte hydrogels based on chitosan and pectin. *Bulletin of Bashkir State University 22(1)*, 72–76.
- [41] Gurina MS, Vildanova RR, Badykova LA, Vlasova NM, Kolesov SV; (2017) Microparticles based on the interpolyelectrolyte complex chitosan-hyaluronic acid, ensuring the stability of aqueous dispersions. *Russ J Appl Chem 90(2)*, 197–202. **DOI:10.1134/S1070427217020100**
- [42] Pilipenko I, Korzhikov-Vlakh V, Sharoyko V, Zhang N, Schäfer-Korting M, Rühl E, Zoschke Ch, Tennikova T; (2019) pH-Sensitive chitosan-heparin nanoparticles for effective delivery of genetic drugs into epithelial cells. *Pharmaceutics 11(7)*, 317. **DOI:10.3390/pharmaceutics11070317**
- [43] Tangsadthakun C, Kanokpanont S, Sanchavanakit N, Banaprasert T, Damrongsakkul S; (2006) Properties of collagen/chitosan scaffolds for skin tissue engineering. *J Met Mat Miner 16(1)*, 37–44.
- [44] Raftery RM, Woods B, Marques ALP, Moreira-Silva J, Silva TH, Cryan S-A, Reis RL, O'Brien FJ; (2016) Multifunctional biomaterials from the sea: assessing the effects of chitosan incorporation into collagen scaffolds on mechanical and biological functionality. *Acta Biomater 43*, 160–169. **DOI:10.1016/j.actbio.2016.07.009**
- [45] Kim SE, Cho YW, Kang EJ, Kwon ICh, Lee EB, Kim JH, Chung H, Jeong SY; (2001) Three-dimensional porous collagen/chitosan complex sponge for tissue engineering. *Fibers Polym 2(2)*, 64–70. **DOI:10.1007/BF02875260**
- [46] Stănescu V, Olteanu M, Florea-Spiroiu M, Rusu M; (2008) Using fractal analysis to describe collagen-chitosan matrices. *Analele Universitatii din Bucuresti. Chimie 17(2)*, 47–51.

- [47] Rył A, Owczarz P; (2018) Influence of fish collagen on viscoelastic properties and sol-gel phase transition of chitosan solutions. *Acta Innovations* 27, 14–23. **DOI:**10.32933/ActaInnovations.27.2
- [48] Morozov RA, Nikitina AV, Romashkin AV, Nevolin VK, Suetina IA; (2016) Atomic force microscopy of fibroblast cells cultured on a collagen-chitosan scaffold. *News from universities. ELECTRONICS* 21(3), 230–234.
- [49] Lewandowska K, Sionkowska A, Grabska S, Michalska M; (2017) Characterisation of chitosan/hyaluronic acid blend films modified by collagen. *Prog Chem Appl Chitin Deriv* 22, 125–134. **DOI:**10.15259/PCACD.22.12
- [50] Mustafa A, Tomescu A, Cadar E, Cherim M, Sirbu R; (2016) Polyelectrolyte complexes based on chitosan and natural polymers. *Eur J Interdiscip Stud* 4(1), 100–107. **DOI:**10.26417/ejis.v4i1.p100-107
- [51] Voronko NG, Derkach SR, Sokolan NI; (2015) Interaction of gelatin with chitosan: influence of polysaccharide concentration. *Proceedings of the MSTU* 18(1), 80–89.
- [52] Lukitowati F, Indrani DJ; (2018) Water absorption of chitosan, collagen, and chitosan/collagen blend membranes exposed to gamma-ray irradiation. *Iran J Pharm Sci* 14 (1), 57–66.
- [53] Ma L, Gao Ch, Mao Zh, Zhou J, Shen J, Hu X, Han Ch; (2003) Collagen/chitosan porous scaffolds with improved biostability for skin tissue engineering. *Biomaterials* 24(26), 4833–4841. **DOI:**10.1016/S0142-9612(03)00374-0
- [54] Fernandes LL, Resende CX, Tavares DS, Soares GA, Castro LO, Granjeiro, JM; (2011) Cytocompatibility of chitosan and collagen-chitosan scaffolds for tissue engineering. *Polymeros* 21(1), 1–6. **DOI:**10.1590/S0104-14282011005000008
- [55] Yan Le-P, Wang Y-J, Ren L, Wu G, Caridade SG, Fan J-B, Wang L-Y, Ji P-H, Oliveira JM, Oliveira JT, Mano JF, Reis RL; (2010) Genipin-cross-linked collagen/chitosan biomimetic scaffolds for articular cartilage tissue engineering applications. *J Biomed Mat Res Part A* 95A(2), 465–475. **DOI:**10.1002/jbm.a.32869
- [56] Mighri N, Mao J, Mighri F, Aji A and Rouabhia M; (2015) Chitosan-coated collagen membranes promote chondrocyte adhesion, growth, and interleukin-6 secretion. *Materials* 8(11), 7673–7689. **DOI:**10.3390/ma8115413
- [57] Faikrua A, Jeenapongsa R, Sila-asna M, Viyoch J; (2009) Properties of β -glycerol phosphate/collagen/chitosan blend scaffolds for application in skin tissue engineering *ScienceAsia* 35(3), 247–254. **DOI:**10.2306/scienceasia1513-1874.2009.35.247
- [58] Lima CGA, de Oliveira RS, Figueiró SD, Wehmann CF, Góes JC, Sombra ASB; (2006) DC conductivity and dielectric permittivity of collagen-chitosan films. *Mater Chem Phys* 99(2-3), 284–288. **DOI:**10.1016/j.matchemphys.2005.10.027
- [59] Wary R, Sivaraj S, Gurukarthikeyan, Pathak KR, Suraj SLM, Dasararaju G, Kannayiram G; (2014) Chitosan gallic acid microsphere incorporated collagen matrix for chronic wounds: biophysical and biochemical characterization. *Int J Pharm Pharm Sci* 6(6), 94–100.
- [60] Holyavka MG, Pankova SM, Vyshkvorkina YuM, Lukin AN, Artyukhov VG; (2019) Investigation of UV modification for free and immobilized on the chitosan matrix collagenase (in Russian). *Rad Biol, Radioecol* 59(1), 63–67. **DOI:**10.1134/S0869803119010041
- [61] Hua Y, Ma Ch, Wei T, Zhang L, Shen J; (2020) Collagen/chitosan complexes: preparation, antioxidant activity, tyrosinase inhibition activity, and melanin synthesis. *Int J Mol Sci* 21(1), 313. **DOI:**10.3390/ijms21010313
- [62] Chen Z, Mo X, Qing F; (2007) Electrospinning of collagen-chitosan complex. *Mater Lett* 61(16), 3490–3494. **DOI:**10.1016/j.matlet.2006.11.104

- [63] Arpornmaeklong P, Suwatwirote N, Pripatnanont P, Oungbho K; (2007) Growth and differentiation of mouse osteoblasts on chitosan-collagen sponges. *Int J Oral Maxillofac Surg* 36(4), 328–337. **DOI:**10.1016/j.ijom.2006.09.023
- [64] Bama P, Vijayalakshimi M, Jayasimman R, Kalaichelvan PT, Deccaraman M, Sankaranarayanan S; (2010) Extraction of collagen from cat fish (*Tachysurus Maculatus*) by pepsin digestion and preparation and characterization of collagen chitosan sheet. *Int J Pharm Pharm Sci* 2(4), 133–137.
- [65] Staroszczyk H, Sztuka K, Wolska J, Wojtasz-Pajak A, Kołodziejska I; (2014) Interactions of fish gelatin and chitosan in uncrosslinked and crosslinked with EDC films: FT-IR study. *Spectrochim Acta A Mol Biomol Spectrosc* 117, 707–712. **DOI:**10.1016/j.saa.2013.09.044
- [66] Kumar BS, Aigal S, Ramesh DV; (2012) Air-dried 3D-collagen-chitosan biocomposite scaffold for tissue engineering application. *Polym Compos* 33(11), 2029–2035. **DOI:**10.1002/pc.22345
- [67] Zotarelli Filho IJ, Frascino LF, Greco OT, de Araújo JD, Bilaqui A, Kassis EN, Ardito RV, Bonilla-Rodriguez GO; (2013) Chitosan-collagen scaffolds can regulate the biological activities of adipose mesenchymal stem cells for tissue engineering. *J Regen Med Tissue Eng* 2, 12. **DOI:**10.7243/2050-1218-2-12
- [68] Lü X, Zhang H, Huang Y, Zhang Y; (2018) A proteomics study to explore the role of adsorbed serum proteins for PC12 cell adhesion and growth on chitosan and collagen/chitosan surfaces. *Regen Biomater* 5(5), 261–273. **DOI:**10.1093/rb/rby017
- [69] Zhu Y, Dong Z, Wejinya UC, Jin S, Ye K; (2011) Determination of mechanical properties of soft tissue scaffolds by atomic force microscopy nanoindentation. *J Biomech* 44(13), 2356–2361. **DOI:**10.1016/j.jbiomech.2011.07.010
- [70] Przybyłek M, Bełdowski P; (2023) Molecular dynamics simulations of the affinity of chitin and chitosan for collagen: the effect of pH and the presence of sodium and calcium cations. *Progr Chem Appl Chitin Deriv* 28, 136–150. **DOI:**10.15259/PCACD.28.013
- [71] Izumrudov VA, Mussabayeva BK, Kassymova ZS, Klivenko AN, Orazzhanova LK; (2019) Interpolyelectrolyte complexes: advances and prospects of application. *Russ Chem Rev* 88(10), 1046–1062. **DOI:**10.1070/rer4877
- [72] Panova I, Drobyazko A, Spiridonov V, Sybachin A, Kydraliev K, Jorobekova S, Yaroslavov A; (2018) Humics-based interpolyelectrolyte complexes for antierosion protection of soil: model investigation. *Land Degrad Dev* 30(3), 337–347. **DOI:**10.1002/ldr.3228
- [73] Kabanov VA; (2005) Polyelectrolyte complexes in solution and in bulk. *Russ Chem Rev* 74(1), 3–20. **DOI:**10.1070/rc2005v074n01abeh001165
- [74] Kodirkhonov MR, Nurgaliev IN, Vokhidova NR; (2023) Modeling the reactivity of chitosan and Na-carboxymethylcellulose for the formation of an interpolymer complex. *Scientific Bulletin of Namangan State University, Uzbekistan*, 103–112.
- [75] Vokhidova NR, Khudoyberdiyev ShSh, Nurgaliev IN, Rashidova SSh; (2023) On obtaining binary polyelectrolyte complexes of chitosan *Bombyx mori* with collagen. *Prog Chem Appl Chitin Deriv* 28, 188–203. **DOI:**10.15259/PCACD.28.017
- [76] Emmanuel M, Pogrebnoi A, Pogrebnyaya T; (2015) Theoretical study of the interaction between chitosan constituents (glucosamine and acetylglucosamine dimers) and Na⁺ ions. *Open Access Library Journal* 2(10), e1978. **DOI:**10.4236/oalib.1101978

- [77] Deka BC, Bhattacharyya PK; (2015) Understanding chitosan as a gene carrier: a DFT study. *Comput Theor Chem* 1051, 35–41. **DOI:**10.1016/j.comptc.2014.10.023
- [78] Donald JE, Kulp DW, DeGrado WF; (2010) Salt bridges: geometrically specific, designable interactions. *Proteins Struct Funct Bioinf* 79(3), 898–915. **DOI:**10.1002/prot.22927
- [79] Bolshakov IN, Krivopalov VA, Kaptyuk GI, Karapetyan AM, Ignatov AV; (2012) Transplantation of a cellular polysaccharide substrate for partial spinal rupture in rats (in Russian). *Fundamental Research* 2, 31–34.
- [80] Trofimovich YuG, Cherdantsev DV, Bolshakov IN, Shestakova LA, Kotikov AR, Kozlov VV; (2013) Experimental substantiation of the use of combined polymer materials for reconstruction of the anterior abdominal wall. *Sib Med Rev* 2, 31–34.
- [81] Chaykin DA, Cherdantsev DV, Chaykin AN, Trofimovich YuG, Bolshakov IN, Dvornichenko PA; (2014) Experimental and clinical reasoning of using the combined endoprosthesis structure for laparoscopic hernia in inguinal hernia patients. *Sib Med Rev* 4, 33–38. **DOI:**10.20333/25000136-2014-4-33-38
- [82] Antonov SF, Paramonov BA, Nikonov BA, Nugaev TSh, Zolina NV, Potokin IL, Sviridov YaG, Abramov NA; (2012) Morphological features of wound regeneration processes during treatment with collagen-chitosan and gelatin-chitosan sponges. *Bull North-West Univ Mech* 4(2), 43–46.
- [83] Bolshakov IN, Yemeyev AV, Cherdantsev DV, Kaskayev AV, Kirichenko AK, Vlasov AA, Sapozhnikov AN; (2011) The biodegradable wound coverings on the basis of polysaccharide polymers in the treatment of extensive burn damage (Clinical research) (In Russian). *Iss Reconstr Plastic Surg* 14(3), 56–62.
- [84] Kirichenko AK, Bolshakov IN, Ali-Rizal AE, Vlasov AA; (2012) Morphological study of burn wound healing with the use of collagen/chitosan wound dressing. *Bull Exp Biol Med* 154(11), 692–696. **DOI:**10.1007/s10517-013-2031-6
- [85] You Ch, Li Q, Wang X, Wu P, Ho JK, Jin R, Zhang L, Shao H, Han Ch; (2017) Silver nanoparticle loaded collagen/chitosan scaffolds promote wound healing via regulating fibroblast migration and macrophage activation. *Sci Rep* 7(1), 10489. **DOI:**10.1038/s41598-017-10481-0
- [86] Winias S, Ernawati DS, Ariani MD, Rahayu RP; (2017) Scaffold combination of chitosan and collagen synthesized from chicken feet induces osteoblast and osteoprotegerin expression in bone healing process of mice. *Dental J* 50(2), 86–90. **DOI:**10.20473/j.djmkg.v50.i2.p86-90
- [87] Chen H, Chen H, Liu L, Yuan P, Zhang Q; (2008) The study of collagen-chitosan complex film containing VCR-microspheres. *Conference materials – Society of Biomaterials*.
- [88] Panarin EF, Nudga LA, Petrova VA, Bocek AM and Pinaev GP; (2010) Composite matrices based on chitin and chitosan for the cultivation of human skin cells. *Cell Transplant Tissue Eng* 5(1), 65–73.
- [89] Shaghiera AD, Widiyanti P, Yusuf H; (2018) Synthesis and characterization of injectable hydrogels with varying collagen-chitosan-thymosin β 4 composition for myocardial infarction therapy. *J Funct Biomater* 9(2), 33. **DOI:**10.3390/jfb9020033
- [90] Kaczmarek B, Sionkowska A; (2018) Chitosan/collagen blends with inorganic and organic additive – a review. *Adv Polym Technol* 37(6), 2367–2376. **DOI:**10.1002/adv.21912

- [91] Intaraprasit S, Faikrua A, Sittichokechaiwut A, Viyoch J; (2012) Efficacy evaluation of the fibroblast-seeded collagen/chitosan scaffold on application in skin tissue engineering. *ScienceAsia* 38, 268–277. **DOI:**10.2306/scienceasia1513-1874.2012.38.268
- [92] Tsai S-P, Hsieh Ch-Y, Hsieh Ch-Y, Wang Da-M, Huang LL-H, Lai J-Y, Hsieh H-J; (2007) Preparation and cell compatibility evaluation of chitosan/collagen composite scaffolds using amino acids as crosslinking bridges. *J Appl Polym Sci* 105(4), 1774–1785. **DOI:**10.1002/app.26157
- [93] Paramonov BA, Antonov SF, Abramov NA, Nugaev TSh, Kozulin DA, Andreev DYu; (2012) The influence of implanted collagen-chitosan and gelatin-chitosan sponges on the state of the rat's body: an experimental study. *Scientific Notes of St Petersburg State Medical University named after IP Pavlova* 3, 78–82.
- [94] Semkin VA, Kuzin AV, Gurin AN, Bezrukov AA; (2016) Modern wound dressings in oral surgery (in Russian). *Stomatologiiia (Mosk)* 95(4), 87–90. **DOI:**10.17116/stomat201695487-90
- [95] Eremeev AV, Svetlakov AV, Bolshakov IN, Vlasov AA, Arapova VA; (2009) Functions of cultured embryonic cells on a collagen-chitosan matrix. *Genes and Cells* IV(2), 55–62.
- [96] Yu L, Huang J, Wang J, Cui L, Sun Y, Chen L, Su Y, Lin S, Li G; (2015) Antler collagen/chitosan scaffolds improve critical calvarial defect healing in rats. *J Biomater Tissue Eng* 5(10), 774–779. **DOI:**10.1166/jbt.2015.1368
- [97] Ansarizadeh M, Mashayekhan Sh, Saadatmand M, Khashabi E; (2017) Empirical modeling of mechanical properties of modified collagen/chitosan membrane by Response Surface Methodology. 24th National and 2nd International Iranian Conference on Biomedical Engineering (ICBME), Tehran, Iran, 1–6. **DOI:**10.1109/ICBME.2017.8430222
- [98] Wang P, Liu J, Zhang T; (2013) *In vitro* biocompatibility of electrospun chitosan/collagen scaffold. *J Nanomater* 2013(1), 958172. **DOI:**10.1155/2013/958172
- [99] Xiumei M, Zonggang Ch, Weber HJ; (2007) Electrospun nanofibers of collagen-chitosan and P(LLA-CL) for tissue engineering. *Front Mater Sci* 1(1), 20–23. **DOI:**10.1007/s11706-007-0004-2
- [100] Kaptyuk G, Ignatov A, Kuznetsov V, Sheina Y, Bolshakov I, Karapetyan A; (2013) Experimental complete transection spinal cord and its bioengineering reconstruction. *J New Med Technol* 20(4), 130–138. **DOI:**10.12737/2748
- [101] Bolshakov IN, Eremeev AV, Sheina YuI, Polstyanoy AM, Medvedeva NN, Zhukov EL, Kaptyuk GI, Krivopalov VA, Ignatov AV, Karapetyan AM; (2011) Use of a polysaccharide substrate with a neuronal microenvironment for bioengineering of the central nervous system in experimental spinal injury in rats. *Fundam Res* 11(2), 266–271.
- [102] Porporatto C, Bianco ID, Cabanillas AM, Correa SG; (2004) Early events associated to the oral co-administration of type II collagen and chitosan: induction of anti-inflammatory cytokines. *Int Immunol* 16(3), 433–441. **DOI:**10.1093/intimm/dxh051
- [103] Cao X, Deng W, Wei Y, Yang Y, Su W, Wei Y, Xu X, Yu J; (2012) Incorporating pTGF- β 1/calcium phosphate nanoparticles with fibronectin into 3-dimensional collagen/chitosan scaffolds: efficient, sustained gene delivery to stem cells for chondrogenic differentiation. *Eur Cells Mater* 23, 81–93. **DOI:**10.22203/ecm.v023a06

- [104] Harikumar K, Nandakumar K, Devadas C, Mathew S; (2014) Collagen-chitosan barrier membrane, a novel, indigenous, and economic material for management of periodontal infrabony defects – a case-control study. *Univers Res J Dent* 4(2), 87–92. **DOI:**10.4103/2249-9725.132971
- [105] Yan F, Li M, Zhang H-Q, Li G-L, Hua Y, Shen Y, Ji X-M, Wu Ch-J, An H, Ren M; (2019) Collagen-chitosan scaffold impregnated with bone marrow mesenchymal stem cells for treatment of traumatic brain injury. *Neural Regen Res* 14(10), 1780–1786. **DOI:**10.4103/1673-5374.257533
- [106] Roffi A, Kon E, Perdisa F, Fini M, Di Martino A, Parrilli A, Salamanna F, Sandri M, Sartori M, Sprio S, Tampieri A, Maracci M, Filardo GA; (2019) A composite chitosan-reinforced scaffold fails to provide osteochondral regeneration. *Int J Mol Sci* 20(9), 2227. **DOI:**10.3390/ijms20092227
- [107] Wang X, Wang G, Liu L, Zhang D; (2016) The mechanism of a chitosan-collagen composite film used as biomaterial support for MC3T3-E1 cell differentiation. *Sci Rep* 6(1), 39322. **DOI:**10.1038/srep39322
- [108] Widiyanti P, Setyadi ED, Rudyardjo DI; (2017) Collagen-chitosan scaffold - lauric acid plasticizer for skin tissue engineering on burn cases. *AIP Conf Proc* 1817(1), 020013. **DOI:**10.1063/1.4976765
- [109] Deng Ch, Zhang P, MD, Vulesevic B, Kuraitis D, Li F, Yang AF, Griffith M, Ruel M, Suuronen EJ; (2010) A collagen-chitosan hydrogel for endothelial differentiation and angiogenesis. *Tissue Eng Part A* 16(10), 3099–3109. **DOI:**10.1089/ten.tea.2009.0504
- [110] Valle JAB, Valle RCSC, Bierhalz ACK, Bezerra FM, Hernandez AP, Arias LMJ; (2012) Chitosan microcapsules: methods of the production and use in the textile finishing. *J Appl Polym Sci* 138(21), 50482. **DOI:**10.1002/app.50482
- [111] Jahit IS, Nazmi NNM, Isa MIN, Sarbon NM; (2016) Preparation and physical properties of gelatin/CMC/chitosan composite films as affected by drying temperature. *Int Food Res J* 23(3), 1068–1074.
- [112] Chernon NK, Ozolina SA, Kapustyan AI; (2010) Chitosan-pectin interpolyelectrolyte complex as a matrix for trypsin immobilization. *J Bioproc biotech of food prod, BAR* 4(13) 40–43.
- [113] Cai X, Hu S, Yu B, Cai Y, Yang J, Li F, Zheng Y, Shi X; (2018) Transglutaminase-catalyzed preparation of crosslinked carboxymethyl chitosan/carboxymethyl cellulose/collagen composite membrane for postsurgical peritoneal adhesion prevention. *Carbohydr Polym* 201, 201–210. **DOI:**10.1016/j.carbpol.2018.08.065
- [114] Nedelcu IA, Ficai A, Ficai D, Voicu G, Albu MG, Andronescu E; (2015) Hybrid collagen-carboxymethylcellulose/hydroxyapatite composite materials for bone tissue regeneration. *U.P.B. Sci Bull Series B* 77, 3–14.
- [115] Aminatun, Hikmawati D, Widiyanti P, Amrillah T, Nia WA, Firdania IT, Che Abdullah ChA; (2020) Study of mechanical and thermal properties in nano-hydroxyapatite/chitosan/carboxymethyl cellulose nanocomposite-based scaffold for bone tissue engineering: the roles of carboxymethyl cellulose. *Appl Sci* 10(19), 6970. **DOI:**10.3390/app10196970
- [116] Liuyun J, Yubao L, Chengdong X; (2009) Preparation and biological properties of a novel composite scaffold of nano-hydroxyapatite/chitosan/ carboxymethyl cellulose for bone tissue engineering. *J Biomed Sci* 16(1), 65. **DOI:**10.1186/1423-0127-16-65
- [117] Wang X, Li Y, Wei J, de Groot K; (2002) Development of biomimetic nano-hydroxyapatite/poly(hexamethylene adipamide) composites. *Biomater* 23(24), 4787–4791. **DOI:**10.1016/s0142-9612(02)00229-6

- [118] Wang XL, Li XD, Wang XM, Lu J, Zhao HC, Zhang XD, Gu ZW; (2007) Investigation of a collagen-chitosan-hydroxyapatite system for novel bone substitutes. *KEM* 330–332, 415–418. **DOI:**10.4028/www.scientific.net/KEM.330-332.415
- [119] Charlena, Bikharudin A, Wahyudi ST, Erizal; (2017) Synthesis and characterization of hydroxyapatite-collagen-chitosan (HA/Col/Chi) composite by using ex-situ wet precipitation method. *Rasayan J Chem* 10(3), 766–770. **DOI:**10.7324/RJC.2017.1031768
- [120] Vokhidova NR, Ergashev KH, Rashidova SSh; (2020) Hydroxyapatite-chitosan *Bombyx mori*: synthesis and physicochemical properties. *J Inorg Organomet Polym Mat* 30, 3357–3368. **DOI:**10.1007/s10904-020-01649-9
- [121] Nandhini DP, Subashini S, Pandimadevi M; (2018) Preparation and characterisation of collagen/chitosan/sodium alginate biocomposite electrospun nanofibers. *World J Pharm Res* 7(01), 1328–1338. **DOI:**10.20959/wjpr20181-10489
- [122] Popryadukhin PV, Yukina GYu, Dobrovolskaya IP, Ivankova EM, Yudin VE; (2018) Porous bioresorbable matrices based on chitosan, alginate and collagen in the wall of the rabbit wall uterine after kesarev section (in Russian). *Int J Appl Fundam Res* 6, 112–119. **DOI:**10.17513/mjpf.12302
- [123] Widiyanti P, Rini NDW, Kirana MN, Astutik T; (2019) Synthesis and characterization of collagen-chitosan-sodium hyaluronates as artificial cornea. *J Phys Conf Ser* 1417, 012035. **DOI:**10.1088/1742-6596/1417/1/012035
- [124] Elango J, Saravanakumar K, Rahman SU, Henrotin Y, Regenstein JM, Wu W, Bao B; (2019) Chitosan-collagen 3D matrix mimics trabecular bone and regulates RANKL-mediated paracrine cues of differentiated osteoblast and mesenchymal stem cells for bone marrow macrophage-derived osteoclastogenesis. *Biomolecules* 9(5) 173. **DOI:**10.3390/biom9050173
- [125] Aminatun, Ibrahim MH, Ady J, Hikmawati D, Yasin M; (2019) Synthesis and characterization of nano-hydroxyapatite/chitosan/carboxymethyl cellulose composite scaffold. *J Int Dent Med Res* 12(1), 31–37.
- [126] Yu B-Y, Chou P-H, Chen C-A, Sun Y-M, Kung S-S; (2007) C3A cell behaviors on micropatterned chitosan-collagen-gelatin membranes. *J Biomater Appl* 22(3), 255–274. **DOI:**10.1177/0885328207076780
- [127] Udhayakumar S, Shankar KG, Sowndarya S, Venkatesh S, Muralidharan Ch, Rose Ch; (2017) L-Arginine intercedes bio-crosslinking of a collagen-chitosan 3D-hybrid scaffold for tissue engineering and regeneration: in silico, *in vitro*, and *in vivo* studies. *RSC Adv* 7(40), 25070–25088. **DOI:**10.1039/c7ra02842c
- [128] Maged A, Abdelkhalek AA, Mahmoud AA, Salah S, Ammar MM, Ghorab MM; (2019) Mesenchymal stem cells associated with chitosan scaffolds loaded with rosuvastatin to improve wound healing. *Eur J Pharm Sci* 127, 185–198. **DOI:**10.1016/j.ejps.2018.11.002
- [129] Widiyanti P, Prastyani R; (2019) Collagen-chitosan-glycerol-HPMC composite as cornea artificial candidate. *J Biomimetics Biomater Biomed Eng* 42, 14–21. **DOI:**10.4028/www.scientific.net/JBBBE.42.14
- [130] Bakry NF, Isa MIN, Sarbon NM; (2017) Effect of sorbitol at different concentrations on the functional properties of gelatin/carboxymethyl cellulose (CMC)/chitosan composite films. *Int Food Res J* 24(4), 1753–1762.
- [131] Pérez-Herrero E, García-García P, Gómez-Morales J, Llabrés M, Delgado A, Évora C; (2019) New injectable two-step forming hydrogel for delivery of bioactive substances in tissue regeneration. *Regener Biomater* 6(3), 149–162. **DOI:**10.1093/rb/rbz018

SYNTHESIS OF CHITOSAN COMPOSITES WITH METHYLENE BLUE, MALACHITE GREEN AND ACID FUCHSIN DYES FOR ENHANCEMENT OF THEIR ANTIMICROBIAL ACTION

Volodymyr Antonyuk^{1,2,a,*}, Nazar Manko^{2,b}, Lidiia Panchak^{1,c}, Semen Khomyak^{3,d}, Oleksandr Gromyko^{4,e}, Rostyslav Stoika^{1,2,4,f}

¹ – Danylo Halytsky Lviv National Medical University, Pekarska 69 Str., 79010 Lviv, Ukraine

^a – ORCID: 0000-0002-3643-4957, ^c – ORCID: 0000-0002-9621-3304,

^f – ORCID: 0000-0001-5719-2187

² – Institute of Cell Biology, NAS Ukraine, Drahomanov 14/16 Str., 79005 Lviv, Ukraine

^b – ORCID: 0000-0003-1203-7479

³ – Lviv Polytechnic National University, Yura Sq. 3/4, 79013 Lviv, Ukraine

^d – ORCID: 0000-0003-1931-1688

⁴ – Ivan Franko National University of Lviv, Hrushevsky 4 Str., 79005 Lviv, Ukraine

^e – ORCID: 0000-0002-8107-0128

*corresponding author: antonyukvo@gmail.com

Abstract

The effect of chitosan oxidation with sodium periodate on the ability to form complexes with the dyes methylene blue, malachite green and acid fuchsin, which have an antiseptic effect, was investigated. A non-covalent interaction occurred for methylene blue and malachite green, while a covalent interaction occurred for acid fuchsin. Fourier-transform infrared spectroscopy confirmed the formation of chitosan composites with these dyes. The antimicrobial effect of these dyes complexed with oxidised chitosan against *Pseudomonas aeruginosa*, *Staphylococcus aureus*, *Bacillus subtilis* and *Escherichia coli* was investigated. The non-covalent attachment of malachite green and methylene blue to chitosan preserved their antimicrobial effect; hence, complexes of these dyes with oxidised chitosan provide a more convenient form that is less staining. However, the covalent conjugation of acid fuchsin with oxidised chitosan caused a significant loss of the antimicrobial activity. The developed method of conjugation of specific dyes with chitosan can be used to create complexes of this biopolymer with a wide range of biologically active organic substances.

Keywords: chitosan; periodate oxidation; methylene blue, malachite green, acid fuchsin; conjugates and adducts; FTIR analysis; antimicrobial action

Received: 03.04.2024

Accepted: 19.04.2024

1. Introduction

In the 19th century, scientists proposed specific dyes for use as histochemical reagents in microscopy. Many of these dyes also possess antimicrobial activity. In 1891, Paul Ehrlich showed that methylene blue was an effective remedy in treatment of malaria [1]. At present, the main areas of application of the dyes methylene blue, acid fuchsin and malachite green are the textile industry as well as microbiological and cytological analysis. They are also used in medicines, albeit to a lesser extent, and exert a wide range of the antimicrobial effects against the infectious agents in skin lesions and mucous membranes, as well as a fungicidal remedy in fungal lesions of the outer coverings (Table 1). For example, fucorcin solution, which contains fuchsin, is prescribed to treat skin diseases caused by various types of dermatomycetes (trichophytons, microsporum and epidermophytons), microbial eczema and oily and mixed forms of seborrhoea.

A major disadvantage of dyes is their intense colour, which can stain clothes and other items that come into contact with them. To mitigate this disadvantage, dyes can be complexed with macromolecules such as chitosan. In addition, one may expect a prolongation of the antimicrobial action of dyes complexed with chitosan. Consistently, we previously showed that after subcutaneous administration to rats, ethacridine lactate complexed with chitosan circulated in the blood for a significantly longer time than the intact ethacridine [2].

The preparation of chitosan iodide composites with methylene blue and fuchsin was described recently [3]. These composites formed porous sponges and films and, therefore, could be used for a variety of applications. They possessed antibacterial activity against antibiotic-resistant gram-positive and gram-negative bacteria. Chitosan obtained from different sources and using different methods can vary in the molecular mass, from ≥ 10 to 1,000 kDa, impurities content, and degree of deacetylation, from 30% to 95% [4, 5].

In this work, we oxidised chitosan with sodium periodate (NaIO_4) and complexed the oxidised product with one of three dyes, namely methylene blue, malachite green and acid fuchsin. We evaluated the physicochemical characteristics of the obtained complexes using viscometric analysis to determine the molecular mass of chitosan and Fourier-transform infrared (FTIR) spectroscopy to determine the structure of chitosan–dye complexes. Finally, we assessed the antimicrobial action of intact and chitosan-conjugated forms of these dyes towards the gram-negative bacteria *Pseudomonas aeruginosa* ATCC 9027 and *Escherichia coli* ATCC 25922 and the gram-positive bacteria *Staphylococcus aureus* ATCC 25923 and *Bacillus subtilis* ATCC 31324.

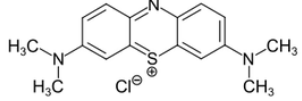
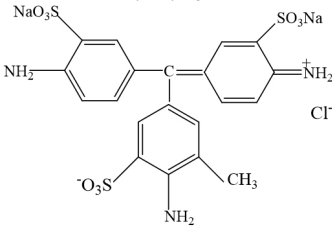
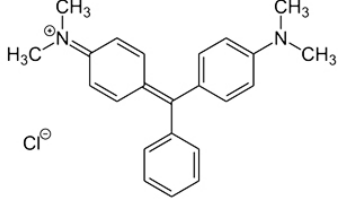
2. Materials and Methods

2.1. Materials

Methylene blue, malachite green and acid fuchsin were obtained from Klebrig (India). Table 1 provides the chemical structure, physicochemical properties and examples of the applications of these dyes.

Shrimp shell chitosan with different molecular masses and degrees of deacetylation – namely, CS-M (502 kDa, 80.8%), CS-S (313 kDa, 85.5%) and CS-L s (739 kDa, 91.3%) – were purchased from Chitopharm (Norway).

Table 1. The physicochemical properties and application of the three dyes used in this work.

Name, structure and physicochemical properties	Application
<p style="text-align: center;">Methylene blue $C_{16}H_{18}ClN_3S \cdot 3H_2O$</p>  <p>Dark green crystals with a bronze lustre; easily soluble in alcohol or hot water, but less soluble in cold water</p>	<p style="text-align: center;">Used as an antiseptic in the form of a water–alcohol solution to treat burns, pyoderma, folliculitis, etc. [1].</p>
<p style="text-align: center;">Fuch sine (rosaniline hydrochloride) $C_{20}H_{20}N_3Cl$</p>  <p>Green crystals with a metallic lustre; aqueous solutions are purple-red; poorly soluble in water, but good solubility in alcohol</p>	<p style="text-align: center;">Treatment of skin diseases, a component of some antiseptics, along with other aniline dyes – diamond green and methylene blue – which are active against staphylococci [6, 7].</p>
<p style="text-align: center;">Malachite green $C_{23}H_{25}ClN_2$</p>  <p>Dark green crystals with a metallic sheen; good solubility in water and ethanol</p>	<p style="text-align: center;">A classic remedy to treat diseases in fish; in most European countries, it is allowed to treat infections of only aquarium fish; corals and other invertebrates in sea and fresh water do not tolerate it [8, 9]</p>

2.2. Methods

The viscosity of chitosan solutions in a mixture of 0.1 M acetic acid and 0.2 M sodium chloride (NaCl) (1:2, v/v) was measured at 25°C with a Ubbelohde VPZh-4 viscometer (Soyuznauchpribor, USSR) with a capillary of diameter = 0.82 mm. The molecular mass of chitosan was determined from this measurement.

2.2.1. Fourier-Transform Infrared Spectroscopy

The FTIR spectra of the samples (chitosan, dyes and chitosan–dye complexes) were recorded on a Spectrum Two spectrometer (PerkinElmer, USA) using a diamond universal attenuated total reflectance (UATR) accessory. The PerkinElmer Spectrum 10 software was used to draw the spectra. The spectra (16 scans per spectrum) of the solutions were collected in the mid-infrared wavenumber range from 4000 to 400 cm^{-1} , with a spectral resolution of 0.4 cm^{-1} .

2.2.2. Preparation of Oxidised Chitosan and Chitosan–Dye Complexes

Finely ground chitosan powder (50 mg) was placed in a centrifuge tube; then, 3.0 ml of 1% sodium bicarbonate (NaHCO_3) solution was added and the mixture was incubated for 30 min. After swelling and impregnation of the chitosan powder, the NaHCO_3 solution was carefully removed with a pipette and 0.4 ml of 5% NaIO_4 was added. The mixture was incubated for 30 min at room temperature. The oxidised chitosan was washed three times with 10 ml of water. Next, 1–2 ml of a 1% dye solution in 0.1 M phosphate buffer (pH 7.0–7.5) was added to the washed oxidised chitosan. The mixture was incubated for 4–16 h, after which time unbound dye was washed away (8–10 times with 10 ml of 6% NaCl solution, and then 2 times with 10 ml of distilled water until complete discoloration of the washing water). In the control, the dye solution was added to the same amount of unoxidised chitosan; the incubation and washing were performed as described above.

2.2.3. Determination of the Bound Dye Content

The washed chitosan powder with dye was dried in an oven at 50–60°C, weighed and then dissolved in 1% acetic acid to a concentration of 1%. The pH of the solution was adjusted to 6.0. Then, the content of the dye in complexes was determined using a colorimetric or spectrophotometric method.

2.2.4. Determination of the Rate of Diffusion in Agar Gel

Filter paper discs (diameter = 5 mm) were impregnated with dye solution (control) or a chitosan–dye complex and dried in an oven at 60°C. Petri dishes were filled with 1% Sabouraud medium agar gel. A disc was placed on the solidified agar gel; after 2, 4 and 10 h, the diameter of the stained zone was measured. The ratio of the diffusion rate of the chitosan–dye complex to the diffusion rate of the pure dye was determined.

2.2.5. Measurement of Antimicrobial Activity

Filter paper discs (diameter = 5 mm) were impregnated with a dye solution (control) or a chitosan–dye complex and dried in an oven at 60°C. Microbial cultures were sown in 100-mm diameter Petri dishes filled with 1% Sabouraud medium agar gel; their growth was monitored and photographed. The experiments were carried out with the strains *P. aeruginosa* ATCC 9027, *S. aureus* ATCC 25923, *B. subtilis* ATCC 31324 and *E. coli* ATCC 25922 obtained from the Collection of microorganisms at the Faculty of Biology of Ivan Franko Lviv National University (Ukraine).

3. Results and Discussion

Table 2 shows the total mass and molecular mass of chitosan before and after oxidation with NaIO_4 .

Table 2. Reduction in the total mass and molecular mass of chitosan after its oxidation with sodium periodate.

Average molecular mass of chitosan [kDa]		Total mass of chitosan [mg]	
Before oxidation	After oxidation	Before oxidation	After oxidation
313	40	50	28 ± 3
502	70	50	32 ± 3
739	110	50	35 ± 3

These results demonstrate that during the treatment of chitosan with NaIO₄, there was oxidation of hydroxyl groups of glucosamine to aldehyde groups and hydrolysis of chitosan chains. Fragments of low-molecular-mass chitosan are probably lost during washing to remove excess NaIO₄. These losses reached 30%–50% of the mass of the chitosan sample, and the average molecular mass decreased by 5–8 times.

Due to the presence of amino groups, chitosan is capable of adsorbing various acidic substances, including dyes. Although unoxidised chitosan remained coloured after treatment with dyes followed by washing to remove unbound dye, the amount of dye it contained was negligible. On the other hand, oxidation of chitosan with NaIO₄ markedly increased the amount of bound dye (Table 3).

Table 3. The content (%) of dye complexed with chitosan (CS) before and after its oxidation with sodium periodate.

Sample	The amount of bound methylene blue [%]		The amount of bound malachite green [%]		The amount of bound acid fuchsin [%]	
	Native (313 kDa)	Oxidised (40 kDa)	Native (313 kDa)	Oxidised (40 kDa)	Native (313 kDa)	Oxidised (40 kDa)
CS-S	0.06	5.7	0.08	7.9	0.024	8.7
	0.06	5.0	0.078	7.7	0.018	6.5
CS-M	0.07	3.2	0.09	6.9	0.021	4.8
	0.07	3.2	0.09	6.9	0.021	4.8

Note. See Section 2.1 for the details of each chitosan.

Filter paper discs (diameter = 5 mm) impregnated with a dye solution (control) or a solution of chitosan–dye complex were examined to determine the rate of dye diffusion in 1% Sabouraud medium agar gel at pH 7.0 (Figure 1). There were no significant differences in the diffusion rate of pure methylene blue and malachite green compared with the chitosan–methylene blue and chitosan–malachite green complexes, respectively. However, the diffusion rate of chitosan–acid fuchsin was reduced markedly compared with pure acid fuchsin. These differences could be due to the bonds formed between the dyes and chitosan. Acid fuchsin binds covalently to oxidised chitosan, leading to a marked reduction in its diffusion. On the other hand, methylene blue and malachite green bind non-covalently. Of note, it is unknown exactly how methylene blue binds to chitosan; the bonds are stronger than those formed between chitosan and malachite green, but weaker than those formed between chitosan and acid fuchsin.

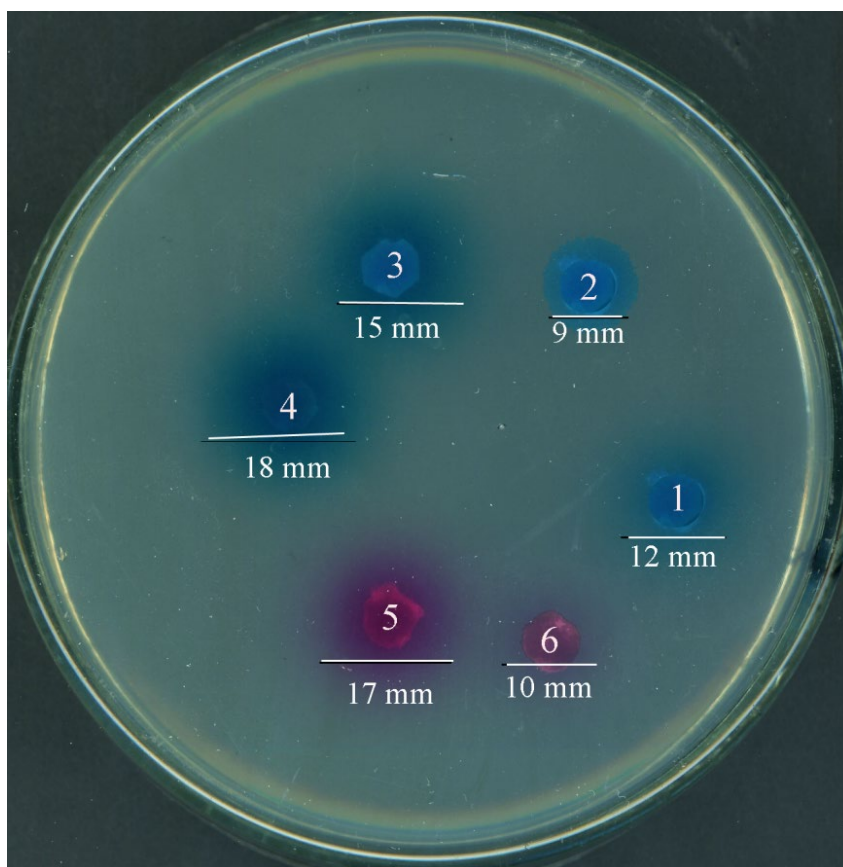


Figure 1. The photograph of a Petri dish containing 1% Sabouraud medium agar gel (pH 7.0) with filter paper discs impregnated with pure dyes of oxidised chitosan–dye complexes incubated for 10 h to allow diffusion. Identities: 1 – methylene blue; 2 – the chitosan–methylene blue complex; 3 – malachite green; 4 – the chitosan–malachite green complex; 5 – acid fuchsin; 6 – the chitosan–acid fuchsin complex.

Next, we compared the antibacterial activities of the pure dyes and the chitosan–dye complexes against gram-negative and gram-positive bacteria (Figure 2). In general, the findings were consistent with the diffusion results: the stronger the interactions between the dye and oxidised chitosan, the weaker the antibacterial activity. Based on the zone of inhibition, for each bacterium pure acid fuchsin (sample 5) presented much stronger antibacterial activity than the chitosan–acid fuchsin complex (sample 6). Pure methylene blue (sample 1) also showed stronger antibacterial activity than the chitosan–methylene blue complex (sample 2), although the difference was not as pronounced as for acid fuchsin. Finally, pure malachite green (sample 3) and the chitosan–malachite green complex (sample 4) showed similar antibacterial activity. Hence, the formation of a covalent complex between chitosan and acid fuchsin (via an unknown mechanism) or a stronger non-covalent complex between chitosan and methylene blue substantially reduces antibacterial activity.

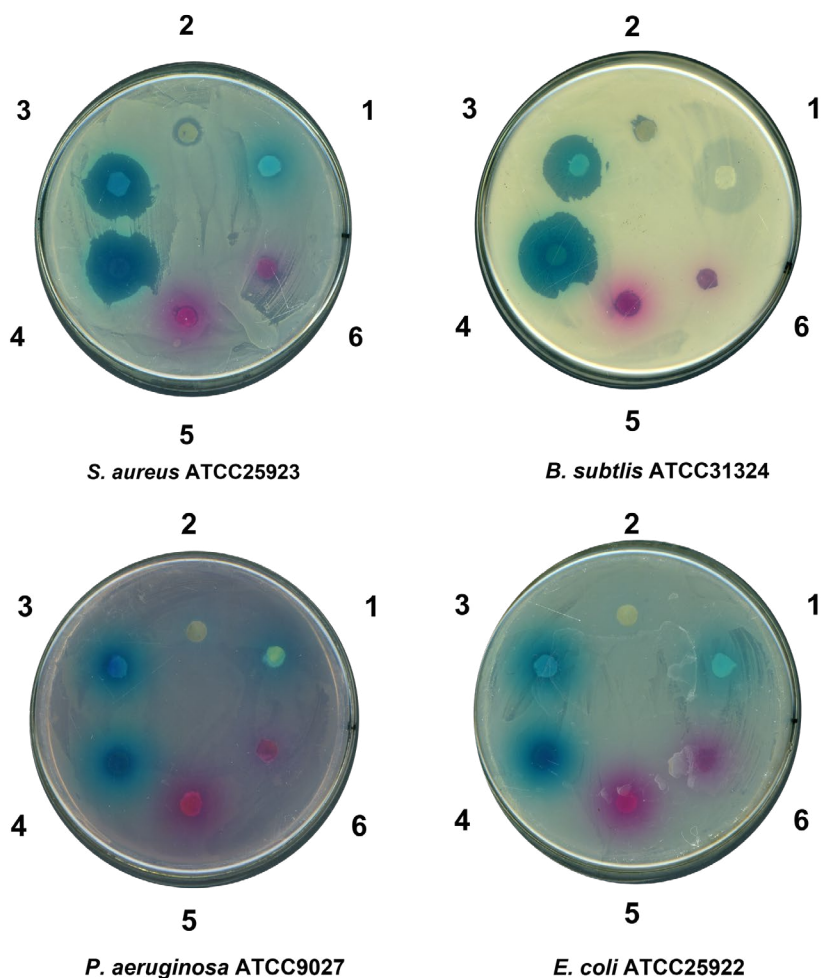


Figure 2. The photographs of the zone of inhibition of the gram-positive bacteria *Staphylococcus aureus* (ATCC25923) and *Bacillus subtilis* (ATCC31324) and the gram-negative bacteria *Pseudomonas aeruginosa* (ATCC9027) and *Escherichia coli* (ATCC25922) in the presence of pure dyes and chitosan–dye complexes. Identities: 1 – methylene blue; 2 – the chitosan–methylene blue complex; 3 – malachite green; 4 – the chitosan–malachite green complex; 5 – acid fuchsin; 6 – the chitosan–acid fuchsin complex.

Next, we used FTIR in an attempt to determine the mechanisms by which the studied dyes form complexes with oxidised chitosan. As shown in Figure 3, we consider that a covalent bond appears between the oxygen atom of oxidised chitosan and the nitrogen atom of the primary amino group of acid fuchsin. Such a change might affect its antimicrobial activity. The possibility of the formation of such a covalent bond does not exist in the case of malachite green (see Table 1). Finally, when methylene blue is added to oxidised chitosan, the aldehyde groups may oxidise to an acid, creating an opportunity for increased binding of methylene blue to oxidised chitosan.

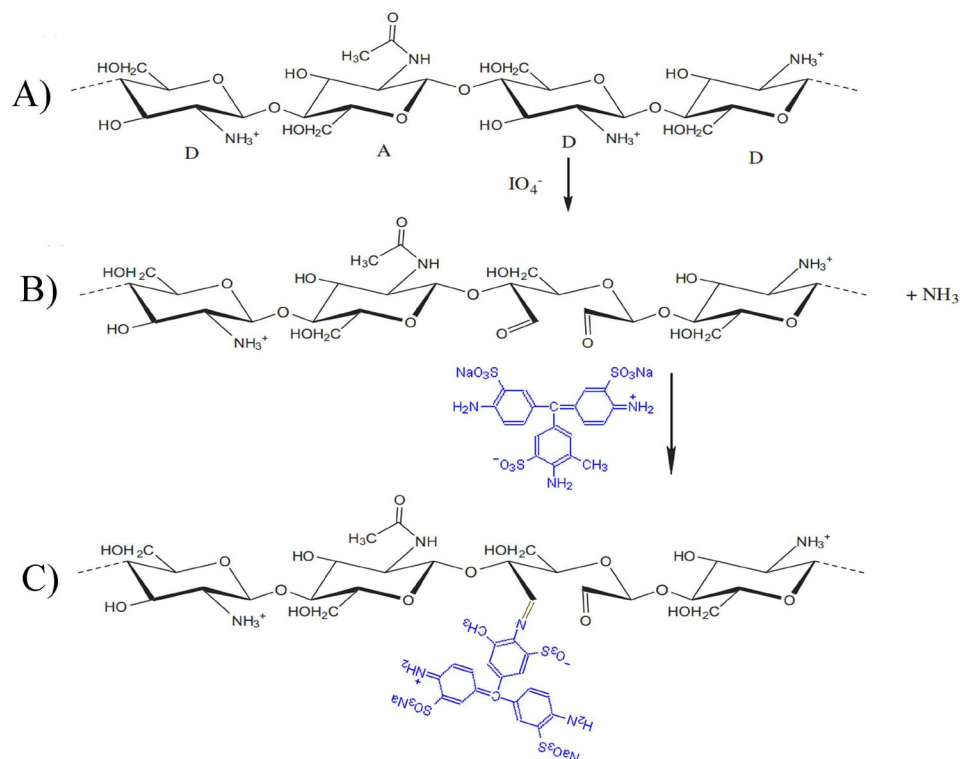


Figure 3. A schematic representation of the interaction between sodium periodate–oxidised chitosan and acid fuchsin.

Acid fuchsin has three amino groups that could interact with oxidised chitosan, while methylene blue and malachite green do not have such chemical groups. However, while malachite green looks to be totally inert for any conjugation, methylene blue has an S(+) atom in its heterocyclic ring. Therefore, it is possible that the aldehyde group of the modified chitosan chain forms a non-covalent bond with the free electron pair of the sulfur atom in methylene blue. It is also possible that when methylene blue is added to oxidised chitosan, there is intramolecular rearrangement of two adjacent aldehyde groups and the formation of hydroxyl and carboxyl groups in their place. This would create an opportunity for enhanced binding of methylene blue to oxidised chitosan through the attraction of sulfur in the phenothiazine ring (positive charge) to carboxyl groups in chitosan (negative charge). Figure 4 presents a scheme of such transformations.

Chitosan oxidation reduces its molecular mass (Table 2). That may increase the number of loci that can interact with other substances. As reported previously, chitosan with a medium molecular mass (135 kDa) and a high degree of deacetylation binds more effectively to substances than chitosan with a high molecular mass [10].

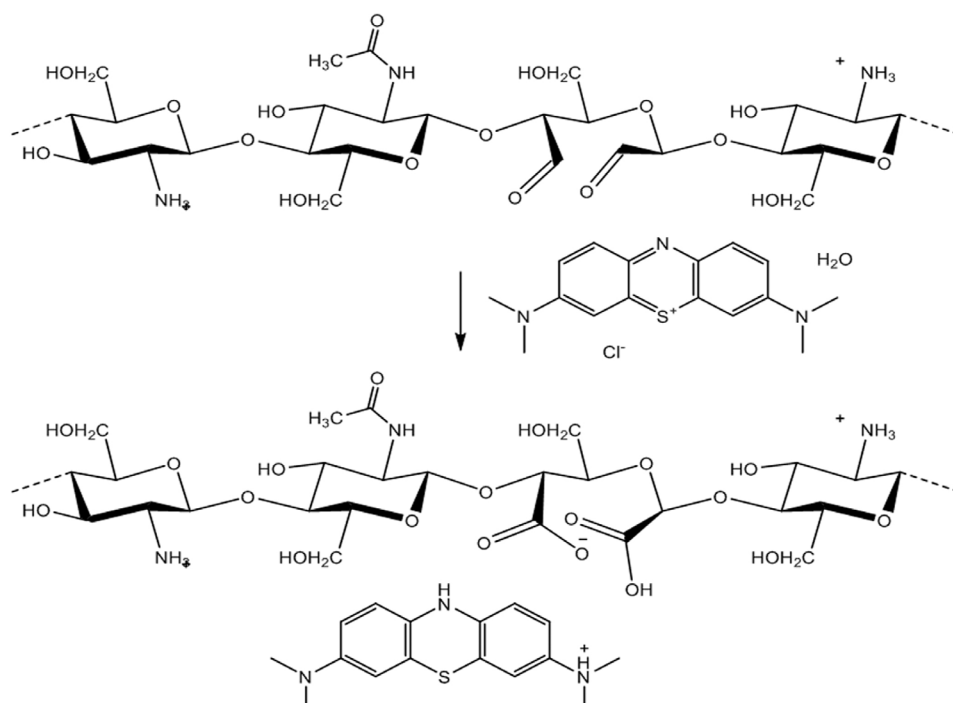


Figure 4. A schematic representation of the possible interaction between sodium periodate–oxidised chitosan and methylene blue.

If the interaction between oxidised chitosan and a dye occurs non-covalently, then the dye can be detached from chitosan with long-term washing with a suitable solvent, or by increasing the temperature or changing the pH or the ionic strength of the solutions. The three dyes attached to oxidised chitosan much better (3.2%–8.7%) than to unoxidised chitosan (0.018%–0.09%; Table 3). As one can see in Figure 1, malachite green was totally released from the chitosan–malachite green complex, while acid fuchsin was almost totally captured by oxidised chitosan. A repeated, more intensive washing of oxidised CS-M containing the absorbed dyes with acidified and alkalisied 80% ethanol led to almost total release of malachite green and methylene blue, which lost their colour, while the release of the attached acid fuchsin was not complete. The dye content after the washing procedure revealed a mean concentration of 0.06% for methylene blue, 0.04% for malachite green and 0.87% for acid fuchsin. Based on these results, we hypothesised that the chitosan–acid fuchsin complex is a mixture of acid fuchsin attached covalently and non-covalently. We tested this assumption by recorded FTIR spectra of chitosan alone and chitosan complexed with the studied dyes.

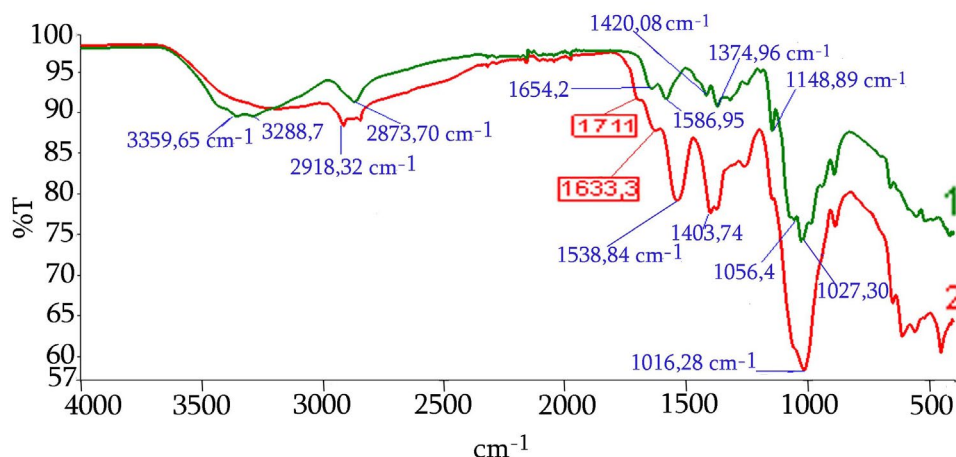


Figure 5. Fourier-transform infrared spectra of chitosan (1, green line) and oxidised chitosan (2, red line).

In general, the FTIR spectra of chitosan, oxidised chitosan and the studied dyes agree with what has been published in the literature [11, 12]. There are three broad absorption bands observed in the FTIR spectra of chitosan and its derivatives (Figure 5). The bands at 1640–1540 cm^{-1} and 1430–1380 cm^{-1} can be attributed to stretching of amide groups and bending of alkyl groups, respectively. The most intense absorption band at 1150–900 cm^{-1} corresponds to C-O-C and C-O-H vibrations. The unmodified chitosan spectrum shows the characteristic absorption bands at 3359 and 3288 cm^{-1} (attributed to O-H and N-H stretching vibrations, respectively), 2873 cm^{-1} (C-H stretching), 1654 cm^{-1} (C=O stretching of amide I), 1586 cm^{-1} (N-H bending of amide II), 1148 cm^{-1} (C-O-C stretching) and 1056 and 1027 cm^{-1} (C-O stretching). The obtained spectrum is consistent with the literature.

The FTIR spectra of chitosan and oxidised chitosan are very similar. The major difference is at 1680–1500 cm^{-1} , where oxidised chitosan shows a shift in the absorption maxima towards short wavelengths and an increase in peak intensity. The only significant difference is the appearance of an absorption band with a low intensity at 1711 cm^{-1} in the FTIR spectrum of oxidised chitosan; it corresponds to stretching vibrations of the aldehyde group formed as a result of oxidation. In addition, a newly formed sharp band at 1633 cm^{-1} derived from a carbonyl group confirms oxidation of chitosan. The changes in the shape and intensity of the stretching vibrations of the hydroxyl band (3200 cm^{-1}) can be explained by the opening of cyclic structure and oxidation of chitosan saccharide units. There are also changes at 1300–1400 cm^{-1} (C-H bending) and 1000–1200 (C-O-C and C-O bending), which prove the effective modification of glucoside rings in chitosan caused by their opening and oxidation at the C2 and C3 positions. Note that in the FTIR spectra of the chitosan–dye complexes, the absorption bands of the dyes are almost absent, probably due to their low concentrations.

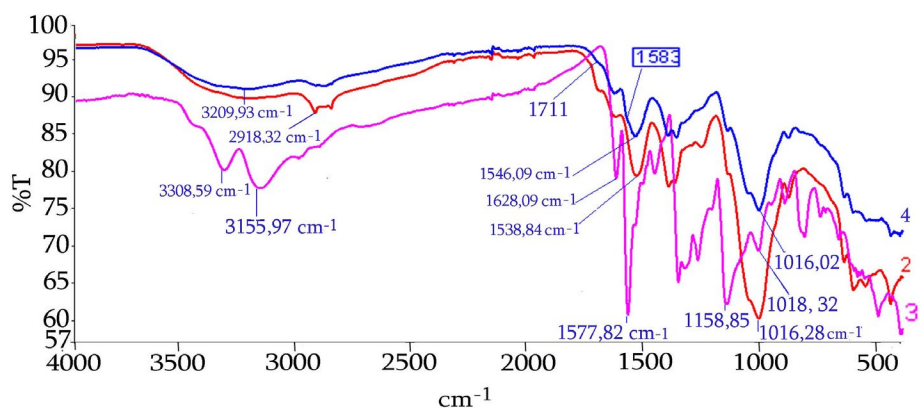


Figure 6. Fourier-transform infrared spectra of oxidised chitosan (2, control, red line), acid fuchsin (3, purple line) and the oxidised chitosan–acid fuchsin complex (4, blue line).

The FTIR spectra of oxidised chitosan and the oxidised chitosan–acid fuchsin complex practically coincide (Figure 6). The only significant difference is the absence of the absorption band at 1711 cm^{-1} (the aldehyde group in the complex). This can be explained by the formation of a covalent bond between the $\text{C}=\text{O}$ group of oxidised chitosan and the amino group of acid fuchsin. The formation of this bond is confirmed by the shift in the absorption bands towards longer wavelengths. Thus, N-H bending in oxidised chitosan shifts from 1538 to 1546 cm^{-1} in the complex. In addition, the complex shows a new shoulder in the absorption band at 1583 cm^{-1} , which corresponds to the vibrations of the new $\text{C}=\text{N}$ covalent bond in the complex. The absorption band at 1546 cm^{-1} is wider due to the intense absorption of acid fuchsin, which entered the adduct.

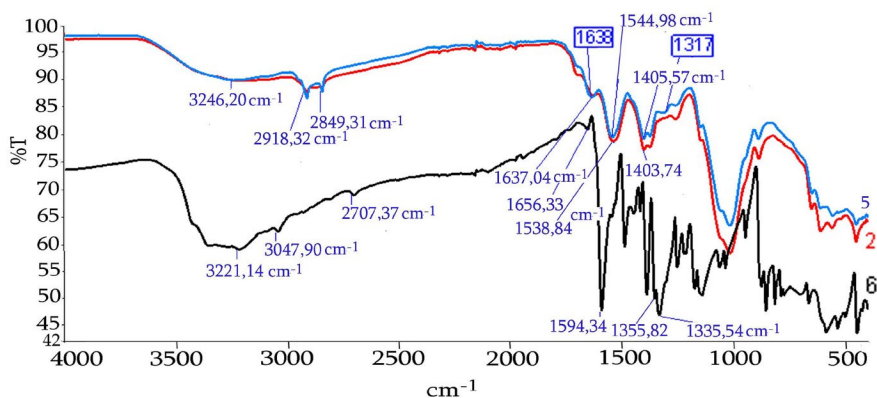


Figure 7. Fourier-transform infrared spectra of oxidised chitosan (2, control, red line), the oxidised chitosan–methylene blue complex (5, blue line) and methylene blue (6, black line).

The FTIR spectra of oxidised chitosan and the oxidised chitosan–methylene blue complex almost coincide (Figure 7). The intensity of the absorption band at 1711 cm^{-1} of the aldehyde group decreases slightly in the complex. It is possible that methylene blue attaches to oxidised chitosan through the free electron pairs of the sulfur atom of the thiazine ring. The formation of such a complex is confirmed in its spectrum by the shift of two absorption bands toward longer wavelengths: N–H bending shifts from 1538 to 1544 cm^{-1} and C–H bending shifts from 1403 to 1405 cm^{-1} . In addition, the complex shows a new absorption band at 1317 cm^{-1} , which corresponds to the vibration of the thiazine ring in methylene blue.

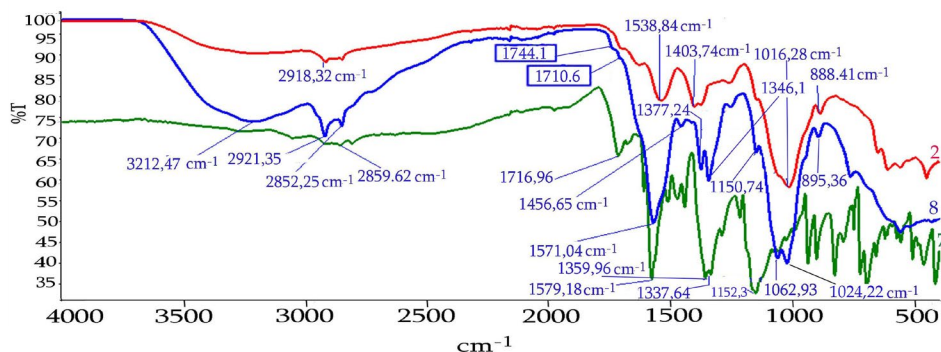


Figure 8. Fourier-transform infrared spectra of oxidised chitosan (2, control, red line), malachite green (7, grey line) and the oxidised chitosan–malachite green complex (8, blue line).

The FTIR spectrum of oxidised chitosan and the oxidised chitosan–malachite green complex are nearly identical (Figure 8). Similarly to the oxidised chitosan–methylene blue complex, the intensity of the absorption band at 1711 cm^{-1} of the aldehyde group decreases slightly. It is possible that the malachite green interacts with oxidised chitosan through the free electron pairs of a nitrogen atom.

Taken together, the technique we developed yields complexes of oxidised chitosan with specific dyes and controls the chemical composition of these complexes. It should be noted that NaIO_4 oxidation of chitosan has been reported previously. The formation of chitosan dialdehyde through NaIO_4 oxidation is particularly interesting. Other conditions of the reaction led to the crosslinking of oxidised chitosan links and an increase in the molecular mass of the formed product, which made it possible to obtain a new material for biometric application [13]. Currently, we are working on the production of chitosan-based hydrogels and ointments with antiseptic dyes to improve wound healing. In addition to such dyes, other biologically active low-molecular-weight compounds, such as the cannabimimetic *N*-stearoylethanolamine, will be conjugated with chitosan to enhance its anti-inflammatory effect [14, 15].

4. Conclusions

Based on the results, we drew the following conclusions

1. Oxidation of chitosan with NaIO_4 leads to chitosan hydrolysis. The conditions used in this paper to oxidise chitosan decreased the total mass by 30%–40% and the average molecular mass by 5.3–8 times.

2. NaIO₄-oxidised chitosan shows an increased ability to absorb dyes. The amount of bound dye per unit of chitosan mass increased 70–360 times (from 0.018%–0.09% to 3.2%–8.7%).
3. FTIR spectroscopy revealed that neither malachite green nor methylene blue bind covalently to oxidised chitosan. This was also evidenced by the release of the dyes from their complexes with chitosan under treatment with alcoholic solutions at an acidic pH.
4. FTIR spectroscopy confirmed that acid fuchsin binds covalently to oxidised chitosan through an amino group. This was evidenced by a decrease in the antimicrobial activity of this complex and the formation of insoluble conjugates (especially with CS-L). The product appears to be a mixture of covalent and non-covalent complexes.
5. The oxidised chitosan–acid fuchsin complex exerted much weaker antimicrobial activity compared with pure acid fuchsin. Thus, the amino group of acid fuchsin might be crucial for its antimicrobial effect.
6. The oxidised chitosan–methylene blue complex showed weaker antimicrobial activity compared with pure methylene blue, although the effect was not as pronounced as for acid fuchsin.
7. The oxidised chitosan–malachite green complex and pure malachite green showed similar antimicrobial activity.

5. Acknowledgements

This work was possible due to a support of Grant #2022.01/0207 awarded by the National Research Foundation of Ukraine (NRFU)

6. References

- [1] Wainwright M, Crossley KB; (2002) Methylene blue—a therapeutic dye for all seasons? *J Chemotherapy* 14(5), 431–443. DOI:10.1179/joc.2002.14.5.431
- [2] Antonyuk V, Manko N, Nektegaev I, Stoika R; (2021) Pharmacokinetics of ethacridine conjugated with chitosan in rats. *Methods Objects Chem* 16(1), 41–47. DOI:10.17721/moca.2021.41-47
- [3] Kalinkevich O, Sklyar A, Kalinkevich A, Chivanov V, Zinchenko Y, Trofimenko Y, Holubnycha V; (2021) Preparation and characterisation of new biomaterials based on chitosan iodide with biologically active dyes. *Prog Chem Appl Chitin Deriv* 26, 121–134. DOI:10.15259/PCACD.26.011
- [4] Cheung RCF, Bun Ng T, Wong JH, Chan WY; (2015) Chitosan: An update on potential biomedical and pharmaceutical applications. *Mar Drugs* 13, 5156–5186. DOI:10.3390/md13085156
- [5] Inmaculada A, Alcántara AR, Concepción CM, Concepción A, Begoña E, Heras CA, Niuris A; (2021) Chitosan: an overview of its properties and applications. *Polymers* 13(19), 3256. DOI:10.3390/polym13193256
- [6] Balabanova M, Popova L, Tchipeva R; (2003) Dyes in dermatology. *Clin Dermatol* 21(1), 2–6. DOI:10.1016/S0738-081X(01)00330-9
- [7] Sarkar R, Sinha S (Eds.); (2019) *World clinics in dermatology: fungal infections*. Jaypee Brothers Medical Publishers, New Delhi.

- [8] Bojarski B, Jurecka P, Szala L, Kondera E, Gaj-Chucher C, Stonawski B, Rombel-Bryzek A; (2023) The influence of methylene blue and malachite green on common carp (*Cyprinus carpio*) blood parameters. *Anim Genet* 19(3), 27–41. **DOI:**10.5604/01.3001.0053.8652
- [9] Yang CW, Chang YT, Hsieh CY, Chang BV; (2021) Effects of malachite green on the microbiomes of milkfish culture. *Water* 13(4), 411. **DOI:**10.3390/w13040411
- [10] Lim C, Hwang DS, Lee DW; (2021) Intermolecular interactions of chitosan: Degree of acetylation and molecular weight. *Carbohydr Polym* 259, 117782. **DOI:**10.1016/j.carbpol.2021.117782
- [11] Antonyuk V, Manko N, Panchak L, Khomyak S, Stoika R; (2022) Chitosan adduct with tranexamic acid and its hemostatic effect. *Prog Chem Appl Chitin Deriv* 27, 35–42. **DOI:**10.15259/PCACD.27.002
- [12] Sherman Hsu CP; (1997) Infrared spectroscopy. In: Settle F (ed), *Handbook of instrumental techniques for analytical chemistry*. Prentice Hall PTR, New York, 249.
- [13] Wegrzynowska-Drzymalska K, Grebicka P, Mlynarczyk DT, Chelminiak-Dudkiewicz D, Kaczmarek H, Goslinski T, Ziegler-Borowska M; (2020) Crosslinking of chitosan with dialdehyde chitosan as a new approach for biomedical applications. *Materials* 13, 3413. **DOI:**10.3390/ma13153413
- [14] Berdyshev AG, Kosiakova HV, Onopchenko OV, Panchuk RR, Stoika RS, Hula NM; (2015) *N*-Stearoyl-ethanolamine suppresses the pro-inflammatory cytokines production by inhibition of NF- κ B translocation. *Prostaglandins Other Lipid Mediat* 121, 91–96. **DOI:**10.1016/j.prostaglandins.2015.05.001
- [15] Manko N, Lootsik M, Antonyuk O, Ivasechko I, Skorokhyd N, Kosiakova H, Mehed’ O, Horid’ko T, Hula N, Klyuchivska O, Panchuk R, Pokhodylo N, Barabash O, Dumych T, Stoika R; (2024) Multifunctional chitosan-based hydrogels: characterization and evaluation of biocompatibility and biodegradability *in vitro*. *Ukr Biochem J* 96(1), 80–95. **DOI:**10.15407/ubj96.01.080

HYGIENIC PAPERS MODIFIED BY FUNCTIONAL BIOPOLYMER-BIOCIDE COMPOSITIONS IN A PILOT RESEARCH INSTALLATION

Mateusz Data¹, Danuta Ciechańska^{1,*}, Łukasz Horajski¹,
Bogumił Brycki^{1,2,a}, Maria Wiśniewska-Wrona^{3,b}, Ewa Kopania^{3,c},
Justyna Wietecha^{3,d}, Dorota Kaźmierczak^{3,e}, Jagoda Jóźwik-Pruska^{3,f}

¹ – EPICOM Sp. z o.o, Zakład Produkcyjny,
Ekologiczna 8 Str., Bogumiłów, 97-410 Kleszczów, Poland

² – Department of Bioactive Products, Faculty of Chemistry, Adam Mickiewicz University,
Uniwersytetu Poznańskiego 8 Str., 61-614 Poznań, Poland

^a – ORCID: 0000-0002-5659-9847

³ – Łukasiewicz Łódź Institute of Technology,

M. Skłodowskiej-Curie 19/27 Str., 90-570 Łódź, Poland

^b – ORCID: 0000-0001-5666-4138, ^c – ORCID: 0000-0001-5855-6878,

^d – ORCID: 0000-0003-3285-074X, ^e – ORCID: 0000-0003-4579-3414,

^f – ORCID: 0000-0003-4517-0057

*corresponding author: danuta.ciechanska@wp.pl

Abstract

*The aim of this work was to demonstrate the process of manufacturing and applying functionalising additives using a pilot research installation. As part of the optimisation evaluation, hygienic papers functionalised with biopolymer-biocide compositions based on chitosan, starch and Gemini surfactants were prepared. The microbiological properties and susceptibility to biodegradation of prototype hygienic papers (prepared in EPICOM) were assessed. In particular, the minimum amount of biopolymer and bioactive agent were determined to ensure the finished product exerted antibacterial activity against *Staphylococcus aureus*, *Bacillus subtilis* and *Escherichia coli* and was more than 90% biodegradable in a compost environment. Under optimal conditions, the hygienic paper exerted excellent antibacterial activity against *S. aureus* and *E. coli* as well as good activity against *B. subtilis*. Moreover, the hygienic paper showed more than 90% biodegradability in compost conditions within 8 weeks.*

Keywords: biodegradable, bioactive hygienic papers, Gemini surfactants, chitosan-starch functional compositions

Received: 05.04.2024

Accepted: 12.06.2024

1. Introduction

Washing hands with soap and drying them with a disposable paper towel is the method recommended by the World Health Organization (WHO) to remove germs. The present study aimed to develop an innovative hygienic paper based on an in-depth analysis of the needs and expectations of recipients/consumers, which include:

- extended functionality including hygiene (a benefit for end users);
- the possibility of recycling using generally available methods (a benefit for the target group);
- pro-ecological solutions, namely a biodegradable product produced from renewable raw materials of natural origin (a benefit for the target group);
- a solution with increased innovation that is the same price as alternative solutions (a benefit for the target group); and
- reduced consumption of raw material.

This paper discusses studies that were carried out as part of a project whose aim was to develop an innovative line of functional paper towels containing strengthening additives obtained from recycled waste and functionalising biopolymer additives that replace water-fixing resins and carry innovative hygienising substances. The innovative functional paper towels developed were enriched with reinforcing additives in the form of nano/micro cellulose fibres obtained from biotechnological treatment of cellulose waste from the production of hygienic paper using specialised enzymatic preparations and functionalising additives based on biopolymers, including chitosan and starch as a carrier of Gemini surfactants. The novel functional paper towels were assumed to have three features compared with other solutions with a similar purpose. First, they have antimicrobial properties, including the ability to inhibit the growth of *Staphylococcus aureus*, *Bacillus subtilis* and *Escherichia coli* over time. This ability would reduce the possibility transmitting microorganisms and allowing them to multiply in workplaces, restaurants, public places, shopping centres, etc., by improving the effectiveness of removing microorganisms when drying hands after washing them (increasing the level of hygiene). Second, they allow the possibility of recycling while maintaining appropriate durability parameters of the product. This ability would reduce the amount of waste in landfills, allow the reuse of materials and raw materials or their processing into new ones, lower energy consumption and expenses and thus reduce the overall burden on natural environments. Finally, they show > 90% biodegradability over a period of 10 days to 8 weeks with over 99% content of biodegradable raw materials. This ability offers a fully environmentally friendly product.

Based on previous experience of the Łukasiewicz Łódź Institute of Technology (LIT) regarding water-fixing paper, chitosan was selected as one of the components of the polymer compositions. This cationic copolymer is composed of glucosamine and *N*-acetyl-glucosamine residues connected by a β -1,4-glycosidic bond. Chitosan has a reactive amino group at C2 and primary and secondary hydroxyl groups present at C3 and C6, thanks to which it has good adsorption properties [1, 2]. The use of chitosan should contribute to the elimination or a significant reduction in the use of resins, mainly polyamide-epichlorohydrin, and thus facilitate the pulping of paper products in the recycling process in an aqueous environment. The choice of chitosan for water-fixing paper was primarily based on its good miscibility with cellulose and a molecular structure that is similar to cellulose, which favours the formation of strong hydrogen bonds and thus increases the mechanical strength of the paper. An important biological property of chitosan is its antibacterial and antifungal activity [3, 4] from its positively charged amino groups, which react with negatively charged lipopolysaccharides and proteins on the surface of microbial cells, leading to disintegration of cell membranes and damage to the bacterial cell wall. The antibacterial effect of chitosan also varies depending on its degree

of deacetylation and molecular weight. High-molecular-weight chitosan can create a polymer film on the surface of the microbial cell wall to prevent the delivery of nutrients and thus causes the death of bacterial cells. However, low-molecular-weight chitosan can penetrate cells and combine with negatively charged intracellular components [5, 6]. A carrier of innovative hygiene substances (Gemini surfactants) developed based on the selected form of chitosan in the form of polymer-biocide mixtures should demonstrate increased antimicrobial activity. Gemini are highly effective against bacteria and microscopic fungi [7, 8]. Introducing both monomeric didecylmethylammonium chloride (DDAC) and dimeric hexamethylene-1,6-bis-(*N,N*-dimethyl-*N*-dodecylammonium bromide) C6 surfactants onto the surface of the paper via coating and spraying would provide good protection against microorganisms.

2. Materials and Methods

2.1. Materials

The following chemicals were used in the experiments: chitosan characterised by a degree of deacetylation of $\geq 90\%$, solubility of $\geq 99\%$ (in 1% acetic acid), a water content of $\leq 10\%$, an ash content of $\leq 1\%$, a protein content that is not detectable, a viscosity of $< 200 \text{ mPa}\cdot\text{s}$, a heavy metal content of $< 10 \text{ ppm}$ (Chemsta, Poland); the Gemini surfactant GEMSUR 12.06 and the cationic surfactant dibromide hexamethylene-1,6-bis-(*N,N*-dimethyl-*N*-dodecylammonium) (MDA, Poland); and starch HI-CAT 3353A (Roquette Group, France).

2.2. Methods

2.2.1. Preparation of Reinforcing Additives at the Laboratory Scale

Laboratory tests on the preparation of cellulose micro/nanofibers for use as reinforcing additives employed post-production waste cellulose materials obtained in the finishing stage of the production of paper towels and toilet paper. Before the enzymatic treatment process, cellulose waste was subjected to preliminary mechanical treatment to modify the structure of the initial waste masses. During this process, the cellulose structure loosens due to internal and external fibrillation due to the breaking of hydrogen and interfibrillar bonds. The following optimal parameters for enzymatic treatment of waste cellulosic materials at the lab scale were determined: for the enzyme, 900 UCMC per gram cellulose; a 2.5% cellulose suspension; and a reaction time of 2 h [9]. Figure 1 shows a scanning electron micrograph of waste cellulosic material after the enzymatic treatment and homogenisation stages.

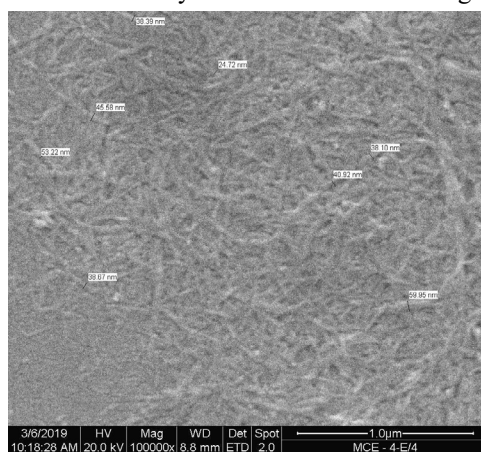


Figure 1. The scanning electron micrograph shows waste cellulosic material after the enzymatic treatment and homogenisation. The numbers indicate the dimensions of the fibres [9, 10].

2.2.2. Preparation of Reinforcing Additives at the Pilot Research Installation

Tests on the production of strengthening additives were carried out based on process assumptions developed under laboratory conditions. Grinding was carried out in a flow device with an actuating element design similar to the grinding head used during the development of the technology under laboratory conditions [9]. The pilot research installation comprised five stages [11].

- Stage I – defibration of production waste generated in the production of toilet paper in a centrifugal pulper. The process parameters were: water volume 700 dm³, paper weight 37 kg, concentration 5.5% and defibration time 15 min.
- Stage II – grinding the paper pulp obtained in Stage I using a centrifugal pulper, a pump transporting the pulp and a mill operating in a closed circuit with full circulation of the pulp. The process parameters were: grinding time 90 min and concentration 4%.
- Stage III – dilution and transport of mass to the enzymatic treatment reactor. The process was carried out using a pump transporting paper pulp and a water supply system. The process parameters were: input concentration 4% and final concentration 2.5%.
- Stage IV : enzymatic treatment of paper pulp in the reactor. The process parameters were: paper pulp concentration 2.5%, dry matter amount 37 kg, pulp volume 1480 dm³, amount of enzyme prepare 0.89 dm³ and enzymatic treatment time 120 min.
- Stage V – dilution and homogenisation using a tank with a mixer and a homogeniser with continuous mixing. The process parameters were: flow through the homogeniser 200 dm³/h and fibre share in the composition 1.25%.

2.2.3. Preparation of Functionalising Additives in Real Conditions

The process to prepare functionalising compositions was developed based on guidelines developed during laboratory work [12]. It comprised four stages [11, 13].

- Stage I – dissolving chitosan in a lactic acid solution using a tank with a mixer, an industrial homogeniser and a circulation pump. The process parameters were: concentration of lactic acid solution 0.45%, amount of solution 80 dm³, chitosan share 2.4%, dissolution process time 20 min and deaeration time 15 min.
- Stage II – preparation of an aqueous starch solution using a tank with a mixer, an industrial homogeniser and a circulation pump. The process parameters were: water volume 80 dm³, starch content 1.2% and process time 20 min.
- Stage III – combining the chitosan solution with the starch solution using two tanks with mixers, a homogeniser and a circulation pump. The process parameters were: process time 20 min, final volume 160 dm³, final percentage of chitosan 1.2% and final percentage of starch 0.6%.
- Stage IV – introducing the Gemini surfactant into the composition using a tank with a mixer, homogeniser and circulation pump. The process parameters were: Gemini surfactant volume 1 dm³, Gemini surfactant concentration 0.6%, final volume 161 dm³, final percentage of chitosan 1.2% and final percentage of starch 0.6%.

2.2.4. Applying Separate Functionalising and Reinforcing Compositions to the Paper Web

Attempts to apply strengthening and functionalising compositions were made using a system of two separate spray collectors. The reinforcing additives were sprayed using

a system powered by peristaltic pumps and a system of rotary nozzles. The composition of functionalising additives was sprayed using flat-jet nozzles. The tests were carried out in the range of linear web speed from 100 to 150 m/min. The process parameters were: share of the composition of functionalising additives 60%, share of the composition of reinforcing additives 40%, spraying efficiency 144 dm³/h, efficiency of spraying functionalising additives 48–64 dm³/h and efficiency of spraying additives strengthening 52.8–74.4 dm³/h [11].

2.2.5. Analytical Methods

Antibacterial activity of the functional hygiene paper samples was assessed at the Accredited Laboratory of Biodegradation and Microbiological Research of Łukasiewicz – ŁIT. The antibacterial activity tests used *E. coli*, *S. aureus* and *B. subtilis*. Specifically, antibacterial activity against *E. coli* ATCC 11229 and *S. aureus* ATCC 6538 were carried out in accordance with PN-EN ISO 20743:2013 by counting on plates [14]. The criteria for assessing antibacterial activity are presented in Annex F of PN-EN ISO 20743:2013. The antibacterial activity against *B. subtilis* ATCC 6633 was tested using the parallel streak method in accordance AATCC Test Method 147:2011.

Biodegradation of the hygienic paper samples was assessed at the Accredited Laboratory of Biodegradation and Microbiological Research of Łukasiewicz – ŁIT. The tests were carried out in accordance with Procedure No. 2 (V Edition of 4 June 2018), ‘Determination of the degree of degradation of plastics and textile products in simulated composting conditions on a laboratory scale. Method for determining mass loss’ based on the following standards: PN-EN 14045:2012, PN-EN 14806:2010 and PN-EN ISO 20200:2016-01.

3. Results and Discussion

The technological tests regarding the production of functional hygienic papers were carried out in real conditions, including development related to optimisation of the scale to semi-technical and technical scale and integrating the application of reinforcing additives, and integrated reinforcing and functionalising compositions. The technological tests aimed at verifying the technological assumptions of the functional paper production process in real conditions using prototype modular devices integrated with a pilot research installation. Tests were carried out using a system with two separate spray collectors. The reinforcing additives were sprayed using a system powered by peristaltic pumps and a system of rotary nozzles. The functionalising additives were sprayed using flat-jet nozzles. Based on the results of previous tests, the only technological parameter that changed was the share of the active substance relative to the mass of the product. During the tests, different linear speeds of the paper ribbon were used to collect information that could to optimise the process technically and economically. The tests were carried out in the range of linear web speed from 100 to 150 m/min. During optimisation, a series of hygienic papers functionalised with biopolymer-biocide compositions based on chitosan, starch and Gemini surfactants were prepared, and the parameters for the production of papers functionalised with biopolymer compositions with expected functional properties were developed [12, 15, 16]. Based on previous experience, three paper samples were selected. Table 1 presents their technological parameters. The share of the active substance used, relative to the weight of the paper produced, was 0.5%, 0.6% and 0.69%. These samples were subjected to assays to assess antimicrobial activity and biodegradability.

Table 1. Technological parameters of hygienic papers modified with reinforcing and functionalising compositions.

Sample symbol	Additives [%]	Nozzle performance [dm ³ /h]	Spraying efficiency [dm ³ /h]	Linear speed of paper web [m/min]	Thickness of sprayed layer [mm]	Percentage of composition [%]	Active substance in composition [%]	Active substance in paper [%]
K2/1	40 Reinforcing	22	52.8	150	0.002560	8.26	6.00	0.50
	60 Functional	12	48.0		0.002608			
K2/2	40 Reinforcing	26	62.4	125	0.003438	11.09	5.40	0.60
	60 Functional	13	52.0		0.002287			
K2/3	40 Reinforcing	31	74.4	100	0.004099	13.22	5.20	0.69
	60 Functional	15	60.0		0.001711			

3.1. Antibacterial Activity Against *S. aureus* and *E. coli*

A specific number of bacteria was applied to the test and control samples. After incubation for 24 h, the change in the number of bacteria on the test and control samples was assessed, and the antibacterial effect was calculated. There were three replicates for each control (paper towel without additives) and test sample (0.4 ± 0.05 g) for each incubation time. The prepared bacterial suspension with a density of 10⁵ cells/mL was inoculated into previously sterilised control and test samples (0.2 ml per 0.4 g of sample; six replicates for each test sample and six replicates for the control sample). Three replicates of each sample were washed immediately, and three replicates of each sample were incubated at 37 ± 1°C for 24 h. After incubation, the bacteria were washed off by shaking in a neutralising Soya Casein Digest Lecithin Polysorbate (SCDLP) Broth solution. Appropriate dilutions were made from the obtained suspension in saline containing peptone. Each dilution was sub-cultured onto Plate Count Agar. The antimicrobial activity of the hygienic papers against *S. aureus* ATCC 6538 and *E. coli* ATCC 11229 are presented in Tables 2–4. The hygienic papers exhibited strong antibacterial activity against both strains.

3.2. Antibacterial Activity Against *B. subtilis*

The test samples were placed linearly on test plates with agar medium inoculated with a bacterial suspension. A paper towel sample with an active agent was used as an active control. A sample without antibacterial additive was used as an inactive control. The samples were incubated at 37°C for 24 h. After incubation, bacterial growth was assessed. A lack of growth under the sample and along the sides of the sample indicates that the sample has a bacteriostatic effect. A paper towel sample with an active agent was used as an active control. A sample without antibacterial additive was used as an inactive

control. Table 5 presents the antimicrobial activity of the hygienic papers against *B. subtilis* ATCC 6633. The hygienic papers exhibited a good antibacterial effect against this strain.

3.3. Biodegradability of the Hygienic Papers in a Compost Environment

The hygienic paper samples were placed in aerobic compost conditions at $58 \pm 2^\circ\text{C}$. The biodegradability was assessed after 4, 6, 8, 10, 12 and 16 weeks based on sample weight loss. The results are presented in Table 6.

Table 2. Assessment of the antibacterial activity of the hygienic paper samples against *Staphylococcus aureus* ATCC 6538.

Evaluated parameter	Requirement	Test results	Study evaluation						
Control sample (without additives)									
Inoculum concentration	$1-3 \times 10^5$ [CFU/ml]	1.6×10^5 [CFU/ml]	Fulfil condition						
Extreme difference in the logarithm of the number of bacteria on the control sample at time 0 and after incubation ($\log C_{\max} - \log C_{\min}$)	$\log < 1$	<table border="1" style="width: 100%;"> <tr> <td style="text-align: center;">Contact time 0 h</td> <td style="text-align: center;">Contact time 18–24 h</td> </tr> <tr> <td style="text-align: center;">$\log C_{0\min} = 4.45$</td> <td style="text-align: center;">$\log C_{T\min} = 6.29$</td> </tr> <tr> <td style="text-align: center;">$\log C_{0\max} = 4.60$</td> <td style="text-align: center;">$\log C_{T\max} = 6.48$</td> </tr> </table>	Contact time 0 h	Contact time 18–24 h	$\log C_{0\min} = 4.45$	$\log C_{T\min} = 6.29$	$\log C_{0\max} = 4.60$	$\log C_{T\max} = 6.48$	-
		Contact time 0 h	Contact time 18–24 h						
$\log C_{0\min} = 4.45$	$\log C_{T\min} = 6.29$								
$\log C_{0\max} = 4.60$	$\log C_{T\max} = 6.48$								
		0.15	0.19						
Growth value for control sample	$\log C_t - \log C_0 = F \geq 1$	1.91	Fulfil condition						
Sample K2/1									
Extreme difference in the logarithm from the number of bacteria on the test sample at time 0 and after incubation ($\log T_{\max} - \log T_{\min}$)	$\log < 2$	<table border="1" style="width: 100%;"> <tr> <td style="text-align: center;">$\log T_{0\min} = 1.3$</td> <td style="text-align: center;">$\log T_{T\min} = 1.3$</td> </tr> <tr> <td style="text-align: center;">$\log T_{0\max} = 1.3$</td> <td style="text-align: center;">$\log T_{T\max} = 1.3$</td> </tr> </table>	$\log T_{0\min} = 1.3$	$\log T_{T\min} = 1.3$	$\log T_{0\max} = 1.3$	$\log T_{T\max} = 1.3$	Fulfil condition		
		$\log T_{0\min} = 1.3$	$\log T_{T\min} = 1.3$						
$\log T_{0\max} = 1.3$	$\log T_{T\max} = 1.3$								
		0.0	0.0						
Growth value for the tested sample	$\log T_t - \log T_0 = G$	0.0	Fulfil condition						

Table 2. (continued) Assessment of the antibacterial activity of the hygienic paper samples against *Staphylococcus aureus* ATCC 6538.

Evaluated parameter	Requirement	Test results		Study evaluation
Sample K2/2				
Extreme difference in the logarithm from the number of bacteria on the test sample at time 0 and after incubation ($\log T_{\max} - \log T_{\min}$)	$\log < 2$	$\log T_{0\min} = 1.3$	$\log T_{T\min} = 1.3$	Fulfil condition
		$\log T_{0\max} = 1.3$	$\log T_{T\max} = 1.3$	
Growth value for the test sample	$\log T_t - \log T_0 = G$	0.0		Fulfil condition
Sample K2/3				
Extreme difference in the logarithm from the number of bacteria on the test sample at time 0 and after incubation ($\log T_{\max} - \log T_{\min}$)	$\log < 2$	$\log T_{0\min} = 1.3$	$\log T_{T\min} = 1.3$	Fulfil condition
		$\log T_{0\max} = 1.3$	$\log T_{T\max} = 1.3$	
Growth value for the test sample	$\log T_t - \log T_0 = G$	0.0		Fulfil condition

Table 3. Assessment of the antibacterial activity of the hygienic paper samples against *Escherichia coli* ATCC 11229.

Evaluated parameter	Requirement	Test results		Study evaluation
Control sample (without additives)				
Inoculum concentration	$1-3 \times 10^5$ [CFU/ml]	2.6×10^5 [CFU/ml]		Fulfil condition
Extreme difference in the logarithm of the number of bacteria on the control sample at time 0 and after incubation ($\log C_{\max} - \log C_{\min}$)	$\log < 1$	Contact time 0 h		-
		$\log C_{0\min} = 4.03$	$\log C_{T\min} = 5.99$	
		$\log C_{0\max} = 4.07$	$\log C_{T\max} = 6.22$	0.23
Growth value for the control sample	$\log C_t - \log C_0 = F \geq 1$	2.02		Fulfil condition
Sample K2/1				
Extreme difference in the logarithm from the number of bacteria on the test sample at time 0 and after incubation ($\log T_{\max} - \log T_{\min}$)	$\log < 2$	0.0		Fulfil condition
		$\log T_{0\min} = 1.3$	$\log T_{T\min} = 1.3$	
		$\log T_{0\max} = 1.3$	$\log T_{T\max} = 1.3$	0.0
Growth value for the test sample	$\log T_t - \log T_0 = G$	0.0		Fulfil condition

Table 3. (continued) Assessment of the antibacterial activity of the hygienic paper samples against *Escherichia coli* ATCC 11229.

Evaluated parameter	Requirement	Test results				Study evaluation
Sample K2/2						
Extreme difference in the logarithm from the number of bacteria on the test sample at time 0 and after incubation ($\log T_{\max} - \log T_{\min}$)	$\log < 2$	$\log T_{0\min} = 1.3$	0.0	$\log T_{T\min} = 1.3$	0.0	Fulflis condition
		$\log T_{0\max} = 1.3$		$\log T_{T\max} = 1.3$		
Growth value for the test sample	$\log T_t - \log T_0 = G$	0.0				Fulflis condition
Sample K2/3						
Extreme difference in the logarithm from the number of bacteria on the test sample at time 0 and after incubation ($\log T_{\max} - \log T_{\min}$)	$\log < 2$	$\log T_{0\min} = 1.3$	0.0	$\log T_{T\min} = 1.3$	0.0	Fulflis condition
		$\log T_{0\max} = 1.3$		$\log T_{T\max} = 1.3$		
Growth value for the test sample	$\log T_t - \log T_0 = G$	0.0				Fulflis condition

Table 4. Antibacterial activity of the hygienic paper samples against *Staphylococcus aureus* ATCC 6538 and *Escherichia coli* ATCC 11229.

Sample	Incubation time [h]	Number of bacteria [CFU/g]	Antibacterial activity of A*	Growth value
<i>Staphylococcus aureus</i> ATCC 6538				
Control	0	3.3×10^4	-	1.91
	24	2.6×10^6		
K2/1	0	< 20	5.1	0.0
	24	< 20		
K2/2	0	< 20	5.1	0.0
	24	< 20		
K2/3	0	< 20	5.1	0.0
	24	< 20		
<i>Escherichia coli</i> ATCC 11229				
Control	0	1.1×10^4	-	2.02
	24	1.2×10^6		
K2/1	0	< 20	4.8	0.0
	24	< 20		
K2/2	0	< 20	4.8	0.0
	24	< 20		
K2/3	0	< 20	4.8	0.0
	24	< 20		

* Effectiveness of antibacterial properties
 Significant
 Strong

Value of antibacterial activity
 $2 \leq A < 3$
 $A \geq 3$

Table 5. Antibacterial activity of the hygienic paper samples against *Bacillus subtilis* ATCC 6633.

Sample	Growth intensity under the sample	Zone of inhibition [mm]	Study evaluation	
Inactive control (tissue sample)	Good	No zone	No antibacterial effect	
Active control (sample of tissue paper with an active agent)	Lack of growth	Average of 8.3	Antibacterial effect	
	K2/1	Pattern	No growth	Good antibacterial effect
		Pattern	No growth	
		Pattern	No growth	
	Dots	Dots	No growth	Good antibacterial effect
		Dots	No growth	
Dots		No growth		
K2/2	Pattern	No growth	Good antibacterial effect	
	Pattern	No growth		
	Pattern	No growth		
	Dots	No growth		
	Dots	No growth		
	Dots	No growth		
K2/3	Pattern	No growth	Good antibacterial effect	
	Pattern	No growth		
	Pattern	No growth		
	Dots	No growth		
	Dots	No growth		
	Dots	No growth		

Table 6. Susceptibility of the modified hygienic paper samples to biodegradation in compost.

	Replicate	Biodegradation time, week [days]				
		4 [28]	6 [42]	7 [49]	8 [56]	9 [63]
K2/1		Weight loss [%]				
	1	46.7	65.6	86.7	96.6	100
	2	21.6	63.1	82.3	78.9	100
	3	34.9	71.7	97.4	100	-
		Average sample weight loss after 8 weeks: 92% Final average sample weight loss after 9 weeks: 100%				
K2/2		Biodegradation time, week [days]				
	1 [7]	4 [28]	8 [56]	12 [84]	16 [112]	
		Weight loss [%]				
	1	5.04	45.0	84.3	79.0	87.0
2	3.49	74.6	75.0	86.5	88.5	
3	1.22	32.1	74.6	83.6	76.5	
		Average sample weight loss after 8 weeks: 78% Final average sample weight loss after 16 weeks: 84%				
K2/3		Biodegradation time, week [days]				
	1 [7]	4 [28]	8 [56]	12 [84]	16 [112]	
		Weight loss [%]				
	1	1.49	30.2	71.2	77.9	91.5
2	1.04	35.0	72.1	85.0	84.4	
3	1.75	30.9	79.2	79.6	82.9	
		Average sample weight loss after 8 weeks: 74% Final average sample weight loss after 16 weeks: 86%				

4. Conclusions

Under optimal conditions, the modified hygienic papers produced at a pilot research installation presented substantial antibacterial activity against *S. aureus* (activity = 5.1, growth value = 0.0) and *E. coli* (activity = 4.8, growth value = 0.0) and good antibacterial activity against *Bacillus subtilis* (zone of inhibition of bacterial growth = 4.7–5.4 mm). Moreover, in compost conditions, > 90% of the samples had degraded within 8 weeks. The possibility of recycling cellulose fibres from production waste as a substitute for water-setting resins in towel paper is important from the point of view of implementing the goals of a circular economy.

5. Acknowledgements

This research was financially supported by the European Regional Development Fund, Smart Growth Operational Program for 2014–2020, sub-measure 1.1.1 'Industrial research and development works carried out by enterprises' for the implementation of the project 'Development of an innovative product line of functional towel papers containing own reinforcing additives obtained from recycled waste and biopolymer functional additives replacing water-setting resins and constituting a carrier of innovative hygienic substances - Gemini surfactants' (POIR.01.01.01-00-1199/17-00).

6. References

- [1] Mucha M; (2010) Chitozan wszechstronny polimer ze źródeł odnawialnych. Wydawnictwo Naukowo-Techniczne, Warszawa.
- [2] Rinaudo M; (2008) Main properties and current applications of some polysaccharides as biomaterials. *Polym Int* 57(3), 397–430. DOI:10.1002/pi.2378
- [3] Sikorski D, Bauer M, Frączyk J, Draczyński Z; (2022) Antibacterial and antifungal properties of modified chitosan nonwovens. *Polymers* 14(9), 1690. DOI:10.3390/polym14091690
- [4] Xing Y, Wang X, Guo X, Yang P, Yu J, Shui Y, Chen C, Li X, Xu Q, Xu L, Bi X, Liu X; (2021) Comparison of antimicrobial activity of chitosan nanoparticles against bacteria and fungi. *Coatings* 11(7), 769. DOI:10.3390/coatings11070769
- [5] Tsai GJ, Su WH; (1999) Antibacterial activity of shrimp chitosan against *Escherichia coli*. *J Food Prot* 62(3) 239–243. DOI:10.4315/0362-028x-62.3.239
- [6] Kim J-S, Shin D-H; (2013) Inhibitory effect on *Streptococcus mutans* and mechanical properties of the chitosan containing composite resin. *Restor Dent Endod* 38(1) 36–42. DOI:10.5395/rde.2013.38.1.36
- [7] Koziróg A, Brycki B; (2015) Monomeric and gemini surfactants as antimicrobial agents - influence on environmental and reference strains. *Acta Biochim Pol* 62, 879–883. DOI:10.18388/abp.2015_1150
- [8] Koziróg A, Brycki B, Olejnik K, Wysocka-Robak A, Dębska-Winkler P; (2019) Cellulose products modified with monomeric and gemini surfactants: antimicrobial aspects. *Cellulose* 26, 5559–5570. DOI:10.1007/s10570-019-02475-0
- [9] Wietecha J, Kopania E; (2019) Report R+D: Opracowanie technologii otrzymywania mikro/nanowłókien celulozowych do zastosowania jako dodatki wzmacniające papiery tissue na etapie konfekcjonowania. POIR.01.01.01-00-1199/17. Łukasiewicz Łódzki Instytut Technologiczny, Łódź.

- [10] Data M, Ciechańska D, Brycki B, Horajski Ł, Wiktorowska M, Kopania E, Wietecha J, Wiśniewska-Wrona M, Kaźmierczak D, Jóźwik-Pruska J; (2022) Biopolimerowe kompozycje funkcjonalno-wzmacniające do papierów ręcznikowych. XX Międzynarodowa Konferencja i Wystawa Papiernicza. Papier w Biogospodarce PROGRESS 2022, Łódź.
- [11] Data M, Horajski Ł; (2022) Report: Próby technologiczne wytwarzania funkcjonalnych papierów higienicznych w warunkach rzeczywistych. EPICOM, Poland.
- [12] Sikora M, Piekarska K, Wiśniewska-Wrona M; (202) Report R+D: Opracowanie technologii otrzymywania mieszanek polimerowo-biocydowych z wykorzystaniem form użytkowych polisacharydów. POIR.01.01.01-00-1199/17. Łukasiewicz Łódzki Instytut Technologiczny, Łódź.
- [13] Data M, Ciechańska D, Horajski Ł, Brycki B, Wiśniewska-Wrona M, Wietecha J, Kaźmierczaka D, Jóźwik-Pruska J; (2023) Hygienic papers modified with the addition of functional biopolymer-biocide compositions produced on a pilot research installation. Proceedings of XXVIII Conference of the Polish Chitin Society 'New Aspects on Chemistry and Application of Chitin and ITS Derivatives', Gdańsk, Poland.
- [14] PN-EN ISO 20743:2013: Tekstylnia. Wyznaczanie aktywności antybakteryjnej wyrobów włókienniczych. Metoda absorpcyjna oznaczana metodą liczenia na płytkach.
- [15] Data M, Horajski Ł, Ciechańska D, Brycki B, Kukuczka Sz, Wiktorowska M; (2023) Biofunkcjonalne papiery ręcznikowe na bazie biopolimerów wytwarzane w warunkach przemysłowych. VII Ogólnopolska Konferencja Naukowa 'BIOPOLIMER. Źródło Nowych Materiałów', Lublin, Poland.
- [16] Patent Application P.442314; (2022) Kompozycja wzmacniająco-funkcjonalizująca i jej sposób nanoszenia oraz sposób wytwarzania kompozycji wzmacniającej.

STUDY OF THE KINETICS OF COPPER ION SORPTION BY CHITOSAN SPHERES

Joanna Dziezic¹, Dorota Biniś^{1,a,*}, Włodzimierz Biniś^{1,b}

¹ – Civil and Environmental Engineering, Faculty of Materials, University of Bielsko-Biala, Willowa 2 Str., 43-309 Bielsko-Biala, Poland

^a – ORCID: 0000-0002-2548-1774, ^b – ORCID: 0000-0002-7260-7739

*corresponding author: dbinias@ubb.edu.pl

Abstract

Chitosan, a polysaccharide derived from chitin, has adsorption capacity, particularly towards heavy metal ions. The aim of this study was to produce chitosan spheres with and without CCP 90 activated carbon and then to evaluate their adsorption ability and kinetics using an aqueous copper(II) solution. The research was conducted using ultraviolet–visible spectrophotometry, examining the surface morphology of the obtained spheres after copper ion (Cu^{2+}) adsorption, along with elemental analysis with an energy dispersive spectrometric probe. The results confirmed an increase in the adsorption of Cu^{2+} on chitosan spheres with CCP 90 activated carbon.

Keywords: chitosan, sorption, hydrogel spheres, UV–Vis

Received: 12.03.2024

Accepted: 20.06.2024

1. Introduction

Industrial waste and sewage pose a threat to the natural environment and living organisms, which necessitates the need to limit their negative impact through effective utilisation or complete neutralisation. Industrial sewage may contain environmentally harmful compounds such as metal ions, including nickel(II), copper(II), lead(II), chromium(III), cadmium(II) and organic substances such as pesticides or dyes. These compounds can be removed using chitosan or modified forms of chitosan [1–10]. Chitosan is a copolymer produced by the deacetylation of chitin, consisting of randomly distributed β -(1 \rightarrow 4)-D-glucosamine and *N*-acetyl-D-glucosamine. It can be used as an adsorbent in engineering and environmental protection. The currently used wastewater treatment methods include mineralisation [11], flotation [12], ion exchange [13], catalysis and photocatalysis [14–17] and adsorption [18, 19]. Adsorption is considered one of the most effective and economical methods of removing metal ion contaminants from watercourse systems. When chitosan is used, its adsorption efficiency is increased by mixing it with various materials – perlite [20], zeolites [21], cellulose [22], diatomaceous earth [23], titanium dioxide [24] and montmorillonite [25], among others. The production of fertilisers, paints and pigments as well as galvanisation processes produce waste containing copper ions (Cu^{2+}), which are harmful to the natural environment. This study aimed to modify chitosan with CCP 90 activated carbon, to produce chitosan hydrogel spheres and evaluate the ability of these spheres to adsorb copper(II) sulfate (CuSO_4).

2. Materials and methods

2.1. Materials

The following reagents were used to produce hydrogel spheres: commercial chitosan ($\text{C}_6\text{H}_{11}\text{NO}_4$)_n (CAS number 9012-76-4) with a deacetylation degree of 90% procured from POL-AURA (Poland); acetic acid (CH_3COOH) and sodium hydroxide (NaOH) obtained from Chempur (Poland); and activated carbon, namely Carbopal CCP 90 from Donauchem (Poland) obtained from carbonisation of coconut shells. The ion adsorption tests used $\text{CuSO}_4 \cdot 5\text{H}_2\text{O}$ from Avantor Performance Materials Poland S.A. (Poland), from which a 1% solution was prepared. All other materials used were of analytical grade.

2.2. Methods

2.2.1. Preparation of Chitosan Hydrogel Spheres

Chitosan hydrogel spheres without and with the addition of 5% and 10% CCP 90 activated carbon were obtained from a 3% chitosan solution prepared in 2% acetic acid. The percentage of activated carbon added was based on the weight of the applied chitosan.

The prepared solutions were placed in a syringe and added to a 10% NaOH solution, which constituted a coagulation bath, using an infusion pump. A mechanical stirrer was used to enhance gelation of the obtained chitosan spheres and to prevent the spheres from sticking to each other. The resulting spheres were rinsed several times with distilled water until a neutral pH was obtained. Figure 1 presents photographs of the obtained chitosan hydrogel spheres. Figure 2 presents photographs of the obtained chitosan spheres after drying at room temperature.

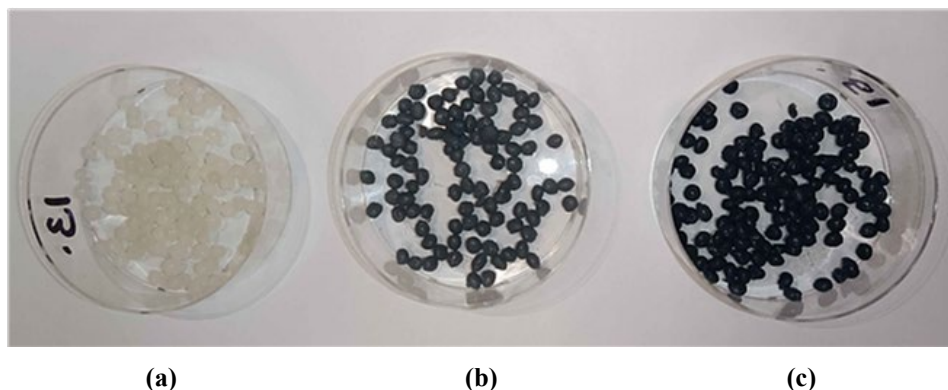


Figure 1. The photographs of chitosan spheres prepared from (a) 3% chitosan solution, (b) 3% chitosan solution with the addition of 5% activated carbon CCP 90, and (c) 3% chitosan solution with the addition of 10% activated carbon CCP 90.

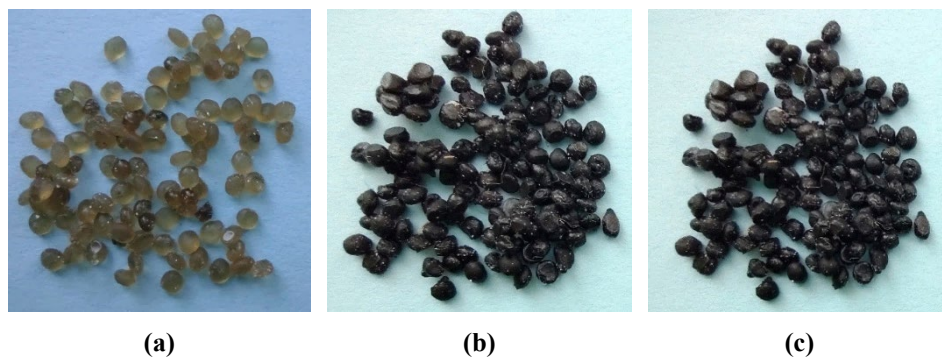


Figure 2. The photographs of chitosan spheres after drying at room temperature. They were prepared from (a) 3% chitosan solution, (b) 3% chitosan solution with the addition of 5% activated carbon CCP 90, and (c) 3% chitosan solution with the addition of 10% activated carbon CCP 90.

2.2.2. Investigation of the Adsorption Properties of the Obtained Chitosan Hydrogel Spheres

The adsorption properties of chitosan hydrogel spheres were tested using a CuSO_4 solution (prepared from 1 g of CuSO_4 in a volume of 100 cm^3). Approximately 2 g of wet chitosan spheres were placed in the beaker and 5 cm^3 of the CuSO_4 solution was added. The tests were carried out at neutral pH. Samples for testing were taken at 1, 2, 5, 10, 30, 60, and 120 min.

2.2.3. Analytical Methods

2.2.3.1. Ultraviolet–Visible Spectrometry

An Evolution™ 300 ultraviolet–visible (UV–Vis) spectrophotometer (Thermo Scientific, USA) was used to measure chitin suspensions in aqueous solutions obtained after the sonication steps. The absorbance was measured in the range of 625–850 nm. The blank was distilled water. The VISION pro™ software (Thermo Scientific, USA) was used to process the spectra.

2.2.3.2. Analysis of Morphology and Elements

A Phenom ProX scanning electron microscope (AM Eindhoven, the Netherlands) with a fully integrated energy dispersive X-ray spectroscopy (EDS) detector and software were used to assess morphology. The distribution of the different elements in the chitosan spheres was evaluated with the element identification (EID) software package and a specially designed and fully integrated energy dispersive spectrometer.

2.2.3.3. Optical Microscopy

The dimensions of the chitosan hydrogel spheres after adsorption were analysed using an optical microscope (Reichert, Austria) equipped with an ARTCAM CCD camera (Olympus, Japan), controlled by the Images Plus 2.0 software (Motic, China).

3. Results and Discussion

Quantitative calculations of the Cu^{2+} adsorption process were conducted based on data extracted from UV–Vis absorption spectra at the characteristic points of the local absorption band maxima, considering background scattering (Figure 3). The absorption value A was determined for the CuSO_4 solution at 820 nm. According to the Beer–Lambert law, the absorption value is directly proportional to the concentration of the solution. For a solution prepared from 1 g of CuSO_4 in 100 cm^3 , the A value was 0.5397, which was the starting value to assess Cu^{2+} adsorption from the CuSO_4 standard solution and the solutions after adsorption on chitosan hydrogel spheres without the addition of carbon for 1, 2, 5, 10, 30, 60 and 120 min. The spectra appeared similar when using chitosan hydrogel spheres containing 5% or 10% CCP 90 activated carbon.

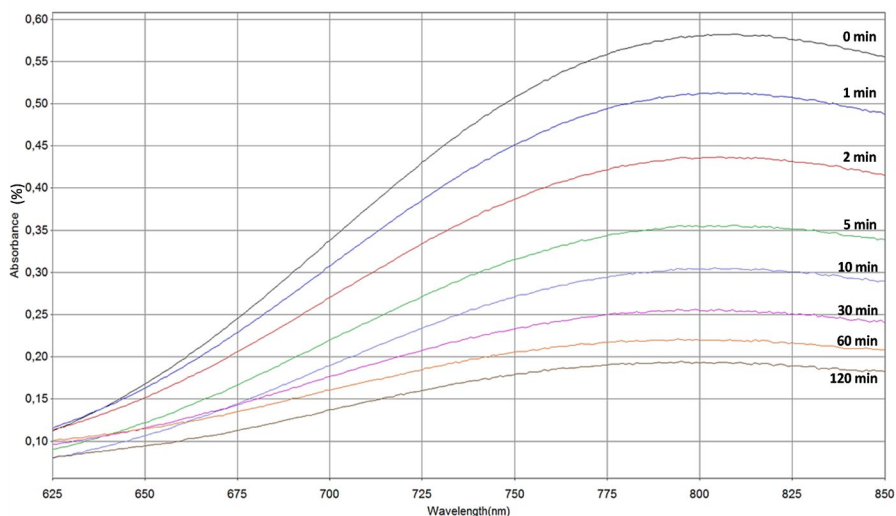


Figure 3. Ultraviolet–visible spectra (625–850 nm) for the standard copper sulfate solution and the solutions after adsorption on chitosan hydrogel spheres without CCP 90 activated carbon for 1, 2, 5, 10, 30, 60 and 120 min.

The adsorption isotherms of Cu^{2+} on chitosan spheres (Figure 4), precipitated in gel form with a significant water content, follow a course similar to the absorption patterns described in the literature [26–28].

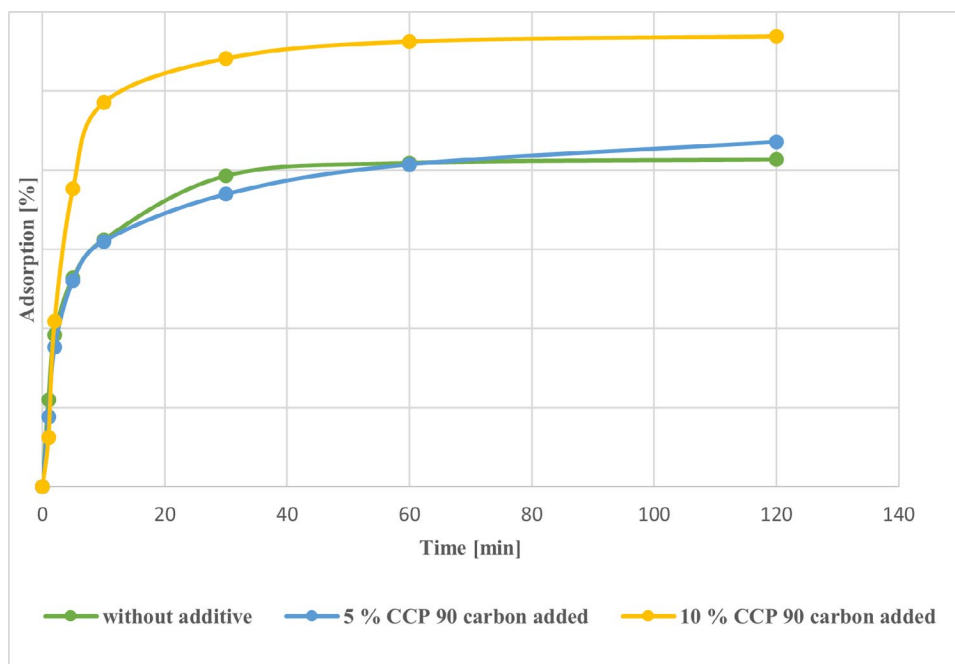


Figure 4. The course of the adsorption process of copper(II) ions for the obtained chitosan hydrogel spheres.

The adsorption value increases proportionally during the adsorption process. As time progresses, its value stabilises, indicating an equilibrium between adsorption and desorption. The adsorbent surface is saturated with the adsorbate layer and the adsorption curve is parallel to the time axis.

The fast speed of the process at the beginning of the process may be the result of strong swelling of chitosan. Interestingly, the addition of 5% activated carbon CCP 90 in the form of micropowder (60–70 μm) did not impact the process. This is probably due to the strong interaction between the ingredients and partial mutual absorption. However, the addition of 10% CCP 90 activated carbon significantly altered the course of absorption, leading to intensification. With the higher amount of activated carbon, there are additional active centres for the adsorption of Cu^{2+} . The tested chitosan hydrogel spheres presented type I isotherms, also known as the Langmuir isotherm, which is characteristic of microporous adsorbents.

Figure 5 shows scanning electron micrographs at different magnifications of the surface of the spheres obtained from a 3% chitosan solution after adsorption of Cu^{2+} , taken at different magnifications. Figure 6 shows the results of EDS analysis of chitosan hydrogel spheres without CCP 90 activated carbon after adsorption of Cu^{2+} . The main identified elements in the tested sample of chitosan sphere after adsorption of copper Cu^{2+} are oxygen (O), carbon (C), nitrogen (N), Cu and sulfur (S) (Table 1).

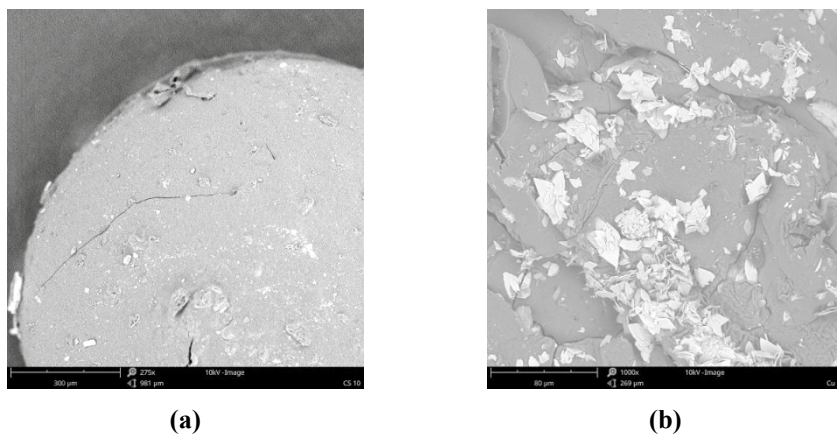


Figure 5. Scanning electron micrographs of the surface of spheres obtained from a 3% chitosan solution after adsorption of copper(II) ions without CCP 90 activated carbon at (a) 275× and (b) 1000× magnification.

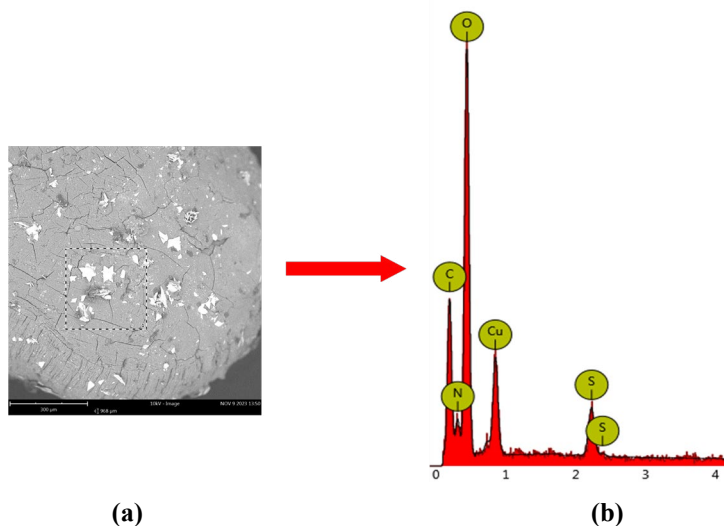


Figure 6. (a) Scanning electron micrograph of the surface of the chitosan spheres without CCP 90 activated carbon; the dashed line shows the scanning path of the energy dispersive X-ray spectroscopy (EDS) probe. (b) EDS analysis of the particles.

Table 1. Energy dispersive X-ray spectroscopy analysis of the chitosan spheres without CCP 90 activated carbon.

Element	Atomic percent [%] in the sample
Oxygen (O)	45.87
Carbon (C)	35.21
Nitrogen (N)	12.60
Copper (Cu)	4.38
Sulfur (S)	1.94

Figure 7 presents scanning electron micrographs of the surface of spheres obtained from a 3% chitosan solution with the addition of 5% CCP 90 activated carbon after adsorption of Cu^{2+} . The results of the EDS analysis are presented in Figure 8 and Table 2. The main identified elements in the tested sample are C, O, N, Cu and S.

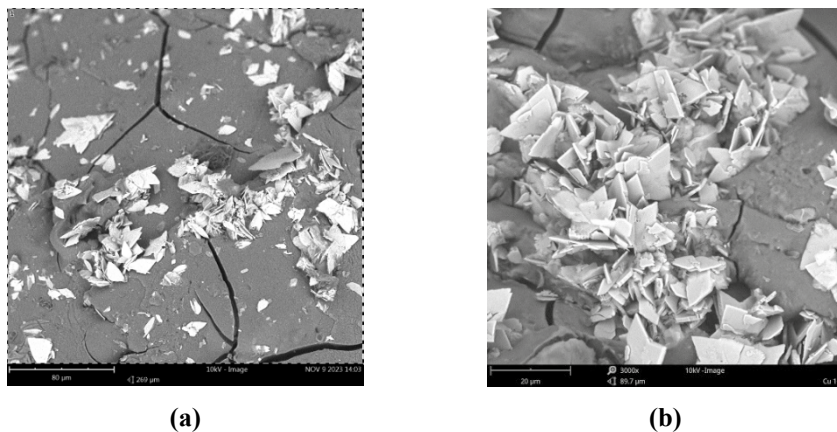


Figure 7. Scanning electron micrographs of the surface of spheres obtained from a 3% chitosan solution with the addition of 5% CCP 90 activated carbon after adsorption of copper(II) ions at (a) 269× and (b) 3000× magnification.

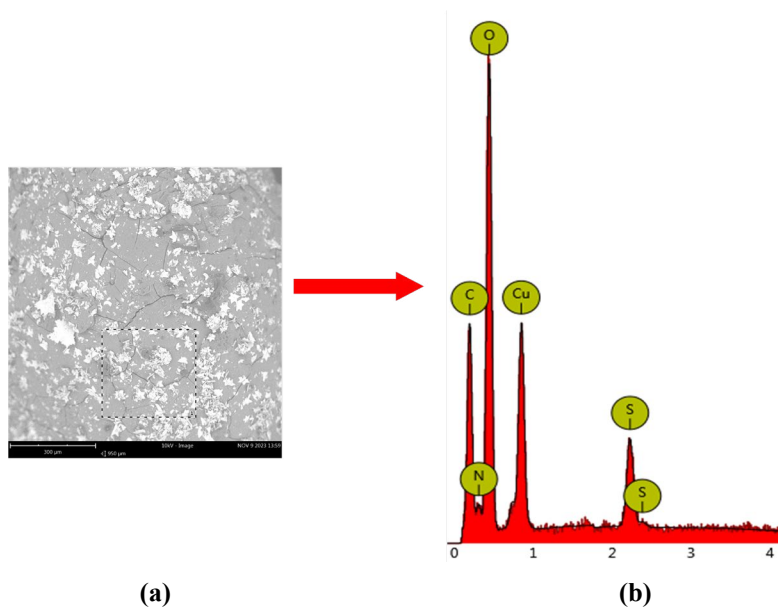


Figure 8. (a) Scanning electron micrograph of the surface of a chitosan hydrogel sphere containing 5% activated carbon; the dashed lines show the scanning area with the energy dispersive X-ray spectroscopy (EDS) probe. (b) EDS analysis of the particles.

Table 2. Energy dispersive X-ray spectroscopy analysis for the chitosan spheres containing 5% CCP 90 activated carbon.

Symbol	Atomic percent [%] in the sample
Carbon (C)	42.01
Oxygen (O)	40.56
Nitrogen (N)	7.89
Copper (Cu)	6.70
Sulfur (S)	2.83

Figure 9 presents scanning electron micrographs of the surface of chitosan spheres containing 10% CCP 90 activated carbon after adsorption of Cu^{2+} .

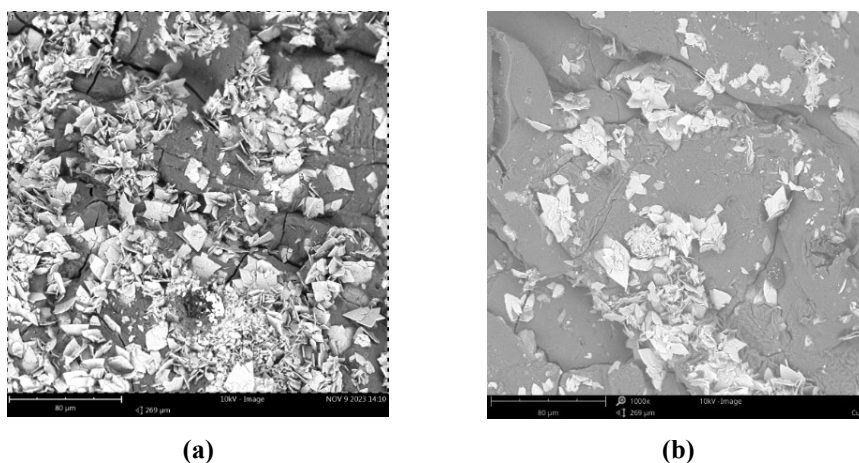


Figure 9. Scanning electron micrograph of the surface of spheres obtained from a 3% chitosan solution and 10% activated carbon after adsorption of copper(II) ions at (a) 269 \times and (b) 1000 \times magnification.

After Cu^{2+} adsorption, there were crystals of hydrated CuSO_4 visible on unmodified dried chitosan spheres. EDS analysis confirmed these observations. The adsorbed ions in the central ion system with chitosan amine ligands constitute a layer with that attracts sulfate anions. The resulting system constitutes the active centres of crystallisation nuclei. Salt probably diffuses from the inside of the hydrated gel spheres to the outside during drying. Stronger and increased diffusion and deposition of crystals outside the spheres may result from modification of the internal structure of the spheres with activated carbon. The number of hydrated CuSO_4 crystals increases with the addition of activated carbon.

EDS analysis was performed for chitosan hydrogel sphere after the addition of 10% CCP 90 activated carbon after adsorption of Cu^{2+} (Figure 10). The main identified elements are O, C, Cu, N and S (Table 3).

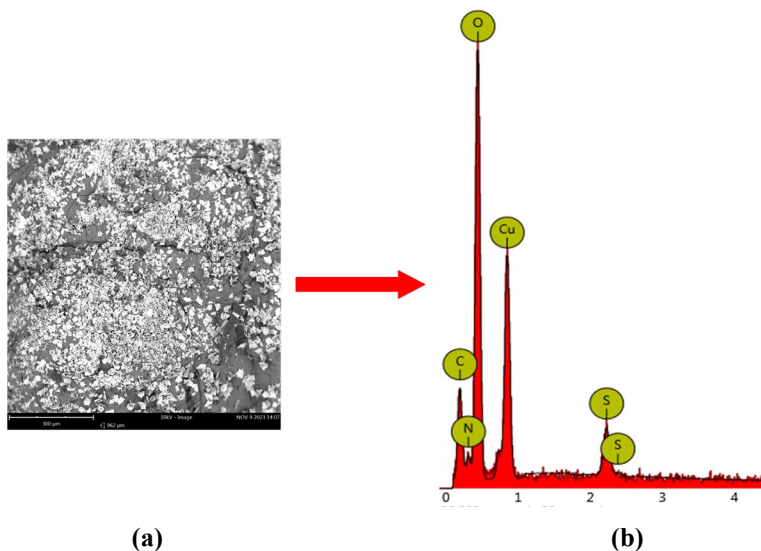


Figure 10. (a) Scanning electron micrograph of the surface of a chitosan sphere containing 10% activated carbon; the dotted lines show the scanning area with the energy dispersive X-ray spectroscopy (EDS) probe. (b) EDS analysis of particles.

Table 3. Energy dispersive X-ray spectroscopy analysis for the chitosan spheres containing 10% CCP 90 activated carbon.

Symbol	Atomic percent [%] in the sample
Oxygen (O)	49.37
Carbon (C)	29.18
Copper (Cu)	11.51
Nitrogen (N)	7.24
Sulfur (S)	2.70

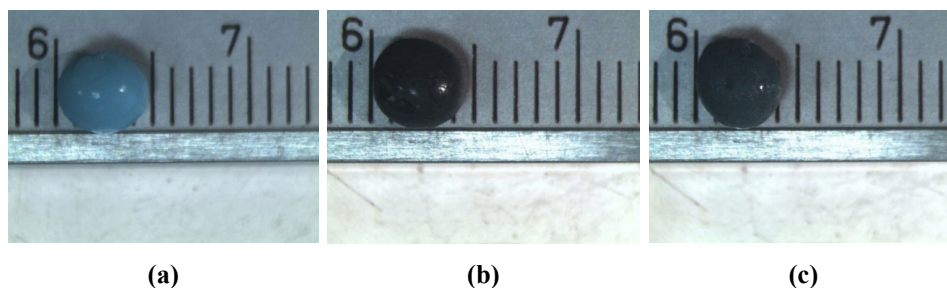


Figure 11. The photographs show chitosan spheres (a) without the addition of CCP 90 activated carbon after adsorption of copper(II) ions, (b) with the addition of 5% CCP 90 after adsorption of copper(II) ions and (c) with the addition of 10% CCP 90 after adsorption of copper(II) ions.

Figure 11 shows the sizes of the chitosan spheres after adsorption of Cu^{2+} . The addition of activated carbon affected the size of the formed chitosan spheres. Chitosan hydrogel spheres without activated carbon were 5 mm (Figure 11a). However, chitosan hydrogel spheres with 5% and 10% activated carbon (Figure 11b, c) were approximately 4.5 mm. There was also a noticeable change in the colour of the chitosan hydrogel sphere after adsorption of Cu^{2+} , from white to blue.

The addition of activated carbon in the form of a colloidal suspension of microparticles was intended to modify the spatial arrangement of chitosan chains through their initial adsorption and the largest possible surface area of chitosan and carbon available for ion migration. The addition of 5% activated carbon did not affect the adsorption of Cu^{2+} by chitosan. It is likely that the entire capacity of activated carbon was blocked by chitosan without blocking the active sites on the amine groups. The addition of 10% CCP 90 activated carbon improved the adsorption of Cu^{2+} due to the additional development of the chitosan adsorption surface or additional active centres on porous particles.

4. Conclusions

Chitosan hydrogel spheres without CCP 90 activated carbon were larger than those containing CCP 90 activated carbon after adsorption of Cu^{2+} . All chitosan hydrogel spheres effectively adsorbed Cu^{2+} . The adsorption of Cu^{2+} was similar for chitosan hydrogel spheres without CCP 90 activated carbon and chitosan hydrogel spheres with 5% CCP 90 activated carbon. However, chitosan hydrogel spheres with 10% CCP 90 activated carbon showed enhanced Cu^{2+} adsorption due to an increase in active centres.

5. References

- [1] Varma A, Deshpande S, Kennedy J; (2004) Metal complexation by chitosan and its derivatives: a review. *Carbohydr Polym* 55(1), 77–93. DOI:10.1016/j.carbpol.2003.08.005
- [2] Modrzejewska Z, Skwarczynska A, Douglas TEL, Binias D, Maniukiewicz W, Sielski J; (2015) Structure of chitosan gels mineralized by sorption. *J Mol Struct* 1098, 101–109. DOI:10.1016/j.molstruc.2015.06.001
- [3] Nikiforova TE, Kozlov VA, Telegin FY; (2021) Chemisorption of copper ions in aqueous acidic solutions by modified chitosan. *Materials Sci Eng B* 263, 114778. DOI:10.1016/j.mseb.2020.114778
- [4] Dragan ES, Dinu MV; (2019) Advances in porous chitosan-based composite hydrogels: Synthesis and applications. *React Funct Polym* 146, 104372. DOI:10.1016/j.reactfunctpolym.2019.104372
- [5] Chen AH, Liu SC, Chen CY, Chen CY; (2008) Comparative adsorption of Cu(II), Zn(II), and Pb(II) ions in aqueous solution on the crosslinked chitosan with epichlorohydrin. *J Hazard Mater* 154, 184–191. DOI:10.1016/j.jhazmat.2007.10.009
- [6] Nikiforova TE, Kozlov VA, Islyaikin M; (2019) Regularities and mechanism of heavy metal cations sorption/proton-desorption by chitosan from water solutions. *Can J Chem* 97, 621–628. DOI:10.1139/cjc-2018-0384
- [7] Kuczajowska-Zadrożna M, Filipkowska U, Józwiak T; (2020) Adsorption of Cu(II) and Cd(II) from aqueous solutions by chitosan immobilized in alginate beads. *J Environ Chem Eng* 8, 103878. DOI:10.1016/j.jece.2020.103878

- [8] Jaworska MM, Filipkowska U, Modrzejewska Z; (2022) Adsorption of the dye Acid Blue 158 premetalized with chromium on chitin/chitosan. *Carbohydr Polym* 298, 120122. **DOI:**10.1016/j.carbpol.2022.120122
- [9] Filipkowska U, Jozwiak T; (2021) Chitosan sorbents used for dye removal. *Desalin Water Treat* 243, 242–261. **DOI:**10.5004/dwt.2021.27850
- [10] Kyzas GZ, Bikiaris DN, Mitropoulos AC; (2017) Chitosan adsorbents for dye removal: a review. *Polym Int* 66, 1800–1811. **DOI:**10.1002/pi.5467
- [11] Lade H, Govindwar S, Paul D; (2015) Mineralization and detoxification of the carcinogenic azo dye Congo red and real textile effluent by a polyurethane foam immobilized microbial consortium in an up flow column bioreactor. *Int J Environ Res Public Health* 12 (6), 6894–6918. **DOI:**10.3390/ijerph120606894
- [12] Polat H, Erdogan D; (2007) Heavy metal removal from waste waters by ion flotation. *J Hazard Mater* 148, 267–273. **DOI:**10.1016/j.jhazmat.2007.02.013
- [13] Jia Y, Ding L, Ren P, Zhong M, Ma J, Fan X; (2020) Performances and mechanism of methyl Orange and Congo red adsorbed on the magnetic ion-exchange resin. *J Chem Eng Data* 65 (2), 725–736. **DOI:**10.1021/acs.jced.9b00951
- [14] Ge J, Zhang Y, Heo YJ, Park SJ; (2019) Advanced design and synthesis of composite photocatalysts for the remediation of wastewater: a review. *Catalysts* 9, 122. **DOI:**10.3390/catal9020122
- [15] Borjigin T, Schmitt M, Morlet-Savary F, Xiao P, Lalevée J; (2022) Low-cost and recyclable Photocatalysts: metal oxide/polymer composites applied in the catalytic breakdown of dyes. *Photochem* 2, 733–751. **DOI:**10.3390/photochem2030047
- [16] Huang C, Wen J, Shen Y, He F, Mi L, Gan Z, Ma J, Liu S, Ma H, Zhang Y; (2018) Dissolution and homogeneous photocatalysis of polymeric carbon nitride. *Chem Sci* 9, 7912–7915. **DOI:**10.1039/c8sc03855d
- [17] Pelosato R, Bolognino I, Fontana F, Sora IN; (2022) Applications of heterogeneous photocatalysis to the degradation of oxytetracycline in water: a review. *Molecules* 27, 2743. **DOI:**10.3390/molecules27092743
- [18] Ghaedi M, Taghavi Moghadam N, Naderi S, Sahraei R, Daneshfar A; (2013) Comparison of removal of bromothymol blue from aqueous solution by multiwalled carbon nanotube and Zn(OH)₂ nanoparticles loaded on activated carbon: a thermodynamic study. *J Ind Eng Chem* 19 (5), 1493–1500. **DOI:**10.1016/j.jiec.2013.01.013
- [19] Nodehi R, Shayesteh H, Kelishami AR; (2020) Enhanced adsorption of Congo red using cationic surfactant functionalized zeolite particles. *Microchem J* 153, 104281. **DOI:**10.1016/j.microc.2019.104281
- [20] Hasan S, Ghosh TK, Viswanath DS, Boddu VM; (2008) Dispersion of chitosan on perlite for enhancement of copper(II) adsorption capacity. *J Hazard Mater* 152, 826–837. **DOI:**10.1016/j.jhazmat.2007.07.078
- [21] Dragan ES, Dinu MV, Timpu D; (2010) Preparation and characterization of novel composites based on chitosan and clinoptilolite with enhanced adsorption properties for Cu²⁺. *Bioresour Technol* 101, 812–817. **DOI:**10.1016/j.biortech.2009.08.077
- [22] Abdul Khalil HPS, Chaturbhuj KS, Adnan AS, Nurul Fazita MR; (2016) A review on chitosan-cellulose blends and nanocellulose reinforced chitosan biocomposites: Properties and their applications. *Carbohydr Polym* 150, 216–226. **DOI:**10.1016/j.carbpol.2016.05.028

- [23] Salih SS, Ghosh TK; (2018) Adsorption of Zn(II) ions by chitosan coated diatomaceous earth. *Int J Biol Macromol* 106, 602–610. **DOI:**10.1016/j.ijbiomac.2017.08.053
- [24] Lipatova IM, Mezina EA; (2012) Synthesis of chitosan-mineral sorbents on fibrous supports and study of their properties. *Russ J Appl Chem* 85, 1059–1063. **DOI:**10.1134/S1070427212070117
- [25] Vieira RM, Vilela PB, Becegato VA, Paulino AT; (2018) Chitosan-based hydrogel and chitosan/acid-activated montmorillonite composite hydrogel for the adsorption and removal of Pb⁺² and Ni⁺² ions accommodated in aqueous solutions. *J Environ Chem Eng* 6, 2713–2723. **DOI:**10.1016/j.jece.2018.04.018
- [26] Hargono H, Sarah AM, Nevrita F, Jos B; (2019) Kinetics and equilibriums adsorption of Cu (II) ion by chitosan and cross-linked chitosan-bentonite. *Reaktor* 19(3), 117–124. **DOI:**10.14710/reaktor.19.3.117-124
- [27] Cheung WH, Ng JCY, Mckay G; (2003) Kinetic analysis of the sorption of copper(II) ions on chitosan. *Chem Technol Biotechnol* 78, 562–571. **DOI:**10.1002/jctb.836
- [28] Cheung WH, Ng JCY, Mckay G; (2002) Equilibrium studies of the sorption of Cu(II) ions onto chitosan. *J Colloid Interf Sci* 255, 64–74. **DOI:**10.1006/jcis.2002.8664

THE COMBINATION OF WASTE PRODUCTS FROM CHITIN AND SAWDUST TO REMOVE ANIONIC AND CATIONIC DYES

Urszula Filipkowska^{1,a,*}, Tomasz Józwiak^{1,b}

¹ – Department of Environmental Engineering, University of Warmia and Mazury in Olsztyn, Warszawska 117 Str., 10-720 Olsztyn, Poland

^a – ORCID: 0000-0003-0140-6558, ^b – ORCID: 0000-0003-3360-9827

*corresponding author: urszula.filipkowska@uwm.edu.pl

Abstract

The application of the immobilisation method – which consists of immobilising modified sawdust in a carrier; a chitosan gel – enabled the development of a new sorbent. By combining waste products from chitin and sawdust, the properties of both adsorbents were utilised. This paper evaluated the adsorption efficiency of four dyes – Reactive Yellow 84, Reactive Black 8, Basic Violet 10 and Basic Green 4 – on four adsorbents – chitin flakes, chitosan flakes, chitosan beads and sawdust immobilised in chitosan beads. The latter adsorbent showed good adsorption properties for both anionic and cationic dyes. The experimental results showed a relationship between the amount of adsorbed and desorbed dye and the type of adsorbent. Chitin flakes showed the lowest adsorption capacity, regardless of the type of dye. The immobilisation of modified sawdust in chitosan had a particularly positive effect on the binding efficiency of cationic dyes.

Keywords: *chitin flakes, chitosan flakes, chitosan beads, modified chitosan in sawdust, cyclic adsorption/desorption*

Received: 25.03.2024

Accepted: 10.06.2024

1. Introduction

The ability of different types of adsorbents to bind to dyes depends on both the type of adsorbent and the structure of the dye; this phenomenon has been well documented in the literature. The practical application of the adsorption process for the removal of dyes from wastewater still faces a number of limitations. Among the most important is the lack of a universal adsorbent that would be highly effective regardless of the type of dye (anionic or cationic) and could be used under flow conditions [1]. The costs associated with separating the adsorbent in the form of powders or flakes from the purified solution also play an important role: if this could be done at a relatively low cost, it would allow the adsorbent to be reused in subsequent adsorption and desorption cycles. These disadvantages can be eliminated by immobilisation.

Agricultural and forestry wastes such as sawdust and bark can be used successfully as adsorbents, mainly due to their wide availability, physicochemical properties and low costs associated mainly with transportation from storage sites to landfills [2–4]. Sawdust is a major by-product of the wood industry; it is mostly used as fuel or as packaging material [5]. Sawdust accounts for about 10% of the wood processed in sawmills. It is also a by-product of cutting and milling, among other activities, in wood-processing companies.

Ligninocellulose biomass is widely available and inexpensive. Its sources include growing resources of coniferous and deciduous trees, reeds, some types of grasses, plantations of fast-growing trees (willows, poplars and eucalyptus), wood waste, straw, hay, crop stalks, wood waste from the pulp and paper industry, corn cobs, waste from the milling industry, the oil industry, waste wood construction materials, and paper and municipal waste. It is estimated that the annual production of terrestrial plant biomass is about 170 billion tonnes. Only about 6 billion tonnes of biomass are used, and only 3% of this amount is used outside the agricultural and food industry [6].

Researchers have described the adsorption of dyes, toxic salts, metals or oils from aqueous solutions using sawdust as a sorbent. Sawdust, which contains organic components such as lignins, cellulose and hemicellulose with polyphenolic groups, is a promising and effective material for the removal of dyes [5, 7–10]. The adsorption capacity achieved by sawdust adsorbents in the published studies show a rather wide range due to the differences in the type of sawdust and the method used for their preparation and modification [11, 12]. The adsorption capacity of raw sawdust can range from 27.4 [13] to 398.8–526 mg/l [8, 14] depending on the tree species, the processing method and the colourant.

The use of chitin and chitosan as adsorbents is economically advantageous. Both chitin and chitosan occur in considerable quantities in nature and their extraction does not involve large financial costs [15–17]. Chitin is obtained from natural resources, while the preparation of chitosan involves the use of inexpensive and widely available chemical reagents [18]. Thanks to this versatility, both chitin and chitosan can be used in various forms: as flakes, in gels, as various types of beads [19–21] or as fibres and membranes [22]. Like chitin, chitosan is easily biodegradable and non-toxic [23]. In addition, it has a number of other properties: high chemical reactivity, high bioactivity, high stability and a high adsorption capacity. The sorption properties of chitosan are used to remove dyes, heavy metals and other toxic substances that pollute water.

Chitosan has attracted particular attention as a complexing agent due to its low cost compared with activated carbon and its numerous functional groups – amino and hydroxyl. Biosorbents based on chitin and chitosan represent effective materials and have a very high affinity for many classes of dyes [9, 20, 21, 24–27]. Chitosan has been used as an adsorbent to remove acid dyes [24, 28–33]. These studies have reported an adsorption capacity of > 1000 mg/g of sorbent, confirming the usefulness of chitosan for the removal

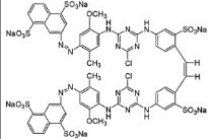
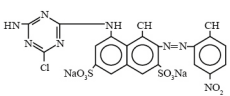
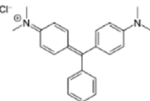
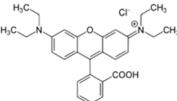
of dyes. The application of the immobilisation method – which consists of immobilising modified sawdust in a carrier, a chitosan gel – enabled the development of a new adsorbent [23, 34, 35]. The combination of waste products from chitin and sawdust utilises the properties of both adsorbents. Immobilised modified sawdust in chitosan gel exhibits good adsorption properties for both anionic and cationic dyes so that the adsorption process can be used to remove dyes under dynamic conditions.

2. Materials and Methods

2.1. Dyes

Dyes from ZPB ‘Boruta’ SA (Poland) were used in this study. Due to their widespread use in industry, anionic (reactive) and cationic (basic) dyes were used. Table 1 shows the chemical characteristics of the dyes employed in this study.

Table 1. The characteristics of the anionic and cationic dyes used in this study.

Name	Reactive Yellow 84 (RY84)	Reactive Black 8 (RB8)	Basic Green 4 (BG4)	Basic Violet 10 (BV10)
Structural formula				
Chemical formula	$C_{52}H_{38}Cl_2N_8O_{26}S_8$	$C_{19}H_{11}ClN_8Na_2O_{10}S_2$	$C_{27}H_{28}N_2O_8$	$C_{28}H_{31}ClN_2O_3$
Molecular mass [g/mol]	1628	657	365	479
λ_{max} [nm]	356	657	618	554
Type of dye	Anionic (reactive)	Anionic (reactive)	Basic (cationic)	Basic (cationic)
Dye class	Double azo dye	Azo dye	Triphenylmethane	Triphenylmethane
Dye application	Dyeing of polyester, cotton and synthetic silk	Dyeing of natural silk and wool	Dyeing of wool, cotton, silk, leather and paper	Dyeing of cotton, paper and leather; production of printing and painting dyes

2.2. Adsorbents

Adsorbent 1 – chitin flakes. Krill chitin from the Institute of Sea Fisheries in Gdynia with a dry matter content of 95.64%, an ash content of 0.32% and a degree of deacetylation of < 3% was used for the study. The commercial chitin flakes were washed with distilled water and 6 N hydrochloric acid (HCl) before adsorption to loosen the structure and to remove calcium and magnesium ions as well as fat residues. It was then rinsed with distilled water to neutralise the pH of the filtrate.

Adsorbent 2 – chitosan flakes. The chitosan used in the study was prepared from chitin, which was washed with distilled water and HCl and then boiled for 3 h in a water bath with a 70% potassium base. After cooling, the flakes were rinsed with distilled water until neutral and drained in a vacuum. The degree of deacetylation was 75%.

Adsorbent 3 – chitosan beads. Chitosan in the form of flakes with a degree of deacetylation of 85%, a viscosity of 100 mPa/s and a dry substance content of 86.8% was obtained from Hepe (Germany). Fifty grams of chitosan, dissolved in 2% acetic acid, was dropped into 5% sodium hydroxide (NaOH) using a micropipette and incubated in the solution for 24 h. The size of the beads was controlled based on the size of the micropipette (3 mm).

Adsorbent 4 – beads of modified oak sawdust immobilised in chitosan. Oak sawdust from the local sawmill in Naterki, a waste product from the treatment of oak wood that has undergone modification, was used. The fibre fractions were determined based on the chemical analysis method according to Van Soest et al. [36]. This method involves the selective isolation of different fractions under specific conditions using surface-active compounds. The characteristics of the raw material, expressed in % (w/w) in relation to the dry mass, are listed in Table 2.

Table 2. Characteristics of the oak sawdust used in this study.

Component	Percent of dry matter content
Cellulose	45.0
Hemicellulose	28.9
Lignins	22.7
Ash	0.1
Extracts and other ingredients	3.3

2.2.1. Modification of the Sawdust

Fifty grams of sawdust was mixed with 50 g of concentrated sulphuric acid (H_2SO_4) and heated at 150°C for 24 h. The sawdust was washed with distilled water and incubated in 1% sodium carbonate for 12 h to remove residual H_2SO_4 . The resulting modified sawdust was dried at 105°C for 24 h and then sieved through a sieve with a mesh size of 1 mm [5, 11].

2.2.2. Preparation of Modified Sawdust Immobilised on Chitosan

Twenty-five grams of modified sawdust was added to 25 g of chitosan dissolved in 5% acetic acid. To create the beads, a mixture of modified sawdust and chitosan was dropped into 5% NaOH using a micropipette and incubated in the solution for 24 h. The resulting beads were drained, washed and stored in distilled water.

2.2.3. Determination of the Efficiency of Dye Adsorption/Desorption

Adsorption and desorption was assessed for Reactive Yellow 84 (RY 84), Reactive Blue 8 (RB8), Basic Violet 10 (BV10) and Basic Green 4 (BG4). For the anionic dyes (RY84 and RB8), adsorption was carried out at pH 5 and desorption was carried out at pH 10. For the cationic dyes (BV10 and BG4), adsorption was carried out at pH 10 and desorption was carried out at pH 3. The reaction of the solutions was adjusted with HCl and NaOH solutions. The concentration of the adsorbent was constant in all experiments (1 g/l). The adsorption (120 min) and desorption (30 min) times were determined using the studies shown in Figures 1 and 2.

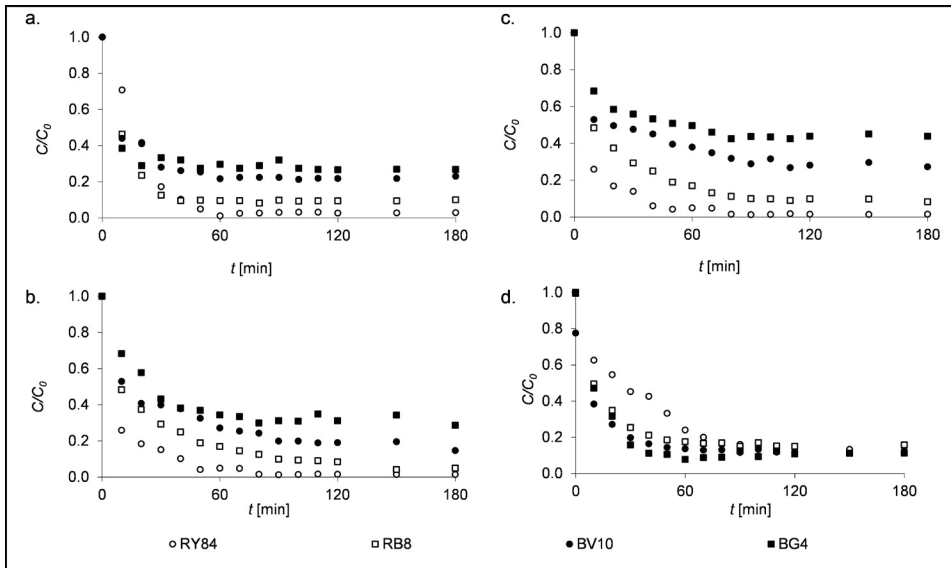


Figure 1. Changes in the dye concentration over time during adsorption on (a) chitin flakes, (b) chitosan flakes, (c) chitosan beads and (d) sawdust immobilised on chitosan beads. Abbreviations: BG4, Basic Green 4; BV10, Basic Violet 10; RB8, Reactive Blue 8; RY84, Reactive Yellow 84.

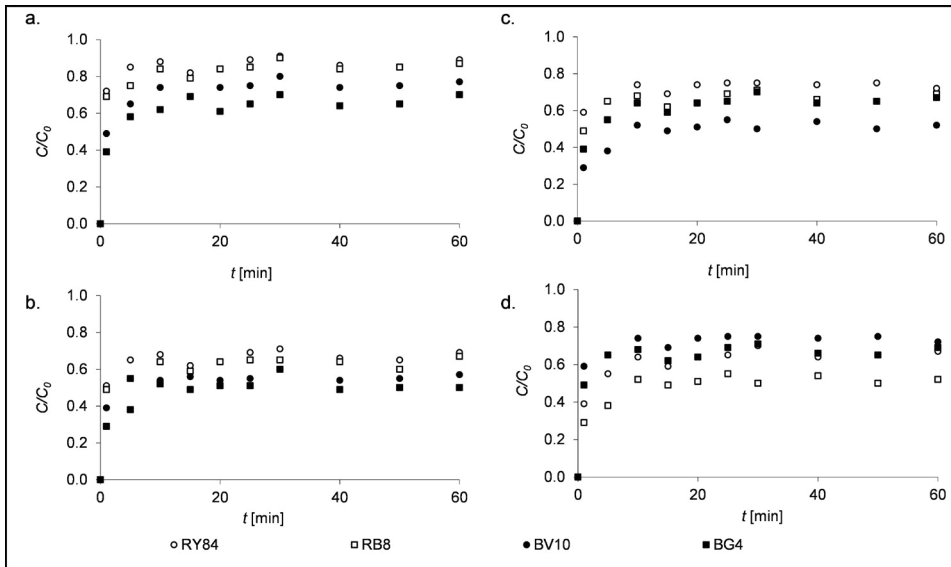


Figure 2. Changes in dye concentration over time during desorption from (a) chitin flakes, (b) chitosan flakes, (c) chitosan beads and (d) sawdust immobilised on chitosan beads. Abbreviations: BG4, Basic Green 4; BV10, Basic Violet 10; RB8, Reactive Blue 8; RY84, Reactive Yellow 84.

2.3. Analytical Methods

The samples taken for analysis were decanted and centrifuged at 10,000 rpm for 15 min. The concentration of dye remaining in the solution was determined using a standard curve prepared with a SP-3000 ultraviolet–visible (UV–Vis) spectrophotometer (VWR In-ter-national LLC., Canada). Distilled water was used as the blank.

2.4. Calculation Methods

The amount of dye adsorbed from the solution was determined by the change in the concentration of dye remaining in the solution and calculated using equation (1):

$$Q_s = \frac{C_0 - C_s}{m} \quad (1)$$

The symbols in this equation mean the following:

- Q_s – amount of adsorbed dye [mg/g dry matter (DM)];
- C_0 – initial concentration of the dye [mg/l];
- C_s – concentration of the dye after adsorption [mg/l];
- m – concentration of mass of the adsorbent in tested sample [g DM/l].

A double-Langmuir model was used to describe the results of the experimental adsorption. The model assumes that the surface of the adsorbent is energetically heterogeneous and has adsorption centra with different binding energies of adsorbates. Each type is described by Langmuir's isotherm equation [37–39] and the active sites are characterised by constants labelled K_1 and b_1 and K_2 and b_2 , respectively, as shown in equation (2). This model has been used successfully to interpret the results of metal adsorption by activated sludge and to evaluate metal adsorption in soils [37].

$$Q = \frac{b_1 \cdot K_1 \cdot C}{1 + K_1 \cdot C} + \frac{b_2 \cdot K_2 \cdot C}{1 + K_2 \cdot C} \quad (2)$$

The symbols in this equation mean the following:

- Q – amount of adsorbed dye [mg/g DM];
- b_1, b_2 – adsorption capacity in active sites of the first and second type [mg/g DM];
- K_1, K_2 – constants in Langmuir's equation [l/mg DM];
- C – concentration of dye in the solution at equilibrium [mg/l].

The total adsorption capacity (b) is equal to the sum of the maximum adsorption capacity determined for the first and second types of active sites ($b = b_1 + b_2$). K_1 and K_2 characterise the adsorption affinity of the dye to the active sites of the first and second types, respectively, and correspond to the reciprocal of the equilibrium concentration of the dye at which the adsorption capacity is more than half the maximum capacity of b_1 or b_2 . A larger K indicates an increase in the adsorption affinity of the dye to the active sites of the adsorbent. The constants K_1 and K_2 and the maximum adsorption capacity (b_1 and b_2) were determined by non-linear regression. The R^2 coefficient was used as a measure of the fit of the curve (with the determined parameters) to the experimental data.

The amount of desorbed dye was calculated from equation (3):

$$Q_d = \frac{C_d - C_s}{m} \quad (3)$$

The symbols in this equation mean the following:

- Q_d – amount of desorbed dye [mg/g DM];
- C_0 – concentration of the dye before desorption [mg/l];
- C_d – concentration of the dye after desorption [mg/l];
- m – concentration of mass of the adsorbent in the tested sample [g DM/l].

The desorption of dyes from aqueous solutions on the tested adsorbents was evaluated based on the relationship between the mass of dye adsorbed on the adsorbent Q (mg/g DM) and its equilibrium concentration C [mg/l].

The single-Langmuir model was used to describe the experimental results of desorption. It is shown in equation (4):

$$Q = \frac{b \cdot K \cdot C}{1 + K \cdot C} \quad (4)$$

The symbols in this equation mean the following:

- Q – amount of adsorbed dye [mg/g DM];
- b – adsorption capacity [mg/g DM];
- K – constant in Langmuir's equation [l/mg DM];
- C – concentration of dye in the solution, at equilibrium [mg/l].

The constants K and b were determined by non-linear regression. R^2 was used as a measure of the fit of the curve (with the determined parameters) to the experimental data.

3. Results and Discussion

The combination of chitin and sawdust via immobilisation of sawdust in chitosan aimed to create an adsorbent that would have good adsorption properties for both anionic and cationic dyes and high adsorption and desorption efficiency. The adsorption and desorption of the dyes was evaluated based on the relationship between the mass of dye adsorbed on the adsorbent (Q) and its equilibrium concentration (C). The double-Langmuir model, equation (2), and the single-Langmuir model, equation (4), were used to describe the experimental results. Figures 3–6 show the relationship between the amount of dye adsorbed and desorbed on adsorbents 1–4, the equilibrium concentration and the Langmuir isotherms. The constants K and b determined from equations (2) and (4) for all dyes tested are presented in Tables 3 and 4, respectively.

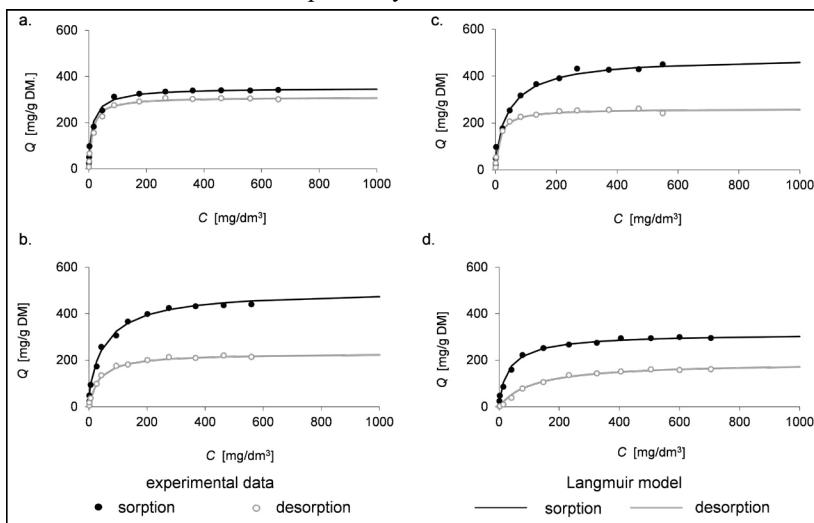


Figure 3. The experimental data compared with the adsorption determined from the double-Langmuir isotherm and the desorption isotherm determined from the Langmuir equation model for Reactive Yellow 84 on (a) chitin flakes, (b) chitosan flakes, (c) chitosan beads and (d) sawdust immobilised on chitosan beads.

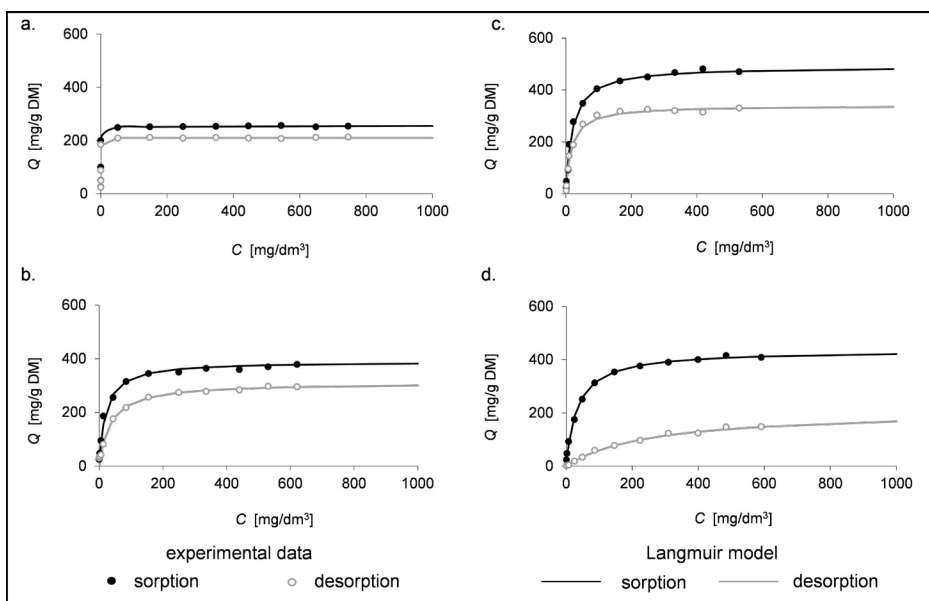


Figure 4. The experimental data compared with the adsorption determined from the double-Langmuir isotherm and the desorption isotherm determined from the Langmuir equation model for Reactive Blue 8 on (a) chitin flakes, (b) chitosan flakes, (c) chitosan beads and (d) sawdust immobilised on chitosan beads.

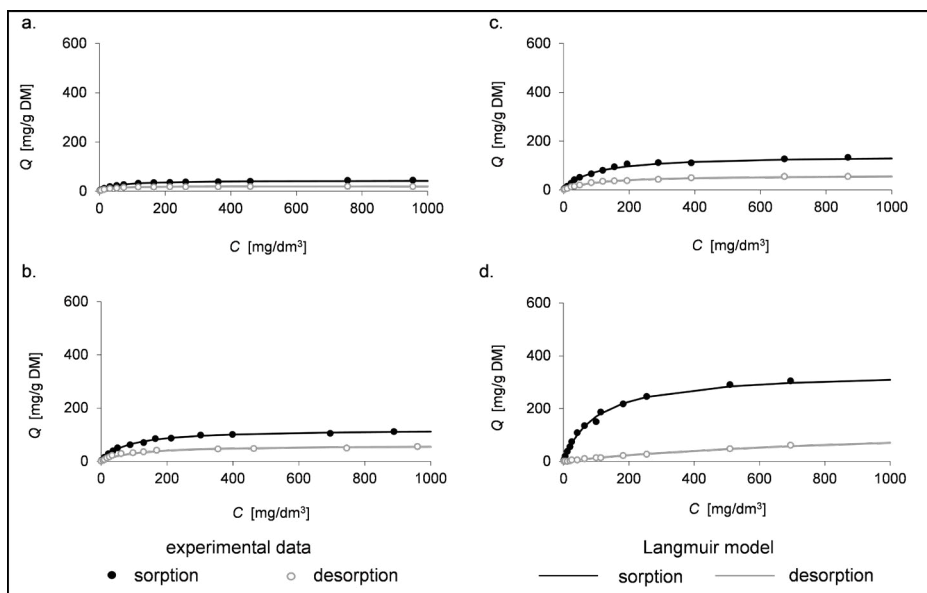


Figure 5. The experimental data compared with the adsorption determined from the double-Langmuir isotherm and the desorption isotherm determined from the Langmuir equation model for Basic Violet 10 on (a) chitin flakes, (b) chitosan flakes, (c) chitosan beads and (d) sawdust immobilised on chitosan beads.

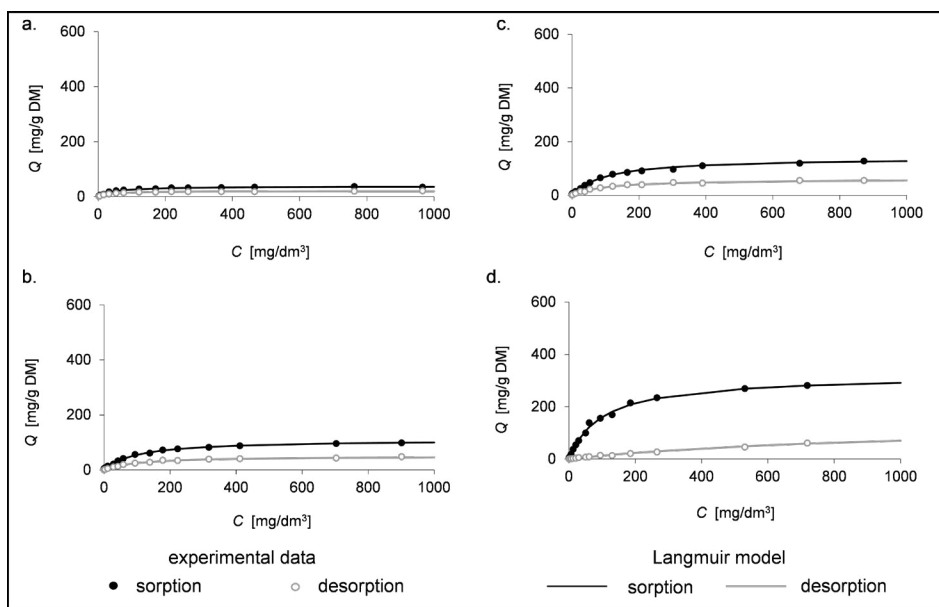


Figure 6. The experimental data compared with the adsorption determined from the double-Langmuir isotherm and the desorption isotherm determined from the Langmuir equation model for Basic Green 4 on (a) chitin flakes, (b) chitosan flakes, (c) chitosan beads and (d) sawdust immobilised on chitosan beads.

Based on the data, regardless of the dye tested, the adsorption capacity of chitin flakes was the lowest compared with the other three adsorbents. Moreover, the efficiency of adsorption on chitin flakes depended strongly on the type of dye. The amount of anionic dyes bound to chitin flakes ranged from 180 mg/g DM (RB8) to 350 mg/g DM (RY84), while for the cationic dyes it was significantly lower, ranging from 38 mg/g DM (BG4) to 44 mg/g DM (BV10) (Table 3). Analysis of the adsorption and desorption isotherms of the tested dyes on chitin flakes revealed a high desorption efficiency. The course of the adsorption and desorption isotherms was very similar.

A higher degree of chitosan deacetylation had a significant effect on the amount of dye removed [40–44]. For chitosan flakes, chitosan beads and sawdust immobilised on chitosan beads, there was an increase in the adsorption capacity of all tested dyes (Figures 3–6, Table 3). Both tested cationic dyes showed the largest increase in the adsorption capacity compared with chitin flakes. The amount of BV10 and BG4 increased to 120 and 110 mg/g DM, respectively, when bound to chitosan flakes (an increase of about 2.8 compared with chitin flakes), to 140 mg/g DM when bound on chitosan beads (a 3.7-fold increase compared with chitin flakes) and to 340 and 320 mg/g DM, respectively, when bound to sawdust immobilised on chitosan beads (an increase of 7.7 and 8.4 times, respectively). The results showed that the modification of chitosan by immobilisation with sawdust increased the adsorption of cationic dyes.

The use of chitosan beads had no effect on the adsorption capacity. The adsorption capacity of the chitosan beads was higher or at a similar level to that of the chitosan flakes for all the tested dyes. The adsorption capacity for the anionic dyes ranged from 390 to 500 mg/g DM for chitosan flakes and from 480 to 490 mg/g DM for chitosan beads. For the cationic dyes BV10 and BG4, the adsorption capacity

was 110 and 140 mg/g DM, respectively. The sawdust immobilised on chitosan beads reduced the adsorption capacity by about 10% compared with chitosan beads.

Analysis of the adsorption and desorption isotherms of chitosan flakes, chitosan beads and sawdust immobilised on chitosan beads revealed that, in case of the anionic dyes, a significant increase in the adsorption capacity did not lead to a corresponding increase in the amount of desorbed dye compared with chitin flakes. The desorption isotherms differed significantly from the adsorption isotherms (Figures 3–6).

A different mechanism of dye binding on the four tested adsorbents is evidenced by the K values, which describe the affinity of the adsorbate to the adsorbent (Table 3). K_1 determined for the chitin flakes was high for RB8 (50 l/mg), which could indicate strong binding of this dye to chitin flakes. K_1 for the cationic dyes BV10 and BG4 determined using the double-Langmuir model was more than 1000 times lower. The adsorption affinity of the tested dyes to the other three adsorbents was significantly lower and there were no significant differences depending on the type of dye. K_1 was between 0.01 and 0.7 l/mg for chitosan flakes, chitosan beads and sawdust immobilised on chitosan beads. K_2 , describing the affinity for the second type of active site, was between 0.01 and 0.05 l/mg regardless of the adsorbent. The only exception was RB8 adsorbed on chitin flakes, for which K_2 was an order of magnitude lower at 0.001 l/mg.

A double-Langmuir model was also used to describe the desorption process, but for all tested dyes and adsorbents, the K_2 and b_2 values were very small; thus, they can be omitted. The desorption of the tested dyes was described successfully with the single-Langmuir model (Table 4).

Table 3. The K and b values determined from the double-Langmuir model, equation (2), for adsorption.

Constants from the double-Langmuir model												
Dye	Chitin flakes						Chitosan flakes					
	K [l/mg DM]		b [mg/g DM]			R^2	K [l/mg DM]		b [mg/g DM]			R^2
	K_1	K_2	b_1	b_2	b		K_1	K_2	b_1	b_2	b	
RY84	1	0.05	90	260	350	0.994	0.70	0.015	80	420	500	0.991
RB8	50	0.001	250	10	260	0.999	0.05	0.05	380	10	390	0.992
BV10	0.04	0.012	25	19	44	0.991	0.01	0.015	40	80	120	0.994
BG4	0.04	0.01	22	16	38	0.991	0.01	0.01	40	70	110	0.994
Dye	Chitosan beads						Sawdust immobilised on chitosan beads					
	K [l/mg DM]		b [mg/g DM]			R^2	K [l/mg DM]		b [mg/g DM]			R^2
	K_1	K_2	b_1	b_2	b		K_1	K_2	b_1	b_2	b	
RY84	0.4	0.017	90	390	480	0.992	0.08	0.02	130	200	380	0.991
RB8	0.05	0.05	480	10	490	0.991	0.03	0.03	380	55	435	0.997
BV10	0.01	0.01	40	100	140	0.992	0.01	0.01	140	200	340	0.996
BG4	0.01	0.01	40	100	140	0.991	0.01	0.01	130	190	320	0.996

Abbreviations: BG4, Basic Green 4; BV10, Basic Violet 10; DM, dry matter; RB8, Reactive Blue 8; RY84, Reactive Yellow 84.

Table 4. The values of K and b determined from the Langmuir model, equation (4), to describe desorption.

Constants from Langmuir equation												
Dye	Chitin flakes			Chitosan flakes			Chitosan beads			Sawdust immobilised on chitosan		
	K	b	R^2	K	b	R^2	K	b	R^2	K	b	R^2
RY84	1	0.05	90	260	350	0.994	0.70	0.015	80	420	500	0.991
RB8	50	0.001	250	10	260	0.999	0.05	0.05	380	10	390	0.992
BV10	0.04	0.012	25	19	44	0.991	0.01	0.015	40	80	120	0.994
BG4	0.04	0.01	22	16	38	0.991	0.01	0.01	40	70	110	0.994

Abbreviations: BG4, Basic Green 4; BV10, Basic Violet 10; DM, dry matter; RB8, Reactive Blue 8; RY84, Reactive Yellow 84.

Based on the K and b values, the significantly higher absorption capacity of the chitosan flakes for the anionic dyes compared with chitin flakes had no effect on the amount of desorbed dye. The desorption of the anionic dyes from chitin flakes was 310 mg/g DM (RY84) and 210 mg/g DM (RB8), which accounted for 89% and 81% of the amount of adsorbed dye, respectively. The shape of the adsorption isotherm and the high K_f values determined for the chitin flakes suggest chemical adsorption. However, this was not confirmed by the desorption results. The chitin flakes showed the highest desorption efficiency regardless of the type of dye. The chitosan flakes, chitosan beads and beads of modified sawdust immobilised on chitosan beads had a significantly lower desorption efficiency for the anionic dyes, ranging from 26% (RB8, chitosan flakes) to 79% (RB8, chitosan flakes).

Dye loss during the dyeing process is estimated to be around 10%–50% for anionic dyes and up to 5% for cationic dyes [20, 21]. Because anionic and cationic dyes can be present in the tanks at the same time, it is important to use adsorbents that allow their simultaneous and effective removal.

Researchers have compared the adsorption capacity of chitosan in the form of flakes and beads, similarly to the present study, but have not provided a clear correlation between the extent of dye binding and the type of adsorbent (flakes and beads). Wu et al. [45] investigated the binding efficiency of Reactive Red 222 (RR222) to flakes and beads of chitosan obtained from shrimp, lobsters and crabs. The capacity was 1026–1106 mg/g for chitosan beads, significantly higher (2–3.8 times) compared with chitosan flakes (293–494 mg/g). Lazaridis and Keenan [46] evaluated the adsorption of RB5 on chitosan beads. The adsorption capacity of 238 mg/g, lower than the capacity of 1000 and 936 mg/g determined by Gibbs et al. [47] and Elwakeel et al. [48] for chitosan flakes.

Kyzas and Lazaridis [49] investigated the adsorption of Reactive Yellow 3RS (RY3RS) and Basic Yellow 37 (BY37), on chitosan flakes and beads. Chitosan flakes showed a higher absorption capacity for both dyes, but this difference was not as significant as in other studies. The adsorption capacity for RY3RS was 373 mg/g for chitosan flakes and 311 mg/g for chitosan beads. The adsorption capacity for BY37 was 254 mg/g for chitosan flakes and 137 mg/g for chitosan beads.

In the present study, sawdust immobilised on chitosan beads showed a good adsorption capacity for the tested anionic and cationic dyes. The adsorption capacity determined for the anionic dyes was slightly lower or comparable to that determined for the chitosan flakes and beads. The decrease in capacity was 12%–21% compared with chitosan beads.

This decrease can be explained by the fact that for sawdust immobilised on chitosan beads, 50% of the weight was chitosan and 50% was modified sawdust. The combination of chitosan and modified sawdust did not affect the binding efficiency of anionic dyes. Sawdust immobilised on chitosan beads had a particularly positive effect on improving the binding efficiency of cationic dyes compared with chitosan beads. Moreover, sawdust immobilised on chitosan beads showed good desorption of all tested dyes.

Based on the K_1 values, the affinity of the chitin flakes for the two tested anionic dyes was markedly higher than the affinity for the two tested cationic dyes. Similarly, Akkaya et al. [33, 50] reported that chitin flakes had a high affinity for Reactive Yellow 2 (RY2) and RB8 as well as indigo carmine and trypan blue based on the adsorption isotherms. The other adsorbents had much lower affinity for all dyes, denoted by the lower K_1 values. The K values in the present study are comparable with the results of Kyzas and Lazaridis [49]. For BY37, the K value was 0.0302 l/mg for chitosan beads and 0.0167 l/mg for chitosan flakes, and for RYG3RS, the K value was 0.0649–0.0542 l/mg. Wu et al. [45] reported a K value of 0.2 l/mg for RR 222 adsorption on spheres, higher than the K value determined for chitosan flakes (0.052 l/mg). The authors explained these results based on the larger adsorption surface and the looser pore structure of the chitosan beads compared with the chitosan flakes, which facilitated the adsorption of RR222. The K_2 values were comparable regardless of the adsorbent and the dye, ranging from 0.001 to 0.05 l/mg. The combination of both immobilised sawdust and chitosan beads resulted in a similar adsorption affinity for both anionic and cationic dyes.

The efficiency of adsorption of anionic and cationic dyes on each component of sawdust immobilised on chitosan beads depends on several factors. The surfaces of cellulosic adsorbents become negatively charged when they come into contact with water. The binding of cationic dyes (e.g. BV10 and BG4) occurs mainly by ion exchange adsorption. On the other hand, the anions of anionic dyes (e.g. RY84 and RB8) are repelled when they approach a negatively charged surface, which is why the removal efficiency is lower. The adsorption process on nitrogen-containing biological adsorbents, which include chitin and chitosan, is different compared with cellulose-containing adsorbents. The chemical structure of these adsorbents enables the binding of anionic dyes by ion exchange adsorption and by hydrogen bonds or intermolecular interactions caused by van der Waals forces, which leads to an increase in adsorption affinity.

The K value can indicate the mechanism of dye binding to the tested adsorbents. Different K_1 and K_2 values may indicate a different type of binding of the dye to the first and second types of active sites of adsorbents. High values indicate strong chemical binding while lower values indicate weaker physical binding. The higher K_1 values in the present study could indicate that there is chemical binding at the first type of active site, especially in case of chitin. On the other hand, the lower K_2 values could indicate weaker physical binding of the second type of active site. This desorption results support this view. The total amount of dye released was equal or close to the amount of dye bound to the second type of active site during adsorption.

An adsorbent may be used in several ways. It may be used once and then disposed of – for example, by incineration or disposal in a landfill – or regenerated. From an economic point of view, methods that allow the regeneration of the adsorbent and the recovery of the desorbed substance are more favourable. Therefore, the efficiency of recovery of the adsorbed components also determines the possibility of using the adsorbent. Repeated use of the adsorbent should maintain its adsorption capacity (maximum adsorption capacity) and not cause physical changes or damage.

In the present study, desorption was carried out by changing the pH of the solution. Although the double-Langmuir model was also used to describe the desorption process,

the K_2 and b_2 values were very small. This indicates that desorption occurs from one type of active site. Consistently, the single-Langmuir model adequately described the data, as confirmed by the R^2 values.

4. Conclusions

This paper presented the production and efficiency of adsorption and desorption of anionic and cationic dyes on chitin flakes, chitosan flakes, chitosan beads and modified sawdust on chitosan beads. Chitin flakes showed the lowest binding efficiency for anionic and cationic dyes, but the highest desorption efficiency. Chitosan flakes and beads showed a much higher adsorption capacity, particularly for the anionic dyes. Compared with chitin flakes, the increase in adsorption efficiency was not associated with an increase in desorption efficiency. In addition, they had a significantly lower adsorption capacity. Based on the results, it can be concluded that the combination of two adsorbents with different properties allowed for the removal of both anionic and cationic dyes, especially the latter, by adsorption with high efficiency.

5. Acknowledgements

This study was financed under Project No. 29.610.023-300 of the University of Warmia and Mazury in Olsztyn, Poland.

6. References

- [1] Sahdev AK, Raorane CJ, Shastri D, Raj V, Singh A, Kim SC; (2022) Update on modified chitosan frameworks and their applications for food, wastewater, toxic heavy metals, dyes treatment and cancer drug delivery. *J Environ Chem Eng* 10, 108656. DOI:10.1016/j.jece.2022.108656
- [2] Palma G, Freer J, Baeza J; (2003) Removal of metal ions by modified *Pinus radiata* bark and tannins from water solutions. *Water Res* 37, 4974–4980. DOI:10.1016/J.WATRES.2003.08.008
- [3] Adegoke KA, Adesina OO, Okon-Akan OA, Adegoke OR, Olabintan AB, Ajala OA, Olagoke H, Maxakato NW, Bello OS; (2022) Sawdust-biomass based materials for sequestration of organic and inorganic pollutants and potential for engineering applications. *Curr Res Green Sustain Chem* 5, 100274. DOI:10.1016/j.crgsc.2022.100274
- [4] Özacar M, Şengil IA; (2005) Adsorption of metal complex dyes from aqueous solutions by pine sawdust *Bioresour Technol* 96, 791–795. DOI:10.1016/J.BIORTECH.2004.07.011
- [5] Garg VK, Amita M, Kumar R, Gupta R; (2004) Basic dye (methylene blue) removal from simulated wastewater by adsorption using Indian Rosewood sawdust: a timber industry waste. *Dyes Pigments* 63, 243–250. DOI:10.1016/J.DYEPIG.2004.03.005
- [6] Mallakpour S, Sirous F, Hussain CM; (2021) Sawdust, a versatile, inexpensive, readily available bio-waste: From mother earth to valuable materials for sustainable remediation technologies. *Adv Colloid Interface Sci* 295, 102492. DOI:10.1016/j.cis.2021.102492
- [7] Shukla A, Zhang YH, Dubey P, Margrave JL, Shukla SS; (2002) The role of sawdust in the removal of unwanted materials from water. *J Hazard Mater* 95, 137–152. DOI:10.1016/S0304-3894(02)00089-4

- [8] Özacar M, Şengil IA; (2005) A kinetic study of metal complex dye sorption onto pine sawdust. *Process Biochem* 40, 565–572. **DOI:**10.1016/J.PROCBIO.2004.01.032
- [9] Ravi Kumar MNV; (2000) A review of chitin and chitosan applications. *React Funct Polym* 46, 1–27. **DOI:**10.1016/S1381-5148(00)00038-9
- [10] Garg VK, Kumar R, Gupta R; (2004) Removal of malachite green dye from aqueous solution by adsorption using agro-industry waste: a case study of *Prosopis cineraria*. *Dyes Pigments* 62, 1–10. **DOI:**10.1016/J.DYEPIG.2003.10.016
- [11] Garg VK, Gupta R, Yadav AB, Kumar R; (2003) Dye removal from aqueous solution by adsorption on treated sawdust. *Bioresour Technol* 89, 121–124. **DOI:**10.1016/S0960-8524(03)00058-0
- [12] Batzias FA, Sidiras DK; (2004) Dye adsorption by calcium chloride treated beech sawdust in batch and fixed-bed systems. *J Hazard Mater* 114, 167–174. **DOI:**10.1016/J.JHAZMAT.2004.08.014
- [13] Witek-Krowiak A, Mitek M, Pokomeda K, Szafran RG; (2010) Biosorption of cationic dyes by beech sawdust ii. Effect of parameters on the process efficiency. *Chem Process Eng* 21, 421–432.
- [14] Dulman V, Cucu-Man SM; (2009) Sorption of some textile dyes by beech wood sawdust. *J Hazard Mater* 162, 1457–1464. **DOI:**10.1016/J.JHAZMAT.2008.06.046
- [15] Bakshi PS, Selvakumar D, Kadirvelu K, Kumar NS; (2020) Chitosan as an environment friendly biomaterial - a review on recent modifications and applications. *Int J Biol Macromol* 150, 1072–1083. **DOI:**10.1016/j.ijbiomac.2019.10.113
- [16] Pal P, Pal A, Nakashima K, Yadav BK; (2021) Applications of chitosan in environmental remediation: a review. *Chemosphere* 266, 128934. **DOI:**10.1016/j.chemosphere.2020.128934
- [17] Azmana M, Mahmood S, Hilles AR, Rahman A, Arfin MAB, Ahmed S; (2021) A review on chitosan and chitosan-based bionanocomposites: promising material for combatting global issues and its applications. *Int J Biol Macromol* 185, 832–848. **DOI:**10.1016/j.ijbiomac.2021.07.023
- [18] Szadkowski B, Marzec A; (2024) Chitosan vs chitin: comparative study of functional pH bioindicators synthesized from natural red dyes and biopolymers as potential packaging additives. *Food Hydrocoll* 150, 109670. **DOI:**10.1016/j.foodhyd.2023.109670
- [19] Cestari AR, Vieira EF, Dos Santos AG, Mota JA, de Almeida VP; (2004) Adsorption of anionic dyes on chitosan beads. 1. The influence of the chemical structures of dyes and temperature on the adsorption kinetics. *J Colloid Interface Sci* 280, 380–386. **DOI:**10.1016/j.jcis.2004.08.007
- [20] Chiou MS, Ho PY, Li HY; (2004) Adsorption of anionic dyes in acid solutions using chemically cross-linked chitosan beads. *Dyes Pigments* 60, 69–84. **DOI:**10.1016/S0143-7208(03)00140-2
- [21] Chiou MS, Li HY; (2003) Adsorption behavior of reactive dye in aqueous solution on chemical cross-linked chitosan beads. *Chemosphere* 50, 1095–1105. **DOI:**10.1016/S0045-6535(02)00636-7
- [22] Vakili M, Rafatullah M, Salamatinia B, Abdullah AZ, Ibrahim MH, Tan KB, Gholami Z, Amouzgar P; (2014) Application of chitosan and its derivatives as adsorbents for dye removal from water and wastewater: a review. *Carbohydr Polym* 113, 115–130. **DOI:**10.1016/j.carbpol.2014.07.007
- [23] Sadiq AC, Olasupo A, Ngah WSW, Rahim NY; (2021) A decade development in the application of chitosan-based materials for dye adsorption: a short review. *Int J Biol Macromol* 191, 1151–1163. **DOI:**10.1016/j.ijbiomac.2021.09.179

- [24] Hasan M, Ahmad AL, Hameed BH; (2008) Adsorption of reactive dye onto cross-linked chitosan/oil palm ash composite beads. *Chem Eng J* 136, 164–172. DOI:10.1016/J.CEJ.2007.03.038
- [25] Wong YC, Szeto YS, Cheung WH, McKay G; (2004) Adsorption of acid dyes on chitosan - equilibrium isotherm analyses. *Process Biochem* 39, 695–704. DOI:10.1016/S0032-9592(03)00152-3
- [26] Chao AC, Shyu SS, Lin YC, Mi FL; (2004) Enzymatic grafting of carboxyl groups on to chitosan - to confer on chitosan the property of a cationic dye adsorbent. *Bioresour Technol* 91, 157–162. DOI:10.1016/S0960-8524(03)00171-8
- [27] Chiou MS, Li HY; (2002) Equilibrium and kinetic modeling of adsorption of reactive dye on cross-linked chitosan beads. *J Hazard Mater* 93, 233–248. DOI:10.1016/S0304-3894(02)00030-4
- [28] Momenzadeh H, Tehrani-Bagha AR, Khosravi A, Gharanjig K; (2011) Reactive dye removal from wastewater using a chitosan nanodispersion. *Desalination* 271, 225–230. DOI:10.1016/j.desal.2010.12.036
- [29] Guibal E, Roussy J; (2007) Coagulation and flocculation of dye-containing solutions using a biopolymer (chitosan). *React Funct Polym* 67, 33–42. DOI:10.1016/J.REACTFUNCTPOLYM.2006.08.008
- [30] Barron-Zambrano J, Szygula A, Ruiz M, Sastre AM, Guibal E; (2010) Biosorption of Reactive Black 5 from aqueous solutions by chitosan: column studies. *J Environ Manage* 91, 2669–2675. DOI:10.1016/J.JENVMAN.2010.07.033
- [31] Szygula A, Guibal E, Palacín MA, Ruiz M; (2009) Removal of an anionic dye (Acid Blue 92) by coagulation - flocculation using chitosan. *J Environ Manage* 90, 2979–2986. DOI:10.1016/J.JENVMAN.2009.04.002
- [32] Dotto GL, Pinto LAA; (2011) Adsorption of food dyes onto chitosan: optimization process and kinetic. *Carbohydr Polym* 84, 231–238. DOI:10.1016/J.CARBPOL.2010.11.028
- [33] Akkaya G, Uzun I, Güzel F; (2007) Kinetics of the adsorption of reactive dyes by chitin. *Dyes Pigments* 73, 168–177. DOI:10.1016/J.DYEPIG.2005.11.005
- [34] Rezakazemi M, Shirazian S; (2019) Lignin-chitosan blend for methylene blue removal: Adsorption modeling. *J Mol Liq* 274, 778–791. DOI:10.1016/j.molliq.2018.11.043
- [35] Arumugam TK, Krishnamoorthy P, Rajagopalan NR, Nanthini S, Vasudevan D; (2019) Removal of malachite green from aqueous solutions using a modified chitosan composite. *Int J Biol Macromol* 128, 655–664. DOI:10.1016/j.ijbiomac.2019.01.185
- [36] Van Soest PJ, Robertson JB, Lewis BA; (1991) Methods for dietary fiber, neutral detergent fiber, and nonstarch polysaccharides in relation to animal nutrition. *J Dairy Sci* 74, 3583–3597. DOI:10.3168/JDS.S0022-0302(91)78551-2
- [37] Machida M, Kikuchi Y, Aikawa M, Tatsumoto H; (2004) Kinetics of adsorption and desorption of Pb(II) in aqueous solution on activated carbon by two-site adsorption model. *Colloids Surf A Physicochem Eng Asp* 240, 179–186. DOI:10.1016/J.COLSURFA.2004.04.046
- [38] Hinz C; (2001) Description of sorption data with isotherm equations. *Geoderma* 99, 225–243. DOI:10.1016/S0016-7061(00)00071-9
- [39] Wang S, Zhu ZH; (2005) Sonochemical treatment of fly ash for dye removal from wastewater. *J Hazard Mater* 126, 91–95. DOI:10.1016/J.JHAZMAT.2005.06.009
- [40] Gonçalves JO, Duarte DA, Dotto GL, Pinto LAA; (2013) Use of chitosan with different deacetylation degrees for the adsorption of food dyes in a binary system. *Clean (Weinh)* 42, 767–774. DOI:10.1002/clen.201200665

- [41] Wu H, Zhou J, Zhang S, Niu P, Li H, Liu Z, Zhang N, Li Ch, Wang L, Wang Y; (2024) A comparative study of removal of acid red 27 by adsorption on four different chitosan morphologies. *Polymers* 16, 1019. **DOI:**10.3390/polym16071019
- [42] Józwiak T, Filipkowska U, Szymczyk P, Zyśk M; (2017) Effect of the form and deacetylation degree of chitosan sorbents on sorption effectiveness of Reactive Black 5 from aqueous solutions. *Int J Biol Macromol* 95, 1169–1178. **DOI:**10.1016/j.ijbiomac.2016.11.007
- [43] Qamar SA, Ashiq M, Jahangeer M, Riasat A, Bilal M; (2020) Chitosan-based hybrid materials as adsorbents for textile dyes - a review. *Case Stud Chem Environ Eng* 2, 100021. **DOI:**10.1016/j.csee.2020.100021
- [44] da Silva Alves DC, Healy B, Pinto LAA, Cadaval TRSJ, Breslin CB; (2021) Recent developments in chitosan-based adsorbents for the removal of pollutants from aqueous environments. *Molecules* 26, 594. **DOI:**10.3390/molecules26030594
- [45] Wu FC, Tseng RL, Juang RS; (2000) Comparative adsorption of metal and dye on flake- and bead-types of chitosans prepared from fishery wastes. *J Hazard Mater* 73, 63–75. **DOI:**10.1016/S0304-3894(99)00168-5
- [46] Lazaridis NK, Keenan H; (2010) Chitosan beads as barriers to the transport of azo dye in soil column. *J Hazard Mater* 173, 144–150. **DOI:**10.1016/J.JHAZMAT.2009.08.062
- [47] Gibbs G, Tobin J, Guibal E; (2004) Influence of Chitosan Preprotonation on Reactive Black 5 Sorption Isotherms and Kinetics. *Ind Eng Chem Res* 43(1), 1-11. **DOI:**10.1021/ie030352p
- [48] Elwakeel KZ; (2009) Removal of Reactive Black 5 from aqueous solutions using magnetic chitosan resins. *J Hazard Mater* 167, 383–392. **DOI:**10.1016/j.jhazmat.2009.01.051
- [49] Kyzas GZ, Lazaridis NK; (2009) Reactive and basic dyes removal by sorption onto chitosan derivatives. *J Colloid Interface Sci* 331, 32–39. **DOI:**10.1016/J.JCIS.2008.11.003
- [50] Akkaya G, Uzun I, Güzel F; (2009) Adsorption of some highly toxic dyestuffs from aqueous solution by chitin and its synthesized derivatives. *Desalination* 249, 1115–1123. **DOI:**10.1016/J.DESAL.2009.05.014

COMPARISON OF THE EFFECTIVENESS OF CHITOSAN AND AUXIN ON *IN VITRO* AND *EX VITRO* ROOTING OF *Vaccinium corymbosum* L.

Marcelina Krupa-Malkiewicz^{1,a,*}, Ireneusz Ochmian^{2,b}

¹ – Department of Plant Genetics, Breeding and Biotechnology, West Pomeranian University of Technology Szczecin, Słowackiego 17 Str., 71-434 Szczecin, Poland

^a – ORCID: 0000-0002-4333-9122

² – Department of Horticulture, West Pomeranian University of Technology Szczecin, Słowackiego 17 Str., 71-434 Szczecin, Poland

^b – ORCID: 0000-0002-3606-1927

*corresponding author: mkrupa@zut.edu.pl

Abstract

A highly efficient micropropagation process can be achieved by using proper conditions for root initiation and growth of regenerated shoots. The efficiency of auxin and chitosan on *in vitro* rhizogenesis of the highbush blueberry (*Vaccinium corymbosum* L.) cv. Liberty was developed. After the multiplication stage, explants were transferred to Woody Plant Medium (WPM) supplemented with 0.1 mg dm⁻³ zeatin and 1.0 or 2.0 mg dm⁻³ of the auxin indole-3-butyric acid (IBA), or chitosan with a molecular weight of 800 kDa at a concentration of 20 or 40 ppm. Among the tested combinations, the maximum mean shoot and root length (6.28 and 1.73 cm, respectively) were recorded for WPM with 0.1 mg dm⁻³ zeatin and 2.0 mg dm⁻³ IBA. The higher chitosan concentration in the WPM medium increased the length of shoots and roots. The highest percentage (100%) of rooted plants was obtained on WPM with the addition of 0.1 mg dm⁻³ zeatin and 40 ppm chitosan. Moreover, leaves of the highbush blueberries from this medium were brighter (*L** from 22% to 36%) and greener (*a** -2.70 and -4.56, respectively) compared with the leaves of plants grown on WPM containing IBA.

Keywords: plant acclimatisation, biopolymer, rhizogenesis, medium, highbush blueberry, Cie *L** *a** *b**

Received: 27.02.2024

Accepted: 24.05.2024

1. Introduction

The blueberry (genus *Vaccinium* L., family Ericaceae Juss.) is a very popular fruit. Its production and consumption have increased globally, characterised in particular by the expansion of production activities into new geographic areas [1]. Poland ranks second in Europe and seventh in the world in blueberry production [2]. The leader in highbush blueberry plantations in terms of cultivated area is the Masovian Voivodeship. According to Cüce and Sökmen [3], the genus *Vaccinium* is more variable than other members of the Ericaceae family. These genetic variations manifest in different growth habits, fruiting times and responses to environmental conditions. *In vitro* culture conditions, including medium composition, need to be adapted to the specific needs of each cultivar to optimise growth and development. Cultivars differ in their ability to cope with the stress associated with tissue culture. Researchers typically perform extensive trials to determine the optimal conditions for each cultivar, including testing different medium compositions and environmental conditions. This ensures that each cultivar grows robustly and healthily, ultimately leading to successful acclimatisation and adaptation to field conditions.

Blueberries have low endogenous hormone levels, and enrichment of the environment with appropriate auxins and organic supplements is a prerequisite for the formation of a good root system [4]. According to Debnath and McRae [5], *Vaccinium macrocarpon* Ait. shoots rooted well *in vitro* in the same media used for shoot proliferation, but without any growth regulators. Tetsumura et al. [6] described that the rooting of shoots of three cultivars of *Vaccinium corymbosum* L. was affected by the multiplication media, namely Murashige and Skoog (MS) [7], Woody Plant Medium (WPM) [8] and a mixture of equal parts of MS and WPM (MW). However, they noticed that the superiority in rooting percentage varied with the cultivar. In other related studies, Ružic et al. [9] examined the effect of the auxin indole-3-butyric acid (IBA) and active charcoal on induction of rhizogenesis in three cultivars of *V. corymbosum*, and Erst et al. [10] investigated the effect of IBA and indole-3-acetic acid (IAA) on *in vitro* rhizogenesis of *Vaccinium uliginosum* L. These researchers confirmed that rooting capacity of shoots varied widely among the tested cultivars.

As is apparent from the literature, the blueberry species *V. corymbosum* and *V. virgatum* root well on propagation medium or on medium without the addition of plant growth regulators. The process of root development can be divided broadly into two primary phases: initiation of roots and their subsequent elongation. During the initiation phase *in vitro*, specific cells undergo dedifferentiation to create root meristems, which then proceed to elongate. Each phase, root initiation and root elongation, has different optimal conditions for plant growth regulators, especially auxin [3]. It is important to consider the potential benefits of using naturally derived, biologically active substances that have a minimal environmental impact and can support both phases of rooting. Due to its characteristics, chitosan is viewed as a biomaterial of interest for plant growth [11, 12]. There are many reports about its positive effects on the growth and yield of plants such as *Dendrobium phalaenopsis* [13], *V. corymbosum* [14], *Lycium chinense* [15], *Vitis vinifera* L. [16] and *Lonicera caerulea* L. [17]. The mechanism of action of chitosan in plant systems is not yet completely clear. According to Lopez-Moya et al. [18], chitosan promotes the accumulation of auxins (mainly IAA) in the root apex of plants, causing strong changes in root cell morphology. Chitosan treatment can induce several biochemical and molecular changes that may be responsible for improving plant growth including rooting, as shown in the examples above [19–21].

The present study compared the effectiveness of chitosan with a molecular weight of 800 kDa (CH₈) and IBA on *in vitro* rooting and *ex vitro* acclimatisation of *V. corymbosum* cv. Liberty explants.

2. Materials and Methods

2.1. Plant Material

V. corymbosum cv. Liberty explants were obtained from the Laboratory of Tissue Culture, West Pomeranian University of Technology, Szczecin, Poland. The shoots with auxiliary buds explants were sub-cultured several times. The stem segments of blueberry explants were cut into several small pieces (approximately 17–20 mm long) and removed from the leaf blades.

2.2. *In Vitro* Rooting Conditions

In a laminar flow cabinet, shoot explants were initiated on Woody Plant Medium (Duchefa Biochemie B.V., the Netherlands) with the addition of 0.1 mg dm⁻³ zeatin (Zea) and CH₈ at a concentration of 20 and 40 ppm, or on WPM supplemented with 0.1 mg dm⁻³ Zea and 1.0 or 2.0 mg dm⁻³ IBA. The pH of each medium was adjusted to 5.7–5.8. Zea, CH₈ and IBA were added to the media before autoclaving.

All media were supplemented with 3% (w/v) sucrose (Chempur, Poland), 0.8% (w/v) agar (Biocorp, Poland) and 100 mg dm⁻³ myo-inositol (Duchefa Biochemie B.V., The Netherlands). Then, they were heated and 30 ml was poured into a 450-ml flask. Next, they were autoclaved at 121°C (0.1 MPa) for the appropriate time (based on the volume of medium in the vessel). Cultures were incubated in a growth room at 24 ± 2°C under a 16-h photoperiod with a photosynthetic photon flux density (PPFD) of 40 μmol m⁻² s⁻¹. Each combination included 32 shoots (8 replicates with 4 explants per flask). After 35 days, the explants were removed and wash with deionised distilled water, and the shoot and root length (cm), the number of new shoots and the colour were assessed. The explants were weighed to determine the fresh mass (g).

2.3. Chitosan

CH₈ was obtained from the Center of Bioimmobilisation and Innovative Packaging Materials, West Pomeranian University of Technology, Szczecin, Poland [22]. It was prepared using the free-radical degradation process. After purification (filtration), it was characterised using high-performance liquid chromatography (SmartLine Knauer, Germany; Tessek Separon HEMA-BIO 40 column, Tessek, Czech Republic). The average degree of deacetylation of the product was 85%.

2.4. *Ex Vitro* Acclimatisation

Explants with developed roots from all combinations of the experiment were removed from the culture vessels and then washed thoroughly with deionised water to remove residual medium. The explants were transferred to plastic pots (10-cm diameter) containing sterile soil (a mixture of 90% peat and 10% perlite). The pots were covered with agro-textile fabric to ensure 90% humidity and incubated in the growth room at 22°C and 73% relative humidity. After acclimatisation for 6 weeks, the percentage survival of the plants was determined.

2.5. Determination of Colour

The leaves from the middle part of the shoot were evaluated using a CM-700d spectrophotometer (Konica Minolta, Japan). Measurements were made in CIE *L*a*b** system [23]. The 10° observer type and D65 illuminant were applied. Colour was measured

in triplicate for each experimental combination. a^* ranges from green ($-a^*$) to red ($+a^*$). b^* describes the colour in the range from yellow ($+b^*$) to blue ($-b^*$). L^* , which represents monochromaticity, ranges from 0 (black) to 100 (white).

2.6. Statistical Analysis

The results were evaluated using the Statistica v.12 software. The results were submitted to variance analysis (ANOVA) followed by Tukey's test. A p value ≤ 0.05 was considered to indicate a statistically significant difference.

3. Results and Discussion

A successful micropropagation system requires the proper conditions for root initiation and growth of regenerated shoots. Healthy roots enable seedlings to establish in the soil and promote normal growth and development. There have been many reports of successful *in vitro* and *ex vitro* rooting of blueberries. Efficient *in vitro* rhizogenesis is generally strongly influenced by the presence of auxins in the medium [10, 24]. Ostrolucká et al. [25] achieved rooted *V. corymbosum* and *Vaccinium vitis-idaea* L. microshoots on Anderson's medium supplemented with 0.8 mg dm^{-3} IBA. Meiners et al. [24] examined IBA and naphthaleneacetic acid (NAA) for their effect on root formation of the *Vaccinium* cultivars Ozarkblue and Red Pearl; they noticed that only IBA was suitable for root induction. Tetsumura et al. [6] compared MS, WPM and MW and observed that the rooting ability of blueberry plants is strictly dependent on the cultivar as well as the multiplication medium. The effectiveness of chitosan on the rooting of highbush blueberry plants remains incompletely investigated. Chitosan is a biopolymer that is completely safe for the environment. It shows positive effects on the growth of many plants, including those propagated *in vitro*. According to Veraplakon et al. [26], chitosan increased the survival percentage and growth rate of *ex vitro* lantana seedlings. Kruczek et al. [15] reported that 20 ppm of chitosan with a molecular weight of 330 kDa was optimal for the initiation of goji explant rhizogenesis *in vitro*. Krupa-Małkiewicz and Ochmian [16] confirmed that 10 ppm of chitosan with a molecular weight of 330 kDa stimulated rhizogenesis of winegrape explants.

Table 1 provides the mean shoot length, number of new shoots, fresh and dry mass of *V. corymbosum* cv. Liberty. WPM containing 0.1 mg dm^{-3} Zea and 2.0 mg dm^{-3} IBA provided the best stimulation of shoot length and root development: compared with the other culture media used, highbush blueberry explants grown on this medium showed longer shoots and roots (6.28 and 1.73 cm, respectively). Good rhizogenesis was correlated with the highest mean fresh and dry mass of the plantlets (0.91 and 0.14 g, respectively). However, there were no significant differences in the number of new explants, which ranged from 1.25 to 1.92. Of the two chitosan concentrations applied in the experiment, 40 ppm was the most efficient in stimulating root growth (Figure 1). Explants grown on WPM containing 40 ppm CH_8 had 44% and 67% longer shoots and roots, respectively, compared with explants grown on WPM containing 20 ppm CH_8 . The inclusion of 40 ppm CH_8 also led to the highest number of new explants (1.92 per plant).

Table 1. The effects of different medium compositions on the morphological traits of *Vaccinium corymbosum* vs. Liberty plants under *in vitro* condition after 35 days of culture (n = 32 shoots per treatment).

Medium	Shoot length [cm]	Number of new explants	Root length [cm]	Fresh mass [g]	Dry mass [g]
WPM + 0.1 mg dm ⁻³ Zea + 1.0 mg dm ⁻³ IBA	2.89 ^b	1.25 ^a	0.88 ^{ab}	0.88 ^a	0.12 ^a
WPM + 0.1 mg dm ⁻³ Zea + 2.0 mg dm ⁻³ IBA	6.28 ^a	1.83 ^a	1.73 ^a	0.91 ^a	0.14 ^a
WPM + 0.1 mg dm ⁻³ Zea + 20 ppm CH ₈	2.57 ^b	1.45 ^a	0.16 ^b	0.16 ^a	0.02 ^b
WPM + 0.1 mg dm ⁻³ Zea + 40 ppm CH ₈	3.56 ^b	1.92 ^a	0.19 ^b	0.28 ^a	0.04 ^b

Note. In each column, means with different superscript letters are significantly different according to Tukey's multiple range test ($p < 0.05$). Abbreviations: CH₈, chitosan with a molecular weight of 800 kDa; IBA, indole-3-butyric acid; WPM, Woody Plant Medium; Zea, zeatin.

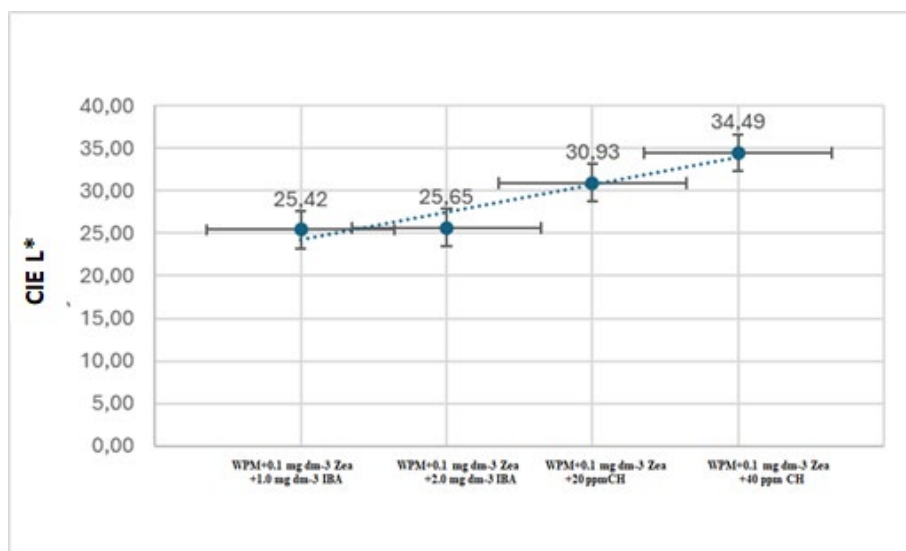


Figure 1. Shoot explants of *Vaccinium corymbosum* L. cv. Liberty after growth for 6 weeks on Woody Plant Medium (WPM) containing (a) 0.1 mg dm⁻³ zeatin (Zea) + 1.0 mg dm⁻³ indole-3-butyric acid (IBA); (b) 0.1 mg dm⁻³ Zea + 2.0 mg dm⁻³ IBA; (c) 0.1 mg dm⁻³ Zea + 20 ppm chitosan with a molecular weight of 800 kDa (CH₈); or (d) 0.1 mg dm⁻³ Zea + 40 ppm CH₈.

Many authors [27–29] have suggested that the contents of photosynthetic pigments in leaves are closely correlated to their colour. The colour of the leaves was analysed in the transmitted mode using the photocolourimetric method in the CIE $L^*a^*b^*$ system [23]. L^* is related to the physiological attributes of visual response [30]. In the present study, the leaves of the explants grown on WPM containing IBA were similar. L^* was 25.42 and 25.65 (Figure 2a). However, the leaves of the explants grown on WPM containing 20 or 40 ppm CH₈ were brighter, as indicated by the 36% and 22% higher L^* values, respectively, compared with the explants grown on WPM containing IBA. Moreover, the explants grown on WPM containing 20 or 40 ppm CH₈ had greener leaves ($a^* = -2.70$

and -4.56, respectively) compared with the leaves of the explants grown on WPM containing IBA (Figure 2b). When higher concentrations of IBA or CH₈ were used in the medium, *b**, which indicates chromaticity, was higher (Figure 2b). Therefore, for the subsequent acclimatisation to greenhouse conditions, only plantlets with well-developed roots and the best rhizogenesis rooted on WPM supplemented with IBA and WPM supplemented with CH₈ were selected.

(a)



(b)

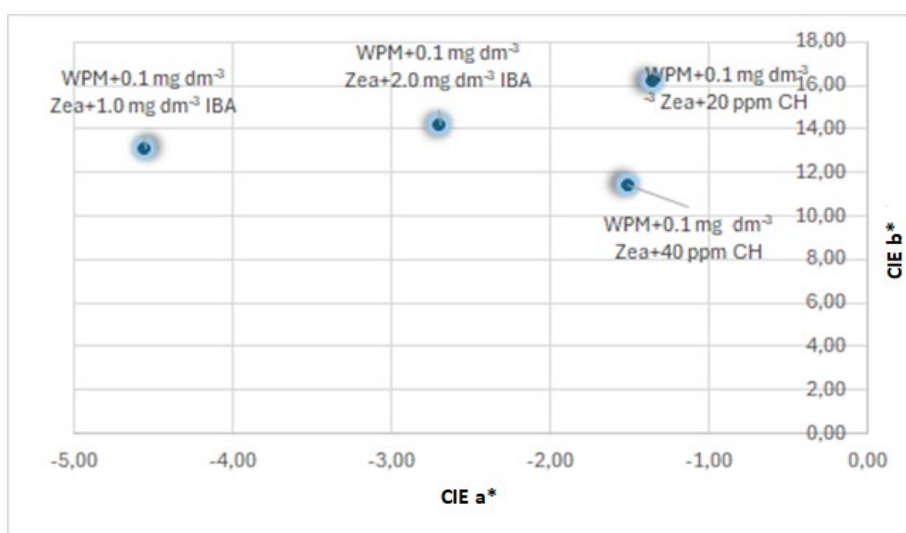


Figure 2. The effect of different medium compositions on the colour of *Vaccinium corymbosum* cv. Liberty leaves ($n = 32$ shoots per treatment) based on the CIE $L^*a^*b^*$ system – (a) L^* , the lightness coefficient and (b) a^* (green colour) and b^* (yellow colour) – at the end of the experiment. Abbreviations: CH₈, chitosan with a molecular weight of 800 kDa; IBA, indole-3-butyric acid; WPM, Woody Plant Medium; Zea, zeatin.

The *ex vitro* rooting rate of *V. corymbosum* cv. Liberty was the highest on WPM containing 0.1 mg dm⁻³ Zea and 2.0 mg dm⁻³ IBA or 40 ppm CH₈ (98% and 100%, respectively) (Figure 3a, b). The lowest rooting efficiency (80%) was observed on WPM containing 0.1 mg dm⁻³ Zea and 20 ppm CH₈ (Figure 4). Ružić et al. [9] obtained a similar *ex vivo* rooting rate for the Goldtraube (91.8%) and Berkeley (66.7%) cultivars. Ostroľucká et al. [31] used Anderson's Rhododendron medium (AN) containing 0.8 mg dm⁻³ IBA and 8 g dm⁻³ charcoal and recorded a rooting percentage of 95%, 90% and 80% for the blueberry cultivars Berkeley, Bluecrop and Brigitta, respectively. In contrast, Erst et al. [10] found that the optimal technique of *in vitro* rooting of *V. uliginosum* involved treating microshoots with an auxin solution for 24 h, followed by transfer to media that did not contain growth regulator. They obtained a 100% rooting percentage for explants of the Golubaya rossyp and Naktarnaya cultivars.

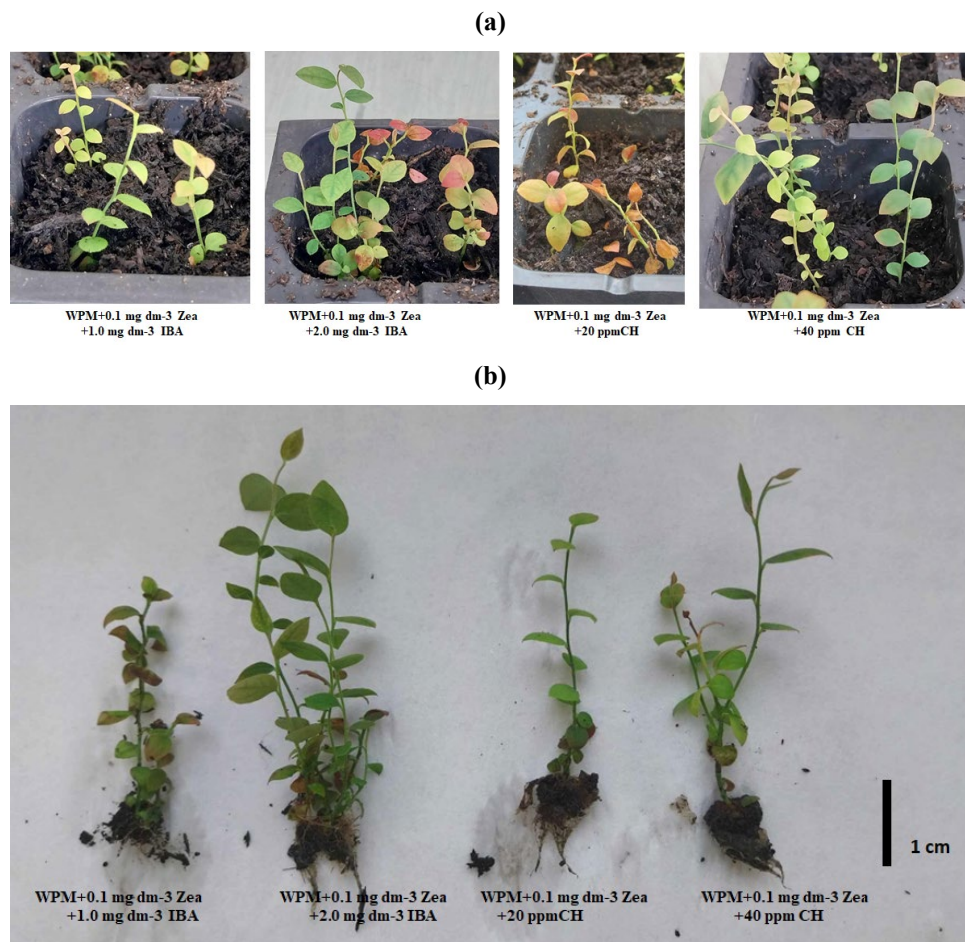


Figure 3. The photographs show *Vaccinium corymbosum* cv. Liberty plants (a) after being acclimatized for 35 days and (b) after transfer to the greenhouse (b). Abbreviations: CH₈, chitosan with a molecular weight of 800 kDa; IBA, indole-3-butyric acid; WPM, Woody Plant Medium; Zea, zeatin.

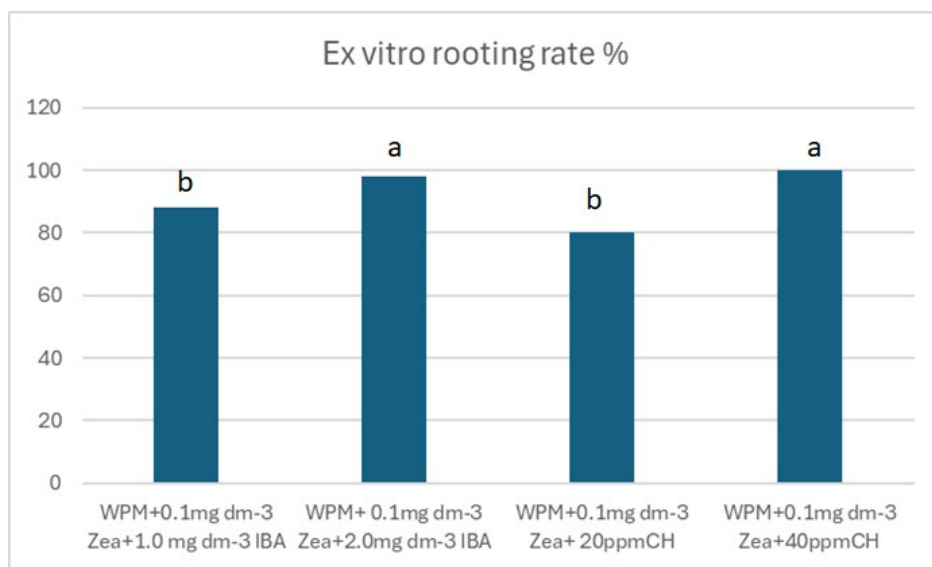


Figure 4. The *ex vitro* rooting rate of *Vaccinium corymbosum* cv. Liberty plants. Abbreviations: CH₈, chitosan with a molecular weight of 800 kDa; IBA, indole-3-butyric acid; WPM, Woody Plant Medium; Zea, zeatin.

4. Conclusions

The obtained results enrich the knowledge on *in vitro* and *ex vitro* rooting of *V. corymbosum* cv. Liberty. Based on the results of this experiment, the addition of CH₈ to WPM resulted in a rooting rate similar to that of the auxin IBA. However, the addition of 40 ppm chitosan to WPM resulted in longer shoots, more new shoots per plant and longer roots compared with the lower chitosan concentration (20 ppm). Moreover, the addition of a higher concentration of IBA to WPM (2.0 mg dm⁻³) resulted in more plants with longer roots. The addition of 40 ppm CH₈ had a positive effect on the percentage of rooted plants. Research into the development of an optimal rooting protocol for *V. corymbosum* should improve plant survival at later stages of adaptation to *ex vitro* conditions.

5. Acknowledgements

This work was supported by the West Pomeranian University of Technology, Szczecin (grant number 518-07-014-3171-03/18).

6. References

- [1] Brazelton C; (2013) World blueberry acreage & production. North American Blueberry Council, Folsom.
- [2] Brazelton C, Young K; (2017) World blueberry statistics and global market analysis. Spring Preview for GBC. 2017. International Blueberry Organization.
- [3] Cüce M, Sökmen A; (2017) *In vitro* production protocol of *Vaccinium uliginosum* L. (Bog bilberry) growing in the Turkish flora. Turkish J Agric Forest 41(4), 294–304. DOI:10.3906/tar-1704-19

- [4] Georgieva M, Kondakova V; (2021) *In vitro* propagation of *Vaccinium corymbosum* L. Bulgarian J Agric Sci 27(2), 323–327.
- [5] Debnath SC, McRae KB; (2001) An efficient *in vitro* shoot propagation of cranberry (*Vaccinium macrocarpon* Ait.) by axillary bud proliferation. In Vitro Cell Dev Biol-Plant 37, 243–249. DOI:10.1079/IVP2000135
- [6] Tetsumura T, Matsumoto Y, Sato M, Honsho C, Yamashita K, Komatsu H, Sugimoto Y, Kunitake H; (2008) Evaluation of basal media for micropropagation of four highbush blueberry cultivars. Sci Hort 119, 72–74. DOI:10.1016/j.scienta.2008.06.028
- [7] Murashige T, Skoog F; (1962) A revised medium for rapid growth and bioassay with tobacco tissue culture. Physiol Plant 15, 473–497.
- [8] Lloyd G, McCown B; (1980) Commercially feasible micropropagation of mountain laurel, *Kalmia latifolia*, by use of shoot-tip culture. Comb Proc Int Plant Propag Soc 30, 421–427.
- [9] Ružić D, Vujović T, Libiakova G, Cerović R, Gajdošova A; (2012) Micropropagation *in vitro* of highbush blueberry (*Vaccinium corymbosum* L.). J Berry Res 2(2), 97–103. DOI:10.3233/JBR-2012-030
- [10] Erst AA, Gorbunov AB, Erst AS; (2018) Effect of concentration, method of auxin application and cultivation conditions on *in vitro* rooting of bog blueberry (*Vaccinium uliginosum* L.). J Berry Res 8(1), 41–53. DOI:10.3233/JBR-170253
- [11] Alenazi MM, El-Ebidy AM, El-Shehaby OA, Seleiman MF, Aldhuwaib KJ, Abdel-Aziz HM; (2024) Chitosan and chitosan nanoparticles differentially alleviate salinity stress in *Phaseolus vulgaris* L. plants. Plants 13(3), 398. DOI:10.3390/plants13030398
- [12] Malerba M, Cerana R; (2016) Chitosan effects on plant systems. Int J Mol Sci 17, 996. DOI:10.3390/ijms17070996
- [13] Nge KL, Nwe N, Chandkrachang S, Stevens WF; (2006) Chitosan as a growth stimulator in orchid tissue culture. Plant Sci 170(6), 1185–1190. DOI:10.1016/j.plantsci.2006.02.006
- [14] Cabrera G, González D, Silva C, Bernardo Y, Gidekel M, Osorio J, Taboada E, Gutierrez A, Cabrera JC; (2010) Effect of chitosan on growth and development of highbush blueberry plants. Adv Chitin Sci 12, 191–195.
- [15] Kruczek A, Krupa-Malkiewicz M, Ochmian I; (2021) Micropropagation, rooting, and acclimatization of two cultivars of goji (*Lycium chinense*). Not Bot Horti Agr Cluj-Napca 49(2), 12271. DOI:10.15835/nbha49212271
- [16] Krupa-Malkiewicz M, Ochmian I; (2023) Chitosan and *meta*-topolin supplementation of the multiplication media of *Vitis vinifera* L. Prog Chem Appl Chitin Deriv 28, 46–55. DOI:10.15259/PCACD.27.011
- [17] Ochmian I, Krupa-Malkiewicz M; (2023) The effects of applying chitosan of different molecular weights on the growth and quality of kamchatka berries (*Lonicera caerulea* L.): part 1. Prog Chem Appl Chitin Deriv 28, 119–127. DOI:10.15259/PCACD.28.011
- [18] Lopez-Moya F, Escudero N, Zavala-Gonzalez EA, Esteve-Bruna D, Blázquez MA, Alabadi D, Lopez-Llorca LV; (2017) Induction of auxin biosynthesis and WOX5 repression mediate changes in root development in *Arabidopsis* exposed to chitosan. Sci Rep 7(1), 16813. DOI:10.1038/s41598-017-16874-5
- [19] Sopalun K, Thammasiri K, Ishikawa K; (2010) Effects of chitosan as the growth stimulator for *Grammatophyllum speciosum in vitro* culture. Int J Innov Res Sci Eng Technol 4(11), 828–830.

- [20] Krupa-Małkiewicz M, Smolik B; (2019) Alleviative effects of chitosan and ascorbic acid on *Petunia* × *atkinsiana* D. Don under salinity. *Eur J Hortic Sci* 84(6), 359–365. **DOI:**10.17660/eJHS.2019/84.6.5
- [21] Coelho N, Romano A; (2022) Impact of chitosan on plant tissue culture: recent applications. *Plant Cell Tissue Org Cult* 148, 1–13. **DOI:**10.1007/s11240-021-02156-6
- [22] Bartkowiak A; (2001) Binary polyelectrolyte microcapsules based on natural polysaccharides. Szczecin University of Technology, Szczecin.
- [23] Hunterlab; (2012) Measuring Colour using Hunter L, a, b versus CIE 1976 L*a*b*. <http://www.hunterlab.com/an-1005b.pdf>.
- [24] Meiners J, Schwab M, Szankowski I; (2007) Efficient *in vitro* regeneration systems for *Vaccinium species*. *Plant Cell Tissue Org Cult* 89, 169–176. **DOI:**10.1007/s11240-007-9230-7
- [25] Ostrolucká MG, Libiaková G, Ondrušková E, Gajdošová A; (2004) *In vitro* propagation of *Vaccinium species*. *Acta Univ Latviensis* 676, 207–676.
- [26] Veraplakorn V, Kudan S; (2021) Chitosan elicitor stimulation of *in vitro* growth and *ex vitro* acclimatization of *Lantana camara* L. *Agr Nat Resour* 55, 431–439. **DOI:**10.34044/j.anres.2021.55.3.13
- [27] Pacewicz K, Gregorczyk A; (2009) Porównanie ocen zawartości chlorofilu chlorofilometrami SPAD-502 i N-Tester. *Folia Pomer Univ Technol Stetin Agric Aliment Pisc Zootech* 269, 49–46. [In Polish]
- [28] Ochmian I, Kubus M, Dobrowolska A; (2013) Description of plants and assessment of chemical properties of three species from the *Amelanchier* genus. *Dendrobiology* 70, 59–64. **DOI:**10.12657/denbio.070.006
- [29] Krupa-Małkiewicz M, Calomme M; (2021) Actisil application affects growth, flowering, and biochemical parameters in petunia *in vitro* and greenhouse. *Plant Cell Tiss Org Cult* 146, 449–459. **DOI:**10.1007/s11240-021-02078-3
- [30] Wrolstad RE, Durst RW, Lee L; (2005) Tracking color and pigment changes in anthocyanin products. *Trends Food Sci Technol* 16, 423–428. **DOI:**10.1016/j.tifs.2005.03.019
- [31] Ostrolucká MG, Gajdošova A, Ondrušková E, Libiakova G; (2009) *In vitro* propagation of several *Vaccinium corymbosum* L. and *Vaccinium vitis-idaea* L. cultivars. *Latvian J Agron/Agronomija Vestis* 12, 75–80.

ALLEVIATIVE EFFECTS OF CHITOSAN AND NANOSILVER ON *Solanum pimpinellifolium* UNDER HEAVY METAL STRESS *IN VITRO*

Marcelina Krupa-Malkiewicz^{1,a,*}, Ireneusz Ochmian^{2,b}

¹ – Department of Plant Genetics, Breeding and Biotechnology, West Pomeranian University of Technology Szczecin, Słowackiego 17 Str., 71-434 Szczecin, Poland

^a – ORCID: 0000-0002-4333-9122

² – Department of Horticulture, West Pomeranian University of Technology Szczecin, Słowackiego 17 Str., 71-434 Szczecin, Poland

^b – ORCID: 0000-0002-3606-1927

*corresponding author: mkrupa@zut.edu.pl

Abstract

This study aimed to investigate the potential mitigation of copper stress in tomato plants (*Solanum pimpinellifolium* L0566) through the addition of chitosan (CH) or nanosilver (nAg) to Murashige and Skoog (MS) medium under *in vitro* conditions. Various growth parameters; the proline, malondialdehyde (MDA), total polyphenol and mineral contents; and CIE L*a*b* colour parameters were evaluated. After the multiplication stage, the explants were transferred to MS medium (control); MS + 20 ppm chitosan with a molecular weight of 3.33 kDa (CH_{3.33}); MS + 6 mg l⁻¹ nAg; MS + 100 μM l⁻¹ copper sulfate (CuSO₄); MS + 20 ppm CH_{3.33} + 100 μM l⁻¹ CuSO₄; or MS + 6 mg l⁻¹ nAg + 100 μM l⁻¹ CuSO₄. The results indicated that while CuSO₄ or CuSO₄-nAg solutions inhibited growth traits, CH_{3.33} stimulated growth, particularly shoot production, and plants treated with CH_{3.33} exhibited better developed roots and a higher fresh mass. Additionally, CH_{3.33} alleviated the negative effects of CuSO₄ on the proline, MDA and total polyphenol contents in tomato plants. Moreover, tomato explants exhibited greener leaves, while those treated with nAg and CuSO₄ showed decreased colour values. CH_{3.33} or nAg positively influenced the mineral content of tomato leaves under heavy metal stress. This study underscores the complex interactions between growth medium components on tomato plant growth, physiology and the mineral content, highlighting the potential of chitosan in mitigating heavy metal stress in tomato plants.

Keywords: tomato, chitosan, *in vitro*, nanoparticle, copper

Received: 01.03.2024

Accepted: 11.06.2024

1. Introduction

The expansion of industrial production activities has led to an alarming increase in environmental pollution from wastewater containing heavy metals. These metals, particularly prevalent in developing countries, are disposed of directly or indirectly into the environment in significant quantities. Due to their non-biodegradable nature, heavy metals tend to accumulate in living organisms, where they create a significant risk of toxicity. When copper (Cu) is present slightly above the optimal tissue levels, it can become toxic to a plant [1, 2]. However, heavy metals as trace elements can play an important role in various oxidation and reduction reactions. For example, Cu acts as a crucial cofactor for various enzymes associated with the oxidative stress response, such as catalase, superoxide dismutase, peroxidase, cytochrome *c* oxidase, ferroxidases, monoamine oxidase and dopamine β -monoxygenase [3, 4]. Heavy metals accumulated in excessive amounts in tissues cause oxidative stress, which contributes to the release of oxygen free radicals. Due to their strong attraction to sulfur-containing peptides and proteins, free radicals reduce enzymatic and non-enzymatic antioxidant levels [5]. Reactive oxygen species (ROS) can potentially cause massive oxidation of membrane proteins and lipids, resulting in increased malondialdehyde (MDA), a by-product of lipid peroxidation [1]. Consistently, following exposure to Cu, there was a notable accumulation of MDA [6].

New solutions are being investigated to alleviate the detrimental impacts of environmental stresses on plants, including the application of biologically active substances and nanotechnology. As a relatively modern field of science, nanotechnology offers various applications in agriculture. The use of nanoparticles in agriculture provides for the elimination of nutrient deficiencies in plant tissues and enhances tolerance to stress, thus contributing to improved growth and increased yield [7]. Many authors [8, 9] have highlighted that nanosilver (nAg) improves seed germination, plant growth and photosynthetic efficiency, and reduces microbial growth on plant bodies. An alternative to the use of synthetic materials to remove heavy metals from the environment is biopolymers, including chitosan, which is widely available. Chitosan is a non-toxic, natural elicitor and biodegradable compound of natural origin, obtained by enzymatic deacetylation of chitin [10, 11]. This biocompatible biopolymer has a variety of applications in agriculture. It improves both qualitative and quantitative crop characteristics by facilitating nutrient uptake by plants [12].

In addition, it stimulates seed germination as well as shoot and root growth [13 and influences numerous metabolic and physiological processes. As a consequence, plants treated with chitosan may show increased resistance to environmental stresses [14].

The tomato, *Solanum pimpinellifolium*, is a widely favoured vegetable within the Solanaceae family. Ranked as the world's second most significant vegetable crop, it is cultivated in nearly every country. Renowned for its taste, nutritional benefits and simple cultivation process, the tomato holds a pivotal place in human diets [15, 16]. Due to the important role of the Solanaceae family in agronomic and ornamental crops, the objective of the present study was to evaluate the effectiveness of chitosan with a molecular weight of 3.33 kDa ($\text{CH}_{3.33}$) and nAg in alleviating the harmful effects of Cu stress on tomato plants under *in vitro* conditions. This study tested the hypothesis that chitosan and nAg alleviate Cu stress by enhancing growth parameters, reducing stress markers and improving mineral content and leaf colouration. Chitosan is expected to have a more pronounced beneficial effect compared with nAg.

2. Materials and Methods

2.1. Plant Materials

S. pimpinellifolium (L0566) seeds were obtained from the Tomato Genetics Resource Centre (University of California, Davis). They were disinfected by soaking in a 70% ethanol solution for 30 s, washed twice with sterile deionised water and submerged in 7% sodium hypochlorite (NaOCl) for 10 min. Then, the seeds were rinsed 3×5 min with sterile and deionised water under a laminar flow hood.

2.2. Medium and Culture Conditions

Sterilised tomato seeds were cultured individually in glass tubes (35×110 mm) containing 15 ml of initiation Murashige and Skoog (MS) medium [17] without plant growth regulators for 4 weeks. Explants were sub-cultured three times. After that, a shoot with auxiliary buds was transferred to a 300-ml flask with 30 ml of MS medium containing 20 ppm $\text{CH}_{3.33}$; MS medium containing 6 mg l^{-1} nAg (nanopowder < 100 nm particle size, Sigma-Aldrich, Germany); MS containing $100 \mu\text{l l}^{-1}$ CuSO_4 ; or MS containing $100 \mu\text{l l}^{-1}$ CuSO_4 , 20 ppm $\text{CH}_{3.33}$ and MS + $100 \mu\text{l l}^{-1}$ CuSO_4 + 6 mg l^{-1} nAg. MS medium without plant growth regulators served as the control. Each combination included 32 shoots (4 explants per flask and 8 replicates).

Following a 35-day incubation period, the explants were carefully removed and cleaned with deionised distilled water. The following parameters were assessed: shoot and root length [cm]; the number of new shoots per explant; the fresh mass [cm]; the proline, MDA and total polyphenol (TP) contents; the macroelement (phosphorus [P], potassium [K], calcium [Ca] and magnesium [Mg]) and microelement (iron [Fe], zinc [Zn], manganese [Mn] and Cu) levels; and CIE $L^*a^*b^*$ colour.

All media contained 30 g l^{-1} sucrose (Chempur, Poland) and 100 mg l^{-1} myo-inositol (Duchefa, the Netherlands) and were solidified using 8 g l^{-1} agar (Biocorp, Poland). The pH was adjusted to 5.8 prior to autoclaving at 121°C and 0.1 MPa. Cultures were incubated in a growth room at $25 \pm 2^\circ\text{C}$ under a 16-h photoperiod, with a photosynthetic flux density (PPFD) of $40 \mu\text{mol m}^{-2} \text{ s}^{-1}$ provided by Narva (Germany) emitting cool white daylight, and maintained at 60%–70% humidity.

2.3. Biochemical Analysis

The proline content of fresh tomato leaves was determined following the method outlined by Bates et al. [18], utilising a spectrophotometer set to 520 nm; it is expressed as micromoles per gram fresh weight. The MDA content was assessed according to Sudhakar et al. [19] based on the absorbance at 600, 532 and 450 nm. The mineral content in dried plant material was evaluated as per the Polish Standard (IUNG 1972) using certified reagents from Chempur and Merck (Germany). The P, K, Ca and Mg contents were measured following wet mineralisation in sulfuric acid (H_2SO_4 , 96%) and perchloric acid (HClO_4 , 70%). The Cu, Zn, Mn and Fe contents were measured following mineralisation in nitric acid (HNO_3 , 65%) and HClO_4 (70%). The K content was measured via atomic emission spectrometry. The Mg, Ca, Cu, Zn, Mn and Fe contents were measured using flame atomic absorption spectroscopy utilising a iCE 3000 Series instrument (Thermo Fisher Scientific, UK). P was assessed using the colourimetric method on a Specol 221 apparatus (Carl Zeiss, Germany) [20]. The TP content was determined spectrophotometrically by employing the Folin–Ciocalteu reagent. The standard curve, calculated using gallic acid as a standard, was measured spectrophotometrically at 700 nm and is expressed as milligrams of gallic acid equivalents (GAE) per gram of plant material.

2.4. Leaf Pigment Estimation

Leaves from the middle part of the shoot were evaluated using a CM-700d spectrophotometer (Konica Minolta, Japan). Measurements were conducted in the CIE $L^*a^*b^*$ system [21], employing the 10° observer type and the D65 illuminant. Colour readings were taken in triplicate for each experimental combination.

2.5. Statistical Analysis

Statistical analyses were conducted using Statistica 13.0 (StatSoft, Poland). The homogeneity of variance and normality of the distribution of the data were determined. Because the data showed a normal distribution, they were submitted to analysis of variance (ANOVA) followed by Tukey's post hoc test. A p value < 0.05 indicated a statistically significant difference. The relationships between macro- and microelements were analysed using agglomerative cluster analysis and classified into hierarchical groups using Ward's method.

3. Results and Discussion

Excessive amounts of heavy metals significantly inhibit plant growth due to physiological changes caused by oxidative stress. Cu toxicity can lead to severe ultrastructural damage, thus affecting key biochemical transformation processes in plants. This study was conducted to analyse the possibility of mitigating Cu stress in tomato plants by adding $\text{CH}_{3,33}$ or nAg to the medium under *in vitro* conditions. Table 1 provides the mean shoot and root length, the number of new shoots per plant and the fresh mass.

Table 1. The effects of different medium compositions on the morphological traits of *Solanum pimpinellifolium* (L0566) plants under *in vitro* condition after 35 days of culture (n = 32 shoots per treatment).

Medium	Shoot length [cm]	Number of new shoots per plant	Root length [cm]	Fresh mass [g]
MS (control)	11.30 ^b	1.6 ^{abc}	8.55 ^{ab}	1.71 ^b
MS + 20 ppm $\text{CH}_{3,33}$	12.95 ^b	2.3 ^c	11.25 ^a	1.98 ^b
MS + 6 mg l ⁻¹ nAg	12.65 ^b	1.5 ^{abc}	6.25 ^b	1.63 ^b
MS + 100 μM l ⁻¹ CuSO_4	11.35 ^b	1.1 ^a	9.35 ^b	1.41 ^{ab}
MS + 100 μM l ⁻¹ CuSO_4 + 20 ppm $\text{CH}_{3,33}$	10.95 ^b	2.1 ^{ab}	6.05 ^b	1.54 ^{ab}
MS + 100 μM l ⁻¹ CuSO_4 + 6 mg l ⁻¹ nAg	5.15 ^a	1.3 ^{bc}	12.30 ^a	0.6 ^b

Note. In each column, means followed by a different superscript letter differ significantly according to Tukey's test (p < 0.05). Abbreviations: $\text{CH}_{3,33}$, chitosan with a molecular weight of 3.33 kDa; CuSO_4 , copper sulfate; MS, Murashige and Skoog; nAg, nanosilver.

There were almost no significant differences between explants grown on different media, except the explants grown on MS containing $100 \mu\text{M l}^{-1} \text{CuSO}_4$ and $6 \text{ mg l}^{-1} \text{nAg}$ were 55% smaller compared with the control (Figure 1a). The explants grown on MS medium containing 20 ppm $\text{CH}_{3,33}$ or MS medium containing $100 \mu\text{M l}^{-1} \text{CuSO}_4$ and 20 ppm $\text{CH}_{3,33}$ showed the highest number of new shoots per plant (144% and 131% of the control, respectively). In contrast, the number of new shoots in the explants grown on MS medium containing $6 \text{ mg l}^{-1} \text{nAg}$ was the same as the control (1.6). Only the addition of CuSO_4 or CuSO_4 and nAg to the MS medium had an inhibitory effect on the number of new shoots, with a 31% and 19% reduction, respectively, compared with the control. However, the explants grown on MS medium containing $100 \mu\text{M l}^{-1} \text{CuSO}_4$ and $6 \text{ mg l}^{-1} \text{nAg}$ had longer roots compared with plants grown on the other media. The exception was explants grown on MS medium containing 20 ppm $\text{CH}_{3,33}$, which had a root length of 11.25 cm. Moreover, the roots of these plants were thicker and developed more adventitious roots (Figure 1b). In contrast, explants grown on MS medium containing $100 \mu\text{M l}^{-1} \text{CuSO}_4$ and 20 ppm $\text{CH}_{3,33}$ showed shorter roots (70% of control). There was a significant decrease in the fresh weight of plants grown on MS medium containing $100 \mu\text{M l}^{-1} \text{CuSO}_4$. However, the explants grown on MS medium containing 20 ppm $\text{CH}_{3,33}$ had the highest fresh mass (116% of control).

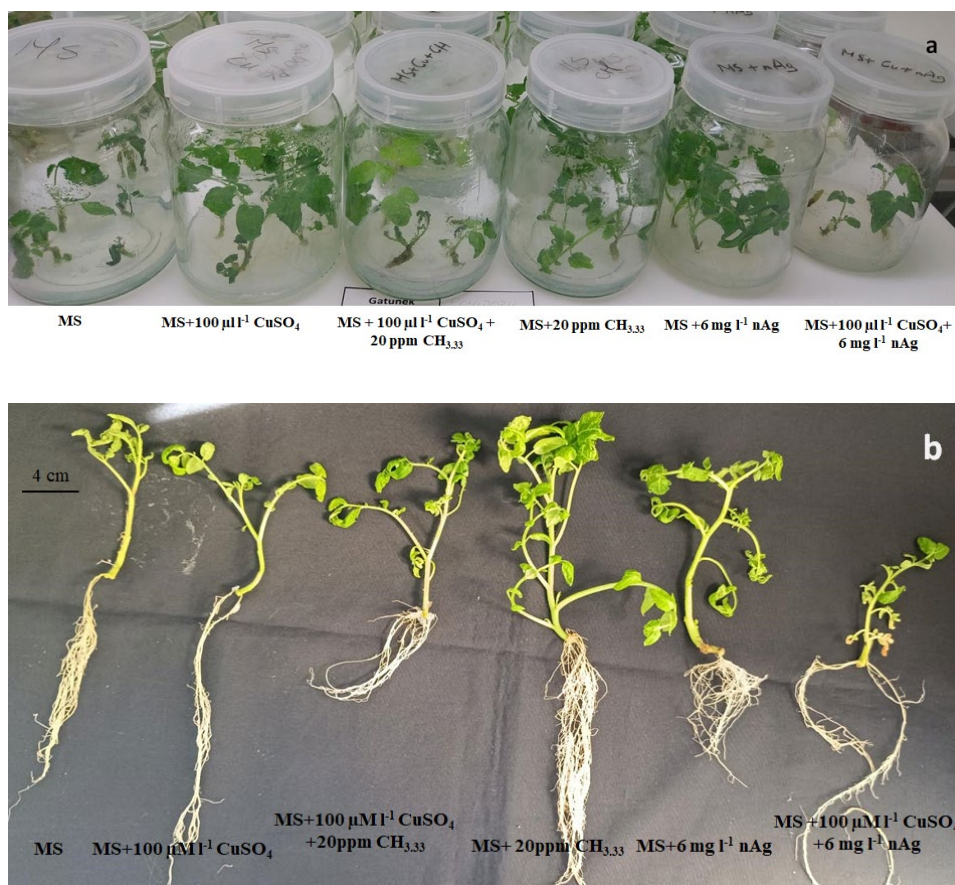


Figure 1. The photographs show the effects of chitosan ($\text{CH}_{3,33}$), nanosilver (nAg) and copper sulfate (CuSO_4) in the Murashige and Skoog (MS) medium on the growth of tomato explants (a) *in vitro* and (b) after 35 days of culture.

The results are consistent with the study by Ernst et al. [22], who observed that the roots of higher plants have some barrier to prevent the translocation of heavy metals to the shoot apices. Hence, there is likely a tolerance mechanism that acts in the root cells. Rostami and Shahsavari [23] demonstrated the impact of nAg on the morphological traits of the explants. Their findings revealed that the addition of 6.0 mg l⁻¹ nAg in MS medium reduced the growth of *Olea europea* L. plants. Krupa-Mańkiewicz et al. [8] showed that the barley cultivar Eunova seedlings with the longest roots grew on MS medium containing 4 or 8 mg l⁻¹ nAg.

The positive effect of chitosan in alleviating environmental stress in plants has been described by Pongprayonn et al. [24] in rice, Jabeen and Ahmad [25] in safflower and sunflower and Krupa-Mańkiewicz and Smolik [26] in *Petunia × atkinsiana* D. Don under salinity stress. The survival of plants growing under environmental stress conditions depends on its effect on biochemical transformation processes. This process depends on the degree of accumulation of inorganic ions and/or organic compounds [26]. According to Jabeen and Ahmad [25] and Krupa-Mańkiewicz and Smolik [26], one of the first symptoms of the effect of stress on plants is an increase in the proline, MDA and TP contents in plant tissue. In the present study, compared with the control, the proline, MDA and TP contents in tomato plants increased by 87%, 82% and 84%, respectively, after application of 100 µM l⁻¹ CuSO₄ (Table 2). The addition of 6 mg l⁻¹ nAg to MS also increased the proline (39% of control), MDA (32% of control) and the TP (12% of control) contents.

Table 2. The effects of chitosan, nanosilver (nAg) and heavy metal treatment on the proline, malondialdehyde (MDA) and total polyphenol contents in *Solanum pimpinellifolium* (L0566) leaves.

Medium	Proline [µmol g ⁻¹]	MDA [nmol g ⁻¹]	Total polyphenol [GAE mg g ⁻¹]
MS (control)	6.1 ^a	22.4 ^a	7.4 ^a
MS+ 20ppm CH _{3.33}	6.3 ^a	21.0 ^a	7.0 ^a
MS+6 mg l ⁻¹ nAg	8.5 ^b	29.5 ^b	8.3 ^b
MS+100 µM l ⁻¹ CuSO ₄	11.40 ^d	40.7 ^d	13.6 ^c
MS+100 µM l ⁻¹ CuSO ₄ + 20 ppm CH _{3.33}	9.0 ^{bc}	32.2 ^{bc}	11.2 ^d
MS+100 µM l ⁻¹ CuSO ₄ + 6 mg l ⁻¹ nAg	9.6 ^c	35.8 ^c	9.4 ^c

Note. In each column, means followed by a different superscript letter differ significantly according to Tukey's test ($p < 0.05$). Abbreviations: CH_{3.33}, chitosan with a molecular weight of 3.33 kDa; CuSO₄, copper sulfate; MS, Murashige and Skoog.

While the addition of 20 ppm CH_{3.33} or 6 mg l⁻¹ nAg alleviated the negative effect of CuSO₄, the former induced the most pronounced decrease in the proline and MDA contents (by 21% and 21%, respectively, compared with the plants treated with 100 µM l⁻¹ CuSO₄). In contrast, the addition of 6 mg l⁻¹ nAg reduced the TP content by 31%, more than the 18% reduction due to the addition of 20 ppm CH_{3.33} compared with the plants treated with 100 µM l⁻¹ CuSO₄. The findings align with those of Mahdavi and Rahimi [14]

and Krupa-Malkiewicz et al. [27], who validated the role of chitosan in regulating plant responses to various abiotic stresses. Additionally, Jabeen and Ahmad [25] highlighted chitosan's efficacy as a biostimulant in mitigating severe stress by reducing enzyme activity through ROS scavenging. Conversely, Sumalia et al. [7] suggested the utility of nanocomposites as agents to remove toxic substances.

The mineral content of plant tissues plays a crucial role in the process of proper growth and development of plants [8]. In the present study, CH_{3,33}, nAg and CuSO₄ had distinct effects on the mineral content of tomato leaves (Table 3). The addition of 100 μM l⁻¹ CuSO₄ to the MS medium decreased most of the minerals compared with the control. The addition of CH_{3,33} or nAg to the MS medium had a minimal effect on the levels of these elements. On the other hand, the addition of CH or nAg to the MS medium containing CuSO₄ had a positive influence on the mineral content of tomato leaves. The results are consistent with what Kahromi and Khara [20, 21] reported, namely that chitosan had a positive effect on the total content of most macronutrients in *Dracocephalum kotschyi*. In contrast, Krupa-Malkiewicz et al. [8] reported that the addition of 6 mg l⁻¹ nAg to the MS medium increased the content of most of minerals (N, Mg, Zn, Cu and P) in the leaves of spring barley.

Table 3. The influence of chitosan, nanosilver (nAg) and heavy metal (CuSO₄) treatment on the mineral content of *Solanum pimpinellifolium* (L0566) leaves.

	MS (control)	MS + 100 μM l ⁻¹ CuSO ₄	MS + 20 ppm CH _{3,33}	MS + 6 mg l ⁻¹ nAg	MS + 100 μM l ⁻¹ CuSO ₄ + 20 ppm CH _{3,33}	MS + 100 μM l ⁻¹ CuSO ₄ + 6 mg l ⁻¹ nAg
[g 100 g ⁻¹]						
P	0.52 ^{bc}	0.44 ^a	0.57 ^d	0.50 ^b	0.55 ^{cd}	0.42 ^a
K	4.11 ^c	4.37 ^c	3.88 ^a	4.05 ^{bc}	3.92 ^{ab}	4.20 ^d
Ca	3.87 ^c	3.36 ^a	4.12 ^e	3.95 ^{cd}	4.04 ^{de}	3.59 ^b
Mg	0.46 ^{bc}	0.51 ^d	0.41 ^a	0.48 ^{bc}	0.45 ^b	0.49 ^{cd}
[mg 1000 g ⁻¹]						
Fe	242 ^{cd}	144 ^a	255 ^d	206 ^b	230 ^c	158 ^a
Zn	27.4 ^c	35.5 ^e	22.6 ^a	25.0 ^b	24.8 ^b	30.0 ^d
Mn	26.5 ^c	12.4 ^a	28.9 ^f	18.3 ^c	22.5 ^d	14.7 ^b
Cu	5.03 ^a	11.19 ^e	5.27 ^a	7.84 ^c	6.18 ^b	9.42 ^d

Note. In each column, means followed by a different superscript letter differ significantly according to Tukey's test (p < 0.05). Abbreviations: CH_{3,33}, chitosan with a molecular weight of 3.33 kDa; CuSO₄, copper sulfate; MS, Murashige and Skoog.

A cluster analysis using Ward's method facilitated the identification of three distinct groups of media with comparable impacts on the micro- and macroelements present in tomato leaves (Figure 2). Group (a) – MS; MS + 20 ppm CH_{3,33}; and MS + 100 μM l⁻¹ CuSO₄

+ 20 ppm $\text{CH}_{3,33}$ – resulted in the highest mineral content. Group (c) – MS + 100 $\mu\text{M l}^{-1}$ CuSO_4 and MS + 100 $\mu\text{M l}^{-1}$ CuSO_4 + 6 mg l^{-1} nAg – led to the lowest mineral content. Finally, group (b) – MS + 6 mg l^{-1} nAg – led to an intermediate mineral content.

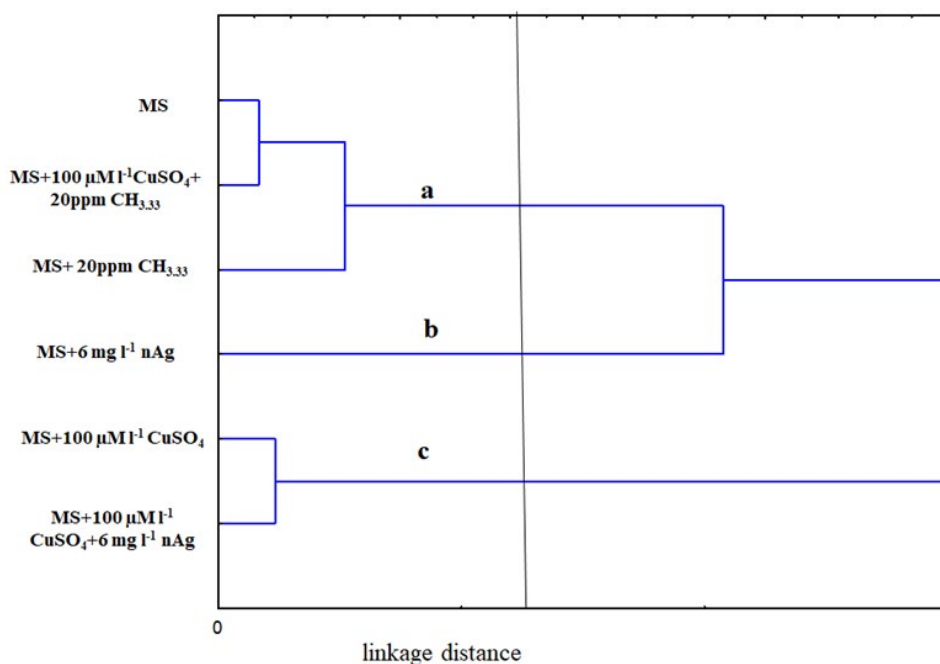


Figure 2. Dendrogram of cluster analysis of the micro- and microelements in *Solanum pimpinellifolium* (L0566) leaves grown on different medium *in vitro*. Abbreviations: $\text{CH}_{3,33}$, chitosan with a molecular weight of 3.33 kDa; CuSO_4 , copper sulfate; MS, Murashige and Skoog; nAg, nanosilver.

The condition of a plant can be assessed by measuring the colour of its leaves [10, 28, 29]. In the present study, the control tomato leaves were the brightest, as determined by L^* . The addition of CuSO_4 and $\text{CH}_{3,33}$ to the MS medium significantly decreased L^* (by 15%) compared with the control (Figure 3a). Otherwise, there were no significant differences between the treatment groups regarding brightness. The leaf surface colour defined by a^* indicates the location along the axis between green and red. The explants grown on MS medium alone or MS medium containing $\text{CH}_{3,33}$ had greener leaves (Figure 3b). In contrast, the explants grown on MS medium containing nAg and CuSO_4 showed a significant decrease in a^* (56% of control). There was a similar relationship for b^* , which indicates the blue/yellow colour. The leaves from the control explants and explants grown in MS medium containing $\text{CH}_{3,33}$ had the highest b^* ; they were more yellow compared with the other treatments (Figure 3b). The leaves from the explants grown in MS medium containing CuSO_4 and nAg had the lowest b^* (24% of control) and were bluer in colour. This change is probably due to a stress response, metal ion interaction or oxidative stress induced by nAg and Cu. These factors may interfere with the synthesis of assimilatory pigments, leading to the observed colour change [8].

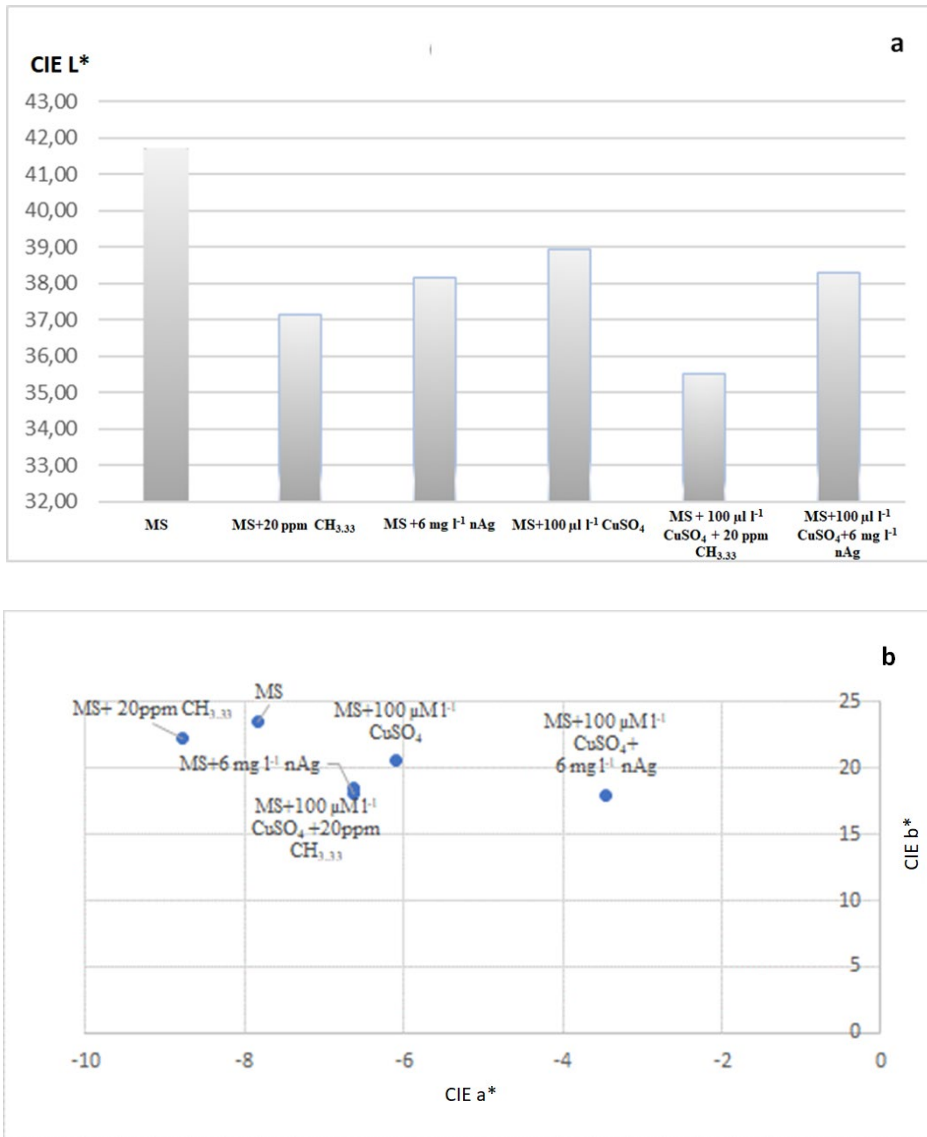


Figure 3. The effects of the medium compositions on the colour of *Solanum pimpinellifolium* (L0566) leaves (n = 32 shoots per treatment), based on the CIE $L^*a^*b^*$ system – (a) L^* , the lightness coefficient and (b) a^* (green colour) and b^* (yellow colour) – at the end of the experiment. Abbreviations: CH_{3,33}, chitosan with a molecular weight of 3.33 kDa; CuSO₄, copper sulfate; MS, Murashige and Skoog; nAg, nanosilver

4. Conclusions

The results highlight the complex interactions between heavy metals, nAg and chitosan on tomato plant growth, physiology and the mineral content, and provide valuable information for further research into optimising tomato plant growth and stress response.

The addition of chitosan to MS medium alleviated some of the harmful effects of heavy metal stress on tomato explants *in vitro* by enhancing their antioxidant defence systems. Specifically, chitosan significantly increased the fresh mass and decreased the proline and MDA contents, indicating a potential reduction in stress responses in tomato plants. Additionally, chitosan improved plant growth and health by stimulating the production of growth-promoting hormones and enhancing nutrient uptake. The effects of nAg appear to be more nuanced compared with chitosan. The addition of nAg to the growth medium did not seem to have a significant impact on shoot growth or fresh mass production, but it did influence root development in tomato plants. Furthermore, the addition of nAg increased the proline, MDA and TP contents, although to a lesser extent than CuSO₄. This suggests that nAg may induce some level of a stress response in tomato plants.

5. Acknowledgements

This work was supported by the West Pomeranian University of Technology, Szczecin (grant number 503-08087-09-0000021). The authors thank Ms. Agata Jurkiewicz, an MSc student at the Biotechnology West Pomeranian University of Technology Szczecin, for technical assistance with the experiments.

6. References

- [1] Mediouni C, Benzarti O, Tray B, Ghorbel MH, Jemal F; (2006) Cadmium and copper toxicity for tomato seedlings. *Agron Sustain Devm* 26(4), 227–232. DOI:10.1051/agro:2006008
- [2] Chamseddine M, Wided BA, Guy H, Marie-Edith C, Fatma J; (2009) Cadmium and copper induction of oxidative stress and antioxidative response in tomato (*Solanum lycopersicon*) leaves. *Plant Growth Regul* 57, 89–99. DOI:10.1007/s10725-008-9324-1
- [3] Stern BR; (2010) Essentiality and toxicity in copper health risk assessment: overview, update and regulatory considerations. *J Toxicol Environ Health Part A* 73(2-3), 114–127. DOI:10.1080/15287390903337100
- [4] Nazir F, Hussain A, Fariduddin Q; (2019) Hydrogen peroxide modulate photosynthesis and antioxidant systems in tomato (*Solanum lycopersicum* L.) plants under copper stress. *Chemosphere* 230, 544–558. DOI:10.1016/j.chemosphere.2019.05.001
- [5] Mishra S, Srivastava S, Tripathi RD, Govindarajan R, Kuriakose SV, Prasad MNV; (2006) Phytochelatin synthesis and response of antioxidants during cadmium stress in *Bacopa monnieri* L. *Plant Physiol Biochem* 44(1), 25–37. DOI:10.1016/j.plaphy.2006.01.007
- [6] Groppa MD, Tomaro ML, Benavides MP; (2001) Polyamines as protectors against cadmium or copper-induced oxidative damage in sunflower leaf discs. *Plant Sci* 161(3), 481–488. DOI:10.1016/S0168-9452(01)00432-0
- [7] Sumaila AO, Sumaila AS, Abdullahi AS, Usman AO, Ekwoba L; (2022) Application of chitosan-silver nanocomposites for heavy metals removal: a review study. *J Mater Environ* 13, 869–883.
- [8] Krupa-Małkiewicz M, Oszmiański J, Lachowicz S, Szczepanek M, Jaśkiewicz B, Pachnowska K, Ochmian I; (2019) Effect of nanosilver (nAg) on disinfection, growth, and chemical composition of young barley leaves under *in vitro* conditions. *J Integr Agric* 18(8), 1871–1881. DOI:10.1016/S2095-3119(18)62146-X

- [9] Ahmed F, Javed B, Razzaq A, Mashwani ZUR; (2021) Applications of copper and silver nanoparticles on wheat plants to induce drought tolerance and increase yield. *IET Nanobiotechnol* 15(1), 68–78. DOI:10.1049/nbt2.12002
- [10] Figiel-Kroczyńska M, Ochmian I, Krupa-Malkiewicz M; (2022) Effect of chitosan-based spraying on the quality of highbush blueberries (Sunrise cultivar). *Prog Chem Appl Chitin Deriv* 27, 67–78. DOI:10.15259/PCACD.27.005
- [11] Ochmian I, Krupa-Malkiewicz M; (2023) The effects of applying chitosan of different molecular weights on the growth and quality of kamchatka berries (*Lonicera caerulea* L.): part 1. *Prog Chem Appl Chitin Deriv* 27, 119–127. DOI:10.15259/PCACD.28.011
- [12] Malerba M, Cerana R; (2016) Chitosan effects on plant systems. *Int J Mol Sci* 17(7), 996. DOI:10.3390/ijms17070996
- [13] Kruczek A, Krupa-Malkiewicz M, Ochmian I; (2021) Micropropagation, rooting, and acclimatization of two cultivars of goji (*Lycium chinense*). *Not Bot Horti Agro Cluj-Napca* 49(2), 12271. DOI:10.15835/nbha49212271
- [14] Mahdavi B, Rahimi A; (2013) Seed priming with chitosan improves the germination and growth performance of ajowan (*Carum copticum*) under salt stress. *Eursia J Biosci* 7, 69–76. DOI:10.5053/ejobios.2013.7.0.9
- [15] Krupa-Malkiewicz M, Kulpa D; (2018) *In vitro* selection of *Solanum pimpinellifolium* plant tolerant to NaCl. *Folia Pomer Univ Technol Stetin Agric Aliment Pisc Zootech* 341(46), 19–28. DOI:10.21005/AAPZ2018.46.2.03
- [16] Ullah N, Basit, A, Ahmad I, Ullah I, Shah ST, Mohamed HI, Javed S; (2020) Mitigation the adverse effect of salinity stress on the performance of the tomato crop by exogenous application of chitosan. *Bull Natl Res Cen* 44, 1–11. DOI:10.1186/s42269-020-00435-4
- [17] Murashige T, Skoog F; (1962) A revised medium, for rapid growth and bioassays with tobacco tissue cultures. *Physiol Plant* 15(3), 473–479. DOI:10.1111/j.1399-3054.1962.tb08052.x
- [18] Bates LS, Waldren R, Teare I; (1973) Rapid determination of free proline for water-stress studies. *Plant Soil* 39(1), 205–207. DOI:10.1007/BF00018060
- [19] Sudhakar C, Lakshim A, Giridarakumar S; (2001) Changes in the antioxidant enzyme efficacy in two high yielding genotypes of mulberry (*Morus alba* L.) under NaCl salinity. *Plant Sci* 161(3), 613–619. DOI:10.1016/S0168-9452(01)00450-2
- [20] Ochmian I, Oszmiański J, Jaśkiewicz B, Szczepanek M; (2018) Soil and highbush blueberry responses to fertilization with urea phosphate. *Folia Hort* 30(2), 295–305. DOI:10.2478/fhort-2018-0025
- [21] Hunterlab: Measuring color using Hunter L, a, b versus CIE 1976 L*a*b* (2012) AN 1005.00, pp. 1-4. www.hunterlab.com/an-1005b.pdf.
- [22] Ernst WHO, Verkleij JAC, Schat H; (1992) Metal tolerance in plants. *Acta Bot Neerl* 41(3), 229–248. DOI:10.1111/j.1438-8677.1992.tb01332.x
- [23] Rostami AA, Shahsavari A; (2009) Nano-silver particles eliminate the *in vitro* contaminations of olive ‘Mission’ explants. *Asian J Plant Sci* 8, 505–509. DOI:10.3923/ajps.2009.505.509
- [24] Pongprayonn W, Roytrakul S, Pichayangkura R, Chadchawan S; (2013) The role of hydrogen peroxide in chitosan-induced resistance to osmotic stress in rice (*Oryza sativa* L.). *Plant Growth Regul* 70, 159–173. DOI:10.1007/s10725-013-9789-4
- [25] Jabeen N, Ahmad R; (2013) The activity of antioxidant enzymes in response to salt stress in safflower (*Carthamus tinctorius* L.) and sunflower (*Helianthus annuus* L.) seedlings raised from seed treated with chitosan. *J Sci Food Agric* 93, 1699–1705. DOI:10.1002/jsfa.5953

- [26] Krupa-Małkiewicz M, Smolik B; (2019) Alleviative effects of chitosan and ascorbic acid on *Petunia×atkinsiana* D. Don under salinity. *Eur J Horti Sci* 84(6), 359–365. **DOI:**10.17660/eJHS.2019/84.6.5
- [27] Krupa-Małkiewicz M, Smolik B, Ostojski D, Sędzik M, Pelc J; (2015) Effect of ascorbic acid on morphological and biochemical parameters in tomato seedling exposure to salt stress. *Environ Protec Natural Res* 26(2), 21–25. **DOI:**10.1515/oszn-2015-0007
- [28] Kahromi S, Khara J; (2021) Chitosan stimulates secondary metabolite production and nutrient uptake in medicinal plant *Dracocephalum kotschyi*. *J Sci Food Agric* 101(9), 3898–3907. **DOI:**10.1002/jsfa.11030
- [29] Krupa-Małkiewicz M, Calomme M; (2021) Actisil application affects growth, flowering, and biochemical parameters in petunia *in vitro* and greenhouse. *Plant Cell, Tiss Org Cult* 146, 449–459. **DOI:**10.1007/s11240-021-02078-3

PROTECTION OF THE OESOPHAGEAL MUCOSA WITH CHITOSAN GELS

Katarzyna Malolepsza-Jarmolowska^{1,a,*}, Hanna Bazan^{2,b}

¹ – Department of Drug Form Technology, Faculty of Pharmacy, The ‘Silesian Piasts’ Memorial Wrocław Medical University, Wrocław Medical University Poland, Borowska 211A Str., 50-556 Wrocław, Poland

^a – ORCID: 0000-0002-0127-835X

² – Faculty of Medicine, The ‘Silesian Piasts’ Memorial Wrocław Medical University, Wrocław Medical University Poland, J. Mikulicza-Radeckiego 5 Str., 50-345 Wrocław, Poland

^b – ORCID: 0009-0006-7699-5309

Abstract

In developed countries, gastro-oesophageal reflux is one of the most frequently diagnosed diseases. Although acid reflux is more well known, alkaline reflux is equally troublesome. In either of the two cases, the oesophageal mucosa is destroyed. The aim of this study was to analyse the possibility of eliminating the problem by using hydrogels containing dextran and chitosan to prevent irritation of the oesophageal mucosa. The addition of chitosan to all tested gels increased their dynamic viscosity, enabling better adhesion and, consequently, better protection of the mucous membrane. The addition of dextran reduced the pH of the tested gels, which allowed for the neutralisation of alkaline reflux. Based on the texture tests, chitosan and dextran increased work of adhesion.

Keywords: *alkaline gastro-oesophageal reflux, physiological gastro-oesophageal environment, hydrophilic gels, oesophageal mucosa, anti-inflammatory drugs, oesophageal infections*

Received: 01.04.2024

Accepted: 05.07.2024

1. Introduction

Gastro-oesophageal reflux disease continues to be a common disease. Indeed, based on the available literature, acid and alkaline reflux have yet to be solved effectively. It is estimated that up to half of adults complain about symptoms of this disease. A potential treatment for this disease is the use of protective gels that can adhere to the mucous membrane for a long time. The tested hydrogels are designed to protect the oesophageal mucosa against harmful factors [1–9].

The aim of the study was to investigate the effect of dextran on the properties of chitosan-containing hydrogels. First, the effect of chitosan on the physicochemical properties of the tested gels was examined. The prepared hydrogels showed a range of pH and rheological properties. Based on the *in vitro* tests, the gels can be assumed to remain at the site of application to protect the oesophageal mucosa against the irritating effects of alkaline reflux. The texture tests showed the influence of dextran concentration on the adhesion of the hydrogels. Moreover, the wide pH range of the hydrogels would allow one to select an optimal hydrogel for each patient. These *in vitro* findings require clinical confirmation.

2. Materials and Methods

2.1. Materials

The following chemicals of analytical grade were used in the experiments: chitosan with a degree of deacetylation of 93.5%, viscosity of 15 mPa·s, 1% in acetic acid (20°C) (Sea Fisheries Institute, Poland); methylcellulose with a viscosity of 400, 1500 and 4000 mPa·s, 2% in H₂O (20°C) (Aldrich Chemical Company Ltd., England); dextran with a molecular weight of 40000 (Sigma-Aldrich Chemie GmbH, Germany); and aqua purificata as required by Farmacopoeia Poland XII.

2.2. Methods

2.2.1. Preparation of Hydrogels

The gel preparation steps were:

1. Methylcellulose (4.0 g) and dextran (0.25, 0.5 or 1.0 g) were combined into a homogeneous mixture. Then, distilled water was added to reach a final mass of 100.0 g (accounting for the mass of chitosan that will be added in step 2). The mixture was cooled to 5–10°C. The resulting homogeneous gel was weighed. The amount of distilled water necessary to obtain the starting mass was added.
2. Chitosan was added to the homogenous gel (1.0 g of micronised powder). The gel was mixed thoroughly. After obtaining a homogeneous mixture, the preparation was cooled to 5–10°C.

2.2.2. Analytical Methods

2.2.2.1. pH Measurement

A potentiometric method was used to measure the pH of the prepared hydrogels at 37°C by immersing an electrode integrated with the CX-742 multifunctional multimeter (ELMETRON, Poland). pH was measured three times; the final result is the average of the three measurements.

2.2.2.2. Dynamic Viscosity

A Rheotest 2 rotational viscometer (Medingen, Germany) was used to determine the rheological properties of the prepared hydrogels. The measurements were carried out in the range Ia and IIa. A K-1 cone with a diameter of 36 mm was also used.

The measurement gap was 0.917 cm at 37°C. The shear angle was measured using 12 shear rates in the increasing direction and 11 shear rates in the decreasing direction. The measurements were carried out three times at 37°C. The result is the average of the three measurements. The dynamic viscosity and shear stress were calculated from the results of the measurements using equations (1)–(4):

- Shear stress for the range Ia: $\tau = c \times \alpha_{(1-12)} = 85.0 \times \alpha_{(1-12)}$ (1)

- Viscosity for the range Ia: $\eta = \frac{\tau}{D(1-12)} \cdot 100 = \frac{85.0 \times \alpha(1-12)}{D(1-12)} \times 100$ (2)

- Shear stress for the range IIa: $\tau = c \times \alpha_{(1-12)} = 820.2 \times \alpha_{(1-12)}$ (3)

- Viscosity for the range IIa: $\eta = \frac{\tau}{D(1-12)} \times 100 = \frac{820.2 \cdot \alpha(1-12)}{D(1-12)} \times 100$ (4)

The symbols in the above equations mean the following:

τ – shear stress [N/m²];

η – viscosity [mPa·s];

α – shear angle [°];

D – shear rate [1/s].

2.2.2.3. Measurement of Adhesion

The texture of the prepared hydrogels was examined using the Exponent TA.XT Texture Analyzer. Plus System (Stable Micro Systems, UK). The measurement tool was a ball-shaped probe (P/1S) made of stainless steel with a diameter of 2.54 cm. The following parameters were used: the speed of the probe was 0.5 mm/s; the probe lifting speed was 10 mm/s; and the height at which the probe was raised was 40 mm. During the test, the maximum allowable force was 100 g, and the probe stayed in the gel for 10 s. The measurement was started by placing the gel in a transparent cylindrical plexiglass vessel. Then, the probe was lowered above the gel surface until it contacted it directly; this contact lasted for 10 s. After selecting the appropriate program parameters, the probe detached from the gel surface and began to rise to a height of 40 mm at 10 mm/s. The preparations were tested three times at 37°C, and the results are presented as the average of three measurements.

2.2.2.4. Measurement of the Ability of the Hydrogel to Coat a Surface

Due to the lack of availability of an appropriate measuring device, a model was constructed to simulate the physiological conditions in the oesophagus [10]. It is a 25-cm-long glass tube, modelled on a water cooler, with double walls and ending with a wide opening on both sides. The entire device is thermostated. Water is maintained at 37°C, the temperature of the human body, through continuous heating and flows constantly between the inner and outer walls of the model. The outer wall of the glass tube is equipped with a measurement scale in millimetres. A plastic medical syringe is placed vertically under the mouth of the glass tube. The syringe has a scale in millimetres on its surface. The plunger is removed from the syringe and its tip is closed with a cap. The hydrogel flowing down the glass walls of the model can be collected in a syringe. With a medical syringe, 5 ml of the prepared hydrogel was applied to the top of the tube in a uniform motion. The time it took the hydrogel to flow 5, 10, 15, 20, and 25 cm and to the bottom of the tube was recorded. Hydrogel that travelled the entire length of the apparatus was collected in a syringe placed under the glass tube. The total measurement time was 10 min. The volume of hydrogel that drained into the syringe was read or the height on the scale of the glass tube at which the preparation stopped was recorded. The results are presented as the average of three measurements.

3. Results and Discussion

3.1. pH

Table 1 presents the pH of the prepared hydrogels. The hydrogels containing 4.0% methylcellulose (400, 1500 or 4000 cp) showed an initial pH range of 5.96 to 5.73. After adding 1.0% chitosan, the pH increased, with a range of 6.60 to 5.82. The addition of dextran (0.25%, 0.5% or 1.0%) decreased the pH, with a range from 5.09 to 4.46 (compared to the previous range of 5.96 to 5.73). Finally, adding both 1.0% chitosan and dextran reduced the pH, with a range of 5.36 to 4.68 (compared with the previous range of 6.60 to 5.82).

Table 1. The influence of chitosan on the pH of hydrogels containing 4.0% methylcellulose (MC) and dextran.

Gel composition	pH	pH of the gel containing 1.0% chitosan
MC 400 cp	5.96	6.60
MC 1500 cp	5.77	5.98
MC 4000 cp	5.73	5.82
MC 400 cp + 0.25% dextran	5.09	5.36
MC 1500 cp + 0.25% dextran	4.79	5.28
MC 4000 cp + 0.25% dextran	4.69	5.15
MC 400 cp + 0.5% dextran	4.82	5.25
MC 1500 cp + 0.5% dextran	4.78	4.99
MC 4000 cp + 0.5% dextran	4.64	4.85
MC 400 cp + 1.0% dextran	4.65	4.82
MC 1500 cp + 1.0% dextran	4.53	4.74
MC 4000 cp + 1.0% dextran	4.46	4.68

The methylcellulose gels enriched with chitosan had a wide pH range (from 4.0 to 7.0) at 37°C, which allows for the selection of hydrogels with physicochemical properties for specific applications. The introduction of dextran reduced the pH. There was a relationship between the dextran concentration and pH: the higher the dextran concentration, the lower the pH. Consistently, gels containing the highest dextran concentration (1.0%) showed the lowest pH. These gels could be used to neutralise the alkaline content in a gentle way, bringing the pH to the physiological level.

3.2. Rheological Tests

Table 2 shows the rheological test results. The hydrogels prepared with methylcellulose (400, 1500 or 4000 cp) showed a dynamic viscosity of 142–365 mPa·s. The addition of 1.0% chitosan increased the dynamic viscosity to 246–457 mPa·s. The addition of dextran (0.25%, 0.5% or 1.0%) also increased the dynamic viscosity to 202–348 mPa·s. Finally, the addition of 1.0% chitosan and dextran (0.25%, 0.5% or 1.0%) increased the dynamic viscosity to 268–540 mPa·s.

Table 2. The influence of chitosan on the dynamic viscosity of hydrogels containing 4.0% methylcellulose (MC) and dextran.

Gel composition	Dynamic viscosity [mPa·s]	Dynamic viscosity of the gel containing 1.0% chitosan [mPa·s]
MC 400 cp	142	246
MC 1500 cp	254	328
MC 4000 cp	365	457
MC 400 cp + 0.25% dextran	202	268
MC 1500 cp + 0.25% dextran	259	354
MC 4000 cp + 0.25% dextran	378	469
MC 400 cp + 0.5% dextran	239	279
MC 1500 cp + 0.5% dextran	265	378
MC 4000 cp + 0.5% dextran	284	480
MC 400 cp + 1.0% dextran	256	325
MC 1500 cp + 1.0% dextran	299	420
MC 4000 cp + 1.0% dextran	348	540

Dextran was added to the gels in an attempt to increase the dynamic viscosity so that the preparations could be used to protect the oesophageal mucosa. The dynamic viscosity of the gels increased as the dextran concentration increased. The addition of chitosan further increased the dynamic viscosity. The increased dynamic viscosity could enhance the ability of the preparation to adhere to the oesophageal mucosa and thus protect it against the harmful effects of alkaline food content.

3.3. Adhesion

Table 3 presents the work of adhesion results. At 37°C, the hydrogels prepared with methylcellulose (400, 1500 or 4000 cp) had a work of adhesion of 39.2–51.9 g/s. The addition of 1.0% chitosan increased the work of adhesion to 74.1–78.0 g/s. Moreover, the addition of dextran (0.25%, 0.5% or 1.0%) increased the work of adhesion to 48.6–66.2 g/s. Finally, the hydrogels containing 1.0% chitosan and 1% dextran had the highest work of adhesion: 82.5–90.0 g/s (Table 3).

Table 3. The influence of chitosan on the work of adhesion of hydrogels containing 4.0% methylcellulose (MC) and dextran.

Gel composition	Work of adhesion [g/s]	Work of adhesion of the gel containing 1.0% chitosan [g/s]
MC 400 cp	39.2	74.1
MC 1500 cp	48.3	76.0
MC 4000 cp	51.9	78.0
MC 400 cp + 0.25% dextran	48.6	82.5
MC 1500 cp + 0.25% dextran	59.1	84.2
MC 4000 cp + 0.25% dextran	59.9	86.9
MC 400 cp + 0.5% dextran	50.6	83.8
MC 1500 cp + 0.5% dextran	61.9	87.5
MC 4000 cp + 0.5% dextran	64.9	88.6
MC 400 cp + 1.0% dextran	59.4	85.2
MC 1500 cp + 1.0% dextran	63.2	88.0
MC 4000 cp + 1.0% dextran	66.2	90.0

A work of adhesion value above 5.0 g/s is indicative of good adhesion. All hydrogels showed good work of adhesion, especially the gels containing chitosan and dextran, indicating the ability to adhere to the oesophageal mucosa. The results showed that it is possible to obtain gels with high adhesive properties to the oesophageal mucosa, with a dynamic viscosity above 100 mPa·s.

3.4. Measurement of the Ability of the Hydrogel to Coat a Surface

At 37°C, the ability of the prepared hydrogels to coat a surface depended on the initial methylcellulose viscosity (400, 1500 or 4000 cp). At 400 cp, 4.5 ml flowed into the syringe; however, at 4000 cp, 4.0 ml flowed into the syringe. After adding 1.0% chitosan, 3.0 ml of the methylcellulose 400 cp gel and 1.7 ml of the methylcellulose 4000 cp gel flowed into the syringe. The addition of dextran (0.25%, 0.5% or 1.0%) further reduced the amount of gel that flowed into the syringe, with a range of 3.0 to 1.1 ml. Finally, the addition of 1.0% chitosan reduced the amount of gel that flowed into the syringe to 2.2 to 0.0 ml. The hydrogels containing 1% chitosan, methylcellulose 4000 cp and 0.5% or 1.0% dextran; 1% chitosan, methylcellulose 1500 cp and 0.5% or 1.0% dextran; or 1% chitosan, methylcellulose 400 cp and 1.0% dextran remained entirely on the test surface (Table 4).

Table 4. The influence of chitosan on the ability of hydrogels containing 4.0% methylcellulose (MC) and dextran to coat a surface.

Gel composition	Surface coating of the gel [cm] after 10 min	Surface coating of the gels containing 1.0% chitosan [cm] after 10 min
MC 400 cp	25.0 + 4.5 ml S	25.0 + 3.0 ml S
MC 1500 cp	25.0 + 4.1ml S	25.0 + 2.5 ml S
MC 4000 cp	25.0 + 4.0 ml S	25.0 + 1.7 ml S
MC 400 cp + 0.25% dextran	25.0 + 3.0 ml S	25.0 + 2.2 ml S
MC 1500 cp + 0.25% dextran	25.0 + 2.7 ml S	25.0 + 1.5 ml S
MC 4000 cp + 0.25% dextran	25.0 + 2.0 ml S	25.0 + 0.9 ml S
MC 400 cp + 0.5% dextran	25.0 + 2.6 ml S	25.0 + 0.5 ml S
MC 1500 cp + 0.5% dextran	25.0 + 2.1 ml S	25.0 + 0.0 ml S
MC 4000 cp + 0.5% dextran	25.0 + 1.3 ml S	25.0 + 0.0 ml S
MC 400 cp + 1.0% dextran	25.0 + 2.0 ml S	25.0 + 0.0 ml S
MC 1500 cp + 1.0% dextran	25.0 + 1.7 ml S	25.0 + 0.0 ml S
MC 4000 cp + 1.0% dextran	25.0 + 1.1 ml S	25.0 + 0.0 ml S

Note. 25.0 + 1.0 ml S means the gel coated the entire 25.0 cm length of the apparatus and 1.0 ml of gel was collected in the syringe. Abbreviation: S, syringe.

4. Conclusions

This study produced hydrogels that could neutralise the alkaline content that irritates the oesophagus. Based on an *in vitro* model, these gels have an excellent adhesion ability and could remain on the oesophageal mucosa for a long time. There was a wide range of dynamic viscosity, allowing for the selection of the appropriate preparation. These results may lead to significant improvements in the treatment of alkaline reflux, including the ability to personalise treatment. The next goal will be to validate the *in vitro* with *in vivo* experiments.

5. Acknowledgements

This research was financially supported by the Ministry of Health subvention from the IT Simple System of Wrocław Medical University (SIMPLE SUBZ.D190.24.070).

6. References

- [1] Sasankan P, Thota PN; (2022) Evaluation and the for diagnosis and management of Gastroesophageal reflux disease: A brief look at the updated guidelines. *Cleve Clin J Med* 89, 700–703. **DOI:**10.3949/ccjm.89a.22059
- [2] Maret-Ouda J, Markar SR, Lagergren J; (2020) Gastroesophageal reflux disease: a review. *JAMA* 324(24), 2536–2547. **DOI:**10.1001/jama.2020.21360
- [3] Katz PO, Gerson LB, Vela MF; (2013) Guidelines for the diagnosis and management of gastroesophageal reflux disease. *Am J Gastroenterol* 108, 308–328. **DOI:**10.1038/ajg.2012.444
- [4] Raban M, Žak A, Litak J, Turska M, Grochowski C; (2017) Gastroesophageal reflux disease - unit description, diagnosis and treatment. *J Educ Health Sport* 7, 215–225. **DOI:**10.5281/zenodo.825357
- [5] Vakil N, van Zanten SV, Kahrilas T; (2006) The Montreal definition and classification of gastroesophageal reflux disease: a global evidence-based consensus. *Am J Gastroenterol* 101, 1900–1920. **DOI:**10.1111/j.1572-0241.2006.00630.x
- [6] Singh M, Lee J, Gupta N, Gaddam S, Smith BK, Wani SB; (2013) Weight loss can lead to resolution of gastroesophageal reflux disease symptoms: a prospective intervention trial. *Obesity (Silver Spring)* 21, 284–290. **DOI:**10.1002/oby.20279
- [7] Jacobson BC, Somers SC, Fuchs CS, Kelly CP, Camargo CAJ; (2006) Body-mass index and symptoms of gastroesophageal reflux in women. *N Engl J Med* 354, 2340–2348. **DOI:**10.1056/NEJMoa054391
- [8] Ze EY, Kim BJ, Kang H, Kim JG; (2017) Abdominal visceral to subcutaneous adipose tissue ratio is associated with increased risk of erosive esophagitis. *Dig Dis Sci* 62, 1265–1271. **DOI:**10.1007/s10620-017-4467-4
- [9] Gao F, Gao Y, Chen X, Qian J, Zhang J; (2017) Comparison of oesophageal function tests between Chinese non-erosive reflux disease and reflux hypersensitivity patients. *BMC Gastroenterol* 17, 67. **DOI:**10.1186/s12876-017-0624-7
- [10] Małolepsza-Jarmołowska K; (2019) Influence of chitosan on the properties of gels protecting of the esophageal mucosa. *Prog Chem Appl Chitin Deriv* 24, 135–144. **DOI:**10.15259/PCACD.24.012

STUDIES ON CHITOSAN GELS WITH POLYVINYL ALCOHOL TO PROTECT THE OESOPHAGEAL MUCOSA

Katarzyna Malolepsza-Jarmołowska^{1,a,*}, Hanna Bazan^{2,b}

¹ – Department of Drug Form Technology, Faculty of Pharmacy, The 'Silesian Piasts' Memorial Wrocław Medical University, Wrocław Medical University Poland, Borowska 211A Str., 50-556 Wrocław, Poland

^a – ORCID: 0000-0002-0127-835X

² – Faculty of Medicine, The 'Silesian Piasts' Memorial Wrocław Medical University, Wrocław Medical University Poland, J. Mikulicza-Radeckiego 5 Str., 50-345 Wrocław, Poland

^b – ORCID: 0009-0006-7699-5309

Abstract

Young children have an incompletely developed digestive tract and they are susceptible to numerous disorders due to the return of acid and alkaline content to the oesophagus. The aim of the study was to analyse the ability of hydrogels containing chitosan and polyvinyl alcohol to prevent irritation of the oesophageal mucosa in children. The addition of chitosan to the tested gels increased their pH, which could be useful to neutralise gastric reflux, and dynamic viscosity. The texture tests revealed that chitosan and polyvinyl alcohol significantly increased the work of adhesion work.

Keywords: *mild treatment of reflux in children, physiological gastro-oesophageal environment, hydrophilic gels, oesophageal mucosa, anti-inflammatory drugs, oesophageal infections*

Received: 01.04.2024

Accepted: 05.07.2024

1. Introduction

Health problems related to the digestive tract affect people of all ages, including children. Diagnosing gastro-oesophageal reflux in children is a difficult task. For a long time, the so-called gold standard in this diagnosis was 24-h oesophageal pH-metry. A more modern method has recently been introduced; it uses the phenomenon of resistance, that is, oesophageal impedance. This method is much more effective than pH-metry because it allows detecting not only acid gastroesophageal reflux, but also episodes of weak acid or alkaline reflux. Research into ways to treat gastro-oesophageal reflux have suggested the possibility of using hydrogels that protect the oesophageal mucosa against harmful factors [1–9].

The aim of the study was to investigate the effect of polyvinyl alcohol on the properties of hydrogels containing chitosan that could be used to treat gastro-oesophageal reflux in children. These gels were designed so that they could be swallowed easily while thoroughly cover the oesophageal mucosa to protect it from the irritating effects of refluxed content. The prepared hydrogels had a range of pH and rheological properties and good adherence to the surface of a device imitating the physiological conditions of the oesophagus. The prepared hydrogels should remain on the oesophageal mucosa for a long time and protect it against the adverse effects of refluxed content. The *in vitro* results require confirmation with *in vivo* tests, which will be performed in subsequent research.

2. Materials and Methods

2.1. Materials

The following chemicals of analytical grade were used in the experiments: chitosan with a degree of deacetylation of 93.5%, viscosity of 15 mPa·s, 1% in acetic acid (20°C) (Sea Fisheries Institute, Poland); methylcellulose with a viscosity of 400, 1500 or 4000 mPa·s, 2% in H₂O (20°C) (Aldrich Chemical Company Ltd., UK), polyvinyl alcohol 87%–90% hydrolysed, average molecular weight 30000–70000, viscosity 4–6 cP, 4% in H₂O (20°C) (Sigma-Aldrich Chemie GmbH, Germany); and aqua purificata as required Farmacopoeia Poland XII.

2.2. Methods

2.2.1. Preparation of Hydrophilic Gel

The gel preparation steps were:

1. Methylcellulose (4.0 g) and polyvinyl alcohol (0.1, 0.3 or 0.5 g) were combined into a homogeneous mixture. Then, distilled water was added to reach a final mass of 100.0 g (accounting for the mass of chitosan that will be added in step 2). The mixture was cooled to 5–10°C. The resulting homogeneous gel was weighed. The amount of distilled water necessary to obtain the starting mass was added.
2. Chitosan was added to the homogenous gel (1.0 g of micronised powder). The gel was mixed thoroughly. After obtaining a homogeneous mixture, the preparation was cooled to 5–10°C.

2.2.2. Analytical Methods

2.2.2.1. pH

A potentiometric method was used to measure the pH of the prepared hydrogels at 37°C by immersing an electrode integrated with the CX-742 multifunctional multimeter (ELMETRON, Poland). pH was measured three times; the final result is the average of the three measurements.

2.2.2.2. Dynamic Viscosity

A Rheotest 2 rotational viscometer (Medingen, Germany) was used to determine the rheological properties of the prepared hydrogels. The measurements were carried out in the range Ia and IIa. A K-1 cone with a diameter of 36 mm was also used. The measurement gap was 0.917 cm at 37°C. The shear angle was measured using 12 shear rates in the increasing direction and 11 shear rates in the decreasing direction. The measurements were carried out three times at 37°C. The result is the average of the three measurements. The dynamic viscosity and shear stress were calculated from the results of the measurements using equations (1)–(4):

- shear stress for the range Ia: $\tau = c \times \alpha_{(1-12)} = 85.0 \times \alpha_{(1-12)}$ (1)

- viscosity for the range Ia: $\eta = \frac{\tau}{D(1-12)} \times 100 = \frac{85.0 \times \alpha_{(1-12)}}{D(1-12)} \times 100$ (2)

- shear stress for the range IIa: $\tau = c \times \alpha_{(1-12)} = 820.2 \times \alpha_{(1-12)}$ (3)

- viscosity for the range IIa: $\eta = \frac{\tau}{D(1-12)} \times 100 = \frac{820.2 \times \alpha_{(1-12)}}{D(1-12)} \times 100$ (4)

The symbols in the above equations mean the following:

τ – shear stress [N/m²];

η – viscosity [mPa·s];

α – shear angle [°];

D – shear rate [1/s].

2.2.2.3. Measurement of Adhesion

The texture of the prepared hydrogels was examined using the Exponent TA.XT Texture Analyzer. Plus System (Stable Micro Systems, UK). The measurement tool was a ball-shaped probe (P/1S) made of stainless steel with a diameter of 2.54 cm. The following parameters were used: the speed of the probe was 0.5 mm/s; the probe lifting speed was 10 mm/s; and the height at which the probe was raised was 40 mm. During the test, the maximum allowable force was 100 g, and the probe stayed in the gel for 10 s. The measurement was started by placing the gel in a transparent cylindrical plexiglass vessel. Then, the probe was lowered above the gel surface until it contacted it directly; this contact lasted for 10 s. After selecting the appropriate program parameters, the probe detached from the gel surface and began to rise to a height of 40 mm at 10 mm/s. The preparations were tested three times at 37°C, and the results are presented as the average of three measurements.

2.2.2.4. Measurement of the Ability of the Hydrogel to Coat a Surface

Due to the lack of availability of an appropriate measuring device, a model was constructed to simulate the physiological conditions in the oesophagus [10]. It is a 25-cm-long glass tube, modelled on a water cooler, with double walls and ending with a wide opening on both sides. The entire device is thermostated. Water is maintained at 37°C, the temperature of the human body, through continuous heating and flows constantly between the inner and outer walls of the model. The outer wall of the glass tube is equipped with a measurement scale in millimetres. A plastic medical syringe is placed vertically under the mouth of the glass tube. The syringe has a scale in millimetres on its surface. The plunger is removed from the syringe and its tip is closed with a cap. The hydrogel flowing down the glass walls of the model can be collected in a syringe. With a medical syringe, 5 ml of the prepared hydrogel was applied to the top of the tube in a uniform motion. The time it took the hydrogel to flow 5, 10, 15, 20, and 25 cm and to the bottom

of the tube was recorded. Hydrogel that travelled the entire length of the apparatus was collected in a syringe placed under the glass tube. The total measurement time was 10 min. The volume of hydrogel that drained into the syringe was read or the height on the scale of the glass tube at which the preparation stopped was recorded. The results are presented as the average of three measurements.

3. Results and Discussion

3.1. pH

Table 1 presents the pH of each prepared hydrogel. The hydrogels containing 4.0% methylcellulose (400, 1500 or 4000 cp) presented a pH that ranged from 5.96 to 5.73. The addition of 1% chitosan increased the pH, with a range from 6.60 to 5.82. The addition of polyvinyl alcohol (0.1%, 0.3% or 0.5%) to the gels containing 4.0% methylcellulose decreased pH, with a range from 5.93 to 5.34 (compared with the previous range from 5.96 to 5.73). Finally, the addition of 1.0% chitosan and polyvinyl alcohol reduced the pH of the gels, with a range from 6.24 to 5.55 (compared with the previous range from 6.60 to 5.82).

The use of methylcellulose along with polyvinyl alcohol provided gels with a wide pH range from 5.0 to 7.0. Of note, these gels fall within the physiological pH range of the oesophagus (4.0–7.0). Hence, gels containing methylcellulose, chitosan and polyvinyl alcohol could be of great importance to neutralise the oesophageal pH and thus treat alkaline reflux in children.

Table 1. The influence of chitosan on the pH of hydrogels containing 4.0% methylcellulose (MC) and polyvinyl alcohol.

Gel composition	pH	pH of the gel containing 1.0% chitosan
MC 400 cp	5.96	6.60
MC 1500 cp	5.77	5.98
MC 4000 cp	5.73	5.82
MC 400 cp + 0.1% polyvinyl alcohol	5.93	6.24
MC 1500 cp + 0.1% polyvinyl alcohol	5.77	6.12
MC 4000 cp + 0.1% polyvinyl alcohol	5.75	5.99
MC 400 cp + 0.3% polyvinyl alcohol	5.70	5.94
MC 1500 cp + 0.3% polyvinyl alcohol	5.63	5.87
MC 4000 cp + 0.3% polyvinyl alcohol	5.58	5.81
MC 400 cp + 0.5% polyvinyl alcohol	5.57	5.78
MC 1500 cp + 0.5% polyvinyl alcohol	5.50	5.70
MC 4000 cp + 0.5% polyvinyl alcohol	5.34	5.55

3.2. Rheological Tests

Table 2 presents the rheological test results. The hydrogels containing methylcellulose (400, 1500 or 4000 cp) had a dynamic viscosity of 142–365 mPa·s. The addition of 1.0% chitosan increased the dynamic viscosity to 246–457 mPa·s. The addition of polyvinyl alcohol (0.1%, 0.3% or 0.5%) to the gels increased the dynamic viscosity to 266–483 mPa·s. Finally, adding 1% chitosan and polyvinyl alcohol increased the dynamic viscosity to 294–579 mPa·s.

The dynamic viscosity of the gels increased as the polyvinyl alcohol concentration increased. Enrichment with chitosan further increased the dynamic viscosity. These data indicate that the gels could potentially adhere to the oesophageal mucosa and thus protect against the harmful effects of alkaline content refluxed into the oesophagus.

Table 2. The influence of chitosan on the viscosity of hydrogels containing 4.0% methylcellulose (MC) and polyvinyl alcohol.

Gel composition	Dynamic viscosity [mPa·s]	Dynamic viscosity of the gel containing 1.0% chitosan [mPa·s]
MC 400 cp	142	246
MC 1500 cp	254	328
MC 4000 cp	365	457
MC 400 cp + 0.1% polyvinyl alcohol	266	294
MC 1500 cp + 0.1% polyvinyl alcohol	298	356
MC 4000 cp + 0.1% polyvinyl alcohol	400	478
MC 400 cp + 0.3% polyvinyl alcohol	280	359
MC 1500 cp + 0.3% polyvinyl alcohol	348	445
MC 4000 cp + 0.3% polyvinyl alcohol	462	512
MC 400 cp + 0.5% polyvinyl alcohol	305	423
MC 1500 cp + 0.5% polyvinyl alcohol	379	487
MC 4000 cp + 0.5% polyvinyl alcohol	483	579

3.3. Adhesion

Table 3 shows the work of adhesion of the prepared hydrogels at 37°C. The hydrogels containing methylcellulose (400, 1500 cp or 4000 cp) had a work of adhesion of 39.2–51.9 g/s. The addition of 1.0% chitosan to these gels increased the work of adhesion to 74.1–78.0 g/s. The addition of polyvinyl alcohol (0.1%, 0.3% or 0.5%) also increased the work of adhesion to 55.4–68.1 g/s. Finally, the addition of 1.0% chitosan and polyvinyl alcohol (0.1%, 0.3% or 0.5%) increased the work of adhesion to 82.5–95.1 g/s.

A work of adhesion value above 5.0 g/s indicates good adhesion. Hence, the obtained gels are characterised by high adhesion to the oesophageal mucosa. The addition of 0.1%, 0.3% or 0.5% polyvinyl alcohol had a positive influence on the work of adhesion. Overall, it was possible to obtain hydrogels with high adhesive properties to the oesophageal mucosa.

Table 3. The influence of chitosan on the work of adhesion of hydrogels containing 4.0% methylcellulose (MC) and polyvinyl alcohol.

Gel composition	Work of adhesion [g/s]	Work of adhesion of gels containing 1.0% chitosan [g/s]
MC 400 cp	39.2	74.1
MC 1500 cp	48.3	76.0
MC 4000 cp	51.9	78.0
MC 400 cp + 0.1% polyvinyl alcohol	55.4	82.5
MC 1500 cp + 0.1% polyvinyl alcohol	58.6	84.2
MC 4000 cp + 0.1% polyvinyl alcohol	62.6	90.6
MC 400 cp + 0.3% polyvinyl alcohol	58.3	85.1
MC 1500 cp + 0.3% polyvinyl alcohol	60.4	87.5
MC 4000 cp + 0.3% polyvinyl alcohol	64.1	90.3
MC 400 cp + 0.5% polyvinyl alcohol	60.8	88.6
MC 1500 cp + 0.5% polyvinyl alcohol	64.5	92.2
MC 4000 cp + 0.5% polyvinyl alcohol	68.1	95.1

3.4. Measurement of the Ability of the Hydrogel to Coat a Surface

The ability of each hydrogel to coat the surface of the *in vitro* model was evaluated at 37°C. The coating properties of the gels depended on the initial static viscosity of methylcellulose (400, 1500 or 4000 cp). At 400 cp, 4.5 ml of the gel flowed into the syringe, while at 4000 cp, 4.0 ml of the gel flowed into the syringe. After adding 1.0% chitosan, 3.0 ml of the methylcellulose 400 cp gel and 1.7 ml of the methylcellulose 4000 cp gel flowed into the syringe. The addition of 0.1%, 0.3% or 0.5% polyvinyl alcohol notable reduced the amount of gel that flowed into the syringe (from 3.0 to 0.2 ml). Finally, of the addition of 1.0% chitosan and polyvinyl alcohol had the greatest impact: the amount of gel that flowed into the syringe ranged from 1.5 to 0.0 ml (Table 4).

Table 4. The influence of chitosan on ability of hydrogels containing 4.0% methylcellulose and polyvinyl alcohol to coat the model surface.

Gel composition	Surface coating with the gel [cm] after 10 min	Surface coating with the gel containing 1.0% chitosan [cm] after 10 min
MC 400 cp	25.0 + 4.5 ml S	25.0 + 3.0 ml S
MC 1500 cp	25.0 + 4.1ml S	25.0 + 2.5 ml S
MC 4000 cp	25.0 + 4.0 ml S	25.0 + 1.7 ml S
MC 400 cp + 0.1% polyvinyl alcohol	25.0 + 3.0 ml S	25.0 + 1.5 ml S
MC 1500 cp + 0.1% polyvinyl alcohol	25.0 + 2.7 ml S	25.0 + 0.6 ml S
MC 4000 cp + 0.1% polyvinyl alcohol	25.0 + 2.2 ml S	25.0 + 0.0 ml S
MC 400 cp + 0.3% polyvinyl alcohol	25.0 + 2.9 ml S	25.0 + 0.5 ml S
MC 1500 cp + 0.3% polyvinyl alcohol	25.0 + 2.0 ml S	25.0 + 0.0 ml S
MC 4000 cp + 0.3% polyvinyl alcohol	25.0 + 1.6 ml S	25.0 + 0.0 ml S
MC 400 cp + 0.5% polyvinyl alcohol	25.0 + 2.5 ml S	25.0 + 0.0 ml S
MC 1500 cp + 0.5% polyvinyl alcohol	25.0 + 0.8 ml S	25.0 + 0.0 ml S
MC 4000 cp + 0.5% polyvinyl alcohol	25.0 + 0.2 ml S	25.0 + 0.0 ml S

Note. 25.0 + 1.0 ml S means the gel coated the entire 25.0 cm length of the apparatus and 1.0 ml of gel was collected in the syringe. Abbreviation: S, syringe.

4. Conclusions

The results of this work showed the significant impact of chitosan and polyvinyl alcohol on several parameters of hydrogels, including the pH, dynamic viscosity, adhesion and *in vitro* coverage of the model surface. The wide pH range of the gels allows for the selection of the optimal gel for each juvenile patient depending on the content that enters the oesophagus. Due to their adhesive properties, the presented hydrogels should remain on the oesophageal mucosa for a long time and protect it against the adverse effects of regurgitation from the stomach. Although these *in vitro* results are very promising, they require verification with *in vivo* experiments. This is the focus of future research.

5. Acknowledgements

This research was financially supported by the Ministry of Health subvention from the IT Simple System of Wrocław Medical University (SIMPLE SUBZ.D190.24.070).

6. References

- [1] Mousa HM, Rosen R, Woodley FW, Orsi M, Armas D, Faure C, Fortunato J, O'Connor J, Scaggs B, Nurko S; (2011) Esophageal impedance monitoring for gastroesophageal reflux. *J Pediatr Gastroenterol Nutr* 52, 129–139. **DOI:**10.1097/MPG.0b013e3181ffde67
- [2] Maret-Ouda J, Markar SR, Lagergren J; (2020) Gastroesophageal reflux disease: a review. *JAMA* 324 (24), 2536–2547. **DOI:**10.1001/jama.2020.21360
- [3] Katz PO, Gerson LB, Vela MF; (2013) Guidelines for the diagnosis and management of gastroesophageal reflux disease. *Am J Gastroenterol* 108, 308–328. **DOI:**10.1038/ajg.2012.444
- [4] Raban M, Žak A, Litak J, Turska M, Grochowski C; (2017) Gastroesophageal reflux disease - unit description, diagnosis and treatment. *J Educ Health Sport* 7, 215–225. **DOI:**10.5281/zenodo.825357
- [5] Vakil N, van Zanten SV, Kahrilas T; (2006) The Montreal definition and classification of gastroesophageal reflux disease: a global evidence - based consensus. *Am J Gastroenterol* 101, 1900–1920. **DOI:**10.1111/j.1572-0241.2006.00630.x
- [6] Singh M, Lee J, Gupta N, Gaddam S, Smith BK, Wani SB; (2013) Weight loss can lead to resolution of gastroesophageal reflux disease symptoms: a prospective intervention trial. *Obesity (Silver Spring)* 21, 284–290. **DOI:**10.1002/oby.20279
- [7] Sasankan P, Thota PN; (2022) Evaluation and the for diagnosis and management of Gastroesophageal reflux disease: a brief look at the updated guidelines. *Cleve Clin J Med* 89, 700–703. **DOI:**10.3949/ccjm.89a.22059
- [8] Ze EY, Kim BJ, Kang H, Kim JG; (2017) Abdominal visceral to subcutaneous adipose tissue ratio is associated with increased risk of erosive esophagitis. *Dig Dis Sci* 62, 1265–1271. **DOI:**10.1007/s10620-017-4467-4
- [9] Gao F, Gao Y, Chen X, Qian J, Zhang J; (2017) Comparison of oesophageal function tests between Chinese non-erosive reflux disease and reflux hypersensitivity patients. *BMC Gastroenterol* 17, 67. **DOI:**10.1186/s12876-017-0624-7
- [10] Małolepsza-Jarmołowska K; (2019) Influence of chitosan on the properties of gels protecting of the esophageal mucosa. *Prog Chem Appl Chitin Deriv* 24, 135–144. **DOI:**10.15259/PCACD.24.012

FEATURES OF THE INTERACTION AND FORMATION OF NANOSTRUCTURED CHITOSAN SYSTEMS DURING IONOTROPIC GELATION

Rakiya Yunusovna Milusheva^{1,a}, Ilnar Nakipovich Nurgaliev^{1,b,*},
Sayora Sharafovna Rashidova^{1,c}

¹ – Institute of Chemistry and Physics of Polymers of Scientific Academy of Uzbekistan,
Tashkent 100128, Uzbekistan

^a – ORCID: 0000-0003-2573-1013, ^b – ORCID: 0000-0002-6983-4375,

^c – ORCID: 0000-0003-3104-6004

*corresponding author: ilnarvodnik@gmail.com

Abstract

Bombyx mori chitosan nanoparticles (ChS NPs) were obtained and the kinetic aspects of their size distribution depending on the degree of nonequilibrium of the synthesis by ionotropic gelation using sodium tripolyphosphate (TPP) were studied. The size of ChS NPs was greatly influenced by the ChS concentration, which varied from 0.5 to 10 mg/ml. The size of the NPs increased from 100 to 300 nm when the ChS concentration increased from 0.5 to 10 mg/ml and while maintaining all other parameters of the reaction. An increase in the ChS to-TPP ratio corresponded to a lower cross-linking density and thus ensured slower kinetics for NP formation alongside the formation of large chitosan/TPP aggregates. There was an almost threefold increase in the particle size when the pH of the medium increased from 3.8 to 4.7; thus, the size of ChS NPs depends on the pH of the solution. There was a slight agglomeration of NPs from 363 to 642 nm with an increase in the NP synthesis time from 4 to 24 h. According to calculations, the maximum interaction energy is 50.4 and 69.4 kcal/mol for deprotonated TPP ($P_3O_{10}^{5-}$); after adiabatic transfer of the proton, the value decreases to 32.9–33.5 kcal/mol. The maximum interaction energy is –12.8 kcal/mol for the initially protonated TPP ($H_4P_3O_{10}^-$).

Keywords: *Bombyx mori* chitosan, tripolyphosphate, nanoparticles, ionic gelation, modelling, interaction energy

Received: 11.12.2023

Accepted: 16.05.2024

1. Introduction

There is extensive research on chitosan-based nanoparticles (ChS NPs), especially for the design and development of new drug-delivery systems. These NPs have numerous beneficial properties such as biocompatibility, biodegradability, bioactivity, mucoadhesion and hydrophilicity, which facilitate the administration of poorly absorbed drugs through various epithelial barriers such as the cornea and the nasal and intestinal mucosa [1]. These systems can be produced under aqueous and fairly mild conditions to preserve the bioactive conformation of sensitive macromolecules (e.g. hormones, antigens, DNA and growth factors) that would otherwise be susceptible to enzymatic degradation and hydrolysis [2, 3]. Usually, ChS NPs are formed according to a ‘bottom-up’ approach as a result of self-assembly or stitching in which molecules are arranged into ordered nanoscale structures due to physical, covalent inter- or intramolecular interactions. A recognised feature of these nanosystems is their ability to protect hydrophilic macromolecules from degradation and to overcome mucosal barriers. One of the ways to create ChS NPs using self-assembly is ionotropic gelation using sodium tripolyphosphate (TPP), which is non-toxic.

ChS is one of the most popular components in the creation of NPs for the delivery of drugs. However, the ability to reproduce ChS NPs consistently is often a problem; therefore, great attention is paid to the purity and accurate characterisation of the source material and to the development of preparatory procedures. The processes used to obtain ChS NPs via ionotropic gelation are quite well known, but the influence of various factors on the particle size requires further investigation. Ionotropic gelation of ChS NPs involves the use of ionic cross-linking agents [4]. When TPP is used as an ionic cross-linking agent, two aqueous phases – one containing ChS and another containing polyanionic TPP – are mixed to form a complex coacervate [5]. The CS/TPP molar ratio and the developed interactions are crucial to ensure NPs exhibit the appropriate size, which can affect the drug release properties. However, the mechanism by which ChS and TPP interact has not been well documented in the literature. It has been suggested that all ionic groups of TPP can participate in interactions with ChS amine groups. However, an oversimplified model of interaction sites lacks accuracy and, to the best of our knowledge, this issue has yet to be addressed.

Electrostatic interactions between the cationic amino groups of ChS and the negatively charged anions of the cross-linker promote the formation of NPs. The size and surface charge of particles can be modified by changing the ratio of ChS and stabiliser [6]. Attempts have been made to optimise the processing parameters of ChS in the process of ionic gelation [7], but there are no unambiguous systematic conclusions in this area of research.

Most research in the field of synthesis of CS NPs is related to raw materials from armoured crustaceans. There has been limited investigation regarding the preparation and specific features of the formation of ChS NPs obtained from the pupae of the silkworm *Bombyx mori*. The present work aimed to generate *B. mori* ChS NPs using ionotropic gelation. Subsequently, the influence of various parameters on the size of the NPs was assessed. We also performed theoretical analysis: we elucidated the aspects of the ChS and TPP interactions, calculated the interaction energy, identified interaction sites and located energetically favourable relative configurations. Of note, the structure of a polymer and its spatial configuration in real experimental conditions depend on numerous factors such as the number of monomers, pH, the ionic strength of the environment, temperature, the solvent type and inter- and intramolecular interactions such as hydrogen bonding, among others. It is practically impossible to simulate such conditions, especially using quantum methods. For this endeavour, we chose to limit the study to the interactions between a ChS pentamer and two types of TPP anions.

2. Materials and Methods

2.1. Obtaining *Bombyx mori* Chitosan Nanoparticles

Purified *B. mori* ChS was dissolved in 2% acetic acid at a concentration of 0.5 mg/ml. A TPP solution (1 mg/ml) was prepared in distilled water. Both solutions were filtered through filters with a pore size of 0.22 μm . Complexation was carried out by adding the TPP solution dropwise to the ChS solution at 25°C with stirring for 20 min on an MS-PA magnetic stirrer (~300 rpm) (HCS Scientific & Chemical Pte Ltd, Singapore). Then, the mixture underwent treatment in an ultrasonic cleaner FSF 020S (FAITHFUL Instrument, China) at a power of 120 W and a frequency of 40 kHz for 2 min immediately before atomic force microscopy (AFM). The NPs were separated from the working solution by centrifugation (7000 rpm) and freeze-dried at -50 to -55°C and 0.4–0.5 mbar for 3–4 h.

2.2. Determination of the Molecular Weight of Chitosan

The molecular weight of ChS was determined by the viscometric method at 25°C. A 0.5% ChS solution in 0.33 M acetate buffer (pH 4.5) was prepared to determine the viscosity (η). The molecular weight was calculated using the Mark–Kuhn–Houwink equation:

$$M\eta = ([\eta]/K)^{1/\alpha}, \quad (1)$$

where K and α are constants for the given polymer-solvent system at $K = 1.4 \times 10^{-4}$ and $\alpha = 0.83$ [8].

2.3. Determination of the Degree of Deacetylation

The degree of deacetylation (DDA) of the ChS samples was determined by conductometric titration on an analytical instrument (Mettler-Toledo, Switzerland) using a 0.1 M sodium hydroxide (NaOH) solution as a titrant for a ChS solution dissolved in 0.1 M hydrochloric acid (HCl). The amount of alkali required to titrate the acid associated with the amino groups was determined from a graph of the dependence of the electrical conductivity of the solution on the volume of alkali. The degree of deacetylation was calculated using equation (2) [9]:

$$\text{Degree of deacetylation} = [(203 \times N_{\text{NH}_2}) / (1400 + 42 N_{\text{NH}_2})] \times 100\%, \quad (2)$$

where N_{NH_2} is the amine nitrogen content, calculated as $N_{\text{NH}_2} = \Delta V \times C_{\text{NaOH}} / m$, where ΔV is the volume of the NaOH solution used for titration of amino groups [ml], C_{NaOH} is the exact concentration of the NaOH solution [mol/l] and m is mass of ChS in the sample [g].

2.4. Determination of the Ash Content

The ash mass fraction was determined using a published procedure [10]. The ash content of the sample (Z) was calculated using equation (3):

$$Z (\%) = m \times 100 / g, \quad (3)$$

where m is the residual mass after combustion [g] and g is the sample weight [g].

2.5. Determination of Solubility

To determine the solubility of ChS, a specific amount of sample was weighed (0.1–0.5 g) and placed into a glass flask. Then, 2% acetic acid (100 ml) was added, and the mixture was stirred until the ChS was dissolved completely. The working solution was filtered through a Schott filter and dried at 104°C for 2 h. Solubility (P) was determined using equation (4):

$$P (\%) = [(g - m) / g] \times 100, \quad (4)$$

where g is the sample weight [g] and m is the amount of substance on the filter [g].

2.6. Fourier-Transform Infrared Spectroscopy

An 'Inventio-S' Fourier-transform infrared (FTIR) spectrometer (Bruker, Germany) was used to measure the spectra of all reaction products in the range of 4000–400 cm^{-1} , because the absorption bands of almost all the functional groups of organic molecules lie in this spectral range. The samples were prepared in the form of tablets with potassium bromide at a pressure of 7×10^8 Pa.

2.7. Determination of the Degree of Crystallinity

X-ray diffraction of the samples were carried out on a Miniflex 600 diffractometer (Rigaku, Japan) with monochromatic $\text{CuK}\alpha$ radiation. The samples were examined in the form of compressed pellets. Scanning was carried out in the 2θ range of 10–35°. The degree of crystallinity was calculated using equation (5):

$$\text{Degree of crystallinity (\%)} = [(I_c - I_a)/I_c] \times 100\%, \quad (5)$$

where I_c and I_a are the intensities of crystal reflection and amorphous scattering, respectively [11].

2.8. Total Nitrogen Content

The nitrogen content in the ChS samples was determined using the Dumas gasometric method by combusting a weighed sample (5–10 mg) in a quartz tube under carbon dioxide (CO_2) flow and measuring the volume of liberated nitrogen. The nitrogen content in the sample was calculated using equation (6) [12]:

$$N = [m \times (V - V') \times 100]/g, \quad (6)$$

where m is the mass of 1 ml of nitrogen at a given temperature and pressure; V is the volume of liberated nitrogen [ml], V' is the correction for a given volume, taking into account the calibration of the gasometer [mL], and g is the weight sample [mg].

2.9. Atomic Force Microscopy

The surface morphology of the samples was analysed by AFM using an Agilent 5500 instrument (USA). Scanning was carried out at room temperature in semi-contact mode in air. Silicon cantilevers with a rigidity of 9.5 N/m and a frequency of 145 kHz were used. The maximum scanning area was $11 \times 11 \mu\text{m}^2$ in the direction of the X, Y coordinates, and 1 μm in the direction of the Z coordinate. The average NP size and coefficient of variation were determined by processing the corresponding images of the sample surface using the Pico image basic software.

The most common method for producing ChS NPs is the ionotropic gelation of ChS with the non-toxic TPP, a small ion with a triple negative charge over the entire pH range [13–15].

2.10. Computational Methods

Geometry was optimised based on all-electron density functional theory (DFT) calculations. The generalised gradient was approximated with the standard 6-31++G (d,p) basis set [16] and the GAUSSIAN 09 software package. Gaussview 5.0.9 was used for visualisation. Fully protonated ChS oligomers were considered, so the overall charge of the ChS pentamers was set to 5e. The interaction energy and maximum interaction energy configurations of ChS with TPP were calculated by scanning the potential energy surface (PES) with respect to different distances and orientations. The PES scans and interaction energy calculations were performed using Grimme's B97-D functional [17], which includes long-range dispersion corrections, with the def-TZVP basis set [18],

which is of triple- ζ quality. Solvation energy was calculated to quantify the reactivity in the aqueous phase using self-consistent field theory and the polarisable continuum model (PCM) [19, 20]. The basis set superposition error (BSSE) was calculated with the counterpoise (CP) method developed by Boys and Bernardi [21]. It requires the keyword CP = N, where N is the number of fragments to be considered (for an A-B system, N = 2) [22, 23].

The first stage of the theoretical calculation was to determine the optimised molecular structures of ChS and TPP. A chain consisting of five monomers was considered to be the structural unit of ChS. The interaction energy ($\Delta E_{\text{interact}}$) was calculated using equation (7):

$$\Delta E_{\text{interact}} = E_{\text{ChS-TPP}} - (E_{\text{ChS}} + E_{\text{TPP}}) + E_{\text{BSSE}} \quad (7)$$

where $E_{\text{ChS-TPP}}$, E_{ChS} and E_{TPP} are the energy of the system for ChS-TPP, ChS and TPP, respectively. E_{BSSE} is a BSSE that was calculated using the CP method. When a CP correction is applied in combination with a solvent reaction field, any basis functions of the ghost atoms lying outside the reaction-field cavity may artificially increase the outlying charge and thus produce erroneous results. Therefore, the interaction energy was computed within the solvation model, the CP method was performed in the gas phase and the interaction energy was subjected to the calculated BSSE corrections.

3. Results and Discussion

3.1. Preparation of Chitosan Nanoparticles

The purity and accurate characterisation of ChS is crucial. ChS is characterised by structural and chemical heterogeneity even after processing under drastic chemical conditions and contains a small amount of mineral and protein impurities, so it is necessary to pay attention to its purification.

Generation of *B. mori* ChS NPs required several steps. First, the technical ChS was pre-dissolved in 2% acetic acid, deposited and coagulated at a certain pH, washed in alcohol, centrifuged and lyophilised [24]. Then, it was subjected to elemental analysis and FTIR spectroscopy. The influence of concentration, the pH of the mediums and the NP synthesis time during the preparation of ChS/TPP NPs was studied to minimise polydispersity in size, to ensure stability and to control the average size of NPs. *B. mori* ChS samples with different molecular weights (No. 1–3, Table 1) – all obtained from a technical sample of ChS – were used to evaluate the production of ChS NPs via ionotropic gelation.

Table 1. Physicochemical characteristics of the Bombyx mori chitosan (ChS) samples.

No.	Sample	Cleaning time [h]	N [%]	Z [%]	P [%]	M η [kDa]	DDA [%]	DC [%]
0	ChS technical	–	7.83	7.17	85.56	194	52.2	40
1	ChS purified-1	6	7.20	1.43	96.7	130	85.8	25
2	ChS purified-2	4	8.32	0.44	99.85	152	96.5	32
3	ChS purified-3	2	8.10	0.79	98.36	165	94.4	30

Note. Abbreviations: DC, degree of crystallinity; DDA, degree of deacetylation; M η , molecular weight; P, solubility; N, nitrogen content; Z, ash content.

The molecular weight of technical *B. mori* ChS, determined by the viscometric method, was 194 kDa (Table 1). When purified, the molecular weight decreased slightly to 130–165 kDa and the degree of deacetylation increased from 52.2% to 85.8%–96.5%. As the degree of deacetylation increased, the solubility of the samples increased from 85.56% to 99.85%. This increased solubility is due to a reduction in the number of acetamide groups of chitin as they are converted into amino groups [25]. Thus, during purification, ChS becomes more structurally homogenous.

As mentioned above, the molecular weight of ChS was determined by the viscometric method (Figure 1). Intrinsic viscosity was calculated using the Huggins equation (top line) and the Kremer equation (bottom line). Their applicability is due to the preservation of the linear dependence of the reduced viscosity on the polymer concentration in solution and the absence of strong intermolecular interactions between the macrochain units.

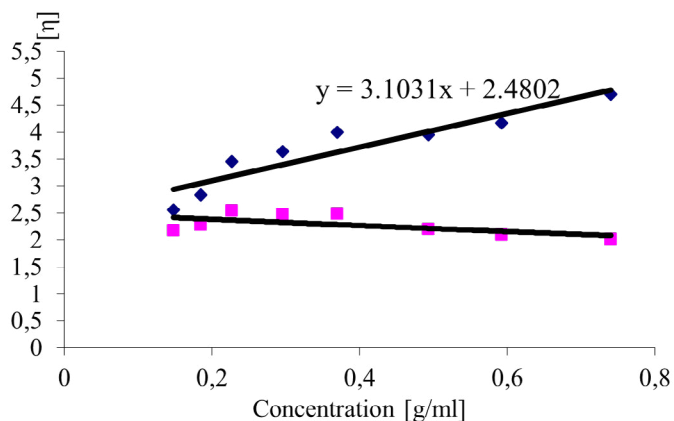


Figure 1. Determination of the molecular weight of sample No. 1 (see Table 1) by the viscometric method: $[\eta] = 2.48 \text{ dl/g}$, $[\eta] = 1.40 \times 10^{-4}$ and $M_n = 130 \text{ kDa}$.

The degree of deacetylation of sample No. 1 (see Table 1) was determined with conductometric titration. It was 85.8% (Figure 2).

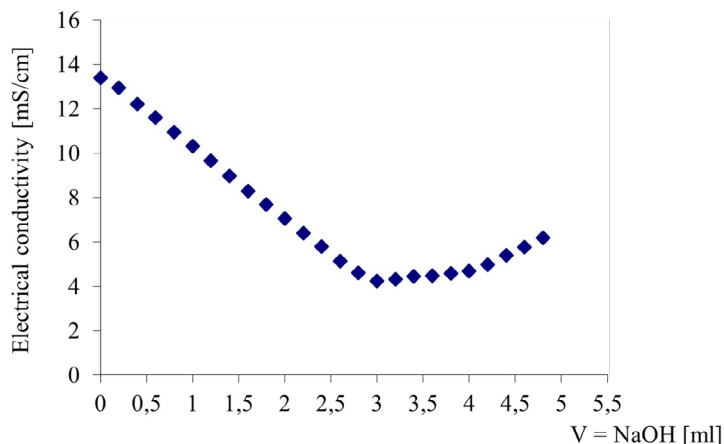


Figure 2. Conductometric titration of sample No. 1 (see Table 1): $M_n = 130 \text{ kDa}$ and degree of deacetylation = 85.8%.

Sample No.1 was also evaluated with FTIR spectroscopy (Figure 3). The intense broad band at 3500–3100 cm^{-1} indicates absorption of $-\text{OH}$ and $-\text{NH}_2$ groups included in hydrogen bonds. There are stretching vibrations of $-\text{CH}$ and $-\text{CH}_2$ groups at 2920 and 2845 cm^{-1} , respectively. There is almost complete absence of an absorption band at 1640 cm^{-1} (amide I) and an intense absorption band at 1579 cm^{-1} , corresponding to the angular deformation of the $-\text{NH}_2$ (amide II). These changes indicate effective purification of the original (technical) ChS. Absorption bands in the range of 900–1150 cm^{-1} are from various deformation vibrations of $=\text{C}-\text{O}-\text{C}=\text{}$, $-\text{NH}$ and $=\text{C}=\text{C}=\text{}$ groups.

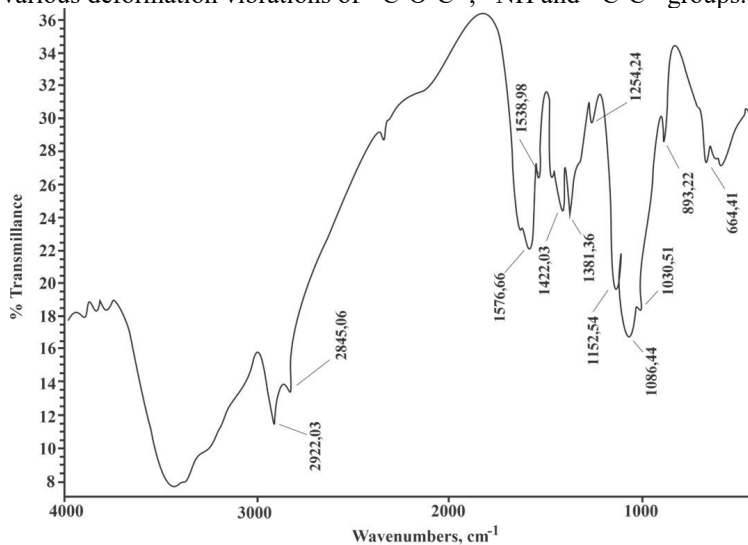


Figure 3. Fourier-transform infrared spectrum of purified *Bombyx mori* chitosan (sample No. 1, see Table 1).

3.2. Effect of the Chitosan Concentration on the Average Size of Nanoparticles

The ChS concentration is an important determinant regarding the finite size of NPs that are formed. The influence of this parameter was studied with the aim of obtaining a narrow NP size distribution and to ensure their stability in solution (Figure 4).

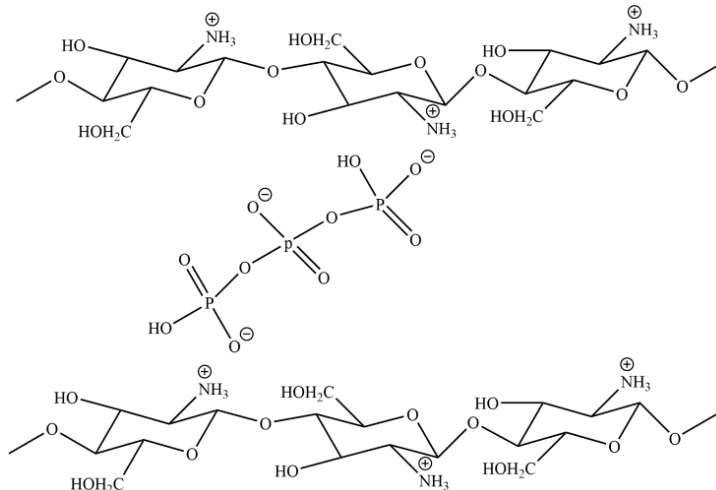


Figure 4. A schematic illustration of negatively charged sodium triphosphate connecting two positively charged chitosan chains.

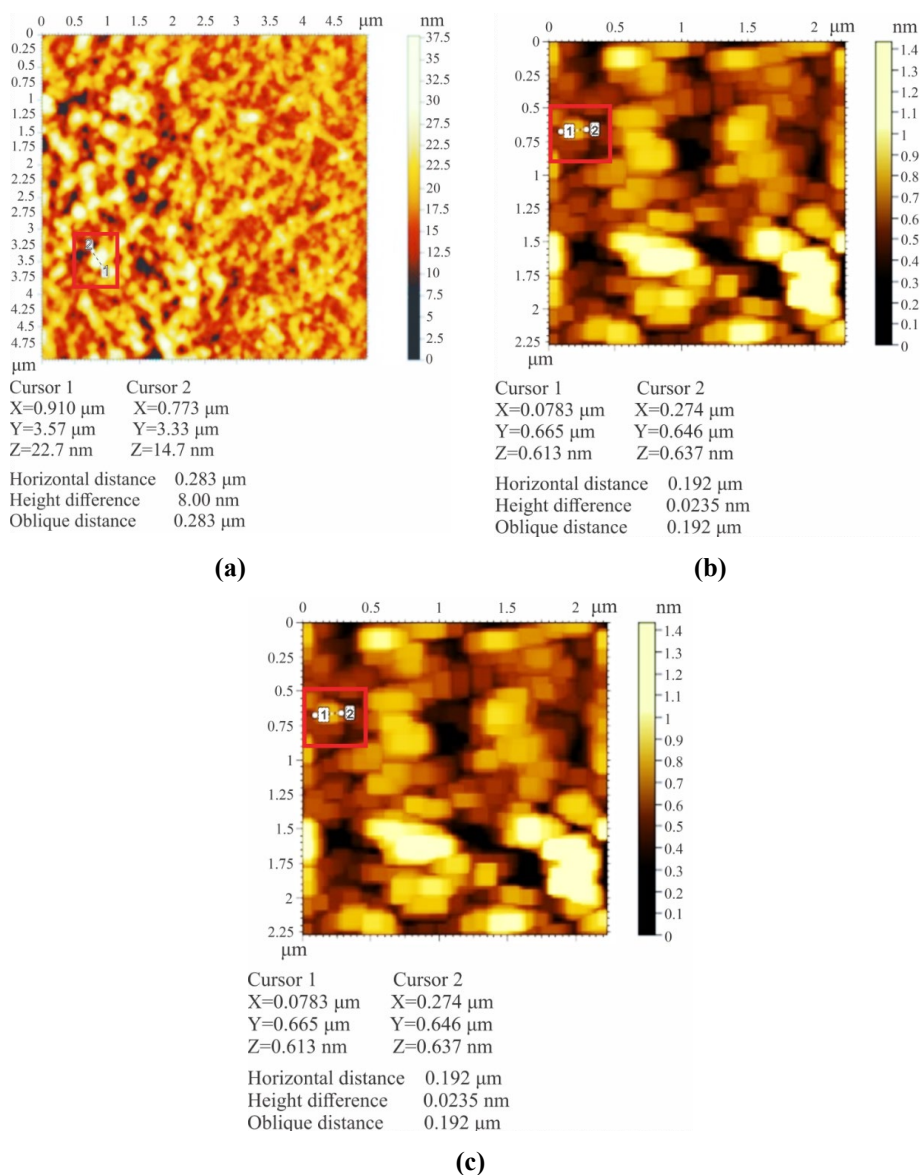


Figure 5. Atomic force micrographs of chitosan nanoparticles (ChS NPs), prepared using sample No. 1 (see Table 1): (a) 10 mg/ml ChS, 1 mg/ml sodium tripolyphosphate (TPP) and a ChS-to-TPP ratio of 1:1 yielded NPs with a size of 283 nm; (b) 1 mg/ml ChS, 1 mg/ml TPP and a ChS-to-TPP ratio of 1:1 yielded NPs with a size of 192 nm; and (c) 0.5 mg/ml ChS, 1 mg/ml TPP and a ChS-to-TPP ratio of 1:1 yielded NPs with a size of 108 nm.

AFM was performed on various samples of purified ChS. With a ChS-to-TPP ratio of 1:1, NPs were a maximum of 283, 333 and 166 nm with a ChS concentration of 10, 1 mg/ml and 0.5 mg/ml (Figure 5, Table 2). The ChS concentration greatly influenced the size of ChS NPs when studying the kinetic aspects of the size distribution of NPs

depending on the degree of nonequilibrium of the synthesis process by the method of ionotropic gelation (Table 2). When the ChS concentration increased from 0.5 mg/ml to 10 mg/ml, the size of the NPs increased from 166 to 283 nm while maintaining all other parameters of the reaction.

Consequently, a high ChS-to-TPP ratio due to a high ChS concentration corresponds to a lower cross-linking density, which ensures a slow NP formation rate and the formation of large ChS/TPP associates. This makes it possible to control the size of NPs with TPP, consistent with previous studies [26, 27].

Table 2. The dependence of the size of chitosan nanoparticles (ChS NPs) on the ChS concentration.

Figure 5 panel	ChS-to-TPP ratio	ChS concentration [mg/ml]	TPP concentration [mg/ml]	Minimum–maximum NP size [nm]
Sample No.1 ($M_n = 130$ kDa)				
(a)	1:1	10	1	50–283
(b)	1:1	1	1	192–333
(c)	1:1	0.5	1	108–166

Note. See Table 1 for details on sample No. 1. Abbreviation: TPP, sodium triphosphate.

3.3. Effect of pH During the Production of the Average Chitosan Nanoparticle Size

Experiments were carried out with ChS with $M_n = 165$ kDa (sample No. 3, see Table 1) to establish how the pH of the production medium affected the ChS NP size distribution. The ChS and TPP concentrations were kept constant at 0.5 and 1 mg/ml, respectively. With a ChS solution pH of 3.8, the NPs were a maximum of 123 nm and oval in shape (Figure 6a, b, Table 3). At pH 4.1, the NPs were a maximum of 239 nm and both oval and irregularly round in shape (Figure 7a, b, Table 3). At pH 4.7, the NPs were a maximum of 388 nm (Figure 7c, Table 3). The results showed that the size of ChS NPs depends on the pH of the solution: the lower the pH of the solution, the smaller the NPs.

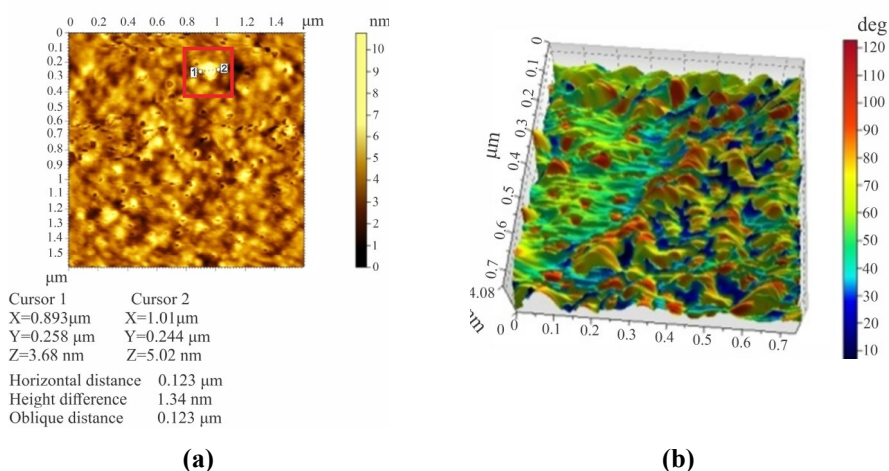


Figure 6. (a) An atomic force micrograph of chitosan nanoparticles prepared at pH 3.8; the NPs were a maximum of 123 nm in size and oval in shape. (b) A topography image of ChS NPs formed at pH 3.8.

Table 3. The dependence of the size of chitosan nanoparticles (ChS NPs) on the pH of the solution.

No.	Sample	pH of the solution	ChS concentration [mg/ml]	Chitosan M η [kDa]	Minimum–maximum NP size [nm]
2	NChS-1	3.8	0.5	165	1.34–123
3	NChS-2	4.1	0.5	165	1.66–239
4	NChS-3	4.7	0.5	165	0.721–388

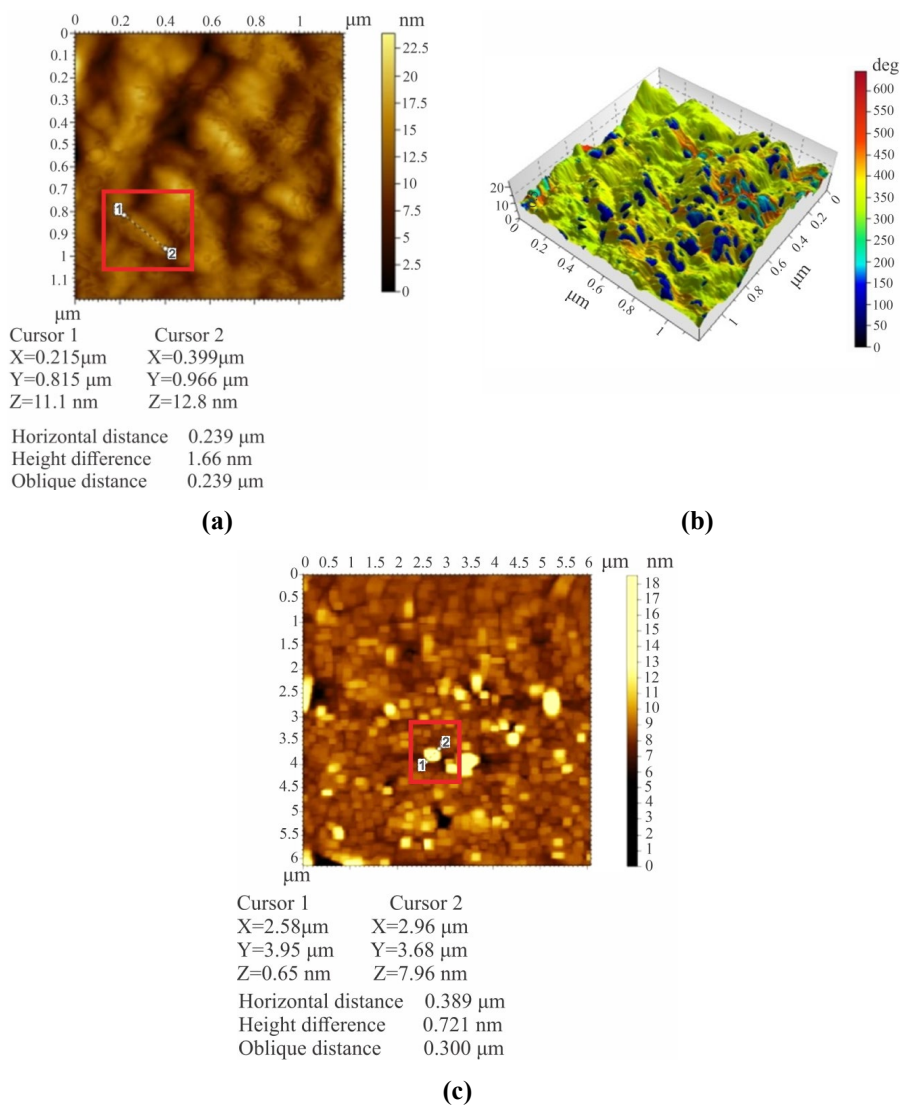


Figure 7. (a) An atomic force micrograph of chitosan nanoparticles (ChS NPs) prepared at pH 4.1; the NPs were a maximum of 239 nm in size. (b) A topography image of ChS NPs formed at pH 4.1. (c) An atomic force micrograph of chitosan nanoparticles prepared at pH 4.7; the NPs were a maximum of 388 nm in size.

3.4. Effect of Time During the Production of Chitosan Nanoparticles on the Average Size

Experiments were carried out using ChS with $M_n = 152$ kDa (sample No. 2, see Table 1) to determine the effect of the amount of time given to form NPs on their size. The maximum size of ChS NPs was 363 nm for a reaction time of 4 h (Figure 8a, Table 4), 564 nm for a reaction time of 8 h (Figure 8c, Table 4) and 642 nm after a reaction time of 24 h (Figure 9a, Table 4). The ChS NP formation is influenced by the reaction time. Apparently, as the synthesis time increases, it is necessary to increase the ChS-to-TPP ratio.

The mechanism of NP formation through ionic gelation has not been well described in the literature. Maintaining the stability of NPs is a very important aspect in the field of pharmaceutical nanotechnology. The NPs must be stable before use; otherwise, the therapeutic efficacy will be lost. The chemical integrity of the drug in NPs is another fundamental aspect of stability [28, 29].

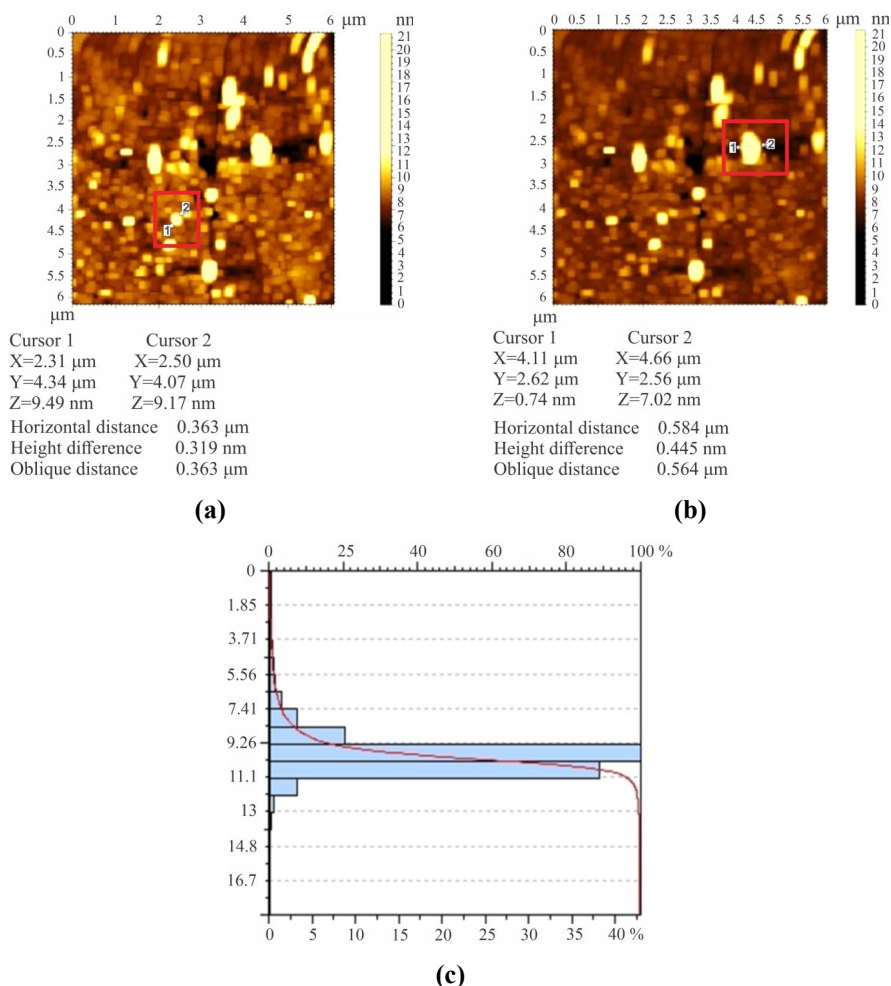


Figure 8. Atomic force micrographs of chitosan nanoparticles (ChS NPs) prepared with ChS sample No. 2 (see Table 1) with (a) a 4-h reaction time, yielding NPs with a maximum size of 363 nm, and (b) an 8-h reaction time, yielding NPs with a maximum size of 564 nm. (c) The histogram shows the NP size distribution for an 8-h reaction time.

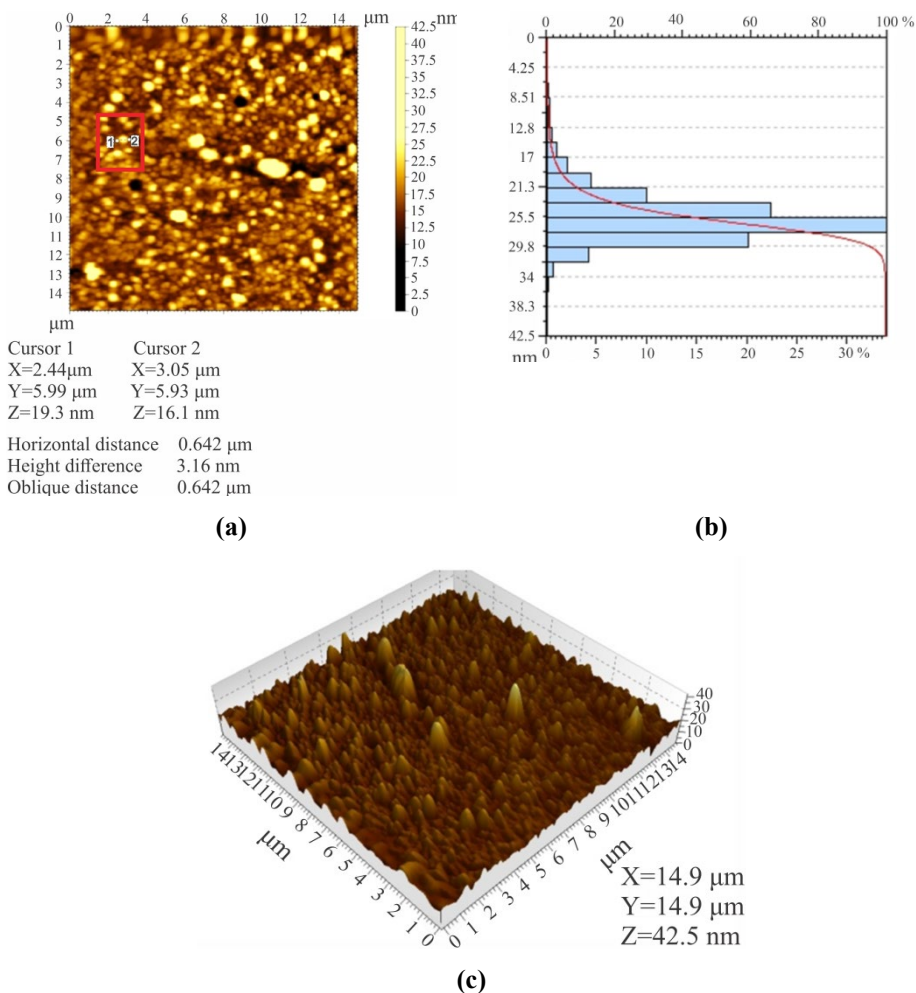


Figure 9. (a) An atomic force micrograph of chitosan nanoparticles (ChS NPs) prepared with ChS sample No. 2 (see Table 1) with a 24-h reaction time, yielding NPs with a maximum size of 642 nm. (b) The histogram shows the NP size distribution after an 24-h reaction time. (c) The surface topography of ChS NPs after a 24-h reaction time.

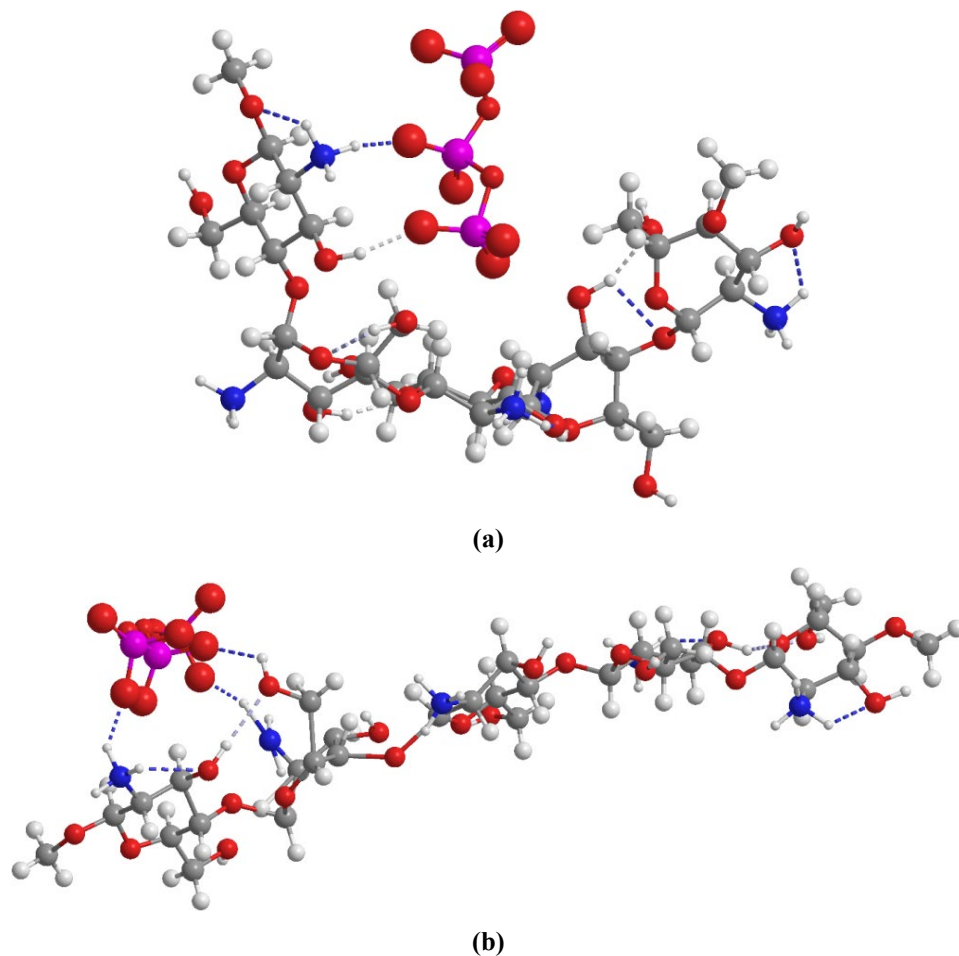
Table 4. The dependence of the size of chitosan nanoparticles (ChS NPs) on the reaction time.

No.	Figure	Synthesis time [h]	Ultrasound time [min]	M η [kDa]	ChS concentration [mg/ml]	Minimum–maximum NP size [nm]
1	Figure 8a	4	2	152	0.5	319–363
2	Figure 8b	8	2	152	0.5	0.445–564
3	Figure 9a	24	2	152	0.5	3.18–642

Experimental work has shown that all ionic groups of TPP can interact with the amino groups of ChS [30–34]. Density functional theory (DFT) calculations also consider the effects of solvation, which is necessary for a correct and accurate quantitative theoretical description of the interactions that occur both during the formation of ChS and TPP NPs and their possible use as drug carriers [35–38]. In the final part of this study, we assessed on aspects of NP formation by determining interaction sites, calculating the interaction energy and searching for energetically favourable configurations between oligomers and oligomer/polyanion complexes.

3.5. Calculation Results

We obtained models of ChS/TPP systems by optimising the geometry for a variety of relative initial configurations, examining both perpendicular and parallel coordination. We focused on the possible interactions between the oxygen and phosphorus atoms of TPP and the amino and hydroxyl groups of ChS. Figure 10 shows four configurations, parallel and perpendicular (Figure 10a, b, respectively), demonstrating the strongest interactions between the completely deprotonated TPP anion ($P_3O_{10}^{5-}$) and the protonated TPP anion ($H_4P_3O_{10}^-$), as well as ChS chains containing protonated amino groups ($-NH_3^+$, Figure 10c, d).



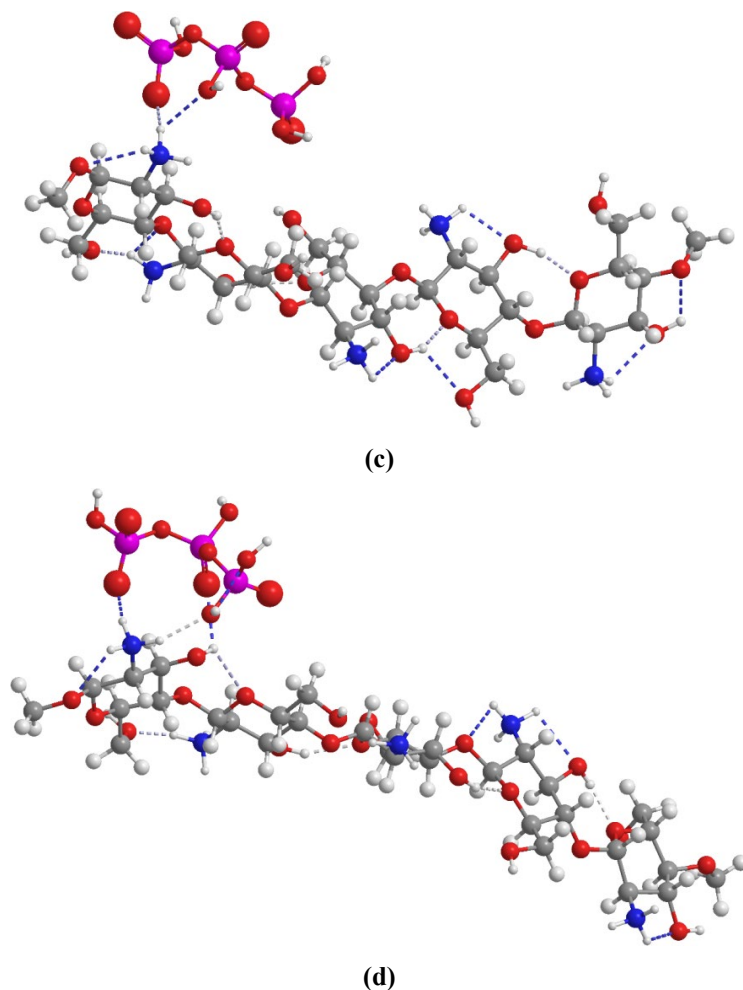
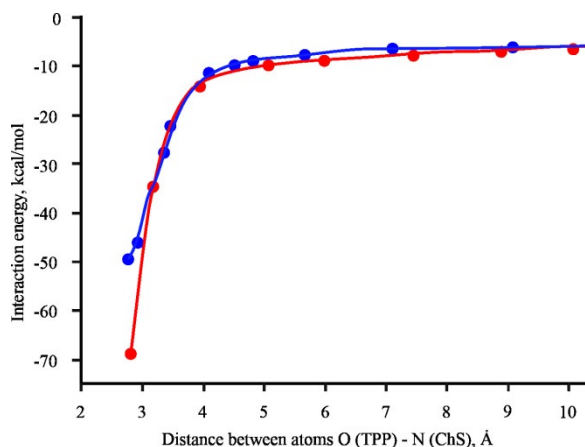
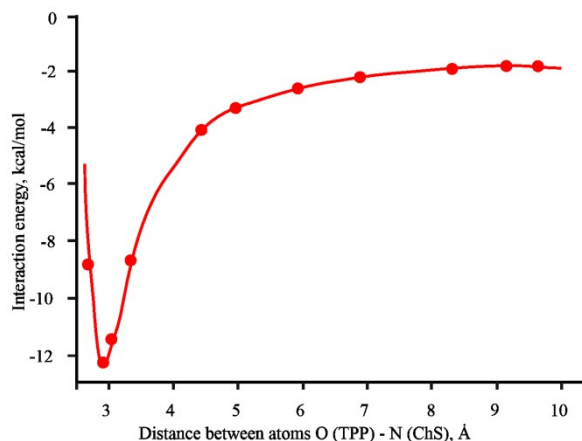


Figure 10. Calculated configurations for the interaction between the chitosan (ChS) pentamer and (a, b) deprotonated sodium triphosphate (TPP, $P_3O_{10}^{5-}$) and (c, d) protonated TPP ($H_4P_3O_{10}^-$): (a) a parallel interaction involving one $-NH_3^+$ group and one $-CH_2OH$ group; (b) a perpendicular interaction involving two $-NH_3^+$ groups and one $-CH_2OH$, the local energy minimum with the ionic cross-linking configuration; (c) one $-NH_3^+$ group of ChS is involved in the interaction; and (d) one $-NH_3^+$ group and one $-CH_2OH$ group of ChS are involved in the interaction (both intra- and intermolecular hydrogen bonds are shown). Hydrogen atoms are white, nitrogen atoms are blue, oxygen atoms are red, carbon atoms are grey and phosphorus atoms are pink.

We calculated the interaction energy for the parallel interaction – the average distance of the TPP oxygen atoms and the ChS nitrogen atoms (two $-NH_3^+$ groups of ChS participate in the interaction) – and for the perpendicular interaction – the oxygen and phosphorus atoms of the TPP and amino and hydroxyl groups of ChS nitrogen (one $-NH_3^+$ group of ChS participates in the interaction). Figure 11 shows the change in the interaction energy as a function of the distance between the interacting atoms.



(a)



(b)

Figure 11. (a) The change in the interaction energy of the deprotonated sodium triphosphate (TPP) polyanion ($P_3O_{10}^{5-}$) for the parallel approach (red line) and the perpendicular approach (blue line) on the distance between the outermost oxygen atom of TPP and the nearest nitrogen atom of ChS. (b) The change in the interaction energy of the initially protonated TPP anion ($H_4P_3O_{10}^-$) for the perpendicular approach depending on the distance between the interacting atoms.

We calculated the interaction energy within the framework of the gas phase model of solvation and applied BSSE corrections. We set the charge of the ChS pentamer to $5e$, that is, with fully protonated amino groups. The maximum interaction energy at the local minimum of the perpendicular configuration is 50.4 kcal/mol. The interaction energy curve becomes very steep at a close distance of interacting $O \cdots N$ atoms of < 3.3 Å. At 2.75 Å, the transfer of a proton from the amino group of ChS to TPP reduces the interaction energy to 28.3 kcal/mol. The configuration with a global maximum interaction has a maximum interaction energy of 69.4 kcal/mol. This energy also decreases at a close distance ($O \cdots N \approx 2.77$ Å) after double proton transfer, in this case to 33.5 kcal/mol. Each of these

two proton transfers occurs between the TPP polyanion and one of the two interacting amino groups (i.e. one transfer of the proton to ChS amino group). In both cases, the drop in the interaction energy is due to proton transfer; hence, the interaction energy is significantly higher than the corresponding value in the case of a perpendicular configuration, but not twice as large as might be expected.

These findings can be explained by two facts. First, the electrostatic component of the interaction decreases unevenly during sequential proton transfer by approximately $[25 - (5 - n)^2]$ for the n -th proton transfer. Second, structural relaxation occurs; in this regard, the process corresponds to adiabatic proton transfer. In both cases, the final maximum interaction energy is significantly higher than what would be expected from the formation of a single $O \cdots HN$ hydrogen bond. In addition to the electrostatic component, a high interaction energy also results in part from long-range and weaker secondary interactions that occur between the alternative oxygen atom of TPP and the nearby hydroxyl group of ChS. We also considered the pH dependence when including the protonated TPP anion in the calculation. To do this, in addition to PES scan calculations of the deprotonated TPP anion, we also performed a similar calculation for the perpendicular approach for the protonated TPP anion ($H_4P_3O_{10}^-$; Figure 11b). In contrast to the previous calculation with the deprotonated TPP anion, the protonated TPP anion does not induce the transfer of the proton from the protonated amino group at a close range. In addition, the calculated maximum interaction energy is -12.8 kcal/mol, which is significantly lower than in the previous case, but higher than what would be expected from the formation of a single $O \cdots HN$ hydrogen bond [39].

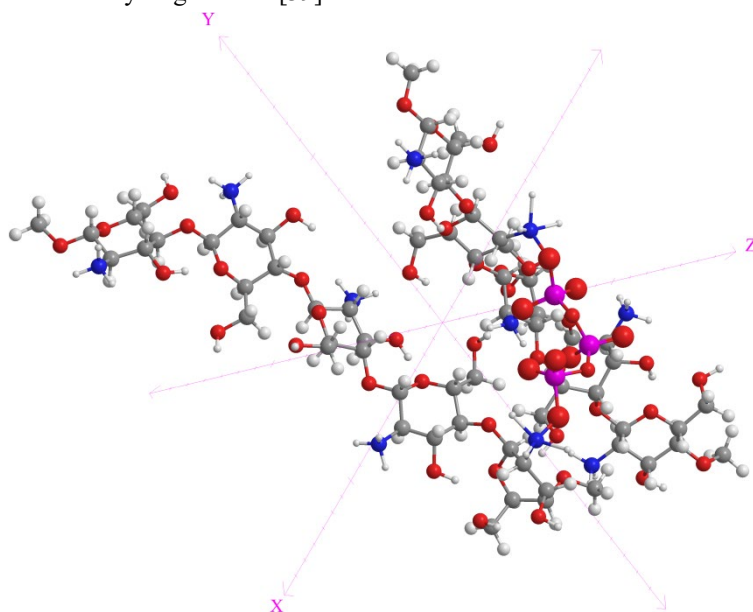


Figure 12. Cross-linked chitosan pentamers with initially deprotonated sodium triphosphate.

After identifying the maximum-interaction configurations and the corresponding energies for the two TPP anions, we investigated two CS pentamers cross-linked with the deprotonated TPP anion. Although the CS oligomers are initially oriented parallel to each other, in every case their final orientation is such that the planes defined by their chain axes and the TPP primary axis form a dihedral angle of 120 – 135° . This situation

induces a bias in the orientation of the cross-linked CS pentamers that is expected to affect the NP formation mechanism, especially at low TPP concentrations. Figure 12 shows the optimal configuration for the ChS pentamers. The two planes correspond to a ChS chain and the TPP anion as described above; they form a dihedral angle of 127.4°

4. Conclusions

We showed that the ChS concentration (0.5–10 mg/ml) has a great influence on the size of ChS NPs when synthesised using ionotropic gelation. When the concentration increases from 0.5 to 10 mg/ml, the size increases from 100 to 300 nm while maintaining all other parameters of the reaction. Thus, an increase in the ChS-to-TPP ratio corresponds to a low cross-linking density and ensures slower kinetics of NP formation alongside the formation of large ChS/TPP associates. The pH of the medium also greatly influences the kinetics of NP formation: the size increases almost threefold, from 123 to 388 nm, when the pH increases from 3.8 to 4.7. Finally, the synthesis time also affects the size of ChS NPs: there is a slight agglomeration of NPs when increasing the time from 4 to 24 h. Apparently, with an increase in the synthesis time, it is necessary to increase the ChS-to-TPP ratio.

We performed DFT calculations to quantify the intermolecular interactions responsible for the ionic cross-linking of ChS with TPP and identified the functional groups responsible for the interaction. Based on PES scanning, the maximum interaction energy is 69.4 kcal/mol for the initially deprotonated TPP anion, decreasing to 33.5 kcal/mol after the adiabatic transfer of the proton to the protonated TPP anion. We found a maximum interaction energy of –12.8 kcal/mol for the initially protonated TPP anion. The electrostatic interaction between ChS and TPP leads to a compound that can be used to obtain NPs and surface modification of films.

5. References

- [1] Barclay TG, Day CM, Petrovsky N, Garg S; (2019) Review of polysaccharide particle-based functional drug delivery. *Carbohydr Polym* 221, 94–112. DOI:10.1016/j.carbpol.2019.05.067
- [2] Janes KA, Calvo P, Alonso MJ; (2001) Polysaccharide colloidal particles as delivery systems for macromolecules. *Adv Drug Deliv Rev* 47, 83–97. DOI:10.1016/s0169-409x(00)00123-x
- [3] Csaba N, Garcia-Fuentes M, Alonso MJ; (2006) The performance of nanocarriers for transmucosal drug delivery. *Expert Opin Drug Deliv* 3, 463–478. DOI:10.1517/17425247.3.4.463
- [4] Janes KA, Fresneau MP, Marazuela A, Fabra A, Alonso MJ; (2001) Chitosan nanoparticles as delivery systems for doxorubicin. *J Control Release* 73, 255–267. DOI:10.1016/s0168-3659(01)00294-2
- [5] Pan Y, Li Y-J, Zhao H-Y, Zheng J-M, Xu H, Wei G, Hao J-s, Cui F-d; (2002) Bioadhesive polysaccharide in protein delivery system: chitosan nanoparticles improve the intestinal absorption of insulin *in vivo*. *Int J Pharm* 249, 139–147. DOI:10.1016/s0378-5173(02)00486-6
- [6] Lopez-Leon T, Carvalho EL, Seijo B, Ortega-Vinuesa JL, Bastos-Gonzalez D; (2005) Physicochemical characterization of chitosan nanoparticles: electrokinetic and stability behavior. *J Colloid Interface Sci* 283, 344–351. DOI:10.1016/j.jcis.2004.08.186

- [7] Koukaras EN, Papadimitriou SA, Bikiaris DN, Froudakis GE; (2012) Insight on the formation of chitosan nanoparticles through ionotropic gelation with tripolyphosphate. *Mol Pharm* 9, 2856–2862. DOI:10.1021/mp300162j
- [8] Gamzazade AI, Shlimak BM, Sklyar AM, Stykova EV, Pavlova SA, Rogozin SV; (1985) Investigation of the hydrodynamic properties of chitosan solutions. *Acta Polym* 36, 421–424. DOI:10.1002/actp.1985.010360805
- [9] Gosudarstvennaya farmakopeya SSSR [State Pharmacopoeia of the USSR], XI edn. 2012, *Meditsina*, Moscow, 24 (in Russian).
- [10] Gosudarstvennaya farmakopeya SSSR [State Pharmacopoeia of the USSR], XI edn. 1987, *Meditsina*, Moscow, 175 (in Russian).
- [11] Martynov MA, Vylegzhanina KA; (1972) Rentgenografiya polimerov: Metodicheskoe posobie dlya promyshlennykh laboratorii [Polymer X-ray spectroscopy: methodological guide for industrial laboratories]. *Khimiya*, Leningrad (in Russian).
- [12] Klimova VA; (2001) Osnovnye mikrometody analiza organicheskikh soedinenii [Basic micromethods for the analysis of organic compounds]. *Khimiya*, Moscow, 75 (in Russian).
- [13] Xiong Y, Feng YX, Chang M, Wang Q, Yin SN, Jian LY, Ren DF; (2023) Formulated chitosan-sodium tripolyphosphate nanoparticles for co-encapsulation of ellagic acid and anti-inflammatory peptide: characterization, stability and anti-inflammatory activity. *J Sci Food Agric* 103, 3447–3456. DOI:10.1002/jsfa.12521
- [14] Maximiliano L, Agazzi M, Rovey FP, Apuzzo E, Herrera SE, Spesia MB, Mercedes de las OM, Azzaroni O; (2023) Lysozyme/tripolyphosphate complex coacervates: Properties, curcumin encapsulation and antibacterial activity. *Food Hydrocoll* 145, 109134. DOI:10.1016/j.foodhyd.2023.109134
- [15] Sulaeman U, Ramadhanti SF, Diastuti H, Iswanto P, Isnaeni I, Yin S; (2023) The enhanced photo-stability of defective Ag_3PO_4 tetrahedron prepared using tripolyphosphate. *Arab J Chem* 161, 104409. DOI:10.1016/j.arabjc.2022.104409
- [16] Becke AD; (1993) Density-functional thermochemistry. III. The role of exact exchange. *J Chem Phys* 98, 5648–5652. DOI:10.1063/1.464913
- [17] Grimme S; (2006) Semiempirical GGA-type density functional constructed with a long-range dispersion correction. *J Comput Chem* 27, 1787–1799. DOI:10.1002/jcc.20495
- [18] Schäfer A, Huber C, Ahlrichs R; (1994) Fully optimized contracted Gaussian basis sets of triple zeta valence quality for atoms Li to Kr. *J Chem Phys* 100, 5829–5836. DOI:10.1063/1.467146
- [19] Miertus S, Scrocco E, Tomasi J; (1981) Electrostatic interaction of a solute with a continuum. A direct utilization of AB initio molecular potentials for the prevision of solvent effects. *Chem Phys* 55, 117–129. DOI:10.1016/0301-0104(81)85090-2
- [20] Mennucci B; (2012) Polarizable continuum model. *Wiley Interdiscip Rev Comput Mol Sci* 2, 386–404. DOI:10.1002/wcms.1086
- [21] Boys SF, Bernardi F; (1970) The calculation of small molecular interactions by the differences of separate total energies. Some procedures with reduced errors. *Mol Phys* 19, 553–566. DOI:10.1080/00268977000101561
- [22] Chalasinski G, Szczesniak MM; (1994) Origins of structure and energetics of van der Waals clusters from ab initio calculations. *Chem Rev* 94, 1723–1765. DOI:10.1021/cr00031a001
- [23] Galano A, Idaboy JRA; (2006) A new approach to counterpoise correction to BSSE. *J Comput Chem* 27, 1203–1210. DOI:10.1002/jcc.20438
- [24] Milusheva RY, Rashidova SS; (2017) Bioactive properties of nanochitosan *Bombyx mori*. *Polym Sci Ser C* 59, 29–34. DOI:10.1134/S1811238217010088

- [25] Muzzarelli R, Muzzarelli S; (2001) Chitosan in pharmacy and chemistry. Publishing House 'Università di Ancona', Ancona.
- [26] Nasti A, Zaki NM, Leonardis Pde, Ungphaiboon S, Sansongsak P, Rimoli MG, Tirelli N; (2009) Chitosan/TPP and chitosan/TPP-hyaluronic acid nanoparticles: systematic optimisation of the preparative process and preliminary biological evaluation. *Pharm Res* 26, 1918–1930. **DOI:**10.1007/s11095-009-9908-0
- [27] Lunkov A, Shagdarova B, Konovalova M, Zhuikova Y, Drozd N, Il'ina A, Varlamov V; (2020) Synthesis of silver nanoparticles using gallic acid-conjugated chitosan derivatives. *Carbohydr Polym* 15, 115916. **DOI:**10.1016/j.carbpol.2020.115916
- [28] Yanat M, Schroën K; (2021) Preparation methods and applications of chitosan nanoparticles; with an outlook toward reinforcement of biodegradable packaging. *React Funct Polym* 161, 04849. **DOI:**10.1016/j.reactfunctpolym.2021.104849
- [29] Nimesh S, Saxena A, Kumar A, Chandra R; (2012) Improved transfection efficiency of chitosan-DNA complexes employing reverse transfection. *J Appl Polym Sci* 124, 1771–1777. **DOI:**10.1002/app.35179
- [30] Lemoine D, Francois C, Kedzierewicz F, Preat V, Hoffman M; (1996) Stability study of nanoparticles of poly (caprolactone), poly(D,L-lactide) and poly(D,L-lactidecoglycolide). *Biomater* 17, 2191–2197. **DOI:**10.1016/0142-9612(96)00049-X
- [31] Yan Q, Li M, Dong L, Luo J, Zhong X, Shi F, Ye G, Zhao L, Fu H, Shu G, Zhao X, Zhang W, Yin H, Li Y, Tang H; (2023) Preparation, characterization and protective effect of chitosan - Tripolyphosphate encapsulated dihydromyricetin nanoparticles on acute kidney injury caused by cisplatin. *Int J Biol Macromol* 245, 125569. **DOI:**10.1016/j.ijbiomac.2023.125569
- [32] Sawtarie N, Cai Y, Lapitsky Y; (2017) Preparation of chitosan/tripolyphosphate nanoparticles with highly tunable size and low polydispersity. *Colloids Surf B* 157, 110–117. **DOI:**10.1016/j.colsurfb.2017.05.055
- [33] Kim ES, Baek Y, Yoo HJ, Lee JS, Lee HG; (2022) Chitosan-tripolyphosphate nanoparticles prepared by ionic gelation improve the antioxidant activities of astaxanthin in the *in vitro* and *in vivo* model. *Antioxidants* 11, 479. **DOI:**10.3390/antiox11030479
- [34] Devi KTR, Paulraj SJ, Shah Y, Kumar SR, Kejamurthy P; (2023) Chitosan-tripolyphosphate nanoparticles encapsulated rutin targeting bacterial growth inhibition and its cytotoxicity on PANC-1 pancreatic adenocarcinoma cell. *J Appl Pharm Sci* 13, 141–148. **DOI:**10.7324/JAPS.2023.41561
- [35] Poureghbal Y, Rahimi M, Akbari M; (2021) Ionic gelation of chitosan with sodium tripolyphosphate using a novel combined nebulizer and falling film system. *Can J Chem Eng* 100, 1547–1557. **DOI:**10.1002/cjce.24234
- [36] Di Santo MC, D' Antoni CL, Rubio APD, Alaimo A, Pérez OE; (2021) Chitosan-tripolyphosphate nanoparticles designed to encapsulate polyphenolic compounds for biomedical and pharmaceutical applications - A review. *Biomed Pharmacother* 142, 111970. **DOI:**10.1016/j.biopha.2021.111970
- [37] Şenol ZM, Çetinkaya S, Yenidünya AF, Başoğlu-Ünal F, Ece A; (2022) Epichlorohydrin and tripolyphosphate-crosslinked chitosan-kaolin composite for Auramine O dye removal from aqueous solutions: experimental study and DFT calculations. *Int J Biol Macromol* 199, 318–330. **DOI:**10.1016/j.ijbiomac.2022.01.008
- [38] Moreno A, Jordana A, Grillo R, Fraceto LF, Jaime C; (2019) A study on the molecular existing interactions in nanoherbicides: a chitoooligosaccharide/tripolyphosphate loaded with paraquat case. *Colloids Surf A Physicochem Eng* 562, 220–228. **DOI:**10.1016/j.colsurfa.2018.11.033
- [39] Řežáč J, Riley KE, Hobza P; (2011) S66: a well-balanced database of benchmark interaction energies relevant to biomolecular structures. *J Chem Theory Comput* 7, 2427–2438. **DOI:**10.1021/ct2002946

***o*-PHTHALALDEHYDE CROSS-LINKED CHITOSAN MEMBRANE AS A QUASI-SOLID-STATE ELECTROLYTE FOR SUPERCAPACITORS**

Krzysztof Nowacki^{1,a,*}, Maciej Galiński^{1,b}

¹ – *Institute of Chemistry and Technical Electrochemistry, Faculty of Chemical Technology, Poznan University of Technology, Berdychowo 4 Str., 60-965 Poznań, Poland*

^a – ORCID: 0000-0002-3664-5463, ^b – ORCID: 0000-0002-0398-5760

*corresponding author: krzysztof.nowacki@put.poznan.pl

Abstract

*This study reports a stepwise formation method of a chitosan membrane cross-linked with *o*-phthalaldehyde and its use as a polymer matrix in a quasi-solid-state-electrolyte-based supercapacitor. The proposed method of cross-linking in chitosan solution and evaporation of the solvent yielded a homogeneous and durable chitosan-*o*-phthalaldehyde membrane, which, after dipping in an aqueous 2 M lithium sulfate solution, formed a quasi-solid-state-electrolyte (CS/OPAQSSE). The prepared CS/OPA-QSSE was then used in an electric double layer capacitor (EDLC) cell to study its electrochemical properties. The electrochemical performance of the EDLC cell was determined by using the electrochemical impedance spectroscopy, cyclic voltammetry and galvanostatic charging/discharging techniques. The results showed that the EDLC cell with the CS/OPA-QSSE is a fully functional and efficient device. The specific capacitance values calculated for the CS/OPA-QSSE EDLC (up to 115 F g⁻¹) always surpassed the reference cell based on a commercial glass fibre separator. Therefore, the proposed chitosan modification can be considered as a future alternative to produce other polysaccharide-based materials for electrochemical use.*

Keywords: *chitosan, *o*-phthalaldehyde, quasi-solid-state electrolyte, hydrogel electrolyte, electric double-layer capacitor, supercapacitor*

Received: 27.02.2024

Accepted: 06.04.2024

1. Introduction

To meet the newest strict environmental regulations [1–3], both science and technology are becoming even more focused on the potential use of renewable materials in all fields. The reasonable demands of sustainable chemistry to design energy storage devices has led to the recognition of polysaccharides as a promising option for the replacement of components made from conventional polymer materials [4, 5]. Among them is the highly abundant marine polysaccharide chitin, which has been widely studied for its nontoxicity, biodegradability and biocompatibility [6, 7]. At the same time, chitosan (CS, the derivative of chitin), which shows good solubility in aqueous solvents, has attracted even more attention in hydrogel science due to its ease of processing and chemical modification [8, 9]. Unfortunately, to form dimensionally stable and mechanically durable CS-based hydrogels, this aminopolysaccharide has to be cross-linked [8–11]. Among all varieties of CS cross-linkers, the dialdehydes (e.g. glutaraldehyde and glyoxal) are the most widely used because permanent imine bonds can be formed easily with the neighbouring CS polymeric chains [12, 13]. Despite the dominance of glutaraldehyde as the most common modifier of CS, using different types of CS cross-linking agents may impact the hydrogel physicochemical properties; therefore, it is possible to tailor the CS hydrogel for different applications by simply changing its cross-linker [14, 15].

In the electrochemical capacitor research field, one of the leading innovations developed to increase the electrochemical performance of these devices is a quasi-solid-state electrolyte (QSSE) [16, 17]. These solid polymer matrices have a liquid electrolyte trapped inside the polymer chain interspaces and use polysaccharides of natural origin (e.g. chitin, cellulose and CS) as a matrix and an aqueous solution of inorganic salt as the dispersed phase. They represent a promising green alternative to conventional solid polymer electrolytes [18, 19]. CS hydrogels have been reported as QSSEs for supercapacitors; they exhibit good electrochemical properties and specific capacitance, even superior to devices with commercially used separators [20]. Moreover, the CS cross-linker type exerts a significant influence on electrochemical capacitor performance [21].

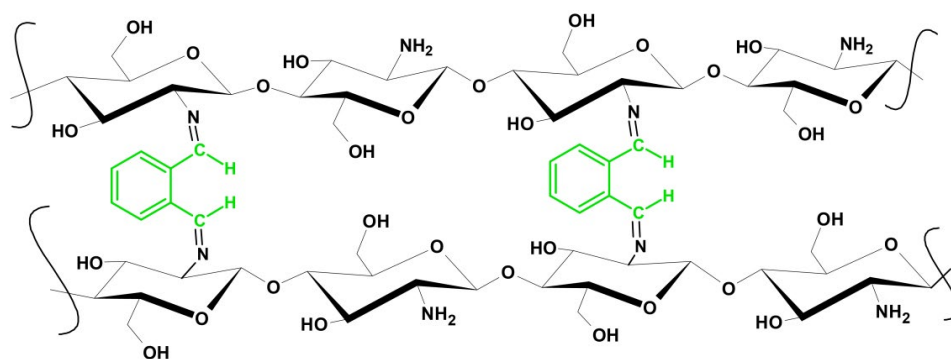


Figure 1. Schematic illustration of chitosan chemical cross-linking using *o*-phthalaldehyde [22].

This study aimed to develop an electrochemical capacitor employing a QSSE based on *o*-phthalaldehyde (OPA) cross-linked CS matrix and an aqueous lithium sulfate (LiSO_4) solution as a dispersed phase. It tested the hypothesis that OPA represents a replacement for glutaraldehyde in terms of cross-linking of the CS matrix (Figure 1) and that the introduction of the aromatic ring with delocalised electrons into

the biopolymer chains interspaces exerts a positive impact on the electrochemical performance of a QSSE-based supercapacitor. The prepared supercapacitor device was evaluated with advanced electrochemical methods and compared with a reference cell containing a commercial separator.

2. Materials and Methods

2.1. Chemicals

Medium-molecular-weight CS in the form of flakes was purchased from Sigma-Aldrich (USA) and dried before use (72 h at 105°C). This polysaccharide had a degree of deacetylation of $83\% \pm 3\%$ and viscosity of 3.6 cP in a 2 wt% solution in 1% acetic acid (25°C). OPA ($\geq 99.0\%$) was purchased from Sigma-Aldrich and used for CS cross-linking. Acetic acid ($\geq 99.5\%$) and anhydrous Li_2SO_4 (≥ 98.5) were also procured from Sigma-Aldrich and used as received. Moreover, re-distilled water was used to prepare all aqueous solutions.

2.2. Preparation of *o*-Phthalaldehyde Cross-linked Chitosan Matrix

A CS-based membrane modified by OPA was used to synthesise a QSSE as a polymer matrix and prepared as follows (Figure 2). First, a 2 wt% CS solution in 1 wt% aqueous acetic acid was prepared by dispersing an appropriate quantity of dry CS flakes in acetic acid. The mixture was stirred at 37°C for 7 days to obtain a transparent, yellowish solution without solid residues. Next, the cross-linking process was initiated by mixing 6 g of homogeneous CS solution with 0.68 g of 0.10 wt% aqueous OPA solution (to obtain 0.5×10^{-5} mol of OPA) and stirred for 1 h at 25°C. The homogeneous solution was hot-cast on a poly(propylene) plate and incubated for 24 h at 37°C to evaporate the solvent.

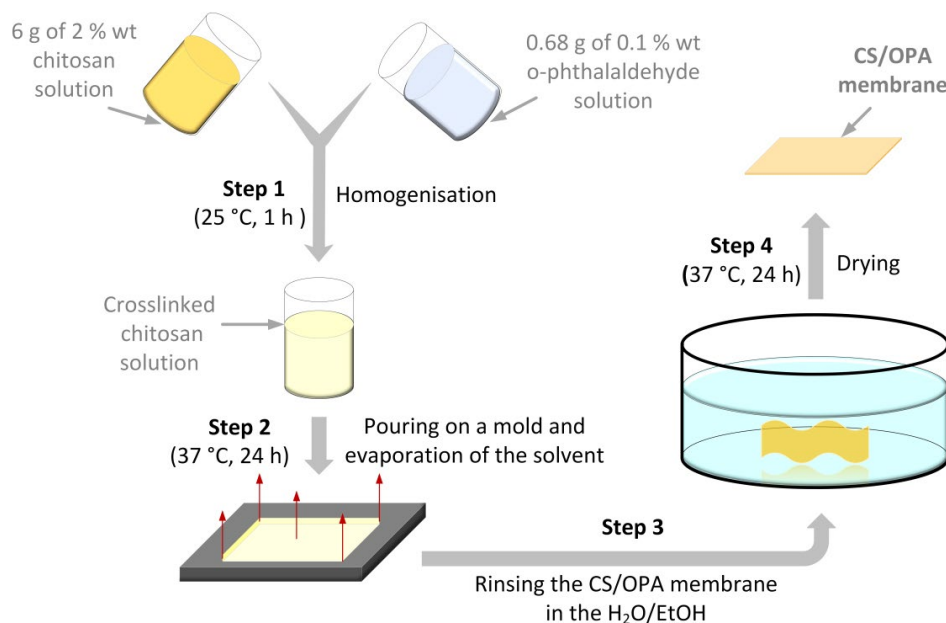


Figure 2. Preparation of the *o*-phthalaldehyde cross-linked chitosan membrane (CS/OPA).

This process yielded a slightly blurred, yellow CS/OPA membrane. It was carefully immersed in a water–ethanol bath (1:3, v/v) to remove acetic acid residues and redundant OPA particles and then dried for 24 h at 37°C.

2.3. Preparation of an *o*-Phthalaldehyde Cross-Linked Chitosan Membrane Quasi-Solid-State Electrolyte

The CS/OPA-QSSE was prepared by immersing a dry CS/OPA matrix in a 2 M Li₂SO₄ aqueous solution for 24 h at 25°C. After the incubation, the hydrogel electrolyte was carefully removed.

2.4. Attenuated Total Reflectance Fourier-Transform Infrared Spectroscopy

Attenuated total reflectance Fourier-transform infrared (ATR-FTIR) spectroscopy was used to identify possible changes in the CS polymer chain functional groups caused by cross-linking by OPA; this technique enables the non-destructive examination of the sample. ATR-FTIR spectra were recorded on a Vertex 70 Series FTIR spectrometer (Bruker, Germany) with a wave number range of 4000–500 cm⁻¹ (resolution of 1 cm⁻¹). Before examination, the samples were dried to the constant mass at 37°C.

2.5. Atomic Force Microscopy

The topography and nanomechanical properties of the dry CS/OPA membrane were determined using atomic force microscopy (AFM). The three-dimensional images of the sample surface were recorded with an NX10 microscope (Park Systems, South Korea). The examined surface area was 20 × 20 μm, scanned with 512 lines per image and a non-contact mode scan speed set at approximately 0.3–0.4 Hz. The nanomechanical properties (adhesion force, energy dissipation and Young's modulus) of the dry CS/OPA membrane were examined in the PINPOINT™ mode. All measurements were performed at 23°C, and the resulting data were analysed using the open-source Gwyddion software and XEI (Park Systems) AFM analysis programs.

2.6. Contact Angle Measurements

The wettability and surface free energy of the dry CS/OPA membrane were examined by static contact angle measurements, with ethylene glycol and diiodomethane as the polar and dispersion components, respectively. Measurements were made using a sessile drop technique at 25°C with a DSA 100E Drop Shape Analyzer (KRÜSS, Germany). The surface free energy was calculated using the Owens–Wendt–Rabel–Kaelble model.

2.7. Swelling Test

The degree of swelling (DS) of the CS/OPA membrane in an aqueous environment was determined using a 2 M Li₂SO₄ aqueous solution. First, a 10-mm disc was cut out from the dry CS/OPA membrane and weighed with an analytical scale (model AS 110.R2, Radwag, Poland). Next, the sample was soaked in 2.0 cm³ of a 2 M Li₂SO₄ aqueous solution for 94 h. After specified times (10, 20 and 30 min, and 1, 2, 4, 8, 24, 48 and 96 h), the sample was removed from the electrolyte, carefully cleaned of the excess surface liquid with filter paper and weighed. DS was calculated using equation (1):

$$DS = \frac{m_w - m_d}{m_d} \times 100\% \quad (1)$$

where m_w is the mass of the wet sample and m_d is the mass of the dry sample. All measurements were performed at 23°C.

2.8. Ionic Conductivity Measurements

The ionic conductivity of the CS/OPA-QSSE was investigated with electrochemical impedance spectroscopy (EIS). The CS/OPA-QSSE sample (a disc with a diameter of 5 mm) in the equilibrium state after swelling in a 2 M Li₂SO₄ aqueous solution for 24 h was placed between two platinum blocking electrodes within a test vessel (a detailed description of the ionic conductivity test vessel is included in a previous publication [23]). All measurements were performed at 25°C and in a frequency range from 100 kHz to 1 Hz with a potential amplitude of 10 mV. The ionic conductivity (σ) of the investigated CS/OPA-QSSE was calculated using equation (2):

$$\sigma = \frac{t_s}{A \times R} \quad (2)$$

where t_s is the thickness of the swollen QSSE, A is the surface area of the working electrode (0.0177 cm²) and R is the resistance of the sample.

2.9. Assembly of an Electric Double Layer Capacitor Test Cell

The applicability of the CS/OPA-QSSE as a hydrogel electrolyte for supercapacitors was evaluated in an electric double layer capacitor (EDLC) test cell. The symmetric EDLC cell was assembled using a two-electrode vessel produced by Swagelok (USA) (Figure 3).

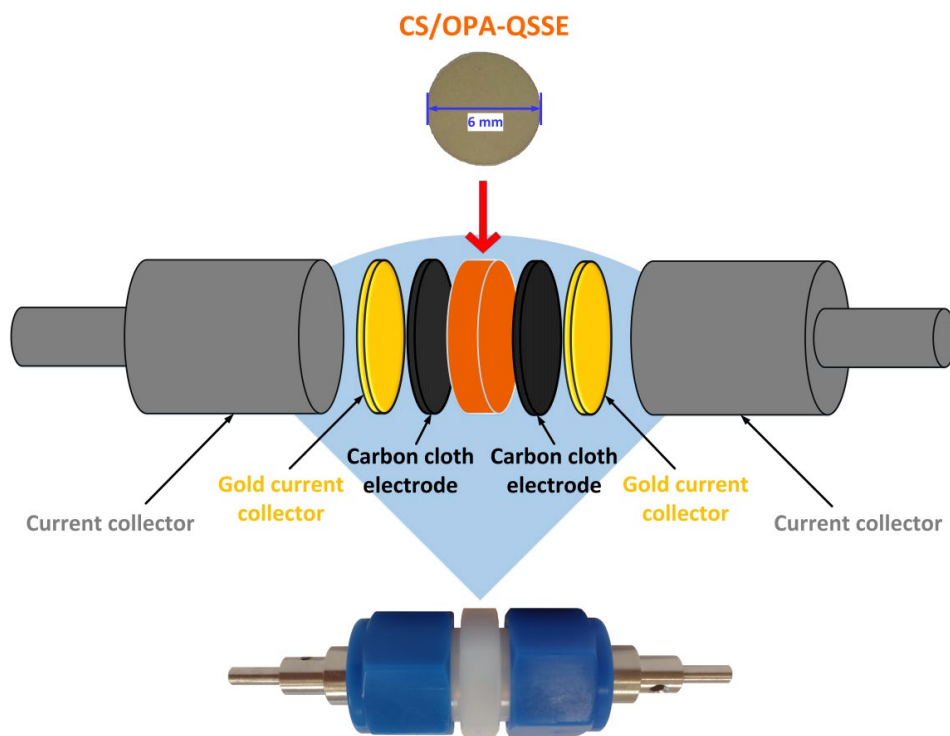


Figure 3. Schematic view of the electric double-layer capacitor assembled in this study using the Swagelok® system. Abbreviation: CS/OPA-QSSE, *o*-phthalaldehyde cross-linked chitosan membrane quasi-solid-state electrolyte.

Activated carbon cloth (2000 m² g⁻¹, No ACC-507-20, Kynol, Japan) and gold discs were used as electrodes and current collectors, respectively. The electrodes were shaped

as discs (diameter = 6 mm), and the mass of a single electrode was 4.8 mg; the CS/OPA-QSSE was also cut into 6-mm discs and placed between them. The reference EDLC cell with a commercial glass fibre separator (pore diameter = 1.6 μm and thickness = 0.3 mm, Whatman GF/A, UK) was assembled using the same electrode material, 2 M Li_2SO_4 solution as a liquid electrolyte and a two-electrode Swagelok vessel.

2.10. Electrochemical Measurements

The EDLC cell electrochemical performance was examined with various advanced electrochemical techniques, including electrochemical impedance spectroscopy (EIS), cyclic voltammetry (CV) and galvanostatic charge/discharge (GCD). EIS was performed using a $\mu\text{AutoLab}$ FRA2 type III electrochemical system (EcoChemie, the Netherlands) in the frequency range from 100 kHz to 0.01 Hz, with a sinusoidal excitation signal of amplitude 10 mV. CV measurements were realised using the same electrochemical system in the potential range of 0–0.8 V and with different scan rates (5–100 mV s^{-1}). GCD was carried out at a constant current of 5 mA with the cell voltage stepped from 0 to 0.8 V, using a Interface 5000 (Gamry Instruments, USA). All electrochemical measurements were performed at 25°C.

3. Results and Discussion

3.1. Attenuated Total Reflectance Fourier-Transform Infrared Spectroscopy

Figure 4 presents the ATR-FTIR spectra obtained for CS standard powder and the CS/OPA membrane.

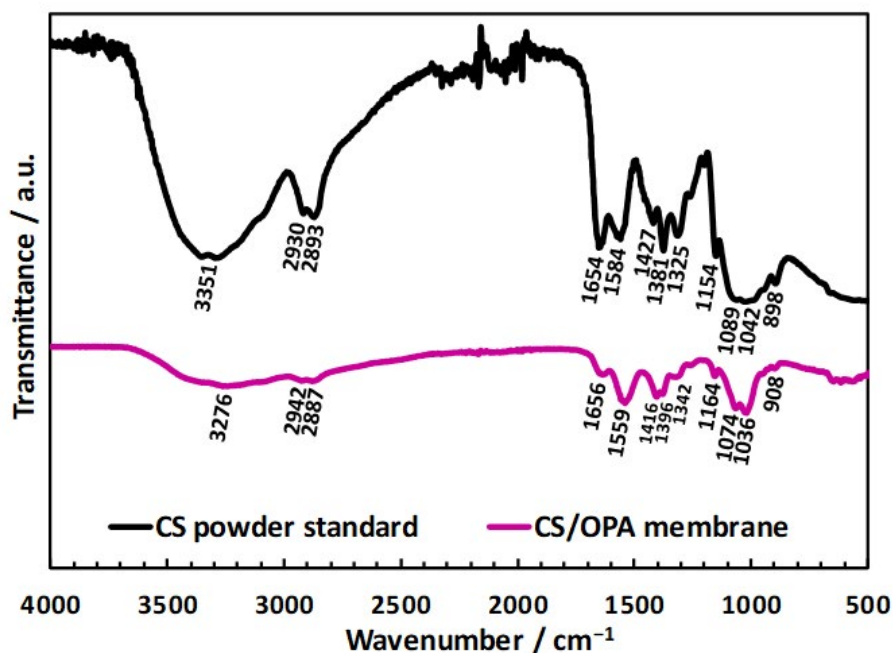


Figure 4. Attenuated total reflectance Fourier-transform infrared spectra of chitosan standard powder (CS, black curve) and the chitosan/*o*-phthalaldehyde (CS/OPA) membrane (purple curve).

The reference sample spectrum (Figure 4, black curve) features characteristic bands for CS, including amide I at 1654 cm^{-1} ($\nu\text{C}=\text{O}$), amide III at 1325 cm^{-1} ($\nu\text{C}-\text{N}$) and the band at around 898 cm^{-1} ($\nu\text{C}-\text{O}-\text{C}$ bridge) [14, 24, 25]. Moreover, there is a distinctive band at 1584 cm^{-1} attributed to the N—H in-plane bending vibrations of the primary amine group. A detailed analysis of the CS/OPA membrane spectrum (Figure 4, purple line) reveals absorption peaks that correspond with the reference sample. However, their wavelengths are shifted slightly and the intensity is markedly lower, which is a frequent phenomenon observed in the spectra of heavily processed CS materials [8, 14, 21, 24, 25]. The cross-linking process caused significant changes in both the wavelength and intensity of the band at 1559 cm^{-1} , which most probably corresponds to the amide II ($\delta\text{N}-\text{H}$) vibrations of the residual *N*-acetyl groups [24]. Such a band confirms the imine bond formation between CS polymeric chains and OPA. In this reaction, the amine groups are consumed (Figure 1); thus, the characteristic band of amide II (overlapped in the reference sample spectrum by the δNH_3^+ vibrations of the primary amine group) can be distinguished.

3.2. Atomic Force Microscopy Characterisation

The topography of the CS/OPA membrane in the dry state and the nanomechanical properties were examined with AFM (Figure 5). The thickness of the investigated sample in the dry state was $30 \pm 1\ \mu\text{m}$.

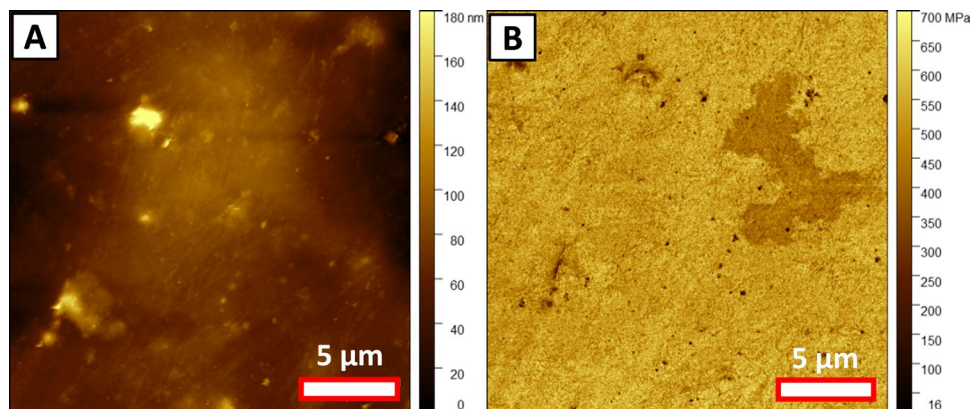


Figure 5. The atomic force micrographs show (A) the surface topography of the chitosan/*o*-phthalaldehyde membrane and (B) the distribution of Young's modulus on the membrane surface.

The general topography of the CS/OPA membrane (Figure 5A) shows a relatively homogeneous and fine-grained surface with an average height of 64.5 nm, an average grain radius of $64.5 \pm 2.8\text{ nm}$ and a mean roughness parameter of 30.74 nm, which are within the wide range of published values for various cross-linked CS membranes [9, 26, 27]. However, a few higher spots are visible (Figure 5A), and the maximum height analysis yielded an h_{max} value of 258.1 nm, which may be caused by the presence of insoluble residues of biomineralised crustacean shell or micro air bubbles congealed during the solvent evaporation process.

The nanomechanical properties – adhesion force, energy dissipation and Young's modulus – were also investigated. The average adhesion force and energy dissipation were $1.85 \pm 0.21\text{ nN}$ and $0.85 \pm 0.03\text{ fJ}$, respectively. Young's modulus showed a relatively

regular distribution of values across the captured image (Figure 5B), with an average of 512.0 ± 2.2 GPa. Further detailed analysis revealed that similarly to the topography image, there are a few areas characterised with lower Young's modulus on the membrane surface. Interestingly, these areas correspond to the spots of inhomogeneity found across the topography image (Figure 5A) and suggest that even small solid inclusions within the CS-based membrane may impact the polymer matrix's mechanical properties.

3.3. Surface Free Energy

Measurement of the contact angle is widely used to determine the wettability of polymer membranes and matrices [23, 28]. In the present study, it was measured to obtain a preliminary evaluation of the applicability of the CS/OPA matrix in polar and non-polar liquid electrolytes. Figure 6 presents a detailed view of the contact angles and shapes of liquid droplets (ethylene glycol and diiodomethane) on the CS/OPA membrane.

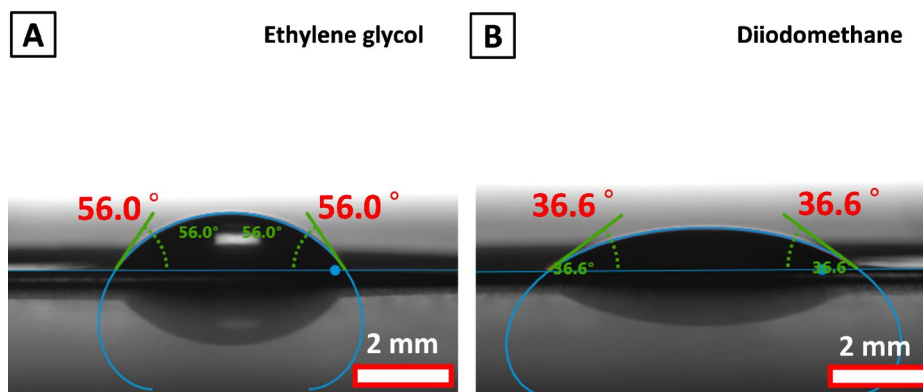


Figure 6. Estimated equilibrium contact angles for the chitosan/*o*-phthalaldehyde membrane with (A) ethylene glycol and (B) diiodomethane as a drop of liquid.

The drop shape analysis revealed that the CS/OPA membrane was well wetted by the non-polar liquid (Figure 6B, contact angle = 36.6°) and wetted slightly less by the polar liquid (Figure 6A, contact angle = 56.0°). Because unmodified CS membranes are often characterised in the literature as extremely wettable by water, it can be assumed that cross-linking CS with OPA decreased its hydrophilic character [8, 9, 21, 28]. The surface free energy dispersive and polar components calculated for the CS/OPA membrane (41.8 and 0.7 mN m^{-1} , respectively) also confirmed that covalent cross-linking of CS reduced its hydrophilicity, possibly by due to the increase in London forces [8, 29]. Thus, the results suggest that CS cross-linked with OPA might be applied for both aqueous and non-aqueous electrolyte systems and simultaneously eliminate the excessive swelling hazard.

3.4. Degree of Swelling and Ionic Conductivity Measurements

The electrolyte uptake test (25°C , 2 M Li_2SO_4) provided essential data for evaluating the effectiveness of the cross-linking process and possible application of the CS/OPA membrane as a QSSE polymer matrix. The non-cross-linked CS membrane was utilised as a reference sample, and the results of this test are shown in Figure 7. Analysis of the DS versus time dependency graph registered for the unmodified CS membrane revealed an extremely high DS (up to 250% by mass, 96 h), which unambiguously implies that without cross-linking of its polymer structure, CS is not applicable as a QSSE matrix due to the excessive swelling and possible electrolyte leakage.

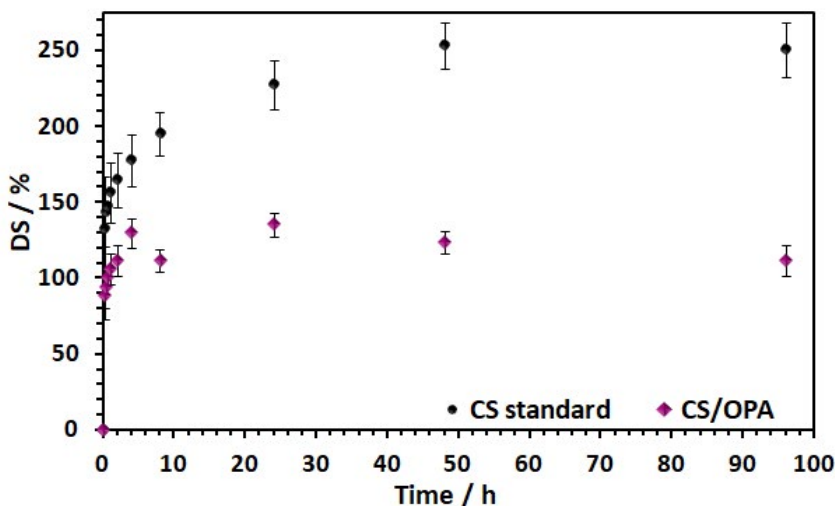


Figure 7. The degree of swelling (DS) versus time in a 2 M lithium sulfate (Li_2SO_4) aqueous solution of unmodified chitosan membrane (CS) and the chitosan/*o*-phthalaldehyde (CS/OPA) membrane.

The swelling curve obtained for the CS/OPA membrane featured a typical cross-linked CS shape, where immediately after the sample contact with neutral aqueous media, there was a dynamic increase in DS. This effect is attributed to the osmotic pressure and the diffusion of water molecules into the polymer network [26, 30]. Next, a small drop in DS can be observed, indicating the relaxation of hydrated CS chains. Finally, the polymer network expands into the solvent until swelling forces balance the osmotic pressure and the CS-based hydrogel reaches its equilibrium state [26, 27, 30]. The maximum DS measured for the CS/OPA hydrogel was 135% by mass (after 24 h), and the equilibrium DS was 112% by mass (after 96 h); both are significantly lower than the respective parameters of the reference sample (Figure 7). Therefore, the CS/OPA membrane used in this study should be recognised as a possible QSSE polymer matrix due to its well-stabilised three-dimensional polymer chain network and balanced swelling behaviour.

One of the most essential factors describing a QSSE is its ionic conductivity. A reduction in electrolyte absorption below a certain level will negatively impact this parameter [21, 31]. Table 1 presents the ionic conductivity, thickness and bulk resistance of the standard glass fibre separator soaked in the 2 M Li_2SO_4 aqueous solution and hydrogel electrolyte used in this study. Based on EIS, the ionic conductivity for CS/OPA QSSE was 26.1 S cm^{-1} , which is comparable to other polysaccharide-based hydrogel electrolytes [21, 23, 32–37].

Table 1. The ionic conductivity (σ), bulk resistance (R), thickness in the swollen state (t_s) and equivalent circuit (EC) used in the electrochemical impedance spectroscopy fitting method.

Electrolyte	σ [mS cm^{-1}]	R [Ω]	t_s [cm]	EC
CS/OPA-QSSE	26.1	15.8 ± 0.8	0.0073 ± 0.0001	$R_1(R_2\text{CPE})$
Whatman GF/A	58.3	11.9 ± 0.4	0.0123 ± 0.0001	$R_1(R_2\text{CPE})$

Note. Abbreviation: CS/OPA-QSSE, *o*-phthalaldehyde cross-linked chitosan membrane quasi-solid-state electrolyte.

3.5. Electrochemical Studies

The applicability of the CS/OPA-QSSE as a component of a supercapacitor was evaluated using standard electrochemical methods, namely EIS, CV and GCD. Moreover, the EDLC was selected as the best system for the electrochemical performance tests of the CS-based hydrogel electrolyte.

Figure 8A and 8B display the Nyquist plots for the CS/OPA-QSSE capacitor and the Whatman GF/A reference cell, respectively, before the GCD test. The shapes of the registered EIS spectra for both investigated devices fit well with the typical EDLC characteristics, including the ability to see the visible arc in the high-frequency area and a straight line parallel to the imaginary part of the impedance axis in the low-frequency range [16, 19, 38].

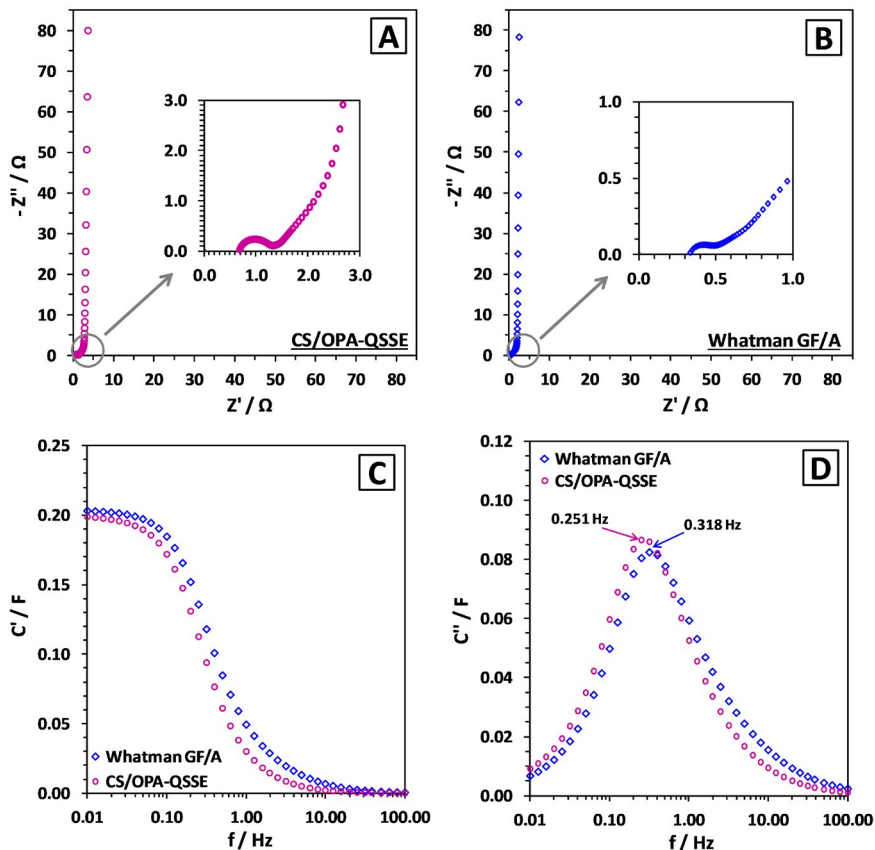


Figure 8. Nyquist plots for the electric double-layer capacitor with (A) the *o*-phthalaldehyde cross-linked chitosan membrane quasi-solid-state electrolyte (CS/OPA-QSSE) and (B) the Whatman GF/A glass fibre separator. (C) Evaluation of the real part of capacitance (C') versus frequency and (D) the imaginary part of capacitance (C'') with characteristic frequencies.

Further detailed analysis of the insets in Figure 8A and 8B provided two crucial parameters: series resistance (R_s) and charge transfer resistance (R_{ct}) [16, 39]. R_s is attributed to the resistance between the working electrode and the counter electrode within the electrochemical device; it can be calculated by extrapolating the high-frequency part of the EIS spectra to the condition $Z' = 0$ [16, 39]. R_{ct} is associated with the ion electron

transfer resistance across the electrode electrolyte interface; it can be extracted as the diameter of the first semi-circle within the Nyquist plot [16, 39]. Therefore, knowing both parameters provides complete information about the internal resistances within the tested EDLC. Table 2 provides the R_s and R_{CT} extracted from Figure 8A and 8B.

Table 2. Series resistance (R_s), charge transfer resistance (R_{CT}) and relaxation time constant (τ_0) extracted from electrochemical impedance spectroscopy.

Electric double-layer capacitor	R_s [Ω]	R_{CT} [Ω]	τ_0 [s]
CS/OPA-QSSE	0.7 ± 0.1	0.7 ± 0.1	4
Whatman GF/A in 2 M Li_2SO_4	0.3 ± 0.1	0.2 ± 0.1	3

Abbreviations: CS/OPA-QSSE, *o*-phthalaldehyde cross-linked chitosan membrane quasi-solid-state electrolyte.

Figure 8C and 8D show the dependence of real (C') and imaginary (C'') parts of capacitance versus frequency registered for the tested EDLCs [38]. Detailed analysis of the $C''(\omega)$ curves, including determining their peak frequencies (Figure 8D), allowed us to calculate another crucial EDLC parameter, namely the relaxation time constant (τ_0), which represents the time during EIS needed for the adsorption and desorption of electrolyte ions in the pores of carbon cloth electrodes [38, 40]. τ_0 was calculated with equation (3):

$$\tau_0 = \frac{1}{f_0} \quad (3)$$

where f_0 is the maximum of the $C''(\omega)$ curve [38, 40]. The results are presented in Table 2.

Summarising the EIS investigation, the internal resistance parameters calculated for the CS/OPA-QSSE test cell were relatively low (R_s and R_{CT} are both $0.7 \pm 0.1 \Omega$) and comparable to the published values for other polysaccharide-based QSSEs [18, 19, 21, 23, 35–37, 41]. However, it should be noted that compared with the Whatman GF/A reference cell ($R_s = 0.3 \pm 0.1 \Omega$ and $R_{CT} = 0.2 \pm 0.1 \Omega$), the resistance between the working electrode and counter electrode was nearly two times higher, a phenomenon that corresponds to diminished ionic conductivity of the CS/OPA-QSSE described earlier. Nonetheless, τ_0 was similar for both EDLCs (3 s for the reference cell and 4 s for the CS/OPA-QSSE); hence, CS/OPA-QSSE should exhibit good capacitive behaviour [16, 40].

The voltammetry curves recorded for both tested EDLCs (a sweep rate of 10 mV s^{-1} in the potential range of 0–0.8 V) are shown in Figure 9. The CS/OPA-QSSE cell exhibited the standard quasi-rectangular shape of the CV curve with no visible redox peaks and good charge propagation (Figure 9A). Thus, the non-Faradic nature of the capacitive processes during the cycling work of the device can be expected [31, 33, 35]. Interestingly, the voltammogram recorded for the Whatman GF/A reference EDLC showed nearly the same shape as the CS/OPA-QSSE cell, consistent with the relatively small differences in the internal resistances of the investigated devices based on the EIS analysis.

Figure 9B shows a comparison of voltammograms registered after 10,000 charging/discharging cycles in the potential range of 0–0.8 V. In general, the recorded CV curves maintained their box-type shape and good charge propagation even after an extended GCD test, which indicates excellent electrochemical stability of the CS/OPA-QSSE in the operational voltage range [18, 19, 21, 23, 35–37, 41].

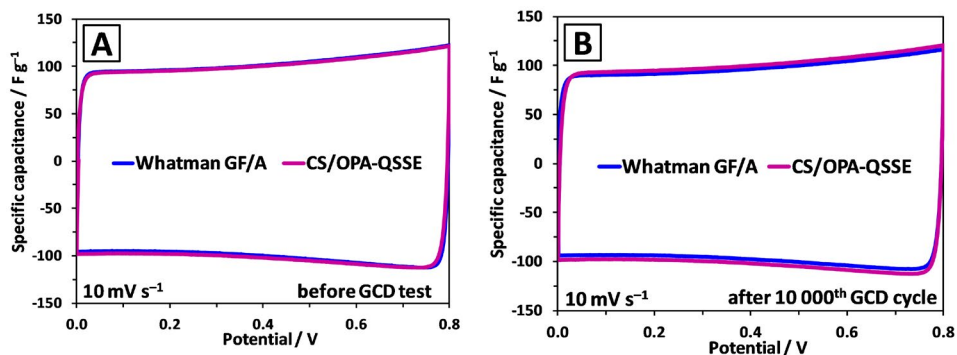


Figure 9. Comparison of the cyclic voltammetry curves recorded at the scan rate 10 mV s^{-1} (A) before the galvanostatic charge/discharge test and (B) after 10,000 charging/discharging cycles.

The cyclic repeatability and the specific discharge capacitance (C_{sp}) of the CS/OPA-QSSE and Whatman GF/A test cells were estimated with the GCD method. Figure 10A and 10B show the potential/time dependency recorded for the 1st and 10,000th charging/discharging cycles of the investigated EDLCs.

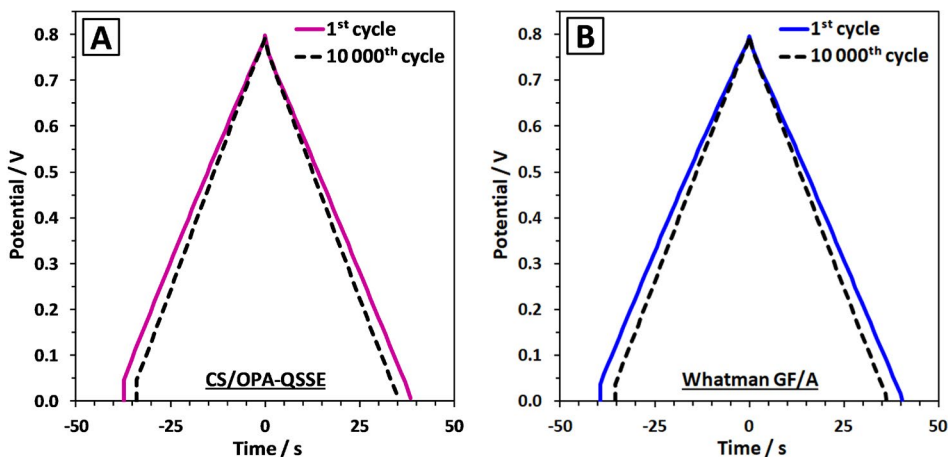


Figure 10. Galvanostatic charge/discharge curves at the 1st and 10,000th cycle for the electric double-layer capacitor test cells with the (A) *o*-phthalaldehyde cross-linked chitosan membrane quasi-solid-state electrolyte (CS/OPA-QSSE) and (B) the Whatman GF/A glass fibre separator.

All registered GCD profiles exhibited a symmetric and triangular shape for both the 1st and 10,000th cycle. This is a typical characteristic of EDLCs, which indicates the non-Faradaic nature of the capacitive processes within the device [33, 35, 41]. Unfortunately, the last GCD profile captured for the CS/OPA-QSSE EDLC did not overlap the initial one, which suggests that the cyclic repeatability of the CS/OPA-QSSE device will be slightly diminished. Nonetheless, the observed

phenomenon (manifested by narrowing the triangle base of the GCD profile) also occurred for the Whatman GF/A reference cell; therefore, it can be considered a frequent EDLC problem caused by clogging of the electrode material pores [42].

Thus, the GCD curves of the CS/OPA-QSSE test cell (Figure 10A) do not depart from the reference cell GCD characteristic (Figure 10B). Because both feature relatively low ohmic drops, their specific capacitance (CSP) can be calculated from equation (4):

$$C_{SP} = \frac{I}{\frac{dU}{dt} \times m_{el}} \quad (4)$$

where I is the discharge current, dU/dt is the slope of the discharge curve and m_{el} is the total mass of the active electrode material.

The CS/OPA-QSSE test cell exhibited the highest specific discharge capacitance values for the 1st and 10,000th cycles (115 and 103 F g⁻¹, respectively). Although the specific discharge capacitance was slightly lower for the Whatman GF/A cell (113 and 101 F g⁻¹ for the 1st and 10,000th cycles, respectively), the electrochemical performance of both EDLCs may be described as comparable with previous data published for analogous systems [33, 37].

Figure 11 provides a visualisation of the repeatability of the CS/OPA-QSSE EDLC. There was good cyclic stability of the investigated capacitors. The CS/OPA-QSSE and Whatman GF/A capacitors had relatively high capacitance retention (89.6% and 89.4%, respectively) [19, 28, 40, 41].

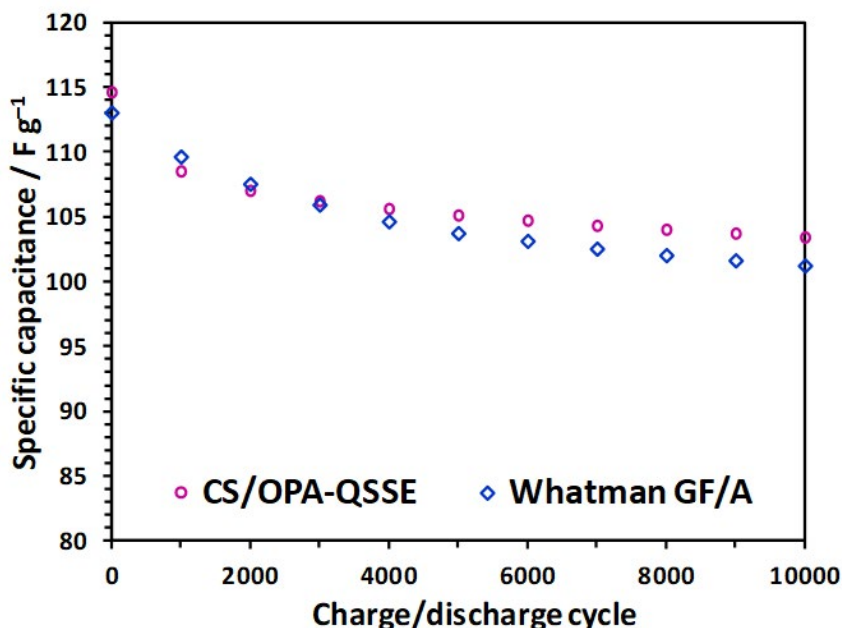


Figure 11. Cyclic stability of the tested electric double-layer capacitors over 10,000 galvanostatic charge/discharge cycles. Abbreviation: CS/OPA-QSSE, *o*-phthalaldehyde cross-linked chitosan membrane quasi-solid-state electrolyte.

Conclusively, the GCD investigation of the CS/OPA-QSSE as a component of a supercapacitor proves that despite its lower ionic conductivity (over two times lower than for the reference separator material), the electrochemical performance of the EDLC that contains it was comparable to the reference cell with a commercial glass fibre separator. These results also suggest that OPA as a CS cross-linker is electrochemically stable (within the 0–0.8 V potential window) and does not cause redox reactions within QSSE. Based on a review of the literature (Table 3), the electrochemical properties of the investigated CS/OPA-QSSE capacitor are in the range of previously published data. Moreover, the specific capacitance calculated for the CS/OPA-QSSE EDLC surpasses the majority of other reported cells with similar architecture.

Table 3. Electrochemical performance of the electric double-layer capacitor systems with the quasi-solid-state-electrolytes based on chitosan matrix reported in the literature.

Polymer matrix	Modifier	Dispersed phase	σ [mS cm ⁻¹]	Voltage window [V]	CSP [F g ⁻¹]	Ref
Chitosan	<i>o</i> -Phthalaldehyde	Li ₂ SO _{4(aq)}	26.1	0–0.8	115 (103)	This work
Chitosan	Glutaraldehyde	CH ₃ COOLi _(aq)	13.0	0–0.8	106.0	[21]
Chitosan	NaOH	CH ₃ COOLi _(aq)	14.3	0–0.8	106.0	[21]
Chitosan	Chitin	CH ₃ COOLi _(aq)	-	0–0.8	98.0	[43]
Chitosan	-	Li ₂ SO _{4(aq)}	39.1	0–0.8	97.0	[37]
Chitosan	Sodium alginate	Li ₂ SO _{4(aq)}	18.7	0–0.8	101.0	[37]
Chitosan	PEG/PPG	H ₂ SO _{4(aq)}	-	0–1.0	132.0	[44]
Chitosan	-	Na ₂ SO _{4(aq)}	-	0–1.6	35.0	[28]
Carboxymethyl chitosan	-	Na ₂ SO _{4(aq)}	-	0–1.8	72.5	[28]
Carboxymethyl chitosan	Acrylic acid/MBA	KOH _(aq)	75.6	0–0.9	39.1	[32]
Carboxymethyl chitosan	Acrylic acid/fecl ₃	KOH _(aq)	47.1	0–0.9	33.5	[32]
Carboxymethyl chitosan	PAM/MBA	Li ₂ SO _{4(aq)}	17.4	0–1.4	31.9	[33]
Chitosan	PC/EC	LiClO _{4(aq)}	5.5	0–1.0	80.0	[34]
Carboxymethyl chitosan	-	HCl _(aq)	86.9	0–0.9	45.9	[35]
Chitosan	PAEK-g-PEG	LiClO _{4(aq)}	8.0	0–1.5	120.8	[36]
Chitosan	Glyoxylic acid	KOH _(aq)	-	0–0.8	95.0	[45]

4. Conclusions

A novel polysaccharide-based QSSE with a polymer matrix – CS cross-linked with OPA – was developed successfully, and a 2 M Li₂SO₄ aqueous solution was utilised as a dispersive phase. Characterisation of the physicochemical properties (using ATR-FTIR

spectroscopy, AFM and contact angle measurements) confirmed that OPA-mediated cross-linking modified the CS matrix. The CS/OPA-QSSE possessed excellent ionic conductivity and, therefore, its applicability as a hydrogel electrolyte in an EDLC was evaluated. The symmetric EDLC based on the CS/OPA-QSSE showed good electrochemical performance (without visible redox processes) and superior specific discharge capacitance (up to 115 F g⁻¹) compared with the reference cell with a commercial Whatman GF/A glass fibre separator (up to 113 F g⁻¹). This study represents the first successful realisation of OPA-cross-linked CS as a QSSE polymer matrix. It can be considered as a future alternative for other polysaccharide-based materials for electrochemical purposes.

5. Acknowledgements

This work was performed with the financial support of the Ministry of Science and Higher Education, Poland (grant no. 0911/SBAD/2402). The authors thank Marcin Wysokowski (Poznan University of Technology, Poland) for technical support during the contact angle measurements.

6. References

- [1] Regulation (EU) 2023/1542 concerning batteries and waste batteries (2023). Off J L191, 1–117.
- [2] Regulation (EU) 2021/1119 establishing the framework for achieving climate neutrality (2021). Off J L243, 1–17.
- [3] Directive 2012/19/EU on waste electrical and electronic equipment (2012). Off J L197, 38–71.
- [4] Musarurwa H, Tavengwa NT; (2022) Application of polysaccharide-based metal organic framework membranes in separation science. *Carbohydr Polym* 275, 118743. DOI:10.1016/j.carbpol.2021.118743
- [5] Shen X, Shamshina JL, Berton P, Gurau G, Rogers RD; (2016) Hydrogels based on cellulose and chitin: fabrication, properties, and applications. *Green Chem* 18, 53–75. DOI:10.1039/C5GC02396C
- [6] Mutsenko VV, Gryshkov O, Lauterboeck L, Rogulska O, Tarusin DN, Bazhenov VV, Schütz K, Brüggemeier S, Gossla E, Akkineni AR, Meißner H, Lode A, Meschke S, Fromont J, Stelling AL, Tabachnik KR, Gelinsky M, Nikulin S, Rodin S, Tonevitsky AG, Petrenko AY, Glasmacher B, Schupp PJ, Ehrlich H; (2017) Novel chitin scaffolds derived from marine sponge *Ianthella basta* for tissue engineering approaches based on human mesenchymal stromal cells: Biocompatibility and cryopreservation. *Int J Biol Macromol* 104, 1955–1965. DOI:10.1016/j.ijbiomac.2017.03.161
- [7] Sahraee S, Milani JM, Ghanbarzadeh B, Hamishehkar H; (2017) Physicochemical and antifungal properties of bio-nanocomposite film based on gelatin-chitin nanoparticles. *Int J Biol Macromol* 97, 373–381. DOI:10.1016/j.ijbiomac.2016.12.066
- [8] Takeshita S, Konishi A, Takebayashi Y, Yoda S, Otake K; (2017) Aldehyde approach to hydrophobic modification of chitosan aerogels. *Biomacromol* 18, 2172–2178. DOI:10.1021/acs.biomac.7b00562
- [9] Gierszewska M, Ostrowska-Czubenko J; (2016) Chitosan-based membranes with different ionic crosslinking density for pharmaceutical and industrial applications. *Carbohydr Polym* 153, 501–511. DOI:10.1016/j.carbpol.2016.07.126

- [10] Yu X, Zhang J, Zheng Y; (2021) Perchlorate adsorption onto epichlorohydrin crosslinked chitosan hydrogel beads. *Sci Total Environ* 761, 143236. **DOI:**10.1016/j.scitotenv.2020.143236
- [11] Vo NTN, Huang L, Lemos H, Mellor AL, Novakovic K; (2021) Genipin-crosslinked chitosan hydrogels: Preliminary evaluation of the *in vitro* biocompatibility and biodegradation. *J Appl Polym Sci* 138(34), 50848. **DOI:**10.1002/app.50848
- [12] Kaczmarek-Szczepańska B, Mazur O, Michalska-Sionkowska M, Łukowicz K, Osyczka AM; (2021) The preparation and characterization of chitosan-based hydrogels cross-linked by glyoxal. *Materials* 14, 2449. **DOI:**10.3390/ma14092449
- [13] Li Q, Su H, Yang Y, Zhang J, Xia C, Guo Z; (2023) Adsorption property and mechanism of glutaraldehyde-crosslinked chitosan for removal of 2,4-dichlorophenoxyacetic acid from water. *Environ Sci* 9(1), 294–307. **DOI:**10.1039/d2ew00638c
- [14] Acharya V, Ghosh A, Chowdhury AR, Datta P; (2021) Tannic acid-crosslinked chitosan matrices enhance osteogenic differentiation and modulate epigenetic status of cultured cells over glutaraldehyde crosslinking. *Soft Mater* 20, 149–160. **DOI:**10.1080/1539445X.2021.1933032
- [15] Józwiak T, Filipkowska U, Szymczyk P, Rodziewicz J, Mielcarek A; (2017) Effect of ionic and covalent crosslinking agents on properties of chitosan beads and sorption effectiveness of Reactive Black 5 dye. *React Funct Polym* 114, 58–74. **DOI:**10.1016/j.reactfunctpolym.2017.03.007
- [16] Hor AA, Yadav N, Hashmi S; (2023) Enhanced energy density quasi-solid-state supercapacitor based on an ionic liquid incorporated aqueous gel polymer electrolyte with a redox-additive trimethyl sulfoxonium iodide. *J Energy Storage* 64, 107227. **DOI:**10.1016/j.est.2023.107227
- [17] Fan L, Tu Q, Geng C, Huang J, Gu Y, Lin J, Huang Y, Wu J; (2020) High energy density and low self-discharge of a quasi-solid-state supercapacitor with carbon nanotubes incorporated redox-active ionic liquid-based gel polymer electrolyte. *Electrochim Acta* 331, 135425. **DOI:**10.1016/j.electacta.2019.135425
- [18] Lin X, Wang M, Zhao J, Wu X, Xie J, Yang J; (2023) Super-tough and self-healable all-cellulose-based electrolyte for fast degradable quasi-solid-state supercapacitor. *Carbohydr Polym* 304, 120502. **DOI:**10.1016/j.carbpol.2022.120502
- [19] Çevik, E, Günday ŞT, Bozkurt A, Iqbal A, Asiri SM, Alqarni AN, Almofleh A; (2022) Scalable, quasi-solid-state bio-polymer hydrogel electrolytes for high-performance supercapacitor applications. *ACS Sustain Chem Eng* 10(33), 10839–10848. **DOI:**10.1021/acssuschemeng.2c02281
- [20] Roy BK, Tahmid I, Rashid TU; (2021) Chitosan-based materials for supercapacitor applications: a review. *J Mater Chem A* 9(33), 17592–17642. **DOI:**10.1039/d1ta02997e
- [21] Nowacki K, Galiński M, Stępnia I; (2019) Synthesis and characterization of modified chitosan membranes for applications in electrochemical capacitor. *Electrochim Acta* 320, 134632. **DOI:**10.1016/j.electacta.2019.134632
- [22] Garg M, Bhullar N, Bajaj B, Sud D; (2021) Terephthalaldehyde as a good crosslinking agent in crosslinked chitosan hydrogel for the selective removal of anionic dyes. *New J Chem* 45(11), 4938–4949. **DOI:**10.1039/d0nj05758d
- [23] Wysokowski M, Nowacki K, Jaworski F, Niemczak M, Bartczak P, Sandomierski M, Piasecki A, Galiński M, Jesionowski T; (2022) Ionic liquid-assisted synthesis of chitin-ethylene glycol hydrogels as electrolyte membranes for sustainable electrochemical capacitors. *Sci Rep* 12(1), 8861. **DOI:**10.1038/s41598-022-12931-w

- [24] Weißpflog J, Vehlow D, Müller M, Kohn B, Scheler U, Boye S, Schwarz S; (2021) Characterization of chitosan with different degree of deacetylation and equal viscosity in dissolved and solid state – insights by various complimentary methods. *Int J Biol Macromol* 171, 242–261. **DOI:**10.1016/j.ijbiomac.2021.01.010
- [25] Klein MP, Hackenhaar CR, Lorenzoni ASG, Rodrigues RC, Costa TMH, Ninow JL, Hertz PF; (2016) Chitosan crosslinked with genipin as support matrix for application in food process: support characterization and β -d-galactosidase immobilization. *Carbohydr Polym* 137, 184–190. **DOI:**10.1016/j.carbpol.2015.10.069
- [26] Ostrowska-Czubenko J, Gierszewska M, Pieróg M; (2015) pH-responsive hydrogel membranes based on modified chitosan: water transport and kinetics of swelling. *J Polym Res* 22(8), 153. **DOI:**10.1007/s10965-015-0786-3
- [27] Węgrzynowska-Drzymalska K, Grebicka P, Młynarczyk DT, Chełminiak-Dudkiewicz D, Kaczmarek H, Gośliński T, Ziegler-Borowska M; (2020) Crosslinking of chitosan with dialdehyde chitosan as a new approach for biomedical applications. *Materials* 13(15), 3413. **DOI:**10.3390/ma13153413
- [28] Lin CY, Wang PH, Lee WN, Li WC, Wen TC; (2021) Chitosan with various degrees of carboxylation as hydrogel electrolyte for pseudo solid-state supercapacitors. *J Power Sources* 494, 229736. **DOI:**10.1016/j.jpowsour.2021.229736
- [29] Takeshita S, Yoda S; (2017) Translucent, hydrophobic, and mechanically tough aerogels constructed from trimethylsilylated chitosan nanofibers. *Nanoscale* 9(34), 12311–12315. **DOI:**10.1039/c7nr04051b
- [30] Zhang X, Wu D, Chu C; (2003) Effect of the crosslinking level on the properties of temperature-sensitive poly(N-isopropylacrylamide) hydrogels. *J Polym Sci B* 41(6), 582–593. **DOI:**10.1002/polb.10388
- [31] Gajewski P, Żyła W, Kazimierczak K, Marcinkowska A; (2023) Hydrogel polymer electrolytes: synthesis, physicochemical characterization and application in electrochemical capacitors. *Gels* 9(7), 527. **DOI:**10.3390/gels9070527
- [32] Zhang Q, Zhao L, Yang H, Kong L, Ran F; (2021) Alkali-tolerant polymeric gel electrolyte membrane based on cross-linked carboxylated chitosan for supercapacitors. *J Mem Sci* 629, 119083. **DOI:**10.1016/j.memsci.2021.119083
- [33] Yang H, Ji X, Tan Y, Liu Y, Ran F; (2019) Modified supramolecular carboxylated chitosan as hydrogel electrolyte for quasi-solid-state supercapacitors. *J Power Sources* 441, 227174. **DOI:**10.1016/j.jpowsour.2019.227174
- [34] Selvakumar M, Bhat DK; (2009) LiClO₄-doped plasticized chitosan as biodegradable polymer gel electrolyte for supercapacitors. *J Appl Polym Sci* 114(4), 2445–2454. **DOI:**10.1002/app.30716
- [35] Yang H, Liu Y, Kong L, Kang L, Ran F; (2019) Biopolymer-based carboxylated chitosan hydrogel film crosslinked by HCl as gel polymer electrolyte for all-solid-state supercapacitors. *J Power Sources* 426, 47–54. **DOI:**10.1016/j.jpowsour.2019.04.023
- [36] Na R, Huo G, Zhang S, Huo P, Du Y, Luan J, Zhu K, Wang G; (2016) A novel poly(ethylene glycol)-grafted poly(arylene ether ketone) blend micro-porous polymer electrolyte for solid-state electric double layer capacitors formed by incorporating a chitosan-based LiClO₄ gel electrolyte. *J Mater Chem A* 4(46), 18116–18127. **DOI:**10.1039/c6ta07846j
- [37] Nowacki K, Galiński M, Stępnik I; (2020) Synthesis and characterization of chitosan/sodium alginate blend membrane for application in an electrochemical capacitor. *Prog Chem Appl Chitin Deriv* 25, 174–191. **DOI:**10.15259/pcacd.25.014

- [38] Taberna P, Simon P, Fauvarque J; (2003) Electrochemical characteristics and impedance spectroscopy studies of carbon-carbon supercapacitors. *J Electrochem Soc* 150(3), A292. **DOI:**10.1149/1.1543948
- [39] Laschuk NO, Easton EB, Zenkina OV; (2021) Reducing the resistance for the use of electrochemical impedance spectroscopy analysis in materials chemistry. *RSC Adv* 11(45), 27925–27936. **DOI:**10.1039/d1ra03785d
- [40] Hor AA, Hashmi S; (2020) Optimization of hierarchical porous carbon derived from a biomass pollen-cone as high-performance electrodes for supercapacitors. *Electrochim Acta* 356, 136826. **DOI:**10.1016/j.electacta.2020.136826
- [41] Kasprzak D, Liu J; (2023) Chitin and cellulose as constituents of efficient, sustainable, and flexible zinc-ion hybrid supercapacitors. *Sustain Mater Technol* 38, e00726. **DOI:**10.1016/j.susmat.2023.e00726
- [42] Yambou EP, Köps L, Kreth FA, Pohlmann S, Varzi A, Brousse T, Balducci A, Presser V; (2023) The many deaths of supercapacitors: degradation, aging, and performance fading. *Adv Energy Mater* 13(29), 2301008. **DOI:**10.1002/aenm.202301008
- [43] Stępniański I, Galiński M, Nowacki K, Wysokowski M, Jakubowska P, Bazhenov VV, Leisegang T, Ehrlich H, Jesionowski T; (2016) A novel chitosan/sponge chitin origin material as a membrane for supercapacitors – preparation and characterization. *RSC Adv* 6(5), 4007–4013. **DOI:**10.1039/c5ra22047e
- [44] Raja M, Balaji S, Ramavath JN, Dhamodharan R, Ramanujam K; (2019) A chitosan/poly(ethylene glycol)-ran-poly(propylene glycol) blend as an eco-benign separator and binder for quasi-solid-state supercapacitor applications. *Sustain Energy Fuels* 3(3), 760–773. **DOI:**10.1039/c8se00530c
- [45] Zallouz S, Meins JL, Ghimbeu CM; (2022) Alkaline hydrogel electrolyte from biosourced chitosan to enhance the rate capability and energy density of carbon-based supercapacitors. *Energy Adv* 1(12), 1051–1064. **DOI:**10.1039/d2ya00250g

RESPONSE OF THE ‘POLESIE’ RASPBERRY CULTIVAR TO FOLIAR APPLICATION OF CHITOSAN WITH DIFFERENT MOLECULAR WEIGHTS

Ireneusz Ochmian^{1,a,*}, Marcelina Krupa-Malkiewicz^{2,b}

¹ – Department of Horticulture, West Pomeranian University of Technology Szczecin, Słowackiego 17 Str., 71-434 Szczecin, Poland

^a – ORCID: 0000-0002-3606-1927

² – Department of Plant Genetics, Breeding and Biotechnology, West Pomeranian University of Technology Szczecin, Słowackiego 17 Str., 71-434 Szczecin, Poland

^b – ORCID: 0000-0002-4333-9122

*corresponding author: iochmian@zut.edu.pl

Abstract

This study explored the effects of chitosan, a biodegradable and non-toxic natural polymer derived from chitin, on the yield and quality of raspberries. Various molecular weights (3.3–950 kDa) were assessed to determine the impact on raspberry plants and fruit development. These applications were made during key growth phases – the start of the vegetation period, during flowering and at the fruit-bearing stage – using a foliar method to ensure full coverage of both leaves and fruit without runoff. The results indicated that chitosan application influenced various parameters of fruit quality, including firmness, colour and antioxidant levels. Notably, chitosan with a molecular weight of 21 and 50 kDa significantly enhanced fruit yield and size compared with the control. Conversely, chitosan with a higher molecular weight (500 and 950 kDa) did not improve yield and appeared to induce stress in plants, although they did contribute to increased fruit firmness and potentially extended the shelf life due to their film-forming capabilities. The findings suggest that while chitosan can improve the yield and quality of raspberries, the effectiveness is highly dependent on its molecular weight. These results support the potential of chitosan as an alternative to traditional chemical treatments, promising a reduction in chemical inputs while sustaining or enhancing agricultural productivity and fruit quality.

Keywords: *antioxidant activity, colour, grey mould, firmness, fruit size, polyphenols*

Received: 18.03.2024

Accepted: 10.06.2024

1. Introduction

Raspberries are grown throughout the world in temperate climates [1]. They are popular because of their taste and nutritional value. In Poland, raspberries are widely grown due to favourable climatic and soil conditions [2].

Raspberries have a unique flavour and many beneficial health-promoting properties. They are rich in antioxidants such as vitamin C, quercetin and anthocyanins [3]. These substances help fight free radicals in the body, which can contribute to protect against heart disease, cancer and cellular ageing [4]. The antioxidant components in raspberries help to reduce inflammation in the body, which may contribute to reduce the risk of many chronic diseases [5].

Raspberries are very tender fruit, susceptible to diseases, especially grey mould, powdery mildew, anthracnose and viral diseases [6–8]. Therefore, preventive measures should be applied to keep the plants in good condition: adequate pruning, irrigation, fertilisation and application of plant-protection products [9, 10].

Intensification of unfavourable factors drastically reduces yield and fruit quality. Many factors influence fruit quality, including climatic conditions such as drought, excessive moisture, frost, heat; diseases and pests; nutrient deficiencies; environmental pollution; and inappropriate cultivation techniques [11–13]. Harvesting the fruit at the right time of ripening ensures the optimal aroma, size colour and firmness. Firmness or mechanical resistance are considered good indicators of raspberry quality [14]. Fruit firmness decreases gradually with ripening. It indicates the suitability of the fruit for harvesting, transport, consumption or freezing as well as the susceptibility of the fruit to fungal diseases [15]. Intensive chemical protection must be applied to produce healthy raspberries. However, the widespread use of chemical plant protection products is one of the causes of environmental degradation.

In recent years, measures have been taken to reduce the over-chemicalisation of agricultural production. Alternative methods are being sought to protect plants from disease. One such natural substance that is being used in agricultural production is chitosan [$\beta(1\rightarrow4)$ -D-glucosamine and *N*-acetyl-D-glucosamine]. It is a non-toxic and biodegradable compound of natural origin, obtained by deacetylation of chitin [16, 17]. Chitin is a key structural component in the exoskeletons of crustaceans such as crabs, shrimp and lobsters; the cell walls of fungi; and the exoskeletons of insects [18]. When applied to plants, chitosan reduces transpiration and induces a number of metabolic changes, increasing their resistance to infection by pathogens [19]. As a natural macromolecular polysaccharide, chitosan is a partially deacetylated chitin product with different molecular weights and degrees of deacetylation [20, 21].

The effectiveness of solutions prepared based on chitosan varies widely and depends on its molecular weight. High-molecular-weight chitosan (360 kDa) delays fruit ripening, but results in higher post-harvest quality compared with low-molecular-weight chitosan (40 kDa) [22]. However, low-molecular-weight chitosan, exemplified by oligomers of chitosan lactate, shows better solubility in water [23]. Therefore, such formulations should be tested for suitability in raspberry cultivation. The present study aimed to investigate the effect of foliar-applied chitosan of different molecular weights on raspberry yield and quality.

2. Materials and Methods

2.1. Characteristics of the Research Area and Plant Material

The experiment was conducted at the Horticulture Department of the West Pomeranian University of Technology, Szczecin, Poland. The Polish raspberry cultivar Polesie was studied. These raspberries are consumed as is and are also frozen and processed into products such as juices. These plants bear raspberries on 1-year-old shoots, a process called repeat fruiting. The cultivar is recommended for ecological cultivation.

Raspberries were harvested successively as they ripened from the production plantation during the harvest. The plants received limited chemical protection according to the accepted rules for organic plantations.

The experiment was established on a precipitous-gley podzolic soil developed from till with a mechanical composition of light clay (26–35 mm fraction < 0.02 mm) [24] under the climatic conditions of north-western Poland [25].

During the experiment, the plants were treated throughout the growing season according to the established rules. The soil was watered using a permanently mounted T-Tape drip line with an emitter capacity of 1 l/h (5 l of water/h over a 1 mb section of the system). The doses and intensity of water emitted were modified according to the degree of soil moisture, determined by contact soil tensiometers.

The orchard used agricultural soil with a natural profile developed from silt-loam with a pH of 6.5. The soil in which the shrubs grew had a high content of phosphorus (P, 88 mg/kg), potassium (K, 145 mg/kg) and magnesium (Mg, 66 mg/kg). Annually, from the start of vegetation (March/April), 90 kg of nitrogen (N) was applied as three equal doses.

2.2. Weather Conditions During the Experiment

Several significant trends and changes can be observed when analysing the data on the temperature and rainfall in Szczecin during the vegetation period from April to October in the years 2020–2022 compared with the long-term period (1951–2012) (Table 1). The temperatures in 2020–2022 were mostly higher than the long-term average, indicating a warming trend. For example, in July and August 2021 and 2022, the temperatures were significantly higher than the long-term average temperatures. The average temperature in 2020–2022 (14.4–14.6°C) was higher than the long-term average (13.7°C). Rainfall in 2020–2022 was generally lower than the long-term average for this period (390.6 mm). For example, the total rainfall in 2020 was 258.1 mm, which is significantly below the norm. There were significant fluctuations in rainfall, especially in July 2021, where rainfall reached 123 mm compared with the long-term average of 69.6 mm. Meanwhile, no rainfall was recorded in June. The higher temperatures and lower rainfall compared with the long-term averages are consistent with general trends of climate change. These changes may pose challenges for agriculture in the Szczecin region and require adjustments in agricultural practices to manage water resources effectively and to maintain healthy conditions for crops.

Table 1. The temperature and rainfall in the period from April to October (vegetation season) in 2020–2022 compared with the long-term period (1951–2012) in Szczecin, Poland.

	Month								
	IV	V	VI	VII	VIII	IX	X	Mean	
Year	Average temperature (°C)								
2020	8.9	11.1	17.7	17.4	20.3	14.6	10.5	14.4	
2021	5.9	11.6	19.3	20.3	16.7	15.1	10.1	14.1	
2022	7.2	13.3	18.1	18.4	20.6	12.9	11.6	14.6	
1951–2012	8.0	13.0	16.4	18.2	17.6	13.8	9.2	13.7	
	Rainfall (mm)								total
2020	20.1	34.0	26.6	21.3	40.0	72.3	43.8	258.1	
2021	4.6	25.1	0.0	123	37.4	17.1	24.7	231.9	
2022	19.9	25.2	27.6	67.5	23.4	39.0	22.2	224.8	
1951–2012	39.7	62.9	48.2	69.6	74.2	58.7	37.3	390.6	

2.3. Edible Coating Preparation and Application of Treatments

Samples with varying molar masses were prepared by controlled radical degradation of chitosan with a molecular mass > 1200 kDa (chitosan HMW, Aldrich, USA) in the Department of Packaging and Biopolymers of the West Pomeranian University of Technology, Szczecin, Poland. Samples were obtained via continuous addition of hydrogen peroxide (0.8–6.4 mM/g of polysaccharide) to 2.5% chitosan solution with pH 3.5–4.0 at 80°C. After degradation, all samples, as chloride salts, had similar polydispersity and a high degree of deacetylation (> 95%). The molar mass of each sample was determined using the high-performance liquid chromatography (HPLC)/gel permeation chromatography (GPC) method (HPLC SmartLine system with an isocratic pump 1000 equipped with an RI Detector 2300; Knauer, Germany).

Raspberry plants were treated with chitosan with the following molecular weights: 3,333 Da (3.3k), 5,000 Da (5k), 12,000 Da (12k), 21,000 Da (21k), 50,000 Da (50k), 125,000 Da (125k), 500,000 Da (500k) and 950,000 Da (950k). Chitosan was dissolved in 300 g of distilled water, and the solution was titrated to a pH of 7.7 by adding 1 M sodium hydroxide (NaOH). Then, the volume was adjusted to 500 g with distilled water, and 500 g of 0.2 M acetic acid was added.

Annually, the plants were sprayed with a 0.2% chitosan solution (0.2 l per metre of row), prepared from the aforementioned chitosan with different molecular weights, ensuring full wetting (without allowing the solution to drip from the plants) of the leaves and, later in the season, both leaves and fruit. The spraying was carried out in the morning using a battery-operated backpack sprayer. The application was planned at the start of the vegetation period, three times during the flowering phase, and three times during the fruit-bearing stage. Conversely, the control plants were sprayed with distilled water. Throughout this study, no additional chemical protections were administered to the plants.

In the experiment, three plots were designated for each treatment/chitosan. Raspberry plants were planted in 2015 with a spacing of 3 × 0.3 m. In the subsequent years, the raspberry rows became denser. Each year, the excess of new plants was reduced: in the spring, they were removed using a rototiller, and during the growing season, plants

that grow in the row spacings were mowed. Each plot consisted of a raspberry plant row section 1 m in length and approximately 30 cm in width. Six hundred litres of solution were applied per hectare, which equals 0.2 l of solution per metre of raspberries.

2.4. General Fruit Parameters

Raspberries were harvested when fully ripe, based on the assessment of their colour, and successively throughout the vegetation season. The yield, weight of 100 raspberries, firmness and colour were measured immediately after harvest. Other analyses were performed on frozen raspberries, after the harvest season had ended. Annually, three composite samples were prepared from individual harvest dates (50 g from each harvest). Raspberries from the first and last harvests were not used for the analyses.

Annual measurements were taken to determine the yield and fruit mass using a RADWAG WPX 4500 scale (RADWAG, Poland, accuracy of ± 0.01 g). The soluble solid content was assessed using a PAL-1 electronic refractometer (Atago, Japan). The acidity level was determined by titrating the water extract with 0.1 N NaOH until reaching a pH of 8.1, using an CX-732 digital multimeter (Elmetron, Poland), as per the PN-2001 standard. The levels of L-ascorbic acid, nitrates and nitrites were analysed using a RQflex 10 reflectometer (Merck, Germany), as documented by Ochmian et al. [25].

2.5. Colour

The colour parameters and indices were determined by averaging 50 measurements using a CM-700d spectrophotometer (Konica Minolta, Japan), as detailed by Ochmian et al. [25], within the CIELab* colour space.

2.6. Firmness

The firmness and puncture resistance of the skin were assessed using a FirmTech2 device (BioWorks, USA) on 100 raspberries chosen at random from three replicates, as described by Ochmian et al. [26]. The results are expressed as the gram force required to cause a 1-mm deformation of the fruit surface.

2.7. Antioxidant Activity

Samples (1 g) were mixed with methanol (80%; 10 ml) and then with hydrochloric acid (1%). This process was performed twice by incubating the above slurry for 20 min under sonication. Next, the slurry was centrifuged at 19,000 g for 10 min, and the supernatant was filtered through a hydrophilic poly(tetrafluoroethylene) (PTFE) 0.20 μm membrane (Merck, Germany) and used for analysis [27].

The 2,2'-azobis(3-ethylbenzothiazoline-6-sulfonic acid) (ABTS) radical scavenging assay was conducted using the method described by Arnao et al. [28]. The 1,1-diphenyl-2-picrylhydrazyl (DPPH) radical scavenging assay was performed in accordance with the protocol established by Brand-Williams et al. [29]. The ferric reducing antioxidant power (FRAP) assay followed the procedure outlined by Benzie and Strain [30].

For the quantification of total polyphenols, supernatants were analysed using the Folin-Ciocalteu method, with absorbance measured at 675 nm, as indicated by Singleton et al. [31].

2.8. Statistical Analysis

Statistical analyses were conducted using Statistica 12.5 (StatSoft Polska, Poland). The data were submitted to one-way analysis of variance (ANOVA) followed by Tukey's least significant difference test. A p value < 0.05 was considered to indicate a statistically significant difference.

3. Results and Discussion

The optimal molecular weight of chitosan appears to vary depending on the developmental stage of the plants. In the early fruit harvesting period (July), the yield was similar to that of the control plants, except for plants sprayed with 500k or 950k chitosan (Figure 1). Moreover, 500k and 950k chitosan did not favour yield, suggesting the existence of a threshold beyond which the efficiency of chitosan may decrease. The yields for 500k and 950k chitosan dropped to 12.1 t/ha and 12.4 t/ha, respectively, compared with 13.3 t/ha for the control (Table 2). The raspberries sprayed with 500k and 950k chitosan were also the smallest. The yield of plants sprayed with 12k chitosan was also low (12.5 t/ha). The 21k and 50k chitosan treatments led to the highest yields: 14.6 and 15 t/ha, respectively. In addition, 21k chitosan had a very positive effect on the size of raspberries, with an average weight of 100 raspberries of 451 g, much higher than the 315 g for the control. A reduction in yield is natural at the end of the growing season. However, treatment with 500k and 950k chitosan sustained higher yields in the first and second decades of October. This confirms the results of previous studies, which also showed that chitosan increased raspberry yield and size [14]. Chitosan can increase fruit mass through various mechanisms that improve health, enhance nutrient uptake, reduce abiotic stress or delay aging and ripening, allowing the fruit to remain on the plant longer and to continue to increase in mass before harvesting [32–34]. During spraying, a coating is formed on the fruit, which may slightly increase their mass by adding an additional layer of material on the surface. However, this coating can also reduce water loss, further affecting the maintenance of fruit mass [35].

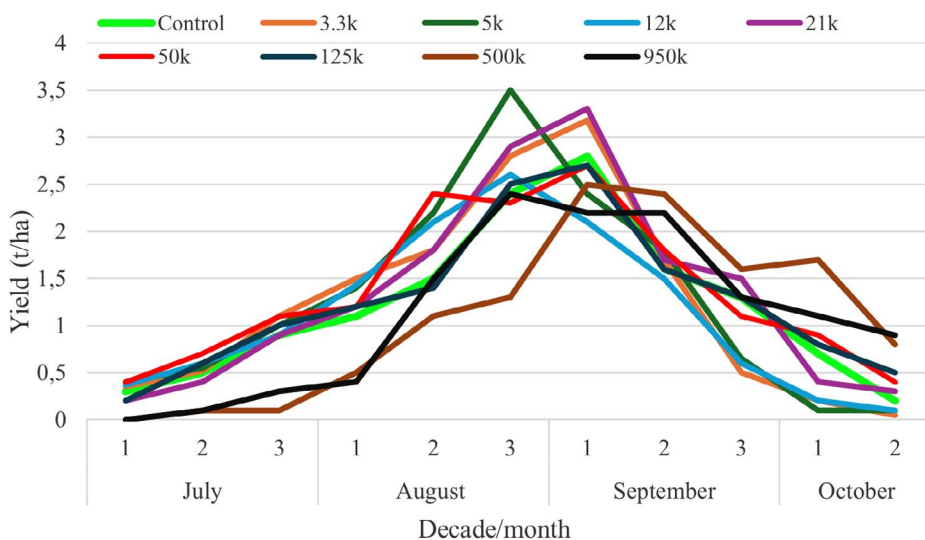


Figure 1. Yield distribution of Polesie raspberries at harvest depending on the chitosan applied. The graph shows the decadal average for 2020–2022.

Table 2. The yield, firmness, mean weight of 100 raspberries and antioxidant properties.

	Chitosan molecular weight								
	Control	3.3k	5k	12k	21k	50k	125k	500k	950k
Total yield [t/ha]	13.3 ^b	13.7 ^{bc}	14.1 ^{cd}	12.5 ^a	14.6 ^{de}	15.0 ^e	13.8 ^c	12.1 ^a	12.4 ^a
Mean weight of 100 raspberries [g]	315 ^{bc}	422 ^f	434 ^{fg}	378 ^e	451 ^g	336 ^{cd}	349 ^d	299 ^b	270 ^a
Firmness of raspberries with a floral base [G mm⁻¹]	152 ^{ab}	137 ^a	146 ^{ab}	158 ^{bc}	134 ^a	160 ^{bc}	153 ^{ab}	175 ^{cd}	189 ^d
Soluble solids [%]	11.3 ^{bc}	12.2 ^f	11.9 ^{ef}	11.5 ^{cd}	11.8 ^{de}	10.6 ^{ce}	11.0 ^b	11.8 ^{de}	11.6 ^{ce}
Titrateable acidity [g 100 g⁻¹]	1.88 ^c	1.55 ^a	1.80 ^{bc}	1.94 ^{cd}	1.79 ^{bc}	2.13 ^d	1.85 ^c	1.61 ^{ab}	1.56 ^a
N-NO₃ [mg 1000 g⁻¹]	72 ^{ab}	118 ^e	102 ^d	91 ^c	75 ^b	64 ^a	88 ^c	97 ^{cd}	112 ^e
N-NO₂ [mg 1000 g⁻¹]	0.09 ^{ab}	0.11 ^{bc}	0.12 ^c	0.11 ^{bc}	0.15 ^d	0.10 ^{ab}	0.10 ^{ab}	0.08 ^a	0.10 ^{ab}
L-ascorbic acid [mg 1000 g⁻¹]	58 ^{bd}	52 ^{ac}	64 ^{de}	70 ^e	55 ^{ad}	49 ^{ab}	60 ^{cd}	51 ^{ac}	46 ^a
Polyphenols [mg/100 g]	113 ^{bc}	122 ^c	105 ^{bc}	125 ^c	99 ^{ab}	82 ^a	94 ^{ab}	171 ^d	164 ^d
DPPH [mmol TE/100 g]	47 ^{ab}	42 ^{bc}	47 ^{ab}	45 ^b	51 ^{ab}	55 ^a	49 ^{ab}	35 ^{cd}	32 ^d
ABTS+ [mmol TE/100 g]	15 ^{bc}	17 ^{av}	19 ^{ab}	20 ^a	14 ^c	15 ^{bc}	19 ^{ab}	16 ^{ac}	16 ^{ac}
FRAP [mmol/100 g]	65 ^{bd}	61 ^{cd}	72 ^a	70 ^{ab}	66 ^{bc}	73 ^a	60 ^{de}	55 ^c	48 ^f
% of fruit infected by grey mould (<i>Botrytis cinerea</i>) after a 3-day shelf life	37 ^a	32 ^{ab}	30 ^b	15 ^d	28 ^b	22 ^c	11 ^d	4 ^e	5 ^e

Note. In each row, means with the same superscript letter do not differ significantly according to Tukey's test ($p > 0.05$). Abbreviations: ABTS, 2,2'-azobis(3-ethylbenzothiazoline-6-sulfonic acid); DPPH, 1,1-diphenyl-2-picrylhydrazyl FRAP, ferric reducing antioxidant power; N-NO₂, nitrite nitrogen; N-NO₃, nitrate nitrogen; TE, Trolox equivalents

The data revealed that raspberry firmness varied depending on the molecular weight of chitosan used. Firmness is an important parameter that affects quality, shelf life and consumer preferences for fruits. In this study, 500k and 950k chitosan increased

raspberry firmness. This ability could be useful in agricultural and processing practices to improve fruit quality. However, the question remains whether the raspberries were firmer due to the application of 500k or 950 k chitosan or due to the negative impact of the treatment on raspberry size. Zhang et al. [36] showed that a coating on fruit made of low-molecular-weight chitosan increased fruit firmness.

Raspberries treated with 3.3k chitosan showed the highest content of soluble solids (12.2%). These raspberries also had the lowest titratable acidity (1.55 g), which gives consumers the impression that they are sweeter. This suggests that chitosan with a lower molecular weight may favour the accumulation of sugars, despite the fact that the raspberries were large and the yield was higher compared with the control. Plants sprayed with 50k chitosan had the lowest amount of sugars and, at the same time, the highest acidity. Meng et al. [37] and Zhang et al. [36] showed that the use of chitosan increased the extract content and slightly reduced the acidity of fruit.

In Poland, there are no established standards that define the level of nitrates and nitrites in fruits. Raspberries accumulated very small amounts of harmful nitrates (maximum 118 mg/1000 g) and nitrites (maximum 0.12 mg/1000 g), regardless of the chitosan used. According to the current regulations, they can be considered safe for consumers. The limits for the nitrate content are defined in European Union (EU) regulations only for green leafy vegetables. For example, fresh lettuce can contain up to 5000 mg nitrates/1000 g. Meanwhile, processed food intended for infants and small children should not exceed 200 mg nitrates/1000 g and 0.07 mg nitrites per kilogram of body weight [38].

Polyphenols are important for the antioxidant properties of fruits. The use of chitosan impacted the polyphenol content and antioxidant activity of raspberries, measured by the DPPH and ABTS radical scavenging assays and the FRAP assay, which measures the antioxidant capacity through the ability to reduce iron. Lower values indicate a better ability to neutralise free radicals. Each of these indicators provides information about the potential health benefits of raspberries, especially in the context of preventing diseases related to oxidative processes. The raspberries treated with 500k and 950k chitosan had the highest polyphenol content, 171 mg/100 g and 164 mg/100 g, respectively. This suggests that higher molecular weights of chitosan may better support the synthesis of polyphenols in raspberries, but also may cause stress in plants. Polyphenols can be synthesised by plants in response to stress. Furthermore, raspberries treated with 500k and 950k chitosan were smaller, and other studies have shown that smaller fruits contain more polyphenols [39].

Raspberries treated with 3.3k and 12k chitosan also showed an elevated polyphenol content compared with the control, although this effect was more moderate. The highest DPPH radical scavenging and FRAP activity correlated with a high polyphenol content. In raspberries collected in Japan, the antioxidant activity measured by FRAP was 18.0 mmol Trolox equivalents (TE)/100 g [40]. The ABTS scavenging assay did not show an effect of the applied chitosan on the antioxidant capacity of raspberries. High- and medium-molecular-weight chitosan had an antioxidant capacity of the fruits similar to that of the control, while low-molecular-weight chitosan even weakened this effect.

Vitamin C, also known as ascorbic acid, is one of the most recognisable and effective antioxidants available in the human diet [41]. The antioxidant capacity of vitamin C is related to its ability to neutralise free radicals and other reactive oxygen species, which can cause cell damage, contribute to the development of cardiovascular diseases and certain types of cancers and accelerate ageing. However, the results did not show a correlation between the content of this compound and the antioxidant capacity. Raspberries sprayed with 950k chitosan had the lowest L-ascorbic acid content. This suggests that the high antioxidant capacity is influenced by polyphenols and not by the content of L-ascorbic

acid. On the contrary, Zhang et al. [36] demonstrated that low-molecular-weight chitosan increased the L-ascorbic acid content.

As a natural polysaccharide, chitosan exhibits a variety of properties that can be particularly useful in the protection of plants and fruits against pests and diseases [36, 42]. Chitosan can induce so-called systemic acquired resistance in plants, which strengthens their natural defence mechanisms. Chitosan also demonstrates direct antifungal action: it can damage the cell walls of fungi by binding to their polymers, leading to disturbances in their growth and development [43]. Additionally, alteration of the environmental pH by chitosan can adversely affect the survival of fungi. When applied to the surface of fruits, chitosan forms a thin, transparent and breathable coating, which can physically limit the access of pathogens to plant tissue, acting as an additional protective barrier [36]. It is difficult to determine which method enhanced the resistance of raspberries against grey mould. Perhaps several defence systems operated simultaneously. All the applied sprays reduced the degree of raspberry infestation compared with the control group. Raspberries treated with 500k and 950k chitosan were the best protected, with only 4%–5% of the fruit being affected. Chitosan 125k was also effective: 11% of the fruit was affected. Badawy and Rabea [44] also found that the effectiveness of chitosan was dependent on its molecular weight.

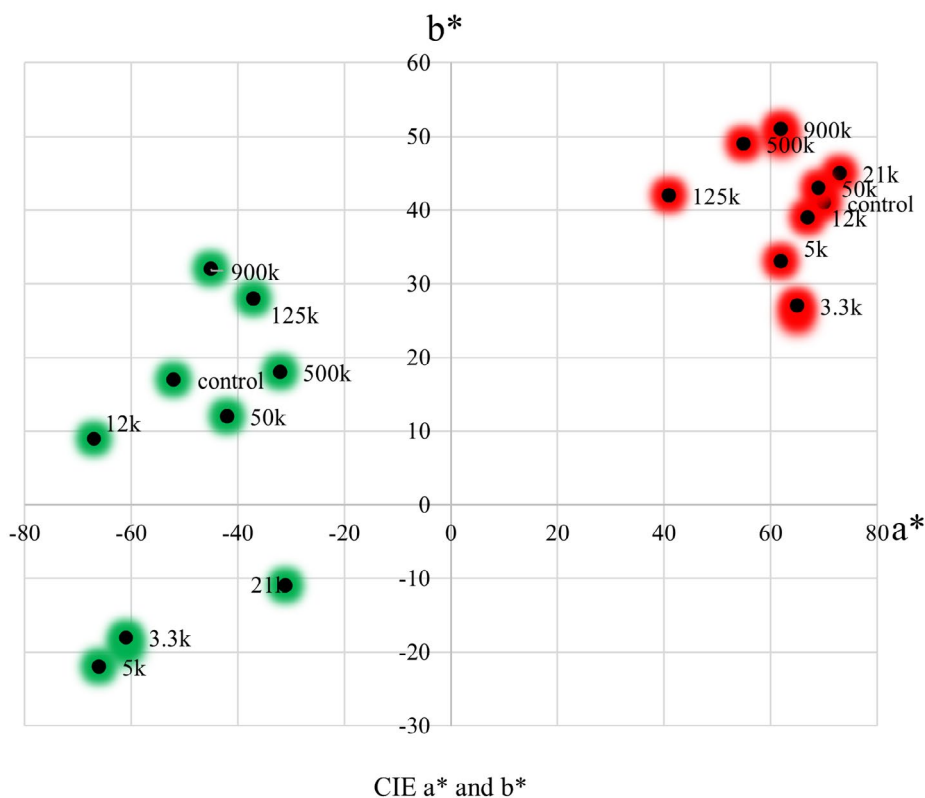


Figure 2. The effects of chitosan on the colour of the leaves and raspberries for the Polesie cultivar. The green markers indicate the values for leaves, while the red markers indicate the values for raspberries.

Chitosan of various molecular weights had a significant impact on the colour of the leaves and raspberries. Treatment with 3.3k chitosan increased the colour intensity of the leaves and raspberries, with a more pronounced effect on the leaves (Figure 2). The b^* parameter took a negative value, meaning that the leaves had an intense green-blue colour, reminiscent of the effect of over-fertilisation with nitrogen. As the chitosan molecular weight increased, this effect was weaker. Treatment with 950k chitosan resulted in the least intensely coloured leaves and raspberries. The opposite effect was observed in strawberries: chitosan with the highest molecular weight produced strawberries with a better colour [45]. Hence, the reaction of different plant species varies, a phenomenon that requires additional research.

4. Conclusions

This study on the impact of chitosan with various molecular weights on the development, quality and health of raspberries highlights the complex interactions between this biopolymer and plants. The results suggest that the optimal molecular weight of chitosan may vary depending on the application goal and the developmental phase of the plants. Treatment with 21k and 50k chitosan resulted in the highest raspberry yield. Moreover, 21k chitosan also impacted raspberry size positively. However, 500k and 950k chitosan reduced the yield compared to the control. On the other hand, chitosan with higher molecular weights favourably influenced the firmness of the raspberries, which is significant from a quality perspective. The raspberries treated with 3.3k chitosan had the highest content of soluble substances and the lowest acidity, which could contribute to the perception of greater sweetness. Raspberries sprayed with chitosan, regardless of its molecular weight, accumulated small amounts of harmful nitrates and nitrites, although they stayed within the established safe limits for consumers. Treatment with 500k and 950k chitosan favoured the accumulation of polyphenols, which may indicate their better properties in supporting the antioxidant capabilities of the fruit, although this could also be related to plant stress. Chitosan, especially 500k and 950k, demonstrated protective action against grey mould. This suggests that chitosan may induce defence mechanisms in plants or create a physical protective barrier on the surface of the fruits. This type of chitosan tends to form stronger and more durable barriers, enhancing plant defence mechanisms against pathogens. In summary, this research indicates the potential benefits from the use of chitosan in agriculture, particularly in increasing yields, improving fruit quality and protecting against diseases. However, selecting the appropriate molecular weight of chitosan is crucial to realising these benefits, an issue that requires further research and refinement.

5. References

- [1] Gevrenova R, Badjakov I, Nikolova M, Doichinova I; (2013) Phenolic derivatives in raspberry (*Rubus L.*) germplasm collection in Bulgaria. *Biochem Syst Ecol* 50, 419–427. DOI:10.1016/j.bse.2013.06.002
- [2] Baranowska A, Radwańska K, Zarzecka K, Gugala M, Mystkowska I; (2015) Właściwości prozdrowotne owoców maliny właściwej (*Rubus idaeus L.*). *Probl Hig Epidemiol* 96(2), 406–409.
- [3] Veljković B, Jakovljević V, Stanković M, Dajić-Stefanović Z; (2019) Phytochemical and antioxidant properties of fresh fruits and some traditional products of wild grown raspberry (*Rubus idaeus L.*). *Not Bot Horti Agrobo* 47(3), 565–573. DOI:10.15835/nbha47311465

- [4] Jiang H, Yang J, Fan Y, Liu Y; (2021) Synergistic effects of unripe raspberry extracts (*Rubus chingii*) and antibiotics against three bacteria. *Food Sci Technol Campinas* 41(2), 482–488. **DOI:**10.1590/fst.04020
- [5] Krauze-Baranowska M, Majdan M, Kula M; (2014) Owoce maliny właściwej i maliny zachodniej źródłem substancji biologicznie aktywnych. *Post Fitoter* 1, 32–39.
- [6] Kozhar O, Larsen MM, Grünwald NJ, Peever TL; (2020) Fungal evolution in anthropogenic environments: *Botrytis cinerea* populations infecting small fruit hosts in the Pacific Northwest rapidly adapt to human-induced selection pressures. *Appl Environ Microbiol* 9, e02908–e2919. **DOI:**10.1128/AEM.02908-19
- [7] Pritts MP; (2020) Raspberries. In: Gough RE, Poling EB (eds), *Small fruits in the home garden*. CRC Press, Boca Raton, 189–225.
- [8] Xu X, Wedgwood E, Berrie AM, Allen J, O'Neill TM; (2012) Management of raspberry and strawberry grey mould in open field and under protection. A review. *Agron Sustain Dev* 32, 531–543. **DOI:**10.1007/s13593-011-0032-2
- [9] Sangiorgio D, Cellini A, Donati I, Pastore C, Onofrietti C, Spinelli F; (2020) Facing climate change: application of microbial biostimulants to mitigate stress in horticultural crops. *Agronomy* 10, 794. **DOI:**10.3390/agronomy10060794
- [10] Krawiec P, Rybczyński R; (2010) Efektywność fertygacji w malinach odmian powtarzających. *Acta Agroph* 16(2), 347–358.
- [11] Glenn DM, Puterka GJ, van der Zwet T, Byers RE, Feldhake C; (1999) Hydrophobic particle films: a new paradigm for suppression of arthropod pests and plant diseases. *J Econ Entom* 92, 759–771. **DOI:**10.1093/jee/92.4.759
- [12] Fereres E, Soriano MA; (2007) Deficit irrigation for reducing agricultural water use. *J Exp Bot* 58(2), 147–159. **DOI:**10.1093/jxb/erl165
- [13] Hopf A, Plotto A, Rizwan R, Zhang C, Boote KJ, Shelia V, Hoogenboom G; (2022) Dynamic prediction of fruit quality traits as a function of environmental and genetic factors. In: XXXI International Horticultural Congress (IHC2022): International Symposium on Integrative Approaches to Product Quality in 1353, 145–152. **DOI:**10.17660/ActaHortic.2022.1353.19
- [14] Grajkowski J, Ochmian I; (2007) Influence of three biostimulants on yielding and fruit quality of three primocane raspberry cultivars. *Acta Sci Pol Hortorum Cultus* 6(2), 29–36.
- [15] Ochmian I, Błaszak M, Lachowowicz S, Piwowarczyk R; (2020) The impact of cultivation systems on the nutritional and phytochemical content, and microbiological contamination of highbush blueberry. *Sci Rep* 10(1), 16696. **DOI:**10.1038/s41598-020-73947-8
- [16] Majeti NV, Ravi Kumar; (2000) A review of chitin and chitosan applications. *React Funct Polym* 46(1), 1–27. **DOI:**10.1016/S1381-5148(00)00038-9
- [17] Prashanth KVH, Tharanathan RN; (2007) Chitin/chitosan: modifications and their unlimited application potential – an overview. *Trends Food Sci Technol* 18, 117–131. **DOI:**10.1016/j.tifs.2006.10.022
- [18] Kaczmarek MB, Struszczyk-Świta K, Li X, Szczesna-Antczak M, Daroch M; (2019) Enzymatic modifications of chitin, chitosan, and chitoooligosaccharides. *Front Bioeng Biotech* 7(2), 43. **DOI:**10.3389/fbioe.2019.00243
- [19] da Silva Lucas AJ, Oreste EQ, Costa HLG, López HM, Saad CDM, Prentice C; (2021) Extraction, physicochemical characterization, and morphological properties of chitin and chitosan from cuticles of edible insects. *Food Chem* 343, 128550. **DOI:**10.1016/j.foodchem.2020.128550

- [20] Zhong Y, Zhuang C, Gu W, Zhao Y; (2019) Effect of molecular weight on the properties of chitosan films prepared using electrostatic spraying technique. *Carbohydr Polym* 212, 197–205. **DOI:**10.1016/j.carbpol.2019.02.048
- [21] Zhuang C, Zhong Y, Zhao Y; (2019) Effect of deacetylation degree on properties of Chitosan films using electrostatic spraying technique. *Food Control* 97, 25–31. **DOI:**10.1016/j.foodcont.2018.10.014
- [22] Jongsri P, Wangsomboondee T, Rojsitthisak T, Seraypheap K; (2016) Effect of molecular weights of chitosan coating on postharvest quality and physicochemical characteristics of mango fruit. *LWT Food Sci Tech* 73, 28–36. **DOI:**10.1016/j.lwt.2016.05.038
- [23] Nguyen TV, Nguyen TTH, Wang SL, Vo TPK, Nguyen AD; (2017) Preparation of chitosan nanoparticles by TPP ionic gelation combined with spray drying, and the antibacterial activity of chitosan nanoparticles and a chitosan nanoparticle - amoxicillin complex. *Res Chem Intermed* 43, 3527–3537. **DOI:**10.1007/s11164-016-2428-8
- [24] Mijowska K, Ochmian I, Oszmiański J; (2016) Impact of cluster zone leaf removal on grapes cv. Regent polyphenol content by the UPLC-PDA/MS method. *Molecules* 21(12), 1688. **DOI:**10.3390/molecules21121688
- [25] Ochmian I, Oszmiański J, Lachowicz S; (2019) Rootstock effect on physico-chemical properties and content of bioactive compounds of four cultivars Cornelian cherry fruits. *Sci Hort* 256, 108588. **DOI:**10.1016/j.scienta.2019.108588
- [26] Ochmian I, Dobrowolska A, Chełpiński P; (2014) Physical parameters and chemical composition of fourteen blackcurrant cultivars (*Ribes nigrum* L.). *Not Bot Horti Agrobot Cluj-Na* 42(1), 160–167. **DOI:**10.15835/nbha4219103
- [27] Lachowicz S, Oszmiański J, Rapak A, Ochmian I; (2020) Profile and content of phenolic compounds in leaves, flowers, roots, and stalks of *Sanguisorba officinalis* L. determined with the LC-DAD-ESI-QTOF-MS/MS analysis and their *in vitro* antioxidant, antidiabetic, antiproliferative potency. *Pharmaceuticals* 13(8), 191. **DOI:**10.3390/ph13080191
- [28] Arnao MB, Cano A, Acosta M; (2001) The hydrophilic and lipophilic contribution to total antioxidant activity. *Food Chem* 73, 239–244. **DOI:**10.1016/S0308-8146(00)00324-1
- [29] Brand-Williams W, Cuvelier ME, Berset C; (1995) Use of a free radical method to evaluate antioxidant activity. *LWT Food Sci Technol* 28, 25–30. **DOI:**10.1016/S0023-6438(95)80008-5
- [30] Benzie IF, Strain JJ; (1996) The ferric reducing ability of plasma (FRAP) as a measure of “antioxidant power”: the FRAP assay. *Analytic Biochem* 239(1), 70–76. **DOI:**10.1006/abio.1996.0292
- [31] Singleton VL, Orthofer R, Lamuela-Raventós RM; (1999) Analysis of total phenols and other oxidation substrates and antioxidants by means of Folin-Ciocalteu reagent. *Method Enzymol* 299, 152–178. **DOI:**10.1016/S0076-6879(99)99017-1
- [32] Salachna P, Bartkowiak A, Mazurkiewicz-Zapałowicz K, Placek M; (2007) Evaluation of the impact of chitosan on yield and health of freesia bulbs (*Freesia Eckl. Ex Klatt*) variety 'Versailles'. *Roczniki Akademii Rolniczej w Poznaniu* 41, 177–181.
- [33] Kananont N, Pichyangkura R, Chanprame S, Chadchawan S, Limpanavech P; (2010) Chitosan specificity for the *in vitro* seed germination of two *Dendrobium* orchids (*Asparagales: Orchidaceae*). *Sci Hort* 124(2), 239–247. **DOI:**10.1016/j.scienta.2009.11.019

- [34] Pichyangkura R, Chadchawan S; (2015) Biostimulant activity of chitosan in horticulture. *Sci Hort* 196, 49–65. **DOI:**10.1016/j.scienta.2015.09.031
- [35] Malerba M, Cerana R; (2018) Recent advances of chitosan applications in plants. *Polymers* 10(2), 118. **DOI:**10.3390/polym10020118
- [36] Zhang H, Li R, Liu W; (2011) Effects of chitin and its derivative chitosan on postharvest decay of fruits: a review. *Int J Mol Sci* 12(2), 917–934. **DOI:**10.3390/ijms12020917
- [37] Meng X, Li B, Liu J, Tian S; (2008) Physiological response and quality attributes of table grape fruits to chitosan preharvest spray and postharvest coating during storage. *Food Chem* 106, 501–508. **DOI:**10.1016/j.foodchem.2007.06.012
- [38] Regulation (EC) no 396/2005 of the European Parliament and of the Council of 23 February 2005 on maximum residue levels of pesticides in or on food and feed of plant and animal origin and amending Council Directive 91/414/EEC - OJ L70, 16.3.2005, 1–16.
- [39] Ochmian I, Kozos K, Chelpiński P, Szczepanek M; (2015) Comparison of berry quality in highbush blueberry cultivars grown according to conventional and organic methods. *Turk J Agric For* 39, 174–181. **DOI:**10.3906/tar-1404-18
- [40] Toshima S, Hirano T, Kunitake H; (2021) Comparison of anthocyanins, polyphenols, and antioxidant capacities among raspberry, blackberry, and Japanese wild Rubus species. *Sci Hort* 285, 110204. **DOI:**10.1016/j.scienta.2021.110204
- [41] Janecka A; (2023) Właściwości, formy i działanie biologiczne witaminy C w terapiach skórnych. *Aesth Cosmetol Med* 12(1), 17–22.
- [42] Romanazzi G, Nigro F, Ippolito A, Di Venere D, Salerno M; (2002) Effects of pre-and postharvest chitosan treatments to control storage gray mould of table grapes. *J Food Sci* 67, 1862–1867. **DOI:**10.1111/j.1365-2621.2002.tb08737.x
- [43] Oh SK, Cho D, Yu SH; (1998) Development of integrated pest management techniques using biomass for organic farming. I. Suppression of late blight and fusarium wilt of tomato by chitosan involving both antifungal and plant activating activities. *Korean J Plant Pathol* 14, 278–285.
- [44] Badawy MEI, Rabea EI; (2009) Potential of the biopolymer chitosan with different molecular weights to control postharvest gray mold of tomato fruit. *Postharvest Biol Technol* 51(1), 110–117. **DOI:**10.1016/j.postharvbio.2008.05.018
- [45] Ochmian I, Lachowicz S, Krupa-Małkiewicz M; (2022) The effect of different molecular weights of chitosan on the yield, quality, and health-promoting properties of strawberries. *Prog Chem Appl Chitin Deriv* 27, 194–203. **DOI:**10.15259/PCACD.27.015

DYNAMIC LIGHT SCATTERING-BASED MICRORHEOLOGY OF THERMOSENSITIVE CHITOSAN HYDROGELS: PRELIMINARY STUDIES

Anna Ryl^{1,a,*}, Piotr Owczarz^{1,b}

¹ – Department of Chemical Engineering, Lodz University of Technology,
Wolczanska 213 Str., 93-005 Łódź, Poland

^a – ORCID: 0000-0003-1741-7905, ^b – ORCID: 0000-0002-3754-3899

*corresponding author: anna.ryl@p.lodz.pl

Abstract

This paper presents a preliminary characterisation of the local mechanical properties of thermosensitive chitosan systems using dynamic light scattering, an endeavour that has not yet been attempted. The tests included solutions of chitosan chloride with the addition of sodium glycerophosphate as well as those without a substance to support the gelation process. There was much better agreement between the data obtained from measurements on the microscopic and macroscopic scales for systems without the addition of glycerophosphate. In most cases, the addition of a pH-neutralising salt resulted in higher values of dynamic moduli than those obtained during microrheological measurements. Therefore, it seems to be possible to use dynamic light scattering to conduct microrheological studies of thermosensitive chitosan systems.

Keywords: *thermosensitive hydrogels, chitosan, DLS, microrheology*

Received: 20.03.2024

Accepted: 10.06.2024

1. Introduction

Assessment of the rheological properties of hydrogels for biomedical applications is crucial because it allows the characterisation of the mechanical properties of the biopolymer matrix during compression (determination of Young's modulus and texture analysis [1]), tension and shear [2, 3]. The use of shear deformation allows for the determination of the mechanical spectrum under isothermal conditions [4] as well as changes in structural properties during measurements with constant deformation under non-isothermal and isothermal conditions [5–7]. The latter are particularly important when characterising thermosensitive media used as injectable biomedical scaffolds [8] that form a spatial polymer network directly in the human body after heating to the physiological temperature. These measurements, although very important at the design stage, only determine the properties of media on a macroscopic scale. From the application point of view, it seems that local mechanical properties [9] are equally important because they directly affect the environment in which the cells multiply, and they may differ from the bulk properties in the case of heterogeneous media.

Microrheological techniques using monodisperse, inert latex tracers of microscopic size represent a way to address these needs. There are passive and active microrheological techniques, which differ depending on the method of forcing the movement of these particles [10–12]. For the former group (also known as thermal), the diffusive movement of tracers is forced by the thermal energy of the system. The most common passive microrheological techniques include video particle tracking and techniques based on monochromatic beam scattering, such as dynamic light scattering (DLS) and diffusing-wave spectroscopy (DWS) [10]. In the case of active (also called forced) techniques, the beads are manipulated by an external force usually generated by a magnetic field (magnetic tweezers [MT]) or by optical beams (optical tweezers [OT]) [10]. Although they have limitations, these techniques enable the characterisation of the medium over a very wide frequency range (10^{-2} to 10^7 Hz) as well as over a wide range of shear moduli (10^{-5} to 10^4 Pa) [10]. The range of low shear modulus values is particularly interesting because it correlates with the range of stresses occurring on the scale of cellular/tissue interactions. DLS is a microrheological tool that uses an inverse approach relative to its classical use to determine the size of the dispersed phase. In this case, based on the scattering intensity signal on tracer particles of a known diameter, rheological properties are determined using mathematical calculations. Briefly, the correlation function on delay time is used to determine the mean square displacement of the tracers as a function of the delay time and finally, using the generalised Stokes–Einstein relation (GSER) and Fourier transform, the course of the storage modulus (G') and the loss modulus (G'') as a function of frequency known as the mechanical spectrum is obtained [13].

This paper presents a preliminary characterisation of the local mechanical properties of thermosensitive chitosan systems using DLS, an endeavour that has not yet been attempted. A critical analysis of the obtained results at the macroscopic and microscopic scales revealed the real potential of using DLS to characterise the tested media, the potential limitations and future research directions.

2. Materials and Methods

2.1. Preparation of Thermosensitive Hydrogels

This study used chitosan of shrimp origin (CAS no. 9012-76-4, Sigma-Aldrich, Germany), whose average molecular weight is 862 kg/mol and degree of deacetylation is 83.4% [3]. Thermosensitive chitosan hydrogels were obtained according to the preparation proposed by Chenite et al. [14]. A chitosan solution was prepared by dissolving 0.4 g

of chitosan powder in 16 ml of 0.1 M hydrochloric acid (CAS no. 7647-01-0, Sigma-Aldrich, Germany) and incubated for 24 h until the polymer had dissolved completely. Subsequently, the solution was incubated at 4°C. In parallel, a suspension of β -disodium glycerophosphate (CAS no. 154804-51-0, Sigma Aldrich, Germany) was prepared by suspending 2 g of powder in 2 ml of distilled water. After cooling, the suspension was added drop by drop to the chitosan solution, then mixed thoroughly and incubated for another 24 h at 4°C before actual measurements.

Monodisperse latex tracers (Magsphere Inc., USA) without surface modification and with a diameter of 210, 500 or 880 nm were added to the pure chitosan solutions and samples with addition of β -disodium glycerophosphate intended for microrheological tests; the final concentration was 0.1% (v/w). The pH of the obtained pure chitosan solutions and systems containing β -disodium glycerophosphate at 20°C was 5.7 and 6.9, respectively [3]. The addition of polystyrene tracers did not change the pH.

2.2. Methods

Bulk mechanical spectra were obtained using a MCR301 rotational rheometer (Anton Paar, Austria) performing a frequency sweep test ($\gamma = 1\%$, $\omega = 0.01 - 500$ rad/s) in the linear viscoelasticity (LVE) range. Microscopic evaluation was performed using the Zetasizer Nano ZS90 analyser (Malvern Panalytical, USA) using the settings proposed by Cai et al. [13]. The tests were carried out at 5, 25 and 37°C, representing the storage temperature, application temperature and human body temperature, respectively. To determine the effect of the tracers on the phase transition time, measurements were carried out at constant deformation ($\gamma = 1\%$, $\omega = 5$ rad/s) under isothermal conditions (37°C) after rapid heating from the storage temperature (5°C). There were 3–5 replicates for each sample. The microrheological test results for each measurement represent the mean of 22 scans for different measurement positions [13]. The discrepancy in the obtained data did not exceed 10%. The mechanical spectra were obtained by analysing the raw data using a code in the Python programming language developed by Krajina et al. [15].

3. Results and Discussion

According to the theory of microrheological measurements, the tracers used should be inert with respect to the medium whose rheological properties are determined. For this reason, the mechanical spectra to determine G' and G'' were compared for samples without and with the addition of tracers (Figure 1).

For the chitosan solutions without β -disodium glycerophosphate, regardless of the measurement temperature, the latex beads did not affect the dynamic modulus values. However, the addition of β -disodium glycerophosphate, which supports the sol-gel phase transition process, affected the tracers' influence on the modulus values, particularly at the lowest temperature (5°C, Figure 1b). The addition of tracers increased the G' and G'' values, indicating an enhancement of both the viscous and elastic properties of the experimental medium.

The dependence of the obtained values on the size of the tracers was non-monotonic, and the highest values were obtained for tracers with a diameter of 500 nm. This means that despite their chemically inert form, they influence the structure of the polymer medium. It should be assumed that they constitute aggregation nuclei which, despite their sol form, strengthen the structure of the medium. However, the differences observed in the G'' values are surprising because if changes are observed, then they should only concern G' , which determines the elastic characteristics of the medium. At 25°C, the tracers only influenced the elastic properties. Again, the addition of latex beads increased G' , with a maximum

value for tracers with a diameter of 500 nm. Surprisingly, after gelation, the presence of latex beads slightly weakened the mechanical properties of the obtained gels. Moreover, it should be emphasised that the spectra obtained in the low frequency range at 37 and 25°C in the case of the medium with β -disodium glycerophosphate, although inconsistent with the course of the universal mechanical spectrum proposed by Kasapis [16], indicate progressive gelation under the influence of shear [5].

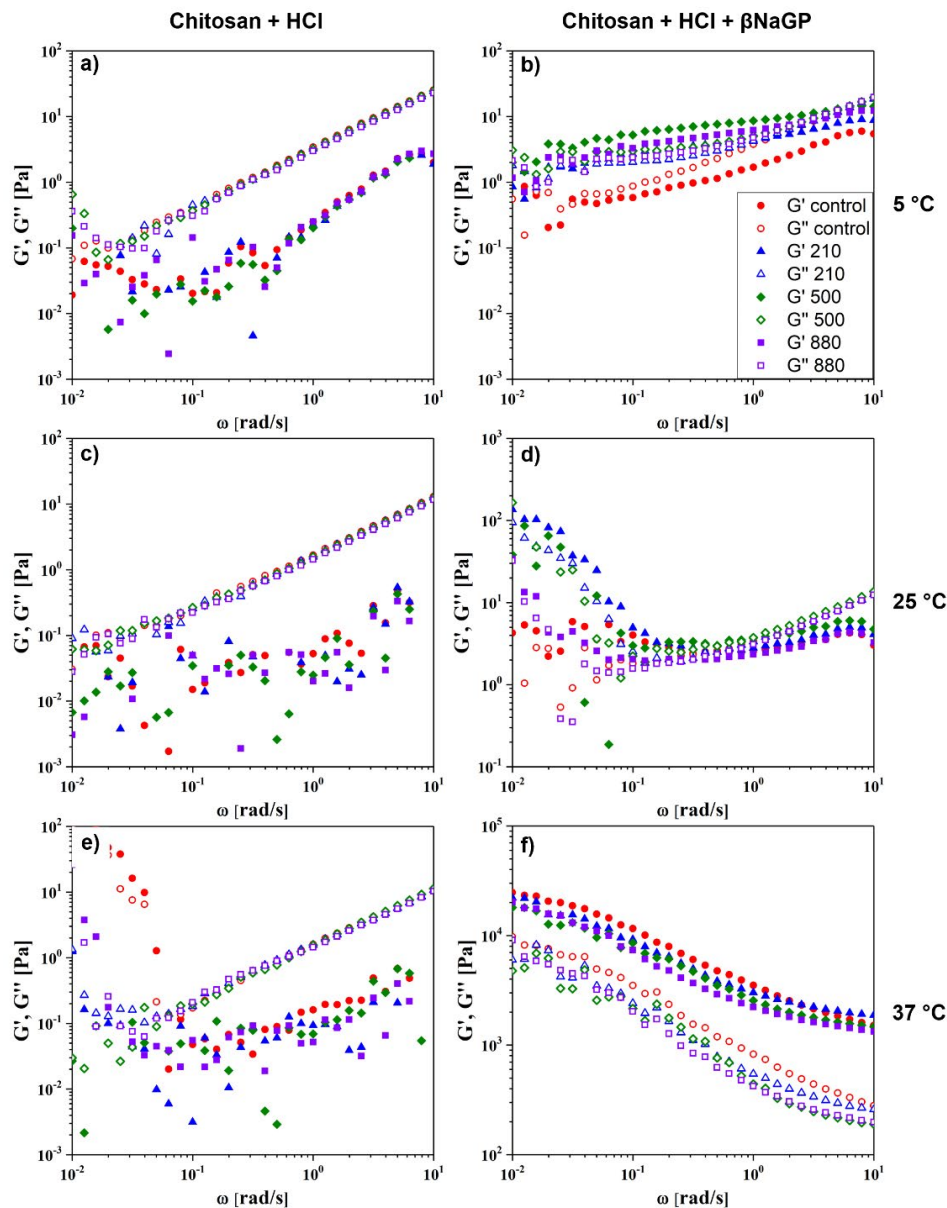


Figure 1. The effect of the tracer diameter on the mechanical spectra of (a, c and e) pure chitosan solutions and (b, d and f) systems with the addition of β -disodium glycerophosphate at 5, 25 and 37°C, respectively. Control samples contained no tracers. The markings 210, 500 and 880 refer to the size of the tracers [nm]. Abbreviations: G' , storage modulus; G'' , loss modulus.

The actual impact of the tracers on the state of the polymer matrix was assessed by determining the kinetics of the phase transition at 37°C. Figure 2 shows the change in G' and G'' over time. Applying the most frequently used method of equalising the values of dynamic moduli to determine the gelation time showed that the presence of tracers did not affect the determined gelation time. Nevertheless, for the media containing latex beads, there was a sharp increase in G' and G'' that occurred much faster compared with the control samples. This proves the faster occurrence of the fast gelation area, where the primary polymer matrix is formed, which is expanded in the slow gelation area.

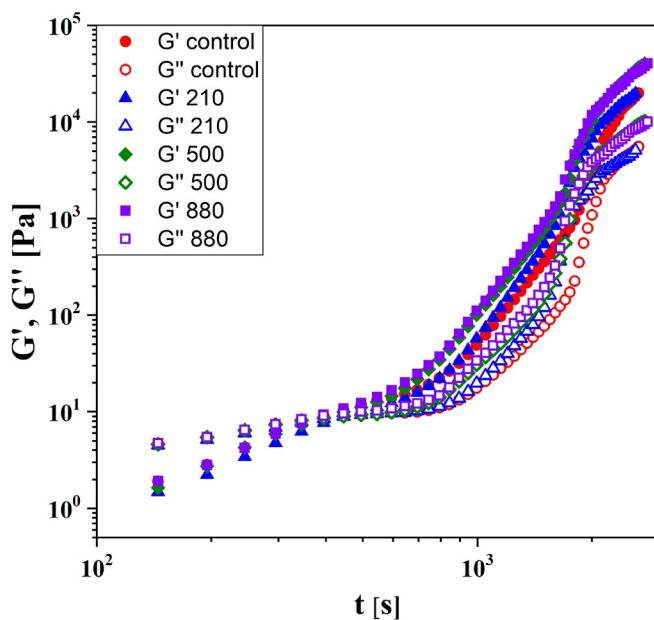


Figure 2. The change in the storage modulus (G') and the loss modulus (G'') over time depending on the tracer diameter at 37°C. The control samples contained no tracers. The markings 210, 500 and 880 refer to diameter of the tracers [nm].

Figure 3 shows mechanical spectra at 5°C obtained as a result of classical bulk tests as well as microrheological tests using DLS. The chitosan solution showed consistency for G' in the low frequency range, while G'' produced inconsistent results (Figure 3a). When using tracers of different sizes, there were similar G' and G'' values at the macroscopic and microscopic scales. For the samples containing β -disodium glycerophosphate, there were much greater discrepancies in the data (Figure 3b). In the case of classical measurements, much higher values of dynamic moduli were obtained. Discrepancy in the results obtained using the two measurement techniques indicates significant heterogeneity of the sample. In this case, microrheological measurements using DLS cannot be used for local characterisation because, despite the use of multiple measurements at different detector positions, the final results are averaged results. It would be more reasonable to use a technique based on video multiple particle tracking.

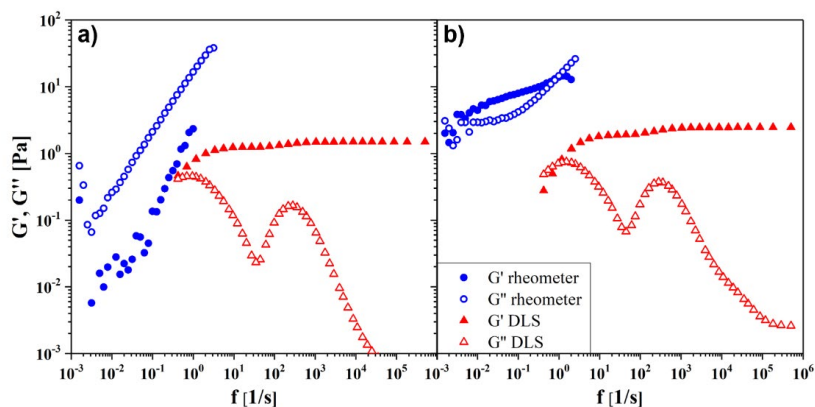


Figure 3. The mechanical spectra of (a) pure chitosan solutions and (b) systems containing β -disodium glycerophosphate at 5°C with the addition of 500 nm tracers determined using a rheometer and dynamic light scattering (DLS). Abbreviations: G' , storage modulus; G'' , loss modulus.

The results of classical oscillatory measurements revealed that despite the low measurement temperature, elastic properties predominated over viscous properties, which should not be the case in the case of a polymer sol. This phenomenon was not observed in the case of a control measurement for a sample without tracers. Despite the predominance of elastic features over viscous features, a gel form was not obtained due to the dependence of both moduli on frequency as well as the flow phenomenon observed during the measurements. In the case of both media, G'' decreased in the frequency range above 300 s^{-1} , a finding inconsistent with theory. This may suggest an incorrect fit of the raw data recorded during the measurements. An undoubted advantage of microrheological measurements is the determination of the G_{N0} value, which is defined as the minimum value of G'' in the highly elastic area in accordance with the Kaspas theory [16].

Figure 4 shows the test results at the macroscopic and microscopic scales at 25°C using tracers with a diameter of 210 nm. In the case of chitosan solutions, G'' showed good compliance in the low frequency range, but G' did not.

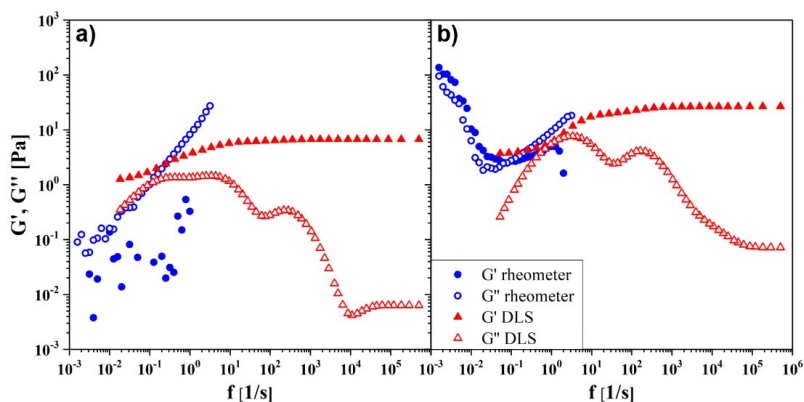


Figure 4. The mechanical spectra of (a) pure chitosan solutions and (b) systems containing β -disodium glycerophosphate at 25°C with the addition of tracers with a diameter of 210 nm determined using a rheometer and dynamic light scattering. Abbreviations: G' , storage modulus; G'' , loss modulus.

In the case of systems containing β -disodium glycerophosphate, there was better convergence of G' and acceptable differences in G'' . This could suggest an increase in homogeneity as the temperature increases. Again, for frequencies above 300 s^{-1} , the obtained data are inconsistent with the literature in the case of G'' . It is worth noting that at the same temperature, the use of larger tracers resulted in a greater divergence of G' and G'' .

Nevertheless, the results obtained using the microrheological technique are very promising because they allow for characterisation over a very wide frequency range (Figure 5), the courses of which are consistent with the theory proposed by Kasapis [16]. This makes it possible to determine all four characteristic regions: starting from the molecular flow and moving through the highly elastic, glass transition and glassy states. Additionally, it is possible to determine the short relaxation time, the relaxation time and the long relaxation time [4], which were 4.1×10^{-4} , 1.2×10^{-2} and 9.8×10^{-2} s, respectively. These times are related to the elastic dynamics of bend relaxation, the internal flexible chain relaxation as well as the total chain relaxation [13]. Consequently, this makes it possible to determine the hierarchy of molecular relaxations. A pure chitosan solution at the frequency range $200\text{--}2400\text{ s}^{-1}$ presented discontinuity in the obtained data and the tendency towards the value of 0 Pa. The authors of the code used in data analysis observed similar discontinuity; they interpreted it as noise occurring in the raw data [15].

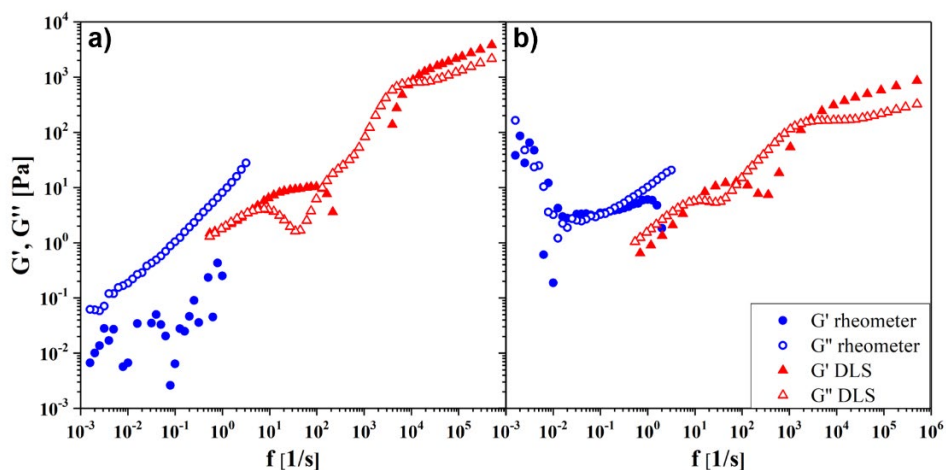


Figure 5. The mechanical spectra of (a) pure chitosan solutions and (b) systems containing β -disodium glycerophosphate at 25°C with the addition of tracers with a diameter of 500 nm, determined using a rheometer and dynamic light scattering (DLS). Abbreviations: G' , storage modulus; G'' , loss modulus.

The results obtained at 37°C strongly depended on the medium tested. In the case of chitosan solutions without sodium glycerophosphate (Figure 6), the size of the tracers had a marked impact on the consistency of the data obtained using both measurement techniques. The use of the smallest tracer with a diameter of 210 nm led to satisfactory convergence for G' . The microrheological measurements revealed discontinuity at high frequencies for both G' and G'' .

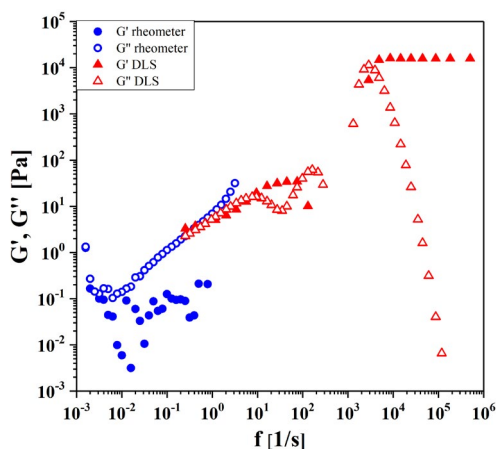


Figure 6. The mechanical spectra of pure chitosan solutions at 37°C with the addition of tracers with a diameter of 210 nm determined using a rheometer and dynamic light scattering (DLS). Abbreviations: G' , storage modulus; G'' , loss modulus.

When using larger tracers (i.e. a diameter of 500 or 880 nm), the experimental data were similar, especially regarding G' . This points to the important issue of selecting tracers for a specific type of measurement. Selecting a tracer that is too small may result in its free diffusion, unrestricted by polymer chains, resulting in a much more reliable measurement of viscous properties during microrheological measurements. On the other hand, the use of larger tracers provides a better characterisation of the elastic properties. Although the tracer diameter does not directly affect the obtained values of the dynamic moduli – because it is considered when analysing the raw data – latex beads with different diameters will interact with polymer chains differently, which results directly from the diffusion rate. This was schematically presented by Li and Mooney [17] when analysing the release rate of active substances from the polymer matrix.

The largest discrepancies between the data obtained from classical rheological measurements and microrheological measurements were obtained for the systems containing β -disodium glycerophosphate at 37°C (Figure 7).

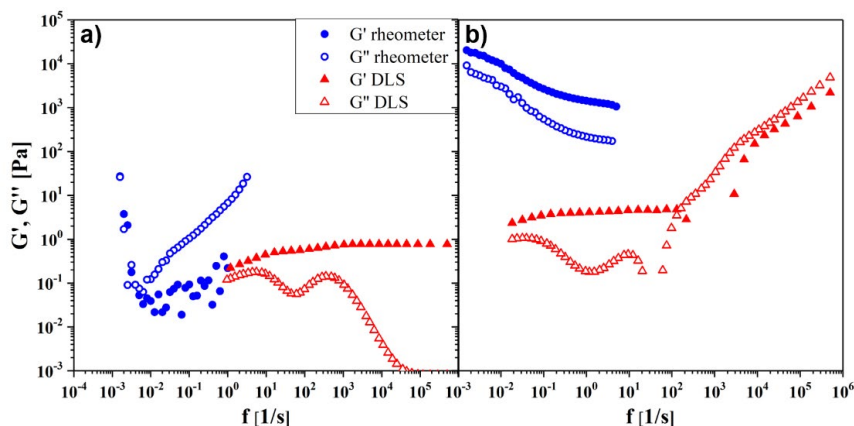


Figure 7. The mechanical spectra of (a) pure chitosan solutions and (b) systems containing β -disodium glycerophosphate at 37°C with the addition of tracers with a diameter of 880 nm determined using a rheometer and dynamic light scattering (DLS). Abbreviations: G' , storage modulus; G'' , loss modulus.

The nature of the observed changes was independent of the size of the tracer used. For the same frequency range, there were much higher G' and G'' values based on classic rheological measurements. This indicates much weaker local properties of the polymer network, which are strengthened throughout the volume, for example, by numerous junction zones. Although measurements were made at several detector positions, the observed discrepancies may result from the non-ergodic state of the medium in which the scattering intensity signal strongly depends on the detector position. In the case of microrheological measurements, two areas are observed on the universal mechanical spectrum curve: a highly elastic area and a glassy transition area. Ultimately, the value of the characteristic time was determined to be 6.7×10^{-3} s. As in the case of measurements at lower temperatures, discontinuities in the courses of both dynamic modules from measurements using the DLS technique are again visible.

4. Conclusions

The results demonstrated much better agreement between the data obtained from measurements at the microscopic and macroscopic scales for systems without β -disodium glycerophosphate. In most cases, the addition of a pH-neutralising salt resulted in higher G' and G'' values than those obtained during microrheological measurements. Moreover, although the polymer tracers are inert from a chemical point of view, they affect the viscoelastic properties, changing the dominant characteristics from viscous to elastic at low temperatures. Moreover, specific crystallisation/aggregation nuclei slightly affect the gelation kinetics by shortening the time after which the rapid gelation area. Ultimately, latex beads of different sizes results in different properties of the tested media. Therefore, it is possible to use DLS to conduct microrheological studies of thermosensitive chitosan systems. However, further research is necessary, including microscopic optical assessment of the state of the polymer matrix and attempts to characterise the tested media using other microrheological techniques such as video multiple particle tracking.

5. Acknowledgments

This work was financed by 'FUPN-Fund for the Improvement of the Skills of Young Scientists' supporting scientific excellence of the Lodz University of Technology (via the grant entitled 'Application of passive optical microrheology techniques to determine the impact of injection application on the local mechanical properties of the polymer network').

6. References

- [1] Owczarz P, Ryl A, Wichlacz Z; (2019) Application of texture profile analysis to investigate the mechanical properties of thermosensitive injectable chitosan hydrogels. *Prog Chem Appl Chitin Deriv* 24, 151–163. DOI:10.15259/PCACD.24.014
- [2] Zuidema JM, Rivet CJ, Gilbert RJ, Morrison FA; (2014) A protocol for rheological characterization of hydrogels for tissue engineering strategies. *J Biomed Mater Res B* 102(5), 1063–1073. DOI:10.1002/jbm.b.33088
- [3] Owczarz P, Ziolkowski P, Modrzejewska Z, Kuberski S, Dziubiński M; (2018) Rheo-kinetic study of sol-gel phase transition of chitosan colloidal systems. *Polymers* 10(1), 47. DOI:10.3390/polym10010047

- [4] Owczarz P, Rył A, Modrzejewska Z, Dziubiński M; (2017) The influence of the addition of collagen on the rheological properties of chitosan chloride solutions. *Prog Chem Appl Chitin Deriv* 22, 176–189. **DOI:**10.15259/PCACD.22.18
- [5] Rył A, Owczarz P; (2021) Thermoinduced aggregation of chitosan systems in perikinetik and orthokinetic regimes. *Carbohydr Polym* 255, 117377. **DOI:**10.1016/j.carbpol.2020.117377
- [6] Rył A, Owczarz P; (2019) Influence of shear direction on gelation ability of colloidal chitosan solutions. *Chem Process Eng* 40(2), 207–212. **DOI:**10.24425/cpe.2019.126113
- [7] Owczarz P, Rył A, Dziubiński M, Sielski J; (2019) Injectable chitosan scaffolds with calcium β -glycerophosphate as the only neutralizing agent. *Processes* 7(5), 297. **DOI:**10.3390/pr7050297
- [8] Rył A, Owczarz P; (2021) Influence of injection application on the sol–gel phase transition conditions of polysaccharide-based hydrogels. *Int J Mol Sci* 22(24), 13208. **DOI:**10.3390/ijms222413208
- [9] Chen DT, Weeks ER, Crocker JC, Islam MF, Verma R, Gruber J, Levine AJ, Lubensky TC, Yodh AG; (2003) Rheological microscopy: local mechanical properties from microrheology. *Phys Rev Lett* 90(10), 108301. **DOI:**10.1103/PhysRevLett.90.108301
- [10] Mao Y, Nielsen P, Ali J; (2022) Passive and active microrheology for biomedical systems. *Front Bioeng Biotechnol* 10, 916354. **DOI:**10.3389/fbioe.2022.916354
- [11] Liu W, Wu C; (2018) Rheological study of soft matters: a review of microrheology and microrheometers. *Macromol Chem Phys* 219(3), 1700307. **DOI:**10.1002/macp.201700307
- [12] Cicuta P, Donald AM; (2007) Microrheology: a review of the method and applications. *Soft Matter* 3(12), 1449–1455. **DOI:**10.1039/B706004C
- [13] Krajina BA, Tropini C, Zhu A, DiGiacomo P, Sonnenburg JL, Heilshorn SC, Spakowitz AJ; (2017) Dynamic light scattering microrheology reveals multiscale viscoelasticity of polymer gels and precious biological materials. *ACS Cent Sci* 3(12), 1294–1303. **DOI:**10.1021/acscentsci.7b00449
- [14] Chenite A, Buschmann M, Wang D, Chaput C, Kandani N; (2001) Rheological characterisation of thermogelling chitosan/glycerol-phosphate solutions. *Carbohydr Polym* 46(1), 39–47. **DOI:**10.1016/S0144-8617(00)00281-2
- [15] Cai PC, Krajina BA, Kratochvil MJ, Zou L, Zhu A, Burgener EB, Bollyky PL, Milla CE, Webber MJ, Spakowitz AJ, Heilshorn SC; (2021) Dynamic light scattering microrheology for soft and living materials. *Soft Matter* 17(7), 1929–1939. **DOI:**10.1039/D0SM01597K
- [16] Kasapis S, Mitchell J, Abeysekera R, MacNaughtan W; (2004) Rubber-to-glass transitions in high sugar/biopolymer mixtures. *Trends Food Sci Tech* 15(6), 298–304. **DOI:**10.1016/j.tifs.2003.09.021
- [17] Li J, Mooney DJ; (2016) Designing hydrogels for controlled drug delivery. *Nature Rev Materials* 1(12), 1–17. **DOI:**10.1038/natrevmats.2016.71

FOLIAR APPLICATION OF DEPOLYMERISED CHITOSAN ENHANCES THE GROWTH AND CONTENT OF POLYPHENOLS AND L-ASCORBIC ACID IN *Eucomis autumnalis*, AN ORNAMENTAL AND MEDICINAL PLANT

Piotr Salachna^{1,a,*}, Agnieszka Zawadzińska^{1,b}

¹ – Department of Horticulture, West Pomeranian University of Technology in Szczecin, Słowackiego 17 Str., 71-434 Szczecin, Poland

^a – ORCID: 0000-0003-0403-8519, ^b – ORCID: 0000-0002-0882-9919

*corresponding author: piotr.salachna@zut.edu.pl

Abstract

Chitosan and its derivatives are promising plant biostimulants with potentially broad applications in agriculture and horticulture. In this study, we determined the effect of the application method and dose of depolymerised chitosan on morphological characteristics and metabolite levels in *Eucomis autumnalis*, a medicinal and ornamental plant. Depolymerised chitosan (molecular weight ~154,500 g/mol, number average molecular weight ~22,800 g/mol and degree of deacetylation ~85%) was used at 50 and 100 mg/l by drenching plants or spraying. In general, depolymerised chitosan increased the length of plant leaves and roots, especially at the dose of 100 mg/l, and also increased the fresh weight of leaves, bulbs and roots, with a more potent effect found when depolymerised chitosan was applied as a foliar spray. In addition, spraying the plants with chitosan solution at 50 and 100 mg/l caused a significant increase in the total chlorophyll content, by 55.4% and 42.0%, respectively, and the total polyphenol content, by 77.7% and 59.0%, respectively, compared with the control. On the other hand, the biosynthesis of carotenoids was most favourably affected by the application of 100 mg/l depolymerised chitosan by drenching and 50 mg/l depolymerised chitosan by spraying. Foliar application of depolymerised chitosan led to an increase in leaf L-ascorbic acid content by an average of 36.4%, regardless of the dose. The results suggest that depolymerised chitosan applied as a foliar spray promoted the growth of *E. autumnalis* and contributed to increased biosynthesis of polyphenols, which may be a future means of obtaining metabolites in this species.

Keywords: polysaccharides, chitosan oligomers, elicitors, phenolic, pineapple lily

Received: 15.03.2024

Accepted: 13.05.2024

1. Introduction

Environmentally friendly biostimulants are increasingly being introduced into conventional crop production following the principles of sustainable development [1]. Chitosan is one of the better-known biostimulants in agriculture and horticulture, and its effects have been widely documented [2]. Chitosan can improve plant growth and yield, modify physiological and metabolic processes, and promote nutrient uptake [3, 4]. Chitosan-based biostimulants have limitations in application, as native high-molecular-weight chitosan does not dissolve in water at pH 7 and has a high viscosity [5]. Due to protonated amino groups, chitosan is susceptible to modification. The degradation of chitosan can produce lower-molecular-weight oligosaccharide derivatives that are soluble in water and often have high biological activity [6, 7]. Depolymerised chitosan can modify plant growth and induce resistance to adverse environmental conditions by enhancing primary and secondary metabolism [8, 9]. The effectiveness of chitosan and its derivatives as a plant biostimulant may depend on the genotype, the physical and chemical properties of the polysaccharide, the solution concentration or the application form [10–12]. Unfortunately, many studies lack basic information about the physicochemical properties of the applied chitosan; hence, it is often difficult to compare the results and conclusions regarding the effect of the biopolymer on plants.

The *Eucomis* genus includes more than a dozen bulbous plant species in South Africa. For a long time, the species *Eucomis autumnalis* has been among the most important medicinal plants in South Africa [13]. Extracts from *E. autumnalis* are used in natural medicine to treat various diseases. The compounds of *E. autumnalis* exhibit antioxidant, anticancer, anti-inflammatory, antibacterial and antifungal properties [14, 15]. In addition to its medicinal properties, *Eucomis* species and varieties are cultivated worldwide as desirable ornamental plants. Due to the excessive harvesting of bulbs from natural sites by local people, endemic *Eucomis* species are threatened with extinction [13]. Therefore, strategies are being sought to propagate and produce *Eucomis* plants easily by using environmentally friendly biostimulants [16]. To date, the few studies using chitosan for *Eucomis* cultivation have focused on using this biostimulant for bulb dressing before planting and propagation by leaf cuttings [17, 18]. So far, the response of *Eucomis* to chitosan treatment during plant growth is unknown.

This study aimed to determine the effect of the dose and method of application of depolymerised chitosan on the morphological parameters, biomass accumulation, pigment content and metabolites of *E. autumnalis* plants obtained from seeds. This study tested the hypothesis that depolymerised chitosan stimulates the growth of *E. autumnalis* and modifies the phytochemical composition of plants.

2. Materials and Methods

2.1. Preparation of Depolymerised Chitosan

Depolymerised chitosan obtained at the Center for Bioimmobilization and Innovative Packaging Materials at West Pomeranian University of Technology in Szczecin was subjected to controlled radical degradation [19] with the continuous addition of hydrogen peroxide at a final concentration of 6.2 mmol to a 2.5% chitosan solution. Depolymerised chitosan was characterised by a molecular weight of ~154,500 g/mol, an number average molecular weight of ~22,800 g/mol and a degree of deacetylation of ~85%.

2.2. Plant Material and Experiment Design

Ten-week-old *E. autumnalis* seedlings obtained from seeds sown in spring under controlled conditions (greenhouse) were repotted one at a time into pots (diameter = 8 cm) filled

with a commercial peat substrate (pH 5.5). Seven days after repotting, the plants were treated with depolymerised chitosan solutions (50 or 100 mg/l) every 7 days for 8 weeks. The solutions were applied by drenching the plants (20 ml of solution per pot) or spraying (5 ml of solution per pot). Control plants were not treated with the biostimulant. The experiment was set up in a randomised block design in four replicates, with five plants per replicate. After 10 weeks of cultivation in the greenhouse (opening the vents at 22°C during the day and 18°C at night), the plants were removed from their pots, washed in water and, after drying, the length and width of the longest leaf and the length of the longest roots were measured, and the fresh weight of all the leaves, the bulb and roots was determined using a PS 200/2000/C/2 balance (RADWAG, Poland) with a reading accuracy of 0.001 g.

2.3. Determination of the Photosynthetic Pigment, Total Polyphenol and L-Ascorbic Acid Contents

Samples (2 g) were taken from fresh leaves for biochemical analyses. The content of assimilation pigments was determined based on absorbance at 441, 646, 652 and 663 nm using a Helios Gamma Spectrophotometer (Thermo Spectronic, UK). The content of each pigment was calculated based on formulas proposed by Lichtenthaler and Buschmann [20] and expressed as mg/g fresh weight. The total polyphenol content in the extracts was determined using the Folin–Ciocalteu reagent by measuring absorbance at 760 nm, and the result is presented in terms of gallic acid equivalents [11]. The content of vitamin C as L-ascorbic acid was determined using the Tillman method based on the reduction of 2,6-dichlorophenolindophenol by L-ascorbic acid [18]. All analyses of plant material were performed triplicate.

2.4. Statistical Analysis

The results were submitted to one-way analysis of variance followed by Tukey's honestly significant difference post hoc using the STATISTICA statistical software (StatSoft, Poland). A p value ≤ 0.05 indicated a statistically significant difference.

3. Results and Discussion

As a result of the application of chitosan and its breakdown products, changes can occur at the morphological and metabolic levels in plants, resulting in increased growth and development [21, 22]. In this study, the dose and the method of application of depolymerised chitosan significantly affected the length and width of leaves and the root length of *E. autumnalis* (Table 1, Figure 1). Both drenching and spraying increased the length and width of the leaves, with spraying showing greater efficacy. Plants sprayed with 100 mg/l depolymerised chitosan had the most extended and widest leaves. The control plants that were not treated with chitosan had the shortest leaves. Treatment with depolymerised chitosan stimulated development of the root system, with the most pronounced effect from spraying with 100 mg/l depolymerised chitosan on the root length. The results confirm the positive effect of foliar treatment of plants with chitosan on morphological traits, consistent with previous studies. Chen et al. [23] showed that spraying *Pinellia ternata* plants with a water-soluble chitosan solution (degree of deacetylation $\geq 90\%$) significantly increased the leaf area and plant height. El-Serafy [24] demonstrated that chitosan oligosaccharides applied as a foliar spray at a dose of 50 mg/l effectively increased the root growth rate of potted *Cordyline terminalis* plants. The beneficial effect of foliar-applied chitosan

on plant growth is most likely due to its easy absorption by the leaves of water-soluble chitosan [3, 4]. Due to the presence of amino groups, chitosan can penetrate the vascular system of plants and activate a number of metabolic and physiological pathways, causing strong changes in their growth and development [25].

Table 1. Influence of the depolymerised chitosan concentration and application method on the morphological characteristics of *Eucomis autumnalis*.

Treatment	Application method	Leaf length [cm]	Leaf width [cm]	Root length [cm]
Control	-	5.00 ± 0.20 ^c	1.80 ± 0.07 ^b	4.63 ± 0.29 ^c
Chitosan 50 mg/l	Soil drench	5.82 ± 0.41 ^b	2.17 ± 0.29 ^{ab}	7.87 ± 0.29 ^b
Chitosan 100 mg/l	Soil drench	5.93 ± 0.51 ^b	2.17 ± 0.29 ^{ab}	7.5 ± 1.04 ^b
Chitosan 50 mg/l	Foliar spray	9.17 ± 0.67 ^a	2.80 ± 0.09 ^a	7.90 ± 0.46 ^b
Chitosan 100 mg/l	Foliar spray	9.47 ± 0.20 ^a	2.77 ± 0.22 ^a	9.97 ± 0.80 ^a

Note. The data are presented as the mean ± standard error of the mean. In each column, means with the same superscript letter are not significantly different based on Tukey's test ($\alpha = 0.05$).

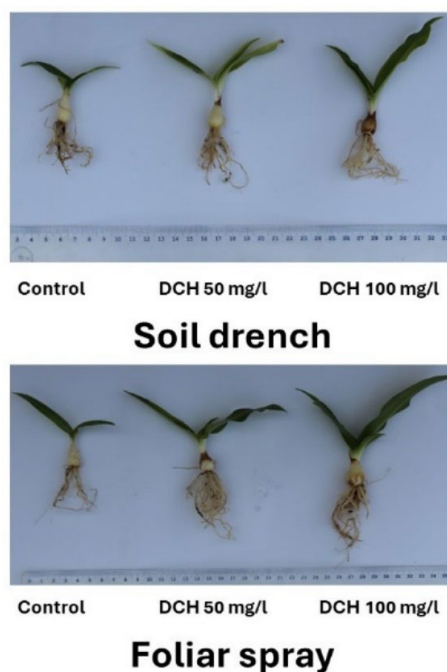


Figure 1. The effects of the depolymerised chitosan (DCH) concentration and application method on *Eucomis autumnalis* growth.

Table 2. The influence of the depolymerised chitosan concentration and application method on the fresh weight of *Eucomis autumnalis*.

Treatment	Application method	Leaf fresh weight [g]	Bulb fresh weight [g]	Root fresh weight [g]
Control	-	0.77 ± 0.13 ^c	0.91 ± 0.01 ^b	0.55 ± 0.05 ^c
Chitosan 50 mg/l	Soil drench	1.08 ± 0.09 ^b	0.96 ± 0.05 ^b	0.70 ± 0.08 ^b
Chitosan 100 mg/l	Soil drench	1.26 ± 0.04 ^b	1.09 ± 0.03 ^b	0.77 ± 0.14 ^b
Chitosan 50 mg/l	Foliar spray	3.18 ± 0.33 ^a	2.70 ± 0.09 ^a	1.47 ± 0.08 ^a
Chitosan 100 mg/l	Foliar spray	3.24 ± 0.24 ^a	2.87 ± 0.14 ^a	1.65 ± 0.08 ^a

Note. The data are presented as the mean ± standard error of the mean. In each column, means with the same superscript letter are not significantly different based on Tukey's test ($\alpha = 0.05$).

Table 2 shows the effect of depolymerised chitosan on plant biomass. The application of depolymerised chitosan significantly increased the fresh weight of leaves, bulbs and roots, with foliar spraying stimulating biomass growth more strongly than application by drenching. For plants treated with depolymerised chitosan at 50 or 100 mg/l via foliar spraying, the average increase in the fresh weight of leaves, bulbs, and roots was 3.2, 2.1 and 1.8 times higher, respectively, compared with the control. There were no significant differences in the leaf, bulb and root biomass depending on the biostimulant dose. In a previous study, researchers reported similar stimulating effects of 50 and 100 mg/l low-molecular-weight chitosan (~5,000 g/mol) applied via drenching on the fresh weight of leaves and roots of *Perilla frutescens* plants [11]. On the other hand, basil (*Ocimum basilicum*) showed an increase in fresh shoot weight when plants were sprayed with a 500 mg/l chitosan lactate solution [26]. The positive effect of chitosan and its derivatives on biomass growth may be related to more efficient uptake and utilisation by plants of macro- and micronutrients, mainly nitrogen, more intense fluorescence of photosystem II in the thylakoid membrane, and an increased rate of plant photosynthesis, which together ultimately lead to increased biomass production [25]. It is also worth noting that low-molecular-weight chitosan contains more nitrogen than non-degraded chitosan and can be a source of this yield-forming macronutrient for plants [3, 27].

The assimilation pigment contents in leaves are important biomarkers that determine the physiological status of plants. There were significant differences in the photosynthetic pigment contents depending on the application method and dose of depolymerised chitosan (Table 3). Both drenching and spraying leaves with the depolymerised chitosan solution stimulated total chlorophyll accumulation in *E. autumnalis*, with spraying exerted a more substantial effect. Relative to the control, foliar application of depolymerised chitosan at 50 and 100 mg/l increased the total chlorophyll content by 55.4% and 42.0%, respectively. Applying 100 mg/l chitosan via drenching and 50 mg/l chitosan via spraying had the most favourable effect on the carotenoid content, with a 21.3% and 22.1% increase compared with the control plants. In a previous study, there were similar results for sage (*Salvia abrotanoides*): after foliar application of chitosan, there was a marked 63% increase in the total chlorophyll content and a 68% increase in the carotenoid content compared with the control plants [28]. In another study, there was a significant increase in leaf accumulation of chlorophyll and carotenoids in potato (*Solanum tuberosum*) plants sprayed with an oligo-chitosan solution (molecular weight ~82.20 kDa) [9]. Chitosan-induced

changes in the content of assimilation pigments are most likely related to the ability of chitosan to stimulate the production of endogenous cytokines and the expression of genes involved in chlorophyll synthesis. Increased synthesis of assimilation pigments may also be related to nitrogen in chitosan, a crucial component of the tetrapyrrole ring of chlorophyll [29, 30].

Table 3. The influence of the depolymerised chitosan concentration and application method on photosynthetic pigments in *Eucomis autumnalis*.

Treatment	Application method	Total chlorophyll content [mg/g fresh weight]	Carotenoid content [mg/g fresh weight]
Control	-	0.45 ± 0.00 ^c	0.17 ± 0.01 ^c
Chitosan 50 mg/l	Soil drench	0.57 ± 0.01 ^b	0.18 ± 0.01 ^{bc}
Chitosan 100 mg/l	Soil drench	0.58 ± 0.01 ^b	0.20 ± 0.00 ^a
Chitosan 50 mg/l	Foliar spray	0.70 ± 0.03 ^a	0.20 ± 0.01 ^a
Chitosan 100 mg/l	Foliar spray	0.64 ± 0.08 ^a	0.19 ± 0.01 ^{ab}

Note. The data are presented as the mean ± standard error of the mean. In each column, means with the same superscript letter are not significantly different based on Tukey's test ($\alpha = 0.05$).

Chitosan is believed to activate the biosynthesis of phytohormones, enzymes and secondary metabolites that help plants fight stresses and pathogens by inducing their defence responses [2, 31]. Table 4 presents the effects of depolymerised chitosan on the metabolite contents of *E. autumnalis* leaves. There was an apparent increase in the total polyphenol content after foliar application of 50 and 100 mg/l depolymerised chitosan – by 77.7% and 59.0%, respectively, compared with the control plants. The total polyphenol content increased significantly by 17% when plants were drenched with 100 mg/l depolymerised chitosan. Moreover, regardless of the dose, foliar treatment of plants with depolymerised chitosan significantly increased the L-ascorbic acid content in leaves by an average of 36.4% compared with the control plants. Application of 100 mg/l depolymerised chitosan by drenching increased the L-ascorbic acid content by 19.6% compared with the control plants, while the dose of 50 mg/l did not affect the L-ascorbic acid content. Chitosan has been shown to increase polyphenol levels in several plants, including Greek oregano (*Origanum vulgare* ssp. *hirtum*) treated with a foliar spray of 50 and 200 mg/l chitosan oligosaccharides (degree of polymerisation = 2–10 and degree of deacetylation > 95%) [8]; medicinal plant *Dracocephalum kotschyi* sprayed with 100 and 400 mg/l chitosan (degree of deacetylation = 85%) [12]; and in sage (*Salvia officinalis*) after foliar application of 0.25 and 0.5 g/l chitosan [21]. Conversely, in tomatoes (*Lycopersicon esculentum*), foliar treatment with chitosan (molecular weight ~ 50–150 kDa) dissolved in different organic acids increased polyphenols by 20%–70% and L-ascorbic acid by 5%–110% [32]. El Amerany et al. [33] also reported the stimulating effect of spraying 1 mg/ml chitosan (molecular weight ~ 318.53 kDa, degree of deacetylation = 4%–17%) on the L-ascorbic acid content in tomatoes.

Table 4. The influence of the depolymerised chitosan concentration and application method on the total polyphenol and L-ascorbic acid contents of *Eucomis autumnalis*.

Treatment	Application method	Total polyphenol content [mg gallic acid equivalents/100 g fresh weight]	L-ascorbic acid content [mg/100 g fresh weight]
Control	-	28.02 ± 0.45 ^c	32.26 ± 0.89 ^c
Chitosan 50 mg/l	Soil drench	30.35 ± 0.66 ^b	29.38 ± 0.82 ^c
Chitosan 100 mg/l	Soil drench	32.77 ± 0.57 ^b	38.59 ± 0.27 ^b
Chitosan 50 mg/l	Foliar spray	49.78 ± 0.91 ^a	43.64 ± 0.90 ^a
Chitosan 100 mg/l	Foliar spray	44.56 ± 1.92 ^{ab}	44.35 ± 0.84 ^a

Note. The data are presented as the mean ± standard error of the mean. In each column, means with the same superscript letter are not significantly different based on Tukey's test ($\alpha = 0.05$).

Chitosan increases the biosynthesis of specific secondary metabolites in plants by acting as a signalling molecule and modulating the expression of genes related to the synthesis of secondary metabolites, including polyphenols, responsible for inducing the plant's defence responses [3, 6, 12]. The results show that foliar treatment with chitosan of immature *E. autumnalis* plants can be an effective method to increase the production of secondary metabolites.

4. Conclusion

In conclusion, foliar application of depolymerised chitosan can stimulate growth and biomass gain and effectively increase the accumulation of chlorophylls, carotenoids, total polyphenols and L-ascorbic acid in *E. autumnalis* leaves. Foliar spraying of 100 g/l depolymerised chitosan provided the most potent biostimulatory effects. In the long term, research is needed to determine how depolymerised chitosan elicits the production of specific substances found in *E. autumnalis* that exhibit biological activity and have potential in the medical, pharmaceutical and food industries.

5. Acknowledgements

This research was funded by the National Science Centre, Poland (Project 2018/02/X/NZ9/03281).

6. References

- [1] Grammenou A, Petropoulos SA, Thalassinou G, Rinklebe J, Shaheen SM, Antoniadis V; (2023) Biostimulants in the soil-plant interface: agro-environmental implications – a review. *Earth Syst Environ* 7(3), 583–600. DOI:10.1007/s41748-023-00349-x
- [2] Stasińska-Jakubas M, Hawrylak-Nowak B; (2022) Protective, biostimulating, and eliciting effects of chitosan and its derivatives on crop plants. *Molecules* 27(9), 2801. DOI:10.3390/molecules27092801
- [3] Ahmed KBM, Khan MMA, Siddiqui H, Jahan A; (2020) Chitosan and its oligosaccharides, a promising option for sustainable crop production – a review. *Carbohydr Polym* 227, 115331. DOI:10.1016/j.carbpol.2019.115331

- [4] Dzung PD, Phu DV, Du BD, Ngoc LS, Duy NN, Hiet HD, Hien NQ; (2017) Effect of foliar application of oligochitosan with different molecular weight on growth promotion and fruit yield enhancement of chili plant. *Plant Prod Sci* 20(4), 389–395. **DOI:**10.1080/1343943X.2017.1399803
- [5] Aranaz I, Alcántara AR, Civera MC, Arias C, Elorza B, Heras Caballero A, Acosta N; (2021) Chitosan: an overview of its properties and applications. *Polymers* 13(19), 3256. **DOI:**10.3390/polym13193256
- [6] Li K, Xing R, Liu S, Li P; (2020) Chitin and chitosan fragments responsible for plant elicitor and growth stimulator. *J Agric Food Chem* 68(44), 12203–12211. **DOI:**10.1021/acs.jafc.0c05316
- [7] Salachna P, Grzeszczuk M, Soból M; (2017) Effects of chitooligosaccharide coating combined with selected ionic polymers on the stimulation of *Ornithogalum saundersiae* growth. *Molecules* 22(11), 1903. **DOI:**10.3390/molecules22111903
- [8] Yin H, Fretté XC, Christensen LP, Grevsen K; (2012) Chitosan oligosaccharides promote the content of polyphenols in Greek oregano (*Origanum vulgare* ssp. *hirtum*). *J Agric Food Chem* 60(1), 136–143. **DOI:**10.1021/jf204376j
- [9] Muley AB, Shingote PR, Patil AP, Dalvi SG, Suprasanna P; (2019) Gamma radiation degradation of chitosan for application in growth promotion and induction of stress tolerance in potato (*Solanum tuberosum* L.). *Carbohydr Polym* 210, 289–301. **DOI:**10.1016/j.carbpol.2019.01.056
- [10] Behboudi F, Tahmasebi-Sarvestani Z, Kassae MZ, Modarres-Sanavy SAM, Sorooshzadeh A, Mokhtassi-Bidgoli A; (2019) Evaluation of chitosan nanoparticles effects with two application methods on wheat under drought stress. *J Plant Nutr* 42(13), 1439–1451. **DOI:**10.1080/01904167.2019.1617308
- [11] Salachna P, Łopusiewicz Ł; (2022) Chitosan oligosaccharide lactate increases productivity and quality of baby leaf red perilla. *Agronomy* 12(5), 1182. **DOI:**10.3390/agronomy12051182
- [12] Kahromi S, Khara J; (2021) Chitosan stimulates secondary metabolite production and nutrient uptake in medicinal plant *Dracocephalum kotschyi*. *J Sci Food Agric* 101(9), 3898–3907. **DOI:**10.1002/jsfa.11030
- [13] Ndhkala AR, Mulaudzi RB, Kulkarni MG, Van Staden J; (2012) Effect of environmental factors on seedling growth, bulb development and pharmacological properties of medicinal *Eucomis autumnalis*. *S Afr J Bot* 79, 1–8. **DOI:**10.1016/j.sajb.2011.10.008
- [14] Masondo NA, Finnie JF, Van Staden J; (2014) Pharmacological potential and conservation prospect of the genus *Eucomis* (Hyacinthaceae) endemic to southern Africa. *J Ethnopharmacol* 151(1), 44–53. **DOI:**10.1016/j.jep.2013.11.002
- [15] Mizieleńska M, Salachna P, Ordon M, Łopusiewicz Ł; (2017) Antimicrobial activity of water and acetone extracts of some *Eucomis* taxa. *Asian Pac J Trop Med* 10(9), 892–895. **DOI:**10.1016/j.apjtm.2017.08.018
- [16] Aremu AO, Plačková L, Gruz J, Bíba O, Novák O, Stirk WA, Van Staden J; (2016) Seaweed-derived biostimulant (Kelpak®) influences endogenous cytokinins and bioactive compounds in hydroponically grown *Eucomis autumnalis*. *J Plant Growth Regul* 35, 151–162. **DOI:**10.1007/s00344-015-9515-8
- [17] Kukla P, Żurawik P; (2022) Physiological status, rooting and bulb yield of leaf cuttings of *Eucomis comosa* (Houtt.) H.R. Wehrh. ‘Sparkling Burgundy’ as affected by chitosan. *Hortic Sci* 49(3), 154–163. **DOI:**10.17221/67/2021-HORTSCI
- [18] Salachna P, Pietrak A; (2021) Evaluation of carrageenan, xanthan gum and depolymerized chitosan based coatings for pineapple lily plant production. *Horticulturae* 7(2), 19. **DOI:**10.3390/horticulturae7020019

- [19] Bartkowiak A; (2001) Binary polyelectrolyte microcapsules based on natural polysaccharides. *Prace Naukowe Politechniki Szczecińskiej* 566(3), 5–102.
- [20] Lichtenthaler HK, Buschmann C; (2001) Chlorophylls and carotenoids: measurement and characterization by UV-VIS spectroscopy. *Curr Prot Food Anal Chem* 1(1), F4.3.1–F4.3.8. **DOI:**10.1002/0471142913.faf0403s0
- [21] Vosoughi N, Gomarian M, Pirbalouti AG, Khaghani S, Malekpoor F; (2018) Essential oil composition and total phenolic, flavonoid contents, and antioxidant activity of sage (*Salvia officinalis* L.) extract under chitosan application and irrigation frequencies. *Ind Crop Prod* 117, 366–374. **DOI:**10.1016/j.indcrop.2018.03.021
- [22] Salachna P; (2023) Mitigation effects of water-soluble chitosan on boron toxicity in pepper plants. *Prog Chem Appl Chitin Deriv* 28, 151–159. **DOI:**10.15259/PCACD.28.014
- [23] Chen F, Li Q, Su Y, Lei Y, Zhang C; (2023) Chitosan spraying enhances the growth, photosynthesis, and resistance of continuous *Pinellia ternata* and promotes its yield and quality. *Molecules* 28(5), 2053. **DOI:**10.3390/molecules28052053
- [24] El-Serafy RS; (2020) Phenotypic plasticity, biomass allocation, and biochemical analysis of cordyline seedlings in response to oligo-chitosan foliar spray. *J Soil Sci Plant Nutr* 20(3), 1503–1514. **DOI:**10.1007/s42729-020-00229-7
- [25] Riseh RS, Vazvani MG, Kennedy JF; (2023) The application of chitosan as a carrier for fertilizer: A review. *Int J Biol Macromol* 252, 126483. **DOI:**10.1016/j.ijbiomac.2023.126483
- [26] Hawrylak-Nowak B, Dresler S, Rubinowska K, Matraszek-Gawron R; (2021) Eliciting effect of foliar application of chitosan lactate on the phytochemical properties of *Ocimum basilicum* L. and *Melissa officinalis* L. *Food Chem* 342, 128358. **DOI:**10.1016/j.foodchem.2020.128358
- [27] Boamah PO, Onumah J, Aduguba WO, Santo KG; (2023) Application of depolymerized chitosan in crop production: a review. *Int J Biol Macromol* 235, 123858. **DOI:**10.1016/j.ijbiomac.2023.123858
- [28] Attaran Dowom S, Karimian Z, Mostafaei Dehnavi M, Samiei L; (2022) Chitosan nanoparticles improve physiological and biochemical responses of *Salvia abrotanoides* (Kar.) under drought stress. *BMC Plant Biol* 22(1), 364. **DOI:**10.1186/s12870-022-03689-4
- [29] dos Reis CO, Magalhães PC, Avila RG, Almeida LG, Rabelo VM, Carvalho DT, de Souza TC; (2019) Action of *N*-succinyl and *N,O*-dicarboxymethyl chitosan derivatives on chlorophyll photosynthesis and fluorescence in drought-sensitive maize. *J Plant Growth Regul* 38, 619–630. **DOI:**10.1007/s00344-018-9877-9
- [30] Zhang X, Li K, Xing R, Liu S; (2017) Metabolite profiling of wheat seedlings induced by chitosan: revelation of the enhanced carbon and nitrogen metabolism. *Front Plant Sci* 8, 296016. **DOI:**10.3389/fpls.2017.02017
- [31] Struszczuk H, Pospieszny H; (2020) New applications of chitin and its derivatives in plant protection. In: Goosen MFA (ed), *Applications of chitin and chitosan*, 1st edn. CRC Press, Boca Raton, 171–184. **DOI:**10.1201/9781003072812
- [32] Attia MS, Osman MS, Mohamed AS, Mahgoub HA, Garada MO, Abdelmouty ES, Abdel Latef AAH; (2021) Impact of foliar application of chitosan dissolved in different organic acids on isozymes, protein patterns and physio-biochemical characteristics of tomato grown under salinity stress. *Plants* 10(2), 388. **DOI:**10.3390/plants10020388
- [33] El Amerany F, Rhazi M, Balcke G, Wahbi S, Meddich A, Taourirte M, Hause B; (2022) The effect of chitosan on plant physiology, wound response, and fruit quality of tomato. *Polymers* 14(22), 5006. **DOI:**10.3390/polym14225006

pH STABILITY AND KINETICS OF pH DEACTIVATION OF CHITIN DEACETYLASE PRODUCED BY *Absidia orchidis*

Barbara M. Stencel^{1,a}, Małgorzata M. Jaworska^{1,b,*}

¹ – Faculty of Chemical and Process Engineering, Warsaw University of Technology,
Waryńskiego 1 Str., 00-645 Warsaw, Poland

^a – ORCID: 0009-0005-2700-9229, ^b – ORCID: 0000-0002-3810-3991

*corresponding author: malgorzata.jaworska@pw.edu.pl

Abstract

*This paper presents the influence of pH on the activity and stability of an extracellular chitin deacetylase produced by *Absidia orchidis*. It showed the highest activity at pH 4.0 and was most stable at pH 9.5. In addition, there was pH deactivation that could be described by first-order irreversible kinetics. The pH deactivation rate constant changed linearly with pH in the range from 4.0 to 9.0.*

Keywords: chitin deacetylase, pH-deactivation, pH-stability

Received: 18.03.2024

Accepted: 04.05.2024

1. Introduction

The optimal pH for an enzyme's activity represents important information because it influences the conditions used for the industrial application of an enzyme. The changes in an enzyme's activity with pH are usually connected with changes in its tertiary conformation and, thus, changes in the conformation of the active centre. Changes in the tertiary conformation of an enzyme are the result of the interaction between its amino acids and the environment. Its optimal conformation at the optimal pH results in the highest activity.

The optimal pH of chitin deacetylase (CDA, EC 3.5.1.41), the only enzyme that deacetylates *N*-acetyl glucosamine units (GlcNAc in chitin and chitosan, depends on the source of the enzyme. For intracellular CDA, the optimal pH is in the range from 4.0 (*Absidia orchidis* [1]) to 5.8 (*Mucor rouxii* [2]), while for extracellular CDA, the optimal pH ranges from 7.0 (*Aspergillus nidulans* [3]) to 12.0 (*Colletotrichum lindemuthianum* [4]). In addition to the influence of pH on the activity of CDA, the pH stability and pH deactivation of this enzyme should be investigated. These parameters are of particular importance due to the desirable industrial applicability of CDA; therefore, it is necessary to determine the pH that ensures the highest CDA activity and the pH that results in the best stability during long-term storage. One must remember that acetic acid is liberated during deacetylation, so changes in the pH of the reaction solution are possible. The present paper aimed to investigate the influence of pH on CDA activity, its pH stability and pH deactivation.

2. Materials and Methods

2.1. Chitin Deacetylase

CDA is not commercially available, so it was partially purified from the culture medium of the fungus *A. orchidis* NCAIM F 00642 (late logarithmic growth phase). This fungus was cultivated on YPG nutrient medium at 26°C and pH 5.5 in a batch culture, according to Jaworska and Konieczna [5]. Culture broth was separated from biomass by centrifugation (3300 g, 10 min) and filtration on membrane filters (0.45 µm, cellulose nitrate). The solution was purified by ultrafiltration using membrane module Vivaflow 50 (Sartorius, cut-off of 30 kDa) followed by diafiltration (with the same module) in hydrochloric acid (HCl, pH 4.0). The enzyme solution was stored at 4°C. The activity (A) of CDA (molecular weight = 70 kDa) was defined as the amount of enzyme that can increase the concentration of acetic acid by 1 nmol/ml during 1 min [1U = (nmol/ml/min)]. When indicated, the activity is expressed as specific activity (A_{sp}): U/mg [(nmol/ml)/(min × mg of protein)].

2.2. Chitosan

Chitosan from shrimp (BioLog Heppel, Germany) with a degree of acetylation of 23% and a medium molecular weight (the viscosity of a 1% solution in 1% acetic acid was 200 mPa), according to the information from the supplier, was used in all experiments. Chitosan (4.0 g) was mixed with 800 ml of pure water, and 1% HCl was added dropwise under pH-controlled conditions (4.0 ± 0.1). The solution was filtered on paper filters with a cut-off of 1 µm to remove insoluble residues. The volume was adjusted to 1000 ml with HCl (pH 4.0). The concentration of the prepared chitosan solution was confirmed by the gravimetric method.

2.3. Reaction Rate

The rate of enzymatic deacetylation of chitosan was determined using the initial rate method. Twenty-five millilitres of chitosan solution was added to a 50-ml reactor and incubated at 45°C for 15 min, with continuous stirring (200 rpm). Two millilitres of CDA solution were added to start the reaction. At appropriate time intervals, 2-ml samples were collected and mixed immediately with 0.1 ml of 1 M sodium hydroxide (NaOH) to stop the reaction. The samples were centrifuged (3300 g, 10 min) to separate the precipitated chitosan. The clear supernatant was collected, and the acetic acid concentration was determined.

2.4. Effect of pH on the Activity and Stability of Chitin Deacetylase

The influence of pH on CDA activity was measured using the method described in Section 2.3, where 25 ml of chitosan solution with a pH of 3.0–6.0 was used. The pH of the chitosan solution was set at a specified level using 0.1 M Tris or 1% HCl before CDA was added. The pH of the CDA solution was identical the reaction mixture and adjusted just before the reaction. The reaction was initiated by adding 2 ml of the CDA solution to the chitosan solution.

For the pH stability evaluation, the CDA solution was divided into fractions, and each fraction was set at a defined pH. The samples were stored for 7 days at 5–8°C in a fridge. The CDA activity was evaluated according to the method described in Section 2.3, using 25 ml of a chitosan solution at pH 4.0. The reaction was initiated by adding 2 ml of the CDA solution. The initial CDA activity (just after isolation, at pH 4.0) was determined and treated as a reference value for each fraction.

2.5. Analytical Methods

The acetic acid concentration was determined using high-performance liquid chromatography (HPLC), as described by Jaworska [1]. The HPLC system consisted of a HyperREZ XP Organic acid column and HyperREZ XO Carbohydrate H⁺ Guard Column (at 60°C). A Varian ProStar 210 isocratic system was used with a Varian ProStar 350 refractometer detector and 0.0025 M sulfuric acid (H₂SO₄, 0.5 ml/min) as an eluent.

The protein concentration was measured using Bradford's method [6] with Coomassie Brilliant Blue (Bio-Rad, USA). The calibration curve was prepared using bovine serum albumin as a standard.

3. Results and Discussion

A. orchidis synthesises intracellular and extracellular CDA [7]. In our earlier experiments, we used intracellular CDA. In the present study, extracellular CDA was used because it is easy to isolate.

3.1. Optimal pH and pH Stability

The activity of CDA was investigated in the pH range from 3.0 to 6.0 (Figure 1). The activity of CDA in neutral pH was very low or even absent in alkaline pH due to precipitation of chitosan; hence, it is not presented in Figure 1.

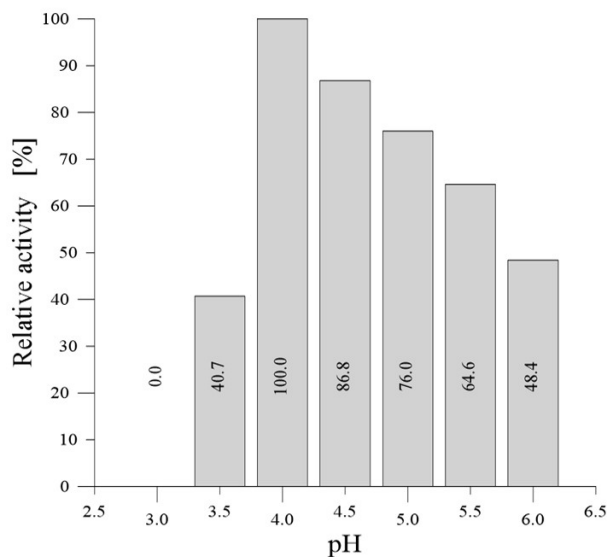


Figure 1. The influence of pH on the activity of chitin deacetylase; the specific activity was 422.8 U/mg at pH 4.0 and 45°C.

The highest activity was observed at pH 4.0 (422.8 U/mg). Of note, CDA was more sensitive to a decrease from this optimal pH to more acidic conditions than an increase to more basic conditions. At pH 3.5, the activity was almost 60% lower than at pH 4.0, and at pH 3.0, CDA was completely inactive. At pH 4.5, CDA's activity was over 90% of that for the optimal pH, and it showed a 10%–15% drop in activity with each 0.5 increase in pH, up to pH 6.0. The experiments were not carried out at higher pHs as chitosan precipitated, and the data would have been difficult to compare due to the different forms of substrate used.

The extracellular CDA used in this study had an optimal pH of 4.0. The optimal pH for extracellular chitin deacetylase has usually been reported in the neutral or alkaline range: pH 7.0 for *A. nidulans* CECT 2544 [3], pH 11.0–12.0 for *C. lindemuthianum* ATCC 56676 [4] and pH 7.5 for *Scopulariopsis brevicaulis* [8]. On the other hand, intracellular enzymes usually have an optimal pH that is slightly acidic – for example, pH 4.5 for the enzyme separated from *M. rouxii* [9] and pH 5.0 for the enzyme separated from *Absidia coerulea* [10]. However, an optimal pH in the alkaline range for extracellular chitin deacetylase is not a rule. Win and Stevens [7] performed experiments with extracellular chitin deacetylase secreted by *A. orchidis* in phosphate buffer with a pH of 5.8. In addition, a chitin deacetylase secreted by *Rhizopus circinans* also had an optimal pH in the acidic range (pH 5.5–6.0) [11].

The pH stability of an enzyme is especially important when it works in an environment that is acidified or alkalinised during the reaction. Additionally, pH stability may play an important role in purification processes where solutions with a pH different from the enzyme's optimal pH are used (e.g. chromatographic purification).

The stability of CDA at different pHs was assessed for 7 days at 5–8°C to avoid thermal deactivation. After storage, the activity of CDA was measured in optimal conditions (pH 4.0) and compared with the initial activity (pH 4.0), which was evaluated just after purification. The changes in CDA activity are presented in Figure 2.

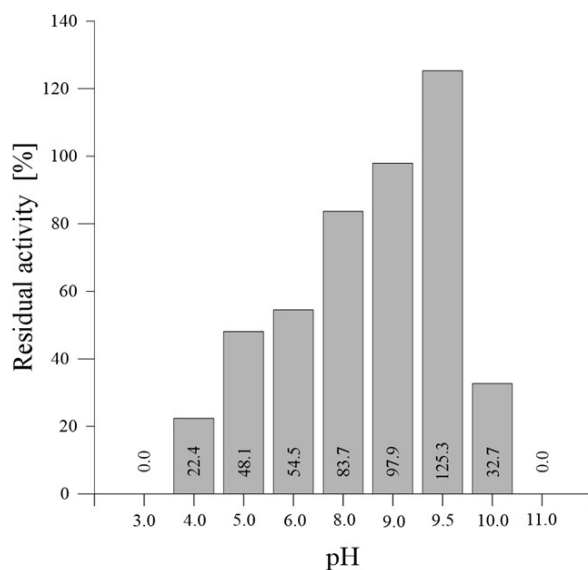


Figure 2. The activity of chitin deacetylase after 7 days of storage at the indicated pH. The initial specific activity was 422.8 U/mg at pH 4.0 and 45°C.

The results showed that CDA was stable in alkaline but not acidic (optimal pH for the reaction) storage conditions. The samples stored at pH 9.5 had the highest activity (125.3% of the initial value), while the samples stored at the optimal pH (4.0) showed activity that decreased to 22% of the initial value. Increasing the storage pH above 9.5 markedly decreased CDA activity: at pH 10.0, it was three times lower than the initial value, and at pH 11.0, CDA was inactivated. This study is the first to report the influence of the storage pH on CDA activity.

3.2. Kinetics of pH Deactivation

Enzymes can be deactivated due to several factors, including high temperature and pH. An enzyme's pH stability and the kinetics of pH deactivation are not often reported in the literature. Based on the pH stability results, the kinetics of pH deactivation was evaluated. The process was assumed to follow first-order irreversible deactivation. This mechanism is described by equation (1):

$$\frac{dU}{dt} = -k_{D,pH} U \quad (1)$$

where U is the enzyme activity [U/mg], t is time [min] and $k_{D,pH}$ is the pH deactivation constant [1/min].

Integration with the initial conditions $U = U_0$ for $t = 0$ yields equation (2):

$$\ln \frac{U}{U_0} = -k_{D,pH} t \quad (2)$$

Based on the linear correlation $\ln(U/U_0)$ versus t , $k_{D,pH}$ the deactivation constant for each pH was evaluated. The dependence of pH on $k_{D,pH}$ is presented in Figure 3. The data point for pH 9.5 was not considered because there was activation rather than deactivation.

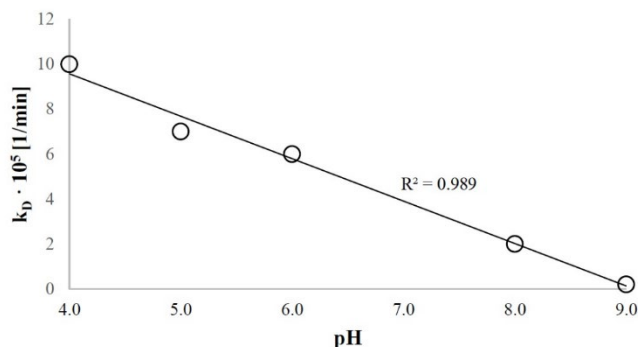


Figure 3. The dependence of the deactivation constant ($k_{D,pH}$) on pH.

The results showed that $k_{D,pH}$ decreased linearly as the pH of the storage solution increased from 4.0 to 9.0. The relation can be approximated by the linear correlation shown in equation (3):

$$k_D = (-1.89 \times 10^{-5}) \times (\text{pH}) + (17.13 \times 10^{-5}) \quad (3)$$

The value of $k_{D,pH}$ is the highest at optimal pH (4.0), which means that the deactivation is the fastest at that pH, while the deactivation rate constant is the lowest for pH 9.0, which means that the enzyme is stable at that pH.

4. Conclusions

Based on the results, pH 4.0 is the optimal pH for the enzymatic deacetylation of chitosan by extracellular CDA of *A. orchidis*. This optimal pH differs from what has been reported for other extracellular enzymes, which are usually in the neutral or alkaline range (pH 7–12). Contrary to our expectations, CDA was more stable in alkaline conditions (pH 9.0–9.5) than in acidic conditions (pH 4.0). High short-term pH stability in neutral or alkaline solutions has also been reported for extracellular chitin deacetylase produced by *Mortierella* sp. [12], *Absidia corymbifera* [13], *Nitratireductor aquimarinus* [14] and *Microbacterium esteraromaticum* [15]; however, contrary to the findings in the present study, those enzymes showed the highest activity in the same pH range. The reason why extracellular CDA from *A. orchidis* shows the highest stability in alkaline conditions but the highest activity is in acidic conditions is unknown and difficult to explain and requires further investigation. Investigation of pH-dependent deactivation showed that the deacetylation process can be described by first-order irreversible kinetics, where the deactivation constant is a linear function of pH in the range from 4.0 to 9.0. The present study represents the first-time results related to pH deactivation and long-term storage pH conditions for any of the chitin deacetylases.

5. Acknowledgement

This work was financed with funds for statutory activity of the Department of Biotechnology and Bioprocess Eng., Faculty of Chemical and Process Engineering, Warsaw University of Technology (Poland).

6. References

- [1] Jaworska MM; (2012) Kinetics of enzymatic deacetylation of chitosan. *Cellulose* 19, 363–369. DOI:10.1007/s10570-012-9650-3
- [2] Kołodziejka I, Malesa-Ciećwierz M, Lerska A, Sikorski Z; (1999) Properties of chitin deacetylase from crude extracts of *Mucor rouxii*. *J Food Biochem* 23, 45–57. DOI:258 10.1111/j.1745-4514.1999.tb00004.x
- [3] Alfonso C, Nuero OM, Santamaria F, Reyes F; (1995) Purification of heat-stabile chitin deacetylase from *Aspergillus nidulans* and its role in cell wall degradation. *Curr Microbiol* 30, 49–54. DOI:10.1007/BF00294524
- [4] Tokuyasu K, Ohnishi-Kameyama M, Hayashi K; (1996) Purification and characterization of extracellular chitin deacetylase from *Colletotrichum lindemutianum*. *Biosci Biotech Biochem* 60, 1598–1603. DOI:10.1271/bbb.60.1598
- [5] Jaworska MM, Konieczna E; (2001) The influence of supplemental components in nutrient medium on chitosan formation by the fungus *Absidia orchidis*. *Appl Microbiol Biotechnol* 56, 220–224. DOI:10.1007/s002530000591
- [6] Bradford MM; (1976) A rapid and sensitive method for the quantitation of microgram quantities of protein utilizing the principle of protein-dye binding. *Analyt Biochem* 72, 248–254. DOI:10.1006/abio.1976.9999
- [7] Win NN, Stevens WF; (2001) Shrimp chitin as substrate for fungal chitin deacetylase. *Appl Microbiol Biotechnol* 57, 334–341. DOI:10.1007/s002530100741
- [8] Cai J, Yang J, Du Y, Fan L, Qiu Y, Li J, Kennedy JF; (2006) Purification and characterization of chitin deacetylase from *Scopulariopsis brevicaulis*. *Carbohydr Polym* 65, 211–217. DOI:10.1016/j.carbpol.2006.01.003
- [9] Kafetzopoulos D, Martinou A, Bouriotis V; (1993) Bioconversion of chitin to chitosan: Purification and characterization of chitin deacetylase from *Mucor rouxii*. *Proc Natl Acad Sci USA* 90, 2564–2568. DOI:10.1073/pnas.90.7.2564
- [10] Gao XD, Katsumoto T, Onodera K; (1995) Purification and Characterization of Chitin Deacetylase from *Absidia coerulea*. *J Biochem* 117, 257–263. DOI:10.1093/jb/117.2.257
- [11] Gauthier C, Clerisse F, Dommes J, Jaspard-Versali MF; (2008) Characterization and cloning of chitin deacetylases from *Rhizopus circinans*. *Protein Expr Purif* 59, 127–137. DOI:10.1016/j.pep.2008.01.013
- [12] Kim YJ, Zhao Y, Oh KT, Nguyen VN, Park RD; (2008) Enzymatic deacetylation of chitin by extracellular chitin deacetylase from a newly screened *Mortierella sp.* DY-52. *J Microbiol Biotechnol* 18, 759–766.
- [13] Zhao Y, Kim YJ, Oh KT, Nguyen VN, Park RD; (2010) Production and Characterization of Extracellular Chitin Deacetylase from *Absidia corymbifera* DY-9. *J Korean Soc Appl Biol Chem* 53(2), 119–126. DOI:10.3839/jksabc.2010.021
- [14] Chai J, Hang J, Zhang Ch, Yang J, Wang S, Liu S, Fang Y; (2020) Purification and characterization of chitin deacetylase active on insoluble chitin from *Nitratireductor aquimarinus* MCDA3-3. *Int J Biol Macromol* 152, 922–929. DOI:10.1016/j.ijbiomac.2020.02.308
- [15] Yang G, Hou X, Lu J, Wang M, Wang Y, Huang Y, Liu O, Liu S, Fang Y; (2022) Enzymatic modification of native chitin and chitin oligosaccharides by an alkaline chitin deacetylase from *Microbacterium esteraromaticum* MCDA02. *Int J Biol Macromol* 203, 671–678. DOI:10.1016/j.ijbiomac.2022.01.167

**THE USE OF ENZYMES
FROM *Mucor circinelloides* IBT-83
IN THE SYNTHESIS OF CHITOLIGOSACCHARIDES
– PRELIMINARY RESEARCH**

Katarzyna Struszczyk-Świta

*Institute of Molecular and Industrial Biotechnology, Faculty of Biotechnology
and Food Sciences, Lodz University of Technology
2/22 Stefanowskiego Str., 90-537 Lodz, Poland
ORCID: 0000-0001-7885-0249
corresponding author: katarzyna.struszczyk@p.lodz.pl*

Abstract

*Chitooligosaccharides (COS) have numerous biological activities, including antibacterial, antifungal, antiviral, anticancer and antioxidant. Unlike high-molecular-weight chitosan, COS have a number of advantages in large-scale commercial applications due to their water solubility and low viscosity. COS are used in the food, agricultural, medical and pharmaceutical industries. The present study demonstrated that intracellular, partially purified enzymes from *Mucor circinelloides* IBT-83 can hydrolyse chitosan and effectively catalyse the synthesis of a heterodimer composed of D-glucosamine and N-acetyl-D-glucosamine (carried out at a 2.5-fold molar excess of N-acetyl-D-glucosamine relative to D-glucosamine in an acetate buffer [pH 5.5] containing 20% ammonium sulfate). The obtained product was analysed using high-performance liquid chromatography.*

Keywords: *chitooligosaccharides, chitosanolytic enzymes, reverse hydrolysis, *Mucor circinelloides**

Received: 10.04.2024

Accepted: 12.06.2024

1. Introduction

Complete hydrolysis of partially *N*-acetylated chitosan to free D-glucosamine (GlcN) and *N*-acetyl-D-glucosamine (GlcNAc) requires the synergistic action of a multienzyme complex composed of both chitosanolytic and chitinolytic enzymes. These include chitosanase [EC 3.2.1.132], which catalyses the hydrolysis of β -1,4-glycosidic bonds between GlcN units occurring inside the biopolymer chain, and exo-1,4- β -D-glucosaminidase [EC 3.2.1.165], which cleaves GlcN monomers from non-reducing ends. Enzymatic hydrolysis of partially acetylated chitosan involves chitinase [EC 3.2.1.14] and β -*N*-acetylhexosaminidase [EC 3.2.1.52]. These enzymes show activity similar to the abovementioned endo- and exo-chitosanases, but they are specific for β -1,4-glycosidic bonds between the GlcNAc units [1]. In addition to hydrolytic activity, chitosanolytic and chitinolytic enzymes have the ability to catalyse the transglycosylation and/or reverse hydrolysis reactions [2, 3].

The possibility of using the aforementioned enzymes to produce oligosaccharides in the transglycosylation or reverse hydrolysis reactions has been confirmed. This enables the production of chitin/chitosan oligomers with the assumed properties, as well as their derivatives. Chitosanase from *Streptomyces griseus* HUT 6037 synthesises two types of oligomers: (GlcN)₂-(GlcNAc)₃ and (GlcN)₃-(GlcNAc)₃ [4]. In turn, chitosanase from *Paenibacillus dendritiformis* produces (GlcN)₆ from smaller chitoooligosaccharides (COS) [5]. Moreover, enzymes with exohydrolytic activity are a promising catalyst for the production of COS with different degrees of polymerisation. Purified exo-1,4- β -D-glucosaminidase from *Aspergillus fumigatus* IIT-004 was used to produce a chitodimer composed of GlcN and GlcNAc [6]. β -*N*-acetylhexosaminidase obtained from *Aspergillus oryzae* was used to produce higher COS (chitohexaose-chitooctaose) from a mixture of smaller chitoooligomers formed by acid hydrolysis of chitin [7].

Previous studies have confirmed that the mycelium of *Mucor circinelloides* IBT-83 is a promising source of enzymes that hydrolyse chitosan. They can be used to produce chitosan oligomers with different degrees of polymerisation: low-molecular weight chitosan, COS and GlcN [8–11]. Moreover, this strain produces intracellular chitin deacetylase [12, 13]. The present study demonstrated that the enzymes from *M. circinelloides* IBT-83 have the ability to effectively catalyse the synthesis of a heterodimer composed of GlcN and GlcNAc.

2. Materials and Methods

2.1. Materials

GlcN and GlcNAc were purchased from Sigma-Aldrich (USA). COS standards (from dimer to hexamer) were purchased from Seikagaku Co. (Japan). Chitosan with a degree of deacetylation of 95% and a viscosity of 1500 mPas was obtained from Heppe Medical Chitosan GmbH (Germany). All other reagents were of analytical grade.

2.2. Microorganisms and Culture Conditions

The filamentous fungus *M. circinelloides* IBT-83 was obtained from the culture collection of the Institute of Molecular and Industrial Biotechnology of Lodz University of Technology (GenBank database with accession numbers KR056084 and KR056083). It was cultured in a 30-l Techfors-S laboratory fermenter (Infors HT, Switzerland). The fermenter was filled with 18 l of culture medium containing corn steep liquor powder (3.7%, w/v)

and rapeseed oil (2.7%, v/v), pH 4.7. The culture medium in the fermenter was inoculated with 5×10^7 cells per 1 ml of medium. The inoculum was grown in a 1000-ml Erlenmeyer flask containing 200 ml of medium at 30°C for 12 h with shaking at 180 rpm. After inoculation, the fungus was cultured at 30°C for 72 h with a stirring speed of 100 rpm and aeration at 1 vvm. After cultivation, the mycelium was harvested by filtration, carefully washed with water, defatted with acetone and air-dried at room temperature.

2.3. Protein Extraction and Salting Out

Protein was extracted from defatted and air-dried mycelium by freezing and grinding the biological material in a 0.5% (w/v) Triton-X100 solution according to the method described by Struszczyk et al. [8]. The homogenate was centrifuged at 10,000 g for 10 min at 4°C, and the supernatant was used as the crude enzyme extract. Protein salting out was performed using ammonium sulfate (saturation degree = 60%). The obtained partially purified enzymes were dissolved in 0.05 M acetate buffer (pH 5.5) and dialysed against the same buffer for 12 h at 4°C in a dialysis bag (regenerated cellulose with a molecular weight cut-off of 10 kDa).

2.4. Chitosanolytic Activity Determination

Chitosanolytic activity was determined based on an increase in the reducing sugar concentration after chitosan hydrolysis, according to the method described previously by Struszczyk et al. [8]. The reaction mixture contained 1 ml of 2% chitosan in 2% acetic acid, 0.85 ml of 1 M sodium acetate and 0.15 ml of enzyme solution (pH 5.5). Chitosan hydrolysis was carried out at 37°C for 60 min and stopped by boiling in a water bath for 5 min. Controls with the same composition as the samples were incubated for 5 min in a boiling water bath to inactivate the enzyme and then incubated at 37°C for 60 min. One unit (U) of chitosanolytic activity (A_{CH}) was equivalent to the amount of enzyme necessary to produce 1 μ mol of reducing sugar per 1 min, [1 U = 1 μ mol/min]. The content of reduced amino chitoooligomers was determined by the Somogyi–Nelson method [14].

2.5. Protein Assay

The protein concentration was determined by the Lowry method [15] using bovine serum albumin as the standard.

2.6. Synthesis Reaction Conditions

The reaction mixture contained 1 mmol GlcN and 2.5 mmol GlcNAc in 50 ml of 0.05 M acetate buffer medium (pH 5.5) containing ammonium sulfate (20%, w/v). The enzyme preparation was introduced at an enzyme-to-reaction medium ratio of 1:25 (v:v). The mixture was incubated at 37°C for 24 h. After the reaction was completed, the sample was freeze-dried. The presence of chitosan oligomers in the sample was analysed using high-performance liquid chromatography (HPLC).

2.7. Analysis of Chitosan Oligomers by High-Performance Liquid Chromatography

HPLC was performed using a Gold Beckman chromatography system equipped with a TSKgel Amide-80 column (4.6 mm \times 25 cm), a precolumn of the same type (3.2 mm \times 1.5 cm) and a refractometer detector. A mixture of acetonitrile, water, methanol, and tetrahydrofuran (THF) (6:2.4:1.5:1.0, v/v/v/v) was used as the mobile phase. The analysis was carried out at 24°C. GlcN, GlcNAc and COS (from dimer to hexamer) were used as standards.

3. Results and Discussion

3.1. Preparation of Chitosanolytic Enzymes From *Mucor circinelloides* IBT-83

The filamentous fungus *M. circinelloides* IBT-83 produces intracellular chitosanase, exo-1,4-β-D-glucosaminidase, and chitin deacetylase [8–13]. We investigated whether the enzymes produced by this strain catalyse the synthesis of COS. First, we extracted intracellular enzymes using a previously developed method (freezing and grinding of mycelium with a 0.5% [w/v] Triton X-100 solution) [8], and then salting out proteins using ammonium sulfate. Table 1 shows the results of the enzyme purification steps. We used partially purified chitosanolytic enzymes as catalysts to synthesise GlcN and GlcNAc oligomers.

Table 1. Salting out proteins using ammonium sulfate precipitation.

Purification step	Total activity [U] × 10 ⁻³	Total protein [mg]	Specific activity [U/g]	Yield [%]	Purification degree [fold]
Crude extract	618.2	98.1	6.3	100	–
Salting out by ammonium sulfate (60%, w/v)	483.9	57.5	8.4	78	1.3

3.2. Chitosanolytic Enzymes in the Oligomer Synthesis Reaction

We prepared reaction mixture variants with both monomers together or separately as substrates. We also tested various GlcN and GlcNAc concentrations. Moreover, we performed the reaction using different ammonium sulfate concentrations. We synthesised oligomers under the optimal conditions for the hydrolytic activity of chitosanase from *M. circinelloides* IBT-83: 37°C and pH 5.5 [8]. The reaction occurred exclusively using 1 mmol GlcN and 2.5 mmol GlcNAc in 50 ml of 0.05 M acetate buffer medium (pH 5.5) containing 20% (w/v) ammonium sulfate. Conducting the reaction for 24 h produced a sample containing a dimer with total consumption of GlcN. Table 2 shows the HPLC analysis of the components of the post-reaction mixture. Of note, the other tested variants of the reaction mixture did not yield oligomers as reaction products.

Figure 1 shows the HPLC chromatogram of the initial sample (containing GlcNAc and GlcN as substrates) and the chromatogram of the reaction product. The post-reaction mixture also contains an unused substrate, namely GlcNAc.

Table 2. Reaction products of chitooligosaccharide synthesis using chitosanolytic enzymes from *Mucor circinelloides* IBT-83.

Sample	Content [%]		
	GlcNAc	GlcN	GlcNAc-GlcN
Components of the initial sample (substrates)	65	32	0
Mixture after synthesis for 12 h	59	26	12
Mixture after synthesis for 24 h	42	0	56

Note. Abbreviations: GlcN, D-glucosamine; GlcNAc, N-acetyl-D-glucosamine.

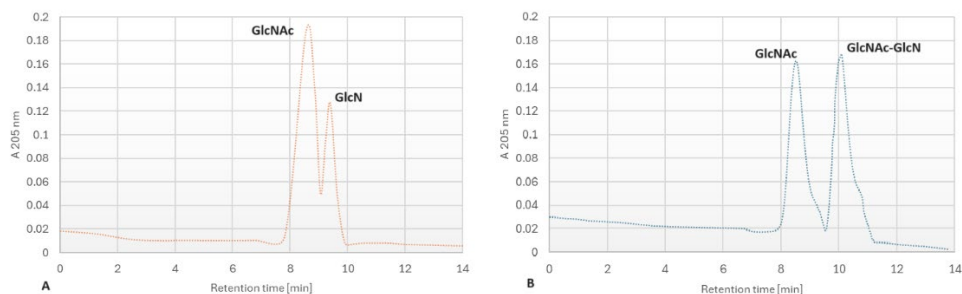


Figure 1. High-performance liquid chromatogram of (A) the components of the initial sample (substrates) and (B) the components of the post-reaction mixture. *Note:* The reaction was carried out according to the methodology described in Section 2.6, reaction time 24 hours. D-Glucosamine (GlcN), *N*-acetyl-D-glucosamine (GlcNAc) and chitooligosaccharides were used as standards.

In the future, it will be necessary to evaluate the possibility of synthesising oligomers with a higher degree of polymerisation. It is also necessary to identify the enzyme that catalyses this reaction, which is related to the need to use highly purified protein in the reaction. Next, attention should be paid to optimising the reaction conditions, including temperature, pH and additives, to increase enzymatic activity. The addition of co-solvents (acetonitrile, dimethylsulfoxide, *N,N* dimethylformamide, dioxane, 1,3-butanediol and 1,2,4-butanetriol), water-soluble solutes, or inorganic, soluble salts (most often ammonium sulfate) can alter water activity, which contributes to increase the synthetic activity of hydrolases [16]. In the present study, we only tested ammonium sulfate. The presence of a high concentration of ammonium sulfate (30%) initiated the conversion of (GlcNAc)₄ into (GlcNAc)₂ (55.7%) and (GlcNAc)₆ (39.6%) using chitinase from *Trichoderma reesei* KDR-11 [17]. Another example is the GlcN-GlcNAc dimer synthesis reaction carried out using exo-1,4- β -D-glucosaminidase from *A. fumigatus* IIT-004 in a 15% ammonium sulfate environment [6]. β -*N*-Acetyl glucosaminidase from *Chitinolyticbacter meiyuanensis* SYBC-H1 has reverse hydrolysis activity towards GlcNAc, synthesising various linked GlcNAc dimers. In this case, the dimer synthesis reaction took place in an environment with a high substrate concentration (10 g/l GlcNAc) [3].

4. Conclusions

This paper includes the preliminary results of research on the activity of intracellular enzymes obtained from *M. circinelloides* IBT-83 towards the synthesis of chitosan oligomers. We confirmed that these enzymes effectively catalyse the synthesis of a heterodimer consisting of GlcN and GlcNAc when using a 2.5-fold molar excess of GlcNAc relative to GlcN and performing the reaction at 37°C and pH 5.5 for 24 h.

5. References

- [1] Kaczmarek MB, Struszczyk-Świta K, Li X, Szczesna-Antczak M, Daroch M; (2019) Enzymatic modifications of chitin, chitosan, and chitooligosaccharides. *Front Bioeng Biotechnol* 7, 243. DOI:10.3389/fbioe.2019.00243
- [2] Jung WJ, Park RD; (2014) Bioproduction of chitooligosaccharides: present and perspectives. *Mar Drugs* 12(11), 5328–5356. DOI:10.3390/md12115328

- [3] Zhang A, Mo X, Zhou N, Wang Y, Wei G, Chen J, Chen K, Ouyang P; (2020) A novel bacterial β -*N*-acetyl glucosaminidase from *Chitinolyticbacter meiyuanensis* possessing transglycosylation and reverse hydrolysis activities. *Biotechnol Biofuels* 13, 115. **DOI:**10.1186/s13068-020-01754-4
- [4] Tanabe T, Morinaga K, Fukamizo T, Mitsutomi M; (2003) Novel chitosanase from *Streptomyces griseus* HUT 6037 with transglycosylation activity. *Biosci Biotechnol Biochem* 67(2), 354–364. **DOI:**10.1271/bbb.67.354
- [5] Sun H, Zhao L, Mao X, Cao R, Liu Q; (2023) Identification of a key loop for tuning transglycosylation activity in the substrate-binding region of a chitosanase. *J Agric Food Chem* 71(14), 5585–5591. **DOI:**10.1021/acs.jafc.3c00110
- [6] Sinha S, Chand S, Tripathi P; (2016) Enzymatic production of glucosamine and chitooligosaccharides using newly isolated *exo*- β -D-glucosaminidase having transglycosylation activity. *3 Biotech* 6(1), 13. **DOI:**10.1007/s13205-015-0330-5
- [7] Dvořáková J, Schmidt D, Huňková Z, Thiem J, Křen V; (2001) Enzymatic rearrangement of chitine hydrolysates with β -*N*-acetylhexosaminidase from *Aspergillus oryzae*. *J Mol Catal B Enzym* 11(4–6), 225–232. **DOI:**10.1016/S1381-1177(00)00075-8
- [8] Struszczyk K, Szczęsna-Antczak M, Walczak M, Pomianowska E, Antczak T; (2009) Isolation and purification of *Mucor circinelloides* intracellular chitosanolytic enzymes. *Carbohydr Polym* 78(1), 16–24. **DOI:**10.1016/j.carbpol.2009.04.010
- [9] Struszczyk K, Szczęsna-Antczak M, Walczak M, Pomianowska E, Wojciechowska J, Antczak T; (2009) Enzymatic preparations from *Mucor* moulds and their application in oligoaminosaccharides production. *Prog Chem Appl Chitin Deriv* 14, 89–100.
- [10] Struszczyk K, Szczęsna-Antczak M, Pomianowska E, Stańczyk Ł, Wojciechowska J, Antczak T; (2010) Process of continuous production of oligoaminosaccharides in a column reactor. *Prog Chem Appl Chitin Deriv* 15, 177–188.
- [11] Struszczyk-Świta K, Stańczyk Ł, Szczęsna-Antczak M, Antczak T; (2017) Scale-up of PUF-immobilized fungal chitosanase-lipase preparation production. *Prep Biochem Biotechnol* 47(9), 909–917. **DOI:**10.1080/10826068.2017.1365240
- [12] Kaczmarek MB, Struszczyk-Świta K, Florczak T, Szczęsna-Antczak M, Antczak T; (2016) Isolation, molecular cloning and characterisation of two genes coding chitin deacetylase from *Mucor circinelloides* IBT-83. *Prog Chem Appl Chitin Deriv* 21, 93–103. **DOI:**10.15259.PCAD.21.09
- [13] Kaczmarek MB, Struszczyk-Świta K, Szczęsna-Antczak MH, Antczak T, Gierszewska M, Steinbuchel A, Daroch M; (2021) Polycistronic expression system for *Pichia pastoris* composed of chitin deacetylase, chitinase, and chitosanase enabling one-pot enzymatic modification of chitin substrates. *Front Bioeng Biotechnol* 9, 710922. **DOI:**10.3389/fbioe.2021.710922
- [14] Nelson W; (1944) A photometric adaptation of the Somogyi method for the determination of glucose. *J Biol Chem* 153, 375–380. **DOI:**10.1016/S0021-9258(18)71980-7
- [15] Lowry OH, Rosenbrough NJ, Farr AL, Randall RJ; (1951) Protein measurement with the Folin phenol reagent. *J Biol Chem* 193, 265–275. **DOI:**10.1016/S0021-9258(19)52451-6
- [16] Muschiol J, Vuillemin M, Meyer AS, Zeuner B; (2020) β -*N*-Acetylhexosaminidases for Carbohydrate Synthesis via Trans-Glycosylation. *Catalysts* 10(4), 365. **DOI:**10.3390/catal10040365
- [17] Usui T, Matsui H, Isobe K; (1990) Enzymic synthesis of useful chito-oligosaccharides utilizing transglycosylation by chitinolytic enzymes in a buffer containing ammonium sulfate. *Carbohydr Res.* 203(1), 65–77. **DOI:**10.1016/0008-6215(90)80046-6

POLYETHYLENE TEREPHTHALATE (PET) COATED WITH CHITOSAN AND CYCLOSPORINE A LAYERS AS A POTENTIAL STENT MATERIAL AND DRUG-DELIVERY SYSTEM

Klaudia Szafran^{1,a}, Małgorzata Jurak^{1,b,*}, Robert Mroczka^{2,c},
Katarzyna Pastuszek^{1,d}, Agnieszka Ewa Wiącek^{1,e}

¹ – Department of Interfacial Phenomena, Institute of Chemical Sciences, Faculty of Chemistry, Maria Curie-Skłodowska University,
Maria Curie-Skłodowska 3 Sq., 20-031 Lublin, Poland

^a – ORCID: 0000-0002-0152-0839, ^b – ORCID: 0000-0002-5365-7677,

^d – ORCID: 0009-0001-9682-0809, ^e – ORCID: 0000-0002-7425-9694

² – Department of Chemistry, Laboratory of X-Ray Optics, Faculty of Medicine,
The John Paul II Catholic University of Lublin, Konstantynów 1J, 20-708 Lublin, Poland
^c – ORCID: 0000-0001-9633-9188

*corresponding author: malgorzata.jurak@mail.umcs.pl

Abstract

The aim of this paper was to design, prepare and characterise chitosan (Ch) and cyclosporine A (CsA) mixed films deposited on a plasma-activated polyethylene terephthalate (PET) polymer surface to be used as a cover for implantable blood vessel stents. The PET polymer coated with Ch and CsA layers was immersed in simulated body fluid (SBF) to examine how the obtained layers can behave in the environment of human body fluids. Time-of-flight secondary ion mass spectrometry was employed to determine the chemical composition of the deposited films and to analyse the spatial distribution of molecules on the PET surface. The results showed the controlled release of CsA from the chitosan matrix. It can be concluded that the modification of the PET polymer with layers of chitosan and CsA has great application potential in the tissue engineering as a biocompatible stent of blood vessels with therapeutic properties.

Keywords: chitosan, CsA, PET, air plasma, Langmuir–Blodgett technique, mass spectrometry

Received: 28.02.2024

Accepted: 20.05.2024

1. Introduction

In recent decades, biomaterials used as implants have gained great importance in regenerative medicine and tissue engineering. Besides properties such as biocompatibility and non-toxicity [1–3], newly designed biomaterials should meet more advanced requirements. One of the unique features can be the ability to deliver and release the drugs in a controlled way. Among the most commonly used materials for the production of blood vessel stents or its coverage is polyethylene terephthalate (PET, Figure 1a) [4, 5]. Despite the appropriate chemical resistance, elasticity and fibre strength, PET causes a negative immune response when it comes in contact with living cells, which can result in rejection of the implant [4]. Thus, coating PET with a natural polymer like chitosan (Figure 1b) can significantly increase its biocompatibility.

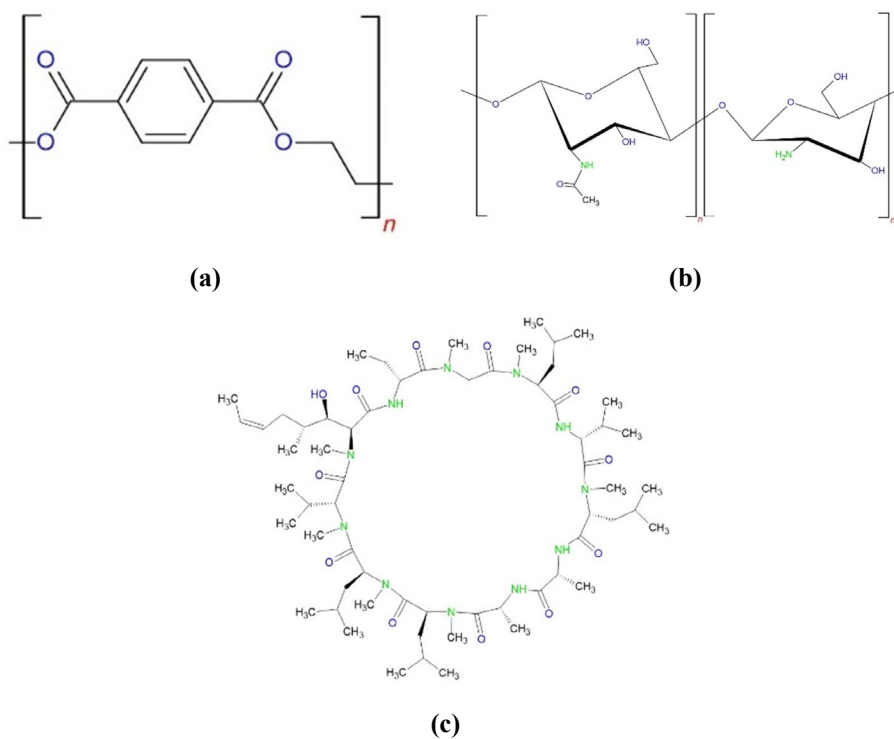


Figure 1. Chemical structure of (a) polyethylene terephthalate (PET), (b) chitosan and (c) cyclosporine A.

Chitosan is a polysaccharide consisting of *N*-acetyl-glucosamine and D-glucosamine monomers [6]. It occurs naturally: it is produced by fungi but it can also be obtained by deacetylation of chitin from shellfish shells [7]. Depending on the conditions of this process, chitosan with a different degree of deacetylation as well as physicochemical properties is obtained. In addition, chitosan is biocompatible and biodegradable, which results in production of oligosaccharides that are harmless to humans and can be easily processed by metabolic pathways and/or excreted by the body [8, 9]. Furthermore, chitosan has mucoadhesive, antimicrobial, antiviral and antifungal properties [6]. Additionally, chitosan is used to design

controlled drug-release systems. This is possible due to the simplicity of changing its properties by the pH, temperature or ionic strength of the solvent adjustments [10, 11]. Therefore, the use of chitosan as a coating of the biomaterial can allow for the delivery of a drug directly to the desired place in the body. Moreover, such coatings slow down the degradation rate and modulate cellular responses and the local release of growth factors from the biomaterial surface. As a result, postoperative complications are minimised [12, 13]. This property is extremely important in the case of strongly hydrophobic substances, whose absorption from the gastrointestinal tract is reduced significantly. However, in the bloodstream, positively charged chitosan ($-NH_3^+$) can interact with negatively charged platelets, provoking clot formation [14]. Thus, the simultaneous use of chitosan with the other substances seems to be appropriate to reduce its charge density and thus make it less thrombogenic.

One of the drugs frequently utilised after placing a biomaterial in the human body is cyclosporine A (CsA, Figure 1c); this cyclic polypeptide consisting of 11 amino acids has strong immunosuppressive properties. CsA works by inhibiting T lymphocyte-dependent immune reactions without affecting bone marrow cells. It also exhibits antifungal, anti-inflammatory and antiparasitic activities [15–17]. CsA is able to permeate membranes via passive diffusion. This process is associated with changes in the CsA conformation, which strictly depends on the polarity of the surrounding medium [18, 19]. However, due to its high molecular weight (1202.61 Da) and the possibility of forming intramolecular hydrogen bonds, CsA is poorly soluble in water and body fluids. Therefore, there are problems with the bioavailability and biocompatibility of CsA, which make oral administration of the drug ineffective (20%–50%) [15–17]. Accordingly, designing a controlled drug-release system that is simultaneously a biomaterial coating could eliminate this disadvantage. Figure 2 illustrates schematically a PET stent coated with chitosan and CsA films placed in a blood vessel.

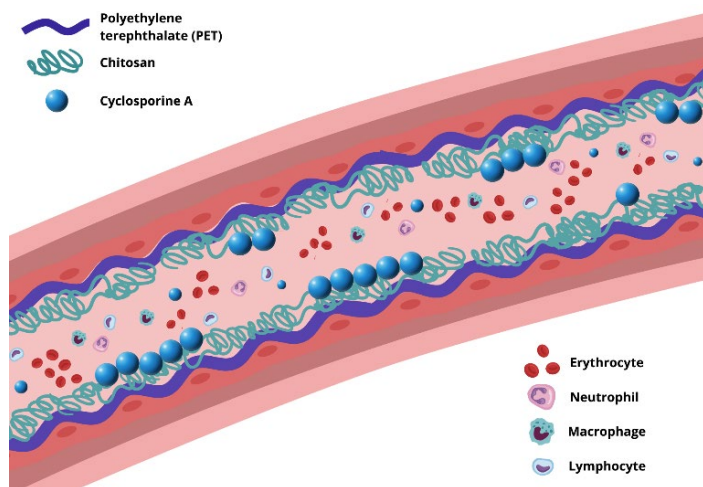


Figure 2. Scheme of the blood vessel with a polyethylene terephthalate stent coated with chitosan and cyclosporine A layers.

De Campos et al. [20] proved that chitosan nanoparticles form a support for CsA and can be applied in ophthalmology. This is possible due to the hydrogen bonds that form between amino groups of chitosan and amide groups of CsA. Additionally,

both acetylated and deacetylated units of chitosan are capable of forming hydrogen bonds [21]. Besides, chitosan membranes loaded with CsA as possible vehicle for local administration of drugs in breast cancer treatment have also been described [22]. It should be emphasised that chitosan increases the permeability of the epithelial membrane that promotes the stability of the drug at the absorption site and its paracellular transport [23].

The aim of this study was to elaborate novel chitosan-based biocoatings for PET stents which can be used for drug delivery, local release and absorption into the blood. For this purpose, the Langmuir–Blodgett technique was employed to prepare CsA monolayer at the chitosan/air interface and deposit it onto the air plasma-activated PET (PET_{air}) support. Additionally, previously prepared samples were immersed in simulated body fluid (SBF). By contacting the biomaterial with a solution containing ions present in body fluids, it was possible to examine how the obtained coatings would behave after grafting them in the human body. Afterwards, the chemical composition of the polymer coating was examined by the time-of-flight secondary ion mass spectrometry (TOF-SIMS).

2. Materials and Methods

2.1. Materials

Plates (20 × 30 × 3 mm³) were cut from commercially available PET (Bayer Material Science, Germany) and used as a solid support. A 0.1 mg ml⁻¹ chitosan solution was prepared by dissolving an appropriate amount of chitosan (molecular weight 100,000–300,000, degree of deacetylation 82% ± 2%, Acrōs Organics, Sweden) in 0.1% acetic acid diluted from concentrated acetic acid (99.5%–99.9%, Avantor Performance Materials Poland S.A., Poland). Additionally, CsA (≥ 99%, Alfa Aesar, Germany) was dissolved in chloroform:methanol mixed in a 4:1 ratio (v:v) to obtain a 1 mg ml⁻¹ concentration (chloroform 99.8%, Macron Fine Chemicals, Avantor Performance Materials Poland S.A., and methanol ≥99.9%, Fluka, Sweden). SBF was prepared according to the procedure described by Kokubo et al. [24]. All used chemicals – NaCl, Na₂CO₃, Na₂HPO₄ × 12H₂O, MgCl₂ × 6H₂O, CaCl₂ (POCh Poland), KCl, Na₂SO₄ (Chempur, Poland) and tris(hydroxymethyl)aminomethane (NH₂C(CH₂OH)₃, Sigma-Aldrich, USA) – were dissolved in Milli-Q water with resistivity of 18.2 MΩ cm (Milli-Q Plus 185 system, Millipore, USA).

2.2. Methods

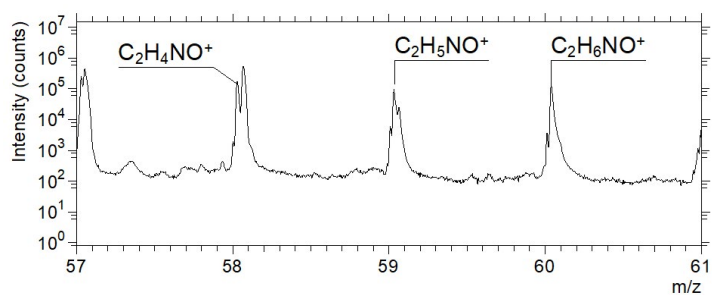
The PET plates were cleaned as described previously [25, 26]. Then, the plates were activated by a low-temperature and low-pressure (0.20 mbar) air plasma (Plasma type system, Diener Electronic, Germany) for 1 min. Immediately after modification, the PET plates were immersed in the chitosan subphase filling the Langmuir–Blodgett trough (KSV 2000 Standard, Finland), which had been purified with acetone (99.5%, Avantor Performance Materials S.A. Poland), methanol and deionised water. The surface tension was measured by the Wilhelmy plate method with an accuracy of 0.1 mN m⁻¹. Subsequently, the proper volume of CsA solution was spread onto the chitosan subphase. After solvent evaporation, symmetrical compression with a constant speed of 20 mm min⁻¹ was performed to achieve a surface pressure of 10 mN m⁻¹ at which the CsA monolayer was found to be the most stable on the liquid subphase [26, 27]. Immediately after reaching the target pressure, the CsA monolayer was transferred onto the PET plate during its withdrawal from the subphase towards the air. Then, the PET substrate with the deposited Langmuir–Blodgett layers was dried to remove traces of water and placed in a dark glass

desiccator before the next stages of the experiment. Afterwards, the samples were immersed in SBF for 3, 10 or 30 min. Subsequently, TOF-SIMS was performed. The modified PET substrates were placed in the ultra-high vacuum chamber of the TOF-SIMS.5 instrument (ION-TOF GmbH, Germany). The primary ion source of bismuth ions (Bi^+) was utilised at 30 keV and corresponded to the 1.0 pA primary beam current in the spectrometry mode where the scanning area of the secondary ions was $200 \times 200 \mu\text{m}^2$ with 256×256 pixels. All measurements were performed under static positive conditions (dose $< 1 \times 10^{12}$ ions cm^{-2}). To neutralise the charge left on the surface, an electron flood gun (20 eV) and a surface potential ($U = -360$ V) were applied. The spectra were calibrated based on the positions of $(\text{CH}_3)^+$, $(\text{C}_2\text{H}_3)^+$ and $(\text{C}_2\text{H}_5)^+$. The intensity of each fragment was normalised to the total intensity.

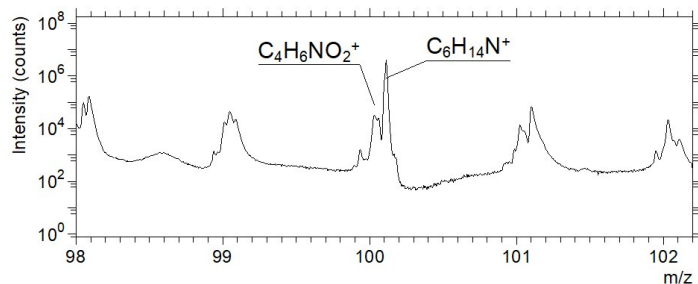
3. Results and Discussion

The design of biocompatible coatings for implants that can be used simultaneously as a controlled drug-release system requires one to examine the chemical composition, which is one of the main properties influencing the host body's immune response [2]. In the present study, the PET surface was activated by plasma leading to generation of new functional groups containing oxygen, nitrogen and carbon ($-\text{OH}$, $\text{C}-\text{O}$, $\text{O}=\text{C}-\text{O}$, $\text{C}=\text{O}$, and $\text{N}-\text{CO}-\text{N}$). Their presence was confirmed by X-ray photoelectron spectroscopy (XPS) from our previous study [26] as well as those studies from other researchers [28–30]. Subsequently, the CsA monolayer was deposited onto the plasma-activated PET (PET_{air}) support by using the Langmuir–Blodgett technique from the chitosan/air interface. This process leads to the formation of new bonds between the activated polymer surface and chitosan [26]. Then, TOF-SIMS was conducted before and after immersion of the PET plates with the deposited chitosan and/or CsA layers in SBF for different periods of time. This technique allows one to determine the chemical structure and fragmentation patterns of molecules based on the mass to charge (m/z) ratio of the molecular fragments formed during ionisation [31]. Due to the fact that only single-charge mass fragments are produced when ionisation is carried out using a bismuth source in the TOF-SIMS spectrometer chamber, the m/z value corresponds practically to the mass of the formed ion. The TOF-SIMS spectra obtained for the mass range of the most characteristic fragments of CsA and chitosan deposited onto the PET_{air} support, along with the whole m/z range from 0 to 1300, are presented in Figure 3.

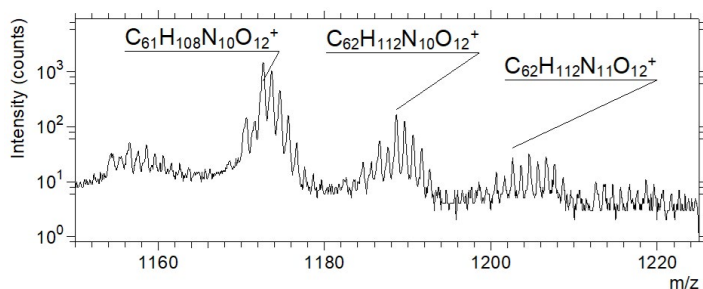
Table 1 summarises the m/z assignment and identification of these fragments. Figures 4 and 5 show the distributions of the fragments. The most prominent ions identified for the single CsA monolayer are $m/z = 100$ ($\text{C}_6\text{H}_{14}\text{N}^+$) (Figure 4a), pseudomolecular $m/z = 1172$ ($\text{C}_{61}\text{H}_{108}\text{N}_{10}\text{O}_{12}^+$) and molecular ion $m/z = 1202$ ($\text{C}_{62}\text{H}_{112}\text{N}_{11}\text{O}_{12}^+$) (Figure 4b); these findings are consistent with our previous papers [25, 26, 32]. We also noted the pseudomolecular ion with $m/z = 1188$ ($\text{C}_{62}\text{H}_{112}\text{N}_{10}\text{O}_{12}^+$). The fragments with $m/z = 1172$ and 1188 come from the molecular ion ($m/z = 1202$) by subtraction of NH_3 and N, respectively. Based on the TOF-SIMS mass spectra, they showed significantly higher intensity (Figure 3c). Thus, we selected the molecular ion ($m/z = 1202$) as the primary meaning and the most intense fragment ($m/z = 1172$) for further analysis; this choice provided better statistical results. The high-mass fragments are typical of the mass patterns of polymers or oligomers (Figure 3c).



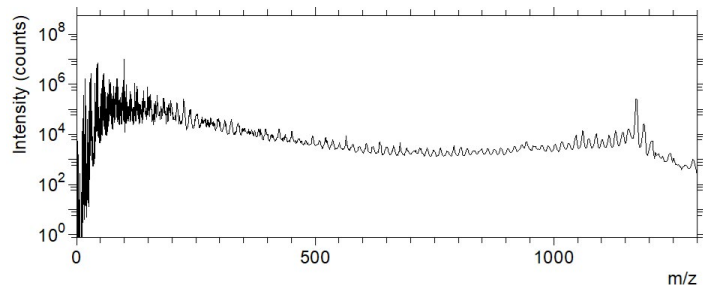
(a)



(b)



(c)



(d)

Figure 3. The time-of-flight secondary ion mass spectra (with a logarithmic scale) for mass range (m/z) (a) from 57 to 61 (peaks characteristic of chitosan), (b) from 98 to 102 (peaks characteristic of chitosan and cyclosporine A), (c) from 1150 to 1224 (the high-mass fragments that results from cyclosporine A) and (d) for the entire mass range from 0 to 1300.

It should be emphasised that the molecular ion is the basic ion identifying a given component of the monolayer and serves as an indicator of its order; it is closely related to the arrangement and/or inclination of the molecules. It is defined as a charged molecule that is formed as a result of ionisation by donating one electron (a positive molecular ion) or, much less often, by taking one electron (a negative molecular ion). Its mass is equal to the molecular weight of the tested compound. Meanwhile, a pseudomolecular ion is created by removing two oxygen or hydrogen atoms from the molecular ion or by adding a foreign metal from the environment.

Table 1. The most characteristic positive fragments in the time-of-flight secondary ion mass spectra obtained for the chitosan (Ch) and cyclosporine A (CsA) layers.

Assignment	m/z	Identification	Reference
$(C_6H_{14}N)^+$	100	CsA	[25, 26, 32]
$(C_{61}H_{108}N_{10}O_{12})^+$ $(CsA-NH_3)^+$	1172	CsA pseudomolecular ion	[25, 26, 32]
$(C_{62}H_{112}N_{10}O_{12})^+$ $(CsA+H-N)^+$	1188	CsA pseudomolecular ion	This study
$(C_{62}H_{112}N_{11}O_{12})^+$ $(CsA+H)^+$	1202	CsA molecular ion	[25, 26, 32]
$(C_2H_4NO)^+$	58	Ch	[26, 33]
$(C_2H_5NO)^+$	59	Ch	[26]
$(C_2H_6NO)^+$	60	Ch	[34]
$(C_4H_6NO_2)^+$	100	Ch	[34]

Other researchers have also identified secondary ions assigned to CsA by TOF-SIMS. Muddiman et al. [35, 36] quantified the $(CsA+Na)^+$ $m/z = 1225$ and $(CsA+Ag)^+$ $m/z = 1309$ fragments on an etched silver substrate with a mass resolution of 8000. In addition, Nicola et al. [37] identified the $(CsA+H)^+$ $m/z = 1202$ and $(CsA+Ag)^+$ $m/z = 1309$ fragments for the CsA layer deposited on silver support previously covered with a cocaine layer. Finally, Biddulph [38] identified the following CsA fragments: $(M+H)^+$ $m/z = 1202$, $m/z = 100$, (leucine) $m/z = 86$, (valine) $m/z = 72$, (alanine) $m/z = 44$, (glycine) $m/z = 30$ and $m/z = 15$. They were yielded by the Au^{3+} primary ion with a relative intensity of 394.5×10^{-5} , 3207.0×10^{-5} , 751.9×10^{-5} , 340.5×10^{-5} , 1205.0×10^{-5} and 81.4×10^{-5} , 37.5×10^{-5} , respectively. For comparison, in the present study the relative intensity of the fragments $m/z = 100$, 1172 and 1202 before immersion in SBF was 0.1×10^{-4} , 8.5×10^{-4} and 1.2×10^{-5} , respectively (Figure 4). Mass resolution was 12652 for the $m/z = 1172$ fragment and 9348 for the $m/z = 1202$ fragment. The former fragment resulted from extraction of $m/z = 30$, which presumably corresponds to C_2H_6 .

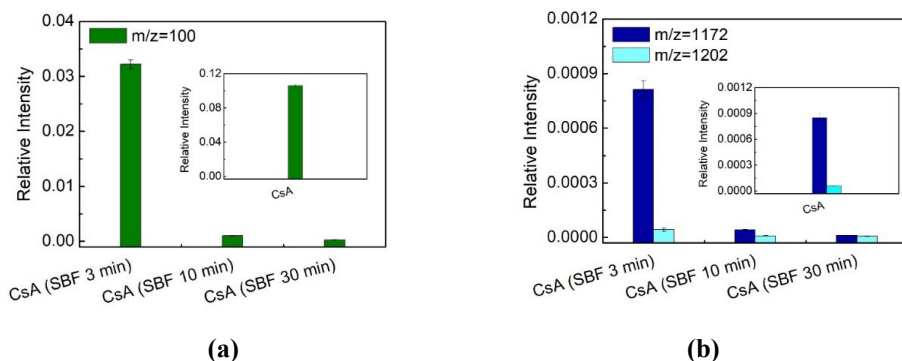


Figure 4. Distribution of the (a) cyclosporine A $m/z = 100$ fragment and the (b) $m/z = 1172$ and 1202 fragments for the air plasma-activated polyethylene terephthalate (PET_{air})/chitosan (Ch)/cyclosporine A (CsA) surface before and after immersion in simulated body fluid (SBF) solution for different periods of time.

As can be seen in Figure 4a,b, the relative intensity of the characteristic CsA fragments was the greatest for the deposited CsA monolayer before immersion in SBF. This correlated with the largest surface coverage. Moreover, the presence of the molecular and pseudomolecular ions confirmed that the obtained monolayer was well ordered. As a result of interactions with the primary ion beam (Bi^+ or Bi^{3+}), the molecules in such a layer are subject to much less fragmentation, which favours high molecular ion efficiency [34]. In other words, in the well-ordered and packed monolayer, the probability of yielding the molecular or pseudomolecular ions ($m/z = 1170$ and 1202) increases significantly. This can be justified by the number of molecules and the intermolecular interactions. Specifically, at very low surface coverage, the CsA molecules are loosely arranged and the interactions between them can be neglected (like in a gas phase) or can be very low (like in a liquid state). Under these circumstances the fragmentation of isolated molecules by primary the Bi^{3+} beam is very high. Hence, the probability of desorption of CsA in their original, unfragmented form is close to zero. When the monolayer is more tightly packed, the intermolecular interactions allow some portion of CsA to be desorbed from the substrate in the unfragmented form and further to be extracted to the analyser chamber of the TOF-SIMS instrument and identified by the detector.

Furthermore, as the CsA monolayer was deposited onto the PET_{air} /chitosan surface, the signal intensity coming from the characteristic fragments of chitosan was the smallest (Figure 5). After immersion of the sample in SBF for 3 min, the relative intensity of the $(C_6H_{14}N)^+$ ion was 3 times smaller with almost the same intensities of the molecular $(C_{62}H_{112}N_{11}O_{12})^+$ and pseudomolecular $(C_{61}H_{108}N_{10}O_{12})^+$ ions (Figure 4b). This can be related to some changes in the CsA molecular organisation due to contact with the liquid. The occurrence of molecular ions proves that CsA monolayer is still present at the PET_{air} /chitosan surface. When the PET_{air} /chitosan/CsA sample was immersed in SBF for a longer time, the relative intensity of CsA molecular ions decreased (Figure 4b). At very low surface coverage with CsA (immersion times of 10 and 30 min), the molecules are too far from each other and thus do not interact. Consequently, the probability of yielding the molecular ion during sputtering by the primary Bi^+ ion beam is strongly diminished. This phenomenon has been well reported in the literature [25, 26, 34, 39]. Thus, the obtained results demonstrate that the packed and ordered CsA monolayer

structure is not retained and most of the CsA molecules can be desorbed into the bulk phase. The intensity of $(C_6H_{14}N)^+$ ion with $m/z = 100$ shows similar behaviour (Figure 4a). This affirms that CsA molecules are still present at the surface.

In the time-of-flight secondary ion mass spectra, the chitosan layer was identified in the form of $(C_2H_4NO)^+$, $(C_2H_5NO)^+$ and $(C_2H_6NO)^+$ (Table 1), consistent with our previous study [26]. Figure 5 shows the intensity distribution of these chitosan fragments. Of note, we obtained the $m/z = 100.04$ fragment assigned to $(C_4H_6NO_2)^+$, which is characteristic of chitosan [34]. Despite the similar $m/z \approx 100$ values, we could distinguish that peak from the most intense CsA fragment $(C_6H_{14}N)^+$, namely $m/z = 100.10$, due to high mass resolution (> 8000). The relative intensity of $(C_4H_6NO_2)^+$ was 1.46×10^{-3} , 5.2×10^{-4} , 2.2×10^{-4} and 3×10^{-4} for samples before immersion in SBF, and after immersion in SBF for 3, 10 and 30 min, respectively. The intensity of this chitosan fragment was significantly lower compared with the others ($m/z = 58, 59$ and 60 , Figure 5). We expected that the intensity would increase after immersion in SBF similarly to $m/z = 60$. Due to the fact that the $m/z = 60$ fragment demonstrated the proper distribution (with a significant increase in intensity after immersion), we used it as an indicator of the chitosan layer. On the other hand, owing to the low intensity and atypical behaviour after immersion of the $m/z = 100.04$ fragment, we did not consider it further.

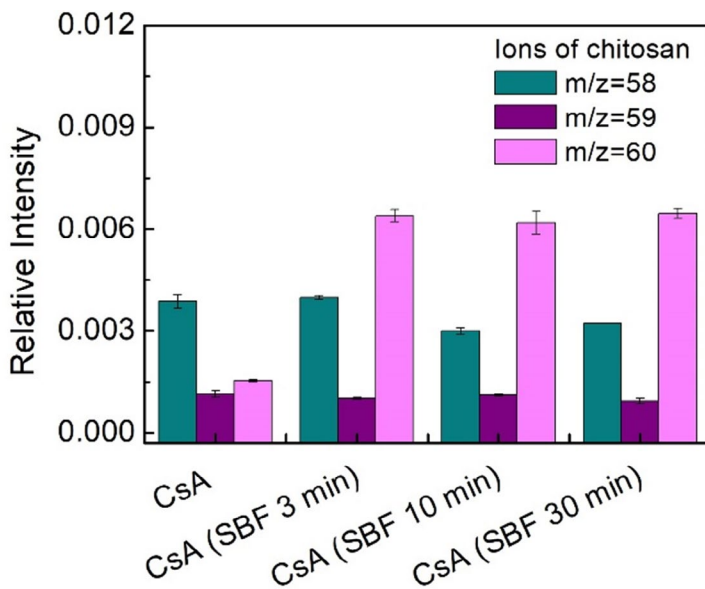


Figure 5. Distribution of the chitosan $m/z = 58, 59$ and 60 fragments for the air plasma-activated polyethylene terephthalate (PET_{air})/chitosan (Ch)/cyclosporine A (CsA) surface before and after immersion in simulated body fluid (SBF) for different periods of time.

As shown in Figure 5, the relative intensity of the $m/z = 58, 59$ and 60 fragments varied depending on the nature of deposited layer and possible post-treatment method. For the untreated Ch/CsA layer, the $(C_2H_4NO)^+$ fragment ($m/z = 58$) showed the highest intensity. On the other hand, the $(C_2H_5NO)^+$ and $(C_2H_6NO)^+$ intensities are roughly similar and two times lower than that of the $(C_2H_4NO)^+$ ion. There were similar results in the recent studies [26, 33, 34]. After immersing the Ch/CsA layer in SBF for 3 min,

the relative intensity of the $m/z = 58$ and 59 fragments remained unchanged. Meanwhile, the relative intensity of the $(C_2H_6NO)^+$ fragment ($m/z = 60$) increased more than 3 times, which corresponds to a decrease in the amount of CsA on the surface (lower intensity of the CsA fragment with mass $m/z = 100$). On the other hand, the intensity of the CsA molecular ions is the same. These results suggest that orientation of the CsA molecules is very likely preserved at even lower surface coverage. A longer immersion in SBF (10 and 30 min) did not influence the relative intensity of the chitosan $(C_2H_6NO)^+$ fragment, but decreased the intensity of the $(C_2H_4NO)^+$ fragment. This reduced intensity of $(C_2H_4NO)^+$ could be the result of a more parallel orientation of CsA at low surface coverage after immersion for 10 and 30 min.

Overall, the greater yield of the $(C_2H_6NO)^+$ fragment after immersion in SBF for 3 min illustrates the chitosan layer covered by patchy CsA layer with polypeptide molecules oriented perpendicularly towards the chitosan underlayer. After immersion for 10 and 30 min, the CsA islands disappear, denoted by disappearance of the molecular ions. This indicates that a very small amount of CsA becomes oriented more parallel towards the chitosan layer. These findings clearly show that the chitosan layer is present at the PET_{air} surface after placing the biomaterial in SBF. This is particularly important in terms of improving and maintaining the biocompatibility of PET surfaces. However, the exact yield mechanism of the chitosan $(C_2H_4NO)^+$, $(C_2H_5NO)^+$ and $(C_2H_6NO)^+$ fragments under different immersion time of the chitosan/CsA layer is beyond the scope of this paper and requires more extensive studies.

The desorption of CsA from the biomaterial surface is related to the fact that CsA does not form chemical bonds with chitosan. Chitosan and CsA may interact via hydrogen bonds and/or Lifshitz–van der Waals forces. It is likely that in the untreated CsA layer, CsA molecules exist mainly in a closed conformation due to the surrounding hydrophobic environment provided by the chitosan backbone. However, immersion in SBF – and thus changing the environment to a polar one – favours the open conformation of CsA, which can then interact more strongly with SBF and weakly with the chitosan layer. This allows CsA to be desorbed from the surface of the biomaterial. The ability of CsA to change its conformation from closed to open depending on the nature of the environment enables its transport through the lipid bilayer according to the mechanism of passive diffusion [18, 19]. Such results are very promising for the design and development of new drug-release systems.

Modification of the PET surface with air plasma and biological films can significantly improve its biocompatibility and minimise side effects associated with the body's response to a foreign material. The presence of chitosan film provides an additional function, namely the controlled release of CsA, a strong immunosuppressant drug that is used to prevent implant rejection.

4. Conclusions

We used TOF-SIMS to analyse the chemical composition and the spatial distribution of molecules in the mixed chitosan and CsA layers. They were deposited by the Langmuir–Blodgett technique on the air plasma-activated PET surface and then immersed in SBF. We identified the most characteristic CsA and chitosan fragments in the time-of-flight secondary ion mass spectra before and after immersing the samples in SBF. The results confirmed the effective PET surface coverage with chitosan and CsA. The chitosan layer was presumably chemically bonded to the activated PET support. Meanwhile, CsA was physically adsorbed on the chitosan layer via hydrogen

bonding and/or Lifshitz van der Waals forces. In the SBF environment, CsA underwent gradual desorption into the bulk phase over time, as indicated by the decreased relative intensity of the $(C_6H_{14}N)^+$, $(C_{61}H_{108}N_{10}O_{12})^+$ and $(C_{62}H_{112}N_{10}O_{12})^+$ fragments. This process was likely due to a change from closed to open conformation of CsA. In effect, the initially well-ordered and packed structure of the CsA monolayer was no longer maintained exposing the chitosan layer. Consistently, there was a significant increase in the relative intensity of the most prominent chitosan fragment, $(C_2H_6NO)^+$, after immersion in SBF.

Our findings are satisfactory from the application point of view. The release of CsA from the PET/chitosan surface can ensure relatively easy delivery of this immunosuppressive drug to living cells directly from the implant surface. Simultaneously, the increased biocompatibility of the PET surface can be maintained due to its durable binding to the polysaccharide. Therefore, designing two-component layers as coatings for implants and/or stents may facilitate the release of CsA, eliminating the problem of its low bioavailability.

5. References

- [1] Williams DF; (2019) Challenges with the development of biomaterials for sustainable tissue engineering. *Front Bioeng Biotechnol* 31, 127. DOI:10.3389/fbioe.2019.00127
- [2] Jurak M, Wiącek AE, Ładniak A, Przykaza K, Szafran K; (2021) What affects the biocompatibility of polymers? *Adv Colloid Interface Sci* 294, 102451. DOI:10.1016/j.cis.2021.102451
- [3] Song X, Tang Z, Liu W, Chen K, Liang J, Yuan B, Lin H, Zhu X, Fan Y, Shi X, Zhao P, Yang L, Zhang K, Mikos AG, Zhang X; (2022) Biomaterials and regulatory science. *J Mater Sci Technol* 128, 221–227. DOI:10.1016/j.jmst.2022.04.018
- [4] Farhatnia, Y, Tan A, Motiwala A, Cousins BG, Seifalian AM; (2013) Evolution of covered stents in the contemporary era: clinical application, materials and manufacturing strategies using nanotechnology. *Biotechnol Adv* 31, 524–542. DOI:10.1016/j.biotechadv.2012.12.010
- [5] Li T, Ma K, Zhang T; (2022) UV-curable semi-interpenetrating matrix for polyester fabric-covered stents. *Progr Org Coat* 172, 107084. DOI:10.1016/j.porgcoat.2022.107084
- [6] Jafarnik K, Ładniak A, Blicharska E, Czarnek K, Ekiert H, Wiącek AE, Szopa A; (2023) Chitosan-based nanoparticles as effective drug delivery systems – a review. *Molecules* 28, 1963. DOI:10.3390/molecules28041963
- [7] Pina S, Oliveira JM, Reis RL; (2015) Natural-based nanocomposites for bone tissue engineering and regenerative medicine: a review. *Adv Mater* 27, 1143–1169. DOI:10.1002/adma.201403354
- [8] Rinaudo M; (2006) Chitin and chitosan: Properties and applications. *Prog Polym Sci* 31, 603–632. DOI:10.1016/j.progpolymsci.2006.06.001
- [9] Ahmed S, Ikram S; (2016) Chitosan based scaffolds and their applications in wound healing. *Achiev Life Sci* 10, 27–37. DOI:10.1016/j.als.2016.04.001
- [10] Carreira AS, Gonçalves FMM, Mendonça PV, Gil MH, Coelho JFJ; (2010) Temperature and pH responsive polymers based on chitosan: applications and new graft copolymerization strategies based on living radical polymerization. *Carbohydr Polym* 80, 618–630. DOI:10.1016/j.carbpol.2009.12.047
- [11] Li J, Cai C, Li J, Li J, Li J, Sun T, Wang L, Wu H, Yu G; (2018) Chitosan-based nanomaterials for drug delivery. *Molecules* 23, 2661. DOI:10.3390/molecules23102661

- [12] Jang TS, Choen KH, Ahn JH, Song EH, Kim HE; (2019) *In-vitro* blood and vascular compatibility of sirolimus-eluting organic/inorganic hybrid stent coatings. *Colloids Surf B Biointerfaces* 179, 405–413. **DOI:**10.1016/j.colsurfb.2019.04.018
- [13] Kersani D, Mugin J, Lopez M, Degoutin S, Tabary N, Cazaux F, Janus L, Maton M, Chai F, Sobocinski J, Blanchemain N, Martel B; (2020) Stent coating by electrospinning with chitosan/poly-cyclodextrin based nanofibers loaded with simvastatin for restenosis prevention. *Eur J Pharm Biopharm* 150, 156–167. **DOI:**10.1016/j.ejpb.2019.12.017
- [14] Baldrick P; (2010) The safety of chitosan as a pharmaceutical excipient. *Regul Toxicol Pharmacol* 56, 290–299. **DOI:**10.1016/j.yrtph.2009.09.015
- [15] Czogalla A; (2008) Oral cyclosporine A - the current picture of its liposomal and other delivery systems. *Cell Mol Biol Lett* 14, 139–152. **DOI:**10.2478/s11658-008-0041-6
- [16] Tedesco D, Haragsim L; (2012) Cyclosporine: a review. *J Transplant* 2012, 230386. **DOI:**10.1155/2012/230386
- [17] Wiącek AE, Jurak M, Ładniak A, Przykaza K, Szafran K; (2020) Cyclosporine CsA - The physicochemical characterization of liposomal and colloidal systems. *Colloids Interfaces* 4, 46. **DOI:**10.3390/colloids4040046
- [18] Witek J, Keller BG, Blatter M, Meissner A, Wagner T, Riniker S; (2016) Kinetic models of cyclosporin A in polar and apolar environments reveal multiple congruent conformational states. *J Chem Inf Model* 56, 1547–1562. **DOI:**10.1021/acs.jcim.6b00251
- [19] Dougherty PG, Sahni A, Pei D; (2019) Understanding cell penetration of cyclic peptides. *Chem Rev* 119, 10241–10287. **DOI:**10.1021/acs.chemrev.9b00008
- [20] De Campos AM, Sánchez A, Alonso MJ; (2001) Chitosan nanoparticles: A new vehicle for the improvement of the delivery of drugs to the ocular surface. Application to cyclosporin A. *Int J Pharm* 224, 159–168. **DOI:**10.1016/S0378-5173(01)00760-8
- [21] Philipova OE, Volkov EV, Sitnikova NL, Khokhlov AR; (2001) Two types of hydrophobic aggregates in aqueous solutions of chitosan and its derivative. *Biomacromol* 2, 483–490. **DOI:**10.1021/bm005649a
- [22] Trombino S, Curcio F, Poerio T, Pellegrino M, Russo R, Cassano R; (2021) Chitosan membranes filled with cyclosporine A as possible devices for local administration of drugs in the treatment of breast cancer. *Molecules* 26, 1889. **DOI:**10.3390/molecules26071889
- [23] Islama MM, Shahruzzamana M, Biswasa S, Sakiba MN, Rashida TU; (2020) Chitosan based bioactive materials in tissue engineering applications - a review. *Bioact Mater* 5, 164–183. **DOI:**10.1016/j.bioactmat.2020.01.012
- [24] Kokubo T, Takadama H; (2006) How useful is SBF in predicting *in vivo* bone bioactivity? *Biomaterials* 27, 2907–2915. **DOI:**10.1016/j.biomaterials.2006.01.017
- [25] Szafran K, Jurak M, Mroczka R, Wiącek AE; (2022) Surface properties of the polyethylene (PET) substrate modified with the phospholipid-polypeptide-antioxidant films: design of functional biocoatings. *Pharmaceutics* 14, 2815. **DOI:**10.3390/pharmaceutics14122815
- [26] Szafran K, Jurak M, Mroczka R, Wiącek AE; (2023) Preparation and characterization of chitosan-based coatings for PET materials. *Molecules* 28, 2375. **DOI:**10.3390/molecules28052375

- [27] Szafran K, Jurak M, Wiącek AE; (2022) Effect of chitosan on the interactions between phospholipid DOPC, cyclosporine A and lauryl gallate in the Langmuir monolayers. *Colloids Surf A Physicochem Eng Asp* 652, 129843. **DOI:**10.1016/j.colsurfa.2022.129843
- [28] Pandiyaraj KN, Selvarajan V, Rhee YH, Kim HW, Shah SI; (2009) Glow discharge plasma-induced immobilization of heparin and insulin on polyethylene film surfaces enhances anti-thrombogenic properties. *Mater Sci Eng C* 3, 796–805. **DOI:**10.1016/j.msec.2008.07.013
- [29] Bui V-T, Liu X, Ko SH, Choi H-S; (2015) Super-amphiphilic surface of nano silica/polyurethane hybrid coated PET film via a plasma treatment. *J Colloid Interface Sci* 453, 209–215. **DOI:**10.1016/j.jcis.2015.04.065
- [30] Abdel-Fattah E; (2022) Surface modifications of PET in argon atmospheric pressure plasma: Gas flow rate effect. *Surf Interface Anal* 54, 794–802. **DOI:**10.1002/sia.7092
- [31] McQuaw CM, Sostarecz AG, Zheng L, Ewing AG, Winograd N; (2005) Lateral heterogeneity of dipalmitoylphosphatidylethanolamine-cholesterol Langmuir-Blodgett films investigated with imaging time-of-flight secondary ion mass spectrometry and atomic force microscopy. *Langmuir* 21, 807–813. **DOI:**10.1021/la0479455
- [32] Przykaza K, Jurak M, Wiącek AE, Mroczka R; (2021) Characteristics of hybrid chitosan/phospholipid-sterol, peptide coatings on plasma activated PEEK polymer. *Mat Sci Eng C* 120, 111658. **DOI:**10.1016/j.msec.2020.111658
- [33] Finšgar M, Ristić T, Fardim P, Zemljič LF; (2018) Time-of-flight secondary ion mass spectrometry analysis of chitosan-treated viscose fibres. *Anal Biochem* 557, 131–141. **DOI:**10.1016/j.ab.2018.07.021
- [34] Jurak M, Wiącek AE, Mroczka R, Łopucki R; (2017) Chitosan/phospholipid coated polyethylene terephthalate (PET) polymer surfaces activated by air plasma. *Colloids Surf A Physicochem Eng Asp* 532, 155–164. **DOI:**10.1016/j.colsurfa.2017.05.061
- [35] Muddiman DC, Gusev AI, Stoppek-Langner K, Proctor A, Herkules DM, Tata P, Venkataramanan R, Diven W; (1995) Simultaneous quantification of cyclosporin A and its major metabolites by time-of-flight secondary-ion mass spectrometry and matrix-assisted laser desorption/ionization mass spectrometry utilizing data analysis techniques: Comparison with high-performance liquid chromatography. *J Mass Spectrom* 30, 1469–1479. **DOI:**10.1002/jms.1190301013
- [36] Muddiman DC, Nicola AJ, Proctor A, Herkules DM; (1996) Important aspects concerning the quantification of biomolecules by time-of-flight secondary-ion mass spectrometry. *Appl Spectrosc* 50, 161–166. **DOI:**10.1366/0003702963906410
- [37] Nicola AJ, Muddiman DC, Hercules DM; (1996) Enhancement of ion intensity in time-of-flight secondary-ionization mass spectrometry. *JASMS* 7, 467–472. **DOI:**10.1016/1044-0305(96)00006-2
- [38] Biddulph GX, Piwowar AM, Fletcher JS, Lockyer NP, Vickerman JC; (2007) Properties of C_{84} and $C_{24}H_{12}$ molecular ion sources for routine TOF-SIMS analysis. *Anal Chem* 79, 7259–7266. **DOI:**10.1021/ac071442x
- [39] Jurak M, Mroczka R, Łopucki R; (2018) Properties of artificial phospholipid membranes containing lauryl gallate or cholesterol. *J Membr Biol* 251, 277–294. **DOI:**10.1007/s00232-018-0025-z

POLYMER BIOCOMPOSITES IN THE FORM OF HYDROGEL USED FOR THE TREATMENT OF PRESSURE SORES

Maria Wiśniewska-Wrona^{1,a,*}, Monika Sikora^{1,b}, Monika Owczarek^{1,c}

¹ – Łukasiewicz Research Network – Łódź Institute of Technology,
M. Skłodowskiej-Curie 19/27 Str., 90-570 Łódź, Poland

^a – ORCID: 0000-0001-5666-4138, ^b – ORCID: 0000-0002-0405-7982,

^c – ORCID: 0000-0003-3758-150x

*corresponding author: maria.wisniewska-wrona@lit.lukasiewicz.gov.pl

Abstract

*This paper presents research related to the development of hydrogel polymer biocomposites (chitosan and alginate) with an analgesic medication (lidocaine hydrochloride). The pharmaceutical availability of lidocaine hydrochloride from the hydrogel preparations was evaluated for transdermal systems in accordance with the Polish Pharmacopoeia, XI Edition. The rheological tests showed that these preparations had the characteristics of non-Newtonian, pseudoplastic liquids, for which the viscosity decreases as the shear rate increases. The developed hydrogel preparations showed bacteriostatic and bactericidal effects against both *Escherichia coli* and *Staphylococcus aureus*. The release of lidocaine hydrochloride from the tested hydrogel was a complex process that followed first-order kinetics. The rate of release could be influenced by appropriate selection of the composition of the biocomposite.*

Keywords: *natural polymers, polymer biocomposite hydrogels, pressure sores, rheological and biological properties, transdermal systems*

Received: 15.04.2024

Accepted: 27.06.2024

1. Introduction

Polymer hydrogels have a characteristic structure, which determines their unusual properties. These materials consist of polymer chains with numerous cross-links between them. Such a system resembles a three-dimensional network whose cross-linking density depends on the number of cross-links. There are free spaces inside the polymer network that are filled by water during the swelling process. This process is possible due to the presence of numerous hydrophilic groups in the polymer chains. In contact with water, hydrophilic groups dissociate, which induces additional electrostatic interactions. There is repulsion of the same ions, which increases the distance between the polymer chains and, consequently, the free space available for water increases [1]. Due to their high water content, appropriate density and plasticity, hydrogels have physical properties similar to those of soft tissues of living organisms. Water in hydrogels acts as a transport medium, thanks to which substances can be 'locked' in them and the rate of their release can be freely manipulated, thus creating a so-called intelligent drug-delivery system. Drugs placed in hydrogel release systems can be administered orally, nasally, rectally, vaginally and into the eyes. The use of hydrogels in the field of medical science is not limited to drug delivery. This type of biomaterial has a very wide range of applications, including the production of soft contact lenses, surgical implants, hybrid organs and biosensors. They are also used in pharmacy, cosmetology, tissue engineering and in the production of surgical tampons and even personal hygiene products [2–5]. The use of polymer biocomposite hydrogels for the treatment of difficult-to-heal wounds provides greater benefits compared with traditional gauze dressings, because they accelerate the wound-healing process, create a protective barrier for newly formed tissues and do not stick to the wound, which facilitates painless dressing replacement and allows following the healing process.

Pressure sores are difficult-to-treat chronic wounds. Their formation may be the result of long-term immobilisation caused by a chronic disease or systemic complications during the course of the underlying disease. Moreover, pressure sores may lead to serious systemic complications, such as dehydration, electrolyte disturbance, osteomyelitis or the development of sepsis [6, 7]. The pressure ulcer healing process is complex and involves regeneration of connective tissue and epidermis. Creating ideal conditions for this healing requires eliminating as many negative factors as possible that may delay or inhibit this process.

Chitosan is a natural cationic polysaccharide consisting of *N*-glucosamine and *N*-acetylglucosamine units linked by a β -1,4-glycosidic bond. Due to its unique biological properties, it has attracted great interest in the field of wound healing. It is an ideal material for the development of new dressings for wounds of various origins (pressure ulcers, burns and difficult-to-heal wounds such as diabetic foot and those infected by bacteria) [8]. Chitosan is used in wound dressings in various forms depending on the application: a hydrogel, membrane, foil, sponge, micro- and nanofibers or powders. As a polycation, chitosan combines with anionic polymers, which allows the creation of two- and three-dimensional structures, each with distinct porosity and mechanical strength. One of the forms mentioned most frequently in the literature is hydrogels. They consist of a three-dimensional network of hydrophilic polymers such as poly(ethylene glycol) (PEG), poly(acrylic acid) (carbomers) and poly(vinyl alcohol) (PVA). The polymer network allows for the absorption of significant amounts of water. Chitosan can be bound to the hydrogel through hydrogen bonds and hydrophobic interactions (physically) or incorporated into the network (chemically), which improves the mechanical strength of the gel [9]. Based on the literature, chitosan hydrogel has great potential in various stages

of the wound-healing process (at various stages): they reduce inflammation and have high sorption properties, thanks to which they retain water and provide a moist environment. Dressings based on chitosan hydrogel have also been described in the literature as a matrix to deliver pharmacological agents such as antibiotics, growth factors and stem cells, among others, which can further accelerate wound healing [10–12].

There is a focus on creating new antibacterial dressings for patients with difficult-to-heal wounds that are infected by antibiotic-resistant pathogenic bacteria. Such wounds are often a consequence of other serious diseases and irregularities in the functioning of our body, such as diabetes, autoimmune diseases, cancer and some medications taken on a permanent basis. Therefore, antibacterial agents, primarily antibiotics, are added to dressings. However, due to the increasing problems with combating antibiotic-resistant infections, there have been numerous attempts to combine polymer matrices with antimicrobial peptides, which may constitute a new direction in the treatment of resistant strains of pathogenic bacteria inhabiting the wound environment. Another innovative approach is the addition of biological factors, including bacteriophages and growth factors. When bacteriophages come into contact with the exudate of an infected wound, they actively fight the bacteria contained therein [13, 14]. Growth factors are often added to accelerate the healing and scarring processes and to improve the ability to repair damaged tissues. One of the most frequently used growth factors is basic fibroblast growth factor (bFGF), a polypeptide that regulates that cell growth, differentiation and angiogenesis [15].

Researchers have attempted to design adhesive nanocomposite hydrogels with photothermal antibacterial properties [10]. In one study, the authors generated a hydrogel dressing made of *N*-carboxyethyl chitosan (CEC) and Pluronic F127/carbon nanotubes (PF127/CNT). *In vivo* studies revealed their great potential as a photothermal therapy (PTT) dressing for infected wounds. The dressings showed adequate haemostatic activity, water absorption capacity, stable mechanical properties and good biodegradability [10]. Hydrogels loaded with the antibiotic moxifloxacin hydrochloride released the antibiotic depending on pH and showed good antibacterial activity. In another study, the researchers generated a chitosan hydrogel with silver nanoparticles that showed a good ability to combat difficult bacterial infections. They compared it with a commercially available reference dressing and found that the chitosan hydrogel had a stronger antibacterial effect, accelerated the healing process and showed very good organoleptic properties and proper adhesion to the wound [16].

This paper presents research related to the development of hydrogels constituting a matrix of dressing material, made of various biopolymers (chitosan and alginates) with an active substance with an analgesic effect (lidocaine hydrochloride [LidCl]). The pharmaceutical availability of LidCl from the hydrogel preparations and the rate of their release from the hydrogel through the membrane into the acceptor fluid were performed as for transdermal systems according to the Polish Pharmacopoeia, XI Edition [17]. Natural polymers from the polysaccharide group were used to construct dressings intended to treat pressure ulcers due to their specific biological properties, namely: biocompatibility; biodegradability; and the ability to accelerate the wound-healing process, to stimulate the body's immune mechanisms and to reduce the risk of infection by limiting bacterial growth [18–25]. The antibacterial activity of the hydrogel preparations against the gram-negative bacterium *Escherichia coli* and the gram-positive bacterium *Staphylococcus aureus* bacteria were assessed according to the JISL 1902:2002 standard).

2. Materials and Methods

2.1. Materials

This research used the following reagents:

- chitosan from Vanson Halo Source (USA) with an average molecular weight of 320.0 kDa, a degree of deacetylation of 77.5% and an ash content of 31 ppm;
- microcrystalline chitosan with a reduced pH of 6.65, a polymer content of 1.8 wt%, an average molecular weight of 284.0 kDa and a degree of deacetylation of 77.5% (created at the Łukasiewicz – Łódź Institute of Technology [ŁIT]);
- sodium alginate (Protanal LF 10/60), FMC BioPolymer (USA);
- glycerine, Fluka (p.a.) (USA), used as a plasticiser;
- lactic acid, Fluka (p.a.);
- sodium tripolyphosphate (TPP; Sigma-Aldrich, USA);
- calcium chloride anhydrous, Avantor Performance Materials Poland S.A. (p.a.) (Poland);
- lidocaine hydrochloride-2-(diethylamino)-*N*-(2,6-dimethylphenyl)acetamide hydrochloride monohydrate (Zakład Farmaceutyczny Amara®). LidCl is a local anaesthetic agent that can be used alone or in combination with sympathotonic amines. This derivative is used more often than LidCl as a pharmaceutical raw material for the production of painkillers [26].

2.2. Research Methodology

2.2.1. Production of Polymer Biocomposite Hydrogels Containing Lidocaine Hydrochloride

A polymer biocomposite in the form of a hydrogel (H/Ch/AlgNa/Ca/liof) was produced with microcrystalline chitosan (with a reduced pH = 6.65 and polymer content = 1.8 wt%) and sodium alginate lyophilisate containing 11 wt% calcium chloride. The chitosan microcrystalline hydrogel (MCCh) used in this research was manufactured by the authors from the raw material obtained from Vanson Halo Source according to the continuous method developed at Łukasiewicz – ŁIT [27, 28].

Two hydrogel mixtures were prepared with two weight contents of microcrystalline chitosan/alginate Na/Ca: 75:25 (H/Ch/AlgNa/Ca/liof/B) and 50:50 (H/Ch/AlgNa/Ca/liof/C). Additionally, the hydrogel preparations were cross-linked with TPP (2.0% by weight based on the dry weight of the composite). Cross-linking was carried out for 3 h at 5.5–6.0°C. In the final stage, a plasticiser (glycerine) was added to each preparation (0.4 parts by weight per 1 part by weight of the composite). LidCl was added separately to the mixtures – 3% by weight based on the dry weight of the polymers contained in the composite, in accordance with the dose recommended in the Polish Pharmacopoeia, XI Edition [17]. Table 1 presents the quantitative composition of the polymer biocomposite hydrogels.

Table 1. Quantitative composition of the chitosan/alginate-sodium-calcium biocomposite hydrogels (H/Ch/AlgNa/Ca/liof).

Sample	Quantitative composition of the hydrogel [wt%]					Total polymer content* [wt%]	pH
	MCCh	AlgNa/Ca	Glycerine	TPP	LidCl		
H/Ch/AlgNa/Ca/liof/B	52.82	17.24	27.59	1.38	–	1.76	6.86
H/Ch/AlgNa/Ca/liof/B/LidCl	51.72	17.24	27.59	1.38	2.07	1.77	6.91
H/Ch/AlgNa/Ca/liof/C	35.21	35.21	28.17	1.41	–	1.82	6.70
H/Ch/AlgNa/Ca/liof/C/LidCl	34.48	34.48	27.59	1.38	2.07	1.83	6.73

Note. *Polymer content (MCCh and AlgNa/Ca) in the composite hydrogel. Abbreviations: AlgNa/Ca, sodium alginate; LidCl, lidocaine hydrochloride; MCCh, chitosan microcrystalline hydrogel; TPP, sodium tripolyphosphate.

2.2.2. Rheological Evaluation of the Polymer Biocomposite Hydrogels Containing Lidocaine Hydrochloride

The dynamic viscosity, shear stress and shear rate were determined using a an RV DV-II digital viscometer with the Rheocalc V3.1-1 program (Brookfield, USA) at 25 and 37°C in accordance with the developed procedure [29]. The CPE-52 and CPE-41 cones were used to measure sample volumes of 0.5 and 2.0 ml, respectively. The thermostating time was 15 min.

2.2.3. Water Release Rate From the Polymer Composite Hydrogels

The rate of water loss from the polymer biocomposite hydrogels was determined. Approximately 1 g of the preparation was weighed with an accuracy of 0.0001 g and incubated at 37°C for the time necessary to obtain a constant mass. The sample was weighed at regular intervals to determine the loss of the initial mass of the preparation. The water loss process is described by equation (1) [30]:

$$m_t = m_a(1 - e^{-kt}) \quad (1)$$

where m_a is the total amount of water in the preparation [g] and m_t is the amount of water that evaporated after time t [g].

2.2.4. Evaluation of the Availability of Lidocaine Hydrochloride From the Polymer Biocomposite Hydrogels

The availability of LidCl from the polymer biocomposite hydrogels was carried out at the Department of Pharmaceutical Pharmacy, Department of Applied Pharmacy, Medical University of Łódź. The tests were performed as for transdermal systems, using a paddle apparatus (Figure 1) and an extraction chamber made of a chemically neutral material (Figure 2), which consisted of a base, an overlay and, if necessary, a semi-permeable membrane (dialysis tubing) made of regenerated cellulose with a pore size approximately 25 Å (Servapor, Sigma-Aldrich, USA). The extraction chamber held the polymer biocomposite hydrogel flat, parallel to the bottom edge of the paddle mixer with the release surface facing upwards. The distance between the paddle mixer

and the surface of the polymer biocomposite hydrogel was constant at 25 ± 2 mm. Each sample weighed approximately 2.5 g. The acceptor fluid was 100 ml of 0.9% sodium chloride (physiological saline). The tests were carried out at $32 \pm 0.5^\circ\text{C}$ and a stirrer speed of 100 rpm. The LidCl concentration in the receptor fluid was determined spectroscopically at 262 nm after 5, 15, 30, 60, 120 and 180 min.



Figure 1. Paddle apparatus for testing *in vitro* the release rate of lidocaine hydrochloride from the polymer biocomposite hydrogels.



Figure 2. Extraction chamber.

2.2.5. Determining the Rate of Lidocaine Hydrochloride Release From the Polymer Composite Hydrogels Into an Acceptor Fluid

The rate of release of LidCl from the polymer biocomposite hydrogels into the acceptor fluid was carried out at the Department of Pharmacy, Department of Applied Pharmacy, Medical University of Łódź. A diffusion apparatus consisting of a donor chamber and an acceptor chamber, separated by a semi-permeable membrane (dialysis tubing) made of regenerated cellulose with a pore size of approximately 25 \AA (Servapor; Figure 3), was used for the tests. A hydrogel preparation weighing approximately 1.0 g was applied to the membrane. Then, 25 ml of physiological saline or phosphate buffer (pH 7.4) was introduced into the acceptor cell. The contact area of the membrane with the acceptor fluid was 0.785 cm^2 . The measurement was performed at $32 \pm 0.5^\circ\text{C}$ with constant stirring

of the acceptor fluid. The amount of the LidCl released was determined spectrophotometrically at 262 nm after 5, 15, 30, 60, 120 and 180 min.

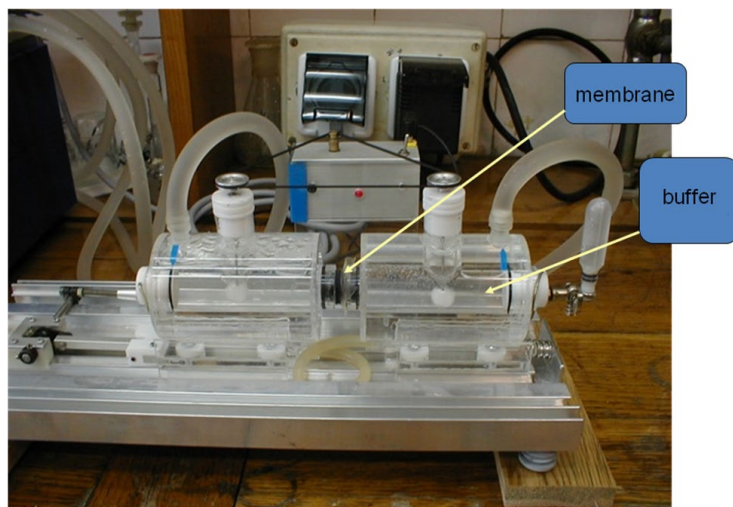


Figure 3. The photograph of a diffusion apparatus used to determine the rate of lidocaine hydrochloride release from the polymer biocomposite hydrogels into the acceptor fluid.

2.2.6. Evaluating the Antibacterial Activity of the Polymer Biocomposite Hydrogels

The antibacterial effect of the polymer biocomposite hydrogels was determined at the Microbiological Laboratory of the Lukasiewicz – ŁIT in accordance with the institution's 'Testing of the antibacterial effect of textile products. Quantitative test' (5th edition) research protocol, developed based on the JIS L 1902:2002 standard. The study consisted of assessing the inhibition of the growth of standard bacterial strains in contact with the tested sample. The number of bacteria on the sample was assessed before and after incubation for 24 h relative to the inactive sample as a control (reference material was cotton).

The number of bacteria (*E. coli* and *S. aureus*) on the control sample before incubation and the number of bacteria that survived on the control sample and test samples after incubation were determined. Based on the number of bacteria, the bacteriostatic and bactericidal activity was determined, calculated according to equations (2) and (3), respectively:

$$S = Mb - Mc, \text{ and} \quad (2)$$

$$L = Ma - Mc. \quad (3)$$

The terms in equations (2) and (3) mean the following:

- S – bacteriostatic activity;
- L – bactericidal activity;
- Ma – common logarithm of the number of bacteria on the sample without the active agent immediately after inoculation;
- Mb – common logarithm of the number of bacteria on the sample without the active agent after incubation for 24 h; and
- Mc – common logarithm of the number of bacteria on the sample with the active agent after incubation for 24 h.

According to the JIS L 1902:2002 standard, $L > 0$ indicates bactericidal activity, while $S > 2$ bacteriostatic activity [31].

3. Results and Discussion

The main goal of this research was to develop a multifunctional dressing in the form of a polymer biocomposite containing the analgesic LidCl and to assess the rheological properties, water-releasing ability and biological activity. The developed dressing is intended for the treatment of difficult-to-heal wounds, in particular, pressure ulcers. Biopolymers such as chitosan and alginates are used to develop dressings due to their specific properties useful in the treatment of difficult-to-heal wounds. Chitosan is a biopolymer with biostimulatory properties that can accelerate the influx of phagocytic cells to the wound site, which cleanse the wound of necrotic tissues and stimulate the migration and proliferation of intraepithelial cells and fibroblasts. This polymer also impairs the growth of bacteria and fungi, which reduces the risk of wound infection. High biological activity predisposes this polymer to the production of modern dressings used to treat difficult-to-heal wounds (bedsores) [23, 32–37]. Alginates are one of the most frequently used natural polymers used to produce dressing materials due to their biological properties: biocompatibility, biodegradability, absorbent properties and the ability to stimulate the growth of fibroblasts. The interaction of alginates, such as sodium alginate, with divalent calcium cations (Ca^{2+}) leads to the formation of gels; this phenomenon has been used in the design and production of active dressings that have haemostatic properties and support the blood coagulation process. The ability to swell and absorb fluids becomes particularly important when using ‘moist wound therapy’. A hydrophilic, moist coating is created on the wound surface, maintaining a warm, healing environment without the adverse effects of occlusion [38–41].

3.1. Assessment of the Rheological Properties of the Polymer Biocomposite Hydrogels

Polymers that have the ability to create hydrogels, retain water in their structure and have adhesive properties to the surface of damaged tissue are valuable materials for the construction of special dressings. The properties of such polymers are determined by the intermolecular forces between the chains and their spatial structure. Intermolecular interactions have a significant impact on the rheological properties of polymer solutions, as well as the rate of release of the medicinal substance from the dressings produced with their participation; moreover, the ability to create gel forms is determined by the formation of hydrogen bridges between the chains of these polymers [42–44]. Therefore, rheological tests play an important role in the development of therapeutic hydrogel dressings containing medicinal substances. The dynamic viscosity, shear stress and shear rate of the polymer biocomposite hydrogels containing LidCl were determined at 25°C (based on the measurement procedure) and at 37°C (the temperature of the human body). The results are presented in Figures 4–7.

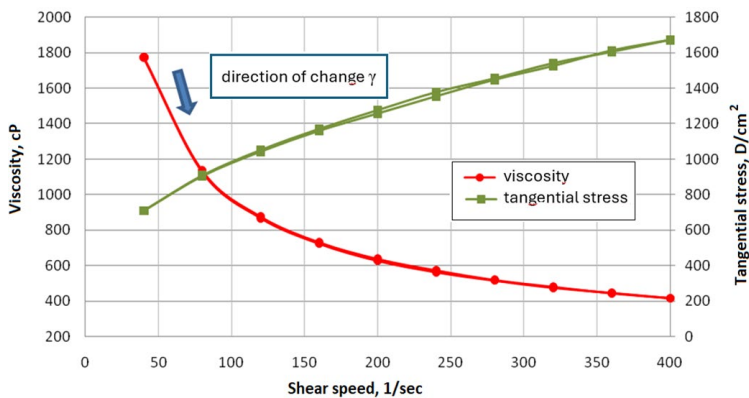


Figure 4. Dependence of viscosity and shear stress on the shear rate (γ) at 25°C for the H/Ch/AlgNa/Ca/liof/B/LidCl hydrogel. See Table 1 for details on the hydrogel.

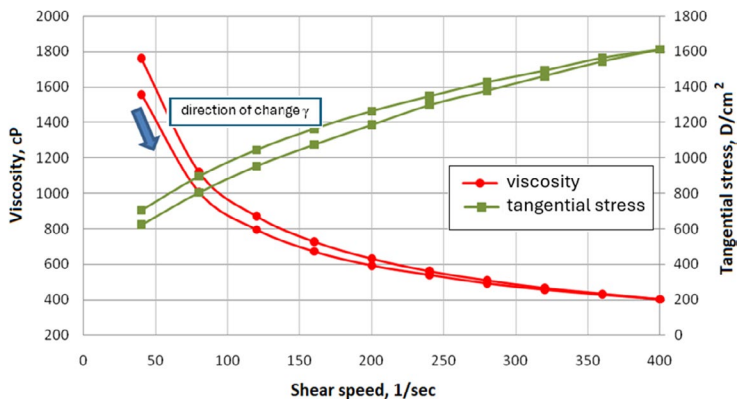


Figure 5. Dependence of viscosity and shear stress on the shear rate (γ) at 37°C for the H/Ch/AlgNa/Ca/liof/B/LidCl hydrogel. See Table 1 for details on the hydrogel.

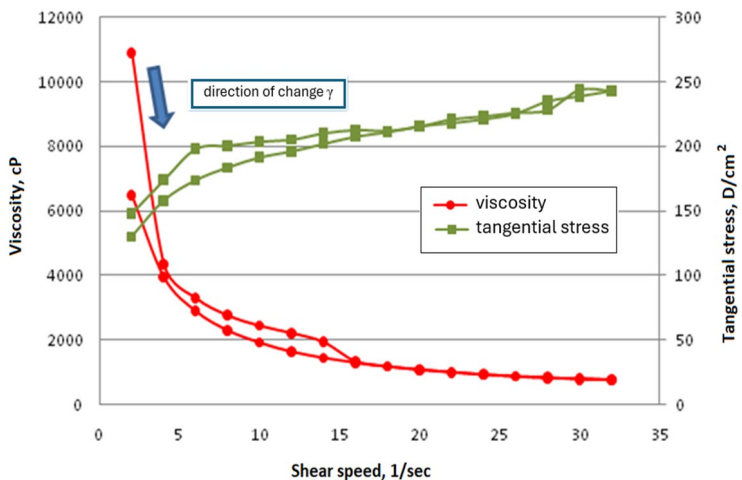


Figure 6. Dependence of viscosity and shear stress on the shear rate (γ) at 25°C for the H/Ch/AlgNa/Ca/liof/C/LidCl hydrogel (diluted to 1%). See Table 1 for details on the hydrogel.

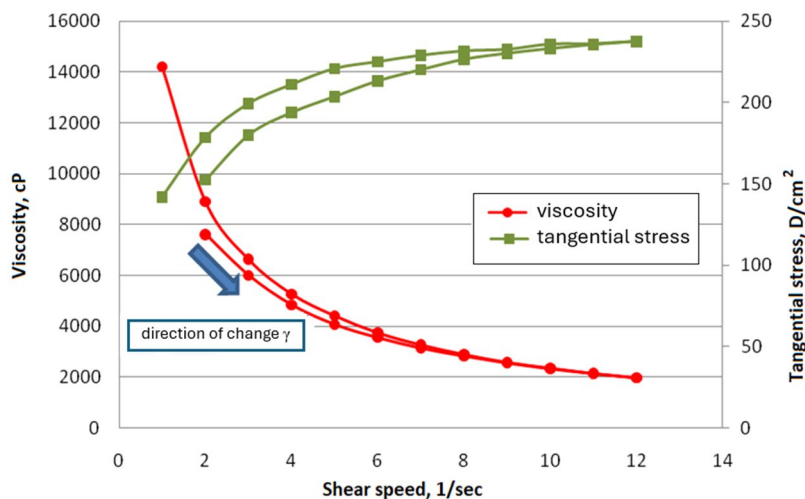


Figure 7. Dependence of viscosity and shear stress on the shear rate (γ) at 37°C for the H/Ch/AlgNa/Ca/liof/C/LidCl hydrogel (diluted to 1%). See Table 1 for details on the hydrogel.

Figures 4–7 show the flow curves of hydrogel preparations in the coordinate system $\eta = f(\gamma)$ and $\tau = f(\gamma)$, where η is the dynamic viscosity [cP], τ is the shear stress [D/cm²] and γ is the shear rate [1/sec]. The tested polymer biocomposite hydrogels varied in terms of composition and showed the characteristics of non-Newtonian, pseudoplastic (shear-thinned) liquids. For most of them, there were hysteresis loops in the flow curve diagrams when the shear rate was increased or decreased. However, the following hydrogel preparations showed an antithixotropic character during shear: H/Ch/AlgNa/Ca/liof/B/LidCl and H/Ch/AlgNa/Ca/liof/C/LidCl (diluted to 1%) at 37°C. Diluting the polymer biocomposite hydrogel with water to a concentration of 1% by weight was necessary to reduce the viscosity so that it could be measured with the instrument (as described in Section 2.2.2). At 25°C, the polymer biocomposite hydrogel (H/Ch/AlgNa/Ca/liof/B/LidCl) was rheologically stable, and its properties did not depend on shear forces. However, the H/Ch/AlgNa/Ca/liof/C/LidCl (diluted to 1%) hydrogel presented the characteristics of a thixotropic liquid thinned by shear when measured at 25°C; the ‘thinning’ effect persisted after the shear forces ceased. The consequence of this phenomenon was the destruction of the molecular structure of the hydrogel.

3.2. Assessment of the Water Release Rate From the Polymer Biocomposite Hydrogels

Functional dressings intended for the treatment of difficult-to-heal wounds – in particular, pressure sores – should ensure the effective action of the medicinal substance contained in them and provide appropriate comfort. An extremely important and desirable feature of dressings is maintaining appropriate moisture in the wound, ensuring greater effectiveness and faster healing. A moist environment ensures better penetration of active substances into the wound and allows easy and painless replacement of the dressing without the risk of damaging the tissue rebuilt as a result of granulation and epithelisation. Figure 8 presents the water release rate from the polymer biocomposite hydrogels.

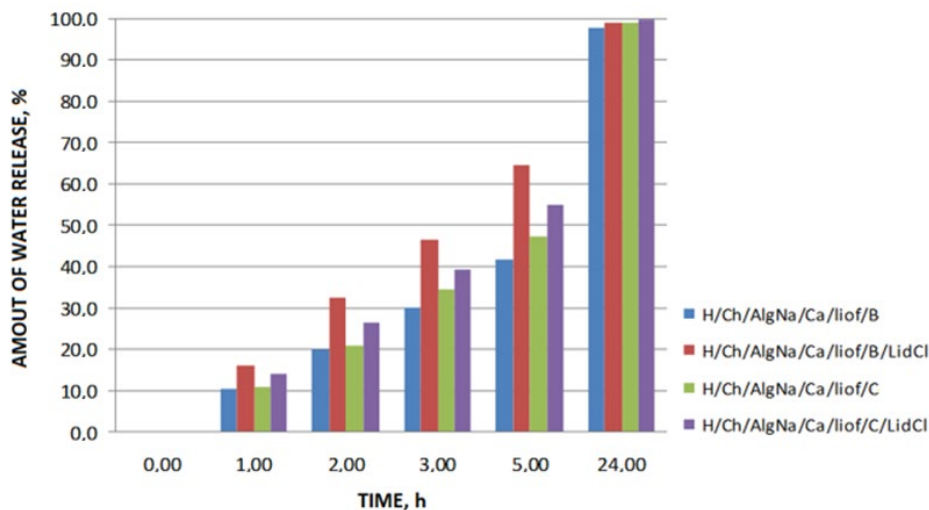


Figure 8. Changes in the amount of water released by the polymer biocomposite hydrogels H/Ch/AlgNa/Ca/liof/B, H/Ch/AlgNa/Ca/liof/B/LidCl, H/Ch/AlgNa/Ca/liof/C and H/Ch/ AlgNa/Ca/liof/C/LidCl as a function of time. See Table 1 for details on the hydrogels.

After 5 h, the polymer biocomposite hydrogels with LidCl released water faster compared with the polymer biocomposite hydrogels without LidCl. After 24 h, almost all water had been released from the polymer biocomposite hydrogels. Therefore, they can be assumed to maintain moisture at the appropriate level and allow appropriate wound healing.

3.3. Availability of Lidocaine Hydrochloride from the Polymer Biocomposite Hydrogels

As described in Section 2.2.4, the availability of LidCl from the polymer biocomposite hydrogels was determined. Table 2 lists the parameters of the kinetic equation describing the release of LidCl from the polymer biocomposite hydrogels, and Figures 9 and 10 show the amount of released LidCl as a function of time.

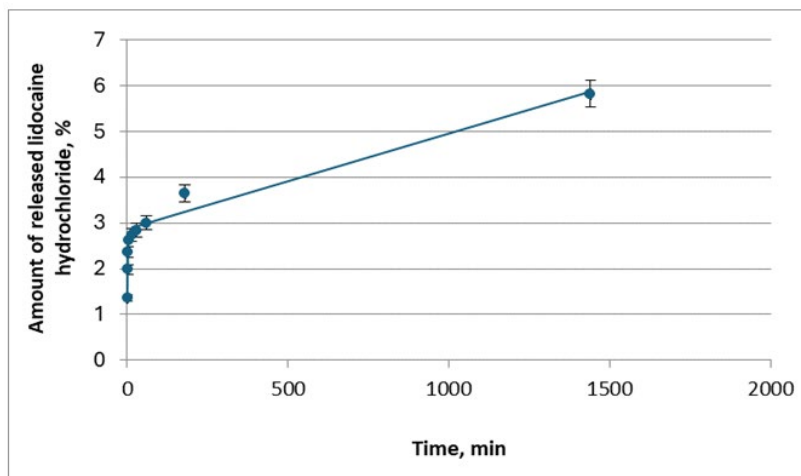


Figure 9. Release kinetics of lidocaine hydrochloride from the H/Ch/AlgNa/Ca/liof/C/LidCl hydrogel. See Table 1 for details on the hydrogel.

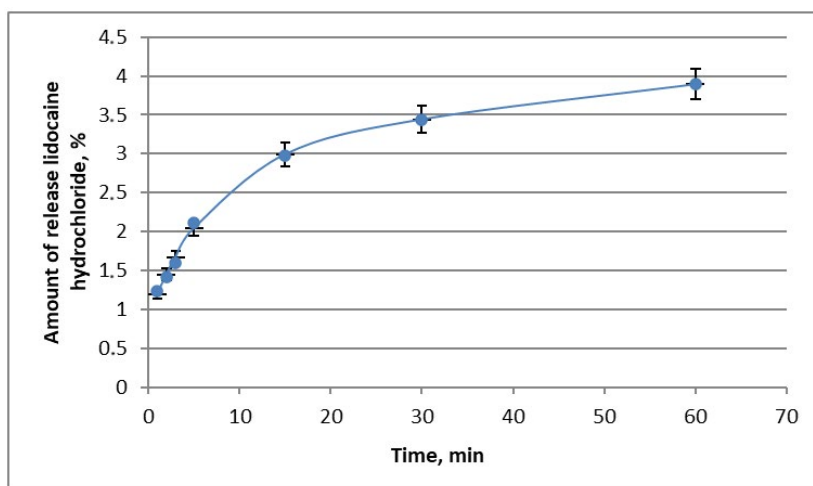


Figure 10. Release kinetics of lidocaine hydrochloride from the H/Ch/AlgNa/Ca/liof/B/LidCl hydrogel. See Table 1 for details on the hydrogel.

Table 2. Parameters of the kinetic equation describing the release rate of lidocaine hydrochloride from the polymer biocomposite hydrogels.

Sample	a_0 [%]	Stage I			Stage II		
		a_1 [%]	k_1 [min ⁻¹]	$t_{0.5}$ [min]	a_2 [%]	$k_2 \times 10^5$ [min ⁻¹]	$t_{0.5}$ [h]
H/Ch/AlgNa/Ca/liof/C/LidCl	0.46	2.40	0.477	1.45	97.14	2.18	530
H/Ch/AlgNa/Ca/liof/B/LidCl	0.91	2.15	0.137	5.07	96.94	14.38	80

Note. See Table 1 for details on the hydrogels. Abbreviations: a_0 , 100 – a_1 – a_2 , the amount of ‘unbound’ lidocaine hydrochloride [%]; a_1 and k_1 , constants describing the first stage; a_2 and k_2 , constants describing the second stage; $t_{0.5}$, release half-life for each stage.

After 1440 min, 5.82% of LidCl had been released from the H/Ch/AlgNa/Ca/liof/C/LidCl hydrogel. After 60 min, approximately 3.89% of LidCl had been released from the H/Ch/AlgNa/Ca/liof/B/LidCl hydrogel.

The H/Ch/AlgNa/Ca/liof/C/LidCl and H/Ch/AlgNa/Ca/liof/B/LidCl hydrogels showed a similar course of LidCl release directly (without membrane usage) into physiological saline. There was a fast initial release, followed by very slow release. This pattern indicates LidCl release follows first-order kinetics and is a complex process. The determined parameters of the kinetic equation revealed a significant slowdown in the release of LidCl from the H/Ch/AlgNa/Ca/liof/C/LidCl hydrogel during the second stage of the process, with a release half-time ($t_{0.5}$) of 530 h.

3.4. Release of Lidocaine Hydrochloride From the Polymer Biocomposite Hydrogels Into an Acceptor Fluid

The developed dressing is a transdermal therapeutic system, which, in addition to the possibility of controlled drug release, allows the administration of drugs that are broken down in the gastrointestinal tract or metabolised in the liver. A diffusion apparatus consisting of donor and acceptor chambers (Figure 4), separated

by a semi-permeable membrane made of regenerated cellulose with a pore size of approximately 25 Å, was used to assess the release of LidCl from the hydrogels to the acceptor fluid, as described in Section 2.2.5. The dressings contained a medicinal substance in the form of lidocaine hydrochloride. Table 3 lists the determined values of the parameters of the kinetic equation describing the rate of release of LidCl, and Figures 11 and 12 show the amount of released LidCl as a function of time.

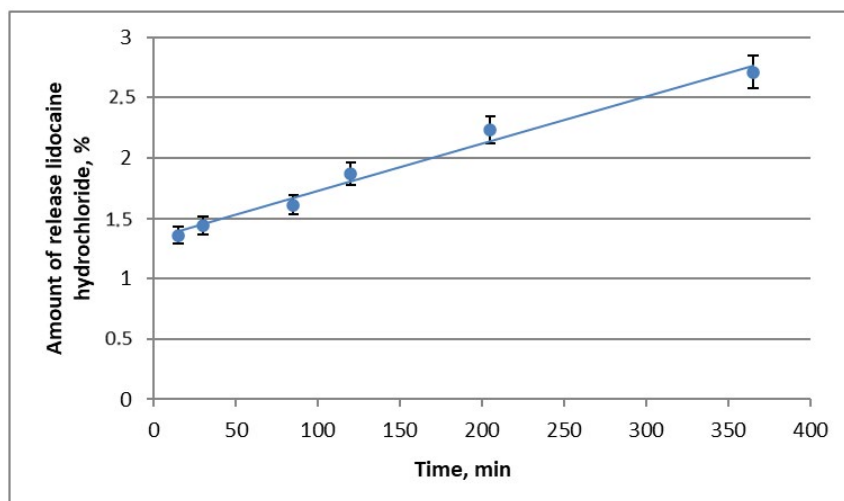


Figure 11. Release kinetics of lidocaine hydrochloride from the H/Ch/AlgNa/Ca/lidf/C/LidCl hydrogel. See Table 1 for details on the hydrogel.

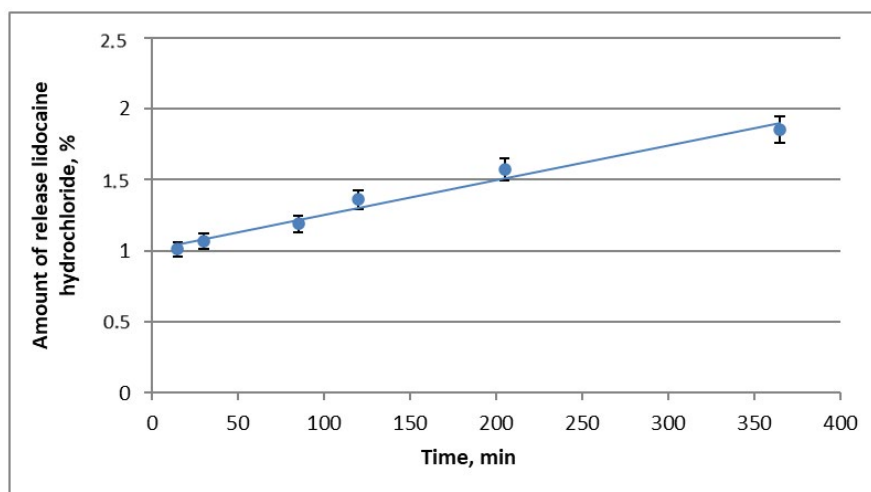


Figure 12. Release kinetics of lidocaine hydrochloride from the H/Ch/AlgNa/Ca/lidf/B/LidCl hydrogel. See Table 1 for details on the hydrogel.

Table 3. Parameters of the kinetic equation describing the release rate of lidocaine hydrochloride from the polymer biocomposite hydrogels.

Hydrogel dressing symbol	a_0 [%]	Stage I			Stage II		
		a_1 [%]	k_1 [min ⁻¹]	$t_{0.5}$ [min]	a_2 [%]	$k_2 \times 10^5$, [min ⁻¹]	$t_{0.5}$ [h]
H/Ch/AlgNa/Ca/liof/C/LidCl	1.33	-	-	-	98.67	4.02	288
H/Ch/AlgNa/Ca/liof/B/LidCl	1.01	-	-	-	98.99	2.47	468

Note. See Table 1 for details on the hydrogels. Abbreviations: a_0 , 100 – a_1 – a_2 , the amount of ‘unbound’ lidocaine hydrochloride [%]; a_1 and k_1 , constants describing the first stage; a_2 and k_2 , constants describing the second stage; $t_{0.5}$, release half-life for each stage.

After 365 min, approximately 1.85% and 2.71% LidCl had been released from the H/Ch/AlgNa/Ca/liof/C/LidCl and H/Ch/AlgNa/Ca/liof/B/LidCl hydrogels, respectively, to the acceptor fluid. These hydrogels had a release process controlled by diffusion through the membrane.

3.5. Assessment of the Antibacterial Activity of the Polymer Biocomposite Hydrogels

The gram-negative bacterium *E. coli* is a natural physiological component of the gastrointestinal flora of humans and animals and but can often cause infections, the clinical symptoms and course of which depend on the place of their occurrence [45]. The gram-positive bacterium *S. aureus* can cause local infections of virtually all tissues and organs as well as a general infection of the body, which is often life-threatening [46]. These bacteria were adopted as model pathogens, approximating the conditions occurring in the wound and causing wound infection, to assess the antibacterial activity of the polymer biocomposite hydrogels. To test the antibacterial activity, the hydrogel preparations were sterilised with ultraviolet radiation for 20 min. Based on the results in Table 4, the tested polymer biocomposite hydrogels showed bacteriostatic and bactericidal properties against *E. coli* bacteria and *S. aureus*.

Table 4. Antibacterial activity of the polymer biocomposite hydrogels containing lidocaine hydrochloride.

Biocomposite symbol	Number of bacteria [cfu/sample]	Bacterium	Bacteriostatic activity (S)	Bactericidal activity (L)
Control (cotton)	1.9×10^4	<i>Escherichia coli</i> ATCC 11229	–	–
H/Ch/AlgNa/Ca/liof/B/LidCl	< 20		7.0	3.0
H/Ch/AlgNa/Ca/liof/C/LidCl	< 20		7.0	3.0
Control (cotton)	1.3×10^4	<i>Staphylococcus aureus</i> ATCC 6538	–	–
H/Ch/AlgNa/Ca/liof/B/LidCl	7.0×10^1		4.4	2.1
H/Ch/AlgNa/Ca/liof/C/LidCl	8.8×10^4		4.9	2.3

Note. See Table 1 for details on the hydrogels. Abbreviation: cfu, colony-forming units.

4. Conclusions

Polymer biocomposite hydrogels based on microcrystalline chitosan with a reduced pH and sodium alginate and carrying the analgesic LidCl, intended for the treatment of difficult-to-heal pressure ulcers, was developed. The hydrogels exhibited the characteristics of non-Newtonian, pseudoplastic (shear-thinned) liquid, for which the dynamic viscosity decreased as the shear rate increased. The hydrogels containing LidCl released water faster than the hydrogels without LidCl. The release of LidCl from the polymer biocomposite hydrogels is a complex process that follows first-order kinetics. By changing the composition and amount of individual polymers in the biocomposite, it will probably be possible to control the release rate of LidCl, or whatever active substance is included in the hydrogel. Finally, the polymer biocomposite hydrogels showed antibacterial activity against the gram-negative bacterium *E. coli* and the gram-positive bacterium *S. aureus*.

5. Acknowledgments

The authors thank Prof. Kazimiera Bodek and Dr Andrzej Bodek for cooperation in the research presented in this publication.

6. References

- [1] Pilarz LP; (2018) Selected technological solutions in medicine. Tygiel Scientific Publishing, Lublin.
- [2] Maciejewski R, Zubrzycki J; (2015) Biomedical engineering. Techniques, technologies, research, monographs. Lublin University of Technology, Lublin.
- [3] Peppas NA, Bures P, Leobandung W, Ichikawa H; (2000) Hydrogels in pharmaceutical formulations. *Eur J Pharm Biopharm* 50, 27–46. DOI:10.1016/s0939-6411(00)00090-4
- [4] Pluta J, Karolewicz B; (2004) Hydrogels: properties and application in the technology of drug form. I. The characteristic hydrogels. *Polim Med* 34(2), 3–19.
- [5] Hoffman AS; (2012) Hydrogels for biomedical applications. *Adv Drug Deliver Rev* 64, 18–23. DOI:10.1016/j.addr.2012.09.010
- [6] Sopata M; (2009) Etiology and pathogenesis of pressure ulcers. *Inforanek* 1(4), 4–5.
- [7] Szewczk MT, Cwajda J; (2005) New generation dressings. *Zakażenia* 5, 94–99.
- [8] Wang K, Pan S, Qi Z, Xia P, Xu H, Kong W, Li H, Xue P, Yang X, Fu Ch; (2020) Recent advances in chitosan-based metal nanocomposites for wound healing applications. *Adv Mater Sci Eng* 2020(1), 3827912. DOI:10.1155/2020/3827912
- [9] Sikora M, Wiśniewska-Wrona M, Arabski M; (2021) Biomedical properties of chitosan: application in tissue engineering. *Postępy Hig Med Dośw* 75(1), 1020–1037. DOI:10.2478/ahem-2021-0015
- [10] Feng P, Luo Y, Ke C, Qiu H, Wang W, Zhu Y, Hou R, Xu L, Wu S; (2021) Chitosan-based functional materials for skin wound repair: mechanisms and applications. *Front Bioeng Biotechnol* 9, 650598. DOI:10.3389/fbioe.2021.650598
- [11] Liu H, Wang Ch, Li Ch, Qui Y, Wan Z, Yang F, Li Z, Wang J; (2018) A functional chitosan-based hydrogel as a wound dressing and drug delivery system in the treatment of wound healing, *RSC Adv* 8(14), 7533–7549. DOI:10.1039/C7RA13510F

- [12] Matica MA, Aachmann FL, Tøndervik A, Sletta H, Ostafe V; (2019) Chitosan as a wound dressing starting material: antimicrobial properties and mode of action. *Int J Mol Sci* 20(23), 5889. **DOI:**10.3390/ijms20235889
- [13] Taute H, Bester MJ, Gaspar ARM; (2019) The dual functionality of antimicrobial peptides Os and Os-C in human leukocytes. *J Pep Sci* 25 (4), e3156. **DOI:**10.1002/psc.3156
- [14] Gómez-Sequeda N, Ruiz J, Ortiz C, Urquiza M, Torres R; (2020) Potent and specific antibacterial activity against *Escherichia coli* O157:H7 and methicillin resistant *Staphylococcus aureus* (MRSA) of G17 and G19 peptides encapsulated into poly-lactic-co-glycolic acid (PLGA) nanoparticles. *Antibiotics* 9(7), 384. **DOI:**10.3390/antibiotics9070384
- [15] Xu H-L, Chen P-P, ZhuGe D-L, Zhu Q-Y, Jin B-H, Shen B-X, Xiao J, Zhao Y-Z (2017) Liposomes with silk fibroin hydrogel core to stabilize bFGF and promote the wound healing of mice with deep second-degree scald. *Adv Healthc Mater* 6(19), 1700344. **DOI:**10.1002/adhm.201700344
- [16] Wang Y, Xie R, Li Q, Dai F, Lan G, Shang S, Lu F; (2020) A self-adapting hydrogel based on chitosan/oxidized konjac glucomannan/AgNPs for repairing irregular wounds. *Biomater Sci* 8, 1910–1922. **DOI:**10.1039/c9bm01635j
- [17] Farmakopea Poland, XI edn.; (2017). PTFarm, Warszawa
- [18] Rinaudo M; (2008) Main properties and current applications of some polysaccharides as biomaterials. *Polym Int* 57, 397–430. **DOI:**10.1002/pi.2378
- [19] Rinaudo M; (2006) Chitin and chitosan: Properties and applications. *Prog Polym Sci* 31(7), 603–632. **DOI:**10.1016/j.progpolymsci.2006.06.001
- [20] Jayakumar R, Prabakaran M, Sudheesh Kumar PT, Nair SV, Tamura H; (2011) Biomaterials based on chitin and chitosan in wound dressing applications. *Biotechnol Adv* 29(3), 322–337. **DOI:**10.1016/j.biotechadv.2011.01.005
- [21] Skoľucka-Szary K, Rieske P, Piaskowski S; (2016) Practical aspects of the use of chitin and its derivatives in wound treatment. *Chemik* 70(2), 89–98.
- [22] Anitha A, Sowmya S, Sudheesh Kumar PT, Deepathi S, Chennazhi KP, Ehrlich H, Tsurkan M, Jayakumar R; (2014) Chitin and chitosan in selected biomedical applications. *Prog Polym Sci* 39(9), 1644–1667. **DOI:**10.1016/j.progpolymsci.2014.02.008
- [23] Kędzierska M, Miłowska K; (2019) The use of chitosan-based biomaterials for the treatment of hard - healing wounds. *Postępy Hig Med Dośw* 73, 768–781. **DOI:**10.5604/01.3001.0013.6823
- [24] Zou P, Yang X, Wang J, Li Y, Yu H, Zhang Y, Liu G; (2016) Advances in characterization and biological activities of chitosan and chitosan oligosaccharides *Food Chem* 190, 1174–1181. **DOI:**10.1016/j.foodchem.2015.06.076
- [25] Xia W, Liu P, Zhang J, Chen J; (2011) Biological activities of chitosan and chitoooligosaccharides. *Food Hydrocoll* 25(2), 170–179. **DOI:**10.1016/j.foodhyd.2010.03.003
- [26] Pawłowski M, Żmudzki P (2009) Rozdział 11: Leki działające na drobnoustroje chorobotwórcze. In: Zejc A, Górczyca M (eds), *Chemia leków*. PZWL Wydawnictwo lekarskie, Warszawa.
- [27] Struszczyk H; (1991) PL 164 247 – Continuous method of producing microcrystalline chitosan.
- [28] Struszczyk H; (1987) Microcrystalline chitosan. I. Preparation and properties of microcrystalline chitosan. *J Appl Polym Sci* 33(1), 177–189. **DOI:**10.1002/app.1987.070330115

- [29] SPR/BPB/25 - Determination of dynamic viscosity of polymer solutions Brookfield's method, according to GLP Nr. G-016 (Lukasiewicz-LIT).
- [30] Bodek KH; (2002) Habilitation thesis. Assessment of the suitability of microcrystalline chitosan as a polymeric drug carrier. Medical Academy.
- [31] Kaźmierczak D, Guzińska K, Dymel M; (2016) Antibacterial activity of PLA fibres estimated by quantitative methods. *Fibres Text East Eur* 24(2), 126–130. DOI:10.5604/12303666.1191437
- [32] Falanga V; (2000) Classifications for wound bed preparation and stimulation of chronic wounds. *Wound Repair Regen* 8(5), 347–352. DOI:10.1111/j.1524-475X.2000.00347.x
- [33] Zarzycki R, Modrzejewska Z, Wylon E; (2004) Chitosan – gentamycin membranes with prolonged antibiotic activity. *Progr Chem Appl Chitin Deriv* 10, 83.
- [34] Guo Y, Qiao D, Zhao S, Liu P, Xie F, Zhang B; (2024) Biofunctional chitosan - biopolymer composites for biomedical applications, *Mat Sci Eng R* 159, 100775. DOI:10.1016/j.mser.2024.100775
- [35] Shah A, Ali Buabeid M, Arafa EA, Hussain I, Li L, Murtaza G; (2019) The wound healing and antibacterial potential of triple-component nanocomposite (chitosan-silver-sericin) films loaded with moxifloxacin. *Int J Pharm* 564, 22–38. DOI:10.1016/j.ijpharm.2019.04.046
- [36] Paul ED, Garba ZN, James DO; (2018) Chitosan, a natural polymer for health. *ATBU J Sci Technol Edu* 6(4).
- [37] Singh R, Shitiz K, Singh A; (2017) Chitin and chitosan: biopolymers for wound management. *Int Wound J* 14, 1276–1289. DOI:10.1111/iwj.12797
- [38] Kashma K, Imai M; (2012) Advanced membrane material from Marine biological polymer and sensitive molecular-size recognition for promising separation technology. In: Ning RY (Ed), *Advancing Desalination*. InTech Open, Rijeka. DOI:10.5772/50734
- [39] Szewczyk MT, Jawień A, Cierzniaowska K, Cwajda J; (2004) Principles of selecting hydrofiber and alginate dressings in the treatment of venous ulcers. *Infections* 6, 158–165.
- [40] Dalheim MØ, Vanacker J, Najmi MA, Aachmann FL, Strand BL, Christensen BE; (2015) Efficient functionalization of alginate biomaterials, *Biomaterials* 80, 146–156. DOI:10.1016/j.biomaterials.2015.11.043
- [41] Wahl EA, Fierro FA, Peavy TR, Hopfner U, Dye JF, Machens HG, Egaña JT, Schenck TL; (2015) *In vitro* evaluation of scaffolds for the delivery of mesenchymal stem cells to wounds. *Biomed Res Int* 2015, 108571. DOI:10.1155/2015/108571
- [42] Górecki M; (1998) Fizykochemiczne problemy układów substancja lecznicza – polimer. *Farm Pol* 54, 590–592.
- [43] Jia B, Li G, Cao E, Luo J, Zhao X, Huang H; (2023) Recent progress of antibacterial hydrogels in wound dressings. *Mat Today Bio* 19, 100582. DOI:10.1016/j.mtbio.2023.100582
- [44] Ramazani A, Aghahosseini H; (2020) Chapter 9 – The biological properties of hydrogels based on natural polymers. In: Chen Y (ed), *Hydrogels based on natural polymers*. Elsevier, 247-269. DOI:10.1016/B978-0-12-816421-1.00009-4
- [45] Kołodynski J; (1998) *Podstawy bakteriologii*. Uniwersytet Wrocławski.
- [46] Szewczyk E; (2007) *Diagnostyka bakteriologiczna*. Polskie Wydawnictwo Naukowe, Warszawa.

EFFECT OF CHITOSAN WITH DIFFERENT MOLECULAR WEIGHT ON THE GROWTH AND BULB YIELD OF ORIENTAL LILY ‘MONA LISA’

Agnieszka Zawadzińska^{1,a,*}, Piotr Salachna^{1,b}

¹ – Department of Horticulture, West Pomeranian University of Technology Szczecin, Słowackiego 17 Str., 71-434 Szczecin, Poland

^a – ORCID: 0000-0002-0882-9919, ^b – ORCID: 0000-0003-0403-8519

*corresponding author: agnieszka.zawadzinska@zut.edu.pl

Abstract

The potential of biodegradable and environmentally friendly substances that exhibit biostimulatory effects on plant growth and yield is now being exploited in horticultural production. This study evaluated the effect of chitosan on the growth, flowering, and yield of bulb of oriental lily ‘Mona Lisa’. Three types of chitosan differing in molecular weight (MW) were used: commercial chitosan (CCh, MW = 50,000–190,000 g/mol) and two forms of depolymerised chitosan (DCh 48, with a MW of ~48,000 g/mol, and DCh 154, with a MW of ~154,500 g/mol). The plants were watered twice with an aqueous solution of chitosan at a concentration of 2 g/l, with 100 ml of solution per pot. The control was plants watered with distilled water. Chitosan had a biostimulatory effect on the growth of lily plants. CCh increased the relative chlorophyll content of leaves (+11.3%), the fresh bulb weight (+11.0%), the bulb diameter (+12.3%) and the number of bulblets (+44.9%) compared with the control plants. DCh 154 significantly increased the fresh aboveground weight of plants (+31.3%), the fresh weight of leaves (+29.0%) and their number (+16.8%), the fresh weight of bulb (+12.3%) and their diameter (+11.0%), and the fresh weight of bulblet (+21.9%). DCh 48 increased the bulb diameter (+12.1%) and the number of bulblets (+45.4%), but decreased the length (-8.6%) and width of tepals (-6.8%) of the lily flowers. Finally, DCh 154 was the most effective in lily production. Using depolymerised chitosan as a biostimulant may contribute to developing new methods to produce high-quality lily plants.

Keywords: oligochitosan, biostimulant, plant propagation, sustainable agriculture

Received: 15.03.2024

Accepted: 13.05.2024

1. Introduction

The production of ornamental plants is a rapidly growing and profitable segment in horticultural production [1]. Among the activities determining the continued development of the floriculture industry is the search for new strategies for growing and propagating plants [2]. Limitations in the use of agrochemicals, as well as economic factors, affect the yield and flower quality. Today, natural biostimulants are increasingly being used to improve the growth and increase the yield of plants [3]. This group includes many substances of natural origin and microorganisms with high biological activity [4]. One of the best-known is chitosan, a natural polysaccharide that consists of molecules of D-glucosamine and N-acetyl-D-glucosamine linked by β -1,4-glycosidic bonds [5]. Chitosan is formed by deacetylation of chitin contained in the chitinous carapaces of transformed crustaceans and the cell walls of fungi [6]. This compound is biodegradable and exhibits numerous biological effects [7]. Du Jardin [8] included chitosan and other polymers in one of seven categories of biostimulants. Studies on ornamental plants have proven that chitosan has a biostimulatory effects on plant growth, flowering and specific physiological processes [9, 10]. It has also been shown to stimulate plant defence mechanisms, inducing plant resistance to pathogenic fungi and bacteria. In addition, chitosan is effective in alleviating the effects of abiotic stresses [11, 12]. It can be applied alone as an aqueous solution for watering and spraying plants or as a component, such as hydrogels for coating seeds [13–15].

After tulips, lilies (*Lilium* spp.) are the most cultivated bulbous plants in the world; they are grown for cut flowers and as very decorative perennials for gardens and potted plants [16]. In addition, some species of lilies are offered as vegetables [17]. These plants are versatile in horticulture, so there is a great demand for their bulbs and improved production methods [18, 19]. Lilies from the group of oriental hybrids have very attractive flowers. They have a relatively long production time and are considered difficult to grow, mainly due to their high susceptibility to diseases, unfavourable growing conditions and low propagation rate [20]. On a production scale, lilies are propagated effectively and without great expense from scales, and growth regulators [21] and biostimulants [22] can be used to increase the yield of adventitious bulblets. Given the versatile properties of chitosan, this study evaluated the effects of chitosan with different molecular weights (MWs) on the growth, flowering and bulb yield of lilies.

2. Materials and Methods

The study was conducted at the West Pomeranian University of Technology in Szczecin (lat. 53°26'17"N, 14°32'32"E). The experiment used 'Mona Lisa' lily bulbs (average circumference 12–13 cm) of the oriental hybrid lily group recommended for growing in pots. The bulbs were imported from Dutch plantations. The bulbs were planted individually in pots (diameter = 16 cm, capacity = 2 dm³) filled with TS1 medium (Klasmann-Deliman, Germany), with pH 6.3, electrical conductivity (EC) 0.63 mS/cm, and the following composition (mg/l): nitrate nitrogen (N-NO₃), 182; phosphorus (P), 131; potassium (K), 402; calcium (Ca), 1646; magnesium (Mg), 172; and chlorine (Cl), 18. Plants were grown for one growing season, from 19 March to 30 July 2019, under natural photoperiod conditions on growing tables in an unheated plastic tunnel covered with double polyethylene film. The average air temperature recorded in the tunnel during lily cultivation was: March, 10.1°C; April, 11.9°C; May, 18.7°C; June, 23.6°C; and July, 21.1°C.

Three types of chitosan were used: commercial chitosan (CCh) with an MW of 50,000–190,000 g/mol (Sigma-Aldrich, Iceland), depolymerised chitosan with a MW

of ~48,000 g/mol (DCh 48) and depolymerised chitosan with a MW of ~154,500 g/mol (DCh 154). DCh 48 and DCh 154 with an average degree of deacetylation of ~85% were obtained by controlled free-radical degradation in the laboratory of the Center for Bioimmobilization and Innovative Packaging Materials at ZUT in Szczecin, Poland [23]. High-performance liquid chromatography (HPLC) was used to determine the DCh 48 and DCh 154 MWs. Chitosan was applied to watered plants as an aqueous solution (in distilled water) at a dose of 2.0 g/l. The dose was determined based on studies on bulbous plants [24]. Lilies were watered twice, after day 30 and 40 of cultivation, each time with 100 ml of chitosan solution per plant. Control plants were watered twice with 100 ml of distilled water. The experiment was set up in a randomised block design with three replicates, each with four plants.

When the first flower was developed, plant height [cm], tepal length [cm] and width [cm] were determined. At this stage, three plants were drawn from each replicate, in which the relative chlorophyll content as an indicator of leaf greenness was determined using the Soil and Plant Analysis Development (SPAD)-502 optical apparatus (Minolta, Japan). Measurements were taken on three fully expanded leaves of each plant. Flowers, buds and leaves were counted, and the fresh weight of the aboveground part of the plant [g] and the fresh weight of the leaves [g] were determined. The fresh weight was measured using an electronic scale (PS 200/2000/C/2, RADWAG, Poland) with an accuracy of 0.001 g.

After flowering, the bulbs removed from the pots were weighed [g], and their diameters [mm] were measured. The bulbs were used to propagate lilies by scales. For this purpose, three bulbs from each variant taken randomly (control, CCh, DCh 48 and DCh 154) were separated into scales, with four replicates per bulb. Scales from individual bulbs were placed separately in plastic bags (capacity = 2 dm³) filled with a moist mixture of acid peat and perlite (1:1, v/v). The scales were stored for 12 weeks without light at 20–22°C, then for 16 weeks at 3–5°C with a relative humidity of approximately 90%. After this period, the number of bulblets formed on scales derived from one bulb and the fresh weight of bulblets [g] were determined.

The experiment was set up in a single-factor, random sub-block design. The results were subjected to analysis of variance (ANOVA) for univariate experiments followed by Tukey's test for multiple comparisons using the Statistica™ Professional 13.3.0 software (TIBCO Statistica, USA). A *p* value ≤ 0.05 was considered to be statistically significant.

3. Results and Discussion

Watering with the DCh 154 solution produced the highest fresh weight of the aboveground part of the plants (Table 1). In this case, the fresh weight gain was increased significantly by 31.3% compared with the control plants. In the available literature, there are no reports on improving oriental lily production technology using chitosan under production conditions. On the other hand, there is information on the beneficial effect of chitosan on the growth of several lily species and their regenerative ability in *in vitro* cultures. Unfortunately, the characterisation of chitosan is generally lacking in these studies. Khalafi et al. [25] added 200 mg/l chitosan to the medium of *Lilium ledebourii* (Baker) Boiss. and noted significantly stimulated plant growth and increased their fresh weight. Pourbeyrami et al. [26] obtained similar results using the same dose of chitosan in *in vitro* cultures of *Lilium regale* E.H. Wilson. In contrast, Kanchanapoom et al. [27] found that the addition of 25 mg/l chitosan to the nutrient solution of *Lilium longiflorum* Thunb. significantly increased the number of multiplied shoots and acted similarly

effectively to the hormone benzyladenine. Shafiee-Masouleh [28] applied chitosan as nano- and magnetic particles at a concentration of 10–15 mg/l and found that it increased the fresh and dry weight of shoots and roots of oriental lily 'Arabian Red'. Based on previous studies [29, 30], it is possible that chitosan acts pleiotropically in cells to activate plant responses through various signalling pathways, transmitters and transcription factors that trigger the stimulatory effect.

Table 1. The effect of chitosan on plant height and the fresh weight of aboveground parts of oriental lily 'Mona Lisa'.

Treatment	Plant height [cm]	Fresh weight of the aboveground parts [g]
Control	46.0 ± 2.00 ^a	44.47 ± 3.10 ^b
CCh	47.5 ± 0.50 ^a	45.23 ± 0.80 ^b
DCh 48	48.8 ± 1.76 ^a	47.50 ± 2.51 ^b
DCh 154	48.1 ± 0.85 ^a	58.37 ± 1.10 ^a
<i>p</i>	0.172	0.0001

Note. The data are presented as the mean ± standard error of the mean. In each column, means followed by the same letter are not significantly different based on Tukey's test ($p \leq 0.05$). Abbreviations: CCh, commercial chitosan; DCh, depolymerised chitosan.

DCh 154 significantly affected the number of leaves and the fresh weight of leaves (Table 2). Compared with the control, plants watered with the DCh 154 solution showed a 16.8% increase in the number of leaves and a 29.0% increase in the fresh weight of leaves. The leaves of plants watered with the CCh solution showed the highest chlorophyll content, with a significant 11.3% increase compared with the control plants. Chamnanmanoontham et al. [31] showed that the elevated chlorophyll content in the leaves of chitosan-treated plants may be the result of increased expression of proteins involved in carbon metabolism and the photosynthetic process, leading to an increase in nutrients, primary metabolites, phytohormones and photosynthetic pigments necessary to stimulate plant growth [29].

Table 2. The effect of chitosan on number and weight of leaves and relative chlorophyll content of oriental lily 'Mona Lisa'.

Treatment	Number of leaves per plant	Leaf fresh weight [g/plant]	Relative chlorophyll content (SPAD)
Control	19.7 ± 1.15 ^b	25.5 ± 1.15 ^b	58.6 ± 0.59 ^b
CCh	20.3 ± 1.53 ^{ab}	26.0 ± 0.89 ^b	65.2 ± 1.34 ^a
DCh 48	22.0 ± 1.00 ^{ab}	26.2 ± 0.93 ^b	51.9 ± 2.64 ^c
DCh 154	23.0 ± 1.00 ^a	32.9 ± 1.36 ^a	62.8 ± 1.98 ^{ab}
<i>p</i>	0.032	0.001	0.001

Note. The data are presented as the mean ± standard error of the mean. In each column, means followed by the same letter are not significantly different based on Tukey's test ($p \leq 0.05$). Abbreviations: CCh, commercial chitosan; DCh, depolymerised chitosan; SPAD, Soil and Plant Analysis Development.

Regardless of its source and MW, chitosan did not affect the number of flowers and buds, but it did affect the length and width of lily petals (Table 3, Figure 1). Watering the plants

with the DCh 48 solution significantly reduced the length and width of perianth tepals by 8.6% and 6.8%, respectively, compared with the control plants. Treatment with the CCh or DCh 154 solution did not significantly affect tepal parameters.

Table 3. The effect of chitosan on the number of flowers and buds and the length and width of the tepals of oriental lily ‘Mona Lisa’.

Treatment	Number of flowers per plant	Number of buds per plant	Tepal length [cm]	Tepal width [cm]
Control	1.83 ± 0.29 ^a	1.67 ± 0.29 ^a	12.8 ± 0.05 ^a	6.50 ± 0.10 ^a
CCh	1.83 ± 0.29 ^a	1.83 ± 0.19 ^a	12.2 ± 0.10 ^{ab}	6.17 ± 0.21 ^{ab}
DCh 48	1.16 ± 0.21 ^a	2.50 ± 0.50 ^a	11.7 ± 0.13 ^b	6.06 ± 0.06 ^b
DCh 154	2.00 ± 0.01 ^a	1.83 ± 0.29 ^a	12.7 ± 0.58 ^a	6.22 ± 0.22 ^{ab}
<i>p</i>	0.055	0.080	0.007	0.046

Note. The data are presented as the mean ± standard error of the mean. In each column, means followed by the same letter are not significantly different based on Tukey’s test ($p \leq 0.05$). Abbreviations: CCh, commercial chitosan; DCh, depolymerised chitosan.

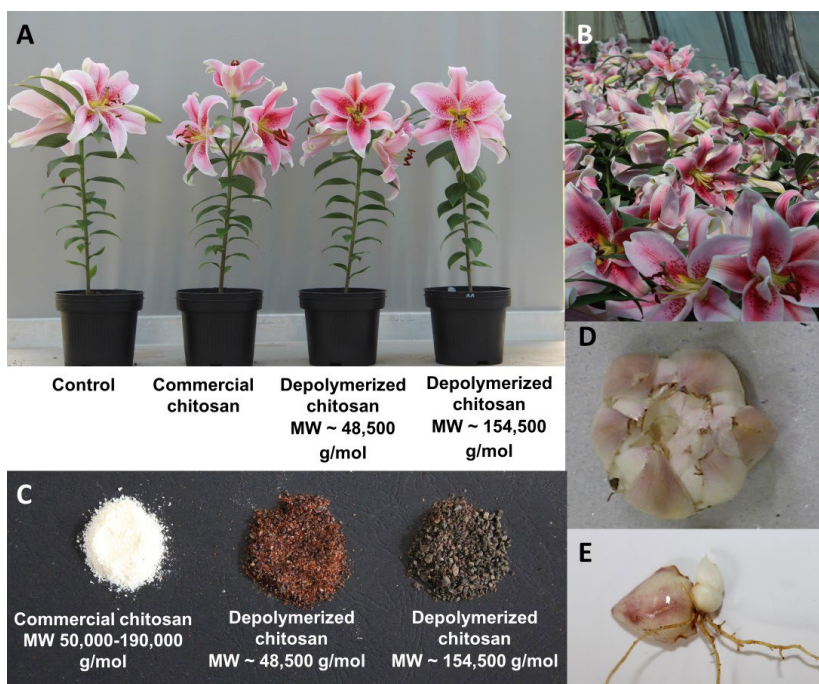


Figure 1. The effect of chitosan on flowering and the bulb yield of oriental lily ‘Mona Lisa’. The photographs show (A) from left to right, an untreated control plant, and plants treated with commercial chitosan (CCh) with a molecular weight (MW) of 50,000–190,000 g/mol, depolymerised chitosan with a MW of ~48,000 g/mol (DCh 48) or depolymerised chitosan with a MW of ~154,500 (DCh 154); (B) flowering lilies in a foil tunnel; (C) chitosan used to the prepare aqueous solutions; (D) a lily bulb; (E) formation of bulblets on a bulb scale.

According to various authors, the response of plants to the type of chitosan used depends on its physical and chemical properties, such as the degree of deacetylation, MW and viscosity [29, 30, 32]. Table 4 shows the significant effect of watering plants with the chitosan solutions on the fresh weight of bulb and bulb diameter of the oriental lily 'Mona Lisa'. Compared with the control plants, bulbs watered with the CCh and DCh 154 solutions had a 11.0% and 12.3% higher fresh weight, respectively. Plants treated with CCh, DCh 48 and DCh 154 developed bulbs with 12.3%, 12.1% and 11.0% larger diameters, respectively, compared with the control plants. Khalafi et al. [25] demonstrated that chitosan significantly increased the yield of *L. ledebourii* bulbs. The authors reported an increased number of bulblets and plant roots after adding 200 mg/l chitosan to the nutrient solution.

Table 4. The effect of chitosan on the fresh weight and diameter of oriental lily 'Mona Lisa' bulb.

Treatment	Bulb fresh weight [g/plant]	Bulb diameter [mm]
Control	34.6 ± 1.83 ^b	47.2 ± 0.88 ^b
CCh	41.9 ± 2.41 ^a	53.0 ± 0.79 ^a
DCh 48	39.9 ± 2.01 ^{ab}	52.9 ± 1.01 ^a
DCh 154	42.5 ± 2.45 ^a	52.4 ± 0.58 ^a
<i>p</i>	0.008	0.001

Note. The data are presented as the mean ± standard error of the mean. In each column, means followed by the same letter are not significantly different based on Tukey's test ($p \leq 0.05$). Abbreviations: CCh, commercial chitosan; DCh, depolymerised chitosan.

Bulbs are organs of vegetative reproduction that show the ability to regenerate the entire plant. Churikoca and Barykina [33] and Feher [34] showed that the main reason for this regenerative ability is the totipotency of bulb cells. When bulbs are placed under conditions of high humidity and temperature without access to light, adventitious bulblets (Figure 1) are formed on the scales from buds in a dormant state. The rate of formation of adventitious bulblets on scales can be increased by using hormones and growth regulators, but with current pro-ecological trends and legal conditions, this approach is increasingly being abandoned [35]. In the present study, the effect of chitosan on bulblet yield – the fresh weight of bulbet and the number of bulblets – was evaluated on the scales of lily bulblets (Table 5). Bulblets formed on scales from bulbs treated with the DCh 154 solution had a 21.9% increase in fresh weight compared with the control. Scales from bulbs treated with the CCh and DCh 48 solutions yielded a significant 44.9% and 45.4% increase in the number of bulblets, respectively. The increased yield of bulblets may indicate a longer accumulation of the biostimulatory agent chitosan in the bulb and its secondary effect on the formation of bulblets on the scales. In addition, the resulting bulblets had no symptoms of disease, which could suggest that chitosan had a protective effect on them. Gong et al. [36] treated lanzhou lily (*Lilium davidii* var. *unicolor*) with chitosan in combination with natamycin to encapsulate the bulb slices. It was effective in maintaining their quality and preventing loss of weight, vitamin C, soluble sugars and proteins. Although there have been many studies, the mechanism of action of chitosan in plant organs is not yet completely clear [37, 38].

Table 5. Post harvest effects of chitosan on fresh weight of bulb and number of bulblets of 'Mona Lisa' lily.

Treatment	Fresh weight of bulblet [g]	Number of bulblets
Control	0.32 ± 0.02 ^b	20.7 ± 8.39 ^b
CCh	0.34 ± 0.02 ^b	30.0 ± 4.58 ^a
DCh 48	0.31 ± 0.02 ^b	30.1 ± 6.56 ^a
DCh 154	0.39 ± 0.01 ^a	24.0 ± 6.93 ^{ab}
<i>p</i>	0.001	0.001

Note. The data are presented as the mean ± standard error of the mean. In each column, means followed by the same letter are not significantly different based on Tukey's test ($p \leq 0.05$). Abbreviations: CCh, commercial chitosan; DCh, depolymerised chitosan.

4. Conclusions

The results presented in this study showed the usefulness of chitosan as a natural biostimulant in the production of oriental lilies. The DCh 154 solution had the strongest effect on growth and yield, with a significant increase in biomass, the number of leaves and leaf weight, of the bulb diameter and the fresh weight of bulb and bulblet. This treatment should be recommended for the production of high-quality lilies. Depolymerised chitosan is particularly important for the horticultural sector as an alternative to environmentally harmful chemicals. The need for integrated plant breeding and the growing interest in organic crops in horticulture may encourage the use of chitosan, also in the production of other bulb crops.

5. References

- [1] Gabellini S, Scaramuzzi S; (2022) Evolving consumption trends, marketing strategies, and governance settings in ornamental horticulture: a grey literature review. *Horticulturae* 8(3), 234. DOI:10.3390/horticulturae8030234
- [2] Cardoso JC, Vendrame WA; (2022). Innovation in propagation and cultivation of ornamental plants. *Horticulturae* 8(3), 229. DOI:10.3390/horticulturae8030229
- [3] Singh R, Singh R, Gehlot A, Akram SV, Priyadarshi N, Twala B; (2022) Horticulture 4.0: adoption of Industry 4.0 technologies in horticulture for meeting sustainable farming. *Appl Sci* 12(24), 12557. DOI:10.3390/app122412557
- [4] Parađiković N, Teklić T, Zeljković S, Lisjak M, Špoljarević M; (2019) Biostimulants research in some horticultural plant species – a review. *Food Energy Secur* 8(2), e00162. DOI:10.1002/fes3.162
- [5] Hossain S, Afrin S, Anika S, Sultana S, Haque P, Shahruzzaman MD; (2022) Synthesis, characterization, and modification of natural polysaccharides. In: Naeem M, Aftab T, Khan MMA (eds), *Radiation-processed polysaccharides*. Academic Press, New York, 29–74. DOI:10.1016/B978-0-323-85672-0.00009-X
- [6] Huq T, Khan A, Brown D, Dhayagude N, He Z, Ni Y; (2022) Sources, production and commercial applications of fungal chitosan: a review. *J Bioresour Bioprod* 7, 85–98. DOI:10.1016/j.jobab.2022.01.002
- [7] Riseh RS, Vazvani MG, Kennedy JF; (2023) The application of chitosan as a carrier for fertilizer: a review. *Int J Biol Macromol* 252, 126483. DOI:10.1016/j.ijbiomac.2023.126483

- [8] Du Jardin P; (2015) Plant biostimulants: Definition, concept, main categories and regulation. *Sci Hortic* 196, 3–14. **DOI:**10.1016/j.scienta.2015.09.021
- [9] Katiyar D, Hemantaranjan A, Singh B; (2015) Chitosan as a promising natural compound to enhance potential physiological responses in plant: a review. *Indian J Plant Physiol* 20, 1–9. **DOI:**10.1007/s40502-015-0139-6
- [10] El Amerany F, Rhazi M, Balcke G, Wahbi S, Meddich A, Taourirte M, Hause B; (2022) The effect of chitosan on plant physiology, wound response, and fruit quality of tomato. *Polymers* 14(22), 5006. **DOI:**10.3390/polym14225006
- [11] Hidangmayum A, Dwivedi P, Katiyar D, Hemantaranjan A; (2019) Application of chitosan on plant responses with special reference to abiotic stress. *Physiol Mol Biol Plants* 25, 313–326. **DOI:**10.1007/s12298-018-0633-1
- [12] Betchem G, Johnson NAN, Wang Y; (2019) The application of chitosan in the control of post-harvest diseases: a review. *J Plant Dis Protect* 126, 495–507. **DOI:**10.1007/s41348-019-00248-2
- [13] Korbecka-Glinka GK, Wiśniewska-Wrona M, Kopania E; (2021) The use of natural polymers for treatments enhancing sowing material. *Polimery* 66(1), 11–20. **DOI:**10.14314/polimery.2021.1.2
- [14] Salachna P, Pietrak A; (2021) Evaluation of carrageenan, xanthan gum and depolymerized chitosan based coatings for pineapple lily plant production. *Horticulturae* 7(2), 19. **DOI:**10.3390/horticulturae7020019
- [15] Jiang Y, Yu L, Hu Y, Zhu Z, Zhuang C, Zhao Y, Zhong Y; (2020) The preservation performance of chitosan coating with different molecular weight on strawberry using electrostatic spraying technique. *Int J Biol Macromol* 151, 278–285. **DOI:**10.1016/j.ijbiomac.2020.02.169
- [16] Tang N, Ju X, Hu Y, Jia R, Tang D; (2020) Effects of temperature and plant growth regulators on the scale propagation of *Lilium davidii* var. unicolor. *HortSci* 55(6), 870–875. **DOI:**10.21273/HORTSCI14916-20
- [17] Zhou J, An R, Huang X; (2021) Genus *Lilium*: A review on traditional uses, phytochemistry and pharmacology. *J Ethnopharmacol* 270, 113852. **DOI:**10.1016/j.jep.2021.113852
- [18] Inamoto K, Nagasuga K, Yano T; (2022) Effect of CO₂ enrichment on the photosynthesis and dry matter accumulation in the Oriental hybrid lily 'Siberia'. *J Hortic* 91(4), 541–550. **DOI:**10.3390/horticulturae9050561
- [19] Chahal D, Malik A, Devi S; (2022) Effect of Different growing conditions and genotypes on growth and bulb parameters of Asiatic lily. *Agric Sci Dig* 42(4), 407–413. **DOI:**10.18805/ag.D-5294
- [20] Treder J; (2003) Effects of supplementary lighting on flowering, plant quality and nutrient requirements of lily 'Laura Lee' during winter forcing. *Sci Hortic* 98(1), 37–47. **DOI:**10.1016/S0304-4238(02)00220-0
- [21] Al-Ajlouni MG, Othman YA, Tala S, Ayad JY; (2023) *Lilium* morphology, physiology, anatomy and postharvest flower quality in response to plant growth regulators. *S Afr J Bot* 156, 43–53. **DOI:**10.1016/j.sajb.2023.03.004
- [22] De Lucia B, Vecchiatti L; (2012) Type of bio-stimulant and application method effects on stem quality and root system growth in LA Lily. *Eur J Hortic Sci* 77(1), 10–15.
- [23] Bartkowiak A; (2001) Binary polyelectrolyte microcapsules based on natural polysaccharides. *Prace Naukowe Politechniki Szczecińskiej* 566(3), 5–102.
- [24] Salachna P, Zawadzińska A; (2014) Effect of chitosan on plant growth, flowering and corms yield of potted freesia. *J Ecol Eng* 15(3), 97–102. **DOI:**10.12911/22998993.1110223

- [25] Khalafi M, Pourbeyrami Hir Y, Chamani E, Maleki Lajayer H; (2022) The effect of chitosan on regeneration and secondary metabolite production of two species of lily flower. *J Plant Res (Iran J Biol)* 35(2), 374–388.
- [26] Pourbeyrami Hir Y, Khalafi M, Chamani E, Maleki Lajayer H; (2021) Effect of chitosan on regeneration and secondary metabolite production of *Lilium regale*. *J Plant Physiol Breed* 11(2), 147–160.
- [27] Kanchanapoom K, Pimolthai P, Kanchanapoom K; (2012) The effect of chitosan on regeneration of lily (*Lilium longiflorum* Thunb. 'Ester Lily') from bulb scale explants cultured *in vitro*. *Propag Ornament Plants* 12(2), 127–129.
- [28] Shafiee-Masouleh SS, Hatamzadeh A, Samizadeh H, Rad-Moghadam K; (2014). Enlarging bulblet by magnetic and chelating structures of nano-chitosan as supplementary fertilizer in *Lilium*. *Hortic Environ Biotechnol* 55, 437–444. **DOI:**10.1007/s13580-014-0175-6
- [29] Ahmed KBM, Khan MMA, Siddiqui H, Jahan A; (2020) Chitosan and its oligosaccharides, a promising option for sustainable crop production - a review. *Carbohydr Polym* 227, 115331. **DOI:**10.1016/j.carbpol.2019.115331
- [30] Zhang X, Li K, Xing R, Liu S, Chen X, Yang H, Li P; (2018) miRNA and mRNA expression profiles reveal insight into chitosan-mediated regulation of plant growth. *J Agric Food Chem* 66(15), 3810–3822. **DOI:**10.1021/acs.jafc.7b06081
- [31] Chamnanmanoontham N, Pongprayoon W, Pichayangkura R, Roytrakul S, Chadchawan S; (2015) Chitosan enhances rice seedling growth via gene expression network between nucleus and chloroplast. *Plant Growth Regul* 75, 101–114. **DOI:**10.1007/s10725-014-9935-7
- [32] Román-Doval R, Torres-Arellanes SP, Tenorio-Barajas AY, Gómez-Sánchez A, Valencia-Lazcano AA; (2023) Chitosan: Properties and its application in agriculture in context of molecular weight. *Polymers* 15(13), 2867. **DOI:**10.3390/polym15132867
- [33] Churikoca OA, Barykina RP; (2015) Microclonal propagation of some bulbous and cormous plants based on regeneration processes in morphological different explants. *Wulfenia* 22, 21–32.
- [34] Feher A; (2019) Callus, dedifferentiation, totipotency, somatic embryogenesis: What these terms mean in the era of molecular plant biology? *Front Plant Sci* 10, 536. **DOI:**10.3390/plants9060702
- [35] Drobek M, Frąc M, Cybulska J; (2019) Plant biostimulants: importance of the quality and yield of horticultural crops and the improvement of plant tolerance to abiotic stress – a review. *Agronomy* 9(6), 335. **DOI:**10.3390/agronomy9060335
- [36] Gong H, Li F, Sun A, Sun M, Tang G; (2016) Effects of natamycin and chitosan coating compounds on fresh-keeping of Lanzhou lily bulb during storage. *Food Ferment Ind* 42(2), 208–212.
- [37] Lopez-Moya F, Suarez-Fernandez M, Lopez-Llorca LV; (2019) Molecular Mechanisms of Chitosan Interactions with Fungi and Plants. *J Mol Sci* 20(2), 332. **DOI:**10.3390/ijms20020332
- [38] Nepthali L, Piater LA, Dubery IA, Patterson V, Huyser J, Burgess K, Tugizimana F; (2020) Biostimulants for plant growth and mitigation of abiotic stresses: a metabolomics perspective. *Metabolites* 10(12), 505. **DOI:**10.3390/metabo10120505